DIRECT TORQUE CONTROL OF INDUCTION MACHINES CONSIDERING THE IRON LOSSES

TRUC PHAM-DINH

A thesis submitted in partial fulfilment of the requirements of Liverpool John Moores University for the degree of Doctor of Philosophy

April 2003

ABSTRACT

Theoretical principles of direct torque control (DTC) for high performance drives were introduced in the second half of the eighties. A DTC scheme requires simple signal processing methods and it entirely relies on the non-ideal nature of the voltage source inverter, since the on-off control of converter switches is used for the decoupling of non-linear structure of the induction machines. Although offering potential for a simple implementation, DTC in practice suffers from a number of shortcomings, related to various segments of the basic control algorithm. An attempt is made in this research project to address some of the problems and provide improved versions of the DTC algorithm.

The research focuses on three particular aspects of direct torque control. The first one is a comparison of performance obtainable with vector control and direct torque control. This issue is addressed at first theoretically and by simulation. It is argued that the most sensible approach is to compare DTC scheme with a very specific stator flux oriented control scheme. Next, an experimental comparison is performed utilising an industrial vector controlled induction motor drive and the commercially available ABB's direct torque controlled drive.

The second aspect is the choice of an appropriate switching table for direct torque control. An attempt is made to improve DTC operation in both low speed and high speed region, by appropriately modifying the inverter switching pattern.

The third aspect is the impact of iron loss existence on accuracy of direct torque control and means for iron loss compensation in sensored and sensorless mode of operation. This aspect has never been addressed before in the existing literature. Both torque mode of operation (which is inherently sensorless) and speed mode of operation (in sensored configuration and sensorless configuration, using two MRAS-based speed estimation schemes) are covered by extensive theoretical considerations and numerous simulations. Torque and speed estimation errors due to iron loss are evaluated and improved schemes for torque and speed estimation, which provide compensation for the iron loss induced detuning, are developed.

An original contribution is offered in relation to all three aspects. The most important contributions of the thesis are believed to be those related to the third aspect.

ACKNOWLEDGEMENTS

I would like to express my sincere gratitude to my Director of Studies, Professor Emil Levi, for his professional guidance and support throughout the course of the project and the presentation of this thesis.

Many thanks go to the technicians Brian Gray and Ron McGovern for their help during the setting up of the experimental rig.

Finally, I would like to thank my parents, my brother, and my sister for their limitless supports and encouragement during the PhD study period.

CONTENTS

CHAPTER 7: SENSORLESS DIRECT TORQUE CONTROL

LIST OF FIGURES

LIST OF TABLES

LIST OF SYMBOLS

$\underline{a}$: Complex spatial operator;

$\underline{v}$: Voltage space vector;

$\underline{i}$: Current space vector;

$\underline{\psi}$: Flux space vector;

v: Voltage;

i: Current;

ψ : Flux;

v_A, v_B, v_C : Leg voltages of voltage source inverter;

v_a, v_b, v_c : Phase to neutral voltages of voltage source inverter;

S_A, S_B, S_C : Switching functions of voltage source inverter;

V_{DC}: DC link voltage of voltage source inverter;

J: Inertia of the induction machine;

L: Inductance;

P: Number of pole pairs;

R: Resistance;

p: Differentiation operator;

T_L : Load torque;

T_e : Electromagnetic torque;

T_r : Rotor time constant;

σ : Leakage coefficient;

ω_r : Angular rotor speed;

ω_s : Angular speed of stator flux space vector;

ω_r^r : Angular speed of rotor flux space vector;

ω_a : Angular speed of common rotating reference frame;

ω_{sl} : Angular slip frequency;

δ : Instantaneous angular position of voltage space vector with respect to phase *a* magnetic axis of stator;

ε : Instantaneous angle between stator and rotor flux space vector;

ϕ : Instantaneous angular position of flux space vector with respect to phase *a* magnetic axis of stator;

γ : Instantaneous angular position of current space vector with respect to phase *a* magnetic axis of stator;

λ : Instantaneous angle between stator current space vector and rotor flux space vector;

θ : Instantaneous rotor angular position with respect to phase *a* magnetic axis of stator;

θ_s : Instantaneous angular position of common rotating reference frame with respect to phase *a* magnetic axis of stator.

θ_r : Instantaneous angular position of common rotating reference frame with respect to phase *a* magnetic axis of rotor.

Superscripts:

'*': Reference values;

' ' ': Rotor quantities referred to stator winding;

'*e*': Estimated quantities;

Subscripts:

A,B,C: Rotor phase variables;

a,b,c: Stator phase variables;

'*s*': Associated with stator winding;

'*r*': Associated with rotor winding;

α,β: Associated with axes of stationary common reference frame;

d,q: Associated with axes of rotating common reference frame;

σ : Leakage inductance;

'm': Associated with magnetising variables;

Fe, iron: Associated with quantities representing iron loss;

CHAPTER 1

INTRODUCTION

1.1 An overview of vector control of induction machines

Vector control has become the most popular control method of induction machines during the last 20 years. It is nowadays widely accepted by the drive manufacturers and there are numerous products on the market that utilise this control principle [Vas (1998)]. Vector control enables induction machines to be utilised in applications where DC machines used to be applied in the past. The advantages of induction machines over DC machines are lower cost of purchase and maintenance, better reliability in hostile environment, higher efficiency, simplicity, ruggedness, absence of brushes, etc [Vas (1998)]. However, vector control method requires more sophisticated hardware and software than the control system of DC machines.

Vector control principles utilise reference frame transformation to refer three phase quantities to a rotating reference frame with fictitious direct and quadrature axes. The new set of differential equations in the new reference frame does not contain time-varying inductances and the decoupling of torque and flux control can be achieved by appropriate selection of the angular speed of rotation of the reference frame [Novotny and Lipo (1996), Krause et al (1995)]. Torque and flux of the machine can be then controlled independently with two different current commands, this being analogous to torque and flux control in DC machines that are used for high dynamic performance. In simple terms, vector control can be defined as a set of control algorithms that enable conversion of an AC machine into its equivalent DC machine counterpart from the control point of view. The means for controlling torque and flux in the rotating reference frame are q-component and d-component of the stator current. There are three possibilities of vector control in induction machines [Trzynadlowski (1994)]:

- Rotor flux oriented control, in which the reference frame is fixed to the rotor flux space vector;
- Stator flux oriented control, with reference frame being fixed to the stator flux space vector;

- Air-gap flux oriented control, with air-gap flux space vector being used for alignment of the d-axis of the reference frame.

The rotor flux oriented control is the most commonly used one among the three, since it requires the least complicated control system configuration [Leonhard (1996)]. Rotor flux oriented control can be realised using direct and indirect control methods for achieving orientation. In one of the direct methods, flux sensors are used to measure the air-gap flux components. These then can be used together with other measured electromagnetic quantities such as phase currents to calculate the magnitude and position of rotor flux. The information regarding instantaneous rotor flux space vector position is required for co-ordinate transformation, since the control system operates in a fictious rotating d-q reference frame, while the machine is supplied with physical three-phase currents in stationary reference frame. The information regarding rotor flux magnitude can be used to estimate the motor torque. By creating closed loop rotor flux and torque control, one is then able to generate references for stator d-q axis current components. This scheme reduces the sensitivity of control to parameter variation effects in the machine [Trzynadlowski (1994)]. However, the high cost of flux sensors and the vulnerability of these devices in hostile environment are the shortcomings of the scheme. Another method of direct field orientation utilises measured stator currents and measured or reconstructed stator voltages in the process of rotor flux position and magnitude estimation. The scheme is sensitive to variation in the stator resistance and in general is not applicable at low and zero speed due to integration problems that occur around zero frequency. In the indirect method, speed position transducers are used to measure the rotor speed position, which is then used for rotor flux position determination together with reference stator current d-q axis components. This scheme gives a better performance at low speed but the sensitivity of the control system to parameter variations is increased [Trzynadlowski (1994)].

Regardless of whether direct or indirect field orientation method is applied, control system generates stator current commands and current controllers are required. Current control can be carried out in stationary reference frame (current-fed machines) or rotating reference frame (voltage-fed machines). In the latter case, two co-ordinate transformations (for measured stator currents and commanded quantities that are now phase voltage references) are necessary.

The idea of rotor flux oriented control can be extended to stator flux oriented control. There are many similarities between the two schemes and stator flux oriented

control enables decoupling of torque and flux control as well. Flux and torque are again controlled independently using d-q axis components of the stator current. However, the essential difference between vector control with rotor flux orientation and the stator flux oriented control is the fact that stator flux oriented control requires an additional decoupling circuit. The simpler configuration (without decoupling circuit in the case of current fed induction machine) has made the rotor flux oriented control preferable and that is the reason why rotor flux oriented control has been in the focus of research for such a long time [Trzynadlowski (1994)]. Recent development of high-speed and low-cost microprocessors has however made the realisation of stator flux orientation possible, and stator flux oriented control of a current-fed induction machine has been studied in detail and implemented successfully [Xu et al (1988a and 1988b)]. However, the industry has not accepted stator flux oriented control as a viable alternative to rotor flux oriented control to this date. The increase in complexity of the control system offsets some advantages, such as easier determination of co-ordinates of the reference flux vector and reduced dependency of control system on accurate knowledge of machine's parameters. In addition to higher complexity, there are some limits concerning achievable torque, this not being the case for rotor flux orientation [Trzynadlowski (1994)].

The air-gap flux oriented control scheme also requires an additional decoupling circuit. However, when the flux sensor is used for measuring the air-gap flux as in one of the direct control methods, this control scheme could be advantageous [De Donker et al (1990)]. Once more, though, commercial products with air-gap flux oriented control are not available on the market.

In general, the main characteristic of vector control is the independent and indirect control of torque and flux by two components of the stator current in a rotating reference frame. This control characteristic is the main advantage of vector control that, together with the low cost, compactness and efficiency of AC machines, makes the application practical in areas where only DC machines were used previously. However, this is achieved by using co-ordinate transformation and current control loops, which make the control system more complicated. The main characteristics and shortcomings of vector control may be summarised as follows [Vas (1998)]:

1. In addition to other controllers, current controllers (in stationary or rotating reference frame) are required.

2. At least one co-ordinate transformation (or two, if current control is in the rotating frame) has to be executed on-line, in real time.
3. A separate PWM block is required for the inverter control (except when hysteresis current control is used).
4. A decoupling circuit is required, unless rotor flux oriented control with current control in stationary reference frame is used.
5. A precise estimate of the instantaneous position of the selected flux space vector is necessary.
6. Depending on the selected control system configuration, flux and torque estimates may or may not be required.
7. In most of the methods of achieving field orientation, information regarding rotor speed (or position) is required for the orientation angle calculation.
8. All the schemes are to some extent affected by variation of induction machine parameters.

One issue that has attracted a lot of interest during the last decade is the possibility of estimating the rotor speed (and/or position) rather than measuring it. As already noted, information regarding machine's speed is required not only for closed loop speed control, but, in many cases, for orientation purposes as well. The utilisation of speed sensor reduces the reliability of the drive and increases cost. Numerous speed estimation schemes have been suggested recently with the idea of eliminating the speed sensors. The speed sensor-less control generally requires more complex hardware configuration and control algorithms. An ideal solution to the problem of speed estimation is still not in sight and is unlikely to exist [Vas (1998)].

1.2 Direct torque control of induction machines

Theoretical principles of direct torque control for high performance drives were introduced in the second half of the eighties [Takahashi and Noguchi (1986), Depenbrock (1985 and 1988)]. Compared with field oriented control, that has its origin in the beginning of the seventies, direct torque control (DTC) is therefore a significantly newer concept. It took almost twenty years for the vector control to gain acceptance by the industry. In contrast to that, the concept of DTC has been taken on board by the industry relative quickly, in only ten years [Schofield (1998) and Tiitinen et al (1995)].

While vector control predominantly relies on mathematical modelling of an induction machine, direct torque control makes direct use of physical interactions that take place within the integrated system of the machine and its supply. The DTC scheme requires simple signal processing methods and it entirely relies on the non-ideal nature of the power source that is used to supply an induction machine within the variable speed drive system (two-level or three-level voltage source inverters, matrix converters, etc.). It can therefore be applied to power electronic converter-fed machines only. The on-off control of converter switches is used for the decoupling of non-linear structure of the induction machine [Kazmierkowski and Tunia (1994)]. The most frequently discussed and used power electronic converter in DTC drives is a voltage source inverter.

Direct torque control takes a different look at the induction machine and the associated power electronic converter. First of all, it recognised that, regardless of how the inverter is controlled, it is by default a voltage source rather than a current source. Next, it dispenses with one of the main characteristics of the vector control, indirect flux and torque control by means of two stator current components. In essence, direct torque control recognises that if flux and torque can be controlled indirectly by these two current components, then there is no reason why it should not be possible to control flux and torque directly, without intermediate current control loops.

Control part of a DTC drive consists of two parallel branches, this being a similarity with vector control. References are the flux set point and the torque set point (which may or may not be the output of the speed controller, depending on whether the drive is torque controlled or speed controlled). Direct torque control asks for estimation of stator flux and the motor torque, so that closed loop flux and torque control can be established. However, the errors between the set and estimated flux and torque values are used in a completely different way, when compared to vector control (where these errors would be used as inputs of the PI controllers, whose outputs are then set points for the stator *d-q* axis current references). The basic idea of DTC is that the existing errors in torque and flux can be used directly to drive the inverter, without any intermediate current control loops or co-ordinate transformation. Flux and torque controllers are of hysteresis types and their outputs are used to determine which of the possible inverter states should be applied to the machine terminals, so that the errors in flux and torque remain within the prescribed hysteresis bands.

Direct torque control is inherently sensorless. Information about actual rotor speed is not necessary in the torque mode of operation because of the absence of co-

ordinate transformation. However, correctness of estimation of stator flux and torque is important for the accurate operation of hysteresis controllers. An accurate mathematical model of an induction machine is therefore essential in DTC. Accuracy of direct torque control is also independent of variations of rotor's parameters. Only variation of stator resistance due to change in thermal operating conditions causes problems for high performance DTC at low speed.

In summary, main features of DTC and differences compared to vector control are the following [Vas (1998)]:

- Direct control of flux and torque.
- Indirect control of stator currents and voltages.
- Absence of co-ordinate transformation.
- Absence of separate voltage modulation block, usually required in vector drives.
- Requirement to know only the sector in which the stator flux linkage space vector is positioned, rather than the exact position of it (necessary in vector drives for co-ordinate transformation).
- Absence of current controllers.
- Inherently sensorless control since speed information is not required at all in the torque mode of operation.
- In its basic form DTC scheme is sensitive to only variation in stator resistance.

1.3 Problems identified in basic DTC scheme for an induction motor

Although being considerably simpler than a vector control scheme, DTC scheme in its basic form [Takahashi and Noguchi (1986)] suffers from a number of potential problems when it comes to an actual implementation. A considerable effort has therefore been put during the last fifteen years into overcoming these shortcomings. A detailed literature survey related to recent improvements in the basic scheme of DTC of an induction motor is provided in chapter 2. It suffices here to say that the main drawbacks of the basic DTC scheme, identified in the literature, are the following:

- Operation of the inverter with a variable switching frequency due to use of hysteresis torque and flux controllers.

- Excursions of stator flux and torque outside the prescribed hysteresis bands in low speed and high speed regions, respectively, when optimum switching table of [Takahashi and Noguchi (1986)] is applied.
- Since stator currents are controlled only indirectly, current limiting is not a straightforward task (in contrast to vector control).
- Integration problem due to offset and drift, encountered in the basic scheme of stator flux and torque estimation from measured stator voltages and stator currents.
- Inaccuracy in the estimation of stator flux and torque in the low speed region due to inevitable variation in stator resistance.
- Rapid ageing of stator winding insulation due to high rate of applied voltage change.

In addition to these well-known problems related to direct torque control of induction machines, one particular issue, which has never before been investigated in conjunction with DTC, is the impact of stator iron loss existence on the motor control and means for its compensation. Stator iron loss is invariably neglected in induction motor models used for the derivation of the DTC algorithm. Its existence therefore affects the accuracy of control and it might be advantageous to provide some means for compensation of its adverse effects. Investigation of this particular topic represents the main theme of this research project and simultaneously is the main original contribution, as discussed in the next section.

1.4 Aims of the research project

1.4.1 Research objectives

Direct torque control is a relatively new method of variable speed operation, which enables simple control of high performance induction motor drives. This is still a rather novel and attractive research area where a lot of work remains to be done. The main aim of this project is to attempt to achieve an improvement over the existing solutions by analysing and solving some of the existing problems. The specific objectives of the project are:

1. *A detailed investigation of various inverter switching algorithms for direct torque control schemes of high performance induction motor drives.*

2. *Investigation of the impact of iron loss on direct torque control and analysis of suitable means for the compensation of their impact on accuracy of control, as applicable to the torque mode of operation.*
3. *Investigation of speed estimation schemes suitable for sensor-less direct torque control of induction machines in the speed mode of operation.*
4. *Investigation of the impact of iron loss on the accuracy of speed estimation in sensorless direct torque control and development of novel compensation method for iron loss, within the speed estimator.*
5. *Realisation of an experimental rig for investigation of performance of an industrial DTC induction motor drive.*

The major advances with respect to the current state of the art are achieved in objectives 2 to 4.

1.4.2 Investigation approaches

A number of approaches have been utilised in order to realise the objectives listed above. The approaches are the following.

Survey of literature on direct torque control is undertaken first. Problems, already listed in the previous section, inherent to the DTC of induction machines are identified in this way and various improvements over the basic [Takahashi and Noguchi (1986)] solution are examined. The lack of any previous research work related to the impact of iron loss on DTC of induction machines and means for its compensation is observed and this is further taken as the main research direction for this particular research work.

Since the whole concept of induction motor DTC entirely relies on the non-ideal nature of the inverter, the main investigation approach taken for further work is dynamic simulation. This approach requires building of dynamic mathematical models for an induction machine. The models used are standard constant parameter machine model and machine models with iron loss representation. Model of voltage source inverter is also constructed. These models are built in Matlab/Simulink, as is the classical direct torque controller for simulation of operation of torque controlled and speed controlled DTC induction motor drive in the base speed region.

A number of different switching tables with different voltage space vector selection schemes are looked at to investigate torque and flux responses. A comparison

of the performance achievable with the classical switching table and with modified switching tables is made.

Simulation of direct torque control of an induction machine with iron loss consideration in both torque mode and speed mode is undertaken next. A novel method for compensation of iron loss in a DTC induction machine is developed for the torque mode of operation and is further verified by simulation.

The research then moved to simulation of sensorless direct torque control of induction machine with model reference adaptive system (MRAS) based speed estimators. Stator flux based MRAS speed estimator and rotor flux based MRAS speed estimator are discussed. Induction machine models with and without iron loss representation are used. Direct torque controllers with and without iron loss compensation are applied in conjunction with the sensorless DTC drive and operation is investigated by simulation.

A novel method of iron loss compensation in speed estimator is then suggested. Simulation of sensorless direct torque control with compensation of iron loss in both direct torque controller and speed estimator is performed and the proposed schemes are verified in this way.

Construction of an experimental rig with ABB industrial DTC drive is finally undertaken and performance is investigated experimentally.

1.4.3 Originality of the research

Existing literature on direct torque control does not contain any discussion of the impact of iron loss on torque and flux control in torque mode of operation and speed mode of operation with and without speed sensor. Literature on the voltage space vector selection schemes in direct torque control is mostly restricted to improvement of the stator flux response in low speed region. The original contributions of this research are:

1. A novel voltage space vector selection scheme is suggested with the idea to improve stator flux response at low speed and reduce torque ripple at high speed.
2. Impact of iron loss on performance of direct torque controlled induction motor in both torque mode and speed mode of operation is evaluated for the first time.
3. A novel method of iron loss compensation in direct torque controller, that improves the accuracy of torque control, is proposed for the first time.

4. Impact of iron loss on performance of a sensorless direct torque control scheme is studied for the first time.
5. A novel method for compensation of iron loss in flux based MRAS speed estimators is developed.
6. A comparison between a DTC drive and a vector controlled drive performance is performed by simulation.

Original research results are discussed in detail in chapters 4,5, 6, and 7.

1.5 Thesis outline

Chapter 2 surveys the existing literature on direct torque control. Origin and nature of DTC are elaborated in section 2.2. Power supplies for DTC are discussed in section 2.3. Section 2.4 reviews switching tables for DTC. Stator flux and torque estimation are covered in section 2.5. Effects of stator resistance variation and on-line stator resistance estimation schemes are introduced in section 2.6. Existing iron loss considerations in induction motor drives, methods of iron loss representation and compensation schemes for vector controlled drives are discussed in section 2.7. Literature on sensorless direct torque control is reviewed in section 2.8.

Chapter 3 discusses dynamic models of induction machines and the voltage source inverter. Constant parameter standard induction machine model in an arbitrary rotating reference frame is described in section 3.2. Dynamic induction machine models with iron loss representation are elaborated in section 3.3. Voltage source inverter model is presented in section 3.4.

Chapter 4 reviews principles of vector control and direct torque control. Section 4.2 summarises principles of rotor flux oriented control and stator flux oriented control together with their control schemes. Section 4.3 discusses principles of direct torque control induction motor, which include torque production mechanism in an induction motor, basic control scheme of DTC method, optimum inverter switching table and stator flux and torque estimation. The chapter concludes with section 4.4 in which a comparative analysis of stator flux oriented control and direct torque control is performed by simulation.

Chapter 5 discusses switching tables for direct torque control. Section 5.2 reviews in detail original optimum switching table suggested by [Takahashi and

Noguchi (1986)] and associated problems experienced in various modes of operation. Section 5.3 describes existing modifications of the original switching table to improve response of torque or stator flux and suggests a novel modification of the switching table which reduces stator flux ripple at low speed and torque ripple at high speed. Section 5.4 presents simulation results of the drive with some of the existing modifications and with the newly suggested modified switching table.

Chapter 6 investigates the impact of iron loss on direct torque control of an induction machine in both torque mode and speed mode (with speed sensor). Section 6.2 details the iron loss representation in induction machine model utilised in this chapter and the simulation procedure. Section 6.3 shows the results of the detuning study related to impact of iron loss on DTC. Section 6.4 suggests a novel way of compensation for iron loss in the direct torque controller and illustrates the improved responses obtainable in this way.

Chapter 7 discusses sensorless direct torque control. Section 7.2 reviews MRAS principles for sensorless control of induction motors. Section 7.3 describes mathematical models of the flux based model reference adaptive system (MRAS) speed estimators with and without compensation for iron loss. Section 7.4 presents simulation results of sensorless direct torque control with stator flux based MRAS speed estimator. Simulations using constant parameter standard machine model and machine model with iron loss representation, with speed estimator with and without iron loss compensation, are carried out. Section 7.5 elaborates sensorless direct torque control with rotor flux based MRAS speed estimator. Similar simulations as in section 7.4 are repeated with the rotor flux based speed estimator with and without iron loss compensation.

Chapter 8 presents experimental investigation of industrial direct torque controlled drive and industrial vector controlled drive. Section 8.2 discusses performance of the vector controlled induction motor drive. Section 8.3 describes the structure of the industrial direct torque controlled drive and presents performance of the drive under no-load and loaded conditions.

Chapter 9 gives the conclusion of the thesis. The theoretical review, mathematical model developments, simulations and practical investigation, carried out in the research project, as well as future work, are summarised and discussed.

CHAPTER 2

LITERATURE SURVEY

2.1 Introduction

This chapter surveys the literature relevant for direct torque control, published in recent past. Various aspects of direct torque control of induction machines are covered. They include the origin and nature of direct torque control, power supply for direct torque controlled drives, switching tables for voltage space vector selection, stator flux and electromagnetic torque estimation, impact of stator resistance variation due to change in thermal operating conditions on accuracy of direct torque control, considerations related to iron loss in high performance drives, and sensorless direct torque control. Mathematical models of induction machines and principles of direct torque control are mentioned only briefly in this chapter, but they will be discussed in detail in chapter 3 and chapter 4, respectively.

2.2 Origin and nature of direct torque control

Direct torque control principle was introduced in the late 1980s by [Takahashi and Noguchi (1986), Depenbrock (1985 and 1988)]. In contrast to vector control, that became accepted by drive manufacturers after 20 years of extensive research, direct torque control needed only just over a decade to really take off. A direct torque controlled induction motor drive has been manufactured commercially by ABB since the mid-nineties [Tiitinen et al (1995)]. In the direct torque controller developed by ABB, the optimum inverter switching pattern is determined in every sampling period (25 μs). The core of the control system in direct torque control is the subsystem containing torque and flux hysteresis controllers and optimal inverter switching logic. An accurate machine model is also very important, since estimation of stator flux and motor torque is based on the machine model and the measurement of the machine input stator voltages and currents. The measurement of actual speed is not required [Tiitinen et al (1995)]. Machine model in stationary reference frame is used to develop DTC

theory. Detailed discussion regarding mathematical modelling of induction machines is presented in the next chapter.

In stationary reference frame, the stator flux linkage is the integral of the stator EMF. If stator voltage drop on stator resistance can be neglected, the stator flux is the integral of applied voltage. Hence in a short period of time, the increments of stator flux are proportional to the applied voltage. It therefore follows that the inverter output voltage space vector directly impresses the stator flux and a desired locus of stator flux can be obtained by selecting the appropriate inverter output voltages [Vas (1998)]. The rotor time constant of induction machines is usually large; therefore the rotor flux linkage changes slowly compared to the stator flux linkage and it can be assumed to be constant in magnitude and speed of rotation during short transients [Vas (1998)]. When the forward active voltage space vectors are applied, the stator flux linkage vector is moved away from the rotor flux linkage vector. This will increase the machine's torque because the torque angle increases. On the other hand, if the zero or backward active voltage space vectors are applied, the torque angle is reduced. The torque is therefore reduced [Kazmierkowski and Tunia (1994)]. It can be seen now that torque can be controlled directly and increased or decreased almost instantly by moving stator flux linkage space vector to the required position (being determined by torque demand), which in turn can be done quickly by selecting the appropriate voltage vector while stator flux linkage magnitude is still kept within the hysteresis band. This is the reason why the control scheme is called direct torque control [Vas (1998)].

Direct torque control requires set points of flux and torque as independent inputs. The estimated values of these quantities are needed to establish closed loop control of flux and torque. However, the errors between the estimates of actual quantities and set points are used in a completely different way compared to vector control. There is no utilisation of current controllers in direct torque control. The torque and flux controllers are two-level or three-level hysteresis controllers, which determine whether an increase or a decrease of flux and/or torque is required, depending on whether or not torque or flux errors fall outside the pre-defined ranges. From this information, together with the knowledge of position of stator flux linkage space vector, an appropriate voltage vector will be selected based on the switching strategy. An accurate knowledge of the magnitude of the stator flux linkage space vector in the machine is needed. However, knowledge of the precise value of the stator flux space vector instantaneous position is not required. The control system only needs to know in

which sector of the voltage vector space (which is a two dimensional complex plane) the flux linkage space vector is. In the case of standard two-level voltage source inverter there are six sectors in the space vector plane corresponding to six active voltage space vectors, with the voltage vectors positioned at the centres of the sectors. Each sector expands 60 degrees so that six of them cover the voltage vector complex plane. Direct torque control is inherently sensorless. Different structures of speed estimators can be incorporated into direct torque controller for sensorless drive operation with closed loop speed control.

2.3 Power supplies for direct torque control

Different kinds of inverters can be used as power supply for induction machines such as: resonant DC link inverter [Habetler and Divan (1991)], multilevel voltage source inverter [Wu and Steimel (1997)] and two level voltage source inverter. The two-level inverter is the most commonly used inverter for low to medium power range applications. Multilevel voltage source inverters are normally applied for high power drives, while utilisation of resonant DC link inverters is still rather limited, especially in commercially available products. Since only low to medium power range induction machines are considered in this research, the two-level voltage source inverter is selected as the power supply. There are only eight on-off combinations of switches in a two-level voltage source inverter (in contrast to multilevel inverters, where the number of combinations is significantly higher). Each on-off combination produces one output voltage vector. There are six non-zero vectors (or active vectors) with equal magnitudes and two zero vectors.

Among the multilevel voltage source inverters to be used in DTC, three-level voltage source inverter has been suggested by many researchers. Although the area of three-level voltage source inverter employment is getting narrower due to the rising working voltage for GTO and IGBT, there is still a wide scope for their utilisation, especially for the high voltage drives [Perelmuter (2000)]. Because the high voltage switches are quite expensive, the employment of an increased number of the cheaper switches is more economical. This also results in a higher number of feasible inverter states, which helps to reduce torque distortions [Perelmuter (2000)]. Current waveform is also improved with three-level inverter although the switching frequency may be

unchanged. Responses with the same quality as the ones with two-level inverters can be obtained with lower switching frequency [Perelmuter (2000)]. The utilisation of three-level neutral-point-clamped voltage source inverter for DTC has also been suggested by [Tan et al (2001)]. Smoother waveform, lower distortion, lower switching frequency and lower cost are the advantages offered by this kind of inverter.

Matrix converter's utilisation for direct torque control has also been proposed by [Casadei et al (1998a and 2001)]. Although there is an increased complexity of the matrix converter topology compared to traditional voltage source inverters, the new control algorithm is rather simple and robust. There are three hysteresis controllers in this control scheme, instead of two as in the traditional one, and they are applied to stator flux, electromagnetic torque and input power. A new switching table is defined based on these hysteresis controllers to select appropriate switching configurations for the matrix converter. This control method can combine the advantages of matrix converters with the advantages of direct torque control [Casadei et al (1998a)]. Because the input phases of the matrix converter are never allowed to be short-circuited and the output currents must never be interrupted, only 27 switching configurations can be used in the matrix converter [Casadei et al (2001)]. These switching configurations can be categorised into three groups, "active" configurations, "zero" configurations and "synchronous" configurations. Only "active" configurations, for which the output voltage vectors have fixed directions but variable amplitudes, and "zero" configurations, for which the output voltage vectors are zero, can be used for DTC. This control method has also been shown by [Casadei et al (2001)] to reduce the harmonic content of the input line current to the matrix converter without any negative effects on the drive performance and the control complexity.

2.4 Voltage space vector selection schemes for direct torque control

There are several different voltage space vector selection strategies. The typical and most popular strategy uses the switching table suggested by [Takahashi and Noguchi (1986)]. The outputs from flux and torque controllers and the information about the sector in which the stator flux space vector is positioned determine the selection of the voltage vectors. This strategy selects forward active voltage space

vectors to increase torque regardless of the direction of the shaft rotation, and zero voltage vectors for torque decrease. While this strategy works well at medium and high speed, it also causes some problems at low speed. At high speed, the selection of zero voltage vectors for torque reduction would reduce the switching frequency of the inverter substantially and give good dynamic performance. The backward active voltage vectors lead to very rapid torque change, and this in turn leads to high switching frequency [Casadei et al (1994)]. At low speed, however, the application of zero voltage vectors will cause cumulative effects, which in turn will decrease the magnitude of stator flux. This results in the flux locus distortion and current waveform distortion [Chen and Li (1999)]. Some other switching strategies, which utilise the backward active voltage vectors for torque decrease, are suggested in [Chen and Li (1999), Kang and Sul (1999), Alfonso et al (1999), Casadei et al (1994)].

Another, rather different, approach to DTC is the one proposed in [Habetler et al (1992)]. Instead of a switching table and hysteresis flux and torque controllers, voltage space vector modulation strategy is applied. The space vector modulation strategy gives the advantage of fixed switching frequency [Habetler et al (1992)]. In this control scheme, torque and flux are controlled in deadbeat fashion by calculating the switching pattern directly. This can be achieved by determining the voltage space vector required to control torque and flux on a cycle-by-cycle basic. The calculation is based on the torque and flux errors sampled from the previous cycle and estimation of the back EMF in the machine. The duty cycle or switching interval is then determined by using voltage space vector PWM [Habetler et al (1992)]. It has to be observed though that although this method does lead to direct torque control, it still involves co-ordinate transformation. The method therefore cannot be considered as a generic DTC method since it does not eliminate the major drawback of vector control, the need to perform a co-ordinate transformation in real time.

Discrete space vector modulation for voltage vector selection in DTC has been proposed by [Casadei et al (1998b and 2000)]. The classical way for determination of switching tables, such as the one in [Takahashi and Noguchi (1986), Casadei et al (1994)], is based on the physical considerations of effects of radial and tangential components of stator voltage space vector on torque and stator flux. Although this approach is simple, it results in unwanted torque variations in some operating conditions. The analysis of electromagnetic behaviour of the induction machines needs to be taken into account to understand the problems of torque variations [Casadei et al

(1997 and 2000), El Hassan et al (1997)]. The solution of increasing the number of voltage space vectors available for selection by using a double three-phase inverter or improvements of traditional power circuit topology, as suggested in [Takahashi and Ohmori (1989), Wu and Steimel (1997)], are only suitable for high power applications, not medium and low power applications because of the increased complexity of the power circuit [Casadei et al (2000)]. Discrete space vector modulation is designed to reduce torque and flux ripples and current distortion. This technique uses a prefixed time interval within each cycle period. A higher number of voltage space vectors are available for the control of torque and flux compared with the classical switching scheme. This new number of voltage space vectors available leads to new definitions of switching tables in which voltage space vectors are selected based on the criteria of rotor speed, torque error and flux error [Casadei et al (2000)]. A new voltage space vector is synthesised from the standard voltage source topology by applying several voltage space vectors for a prefixed time interval during each sampling period. The more voltage space vectors are available, the lower are the amplitudes of torque and flux ripples, but the more complicated are the switching tables. A good compromise should be made between the compensation of ripples and complication of voltage vector selection. This compromise is achieved by sub-dividing the sampling period into three equal time intervals. A substantial torque and flux ripple reduction is obtained with this discrete space vector modulation [Casadei et al (2000)].

A new space vector modulation technique, which is independent of co-ordinate transformation, is also suggested by [Monmasson et al (2001)] to improve the performance of DTC at low speed. The DTC concept has been redrawn so that the switching table is no longer necessary (the variations of stator flux and torque due to the applied voltage space vector are independent of the positions of stator flux space vector in the complex plane). Then, a new space vector modulation function is introduced to generate accurately the voltage vector direction required. An attempt to reduce flux and torque ripple in DTC by space vector modulation is also carried out by [Tang and Rahman (2001)]. Required voltage space vector is synthesised from the adjacent basic voltage space vectors of a standard voltage source inverter topology. The selection rules based on the stator flux regions of complex plane are not used. Instead of switching table and hysteresis controllers, a PI controller and numeric calculation are used to determine the intervals for which the basic voltage space vectors are used to synthesise the required voltage space vector. Predictive pulse width control for reduction of stator

flux and torque ripple is also carried out by [Nillesen et al (2000)]. This control method aims at improving performance of torque and flux responses of DTC in high power applications where switching frequency has to remain low. The basic stator voltage space vectors of the voltage source inverter are not applied to the machine for the whole sampling period. Instead a duty cycle for which the stator flux reaches the boundaries of the hysteresis bands is calculated from the stator voltage values collected at the beginning of the sampling period and stator current values collected at the previous sampling period. At the end of the duty cycle, when stator flux already reaches the boundaries, other non zero voltage space vector, which diverts the direction of stator flux space vector but continues the desired torque change, is applied until the end of the sampling period [Nillesen et al (2000)].

In majority of the switching instants, the applied voltage space vector is not the same as an ideal voltage space vector should be for the desired changes of torque and stator flux linkage. Therefore, there are ripples in torque and flux responses of the induction machine. These ripples can be reduced by various techniques, such as higher switching frequency, change of inverter topology or duty ratio control [Vas (1998)].

The increase of switching frequency has some drawbacks, for example an increase in switching losses, which leads to reduce efficiency, and an increase in stress on semiconductor devices of the inverter. It has the advantage of improving the harmonic content of stator current and torque [Vas (1998)].

The change of topology means that the number of switches in the inverter increases, thus increasing the cost. The benefit is that the number of active (non-zero) voltage space vectors is increased. The idea is well suited to high power region, where use of already mentioned multi-level inverters is usually necessary anyway.

Multilevel hysteresis comparators can also be used to reduce the ripples. This would avoid the use of active backward voltage space vectors. These vector are inevitably selected in the standard DTC look-up table and they cause large torque undershoots when applied to the machine [Purcell and Acarnley (1998)]. Two new forms of hysteresis comparators have been proposed [Purcell and Acarnley (1998)], they are quasi and offset hysteresis comparators. The first one allows backward voltage vectors to be used as long as the torque error has not passed below the reference level. When this happens, only forward active voltage vectors are applied. The second form could be used when switching oscillations happen in the first form.

The third possibility is duty cycle control. During a switching cycle, an active voltage space vector and a zero voltage space vector are applied. The active vector is now applied to the machine for a part of the switching period, rather than for an entire period as before. For the rest of the period, the zero vector is applied. This could reduce the torque or flux error when it exceeds the hysteresis band early in the switching period. The electromagnetic torque is almost unchanged or slightly reduced during the time the zero voltage vector is applied, therefore, torque ripples are reduced [Vas (1998)]. The duty ratio for each switching period is a non-linear function of torque error and stator flux linkage error. It can be selected to make the RMS value of torque ripple minimum as suggested in [Kang and Sul (1999)].

A number of modified switching tables for DTC of an induction motor drive will be reviewed in detail in chapter 5.

2.5 Stator flux and torque estimation

Direct torque control requires estimation of stator flux and torque for determining torque and flux errors. The flux estimation is obtained by integration of back EMF. The accuracy of this method depends on stator resistance variation, integrating technique, and accuracy of stator voltage and current measurement [Vas (1998)]. Stator resistance varies due to change in operating temperature [Mir et al (1998)]. At low speed, the effects of stator resistance variation become more significant, since the stator voltage is very small at low frequency, and the ohmic drop is therefore more dominant. Thus, an accurate value of stator resistance is more important because a small variation of the resistance could result in a significant error in flux estimation [Vas (1998), Mir et al (1998)]. The problems of voltage and current monitoring are the following: phase shift in the obtained values due to the sensors, magnitude errors due to gain and conversion factors, offset in measurement equipment, quantisation errors of digital converters, etc. [Vas (1998)]. The practical implementation of the integration needs drift compensation because drift can result in large errors in flux position estimate [Vas (1998)]. Pure integrators always have DC drift and initial value problems and a DC component in monitored back EMF is practically inevitable [Hu and Wu (1998), Wu and Slemon (1991)]. This DC offset can drive the integration into saturation and the initial value problems can result in a DC offset in estimated flux linkage, which does

not exist in real operation of the machine [Hu and Wu (1998)]. The improved integration methods for stator flux estimation are suggested in [Hu and Wu (1998), Hurst et al (1998)].

A low pass filter can be used instead of a pure integrator. This provides good approximation of the pure integrator over a wide speed range (excluding zero and low speeds) [Vas (1998)].

A modification of low pass filter integrator using, in principle, a combination of low-pass filter and saturation feedback, is suggested in [Hu and Wu (1998)]. The integrator is then further modified by adding the amplitude limiter for drives that require constant flux linkage during operation and to eliminate non-linear distortion occurring in the operation of the modified integrator. Alternatively, an adaptive controller is added for wide range of industrial applications. The last version produces superior performance compared to the first two modifications in both transients and steady states [Hu and Wu (1998)].

The drift problem of pure integrator can also be avoided by using the first order delay element, which integrates band-limited high frequency components and replaces the flux estimation at low frequency (prone to DC drift and initial problems) by reference flux value in a smooth transition [Vas (1998)].

The input into the first order delay element is not the induced EMF space vector, as the case is with pure integrator. Instead, it is the sum of reference flux space vector and the product of induced EMF vector and a chosen time constant. At low frequency, the low-frequency components of the EMF will be cut off by the low-pass filter. The output of the estimator will be the reference value of the stator flux linkage. At high frequency, the estimator functions like a pure integrator [Vas (1998)].

Both stator voltage equation and rotor voltage equation can be used leading to the so-called hybrid estimator. The significant drawback of the method is that, since rotor voltage equation (so-called current model) is utilised, sensitivity to immeasurable rotor parameters appears in the estimation process. The idea is based on the fact that the stator voltage model gives good estimation at high speed while the rotor voltage model gives good estimation at low speeds. A smooth transition should be used to link the two models. This problem is easier to solve when speed sensor is used [Vas (1998)].

Observers (such as Luenberger, extended Kalman filter) can be used to estimate the stator flux linkage. The estimation is less sensitive to parameter variations. Machine's parameters and rotor speed can also be estimated together with stator flux

linkage when extended Kalman filter is used [Vas (1998)]. The artificial intelligent techniques, such as neural network based estimators and fuzzy-neutral estimators, are yet another possibility.

2.6 Stator resistance estimation

Stator resistance varies with the operating temperature. An incorrect value of stator resistance results in significant errors in estimation of stator flux linkage and torque at a low speed region, where the magnitude of supply voltage is small. The stator resistance voltage becomes dominant. Hence, any small error in stator resistance can lead to incorrect values of estimated stator flux components, which, in turn, will cause errors in estimated magnitude and position of flux linkage.

Impact of stator resistance variation diminishes as speed increases in the base speed region. However, at high speed in the field-weakening region, an error in stator resistance causes the motor voltage to be below its rated value in the field-weakening region [Habetler et al (1998)].

On-line identification strategies for stator resistance estimation are suggested in [Mir et al (1998), Habetler et al (1998), Kerkman et al (1996)]. On-line estimation of stator resistance utilising zero-sequence model of the induction machine is suggested by [Jacobina et al (2000)]. The technique is based on machine behaviour with respect to zero sequence quantities. Least square minimisation is used to find the estimate of stator resistance as well as leakage inductance of the stator. In this method, neutral point of induction machine is connected to the central tap of the capacitor bank in the voltage source inverter through a triac. The technique also requires the measurement of phase stator voltage and phase current. However, only one current sensor and one voltage sensor are used instead of three for each of them when the zero-sequence quantities are measured directly. This technique provides a mean to estimate stator resistance independently of machine parameters and drive's control strategy [Jacobina et al (2000)].

A method for on-line tuning of stator resistance, suggested in [Habetler et al (1998)] uses current model to calculate stator flux at low speed and voltage model to calculate stator flux at high speed. At low speed, the rotor flux is at first determined from machine speed and current measurement and rotor time constant, and then it is

used to calculate the stator flux. This value of stator flux is used for updating the stator resistance, which is consequently used at high speed. At high speed the rotor flux is calculated from stator flux and then used for tuning the rotor resistance [Habetler et al (1998)]. By using the current model at low speed in the above method, the sensitivity of the control to stator resistance variation is eliminated. Current model, however, is highly sensitive to rotor time constant variation due to temperature variations and the accuracy of measured speed. Therefore, voltage model is used at high speed. Smooth transition from current model to voltage model is achieved in this method by forcing both models to track one other [Habetler et al (1998)].

Application of fuzzy logic for stator resistance estimation and tuning is presented in [Mir et al (1998)]. Another technique, back electromotive force detector, aimed at reducing the impact of stator resistance variation on the control and estimating the stator resistance is described in [Kerkman et al (1996)].

Direct torque controlled induction motor drives with self-commissioning are also suggested by [Lai et al (2000)]. Machine's parameters and controller's parameters are determined during the self-commissioning process. The machine's parameters include stator resistance, inertia and friction coefficient. The stator resistance is measured first at standstill, then follow the identification of inertia and friction coefficient. The controller's parameters are determined by pole placement method. Taguchi methodology is used in the identification process. This methodology is widely used in quality control engineering [Lai et al (2000)].

Model reference adaptive systems, which are often used for speed estimation in induction motor drives, can also be used for stator and/or rotor resistance estimation to improve performance of sensorless drives in low speed region [Zhen and Xu (1998)]. Rotor resistance estimation is normally not necessary in direct torque control. However, the estimated values of rotor resistance and rotor flux, which are obtained from a model reference adaptive system independent of stator resistance, can be used to estimate stator resistance in a stator flux oriented reference frame [Lee et al (2000)]. This method may have difficulty to estimate accurately stator resistance at high speed because stator resistance identification is more sensitive to errors in motor parameters and variables when speed increases. But the variation of stator resistance at low speed is more important in direct torque control. Stator voltage equation for q-axis in stator flux oriented reference frame is used to estimate the stator resistance. The method suggested by [Lee et al (2000)] does not require integration or differentiation in estimation of

stator resistance. Numerical integration is undesirable as explained before, differentiation is also undesirable because it amplifies noise [Lee et al (2000)]. The voltage equation in *q*-axis also requires estimated values of stator voltage, stator current, and stator flux. Estimation of stator flux can be carried out independently of stator resistance from the estimated rotor flux obtained from the model reference adaptive system estimator. This method has been showed by [Lee et al (2000)] to be insensitive to variation of machine parameters and it provides an accurate estimation of stator resistance. This method was proposed originally for thermal monitoring of induction machines, but it can be well used for direct torque control.

2.7 Iron loss considerations in high performance induction motor drives

Principles of operation of direct torque control scheme are based on the assumption that the existence of the iron loss in an induction machine may be neglected. The same applies to all the standard vector control schemes as well and is a consequence of the lack of possibility of adequate modelling of the iron loss within the standard general theory of electrical machines. Probably the first attempt to represent the iron loss within the orthogonal axis models of electric machines is the one by [Boldea and Nasar (1987)], where fictitious 'iron loss' windings are added for this purpose. This model has been developed for sinusoidal feeding conditions and has subsequently been extensively used in evaluation of the iron loss impact on behaviour of vector controlled induction machines.

Among all the phenomena that lead to detuned operation of field oriented induction machines, iron loss was the last to attract attention. Initial proposals for compensation of the iron loss within rotor flux orientation schemes were given in the early nineties [Mizuno et al (1990), Kubota and Matsuse (1992), Hintze and Schroder (1992)]. This was further followed by detailed investigations of iron loss induced detuning effects in rotor flux oriented, stator flux oriented and air gap flux oriented induction motor drives [Garcia et al (1994), Levi (1994), Levi (1996), Levi et al (1996), Moulahoum et al (1998), Sokola (1998)]. In general, the existence of the iron loss in the machine leads to an orientation angle error and discrepancies between the reference and actual values of the relevant flux and motor torque in steady state operation. As far as

dynamics are concerned, the net consequence of the iron loss is a slower acceleration (since iron loss reduces the output torque in motoring) and faster deceleration (since shaft torque is higher in braking than estimated).

The problem of the discrepancy between actual and the reference torque appears to be very important when efficiency is the primary concern, such as in electric vehicles [Matsuse et al (1999b), Jung and Nam (1998)]. The impact of iron loss is also important when high performance and accuracy in torque control is required, like in tension control for winding applications [Wieser (1995 and 1998), Noguchi et al (1997)]. The torque error caused by iron loss can be even up to 5-7% of the rated torque when a conventional field oriented vector controlled drive is used [Noguchi and Hiraishi (1999)].

The most frequently used approach to model the iron loss [Hintze and Schroder (1992), Levi (1994), Levi (1996), Levi et al (1996), Moulahoum et al (1998)] is a simplification of the model of [Boldea and Nasar (1987)] and is based on representation of the iron loss with an equivalent iron loss resistance, placed in parallel to the magnetising branch of the motor within the dynamic equivalent circuit. Alternatively, equivalent iron loss resistance can be placed immediately after the stator resistance [Noguchi et al (1997), Dittrich (1998)]. The two possibilities yield identical results as long as the correct correlation between the two equivalent iron loss resistors is maintained. The disadvantage of the iron loss modelling with a parallel equivalent resistance is an increase in the number of state space variables. This shortcoming can be overcome by the application of a series iron loss model, in which the equivalent iron loss resistance is connected in series with the magnetising inductance [Jung and Nam (1998)].

Means for compensation of detuning caused by the iron loss existence are nowadays available for a variety of vector control schemes. These include indirect feed-forward rotor flux oriented (RFO) control of a current fed induction machine [Levi (1995), Levi (1996)], RFO control of a current fed induction machine with rotor flux position estimation from measured variables [Choi et al (1996), Hintze and Schroder (1992), Levi et al (1995), Levi et al (1996), Matsuse et al (1999a), Weiser (1998)], direct RFO control of a voltage fed machine [Noguchi et al (1997), Jung and Nam (1998)], indirect feed-forward RFO control of a voltage fed machine [Moulahoum et al (1998)], and indirect feed-forward stator flux oriented control of a voltage fed machine [Moulahoum et al (1998)].

A common feature of all these studies is that they apply to vector control schemes with speed (position) sensor. Hence the process of iron loss compensation requires modifications of the vector controller and the rotor (stator) flux position (and flux amplitude and torque, if applicable) estimation algorithm. Recent emphasis on sensorless control has initiated an interest in evaluation of the iron loss impact on sensorless vector control and investigation of the means for compensation [Matsuse et al (1999b), Wang et al (1999), Wee et al (1999)]. If speed estimation is performed using a model based approach (induction motor model only, MRAS based speed estimation, observer and EKF based speed estimators), compensation of iron loss within the vector controller and flux position estimator does not provide satisfactory drive operation [Wang et al (1999)]. The accuracy of speed estimation is affected by the iron loss as well and therefore it becomes necessary to additionally compensate for the iron loss within the speed estimator. Since different methods of speed estimation are affected by the iron loss in a different way, it is necessary to modify each speed estimation algorithm individually. In other words, detuning effects in a sensorless vector controlled drive with iron loss compensation within the vector controller and the flux position estimator become dependent on the applied algorithm of the speed estimation.

Evaluation of the influence of the iron loss on behaviour of a control scheme and subsequent analysis of compensation methods require knowledge of the iron loss variation during the drive operation. This means that the iron loss has to be identified beforehand, experimentally. A universally valid method is the one described in [Levi et al (1996)]. It consists of a number of no-load tests that are executed using the PWM inverter supply at different operating frequencies during commissioning of the drive. Some alternative methods, applicable to either vector control schemes or in special control scheme configurations, have been proposed as well. The method suggested in [Dittrich (1998), Rasmussen et al (1999)] relies on utilisation of the d-axis stator voltage error within the rotor flux oriented control scheme to identify the iron loss and is therefore not applicable in DTC. An alternative method, proposed in [Choi et al (1996)], identifies the iron loss on the basis of the torque error. Its application requires existence of a mechanical subsystem observer that estimates the actual motor output torque.

On the basis of the survey presented above one can conclude that the impact of iron loss on operation of a vector controlled induction motor drive is nowadays well understood and that the appropriate means for compensation are readily available. It appears, however, that studies related to the impact of the iron loss on induction motor

direct torque control have never been performed, nor are any compensation schemes available.

2.8 Sensorless direct torque control

As already noted, DTC itself does not require information regarding rotor speed and/or position. However, if a DTC algorithm is applied as a part of a drive with closed loop speed control, information regarding actual speed of rotation becomes necessary.

Speed-sensor-less direct torque controlled drive can be implemented by using the same speed estimation techniques as for vector control. All the speed estimation techniques fall into one of the following three categories [Vas (1998)]:

1. Speed estimation from stator current (or voltage) spectrum;
2. Speed estimation based on induction machine model:
    i. Open-loop estimators that use model equations only;
    ii. Closed-loop estimators that utilise an induction motor model and some additional corrective action (observers, extended Kalman filter and model reference adaptive system);
3. Speed estimation based on artificial intelligence techniques (artificial neural networks, neuro-fuzzy systems, etc).

The good feature of methods belonging to the first category is that they do not depend on the machine equivalent circuit parameters. However, they require significant amount of signal processing (that leads to limited accuracy in transient operation) and the level of signal from which speed information is extracted can be very low (or indeed insufficient). Methods of the second category are rather easy to implement (except for the extended Kalman filter), but they are all to some extent affected by parameter variation effects in the machine. The artificial intelligence based estimators are expected to be widely used in the future. They are less sensitive to parameter variations and are currently under extensive development [Vas (1998)].

Sensor-less variable speed high performance drives offer in general reduction of hardware complexity, improved reliability in hostile environment, increased mechanical robustness, decreased maintenance requirement, and reduced cost [Vas and Rashed (1999)].

Many speed prediction techniques have been suggested for sensorless control of induction motors over the years. The original techniques were designed to extract the information regarding the rotor speed from stator voltage and stator current only in steady state operation. These techniques can be used for low cost induction motor drives for applications that do not require highly dynamic performance [Abbondanti and Brennen (1975)]. More sophisticated speed estimation techniques have been suggested for high performance induction motor drives. This section reviews the speed estimation methods of the first group, using the spatial-saturation stator phase third-harmonic voltage, using saliency (geometrical, saturation) effects, and the estimation methods of the second group, using machine model (including open-loop speed estimators and closed-loop estimators).

The first technique utilises saturation phenomena to obtain the rotor speed of an induction motor and also the position and magnitude of the magnetising flux space vector [Vas (1998)]. The spatial saturation third-harmonic voltage component, which is due to main flux saturation, is obtained by monitoring the sum of the phase stator voltages in a symmetrical three-phase induction motor. The third-harmonic voltage component is then integrated to obtain the third-harmonic flux. The fundamental is further calculated by using a saturation function, which can be determined experimentally [Vas (1998)].

The angle of the magnetising flux space angle is also obtained from the monitored third-harmonic voltage. To obtain this information, a phase stator current of the induction motor has to be monitored as well. Then the displacement angle between this stator current maximum and the maximum of the fundamental magnetising flux is found. From the information about the angle of the fundamental magnetising flux with respect to the stator current space vector and the angle of the stator current space vector with respect to the direct axis of the stationary reference frame, the angle of the fundamental magnetising flux space vector with respect to the direct axis of the stationary reference frame can be obtained [Vas (1998)].

Once when the fundamental magnetising flux space vector's modulus and phase angle with respect to the direct axis of the stationary reference frame are known they can then be used to determine the stator flux space vector and rotor flux space vector. The rotor speed then can be determined by differentiating the phase angle of stator flux space vector and deducting the angular slip frequency. The obtained magnetising flux

space vector, stator flux space vector and rotor flux space vector can also be used in vector control [Vas (1998)].

As already mentioned, spatial saturation (zero sequence) third-harmonic voltage is required to obtain the fundamental of the magnetising flux. The third-harmonic voltage can be obtained in two ways [Consoli et al (2000)]. In the first approach, the summation of stator phase voltages is performed. This is carried out in a three-phase induction motor with wye-connected stator windings without a neutral point by using three wye-connected resistors in parallel to the machine, whose voltages are measured and summed. The resultant voltage of the summation contains a zero-sequence third-harmonic voltage component and the high frequency slot harmonic component. The third harmonic component is dominant, since the fundamental and the other non-triple harmonic components, which could be present in the air-gap magneto-motive force and magnetising flux, will cancel out. The slot harmonic component is then filtered out by using an analogue or digital filter [Vas (1998)]. In an alternative approach, the third harmonic voltage is evaluated directly by measuring the voltage across the midpoint of the DC bus and the neutral point of the machine. A cleaner third-harmonic signal can be obtained in this way because of the reference to a more stable potential point [Consoli et al (2000)]. If the induction motor's stator windings are wye connected without a neutral point, there is no flowing of the zero-sequence components of stator current in the motor. This will eliminate any influence of the third-harmonic component of the air-gap flux on the torque production [Consoli et al (2000)]. Phase shift of the third-harmonic voltage due to load currents is also avoided with the absence of zero-sequence stator currents. This guarantees the orthogonality between the third-harmonic components of stator voltage and air-gap flux [Consoli et al (2000)].

Modern induction machines are designed to operate in the saturated region of the magnetising characteristic for better utilisation [Vas (1998)]. When the machines are saturated, the sinusoidal distribution of air-gap flux density, which is caused by the sinusoidally distributed magneto-motive force in a symmetrical three-phase induction machine, is distorted. A speed predicting technique can therefore utilise the phenomenon of saturation in the induction motors [Vas (1998)]. The saturation will result in the spatial distribution of the air-gap flux in a form of flattened non-sinusoidal waveform. The harmonic content of the waveform is characterised by the odd components but with the dominance of the third harmonic [Consoli et al (2000)]. The third-harmonic component of the zero-sequence component of stator voltage is always

in quadrature with the third-harmonic flux component, without being affected by the load current variations [Consoli et al (2000)].

Speed predicting techniques based on the estimation of air-gap flux position by utilising the spatial saturation third-harmonic voltage are developed to improve the performance of back-EMF based direct field oriented control of induction motor drives [Moreira and Lipo (1990), Kreindler et al (1992)]. Traditional direct field oriented control using back EMF measurement fails at low and zero speed because of low induced voltages, which are practically difficult to measure correctly, and no voltage being induced in the stator winding at zero frequency. The reasons for failure also include motor asymmetries, stator voltage variation and electromagnetic noise, which prevent correct calculation [Consoli et al (2000)]. The harmonic based speed estimation techniques do not require any modification of the motor design. They are easy to implement and insensitive to parameter variations and also allow the low speed sensorless operations. However, the methods still fail at low and zero speed because of insufficient amplitude of the third-harmonic voltage. Detection of flux position at zero speed is impossible with third-harmonic voltage measurement because the third-harmonic component is already too low to be utilised effectively when motor's speed is below 1% of the rated speed [Consoli et al (2000)].

Suggestions for improvement of the technique by injection of a high frequency signal into stator voltage components have been set forth [Consoli (2000), Schroedl (1992)]. The additional voltage components are used to create high frequency current components with amplitudes being related to the spatial air-gap flux distribution inside the motor [Jansen and Lorenz (1995a and 1995b)]. The frequencies of the current and voltage harmonics created by the introduction of a high frequency signal in the stator voltage are related to the frequency of the injected signal and that of the fundamental rotating field [Consoli (2000)]. Demodulation of the high frequency current components will help to detect the angular position of the air-gap flux. The techniques have been verified successfully on salient AC machines [Degner and Lorenz (1998), Consoli et al (1999a)] and are being under development for the application in non-salient machines, such as induction motors where saturation produces a small saliency effect on the direction of air-gap flux [Consoli et al (1999b), Manjrekar et al (1998)].

Rotor speed in the induction machines can also be estimated by utilising different types of geometrical effects (such as normal slotting, inherent air-gap asymmetry, intentional rotor magnetic saliency caused by spatial modulation of rotor-

slot leakage inductance or rotor resistance) and saliency effects as a result of saturation, especially with the squirrel-cage induction motors [Vas (1998)]. The first of several speed predicting techniques using saliency effects discussed here is speed estimating technique utilising rotor slot harmonics. Rotor and stator slots in induction machines produce variations in the air gap permanence, that then interact with the stator winding distribution to result in inductance variations, as reviewed in [Degner and Lorenz (2000)]. This technique, up to now, is not directly used for rotor speed estimation. It is however used for tuning the parameters of speed estimators based on model reference adaptive systems [Vas (1998)]. The advantage of this technique is that its accuracy of estimation is not influenced by the variation of the machine's parameters and it is reliable for all loads. The rotor slot harmonics can be obtained by using either monitored stator voltage or monitored stator current. The latter is preferable because it is anyway necessary to measure stator current in high performance drives, so that the monitoring of stator voltage can be avoided [Vas (1998)].

The slot harmonics detection using stator voltage monitoring utilises the slot harmonic voltages induced in the stator winding of the induction motor. The slot harmonic voltages are induced in the stator winding when the rotor is rotating because of the presence of slot harmonics in the air-gap magneto-motive force. These harmonics are produced due to the variation of the reluctance caused by the stator or rotor slots, and are therefore called stator or rotor slot harmonics, respectively [Vas (1998)]. Both amplitudes and frequencies of slot harmonic voltages depend on the rotor speed. However, only the frequencies are used to estimate the rotor speed because the amplitudes also depend on loading conditions and flux levels [Vas (1998)]. Stronger slot harmonics can be produced in the induction machines without the skewed rotor slots. However, skewed rotor slots are normally created inside the machine to reduce audible noise and eliminate the asynchronous crawling during the line starting [Vas (1998)].

During the monitoring of stator voltages to detect rotor slot harmonics, summation of stator phase voltages is carried out. It has been shown that the summation voltage contains a slot harmonic component and a third-harmonic component, due to main flux saturation. When the stator voltage is supplied by an inverter, the summation voltage also contains extra time harmonic voltages [Vas (1998)]. It has also been shown that the frequency of the slot harmonic voltage depends on angular stator frequency, slip frequency and the number of rotor slots per pole pair [Vas (1998)]. The slot harmonic

voltage in the summation voltage is obtained by removing the third-harmonic voltage and extra harmonic voltages. The removal can be carried out by employing various circuits [Vas (1993)]. The frequency of slot harmonic voltage is then evaluated. With the help of available information regarding the stator angular frequency and the number of slots per pole pair, the rotor speed of the induction motor is finally calculated. However, when the induction motor is running in the low speed region, special considerations are required for this speed estimation technique, because amplitude of the slot harmonic voltage decreases at low speed [Vas (1998)]. Speed estimation can also be done with the machine terminal voltage spectrum obtained from tapped stator windings of an induction machine [Zinger et al (1990)].

Speed estimation technique using monitored stator current is preferable. Harmonic spectral estimation is carried out on the obtained signal of the stator current [Vas (1998)]. The measured signal is scaled and low-pass filtered to eliminate high frequency pulse width modulation harmonics (when the power supplies for the induction motors are the voltage source inverters). Digital Fast Fourier Transform is then performed to find the rotor slot harmonic [Ferrah et al (1992a)]. When the rotor slot harmonic frequency is found and if the information about the angular stator frequency and the number of rotor slots per pole pair are available, rotor speed can be estimated. The accuracy of the speed estimation depends therefore on the accuracy of the rotor slot harmonic frequency and the angular stator frequency. Angular stator frequency is obtained by differentiating the angle of the rotor flux space vector when the rotor flux oriented control is used for the drive. The five main steps for the estimation of rotor slot harmonic frequency are summarised as follows [Vas (1998)]:

1. Identification of angular stator frequency.
2. Determination of the no-load slot harmonic around a specific stator harmonic.
3. Definition of the width of the slot harmonic tracking window. Difference window placement for motoring or generating operation of the motor.
4. Search for the harmonic with the highest amplitude (highest spectrum line), which is a non-triple harmonic of angular stator frequency, in the window.
5. An increase in the accuracy of the rotor slot harmonic frequency.

When an adequate frequency resolution is employed, rotor slot harmonic can be identified from the neighbouring harmonics at no-load and load and over a wide range of speed. Real value Fast Fourier Transform based on the split-radix algorithm is

suitable for digital implementation of the estimator. Digital Fast Fourier Transform can give a good result of the estimation when the operating frequency is over a few Hz. However, when the speed of the motor is too low, noise can affect the accuracy of the speed estimation [Vas (1998)]. Accuracy of the estimating process can be increased by employing appropriate windowing (such as Hanning data window, Hamming window or rectangular window) and interpolation techniques. This means that the signals are analysed and processed for a short length (or window) of the sampled data by the Fast Fourier Transform analyser. However, when signals are transformed into frequency domain, false results could be obtained due to the discontinuities at the window's edges [Vas (1998)].

Fast Fourier Transform has been used to obtain rotor slot harmonic in a speed predicting technique proposed by [Ferrah et al (1992b)]. The speed estimation only considers slotting harmonics and saturation harmonics. This technique gives satisfactory results over a wide speed range, down to 2 Hz. Attempts of estimating the rotor speed by this technique give relatively poor dynamic performance due to the limitation of processing power and sampling rate of the hardware. Estimation of slip speed of the motor based on slot harmonic frequency identification (instead of estimation of rotor speed) is also suggested by [Beguenane et al (1995 and 1996)]. Real time adaptive filters with recursive maximum likelihood technique can also be used for tracking slot harmonics [Cilia et al (1998), Ferrah et al (1996 and 1998)]. They give an error of less than 0.1% for the estimated speed. The parameters of the control system are updated regularly with recursive algorithm for rotor slot harmonic analysis to give a better performance.

Insufficiency of the measurement's bandwidth, the main limitation of this method for its use as an effective speed feedback signal in the past, has been overcome recently [Ferrah et al (1996 and 1998)]. Rotor slot harmonic approach can be used to tune the parameters of a sensorless induction motor drive with speed estimation based on machine models as well [Jiang and Holtz (1997), Hurst et al (1994, 1997)]. The algorithm uses digital signal processing techniques to obtain the speed related harmonic frequency signal induced in the motor by rotor slots and rotor eccentricity. The estimation is then used for tuning the parameters of the machine model and load model [Turl et al (2001)]. Speed estimator based on a mechanical model gives speed feedback signal to sensorless control of the motor. Because the estimated speed signal obtained

from rotor slot harmonics analysis is parameter independent, the sensorless control can give good performance at very low speed [Hurst et al (1994)].

Speed estimation techniques based on inductance variation due to saturation and geometrical effects have been used for sensorless vector control of permanent magnet synchronous machines and synchronous reluctance machines. The technique can also be applied to sensorless control of induction motors even when the motor is at standstill [Schroedl (1988)]. In permanent magnet synchronous machines, stator inductance is a function of the rotor position because of saturation effects. This can be used for estimation of the rotor position or speed. It has also been shown that stator inductance depends on the angle of the magnet flux, with respect to the stator voltage space vector [Schroedl (1993)]. In synchronous reluctance machines, the stator inductance is a function of rotor position because of rotor saliency. Therefore, rotor position and speed can be estimated with high accuracy by using the inductance variation due to geometrical effects. This method is especially useful for speed estimation at zero and low speed. The speed estimation can be carried out either by monitoring the stator current ripple or by injecting a suitable test stator voltage signal [Vas (1998)].

The speed predicting techniques based on variation of inductance due to saliency or geometrical effects can be used for sensorless control of induction motors because the stator inductance in induction motors is dependent on the level of saturation as well as the position of main flux. This dependency is caused by the saturation of stator and rotor teeth. In a saturated induction machine at standstill, the rate of change of stator currents is dependent on the stator voltage space vector and stator transient inductance. The magnitude and angle of this inductance also depend on the magnetic operating point and the direction of the magnetising flux space vector. Application of appropriate test voltage signal would give the rate of change of stator currents at test signal frequency. The angle of magnetising flux space vector is then found, which will be used to extract the information about rotor speed, because the minimum of the ellipse locus of the modulus of complex transient inductance is in the direction of the magnetising flux space vector [Vas (1998)]. Estimation of the flux space vector's position can also be carried out by tracking the high frequency magnetic saliency caused by magnetic saturation at zero or low speed, with the injection of high frequency voltages (or currents) into the stator [Jansen and Lorenz (1995a), Briz et al (2001)].

High frequency magnetic saliency caused by magnetic saturation (main flux or leakage flux saturation) can also be used for speed estimation at zero and low speed. A

high frequency signal is injected into the stator winding to create high frequency current with speed related harmonics [Jansen and Lorenz (1996), Degner and Lorenz (1997)]. The technique of combining rotor slot harmonic method and carrier frequency signal injection to estimate rotor speed gives robust response over a wide range of speeds, even at low or zero speed. Multiple saliency, although not desirable, could also be used for speed estimation, by developing an induction machine model with multiple spatial saliencies [Degner and Lorenz (1998)].

A comparative study carried out by [Hurst and Habetler (1997)] has pointed out a significant limitation of all the speed estimation techniques with spectrum analysis discussed so far. It is the lack of robust performance with respect to machine specific structural characteristics. For example, rotor slot harmonic analysis depends on the number of rotor slots, which is a typically unknown parameter. The control schemes then have to be programmed again for each different induction machine. In addition to that, the estimation techniques are intensive computationally, therefore they are only suitable for speed estimation in steady state operation. Robust and fast hardware is required for speed estimation in transient state, and only a limited accuracy can be obtained.

Estimation of rotor speed of induction machines, especially at zero and low speed, can be achieved by utilisation of saliency effects intentionally created by the special design of the rotor, which gives rise to spatial modulation of rotor leakage inductance or rotor resistance [Vas (1998)]. Rotor eccentricity, which is always present in induction motors because of the compromise between cost and performance, can also be used for speed estimation [Holliday et al (1995)]. Specially designed rotor eccentricity will give position signal more robust than those obtained from dynamic eccentricity [Vas (1998)].

The special designs of the rotor may include variation of the rotor slot openings or variation of the depths of rotor slot openings [Jansen and Lorenz (1995a)]. Specially designed asymmetry of rotor resistance can also be used for speed estimation. The asymmetry is created to make rotor position harmonics dependent on the machine flux and load conditions [Cilia et al (1997)]. The speed estimation techniques discussed previously can again be used here, the only difference is that the saliency is created by physically existing asymmetry, not by saturation. Similarly to those techniques, symmetrical three phase high frequency voltages are injected into stator to track the saliency. It has been proven that when the special designs of the rotor are employed, the

stator transient inductance is position-dependent because of physical asymmetry. This dependency will make stator currents position-dependent when the high frequency stator voltages are applied to the machines. Therefore, information about rotor position and speed can be obtained by monitoring and analysing the currents [Vas (1998)]. An attempt of rotor speed estimation using spatial modulation of the rotor leakage inductance, created by periodic variation of rotor slot opening width, has been made by [Jansen and Lorenz (1995b)]. Addition of specific irregularities to the rotor to create small air gap variations in the machine for the purpose of speed estimation has also been suggested. The irregularities are detected by injection of high frequency signal into the stator currents. These irregularities produce amplitude oscillations in the stator currents generated by the high frequency carrier, and the oscillations are proportional to the rotor position [Dixon and Rivarola (1996)].

However, the variation of rotor slot opening width may cause adverse effects on the magnetising inductance and this could result in torque pulsation. Variation of the depths of rotor slot openings to spatially modulate the rotor leakage inductance will almost have no effect on the magnetising inductance, but the rotor lamination asymmetry may not be desirable by the manufacturers. Variation in rotor slot opening fill can help to obtain leakage inductance modulation. However, it could also have some other adverse effects [Vas (1998)]. Iron saturation in induction machines also degrades the performance of speed estimation technique using rotor asymmetry (such as variation of rotor resistance, variation of rotor leakage inductance or rotor eccentricity) because it causes some degree of saliency in addition to the saliency used to estimate the speed [Staines et al (1998)]. Periodic high frequency voltage burst is injected into the machine instead of continuous high frequency voltage to avoid the saturation.

An entirely different approach to induction machine speed estimation is the one that relies on the induction machine model. An open loop speed estimator that utilises only the induction machine equations and has no corrective action will be explained in more detail in section 4.3.5. The other model based speed estimators reviewed further on are of closed-loop structure, where apart from an induction motor model equations some corrective action is introduced to improve the accuracy of the speed estimate.

Closed-loop speed estimators based on machine models can give satisfactory performance in sensorless induction machine drives. Speed estimators using model reference adaptive system (MRAS) are one category of the closed-loop machine-model based estimators, which can give reliable estimation and good performance for speed

sensorless induction motor drives [Griva et al (2001)]. Measured stator voltages and currents are used in these estimators for extracting the information about speed from two machine models. In the first model, certain state or other variable of the induction machine is calculated independently of the rotor speed, and the model is called reference model. In the second model, the same variable is calculated from a different machine model that is dependent on the rotor speed. The estimated rotor speed is used in the second model as feedback signal. The second model is called adaptive model. The difference between the variables from the two models is used to find the estimated value of the rotor speed through an adaptation mechanism. The adaptation mechanism tunes the adaptive model to obtain a satisfactory estimation of speed [Vas (1998)].

The adaptation mechanism can be derived by using Popov's criterion of hyper-stability, which results in a stable and fast response system [Vas (1998)]. The difference between the state variables mentioned above is formulated into an error signal. This signal is used as input into a PI controller, whose output is the estimated speed. The variables of an induction machine that have been used so far for MRAS speed estimators are rotor flux, back EMF, reactive power and air gap power. Rotor flux based MRAS speed estimator is, however, the most frequently used MRAS speed estimator [Schauder (1992), Tajima and Hori (1993)]. Each of these variables will give different performance characteristics of the speed estimator.

It has been shown that rotor flux based MRAS speed estimator gives good estimation in medium performance sensorless drives over a wide range of speed excluding zero and near-zero speed [Conroy et al (1995)]. Back EMF based estimator also produces good estimation over a wide range of speed but the performance at low speed is affected by the inaccuracy of stator resistance [Conroy et al (1995)]. Reactive power based estimator has the advantage of eliminating the dependency on stator resistance [Peng and Fukao (1994)]. It is, however, characterised with difficulty in obtaining stable control under all operating conditions and it still depends on stator transient inductance [Conroy et al (1995)]. Air gap power based speed estimator is independent of the stator transient inductance. Nonetheless, stator resistance variation affects the performance at low speed and an on-line identification scheme for stator resistance is needed to have accurate estimated speed [Conroy et al (1995), Zhen and Xu (1995)].

The transient response of MRAS based sensorless vector control is similar to the response of vector control with speed measurement [Wang (1999)]. Rotor flux based

MRAS speed estimator offers advantages in terms of hardware implementation requirements, when compared to other MRAS based schemes [Marwali and Keyhani (1997)].

Artificial-intelligence-based MRAS speed estimators, which do not require mathematical model and whose adaptation mechanism is a part of the tuning system of an appropriate artificial intelligence network, can also offer good performance, especially at low and very low speed [Vas (1998)]. The problems experienced with the MRAS speed estimators in the low speed region can be therefore avoided.

A closed loop speed estimator can be defined as an observer [Vas (1998)]. A closed loop estimator contains a correction term, which involves the estimation error. This correction term is used to adjust the response of the observer. The observer is more robust than an open loop estimator in terms of immunisation against deviations of parameters and noise, both in steady state and transient states. Observers can be classified as deterministic observers or stochastic observers according to the representation of the systems, for which they are used to estimate variables or parameters [Vas (1998)]. Luenberger observers and Kalman filters are the most commonly used closed loop estimators [Du et al (1994)]. Luenberger observers are of deterministic type and Kalman filters are of stochastic type. The basic forms of both types of observers can only be used with a linear system. For non-linear systems, the extended forms of these observers have to be used [Vas (1998)].

Many kinds of observers can be used for speed sensorless high performance induction motor drive, such as full order adaptive state observer (which is built from the equations of an induction machine in a stationary reference frame and additional error compensators [Vas (1998)]), extended Kalman filters (EKF) and extended Luenberger observers (ELO). While in a full order adaptive state observer rotor speed is a parameter, it is a state variable in EKF and ELO. When an appropriate speed observer is used in speed sensorless high performance induction motor drive, stable operation can be achieved over a wide speed range, even at very low speed. The observers have been used widely in industrial applications of induction motor drives and will have an increasing role in the future [Vas (1998)].

Full order (fourth order) adaptive state observer can be obtained by modification of a rotor flux estimator to give a speed signal. The stability of the system can be assured by deriving the adaptation mechanism of the system from state error dynamic equations of the induction machine and Lyapunov's stability theorem [Vas (1998)].

Adaptive state observers can be used for estimation of states and/or parameters of a non-linear system in real time. During the calculation, the states are estimated based on a mathematical model. The predicted states are continuously adjusted by a feedback correction scheme [Vas (1998)]. Extended Kalman filters, when used in conjunction with speed sensorless induction motor drives, can give high accuracy of estimated speed over a wide range of speeds and joint estimation of other state variables and parameters can also be incorporated in the control scheme [Vas (1998)]. However, the intensive computational task is the most important drawback of the method. It requires powerful hardware to provide fast response and it is not preferable in terms of economy. EKF is a recursive stochastic state estimator, which can be used for non-linear dynamic systems by utilising the monitored signals disturbed by random noises [Vas (1998)]. It is also assumed that the measurement noise and disturbance noise are not correlated. Inaccuracy in modelling and measurement is also accounted for through the noise.

Extended Luenberger observers are used for the control schemes with joint estimation of flux and speed. They are applicable to non-linear time-varying deterministic systems [Vas (1998)]. ELO is used for replacement of EKF for the joint estimation in a high performance induction motor drive. Extended Kalman filters expose inherent problems created by the stochastic approach [Vas (1998)]. An EKF has problems when the noise contents of the system and the measurements are too low [Vas (1998)]. Unlike standard linear Kalman filter, extended Kalman filters are not optimal. There may be a problem of biasing when the assumed characteristics of stochastic noise do not match those of the real noises [Vas (1998)]. Extended Luenberger observers also give better performance at steady state with the higher accuracy of the estimated speed [Vas (1998)].

2.9 Summary

Literature regarding direct torque control and related problems and the solutions has been discussed in this chapter. The literature has been categorised into seven main subsections. They are origin and nature of direct torque control, power supplies used in direct torque control, voltage space vector selection schemes for direct torque control, stator flux and torque estimation, stator resistance estimation, iron loss considerations in high performance induction motor drives, and sensorless direct torque control. The

subsection related to the iron loss considerations in high performance indicates that investigation of iron loss impact on direct torque control has not been carried out so far in the contemporary literature.

CHAPTER 3

INDUCTION MOTOR AND VOLTAGE SOURCE INVERTER MODELLING

3.1 Introduction

A mathematical model of an induction machine suitable for transient operation study is at first developed in this chapter. The model is formed in a common reference frame rotating with an arbitrary angular speed. The model of an induction machine in phase domain is the starting point for the development of this dynamic machine model.

Iron loss and main flux saturation are ignored in the development of the constant parameter machine model in an arbitrary reference frame. However, iron loss and main flux saturation do exist in reality and they affect operation of high performance drives. While inclusion of main flux saturation into the induction machine model may be of substantial importance in certain schemes of vector control [Wang (1999)], it is of no importance in direct torque control. This is so since DTC in its basic form controls stator flux and stator flux is estimated from stator voltages and currents. Hence any variation of the actual degree of main flux saturation in the machine is automatically accounted for in the process of stator flux and torque estimation.

Situation with respect to iron loss is however different. Both vector control schemes and DTC schemes are affected by the existence of the iron loss, which is neglected in the development of control structures. It is for this reason that machine models with iron loss representation are presented further on in this chapter.

Ideal model of a voltage source inverter is finally discussed. The power semiconductor switches of the inverter are assumed to be ideal and inverter operation is modelled using the concept of switching functions.

3.2 Constant parameter model of an induction motor in an arbitrary rotating common reference frame

An induction machine with perfectly smooth air gap is considered. The phase windings of the machine are assumed to be physically 120 degrees apart for both stator

and rotor. Winding resistances and leakage inductances are assumed to be constant. All the parasitic phenomena such as iron loss and main flux saturation are ignored at this stage. The induction machine under consideration is therefore an ideal smooth air gap machine with sinusoidal distribution of windings and all the effects of MMF harmonics are also neglected [Vas (1992), Boldea and Nasar (1992)]. A schematic representation of the machine is shown in figure 3.1.

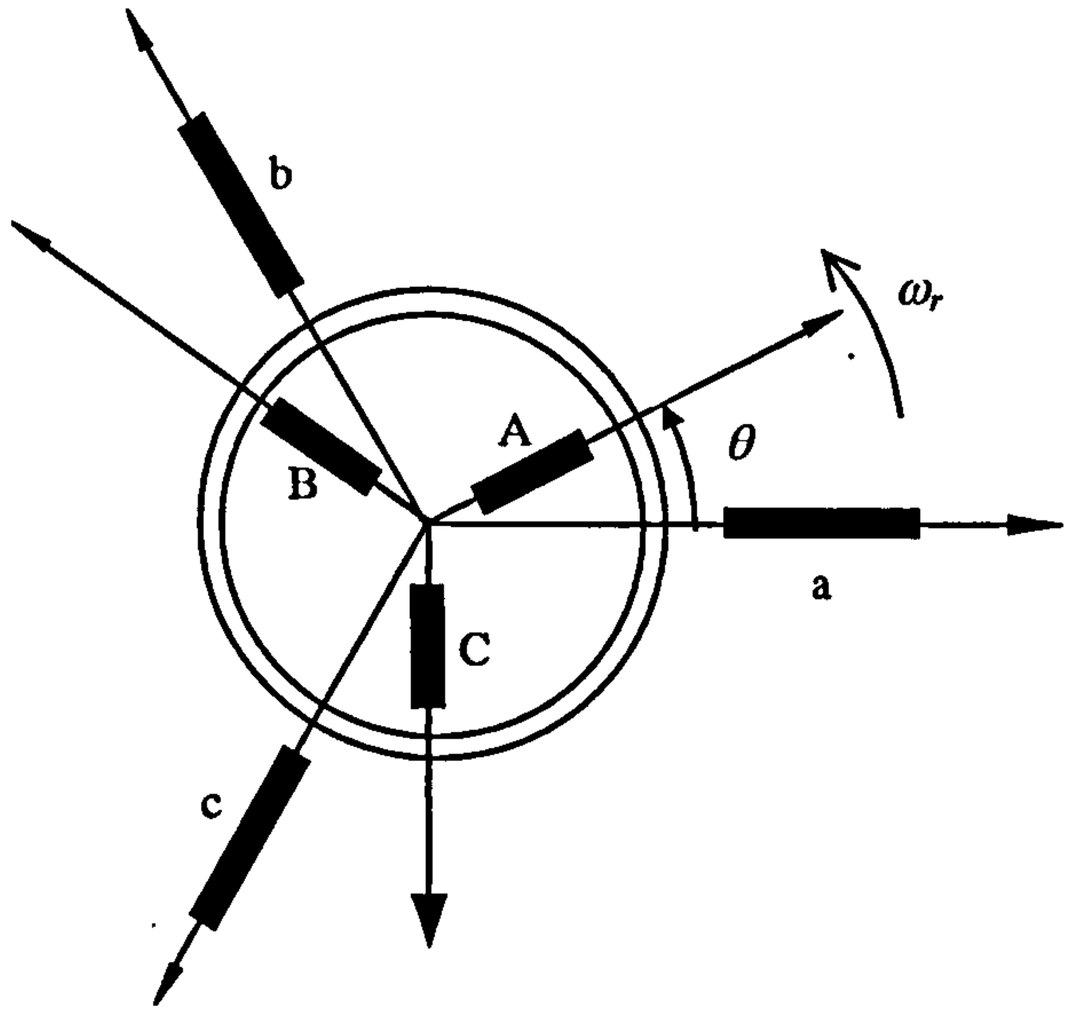

Figure 3.1: Schematic representation of an induction machine with sinusoidal distribution of windings and smooth air gap.

The stator and rotor voltage equations, and the stator and rotor flux linkage equations can be by expressed using matrix notation as follows [Vas (1990)]:

$$\begin{aligned}
[\underline{v}_{abc}] &= [\underline{R}_s][\underline{i}_{abc}] + d[\underline{\psi}_{abc}]/dt \\
[\underline{v}_{ABC}] &= [\underline{R}_r][\underline{i}_{ABC}] + d[\underline{\psi}_{ABC}]/dt
\end{aligned} \tag{3.1}$$

$$[\underline{\psi}_{abc}] = [\underline{L}_s][\underline{i}_{abc}] + [\underline{L}_{sr}][\underline{i}_{ABC}] \tag{3.2}$$

$$[\underline{\psi}_{ABC}] = [\underline{L}_r][\underline{i}_{ABC}] + [\underline{L}_{sr}^t][\underline{i}_{abc}]$$

where

$$[\underline{v}_{abc}] = \begin{bmatrix} v_a \\ v_b \\ v_c \end{bmatrix} \quad [\underline{i}_{abc}] = \begin{bmatrix} i_a \\ i_b \\ i_c \end{bmatrix} \quad [\underline{v}_{ABC}] = \begin{bmatrix} v_A \\ v_B \\ v_C \end{bmatrix} \quad [\underline{i}_{ABC}] = \begin{bmatrix} i_A \\ i_B \\ i_C \end{bmatrix} \tag{3.3}$$

$$[\underline{L}_{sr}] = L_{aA}\begin{bmatrix} \cos\theta & \cos(\theta+2\pi/3) & \cos(\theta+4\pi/3) \\ \cos(\theta+4\pi/3) & \cos\theta & \cos(\theta+2\pi/3) \\ \cos(\theta+2\pi/3) & \cos(\theta+4\pi/3) & \cos\theta \end{bmatrix} \tag{3.4}$$

$$[\underline{L}_s] = \begin{bmatrix} L_{aa} & L_{ab} & L_{ac} \\ L_{ba} & L_{bb} & L_{bc} \\ L_{ca} & L_{cb} & L_{cc} \end{bmatrix} \qquad [\underline{L}_r] = \begin{bmatrix} L_{AA} & L_{AB} & L_{AC} \\ L_{BA} & L_{BB} & L_{BC} \\ L_{CA} & L_{CB} & L_{CC} \end{bmatrix} \tag{3.5}$$

$$[\underline{R}_s] = diag(R_s) \qquad [\underline{R}_r] = diag(R_r) \tag{3.6}$$

Here indices *a, b, c* and *A, B, C* identify the three stator and rotor phases, respectively. The following holds true in (3.5):

$$\begin{aligned} &L_{aa} = L_{bb} = L_{cc} \\ &L_{ab} = L_{bc} = L_{ca} = L_{ba} = L_{cb} = L_{ac} \\ &L_{AA} = L_{BB} = L_{CC} \\ &L_{AB} = L_{BC} = L_{CA} = L_{BA} = L_{CB} = L_{AC} \end{aligned} \tag{3.7}$$

The electromagnetic torque of the motor is given in terms of stator and rotor currents with

$$\begin{aligned} T_e = -L_{aA}[&\sin\theta(i_a i_A + i_b i_B + i_c i_C) + \sin(\theta+4\pi/3)(i_a i_C + i_b i_A + i_c i_B) \\ &+ \sin(\theta+2\pi/3)(i_a i_B + i_b i_C + i_c i_A)] \end{aligned} \tag{3.8}$$

The angle θ is the instantaneous angle between phase A magnetic axis of rotor and stationary phase *a* magnetic axis of stator. The equation of rotor angular motion is as following:

$$T_e - T_L = \frac{J}{P}\frac{d\omega_r}{dt} \tag{3.9}$$

where T_e, T_L are the electromagnetic torque and load torque, respectively, P is the number of pole pairs, J is the inertia constant and ω_r is the electrical angular speed of rotor, which is the derivative of the instantaneous rotor angular position.

$$\omega_r = \frac{d\theta}{dt} \tag{3.10}$$

The model in terms of phase variable is inconvenient for simulation since it is composed of a set of seven first order non-linear differential equations with time varying coefficients.

The rotor winding is at first referred to stator winding and the stator and rotor equations are further transformed to a common rotating reference frame with the perpendicular axes and an arbitrary angular speed of ω_a. The transformation is carried

out by the application of two transformation matrices to stator and rotor equations, respectively. The transformation matrices are [Vas (1990)]:

$$[\underline{A}_s] = \frac{2}{3}\begin{bmatrix} \cos\theta_s & \cos(\theta_s - 2\pi/3) & \cos(\theta_s + 2\pi/3) \\ -\sin\theta_s & -\sin(\theta_s - 2\pi/3) & -\sin(\theta_s + 2\pi/3) \\ 1/2 & 1/2 & 1/2 \end{bmatrix} \tag{3.11}$$

$$[\underline{A}_r] = \frac{2}{3}\begin{bmatrix} \cos\theta_r & \cos(\theta_r - 2\pi/3) & \cos(\theta_r + 2\pi/3) \\ -\sin\theta_r & -\sin(\theta_r - 2\pi/3) & -\sin(\theta_r + 2\pi/3) \\ 1/2 & 1/2 & 1/2 \end{bmatrix} \tag{3.12}$$

where the angles θ_s and θ_r are shown in figure 3.2 and the relation between these two angles is: $\theta_r = \theta_s - \theta$. The relations between the new quantities and the phase quantities are:

$$\begin{aligned} &[\underline{v}_{dqs}] = [\underline{A}_s][\underline{v}_{abc}] \qquad [\underline{v}_{dqr}] = [\underline{A}_r][\underline{v}_{ABC}] \qquad [\underline{\psi}_{dqs}] = [\underline{A}_s][\underline{\psi}_{abc}] \\ &[\underline{i}_{dqs}] = [\underline{A}_s][\underline{i}_{abc}] \qquad [\underline{i}_{dqr}] = [\underline{A}_r][\underline{i}_{ABC}] \qquad [\underline{\psi}_{dqr}] = [\underline{A}_r][\underline{\psi}_{ABC}] \end{aligned} \tag{3.13}$$

where

$$[\underline{v}_{dqs}] = \begin{bmatrix} v_{ds} \\ v_{qs} \\ v_{os} \end{bmatrix} \qquad [\underline{i}_{dqs}] = \begin{bmatrix} i_{ds} \\ i_{qs} \\ i_{os} \end{bmatrix} \qquad [\underline{v}_{dqr}] = \begin{bmatrix} v_{dr} \\ v_{qr} \\ v_{or} \end{bmatrix} \qquad [\underline{i}_{dqr}] = \begin{bmatrix} i_{dr} \\ i_{qr} \\ i_{or} \end{bmatrix} \tag{3.14}$$

The indices '*s*' and '*r*' denote the stator and rotor quantities, respectively. The schematic illustration of relationship between the reference frames is shown in figure 3.2.

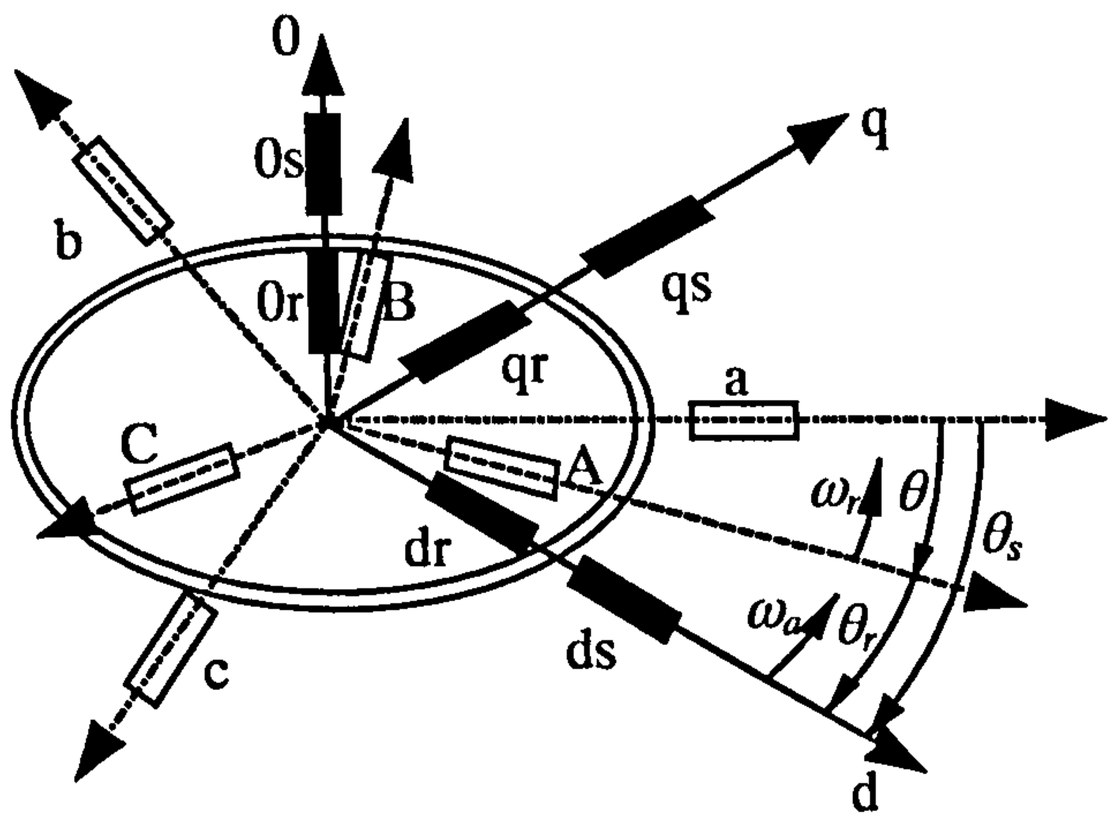

Figure 3.2: Winding transformation from three-phase domain to an arbitrary rotating common reference frame.

The induction machine considered in this research is assumed to be star connected with isolated neutral point and rotor winding is short-circuited. Therefore, the zero-sequence components of both stator and rotor voltages, currents and flux linkages are all zero.

After the transformation, the stator and rotor voltage equations of an induction machine are the following:

$$\begin{aligned} v_{ds} &= R_s i_{ds} + \frac{d\psi_{ds}}{dt} - \omega_a \psi_{qs} \\ v_{qs} &= R_s i_{qs} + \frac{d\psi_{qs}}{dt} + \omega_a \psi_{ds} \end{aligned} \tag{3.15}$$

$$\begin{aligned} v_{dr} &= R_r i_{dr} + \frac{d\psi_{dr}}{dt} - (\omega_a - \omega_r)\psi_{qr} \\ v_{qr} &= R_r i_{qr} + \frac{d\psi_{qr}}{dt} + (\omega_a - \omega_r)\psi_{dr} \end{aligned} \tag{3.16}$$

The flux linkages are:

$$\begin{aligned} \psi_{ds} &= L_s i_{ds} + L_m i_{dr} \\ \psi_{qs} &= L_s i_{qs} + L_m i_{qr} \end{aligned} \tag{3.17}$$

$$\begin{aligned} \psi_{dr} &= L_r i_{dr} + L_m i_{ds} \\ \psi_{qr} &= L_r i_{qr} + L_m i_{qs} \end{aligned} \tag{3.18}$$

Symbols L_s and L_r denote stator and rotor self-inductance, respectively, while L_m is the magnetising inductance. The relationship between the stator, rotor and magnetising inductances and the three-phase model self and mutual inductances are:

$$\begin{aligned} L_s &= L_{aa} - L_{ab} = L_{\sigma s} + L_m \\ L_r &= L'_{AA} - L'_{AB} = L_{\sigma r} + L_m \\ L_m &= (3/2)L'_{aA} \end{aligned} \tag{3.19}$$

where $L_{\sigma s}$ and $L_{\sigma r}$ are stator and rotor leakage inductances, respectively, and superscript ' denotes quantities referred to stator winding.

The equation of mechanical motion remains as in (3.9). Electromagnetic torque can be expressed in terms of d-q components of stator flux and stator current as

$$T_e = \frac{3}{2} P\left(\psi_{ds} i_{qs} - \psi_{qs} i_{ds}\right) \tag{3.20}$$

The correlation between stator quantities in an arbitrary rotating common reference frame and in three-phase domain in the general form is:

$$f_{ds} = \frac{2}{3}[f_a \cos\theta_s + f_b \cos(\theta_s - 2\pi/3) + f_c \cos(\theta_s + 2\pi/3)]$$
$$f_{qs} = -\frac{2}{3}[f_a \sin\theta_s + f_b \sin(\theta_s - 2\pi/3) + f_c \sin(\theta_s + 2\pi/3)] \quad (3.21)$$

where f can be voltage, current or stator flux. The inverse relation is:

$$f_a = f_{ds}\cos\theta_s - f_{qs}\sin\theta_s$$
$$f_b = f_{ds}\cos(\theta_s - 2\pi/3) - f_{qs}\sin(\theta_s - 2\pi/3) \quad (3.22)$$
$$f_c = f_{ds}\cos(\theta_s + 2\pi/3) - f_{qs}\sin(\theta_s + 2\pi/3)$$

The complexity of the induction machine model has been significantly reduced by the transformation to an arbitrary rotating common reference frame. In particular, time varying coefficients present in the phase variable model, have been eliminated. Furthermore, since the *d-q* system of axis is a rectangular co-ordinate system, *d*-axis flux linkage equations are decoupled from *q*-axis currents. The same holds true for *q*-axis flux linkage equations in relation to *d*-axis currents.

If the angular speed of the common reference frame is selected as zero ($\omega_a = 0$), the equations for induction machine model in stationary α-β system of axes (index *d* is changed to α and *q* is changed to β) are obtained:

$$v_{\alpha s} = R_s i_{\alpha s} + \frac{d\psi_{\alpha s}}{dt}$$
$$v_{\beta s} = R_s i_{\beta s} + \frac{d\psi_{\beta s}}{dt} \quad (3.23)$$

$$v_{\alpha r} = R_r i_{\alpha r} + \frac{d\psi_{\alpha r}}{dt} + \omega_r \psi_{\beta r}$$
$$v_{\beta r} = R_r i_{\beta r} + \frac{d\psi_{\beta r}}{dt} - \omega_r \psi_{\alpha r} \quad (3.24)$$

Flux linkage relations in equations (3.17) and (3.18) and torque equation (3.20) remain to be valid. Because of the short-circuiting of rotor winding in a squirrel-cage induction machine, rotor voltage components are zero. Transformation angles are now $\theta_s = 0$ and $\theta_r = -\theta$. The correlation given in equations (3.21) and (3.22) is still valid with substitution $\theta_s = 0$.

Since the machine equations are transformed into an orthogonal system of axis, the d-axis of the common reference frame can be regarded as the real axis of a complex plane, while q-axis takes the role of the imaginary axis. Complex variables, or space vector, can then be introduced. The complex variables in stationary reference frame are defined as follows:

$$\underline{v}_s^s = v_{\alpha s} + jv_{\beta s} = v_s e^{j\delta_s} = \frac{2}{3}\left(v_a + \underline{a}v_b + \underline{a}^2 v_c\right) \tag{3.25a}$$

$$\underline{i}_s^s = i_{\alpha s} + ji_{\beta s} = i_s e^{j\gamma_s} = \frac{2}{3}\left(i_a + \underline{a}i_b + \underline{a}^2 i_c\right) \tag{3.25b}$$

where $\underline{a} = e^{j2\pi/3}$.

Stator voltage and stator current in an arbitrary rotating reference frame can be expressed in space vector form using the concept of a vector rotator:

$$\begin{aligned} \underline{v}_s &= \underline{v}_s^s e^{-j\theta_s} = v_s e^{j(\delta_s - \theta_s)} = v_{ds} + jv_{qs} \\ \underline{i}_s &= \underline{i}_s^s e^{-j\theta_s} = i_s e^{j(\gamma_s - \theta_s)} = i_{ds} + ji_{qs} \end{aligned} \tag{3.26}$$

From the equations (3.15)-(3.18) and (3.26), the dynamic model of an induction machine in an arbitrary reference frame can be expressed in space vector form as follows:

$$\begin{aligned} \underline{v}_s &= R_s \underline{i}_s + \frac{d\underline{\psi}_s}{dt} + j\omega_a \underline{\psi}_s \\ 0 &= R_r \underline{i}_r + \frac{d\underline{\psi}_r}{dt} + j(\omega_a - \omega_r)\underline{\psi}_r \end{aligned} \tag{3.27}$$

$$\begin{aligned} \underline{\psi}_s &= L_s \underline{i}_s + L_m \underline{i}_r \\ \underline{\psi}_r &= L_r \underline{i}_r + L_m \underline{i}_s \end{aligned} \tag{3.28}$$

where

$$\begin{aligned} \underline{\psi}_s &= \psi_s e^{j(\phi_s - \theta_s)} \\ \underline{\psi}_r &= \psi_r e^{j(\phi_r - \theta_s)} \\ \underline{i}_r &= i_r e^{j(\gamma_r - \theta_s)} \end{aligned} \tag{3.29}$$

The angles $\delta_s, \gamma_s, \phi_s, \phi_r$ and γ_r in (3.25a), (3.25b), (3.26) and (3.29) are the instantaneous angular positions of stator voltage, stator current, stator flux, rotor flux and rotor current space vector, respectively, with respect to the stator phase *a* magnetic axis. Electromagnetic torque equation of the induction machine can be expressed in terms of space vectors as

$$T_e = \frac{3}{2} P \,\mathrm{Im}\left(\underline{i}_s \underline{\psi}_s^*\right) \tag{3.30}$$

where '*' denotes the complex conjugation. An electrical dynamic equivalent circuit of an induction machine in an arbitrary rotating common reference frame is built using the equations (3.27) and (3.28). This equivalent circuit is shown in figure 3.3.

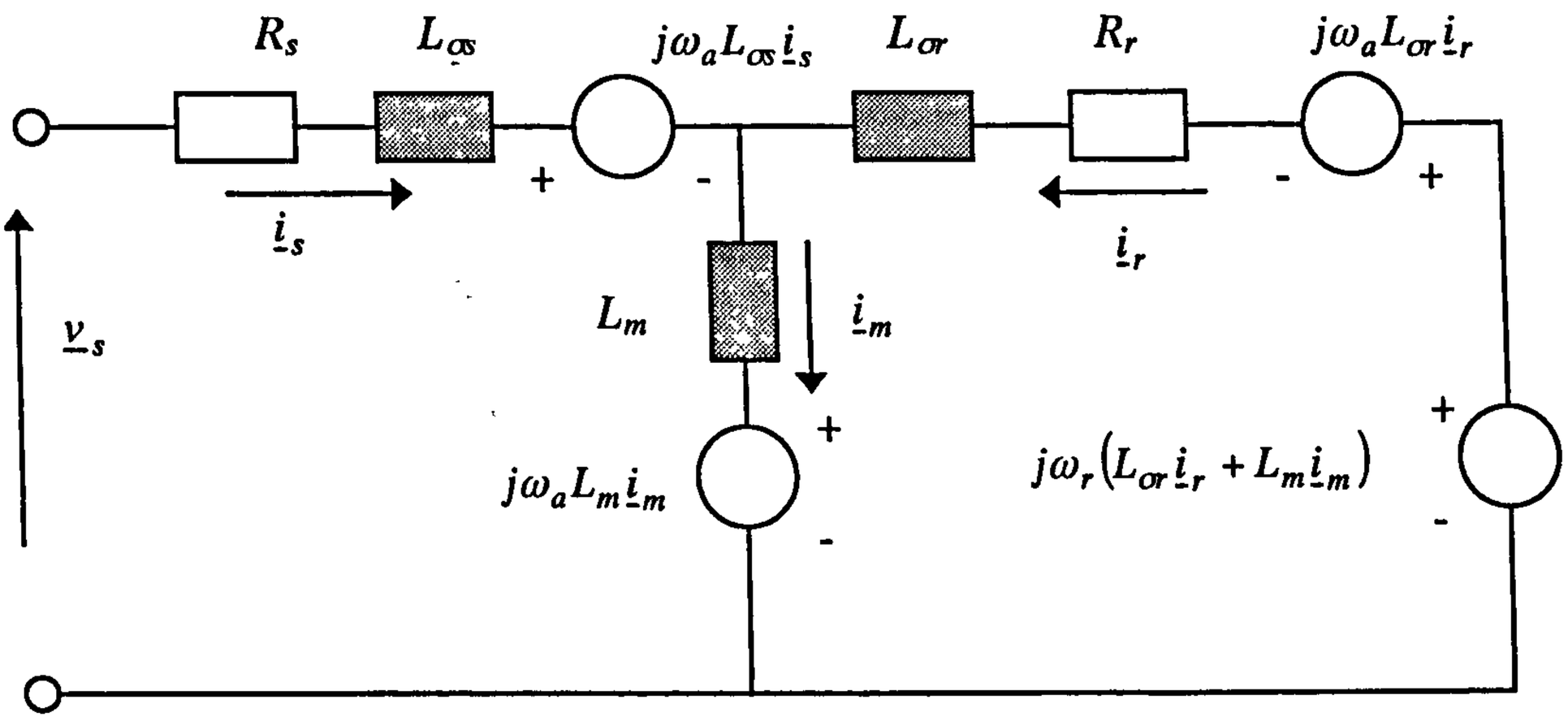

Figure 3.3: Dynamic equivalent circuit of an induction machine in an arbitrary rotating common reference frame.

The induction machine model used further on in this project for simulation purpose is the machine model in stationary reference frame. Components of stator current and rotor current and angular electrical speed ω_r are used as state-space variables in the fifth-order differential equation system. The stator and rotor voltage equations with stator current, rotor current and rotor angular speed as state-space variables are obtained by using equations (3.9), (3.17), (3.18), (3.20) and (3.23)-(3.24):

$$\begin{aligned} v_{\alpha s} &= R_s i_{\alpha s} + L_s \frac{di_{\alpha s}}{dt} + L_m \frac{di_{\alpha r}}{dt} \\ v_{\beta s} &= R_s i_{\beta s} + L_s \frac{di_{\beta s}}{dt} + L_m \frac{di_{\beta r}}{dt} \end{aligned} \tag{3.31}$$

$$\begin{aligned} 0 &= L_m \frac{di_{\alpha s}}{dt} + \omega_r L_m i_{\beta s} + R_r i_{\alpha r} + L_r \frac{di_{\alpha r}}{dt} + \omega_r L_r i_{\beta r} \\ 0 &= -\omega_r L_m i_{\alpha s} + L_m \frac{di_{\beta s}}{dt} - \omega_r L_r i_{\alpha r} + R_r i_{\beta r} + L_r \frac{di_{\beta r}}{dt} \end{aligned} \tag{3.32}$$

$$\frac{J}{P}\frac{d\omega_r}{dt} = \frac{3}{2}P\left[i_{\beta s}\left(L_s i_{\alpha s} + L_m i_{\alpha r}\right) - i_{\alpha s}\left(L_s i_{\beta s} + L_m i_{\beta r}\right)\right] - T_L \tag{3.33}$$

These differential equations will be used for building the induction machine model in Matlab/Simulink for simulation of performance of a DTC induction motor drive.

3.3 Dynamic induction machine models with iron loss representation

The induction machine model presented in previous section ignores iron loss. The machine is assumed to operate in an idealised magnetic condition. Iron loss, however, exists in practical operating conditions of induction machines and it can have undesirable effects on the drive behaviour. A more accurate dynamic model of an induction machine is therefore necessary to study this effect. Many improved dynamic induction motor models have been suggested in the past. Some models account for iron loss or main flux saturation only, while other models consider both iron loss and saturation. Because only iron loss is of relevance for DTC, dynamic models of an induction machine with iron loss representation only are discussed in this section. Two such models are presented further on.

3.3.1 Dynamic model of an induction machine with iron loss resistance placed in parallel to the magnetising branch

All the equations for this dynamic model are shown in an arbitrary rotating common reference frame. The equivalent iron loss resistance is placed in parallel to the magnetising branch, as shown in figure 3.4. The value of the iron loss resistance is determined experimentally in [Levi et al (1996)]. The space vector equations for the new machine model in an arbitrary reference frame follow from figure 3.4 in the form [Levi (1994, 1995)]:

$$\begin{aligned} \underline{v}_s &= R_s \underline{i}_s + \frac{d\underline{\psi}_s}{dt} + j\omega_a \underline{\psi}_s \\ 0 &= R_r \underline{i}_r + \frac{d\underline{\psi}_r}{dt} + j(\omega_a - \omega_r)\underline{\psi}_r \end{aligned} \tag{3.34}$$

$$\begin{aligned} \underline{\psi}_s &= L_{\sigma s}\underline{i}_s + L_m \underline{i}_m = L_{\sigma s}\underline{i}_s + \underline{\psi}_m \\ \underline{\psi}_r &= L_{\sigma r}\underline{i}_r + L_m \underline{i}_m = L_{\sigma r}\underline{i}_r + \underline{\psi}_m \end{aligned} \tag{3.35}$$

$$R_{Fe}\underline{i}_{Fe} = L_m \frac{d\underline{i}_m}{dt} + j\omega_a L_m \underline{i}_m \tag{3.36}$$

$$\underline{i}_m + \underline{i}_{Fe} = \underline{i}_s + \underline{i}_r \tag{3.37}$$

$$T_e = \frac{3}{2} P \frac{L_m}{L_{\sigma r}} (\psi_{dr} i_{qm} - \psi_{qr} i_{dm}) \tag{3.38}$$

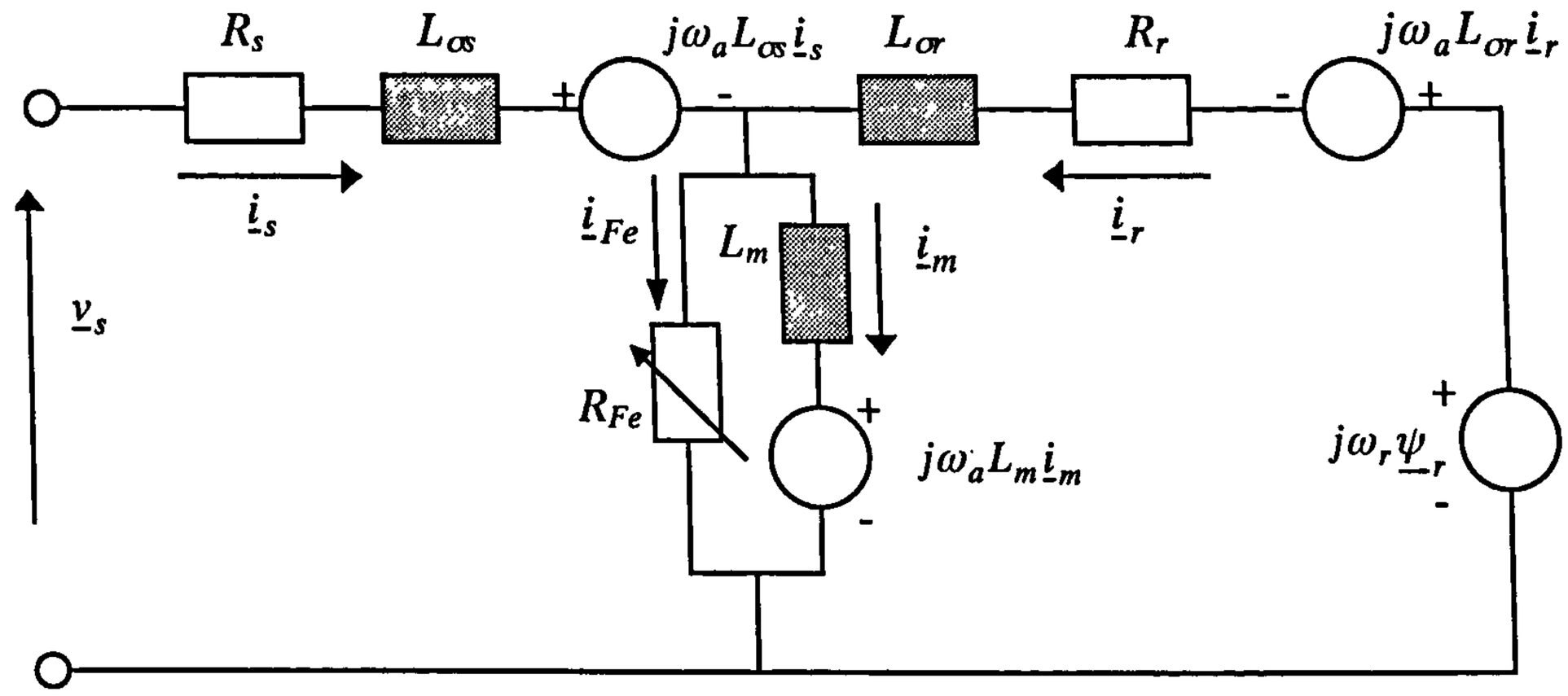

Figure 3.4: Equivalent circuit of induction machine with iron loss consideration in space vector form in an arbitrary rotating reference frame.

The equivalent iron loss resistance is considered as a non-linear function of fundamental frequency only in the machine model above, so that $R_{Fe} = f(f)$. Actually, equivalent iron loss resistance is a function of both flux density and frequency. However, the experimental method of its determination in [Levi et al (1996)] has already taken into account the dependency on flux density.

This dynamic model only takes into consideration the fundamental component of the actual iron loss. This is so because the equivalent iron loss resistance in figure 3.4 models only the fundamental component of the iron loss. The value of the equivalent iron loss resistance is calculated using a variable-frequency no-load test where voltage magnitude is varied using *V/f* = *const.* control law. The source used in the experiment can be either an ideal sinusoidal voltage source (e.g. a synchronous generator) or a PWM voltage source inverter, in which case measurement of the fundamental component of the input power and current is required. In real operation with PWM voltage source inverter, there will be higher order voltage harmonics in the supply voltage. These harmonics will "see" the fundamental equivalent iron loss resistance when the model of figure 3.4 is used in dynamic simulation of a DTC induction motor drive, since the inverter model will be included. This is an inherent limitation of the model (3.34)-(3.38), which is of no consequence when vector control is considered. In simulation of the vector controlled drives the voltage source can be assumed to be ideal sinusoidal (i.e. inverter does not have to be included), so that the fundamental equivalent iron loss resistance suffices. This is however not the case in DTC, where inverter model has to be included in the study. Since use of the fundamental equivalent

iron loss resistance for higher order voltage harmonic is of questionable accuracy, simulation results obtained with the model of figure 3.4 will exhibit a change in the torque ripple characteristic. The issue will be discussed in more detail in chapter 6.

The complete model in the stationary reference frame, convenient for dynamic simulation, is obtained from (3.34)-(3.38) in the following form:

$$v_{\alpha s} = R_s i_{\alpha s} + L_{\sigma s}\frac{di_{\alpha s}}{dt} + L_m\frac{di_{\alpha m}}{dt}$$
$$v_{\beta s} = R_s i_{\beta s} + L_{\sigma s}\frac{di_{\beta s}}{dt} + L_m\frac{di_{\beta m}}{dt} \qquad (3.39)$$

$$0 = R_r i_{\alpha r} + L_{\sigma r}\frac{di_{\alpha r}}{dt} + L_m\frac{di_{\alpha m}}{dt} + \omega_r\left(L_{\sigma r} i_{\beta r} + L_m i_{\beta m}\right)$$
$$0 = R_r i_{\beta r} + L_{\sigma r}\frac{di_{\beta r}}{dt} + L_m\frac{di_{\beta m}}{dt} - \omega_r\left(L_{\sigma r} i_{\alpha r} + L_m i_{\alpha m}\right) \qquad (3.40)$$

$$i_{\alpha m} + i_{\alpha Fe} = i_{\alpha s} + i_{\alpha r} \qquad i_{\beta m} + i_{\beta Fe} = i_{\beta s} + i_{\beta r} \qquad (3.41)$$

$$R_{Fe} i_{\alpha Fe} = L_m\frac{di_{\alpha m}}{dt} \qquad R_{Fe} i_{\beta Fe} = L_m\frac{di_{\beta m}}{dt} \qquad (3.42)$$

$$T_e = \frac{3}{2}P\frac{L_m}{L_{\sigma r}}\left[i_{\beta m}\left(L_{\sigma r} i_{\alpha r} + L_m i_{\alpha m}\right) - i_{\alpha m}\left(L_{\sigma r} i_{\beta r} + L_m i_{\beta m}\right)\right] \qquad (3.43)$$

$$T_e - T_L = \frac{J}{P}\frac{d\omega_r}{dt} \qquad (3.44)$$

Actual variation of the equivalent iron loss resistance with fundamental frequency will be given in chapter 6.

The state-space variables of the differential equations are selected as α-β components of stator current, rotor current and magnetising current, and angular electrical speed of rotor. The final set of differential equations is derived from the equations (3.39)-(3.44) in a straightforward manner, by eliminating iron loss current components from (3.41) using (3.42).

3.3.2 Dynamic model of an induction machine with parallel iron loss resistance placed immediately after stator resistance

Another possible way of taking iron loss into consideration is to place the parallel equivalent iron loss resistor right after stator resistance in the space vector equivalent circuit of an induction motor. This equivalent circuit in an arbitrary rotating common reference frame is shown in figure 3.5.

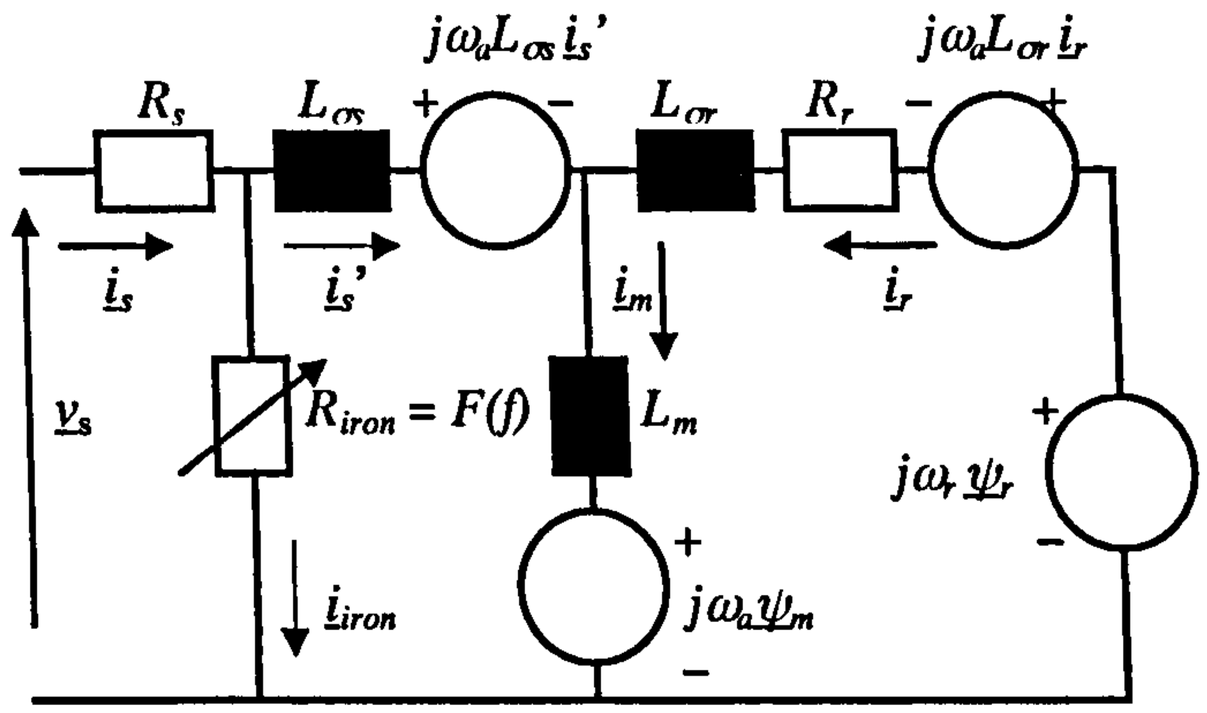

Figure 3.5: Alternative placement of the iron loss resistance in the space vector dynamic equivalent circuit of an induction motor.

A new variable is introduced in the circuit, $\underline{i}_s'$, which is the current flowing through stator leakage inductance. Stator leakage inductance and the rest of the circuit now see $\underline{i}_s'$ instead of $\underline{i}_s$. The equivalent iron loss resistance in this circuit is again a function of frequency and it can be calculated on the basis of R_{Fe} of figure 3.4. This equivalent iron loss resistance will be given for the motor used in the project in chapter 7.

The mathematical model that corresponds to figure 3.5 is described with the following equations:

$$\underline{v}_s = R_s \underline{i}_s + \frac{d\underline{\psi}_s}{dt} + j\omega_a \underline{\psi}_s$$
$$0 = R_r \underline{i}_r + \frac{d\underline{\psi}_r}{dt} + j(\omega_a - \omega_r)\underline{\psi}_r \qquad (3.45)$$

$$\underline{\psi}_s = L_{\sigma s}\underline{i}_s' + L_m \underline{i}_m = L_{\sigma s}\underline{i}_s' + \underline{\psi}_m = L_s \underline{i}_s' + L_m \underline{i}_r$$
$$\underline{\psi}_r = L_{\sigma r}\underline{i}_r + L_m \underline{i}_m = L_{\sigma r}\underline{i}_r + \underline{\psi}_m = L_r \underline{i}_r + L_m \underline{i}_s' \qquad (3.46)$$

$$\underline{i}_s' = \underline{i}_s - \underline{i}_{iron} \qquad (3.47)$$

$$\underline{i}_m = \underline{i}_s' + \underline{i}_r \qquad (3.48)$$

$$\underline{i}_{iron} = (\underline{v}_s - R_s \underline{i}_s)/R_{iron} \qquad (3.49)$$

$$T_e = \frac{3}{2} P\left(\psi_{ds} i_{qs}' - \psi_{qs} i_{ds}'\right) \qquad (3.50)$$

$$T_e - T_L = \frac{J}{P}\frac{d\omega}{dt} \qquad (3.51)$$

Representation of an induction motor with iron loss for simulation purposes will, in subsequent chapters, always utilise the model of section 3.3.1. The model of this section will be however shown to be a better starting point for development of modified speed estimators with iron loss compensation in chapter 7.

3.4 Voltage source inverter model

Variable voltage, variable frequency operation of induction machines is realised utilising autonomous inverters, in conjunction with a rectifier and a DC link circuit. There are two generic structures of autonomous inverters, voltage source inverter (VSI) and current source inverter (CSI). The first one, voltage source inverter, is the most frequently applied power supply source for V/f control of induction motors. Only VSI is used in this research project. Therefore, current source inverter is not discussed here.

Three-phase version of a VSI contains three inverter legs. Input voltage for a three-phase VSI is provided by a three-phase (or single-phase) bridge rectifier with capacitor placed at the output. The capacitor provides smoothing of the DC voltage and, for sufficiently large capacitance, DC voltage at the rectifier output approaches a constant value. It will therefore be assumed that inverter input voltage is constant in the model of VSI throughout the research.

Power circuit of a six-step voltage source inverter is shown in figure 3.6. Each switch in the inverter circuit is composed of two back-to-back connected semiconductor devices. One of these two is a controllable switch (say, BJT), while the other one is a diode. Diode is essential for correct operation of the VSI as output voltage and current are out of phase due to inductive nature of the machine. It enables current flow when one switch in given inverter leg is turned off and the other one turned on, while the current still flows in the previous direction. The switches operate in such a manner that only one switch in every leg is on at any time. The other switch in the same leg is off during that period. This gives eight combinations of on/off switch states in three legs to create eight output voltage space vectors of three-phase VSI. Among the output voltage vectors, six are nonzero vectors and two are zero vectors.

Leg voltages (voltages between points A, B and C and the negative rail of the DC supply 'n') are denoted in what follows with v_A, v_B, v_C. It follows that the space vector of leg voltages will have eight distinct and discrete values and that, instead of

uniformly rotating in the complex plane, it will be jumping from one position to the other. Table 3.1 summarises values of leg voltages with the eight combinations of on/off switch states, lists switches that are on, and defines a corresponding space vector for each combination.

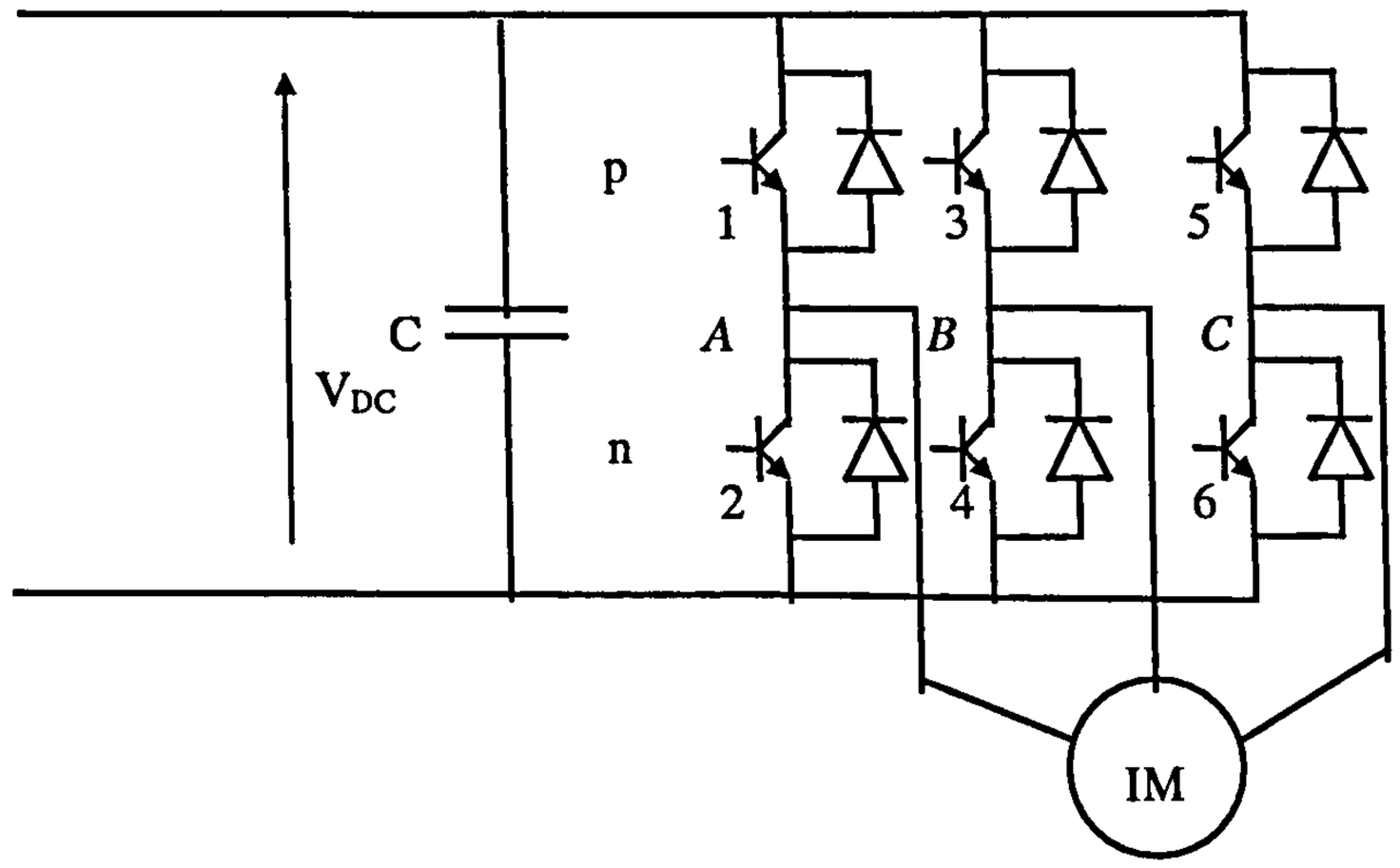

Figure 3.6: Power circuit of the voltage source inverter.

Table 3.1: Leg voltages of voltage source inverter.

switching state	switches on	space vector	Leg voltage v_A	Leg voltage v_B	Leg voltage v_C
1	1,4,6	$\underline{v}_1(100)$	V_{DC}	0	0
2	1,3,6	$\underline{v}_2(110)$	V_{DC}	V_{DC}	0
3	2,3,6	$\underline{v}_3(010)$	0	V_{DC}	0
4	2,3,5	$\underline{v}_4(011)$	0	V_{DC}	V_{DC}
5	2,4,5	$\underline{v}_5(001)$	0	0	V_{DC}
6	1,4,5	$\underline{v}_6(101)$	V_{DC}	0	V_{DC}
7	1,3,5	$\underline{v}_7(111)$	V_{DC}	V_{DC}	V_{DC}
8	2,4,6	$\underline{v}_8(000)$	0	0	0

The two zero vectors describe the condition when the induction motor terminals are short-circuited either through the positive rail of the dc supply (vector 7) or through the negative rail of the dc supply (vector 8). Calculation of the leg voltage space vectors can be carried out by using the definition of the voltage space vector in (3.25a). One gets by substitution of individual leg voltages of table 3.1 for each of the eight combinations of switch states the following:

$$\underline{v}_1 = \frac{2}{3}V_{DC};\ \underline{v}_2 = \frac{2}{3}V_{DC}e^{(j\pi/3)};\ \underline{v}_3 = \frac{2}{3}V_{DC}e^{(j2\pi/3)};\ \underline{v}_4 = \frac{2}{3}V_{DC}e^{(j\pi)};$$
$$\underline{v}_5 = \frac{2}{3}V_{DC}e^{(j4\pi/3)};\ \underline{v}_6 = \frac{2}{3}V_{DC}e^{(j5\pi/3)};\ \underline{v}_7 = \underline{v}_8 = 0 \tag{3.52}$$

The two space vectors $\underline{v}_7, \underline{v}_8$ are identically equal to zero as either all the leg voltages are zero or all the leg voltages have the same value ($1+\underline{a}+\underline{a}^2 = 0$). It follows from (3.52) that all the non-zero space vectors have identical amplitudes. However, they are stationary, indicating that only discrete values of the leg voltage space vector are possible in a VSI. Space vector values for the leg voltages are shown in figure 3.7.

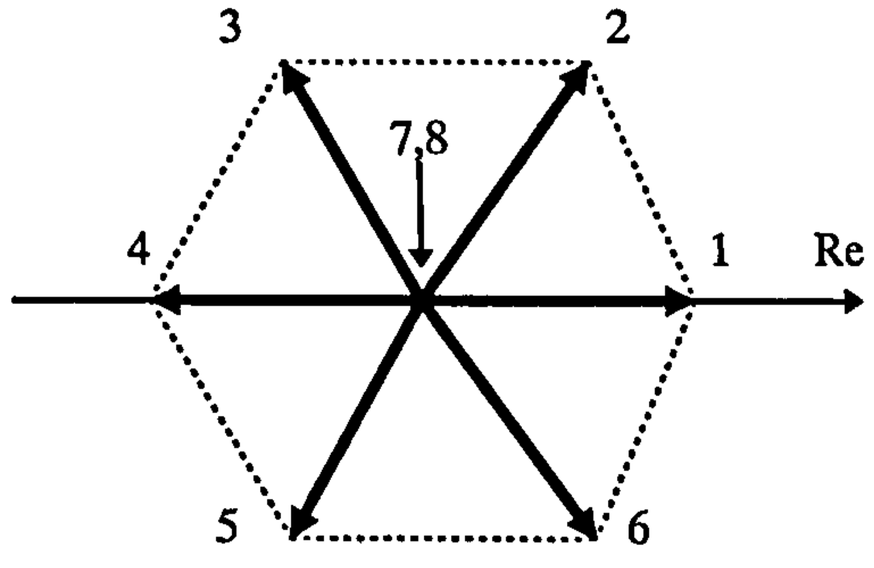

Figure 3.7: Discrete values of the leg voltage space vector and of the phase-to-neutral voltage space vector.

Assuming that load is star connected with isolated neutral, phase-to-neutral voltages of the load are related to the leg voltages through the following expressions [Krause et al (1995)].

$$v_a = \frac{2}{3}v_A - \frac{1}{3}(v_B + v_C)$$
$$v_b = \frac{2}{3}v_B - \frac{1}{3}(v_A + v_C) \tag{3.53}$$
$$v_c = \frac{2}{3}v_C - \frac{1}{3}(v_A + v_B)$$

Table 3.2 summarises values of phase to neutral voltages for the eight inverter switching states. Applying once more the same procedure, one finds the values of the space vector of the phase voltages as equal to those already given in (3.52) for leg voltages.

For simulation purposes the inverter switches are assumed to be ideal and the inverter input DC voltage is kept at constant value. The required phase voltage space

vector, that is to be applied to the induction motor in any particular instant in time, is determined by the DTC algorithm, described in chapter 4. The motor input phase voltages are then calculated using (3.53) and switching functions,

$$\begin{aligned} v_a &= \frac{1}{3}V_{DC}[2S_A - (S_B + S_C)] \\ v_b &= \frac{1}{3}V_{DC}[2S_B - (S_A + S_C)] \\ v_c &= \frac{1}{3}V_{DC}[2S_C - (S_A + S_B)] \end{aligned} \tag{3.54}$$

where switching functions S_A, S_B, S_C take the value of 1 if the upper switch in the given leg is on and value of 0 if the lower switch in the given leg is on.

Table 3.2: Phase to neutral voltages.

Switching state	switches on	space vector	Phase voltage v_a	Phase voltage v_b	Phase voltage v_c
1	1,4,6	$\underline{v}_{1phase}$ (100)	$(2/3)V_{DC}$	$-(1/3)V_{DC}$	$-(1/3)V_{DC}$
2	1,3,6	$\underline{v}_{2phase}$ (110)	$(1/3)V_{DC}$	$(1/3)V_{DC}$	$-(2/3)V_{DC}$
3	2,3,6	$\underline{v}_{3phase}$ (010)	$-(1/3)V_{DC}$	$(2/3)V_{DC}$	$-(1/3)V_{DC}$
4	2,3,5	$\underline{v}_{4phase}$ (011)	$-(2/3)V_{DC}$	$(1/3)V_{DC}$	$(1/3)V_{DC}$
5	2,4,5	$\underline{v}_{5phase}$ (001)	$-(1/3)V_{DC}$	$-(1/3)V_{DC}$	$(2/3)V_{DC}$
6	1,4,5	$\underline{v}_{6phase}$ (101)	$(1/3)V_{DC}$	$-(2/3)V_{DC}$	$(1/3)V_{DC}$
7	1,3,5	$\underline{v}_{7phase}$ (111)	0	0	0
8	2,4,6	$\underline{v}_{8phase}$ (000)	0	0	0

3.5 Summary

The models of an induction machine, which will be used to simulate DTC of induction motor and investigate the effects of core loss on direct torque controlled induction motor drive operation, have been presented. The models in question are the constant parameter induction machine model with neglected iron loss, induction machine model with equivalent iron loss resistance placed in parallel to the magnetising branch of the equivalent circuit and the induction machine model with parallel equivalent iron loss resistance placed immediately after stator resistance. A model of voltage source inverter with constant DC input voltage and ideal semiconductor switches is also discussed. The next chapter will discuss the principles of vector control and direct torque control of induction machines.

CHAPTER 4

PRINCIPLES OF VECTOR CONTROL AND DIRECT TORQUE CONTROL

4.1 Introduction

Principles of vector control and direct torque control are discussed at first in this chapter in sections 4.2 and 4.3. Both stator flux oriented control and rotor flux oriented control are considered. The principles are developed using the standard machine model presented in section 3.2. Upon deliberation of principles of these two control methods, results of a comparative analysis of direct torque control and stator flux oriented control are given in section 4.4.

4.2 Principles of vector control

4.2.1 Rotor flux oriented vector control

In rotor flux oriented vector control, the angular speed of the reference frame is equal, at all times, to the angular speed of rotation of the rotor flux space vector ω_r^r, and *d*-axis of the reference frame, at all times, coincides with the rotor flux space vector [Vas (1990)]. Figure 4.1 illustrates the relative position of the reference frame and the rotor flux space vector. The stator transformation angle θ_s is now equal to the rotor flux space vector angular position ϕ_r. Because *d*-axis of the reference frame is fixed to the rotor flux space vector, the following relations hold true:

$$\theta_s = \phi_r, \quad \theta_r = \phi_r - \theta, \quad \omega_a = \omega_r^r, \quad \omega_r^r = d\phi_r / dt \tag{4.1}$$

and

$$\underline{\psi}_r = \psi_{dr} + j\psi_{qr} = \psi_r \quad \text{or} \quad \psi_{dr} = \psi_r, \quad \psi_{qr} = 0, \quad d\psi_{qr}/dt = 0 \tag{4.2}$$

Electromagnetic torque equation (3.30) now becomes:

$$T_e = \frac{3}{2} P \frac{L_m}{L_r} \mathrm{Im}\left(\underline{i}_s \underline{\psi}_r^*\right) = \frac{3}{2} P \frac{L_m}{L_r} \psi_r i_{qs} \tag{4.3}$$

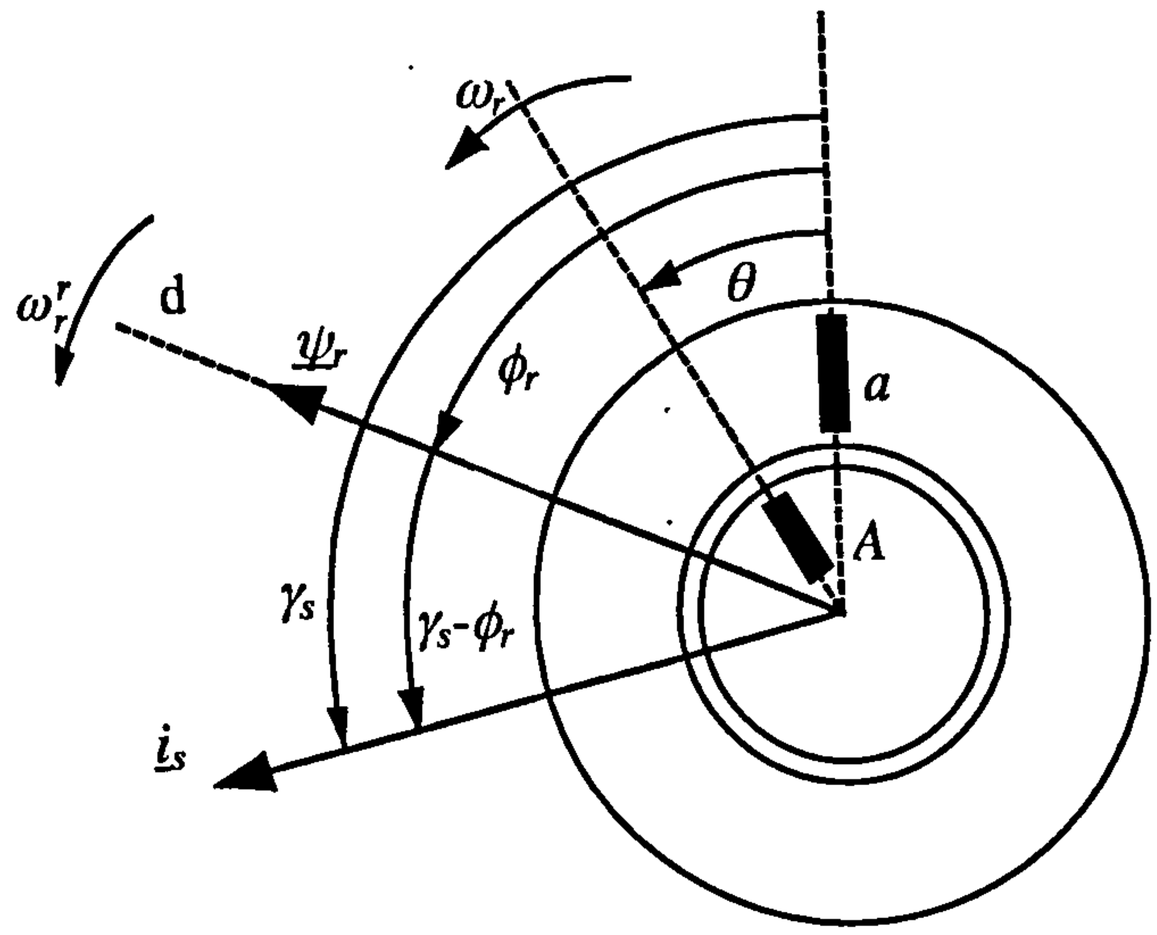

Figure 4.1: Space vectors in rotating reference frame fixed to the rotor flux space vector.

If it can be assumed that the induction machine is supplied from an ideal current source, stator currents are directly controlled variables and stator voltage equation in (3.27) can be omitted from further consideration. The induction motor is treated as a current-fed machine and this significantly simplifies the vector control system [Vas (1990)]. In practice, current-fed induction motor drive is obtained by controlling the voltage source inverter switching instants on the basis of motor phase current closed-loop control [Boldea and Nasar (1992), Vas (1990), Novotny and Lipo (1996), Kazmierkowski and Tunia (1994)]. Hysteresis current control is one possible method of stator phase current closed-loop control.

Substituting the equations (4.1)-(4.2) into the equation (3.27), the rotor voltage equation becomes:

$$0 = \frac{1}{T_r}\psi_r + \frac{d\psi_r}{dt} + j\left(\omega_r^r - \omega_r\right)\psi_r - \frac{1}{T_r}L_m\underline{i}_s \tag{4.4}$$

Rotor time constant is introduced as $T_r = L_r/R_r$. The equation (4.4) can be expressed in terms of *d-q* components as follows:

$$\begin{aligned}\psi_r + T_r\frac{d\psi_r}{dt} &= L_m i_{ds}\\ \left(\omega_r^r - \omega_r\right)\psi_r T_r &= L_m i_{qs}\end{aligned} \tag{4.5}$$

Angular slip frequency is defined as $\omega_{sl} = \omega_r^r - \omega_r$. The equations (4.3) and (4.5) fully describe a current-fed induction motor in the rotor flux oriented reference frame. Equation (4.5) shows that rotor flux can be controlled by stator *d*-axis current only. Because electromagnetic torque is proportional to rotor flux (equation (4.3)), if stator *d*-

axis current is constant, electromagnetic torque depends on stator q-axis current only. Rotor flux is therefore controllable by d-component of stator current and is constant if i_{ds} is constant. Torque is then controllable directly by q-component of stator current. Component of stator current i_{ds} plays the role equivalent to excitation current in a DC machine, while i_{qs} corresponds to armature current in a DC machine. The induction motor has therefore been converted into its DC machine equivalent in this rotating reference frame.

It is important to note that decoupled rotor flux and torque control, described by (4.3) and (4.5), are obtained only if the motor can be regarded as being fed from a current source. If the machine can not be considered as being current-fed, it becomes necessary to take into account the stator voltage equation as well. The control scheme becomes significantly more complicated as correlation between stator d-q axis voltages and currents has to be taken into account. For the reasons to be explained in section 4.4, only current-fed induction machine is discussed here.

4.2.2 Stator flux oriented vector control

Vector control of induction machine can be carried out with orientation along one of the three flux space vectors, stator flux space vector, magnetising flux space vector and rotor flux space vector. When the reference frame is fixed to stator flux space vector, stator flux oriented control of an induction machine results [Vas (1990), Novotny and Lipo (1996)]. The angular rotating speed of the reference frame is now equal to the angular rotating speed of the stator flux space vector, ω_s, and the d-axis of the reference frame coincides with stator flux space vector.

The principles of stator flux oriented control can be again derived using the equations of the constant parameter ideal machine model in an arbitrary rotating reference frame (equations (3.27) and (3.28)). The equations for angular positions and angular speed are the following:

$$\theta_s = \phi_s, \quad \theta_r = \phi_s - \theta, \quad \omega_a = \omega_s, \quad \omega_s = d\phi_s/dt \tag{4.6}$$

And

$$\underline{\psi}_s = \psi_{ds} + j\psi_{qs} = \psi_s \quad \text{or} \quad \psi_{ds} = \psi_s, \quad \psi_{qs} = 0, \quad d\psi_{qs}/dt = 0 \tag{4.7}$$

The equations for rotor current and rotor flux space vector are:

$$\underline{i}_r = \frac{1}{L_m}\left(\psi_s - L_s \underline{i}_s\right) \tag{4.8}$$

$$\underline{\psi}_r = \frac{L_r}{L_m}\left(\psi_s - L_s \underline{i}_s\right) + L_m \underline{i}_s \tag{4.9}$$

The rotor voltage equation in (3.27) can now be expressed, using (4.8) and (4.9), as

$$0 = R_r\left(\frac{\psi_s}{L_m} - \frac{L_s}{L_m}\underline{i}_s\right) + \frac{L_r}{L_m}\frac{d\psi_s}{dt} - \frac{L_s L_r}{L_m}\frac{d\underline{i}_s}{dt} + L_m\frac{d\underline{i}_s}{dt} + j\omega_{sl}\left[\frac{L_r}{L_m}\left(\psi_s - L_s\underline{i}_s\right) + L_m\underline{i}_s\right] \tag{4.10}$$

The definition of slip angular frequency is now $\omega_{sl} = \omega_s - \omega_r$. The relative positions of the space vectors are shown in figure 4.2.

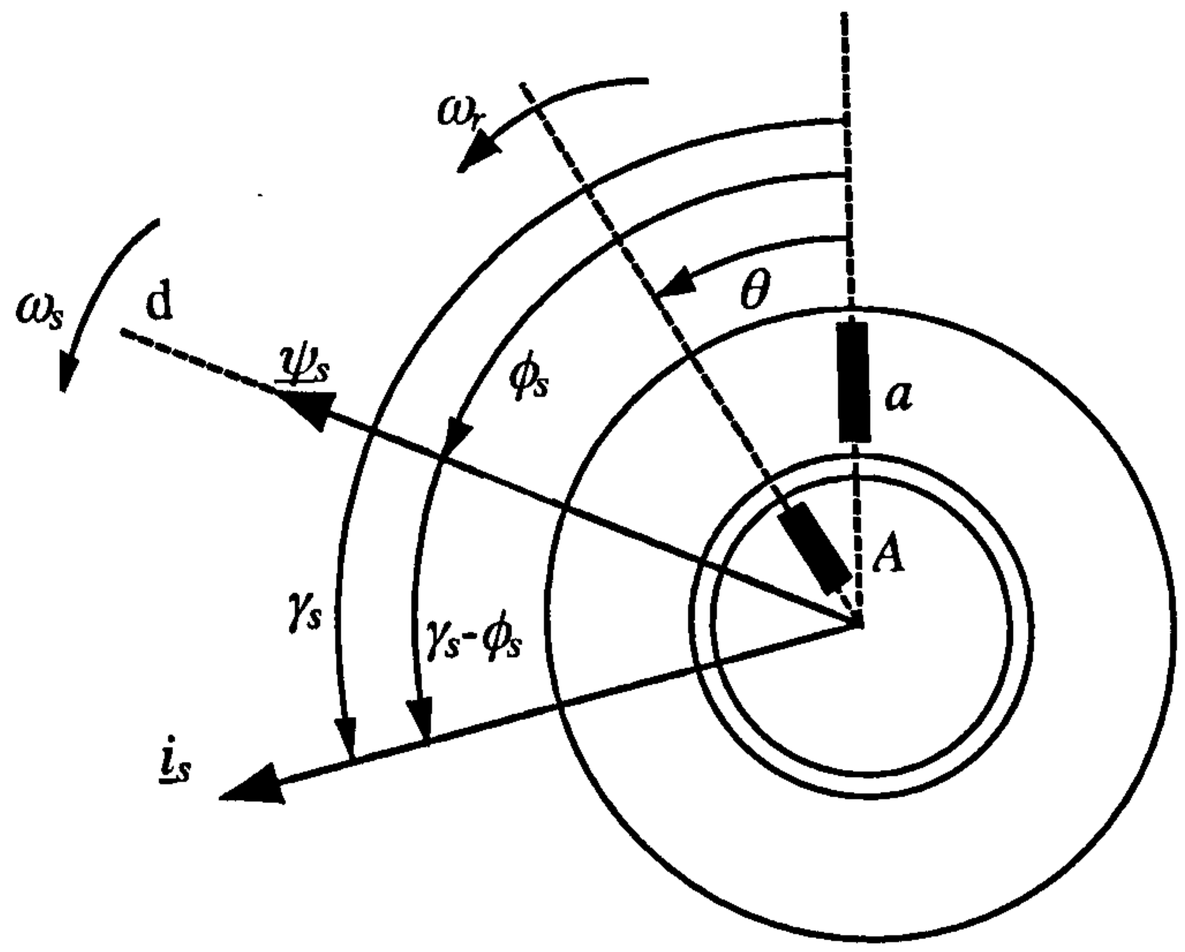

Figure 4.2: Space vectors in rotating reference frame fixed to the stator flux space vector.

The equation for electromagnetic torque (3.30) reduces to:

$$T_e = (3/2)P\psi_s i_{qs} \tag{4.11}$$

Stator voltage equation can again be omitted because of the assumption of ideal current feeding. The rotor voltage equation (4.10) is clearly more complicated than the one in rotor flux oriented reference frame. Therefore, practical implementation of stator flux oriented control will be more computationally demanding. This is the main reason why stator flux oriented vector control is less frequently used in industrial applications.

Rotor voltage equations in terms of *d-q* components result from (4.10):

$$\begin{aligned} \psi_s + T_r\frac{d\psi_s}{dt} &= L_s i_{ds} + \left(L_s T_r - \frac{L_m^2}{R_r}\right)\left(\frac{di_{ds}}{dt} - \omega_{sl} i_{qs}\right) \\ L_s i_{qs} &= \omega_{sl} T_r \psi_s - \left(L_s T_r - \frac{L_m^2}{R_r}\right)\left(\frac{di_{qs}}{dt} - \omega_{sl} i_{ds}\right) \end{aligned} \tag{4.12}$$

Equations (4.12) show that there exists a coupling between the torque producing stator current component i_{qs} and the stator flux producing current component i_{ds} in this reference frame. In order to eliminate the cross-coupling between these two current components, a decoupling circuit has to be used. If the leakage coefficient is introduced as $\sigma = 1 - L_m^2/(L_s L_r)$, the equations (4.12) can be expressed as.

$$\begin{aligned} \psi_s + T_r \frac{d\psi_s}{dt} &= L_s\left(i_{ds} + \sigma T_r \frac{di_{ds}}{dt}\right) - \sigma L_s T_r \omega_{sl} i_{qs} \\ i_{qs} + \sigma T_r \frac{di_{qs}}{dt} &= \omega_{sl} \frac{T_r}{L_s}\left(\psi_s - \sigma L_s i_{qs}\right) \end{aligned} \tag{4.13}$$

4.2.3 Indirect and direct vector control schemes

There are basically two different types of vector control, direct and indirect control. The direct schemes are based on estimation of the rotor flux or stator flux vector amplitude and position, using measured electromagnetic quantities, such as stator currents and stator voltages. The indirect methods use machine model in the feed-forward manner and perform calculations on the basis of references. The indirect methods are highly sensitive to variation of machine parameters. Most of the industrial vector drives utilise indirect rotor flux oriented schemes, since they require relatively simpler hardware and software.

4.2.3.1 Indirect feed-forward rotor flux oriented control

Depending on whether the drive is operated in the speed mode or the torque mode, the input into the control system will be, apart from the flux reference, either speed reference or torque reference, respectively. Torque mode is discussed here, since this mode of operation will be encompassed by the comparative study in section 4.4. In indirect rotor flux oriented control scheme the equations (4.3) and (4.5) are used to build the controller. Taking as independent inputs reference rotor flux and reference torque (ψ_r^* and T_e^*) one has from (4.3) and (4.5)

$$\begin{aligned} i_{qs}^* &= T_e^* \Big/ \left(\frac{3}{2} P \frac{L_m}{L_r} \psi_r^*\right) \\ i_{ds}^* &= \frac{1}{L_m}\left(\psi_r^* + T_r \frac{d\psi_r^*}{dt}\right) \end{aligned} \tag{4.14}$$

$$\omega_{se}^{*} = \frac{L_m i_{qs}^{*}}{T_r \psi_r^{*}}$$

If the drive is aimed at operation in the base speed region, rotor flux reference is kept at constant rated value and stator *d*-axis reference is equal to

$$i_{ds}^{*} = \psi_r^{*} / L_m \tag{4.15}$$

The instantaneous rotor flux space vector position is obtained using measured rotor speed (or position) according to

$$\phi_r = \int \omega_r^{r^{*}} dt = \int \left(\omega_{sl}^{*} + \omega_r\right) dt \tag{4.16}$$

The control scheme of indirect feed-forward rotor flux oriented control is shown in figure 4.3. As already noted, it is assumed that the drive operates in the base speed region only, so that rotor flux reference is constant and equal to rated rotor flux value. Figure 4.3 applies to torque mode of operation.

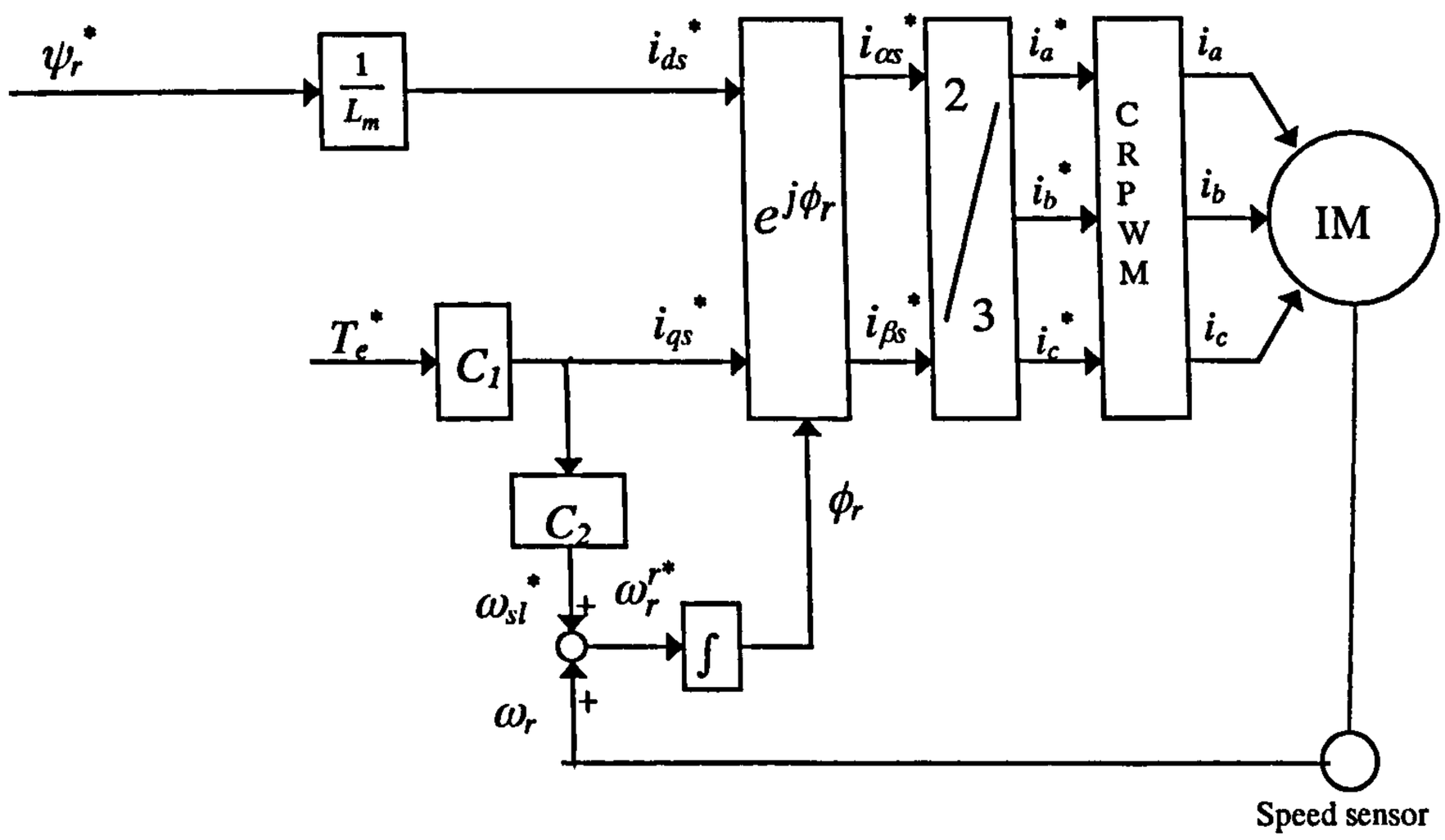

$$C_1 = \left(\frac{3}{2} P \frac{L_m}{L_r} \psi_r^{*}\right)^{-1} \qquad C_2 = \frac{L_m}{T_r \psi_r^{*}}$$

Figure 4.3: Indirect feed-forward rotor flux oriented vector control of an induction machine (CRPWM: Current regulated pulse width modulated inverter).

The induction machine is assumed to be current-fed using an ideal current regulated PWM inverter. Hence $i_a^{*} = i_a, i_b^{*} = i_b, i_c^{*} = i_c$. The two *d-q* axis current references are transformed into phase stator current references in the stationary

reference frame. The phase stator current references can be obtained using (3.22), with instantaneous rotor flux space vector position of (4.16) as the transformation angle.

4.2.3.2 Indirect feed forward stator flux oriented control

From the equations in (4.11) and (4.13), the reference values of *d*-component and *q*-component of stator current and the reference value of angular slip frequency can be expressed as follows:

$$
\begin{aligned}
i_{qs}^{*} &= \frac{T_e^{*}}{\left(\frac{3}{2}P\right)\psi_s^{*}} \\
i_{ds}^{*} &= \frac{1}{1+p\sigma T_r}\left[(1+pT_r)\frac{\psi_s^{*}}{L_s} + \sigma T_r \omega_{sl}^{*} i_{qs}^{*}\right] \\
\omega_{sl}^{*} &= \frac{(1+p\sigma T_r) i_{qs}^{*}}{\psi_s^{*} T_r / L_s - \sigma T_r i_{ds}^{*}}
\end{aligned}
\tag{4.17}
$$

where $p=d/dt$, and the asterisk denotes once more reference quantities.

The equations (4.17) define the indirect stator flux oriented controller and the required decoupling circuit. Thus, when the correct machine parameters are used in these equations, the correct value of i_{ds}^{*} is obtained for a given value of i_{qs}^{*}, and stator flux ψ_s is not altered by any changes in the torque current reference.

For operation in the base speed region, stator flux reference is kept at constant rated value. Hence from (4.17)

$$
\begin{aligned}
i_{qs}^{*} &= \frac{T_e^{*}}{(3/2)P\psi_s^{*}} \\
i_{ds}^{*} &= \frac{1}{1+p\sigma T_r}\left(\frac{\psi_s^{*}}{L_s} + \sigma T_r \omega_{se}^{*} i_{qs}^{*}\right) \\
\omega_{se}^{*} &= \frac{(1+p\sigma T_r) i_{qs}^{*}}{\psi_s^{*}(T_r/L_s) - \sigma T_r i_{ds}^{*}}
\end{aligned}
\tag{4.17a}
$$

The instantaneous position of the stator flux space vector, required for co-ordinate transformation, is obtained using reference angular slip frequency and the measured rotor speed (or position),

$$\phi_s = \int \omega_s^{*} dt = \int (\omega_{sl}^{*} + \omega) dt \tag{4.18}$$

and stator phase current references are again created by means of (3.22).

Figure 4.4 shows schematic of an indirect stator flux oriented induction machine, supplied by a current-regulated pulse width modulation (CRPWM) inverter [Späth (1983)]. The blocks "$e^{j\phi_s}$" and "2/3" describe again inverse co-ordinate transformation, given in (3.22), as a two-step transformation.

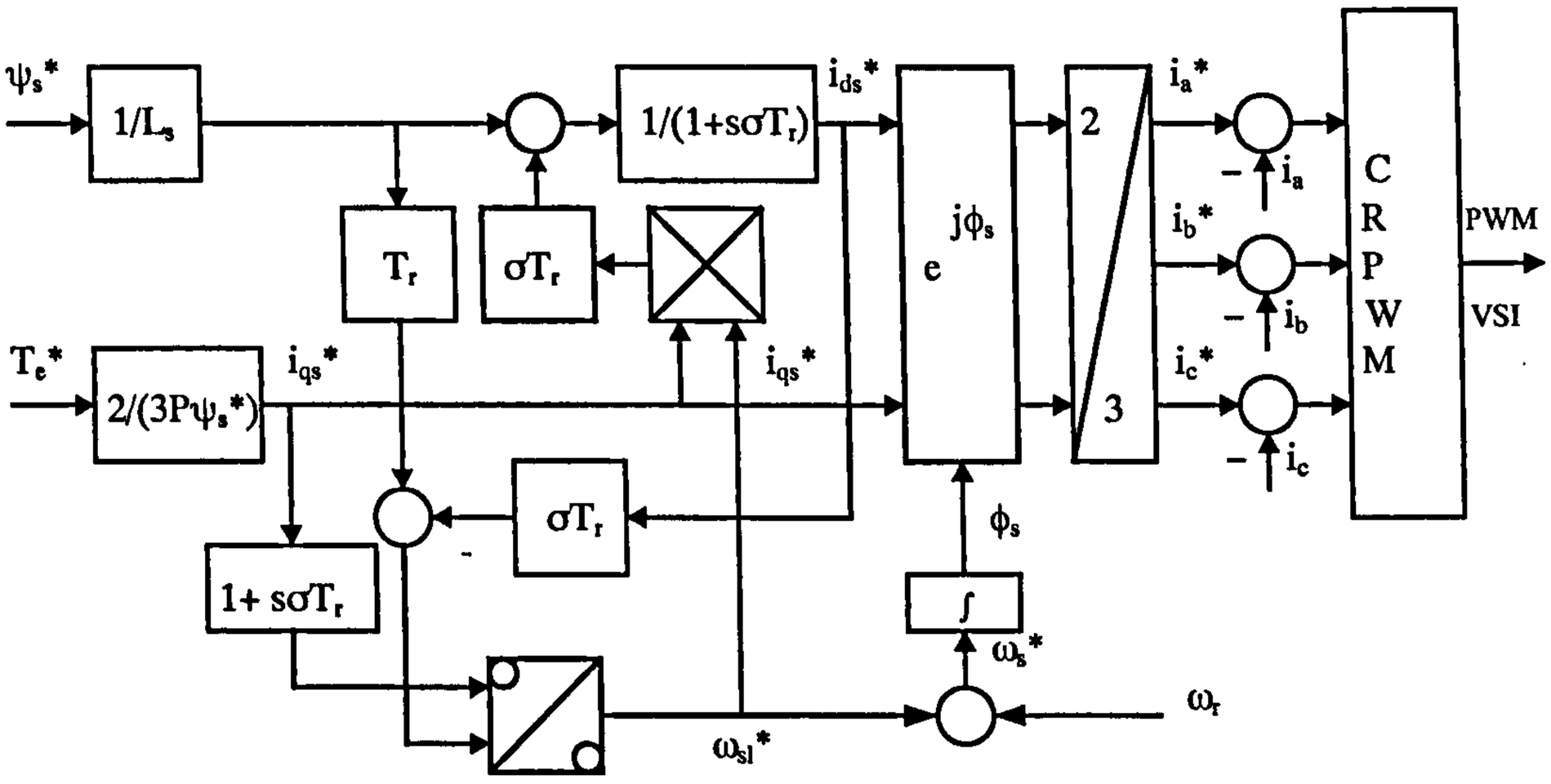

Figure 4.4: Indirect stator flux oriented control scheme with feed-forward decoupling circuit.

4.2.3.3 Direct feedback vector control

In direct vector control, the relevant flux space vector position is estimated directly from measured quantities. Figure 4.5 shows the schematic of the drive with a current-fed induction machine employing direct vector control.

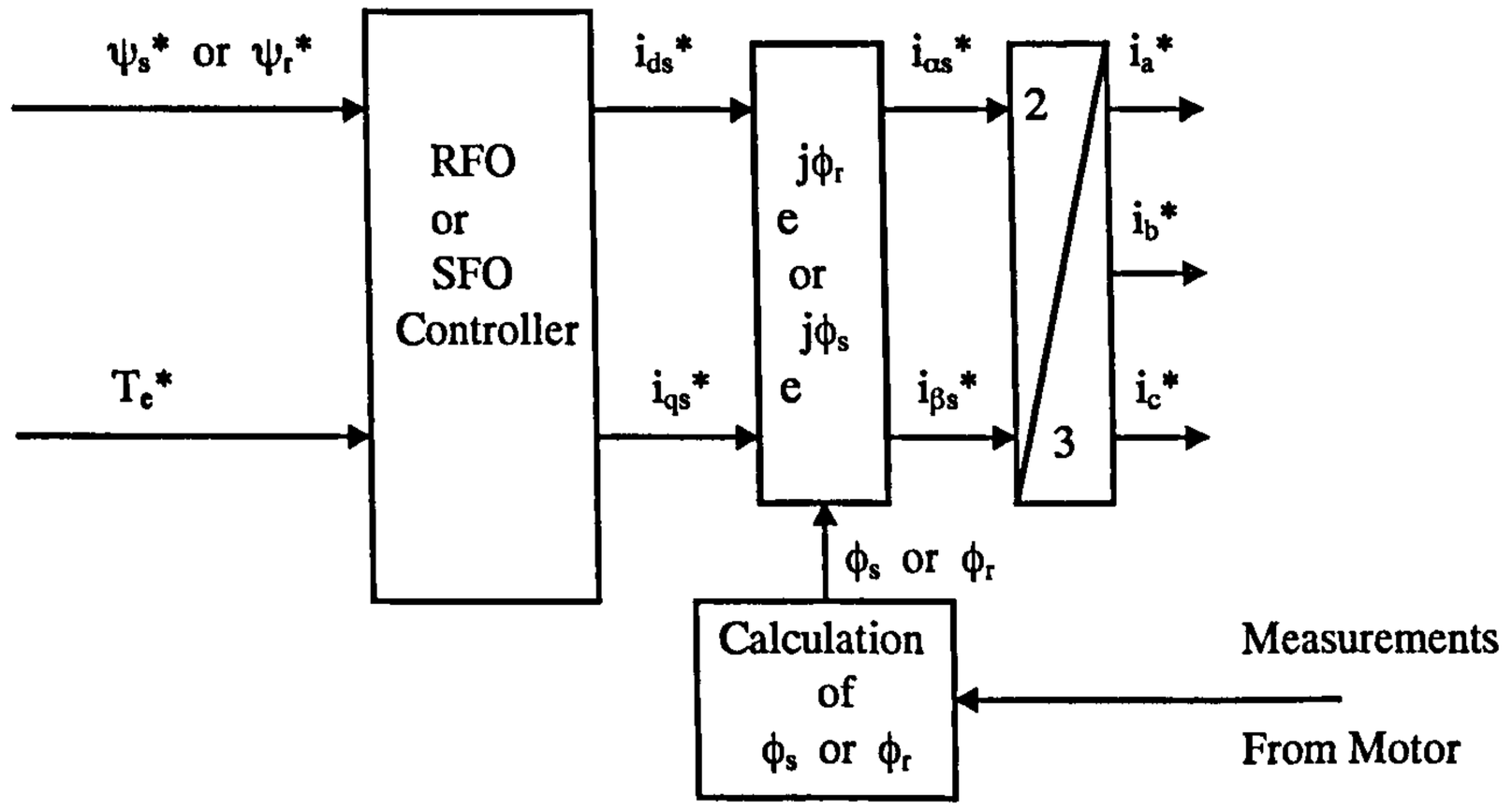

Figure 4.5: Direct feedback vector control scheme.

Configuration of RFO or SFO controller in figure 4.5 can take different forms, depending on how the drive is realised. In its simplest form it may encompass the

relevant parts of figures 4.3 and 4.4, respectively. Alternatively, it may contain flux and torque controller as well, in which case these two variables have to be estimated along with the flux space vector position. Decoupling circuit for SFOC may operate on the basis of reference stator d-q current components or on the basis of measured (and transformed) stator currents.

In the drive scheme of figure 4.5, the relevant flux space vector can be estimated in a number of ways. One particularly relevant method of flux position estimation is based on measured stator currents and measured (or reconstructed) stator voltages.

From the equations (3.23) and (3.17)-(3.18) of the machine model, the estimation of both stator flux position and rotor flux position can be carried out by using the following equations:

$$\psi_{\alpha s} = \int (v_{\alpha s} - R_s i_{\alpha s})dt$$
$$\psi_{\beta s} = \int (v_{\beta s} - R_s i_{\beta s})dt \qquad (4.19)$$
$$\psi_s = \sqrt{\psi_{\alpha s}^2 + \psi_{\beta s}^2} \qquad \cos\phi_s = \psi_{\alpha s}/\psi_s \qquad \sin\phi_s = \psi_{\beta s}/\psi$$

$$\psi_{\alpha r} = (1+\sigma_r)\psi_{\alpha s} - \sigma\frac{L_s L_r}{L_m} i_{\alpha s}$$
$$\psi_{\beta r} = (1+\sigma_r)\psi_{\beta s} - \sigma\frac{L_s L_r}{L_m} i_{\beta s} \qquad (4.20)$$
$$\psi_r = \sqrt{\psi_{\alpha r}^2 + \psi_{\beta r}^2} \qquad \cos\varphi_r = \psi_{\alpha r}/\psi_r \qquad \sin\varphi_r = \psi_{\beta r}/\psi_r$$

where $\sigma_r = L_{\sigma r}/L_m$.

The electromagnetic torque can in both cases be calculated as.

$$T_e = \frac{3}{2} P(\psi_{\alpha s} i_{\beta s} - \psi_{\beta s} i_{\alpha s}) \qquad (4.21)$$

The main difference between direct and indirect field orientation is the method used to calculate relevant flux spatial position. In the indirect scheme, this calculation does not require measurement of electromagnetic quantities. Only speed (or position) measurement is required for orientation purposes. In the direct schemes, flux angle estimation requires measurement of electromagnetic variables such as stator currents and voltages. Apart from the scheme based on stator voltage and current measurement, another frequently employed method in rotor flux oriented control relies on stator current and rotor speed (position) measurement.

4.3 Principles of direct torque control

4.3.1 Torque production in a direct torque controlled drive

In a direct torque controlled induction motor drive, supplied by a voltage source inverter, it is possible to control directly the stator flux linkage and the electromagnetic torque by the selection of the optimum stator voltage space vectors in the inverter. The selection of the most appropriate voltage vector is done in such a way that the flux and torque errors are restricted within respective flux and torque hysteresis bands, fast torque response is obtained, and the inverter switching frequency is kept at as low as possible level.

In the case of rotor flux oriented control of an induction motor, the electromagnetic torque developed by the motor is described with

$$T_e = (3/2)P(L_m/L_r)\psi_r i_{qs} \tag{4.3}$$

where stator q-axis current is the imaginary component of the stator current space vector in the co-ordinate system fixed to the rotor flux space vector, as shown figure 4.6a.

Torque equation (4.3) can be written in terms of the amplitude and phase of the stator current space vector with respect to the d-axis of the reference frame as

$$T_e = K\psi_r|\underline{i}_s|\sin\lambda \tag{4.22}$$

Instantaneous change of the torque requires, according to (4.22) change in the amplitude and phase of the stator current space vector, such that d-axis current component remains the same (so that rotor flux is constant) while the torque is stepped to the new appropriate value by the change in stator q-axis current component.

An alternative expression for the torque utilises stator flux space vector and stator current space vector. Regardless of the applied method of control, torque developed by the motor can be written as

$$T_e = \frac{3}{2}P|\underline{\psi}_s||\underline{i}_s|\sin\alpha \tag{4.23}$$

where angle α is the instantaneous value of the angle between the stator current and stator flux space vectors. Figure 4.6b shows the stator current space vector and stator flux space vector's relative positions.

It can be shown [Vas (1998)] that at certain rotor speed, if the amplitude of stator flux is kept constant, electromagnetic torque can be changed rapidly by changing

rapidly its instantaneous position, so that angle α in (4.23) is rapidly changed. In other words, if such stator voltages are imposed on the motor, which keep the stator flux constant (at the set value), but which quickly rotate the stator flux space vector into the required position (determined by the torque command), then fast torque control is obtained. It follows that if in the direct torque control (DTC) drive the developed torque is smaller than the reference, the torque should be increased by using maximum possible rate of change of the stator flux space vector position ϕ_s. If the stator flux space vector is accelerated in the forward direction, an increase in torque is produced. When it is decelerated backwards, a decrease in torque results. The stator flux space vector can be adjusted by using the appropriate stator voltage space vectors, obtainable from the VSI operated in the PWM mode. Thus there is direct stator flux and torque control achieved by means of the voltage source - hence the name direct torque control. Another form of the torque equation (figure 4.7) is the one given in terms of stator and rotor flux,

$$T_e = \frac{3}{2} P \frac{L_m}{\sigma L_s L_r} |\underline{\psi}_r| |\underline{\psi}_s| \sin \varepsilon \tag{4.24}$$

where ε is the angle between stator flux and rotor flux space vectors.

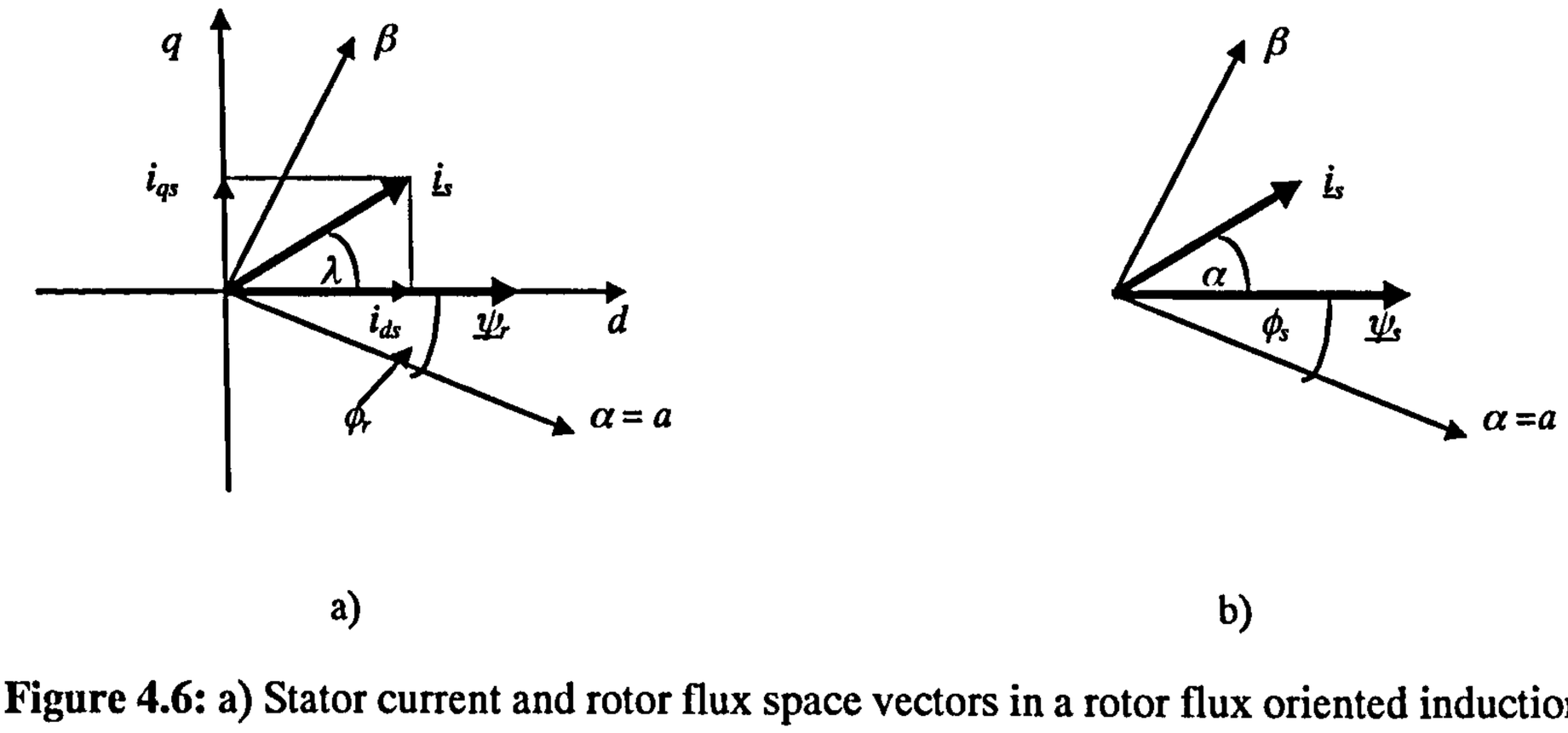

a) b)

Figure 4.6: a) Stator current and rotor flux space vectors in a rotor flux oriented induction machine, b) stator current and stator flux's relative position in an induction machine.

Rotor flux changes slowly because its rate of change depends on a relatively large rotor time constant. Therefore, it can be assumed to be constant in a short period of time. The stator flux amplitude is also kept constant in the DTC control scheme, hence both the vectors in the equation (4.24) have constant amplitudes. Rapid change of

torque can be obtained if instantaneous position of stator flux space vector is change quickly, so that ε is quickly varied. This is the essence of DTC. The instantaneous change of ε can be obtained by switching on appropriate stator voltage space vector of the VSI.

If stator resistance voltage drop is neglected, the stator voltage equation in stationary reference frame is from (3.27)

$$\underline{v}_s = d\underline{\psi}_s / dt \tag{4.25}$$

Hence the applied stator voltage directly impresses stator flux. If the voltage abruptly changes, then stator flux will change accordingly to satisfy the equation (4.25). The variation of stator flux during a short period of time when the stator voltage is changed is $\Delta\underline{\psi}_s = \underline{v}_s \Delta t$. This shows that the stator flux space vector moves in the direction of the applied stator voltage space vector during this period. By selecting appropriate stator voltage space vectors in subsequent time intervals, it is then possible to change the stator flux in the desired way. Decoupled control of the stator flux and torque is achieved by acting on radial and tangential components of the stator flux space vector. These two components are directly proportional to the components of the stator voltage space vector in the same directions.

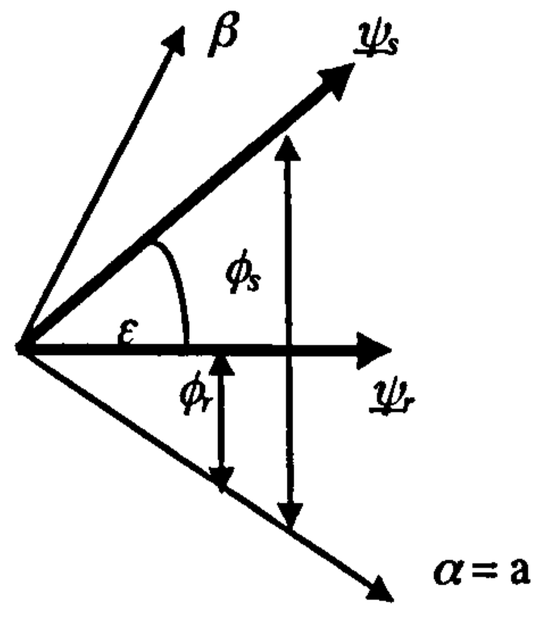

Figure 4.7: Relative positions of stator flux and rotor flux space vectors.

The angle ε between stator and rotor flux space vectors is important in torque production. Assume that the rotor flux space vector is travelling at a given speed, at certain point in the steady-state operation (this speed is initially equal to the average one of the stator flux space vector). The induction motor is accelerated. Appropriate stator

voltage vector is applied to increase torque, and quick rotation of stator flux space vector happens. Rotor flux space vector amplitude, however, does not change appreciably, because of the significant rotor time constant. Rotor flux space vector's speed of rotation is not changed abruptly either (recall that speed of rotation of this vector can be given in terms of rotor flux components and their derivatives; if rotor flux components do not change due to the large time constant, the angular speed of rotor flux space vector does not change either). This will result in an increase of ε to increase the motor's torque. If deceleration is required, an appropriate voltage vector will be applied to reduce the angle ε and therefore the torque developed by the motor. The application of zero voltage vectors will almost stop the rotation of the stator flux space vector. If the angle ε becomes negative, torque will change sign and braking process takes place.

4.3.2 Basic control scheme of direct torque controlled induction motor

Since $\Delta\underline{\psi}_s = \underline{v}_s \Delta t$, then stator flux space vector will move fast if non-zero voltage vectors are applied to the motor. It will almost stop if zero voltage vectors are applied. In DTC drives, at every sampling period, stator voltage vectors are selected on the basis of keeping the stator flux amplitude error and torque error within the prescribed hysteresis bands. The size of the hysteresis bands will significantly affect the inverter switching frequency. In general, the larger the hysteresis band, the lower the switching frequency and the poorer the response of the drive to change in reference. As the stator flux space vector is the integral of the stator voltage vector, then it will move in the direction of the stator voltage space vector for as long as this voltage vector is applied to the motor.

Basic control schemes of a DTC induction motor drive are shown in figure 4.8 and figure 4.9, for torque mode and speed mode of operation, respectively. In each figure, there are two parallel branches, one for stator flux amplitude and the other for the torque control. Torque reference is either an independent input (for a torque-controlled drive, figure 4.8) or the output of the speed controller (in a speed-controlled drive, figure 4.9). Both the stator flux and the torque controllers are of hysteresis type. The drive requires appropriate measurements that will enable estimation of stator flux and torque for closed loop control of these two quantities. Stator currents and measured or reconstructed stator voltage are used for the estimation, as given by (4.19) and (4.21).

Additionally, an estimate of the speed of rotation is required for closed loop speed control in sensorless DTC drive. Note that the DTC induction motor drive inherently lends itself to sensorless operation, since no co-ordinate transformation is involved and speed signal is only needed for closing the speed loop.

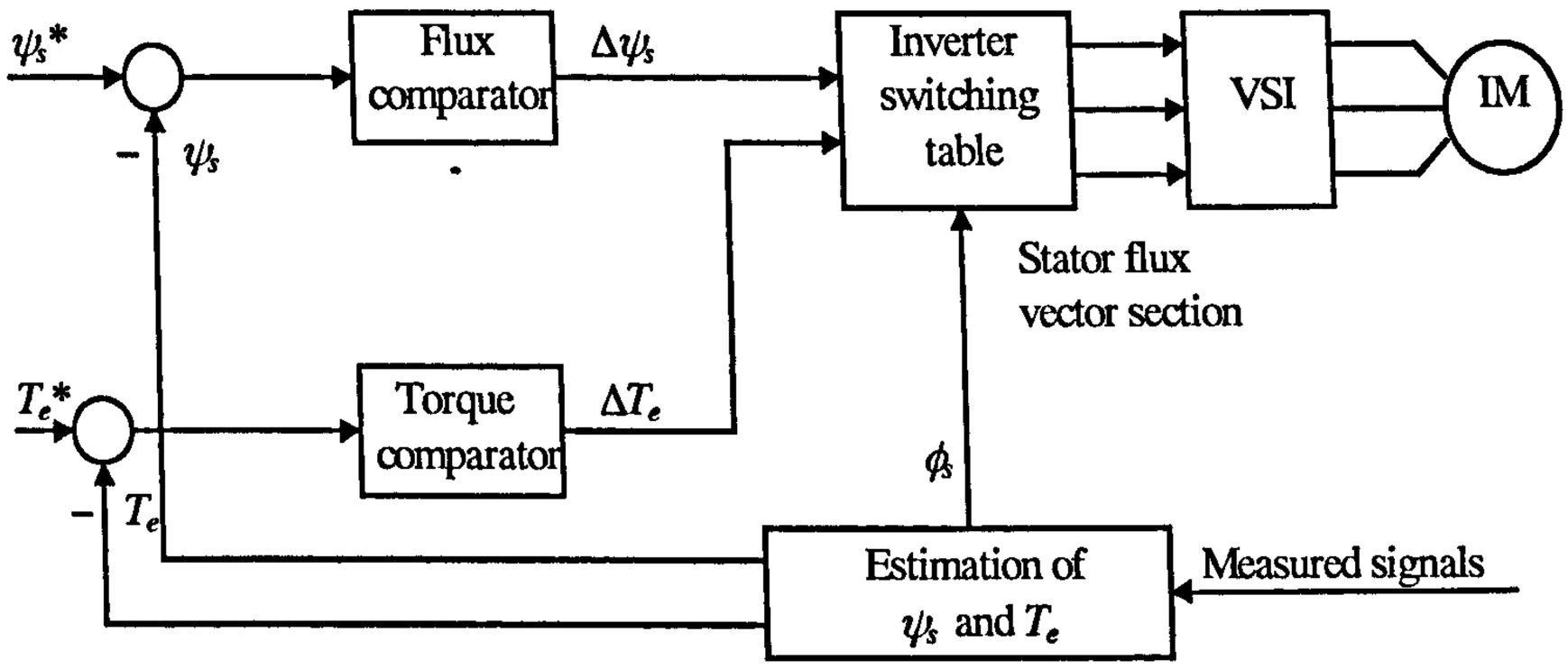

Figure 4.8: Control scheme of a DTC induction motor drive for torque mode of operation.

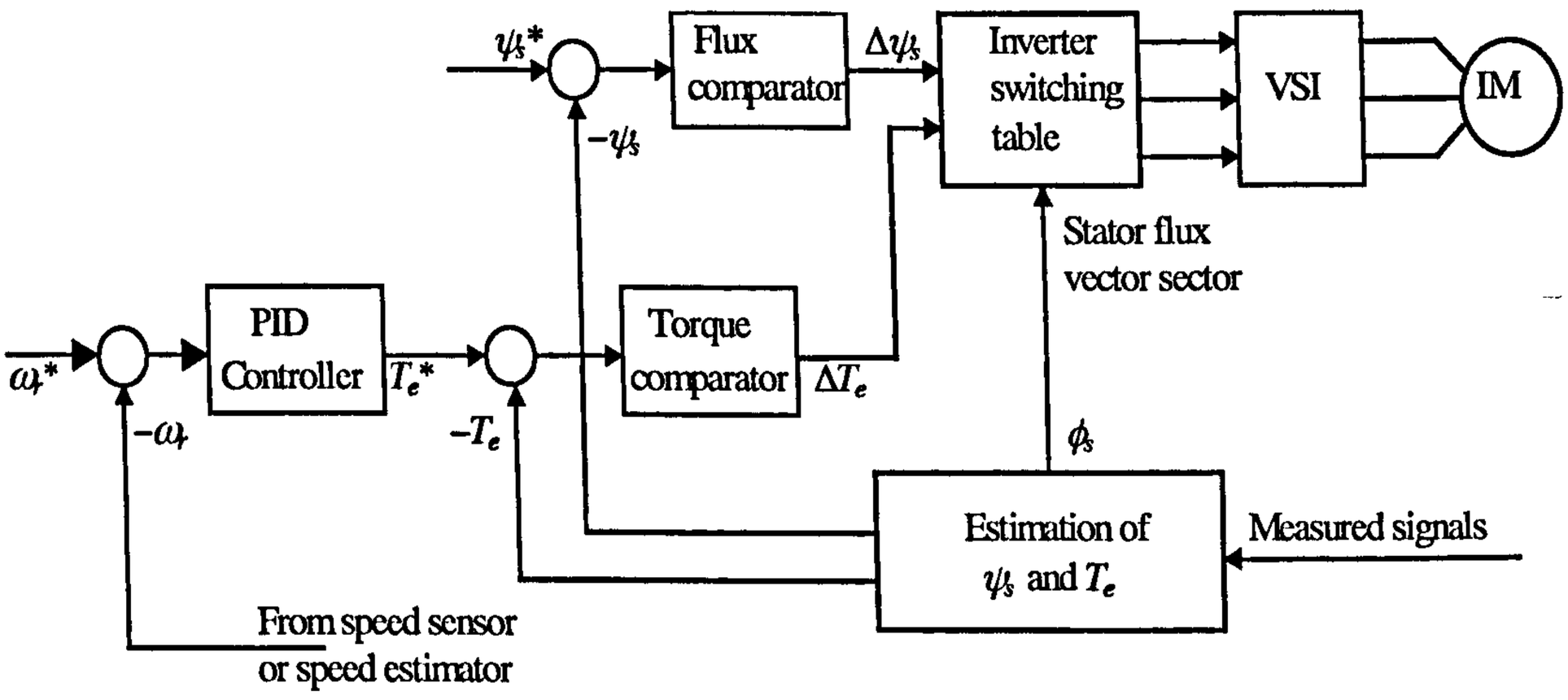

Figure 4.9: Control scheme of DTC induction motor drive for speed mode of operation with or without speed sensor.

4.3.3 Inverter switching table

A number of methods for selection of optimum voltage space vectors for DTC have already been mentioned, for example [Takahashi and Noguchi (1986), Chen and Li (1999), Kang and Sul (1999), Alfonso et al (1999), Casadei et al (1994 and 1998a)]. However, this subsection only discusses the classical one originally suggested by

[Takahashi and Noguchi (1986)]. Further work related to various inverter switching tables is described in chapter 5. Space vectors of inverter output phase voltages are shown again in figure 4.10 for the convenience of explanation. Additionally, sections of the plane, identified with Roman numbers I to VI, are included as well. The sectors are all of sixty degrees, and they are distributed $\pm 30°$ around the corresponding voltage space vector. If the stator flux space vector lies in the *k-th* sector, where $k = 1,2,3,4,5,6$, its magnitude can be increased by using the voltage vectors *k, k+1, k-1*. Its magnitude can be decreased by using *k+2, k-2* and *k+3* vectors. In other words, stator flux will be increased if either the voltage vector belonging to the sector or any of the two adjacent voltage vectors are applied. It will be decreased if the remaining three active voltage vectors are applied. Vectors *k+1* and *k+2* are called active forward voltage vectors, vectors *k-1* and *k-2* are called active backward voltage vectors.

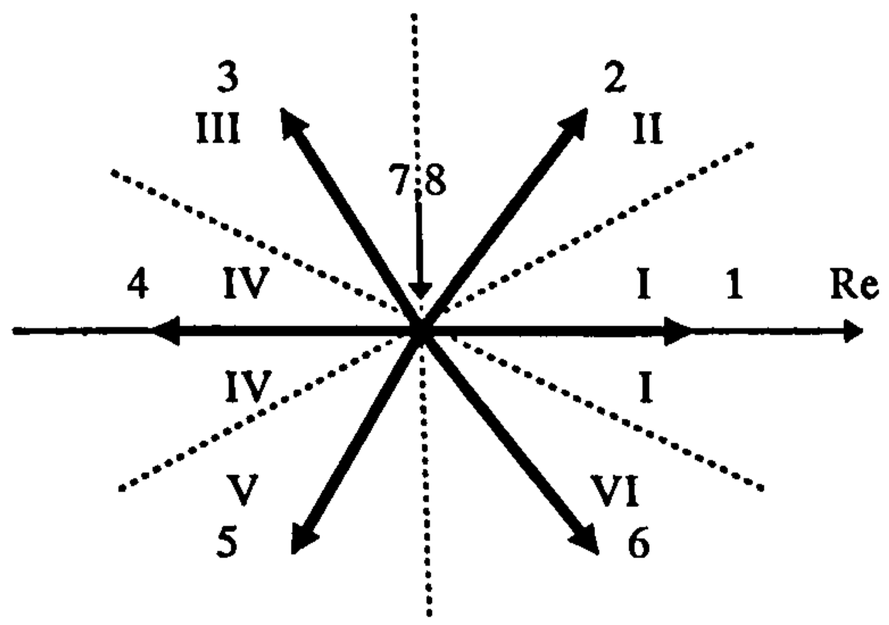

Figure 4.10: Phase voltage space vectors and appropriate sectors.

The selected voltage vector, however, will also affect the torque production of the induction motor. Additionally, switching frequency will be affected as well. The idea is to keep always the switching frequency as low as possible, so that the most appropriate voltage space vector is the one that requires the minimum number of switchings and simultaneously drives both the stator flux and the torque errors in the desired direction. From table 3.2, where inverter switching states are defined as a set of binary signals for each of the six possible non-zero space vectors, one sees that progressing from state one towards state six requires only switching in one of three inverter legs. Hence, if the inverter operates with vector whose state is 100, then the most appropriate subsequent vectors are 110, 101 and 000 (zero vector number 8) as these vectors require switching in a single inverter leg. Minimum switching frequency is

achieved in this way. Which of the three possible vectors will be applied depends on the flux and torque errors.

An illustration of the switching process is given in figure 4.11. Operation in the base speed region is assumed, so that the stator flux reference is constant and equal to the rated stator flux. A deviation by hysteresis band equal to $\pm\Delta\psi_s$ is allowed for the actual flux with respect to the reference. It is assumed that in certain time instant stator flux is in the first sector and has just reached the outer boundary of the allowed deviation (point A). Inverter switching state therefore has to be changed, since stator flux must be reduced. Direction of rotation is anticlockwise. As stator flux is in sector one, then application of voltage vectors 1, 2 and 6 would further increase the flux. Reduction in flux can be obtained using vectors 3, 4 and 5. Out of these three, vector 3 is the only one that asks for switching in only one of the inverter legs. Vector 3 is therefore applied, and it drives stator flux towards point B, where stator flux again reaches upper hysteresis band. As stator flux is now in sector 2, and it again needs to be reduced, possible voltage vectors that will lead to reduction in the stator flux are vectors 4, 5 and 6. Vector 4 is the only one that asks for switching in a single inverter leg. Voltage vector 4 is therefore applied, and it drives stator flux towards lower boundary of the allowed deviation (point C). In point C stator flux is still in the second sector and it needs to be increased. An increase can be obtained using vectors 1, 2 and 3. As vector 3 asks for a single switching, this vector will be applied again. The process continues as time goes by.

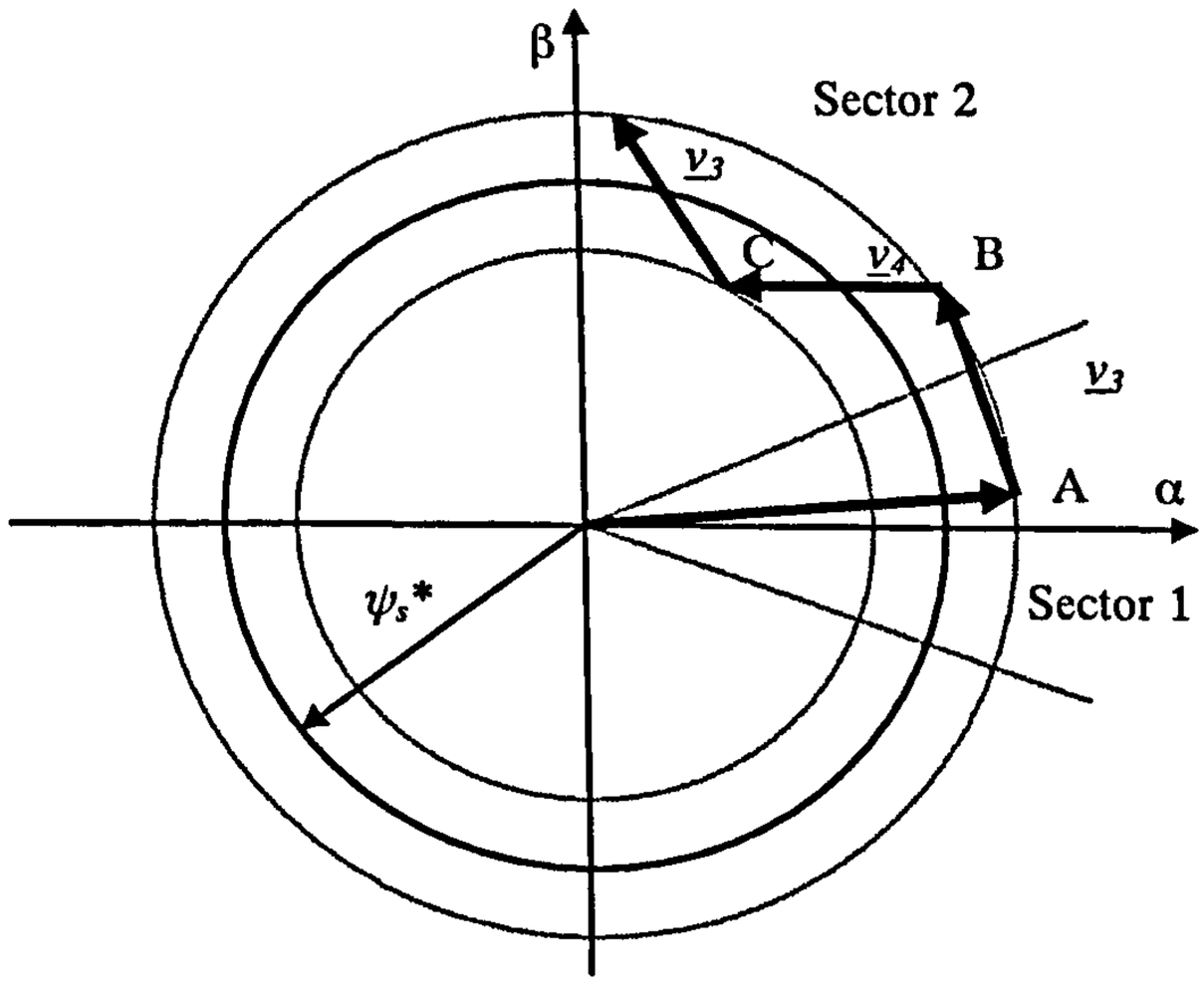

Figure 4.11: Control of stator flux space vector by means of appropriate voltage vector application [Vas (1998)].

Previous consideration did not take into account the impact of torque error on the selection of the switching state. Stopping the rotation of the stator flux space vector corresponds to the case when the torque does not have to be changed (actual value of the torque is within prescribed hysteresis bands). However, when the torque has to be changed (in the clockwise or anticlockwise direction corresponding to negative or positive torque variation), then the stator flux space vector has to be rotated in an appropriate direction. In general, if an increase in torque is required, then the torque is controlled by applying voltage vectors that advance the stator flux space vector in the direction of rotation. If a decrease is required, voltage vectors are applied which oppose the direction of rotation of stator flux space vector. If zero change in torque is required then zero vectors are applied. It follows that the angle of stator flux space vector is controlled indirectly through the flux amplitude and torque control. Torque demands are reduced to choices of increase, decrease or zero. Similarly, the stator flux amplitude control is limited to the choice of increase and decrease. Figure 4.12 illustrates selection of the optimum voltage vector as function of the required change in flux and torque. The situation is shown for anticlockwise direction of rotation of stator flux space vector and for the initial position of the stator flux space vector in the first two sectors. Similar figures can be constructed for other sectors.

The result of these considerations can be represented in a form of table, called optimum voltage vector selection table (table 4.1) or inverter switching table. This gives the optimum selection of the voltage vectors for all the possible stator flux space vector positions (in terms of sectors) and the desired control inputs, which are the output of the torque and flux hysteresis comparator, respectively. The outputs will give commands of increase or decrease for torque and stator flux in order to keep both of them within the respective hysteresis band. If a stator flux increase is required then $\Delta\psi_s = 1$, if a stator flux decrease is required then $\Delta\psi_s = 0$. This notation corresponds to the fact that the digital output signals of a two-level flux hysteresis comparator are

$$\begin{aligned} &\Delta\psi_s = 1 \quad \text{if} \quad |\underline{\psi}_s| \le |\underline{\psi}_s{}^*| - |\text{hysteresis band}| \\ &\Delta\psi_s = 0 \quad \text{if} \quad |\underline{\psi}_s| \ge |\underline{\psi}_s{}^*| + |\text{hysteresis band}| \end{aligned} \tag{4.26}$$

Similarly, if a torque increase is required then $\Delta T_e = 1$, if a torque decrease is required then $\Delta T_e = -1$, and if no change in torque is required then $\Delta T_e = 0$. The notation corresponds to the fact that the digital outputs of a three-level hysteresis comparator are

$$\begin{aligned} \Delta T_e &= 1 \quad \text{if} \quad T_e \leq T_e^* - |\text{hysteresis band}| \\ \Delta T_e &= 0 \quad \text{if} \quad T_e = T_e^* \\ \Delta T_e &= -1 \quad \text{if} \quad T_e \geq T_e^* + |\text{hysteresis band}| \end{aligned} \tag{4.27}$$

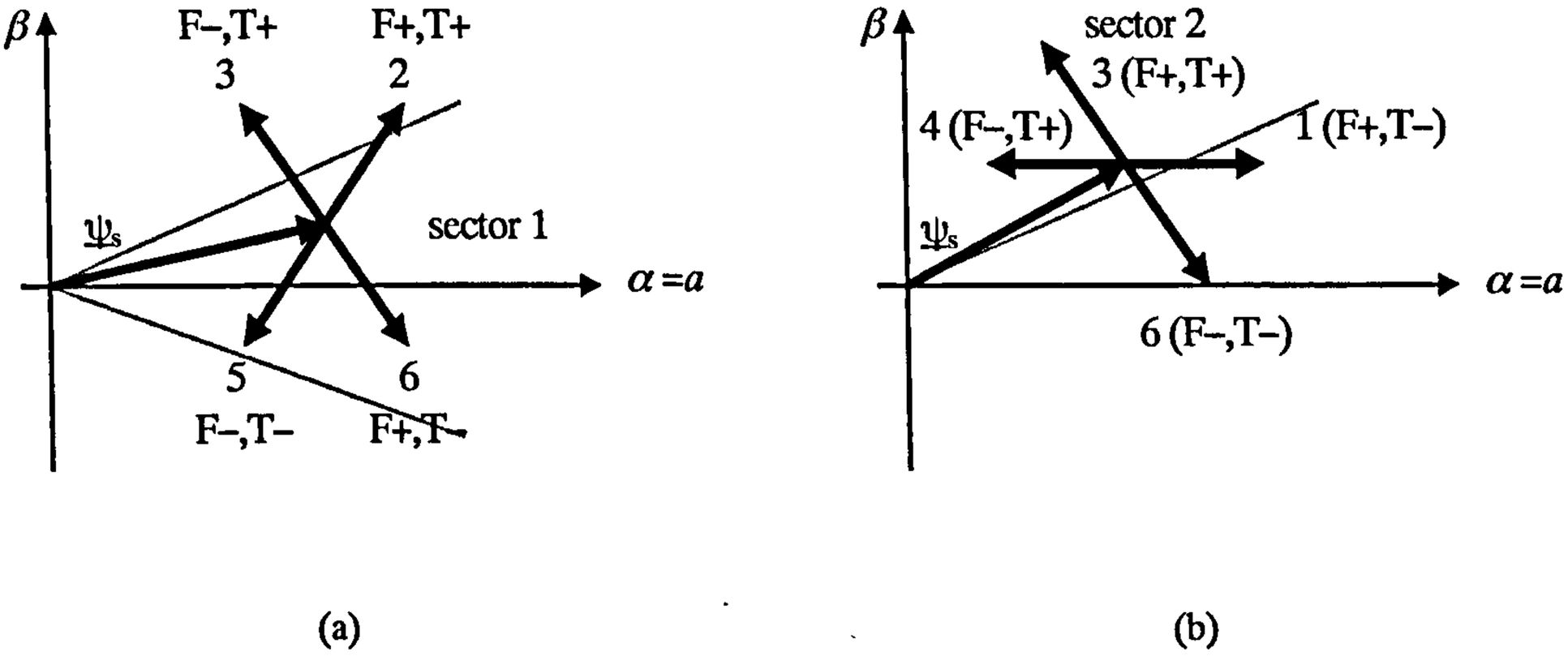

(a) (b)

Figure 4.12: Selection of the appropriate voltage vector for required changes in stator flux and torque: a) when the stator flux is in sector 1, b) when the stator flux is in sector 2 (F ≡ flux, T ≡ torque).

Table 4.1: Optimum voltage vector look-up table.

$\Delta\psi_s$	ΔT_e	sector 1	sector 2	Sector 3	sector 4	Sector 5	sector 6
1	1	$\underline{v_2}$	$\underline{v_3}$	$\underline{V_4}$	$\underline{v_5}$	$\underline{v_6}$	$\underline{v_1}$
	0	$\underline{v_7}$	$\underline{v_8}$	$\underline{v_7}$	$\underline{v_8}$	$\underline{v_7}$	$\underline{v_8}$
	-1	$\underline{v_6}$	$\underline{v_1}$	$\underline{v_2}$	$\underline{v_3}$	$\underline{v_4}$	$\underline{v_5}$
0	1	$\underline{v_3}$	$\underline{v_4}$	$\underline{V_5}$	$\underline{v_6}$	$\underline{v_1}$	$\underline{v_2}$
	0	$\underline{v_8}$	$\underline{v_7}$	$\underline{v_8}$	$\underline{v_7}$	$\underline{v_8}$	$\underline{v_7}$
	-1	$\underline{v_5}$	$\underline{v_6}$	$\underline{v_1}$	$\underline{v_2}$	$\underline{v_3}$	$\underline{v_4}$

Active voltage vectors: 1 (100), 2 (110), 3 (010), 4 (011), 5 (001), 6 (101)
Zero voltage vectors: 7 (111); 8 (000)

4.3.4 Stator flux and torque estimation

From the considerations of the previous subsection, it follows that for successful operation of a DTC scheme it is necessary to have accurate estimates of the stator flux amplitude and the electromagnetic torque. In addition, it is necessary to estimate in which sector of the complex plane the stator flux space vector is situated. As already

shown in subsection 4.2.3.3, stator flux amplitude and torque can be obtained in a rather straightforward manner if stator currents are measured and stator voltages are reconstructed (or measured). Stator flux components and stator flux amplitude are then given with essentially (4.19)

$$\begin{aligned} \psi_{\alpha s}^{e} &= \int (v_{\alpha s} - R_s i_{\alpha s})dt \\ \psi_{\beta s}^{e} &= \int (v_{\beta s} - R_s i_{\beta s})dt \\ \psi_{s}^{e} &= \sqrt{(\psi_{\alpha s}^{e})^2 + (\psi_{\beta s}^{e})^2} \end{aligned} \tag{4.19}$$

where the superscript '*e*' indicates the estimated quantities. Electromagnetic torque is estimated using equation (4.21)

$$T_e^e = (3/2)P(\psi_{\alpha s}^{e} i_{\beta s} - \psi_{\beta s}^{e} i_{\alpha s}) \tag{4.21}$$

The two problems encountered in the process of stator flux and torque estimation are the requirement for the pure integration and temperature related variation in stator resistance in the equation (4.19). Stator resistance related voltage drop is significant at low speed of operation. The accuracy of the estimation at low frequency depends on the accuracy of stator resistance value. An open loop stator flux estimator can work well down to 1-2 Hz but not below this frequency [Vas (1998)].

The equation (4.19) can also be used to find the location of the stator flux space vector in the complex plane,

$$\phi_s^e = \tan^{-1}(\psi_{\beta s}/\psi_{\alpha s}) \tag{4.28}$$

The exact position of the stator flux space vector is not needed in DTC induction motor drives. It is only necessary to know in which sector (out of six possible ones) of the complex plane the vector is located. The equation (4.28) will be used in the simulations for determining the sector containing the stator flux space vector. Determination of the sector of the complex plane containing the stator flux space vector can be done by using the algebraic signs of the stator flux α-β components obtained from equation (4.19) and the sign of the phase '*b*' stator flux (which is obtained by using $\psi_{bs} = -0.5\psi_{\alpha s} + 0.5\sqrt{3}\psi_{\beta s}$), as discussed in [Vas (1998)].

4.3.5 Speed sensorless operation of a DTC induction motor drive

Considerations of the principles of the DTC scheme clearly show that speed information is not required for any other purpose except for closing the speed loop (in contrast to indirect vector control, where speed information is required for calculation of

the relevant flux space vector position as well). DTC scheme is therefore inherently well-suited to sensorless operation. If the drive is operating in the torque mode, the speed information is not needed at all. If the drive operates in closed loop speed mode, speed measurement or an estimate of the speed of rotation is required. In principle, all the methods of speed estimation are equally applicable to all vector drives and a DTC drive. Detailed survey of existing speed estimation methods has been provided in section 2.8.

The already mentioned commercially available DTC drive [Schofield (1998), Tiitinen (1996)], manufactured by ABB, utilises an open loop speed estimator (model based method with no corrective part). Stator voltages are reconstructed, stator currents are measured and stator flux α-β components and torque are at first estimated using (4.19) and (4.21). Rotor flux components, their derivatives and rotor flux amplitude are calculated next,

$$\begin{aligned}\frac{d\psi_{\alpha r}^{e}}{dt} &= \frac{L_r}{L_m}\left(v_{\alpha s} - R_s i_{\alpha s} - \sigma L_s \frac{di_{\alpha s}}{dt}\right)\\ \frac{d\psi_{\beta r}^{e}}{dt} &= \frac{L_r}{L_m}\left(v_{\beta s} - R_s i_{\beta s} - \sigma L_s \frac{di_{\beta s}}{dt}\right)\end{aligned} \tag{4.29}$$

$$\begin{aligned}\psi_{\alpha r}^{e} &= \frac{L_r}{L_m}\left[\int\left(v_{\alpha s} - R_s i_{\alpha s}\right)dt - \sigma L_s i_{\alpha s}\right]\\ \psi_{\beta r}^{e} &= \frac{L_r}{L_m}\left[\int\left(v_{\beta s} - R_s i_{\beta s}\right)dt - \sigma L_s i_{\beta s}\right]\\ \psi_{r}^{e} &= \sqrt{\left(\psi_{\alpha r}^{e}\right)^2 + \left(\psi_{\beta r}^{e}\right)^2}\end{aligned} \tag{4.30}$$

Angular speed of rotor is estimated from angular frequency of the rotor flux space vector, ω_r^{re}, and slip frequency as follows:

$$\omega_r^{e} = \omega_r^{re} - \omega_{sl}^{e} = \frac{\psi_{\alpha r}^{e}\dfrac{d\psi_{\beta r}^{e}}{dt} - \psi_{\beta r}^{e}\dfrac{d\psi_{\alpha r}^{e}}{dt}}{\left(\psi_{\alpha r}^{e}\right)^2 + \left(\psi_{\beta r}^{e}\right)^2} - \frac{L_m}{T_r}\frac{1}{\psi_r^2}\left(\psi_{\alpha r}^{e} i_{\beta s} - \psi_{\beta r}^{e} i_{\alpha s}\right) \tag{4.31}$$

Speed estimation method described with (4.30)-(4.32) is just one possibility, among many. As already noted, numerous speed estimation schemes have already been reviewed in section 2.8. Two specific speed estimation methods, based on the utilisation of the MRAS principle, will be examined in detail in chapter 7.

4.4 A comparison of stator flux oriented control and direct torque control

As already noted, vector control is 30 years old and a variety of different schemes exist. Orientation of the stator current space vector can be performed along stator, air-gap or rotor flux space vector. Current control can be implemented either in the stationary frame (current-fed machine) or in the rotating reference frame (voltage-fed machine). Estimation of the selected flux space vector position can be based on either indirect or direct methods. Such a variety of vector control schemes leads to an interesting question: which scheme is the most appropriate one to be compared with DTC? It is argued here that DTC needs to be compared with SFO control of a current fed induction machine, with hysteresis current control in the stationary reference frame. The reasoning behind this selection is explained further on.

The existing comparisons of DTC and vector control [Le-Huy (1999), Attaianese et al (1999), Ludtke and Jayne (1995)] predominantly deal with indirect rotor flux oriented control. The justification behind such a selection is that the indirect rotor flux oriented control is the solution widely accepted by industry. While this is undoubtedly true, it is not the best choice from the theoretical point of view. The most detailed comparison [Le-Huy (1999)], based on simulations, leads to the conclusion that the two schemes achieve very similar performance and that neither rotor flux oriented control nor DTC has a clear superiority over the other. In contrast to this, experimental results presented in [Attaianese et al (1999)] suggest that DTC offers enormous improvement in dynamic performance. Finally, the conclusion of comparison of [Ludtke and Jayne (1995)] (based on simulations), where some consideration is given to the SFO control as well, is that DTC is superior to vector control.

The considered DTC scheme is the one of figure 4.8. The inputs into the control system are the stator flux reference (that is here kept at constant rated value since the base speed region is analysed only) and the torque reference. Estimation of the stator flux and torque, as well as stator flux position estimation are achieved using (4.19) and (4.21). The optimum inverter switching table given in table 4.1 is used.

DTC relies on control of the stator flux. Hence it seems natural to select for comparison an appropriate SFO control scheme. Next, DTC of figure 4.8 requires estimates of the stator flux magnitude and position, and torque that are obtained from (4.19) and (4.21). It therefore seems as the most adequate to select SFO control scheme

that will use the same principle of stator flux position calculation. Hence position of the stator flux space vector is determined using (4.19). DTC scheme utilises only hysteresis flux and torque controllers and there are not any PI controllers. A SFO control scheme should not therefore have any PI controllers either and hysteresis current control in the stationary reference frame is selected. Finally, since DTC is a torque control scheme, closed loop speed control should not be addressed in the comparison, only torque mode of operation needs to be compared. On the basis of these considerations, the SFO control scheme, selected for analysis, becomes as shown in figure 4.13. It is a combination of schemes shown in figure 4.4 and 4.5, where decoupling circuit operates in the feed-forward manner, while orientation is performed using feedback (direct) method.

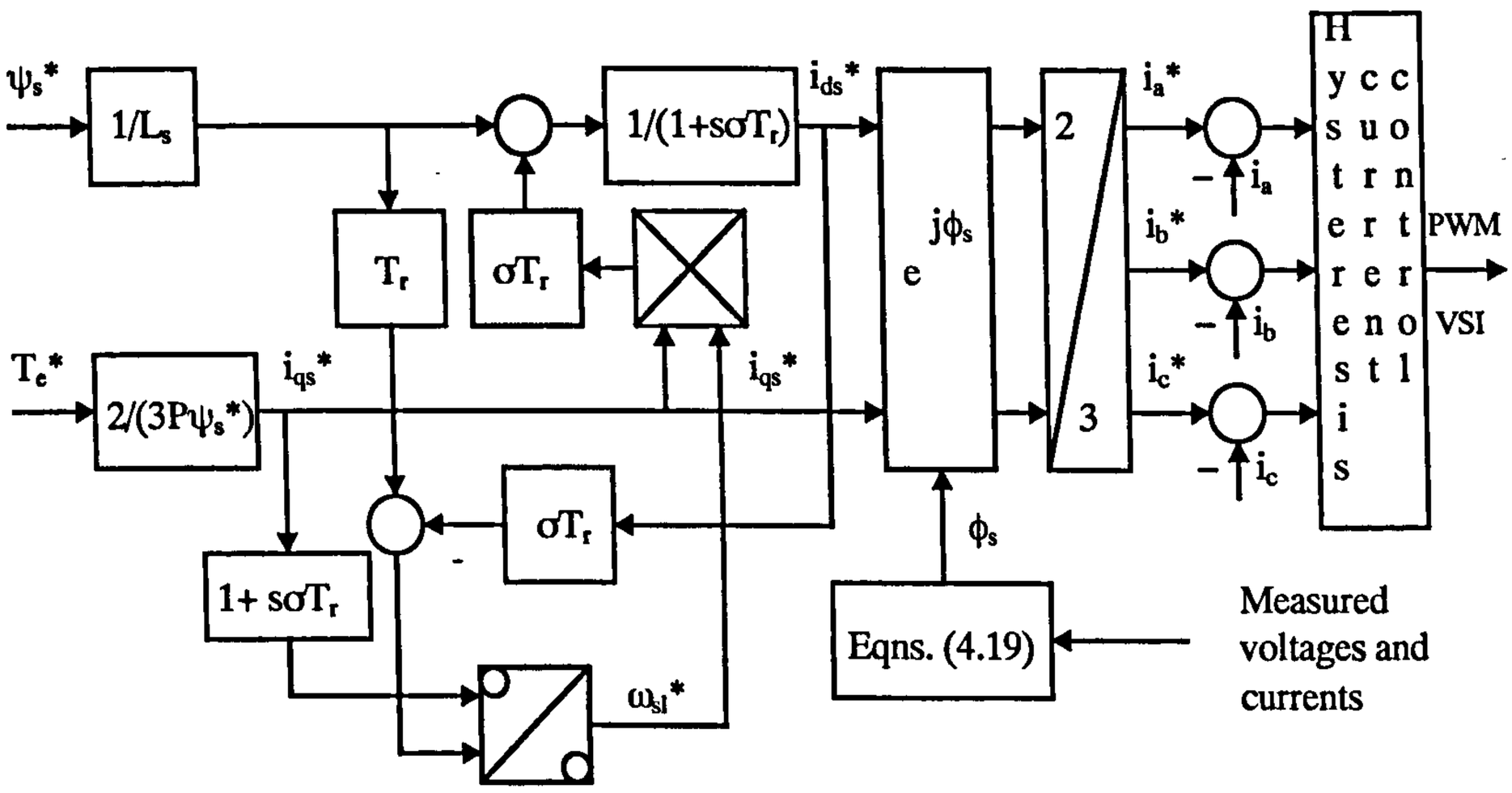

Figure 4.13: Stator flux oriented control scheme with feed-forward decoupling circuit, hysteresis current control and stator flux angle calculation according to (4.19).

The two control schemes are implemented in Simulink software. The model of the inverter is included in both cases, with semiconductor devices being treated as ideal switches (section 3.4). A 4 kW, 380 V, 8.7 A, 4-pole, 50 Hz, 26.5 Nm motor is used (peak rated stator flux is 0.8998 Wb), the same motor is used in subsequent chapter as well (all data in Appendix A). Standard constant parameter model of section 3.2 is utilised. DC link voltage is fixed to the value of 580 V for both schemes. A small voltage margin is therefore provided for operation at rated speed. Hysteresis bands in

DTC are set to ±1% of the rated torque and rated flux (peak) values. Hysteresis band for current controllers in SFO control is ±1% of the rated (peak) current (±0.123 A).

DTC is known to suffer from problems associated with initial magnetisation and zero speed operation. On the other hand, SFO control scheme enables easy pre-magnetisation of the machine. However, since the flux and torque estimator described with (4.19) and (4.21) is used, the problem of zero and very low speed operation remains. The following approach is therefore adopted. SFO machine is pre-excited to the rated stator flux value. Rated torque reference is then applied under no-load conditions. After an appropriate time interval rated load torque is applied, so that steady state operation at 5% of the rated speed is established. In the case of DTC, stator flux reference and torque reference (both equal to rated values) are applied in the same instant. Rated load torque is again applied after appropriate time interval, so that steady state operation at 5% of rated speed is achieved. All the results and observations reported further on start from the initial steady state operation at 5% of rated speed, with rated values of stator flux and torque references and rated load torque.

Figures 4.14 and 4.15 illustrate dynamics of the drive with SFO control and DTC, respectively, during acceleration and deceleration transients. Motor torque, load torque, rotor speed and stator flux are shown. The machine is accelerated from 5% of the rated speed to rated speed, and is then decelerated by setting the torque command to zero while retaining the rated load torque. Steady state operation at one half of the rated speed and at rated speed is encompassed in these figure and is achieved by applying the rated load torque during operation with the torque command equal to rated.

Comparison of the speed traces leads to the conclusion that they are essentially the same. Stator flux and torque dynamic behaviour appears to be the same as well. However, substantial differences exist in the stator flux and the motor torque ripples. Stator flux ripple in SFO control is much smaller than the one with DTC. In addition, flux ripple in DTC significantly exceeds prescribed hysteresis band at low speeds. As far as the torque response is concerned, DTC has smaller torque ripple than SFO in low and medium speed regions. Once when the rated speed is approached, ripple with DTC starts falling outside the hysteresis band and becomes rather significant.

In order to enable a more detailed insight into the behaviour of the two control schemes, steady state operation at one half of the rated speed and at rated speed is further compared. Figures 4.16 and 4.18a, 4.19b, 4.20a illustrate behaviour of the SFO

control, while figures 4.17 and 4.18b, 4.19b, 4.20b apply to DTC at these two operating speeds. Stator phase currents are included in figure 4.20 in addition to the traces of torque and stator flux. Maximum value of the torque ripple is around 2.6% (of the rated value) in the case of SFO control, at both operating speeds. In contrast to this, torque ripple with the DTC is held within the prescribed 1% hysteresis band at medium 0.5 p.u. speed. However, at rated speed the DTC torque ripple significantly increases and attains the value of 6%. Stator flux ripple with SFO control is around 0.3% (of the rated peak value) at medium speed and 0.2% at rated speed. At medium 0.5 p.u. speed, flux ripple with DTC is within prescribed 1% hysteresis band, except in vicinity of the borders of different sectors, while it is completely within the 1% hysteresis band at rated speed.

Phase current ripple at rated speed with SFO control is just over 1% hysteresis band (1.2%), while the current ripple in DTC is higher and is around 3.7%. The ripples at 0.5 p.u. speed are 1.5% and 4.5%, respectively.

As a final result in this comparison, figure 4.21 shows zoomed extracts from figures 4.14a and 4.15a, illustrating the dynamics of the motor torque change after step-wise change of torque reference from rated value to one half of the rated value. It can be concluded from this figure that direct torque control offers a considerably faster torque response than the stator flux oriented control. This is indeed the most frequently cited advantage of DTC over vector control. It should be noted that the irregular torque ripple behaviour in figure 4.21b is only apparent and is the consequence of the low sampling frequency used for plotting purposes in figures 4.14 and 4.15.

Described comparison between SFO control and DTC of an induction motor leads to the following conclusions:

- Faster dynamic torque response in DTC.
- Stator flux and stator current ripples are considerably smaller with SFO control.
- Torque ripple is substantially smaller with DTC in low and medium speed regions, while at high speed torque ripple with DTC exceeds the one of SFO control.

Presented results of this study can be found in [Pham-Dinh and Levi (2000)]. One particular issue that seems appropriate to address at this stage is the problem of stator current limiting. While this is a straightforward task in the case of vector control since stator currents are controlled directly, it is a rather involved problem in DTC since stator currents are controlled only indirectly. On the other hand, stator current has to be limited in order to avoid damage to the inverter during rapid transients. Problem of

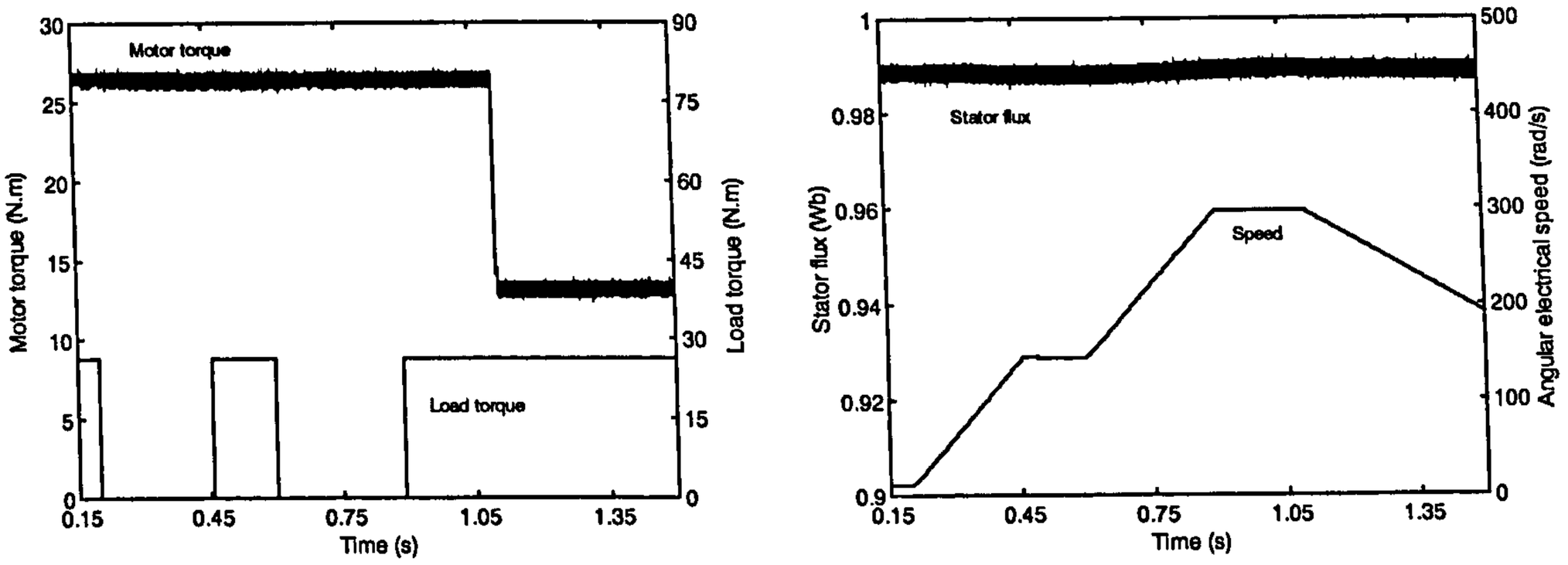

a) b)

Figure 4.14: Dynamic responses of stator flux oriented control: a) Motor torque and load torque, b) Stator flux and rotor speed.

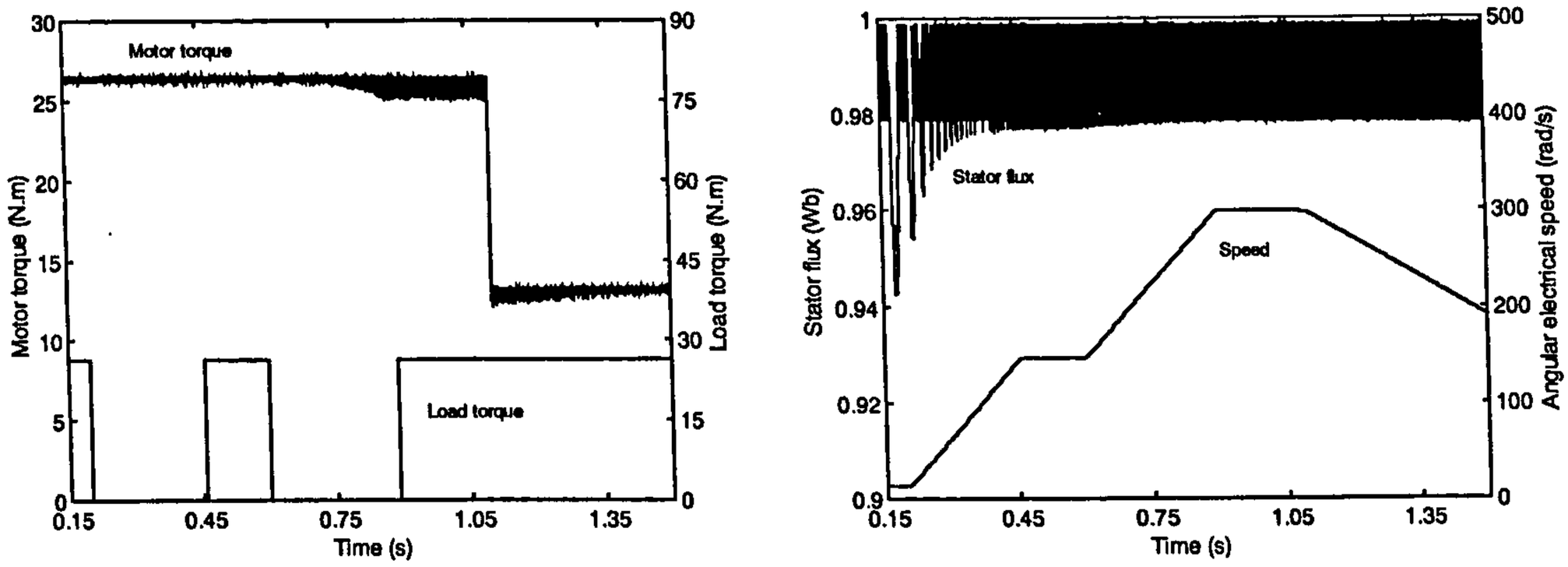

a) b)

Figure 4.15: Dynamic responses of direct torque control: a) Motor torque and load torque, b) Stator flux and rotor speed.

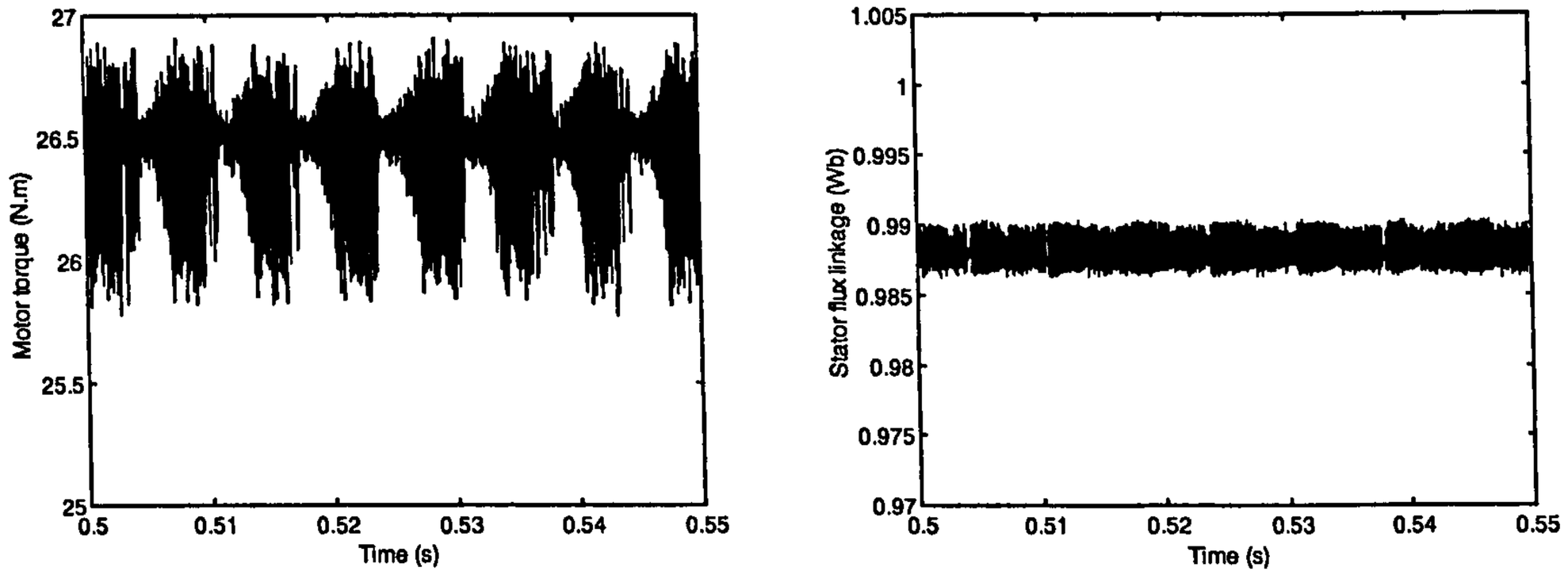

a) b)

Figure 4.16: Steady states at one half of rated speed in stator flux oriented control: a) Torque response, b) Flux response.

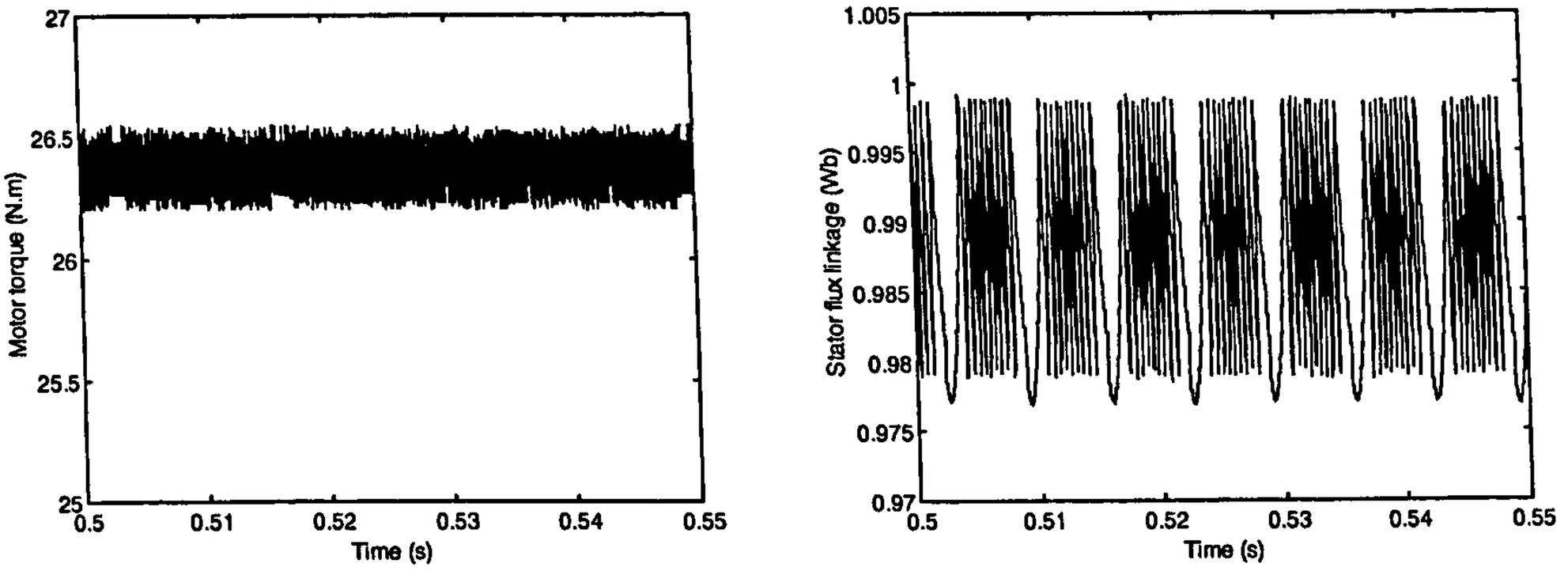

a) b)

Figure 4.17: Steady states at one half of rated speed in direct torque control: a) Torque response, b) Flux response.

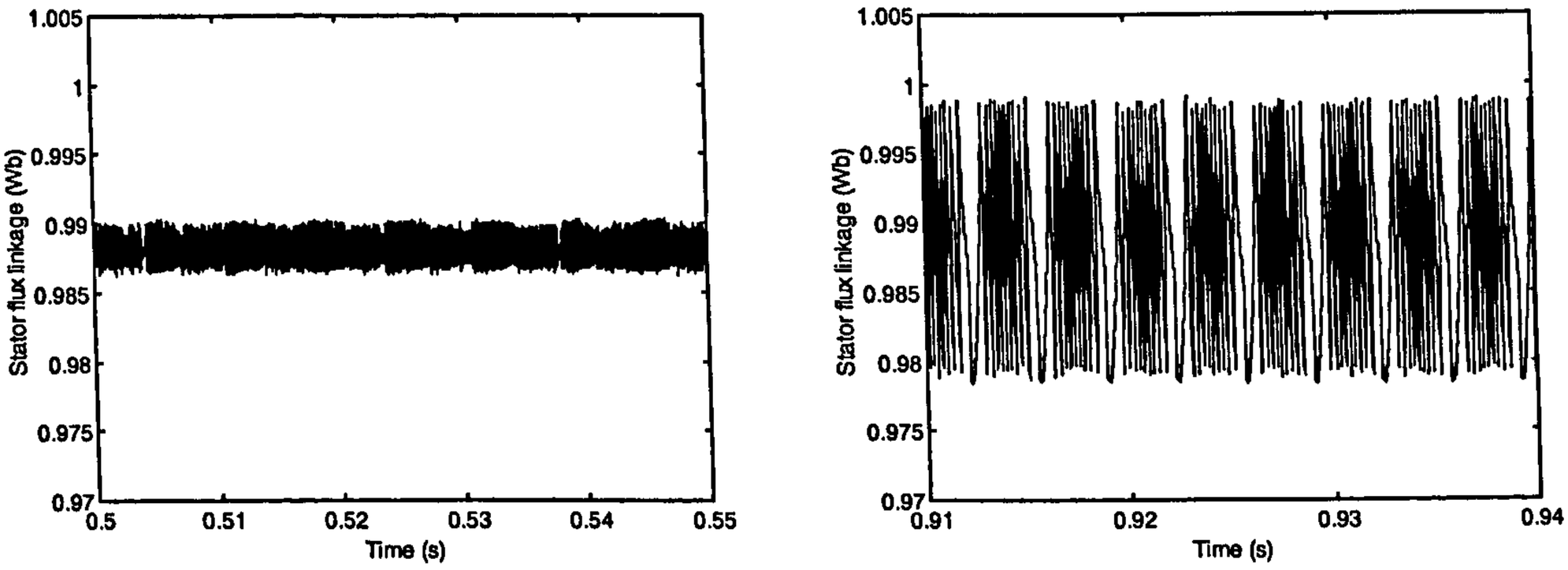

a) b)

Figure 4.18: Steady state responses of stator flux linkage at rated speed: a) Stator flux oriented control, b) Direct torque control.

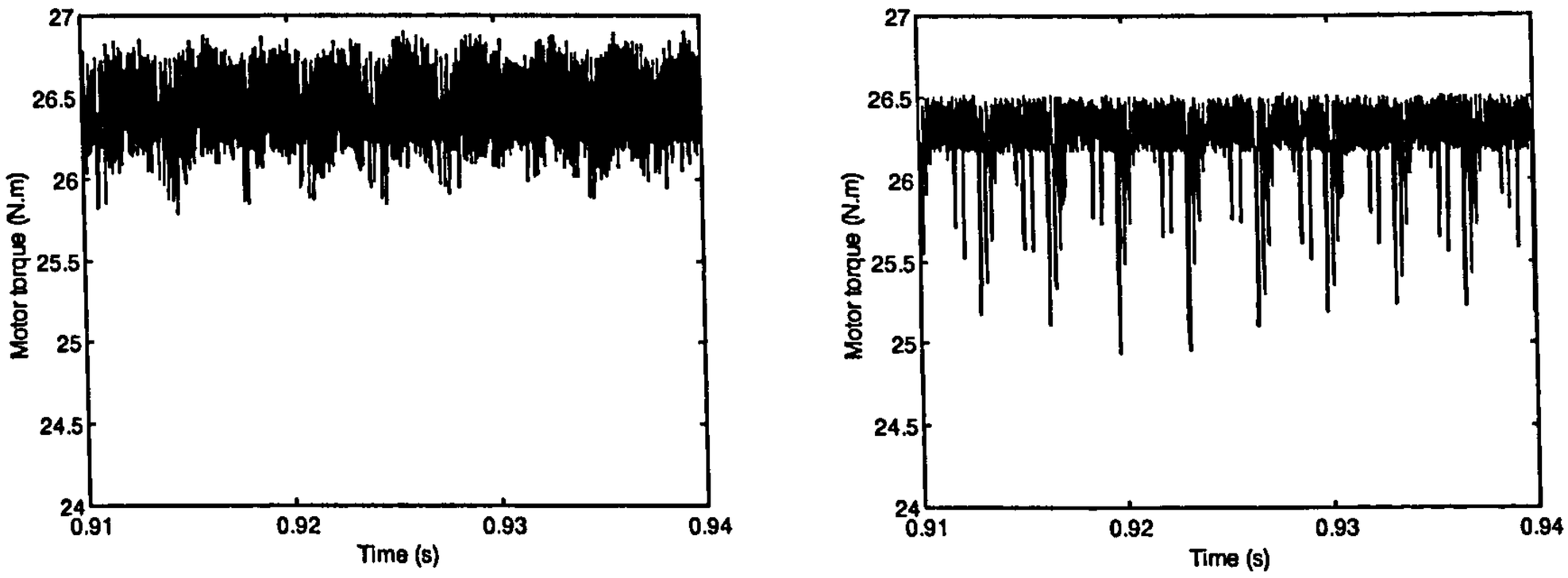

a) b)

Figure 4.19: Steady state responses of motor torque at rated speed: a) Stator flux oriented control, b) Direct torque control.

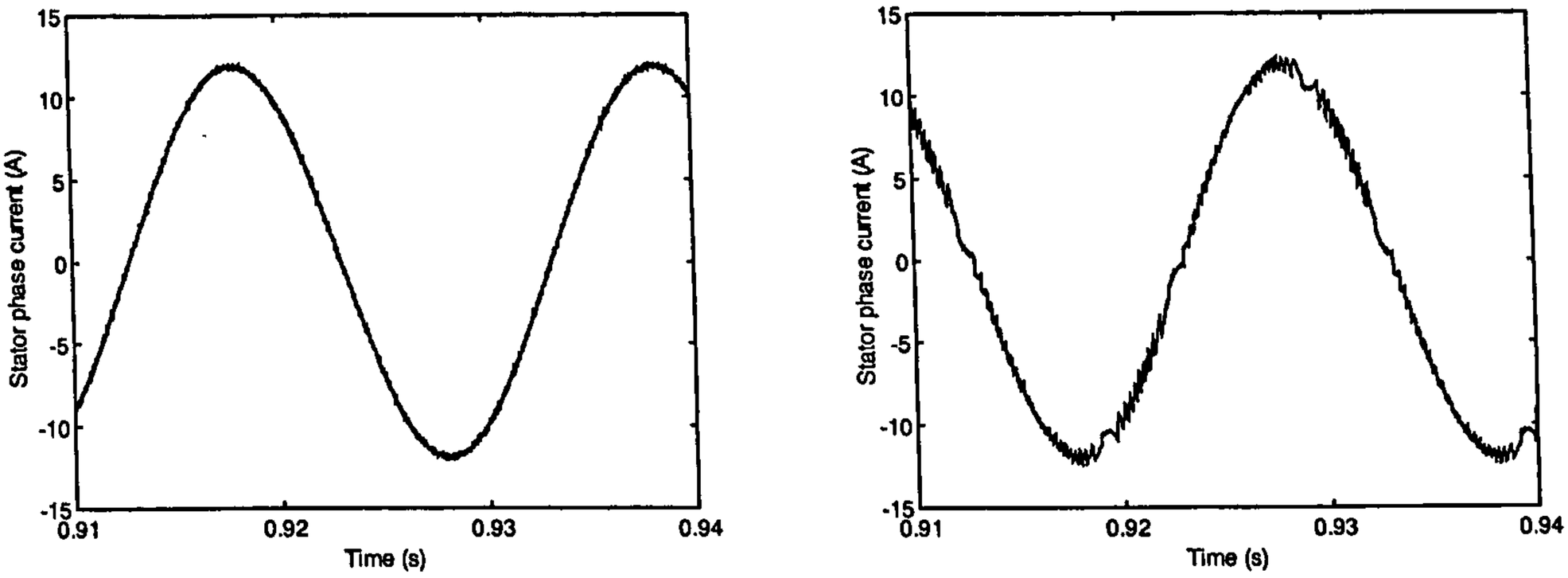

a) b)

Figure 4.20: Steady state responses of stator phase current at rated speed: a) Stator flux oriented control, b) Direct torque control.

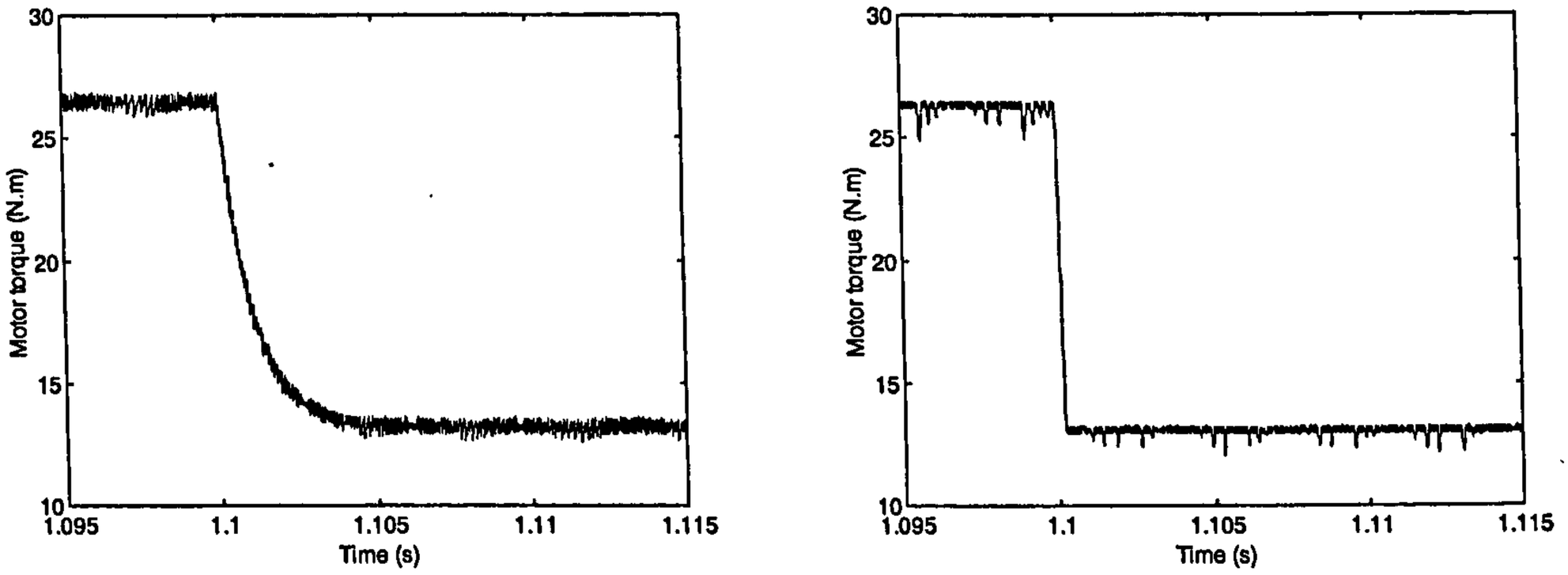

a) b)

Figure 4.21: Dynamics of motor torque change for: a) stator flux oriented control, b) direct torque control.

current limiting in DTC has been discussed in a number of existing publications and various solutions have been proposed [Chapuis and Roye (1998), Casadei et al (1995)]. The issue of stator current limiting is however not of any importance for the research conducted here and the simulation model of DTC induction motor drive used in this section does not include a current limiter. The same applies to all the other simulation models used in chapters 5 to 7.

4.5 Summary

Principles of vector control and direct torque control for induction motor drives have been reviewed in this chapter. The principles rely on the mathematical model of an induction motor, discussed in chapter 3. Two commonly used orientations of the rotating reference frames for vector control have been presented. The first one, which is also the most frequently used vector control method in industry, is rotor flux oriented control. This method of vector control requires minimum number of calculations to decouple the torque and flux control in an induction motor. Therefore, this method requires simple hardware and the computational burden imposed on the hardware is not highly demanding. The second orientation of the rotating reference frame for vector control is stator flux orientation. This method requires more complicated decoupling circuit to control torque and flux independently. Computational capacity of the hardware for this control scheme therefore needs to be higher. Indirect rotor flux oriented control and indirect stator flux oriented control are discussed next, in conjunction with a current fed induction machine. Direct vector control is briefly reviewed, with emphasis on relevant flux estimation from measured stator currents and voltages.

Next, principles of direct torque control, which is based on the mathematical model of an induction motor in the stationary reference frame, are discussed. This control method utilises the non-ideal nature of a voltage source inverter to produce fast and robust response of torque and stator flux. Decoupling of torque and flux is achieved without on line co-ordinate transformation and complicated hardware with high computational capacity. Sensorless DTC drive is briefly addressed as well.

The last section of this chapter presents results of a simulation study related to a comparison between a vector controlled and a direct torque controlled induction motor drive. For the reasons explained in the section, a specific structure of a stator flux oriented induction motor drive is selected among a variety of possibilities for this comparative analysis. The comparison shows that the performance of the two drives is of very much the same quality and this finding to some extent contradicts the previously published results. The reason for this discrepancy is that the previous studies have not compared 'like-for-like', since all were using a rotor flux oriented induction motor drive as a starting point.

CHAPTER 5

SWITCHING TABLES FOR DIRECT TORQUE CONTROL

5.1 Introduction

Quality of direct torque control depends on an appropriate selection of the voltage space vector that will be applied to the motor. This selection is made according to the demands on increase or decrease in stator flux and torque. Other criteria for voltage vector selection such as minimum switching frequency (which reduces switching losses), relatively small flux and torque ripple (which reduces the acoustic noise and harmonic losses) or fast torque response [Takahashi and Noguchi (1986)] are also taken into account. Different criteria lead to different switching tables. The inputs of the switching tables are usually torque and flux comparator's outputs and the sector of the complex plane where the stator flux space vector lies. The output of these tables is the optimum voltage space vector to be applied to the motor based on the feedback data and adopted criteria.

In this chapter, an investigation related to the switching table originally suggested by [Takahashi and Noguchi (1986)] is presented first. Modifications of this original switching table are discussed next. A comparative investigation of the DTC induction motor drive behaviour when different switching tables are used is then conducted. A novel switching table is proposed in this chapter and is verified by simulation.

5.2 Direct torque control with Takahashi's switching table

5.2.1 Original switching table

This particular switching table has already been introduced in subsection 4.3.3. Further more detailed considerations related to the Takahashi's switching table are provided in this subsection. The switching table is designed to give fast torque response, low inverter switching frequency and low harmonic losses [Takahashi and Noguchi

(1986)]. All eight voltage space vectors are used (six active voltage vectors and two zero voltage vectors). The active-forward voltage vectors (v_{k+1}, v_{k+2}, where k is the sector in which the flux space vector is located) are used to increase torque and zero vectors are used to reduce torque when the speed is positive. Similarly, when the speed is negative, active-backward voltage vectors (v_{k-1}, v_{k-2}) are used to decrease torque (by absolute value) and zero voltage vectors are used to increase torque (absolute value). The radial vectors (v_k, v_{k+3}) are not used in this switching table. The torque and flux errors are processed through hysteresis comparators, whose outputs are fed into the switching table. The voltage vector selection is made based on the outputs of hysteresis comparators and on the sector of the plane containing the stator flux space vector.

As already noted, the complex α-β plane is divided into six sectors because of the periodical change of the inverter output voltage vectors after every $\pi/3$ radians [Takahashi and Noguchi (1986)]. The complex plane with the sectors and eight possible output voltage vectors of the inverter has already been shown in figure 4.10, while the switching table suggested by Takahashi has already been given in table 4.1.

Tangential component of the voltage vector does not change the magnitude of the stator flux voltage vector. It causes an instantaneous increase or decrease in the angle between stator flux and rotor flux, which is assumed to be stationary during a short period of time because of the time delay in response [Bertoluzzo et al (1999)]. These changes of the angle cause the electromagnetic torque increase or decrease, respectively. However, the radial component of the voltage vector changes the amplitude of the stator flux space vector. It is therefore used to increase or decrease the stator flux. It has no effect on the electromagnetic torque of the motor, because the components of voltage vectors affect stator flux and torque in the described manner. Application of the voltage vectors over a short time interval can cause quick response of both torque and stator flux to meet demands imposed by the hysteresis comparators.

In the described switching strategy, only one voltage space vector is applied during one sampling period. Therefore, the instantaneous errors of flux and torque cannot be controlled during this period and they will reach their maximal values before another voltage vector is applied for error correction. These errors are proportional to the sampling period [Chen and Li (1999)]. This will cause problems such as asymmetry of torque error, which leads to low frequency torque ripple, and stator flux locus

distortion [Chen and Li (1999)]. Torque variation equations for the cases of increasing and decreasing torque are obtained by [Chen and Li (1999)] in the following form:

$$\begin{aligned}\Delta T_e \uparrow &= [P(\underline{\psi}_r \otimes \underline{v}_s) - P\omega_r \underline{\psi}_s \circ \underline{\psi}_r - R_m T_e] T_f / L_\sigma \\ \Delta T_e \downarrow &= [-P\omega_r \underline{\psi}_s \circ \underline{\psi}_r - R_m T_e] T_f / L_\sigma\end{aligned} \tag{5.1}$$

where T_f is the sampling period, $\otimes$ stands for vector product while $\circ$ denotes scalar product, and

$$R_m = (L_r R_s + L_s R_r)/L_m$$
$$L_\sigma = (L_s L_r - L_m^2)/L_m$$

From the equation above, when $|\Delta T_e \uparrow| < |\Delta T_e \downarrow|$, the average torque will have a negative deviation. This case generally happens at high speed [Chen and Li (1999)]. When $|\Delta T_e \uparrow| \sim |\Delta T_e \downarrow|$, the average torque does not deviate significantly. This usually happens in the medium speed region. When $|\Delta T_e \uparrow| > |\Delta T_e \downarrow|$, the average torque has a positive deviation. This case happens at low speed.

The drawbacks of the switching scheme proposed by Takahashi regarding flux response are also analysed by [Chen and Li (1999)]. Stator flux increment after one sampling period is:

$$\underline{\psi}_s(n) \sim \underline{\psi}_s(n-1) + \underline{v}_s(n-1) \cdot T_f \tag{5.2}$$

The sampling period T_f is usually small. Therefore, it can be assumed that:

$$|\underline{\psi}_s(n-1)| \sim |\underline{\psi}_s(n)| \tag{5.3}$$

From the above assumption, the equation for stator flux variation in terms of applied voltage space vector, sampling period and the angle between the current stator flux space vector and the applied voltage space vector can be obtained as follows:

$$\Delta\psi_s = |\underline{\psi}_s(n)| - |\underline{\psi}_s(n-1)| \sim |\underline{v}_s(n-1)| T_f \cos(\delta_s - \phi_s) \tag{5.4}$$

Here δ_s is the instantaneous angle of stator voltage space vector and ϕ_s is the instantaneous angle of stator flux space vector with respect to phase a magnetic axis of stator. At positive speed, when the stator flux space vector is in the k-th sector and the non-zero voltage space vectors are applied, the following two cases can happen.

Case 1: When voltage vector v_{k+1} is selected, the flux increment equation is:

$$\Delta\psi_s \uparrow = |\underline{v}_{k+1}| T_f \cos(\pi/3 - \phi_s) \tag{5.5}$$

Case 2: When voltage vector v_{k+2} is selected, the flux increment equation is:

$$\Delta\psi_s \downarrow = |\underline{v}_{k+2}| T_f \cos(2\pi/3 - \phi_s) \tag{5.6}$$

Figure 5.1 shows the relationship between stator flux space vector and voltage space vectors. In figure 5.1a, the variation of stator flux space vector due to voltage space vector application after one sampling period is shown. In figure 5.1b, the stator flux space vector in *k*-th sector and voltage space vectors v_{k+1}, v_{k+2} are illustrated.

Figure 5.2 shows the flux variation with position of the stator flux space vector in the *k*-th sector when angle is varied from $30(2k-3)$ degrees to $30(2k-1)$ degrees, where *k* is set to 1. Figure 5.2 is obtained by direct application of equations (5.5) and (5.6). The variation is shown in per unit with the base value being $|\underline{v}_s| T_f$, because all the non-zero voltage vectors have the same magnitude. Figure 5.2(a) shows the case when v_{k+1} is applied and figure 5.2(b) shows the case when v_{k+2} is applied. The graphs show that v_{k+1} application results in a small increase of flux at the border between the *(k-1)*-th sector and the *k*-th sector and a big increase in flux at the proximity of the border between the *k*-th sector and the *(k+1)*-th sector [Chen and Li (1999)]. On the other hand, v_{k+2} application results in a big decrease of flux at the border between the *(k-1)*-th sector and the *kth* sector and a small decrease in flux in the proximity of the border between the *kth* sector and the *(k+1)*-th sector [Chen and Li (1999)]. This also means that when flux space vector is in the proximity of the border between the *k*-th sector and the *(k+1)*-th sector, applying v_{k+1} will cause the flux to increase substantially, especially at low speed, while applying v_{k+2} will cause the flux to decrease insignificantly. Therefore, it would take several sampling period of applying voltage space vector v_{k+2} to compensate the flux deviation caused by applying voltage vector v_{k+1} in one sampling period [Chen and Li (1999)]. This is the reason for demagnetisation at low speed in direct torque control when stator flux space vector is in the proximity of the borders between consecutive sectors. The flux locus in the complex plane in this case is a straight line instead of an arc [Chen and Li (1999)]. The application of zero vectors in the low speed region also causes a decrease in the magnitude of stator flux space vector [Chen and Li (1999)].

The utilisation of zero vectors to decrease torque helps to reduce the switching frequency, because the slowest torque-reducing operation can be obtained with these vectors [Takahashi and Noguchi (1986)]. Switching losses are also reduced by switching only one switch to change the applied voltage space vector in the two

consecutive switching periods [Vas (1998)]. However, at low speed, zero voltage vectors are applied to the induction motor for a long time and this causes de-magnetisation of stator flux in the low speed region [Alfonso et al (1999), Casadei et al (1994)]. When zero voltage vectors are applied to an induction machine, both the amplitude and position of stator flux space vector remain the same [Bertoluzzo et al (1999)]. However, if the machine is in motoring mode, the voltage drop across stator resistance and the inertial movement of rotor flux space vector slowly reduce the stator flux space vector amplitude and the angle between these two vectors (rotor flux and stator flux), which in turn decreases electromagnetic torque of the machine. The rate of torque decrease depends on the speed of the machine [Bertoluzzo et al (1999)]. These are the reasons for stator flux demagnetisation at low speed and high torque ripple at high speed, especially when the flux and torque are required to increase and decrease, respectively, at the same time [Bertoluzzo et al (1999)]. The problems of direct torque control with Takahashi's switching table at low speed will be pronounced at start-up and during braking operation of an induction motor.

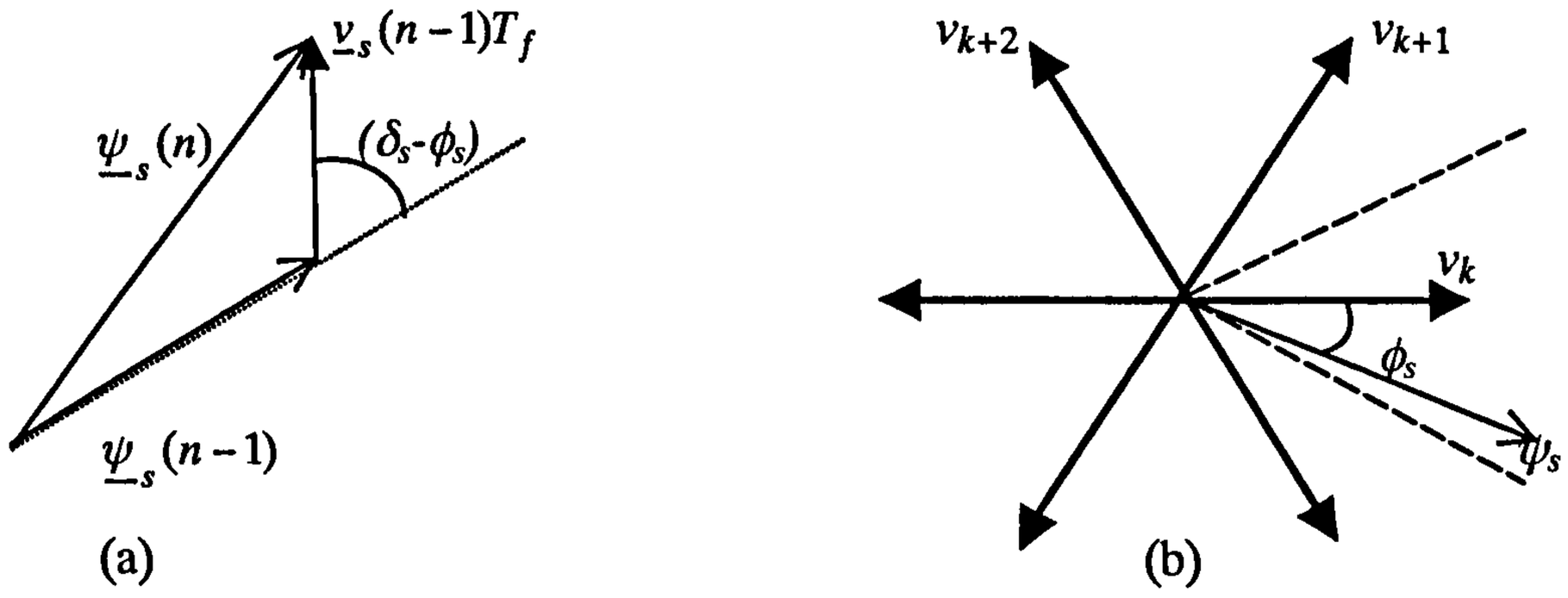

Figure 5.1: Relationship between voltage space vectors and stator flux space vector variation, (a) variation of stator flux after one sampling period, (b) stator flux position and voltage space vectors.

The electromagnetic torque error and stator flux errors (the errors are the differences between reference quantities and estimated quantities) are treated in the same manner with regard to the steady state and transient state. The large errors (which happen at start-up) and the small errors (in steady state) are also treated equally in this switching table [Vas (1998)]. This limits motor speed reversal capability.

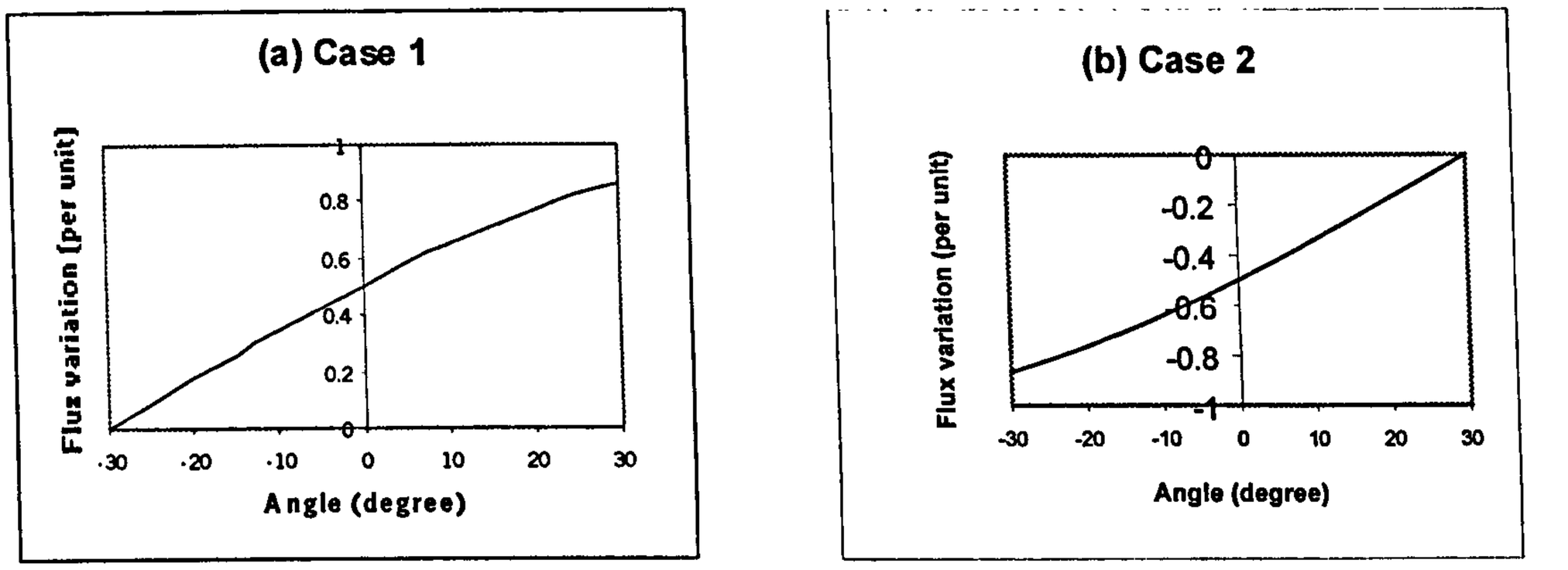

Figure 5.2: Stator flux variation for different positions of stator flux space vector in the *k*-th sector: (a) when vector v_{k+1} is applied, (b) when vector v_{k+2} is applied.

The sampling frequency is assumed to be constant during the operation of the system [Takahashi and Noguchi (1986)]. The voltage space vector selection is based only on the errors (torque and flux) and location (or the sector) of the stator flux [Takahashi and Noguchi (1986)]. The speed of rotation of the machine is not taken into account when applying the voltage vectors; therefore, the same voltage vector could be applied to the induction machine at both low and high speed for the same period of time. This could cause unwanted results at low or high speed in both torque and flux responses [Bertoluzzo et al (1999), Kazmierkowski and Tunia (1994), Kazmierkowski and Kasprowicz (1995)].

The dynamic effects of voltage space vectors are also analysed by [Bertoluzzo et al (1999)]. These dynamic effects on electromagnetic torque and stator flux depend on the rotating speed of the motor. At low speed, the effects of the voltage vectors on torque and stator flux are similar and they depend on tangential and radial components of the voltage vectors. However, at high speed, the effects are not proportional to the components and the voltage vector applied to increase torque may reduce torque instead. The mathematical analysis of these effects is discussed in the above referenced paper. Tangential variation of the stator flux space vector also reduces the impact of voltage space vector on torque response of an induction machine. It can cause torque reduction while the torque-increasing voltage vectors are applied to the machine [Chapuis et al (1998)]. This variation of stator flux space vector is not taken into account in Takahashi's switching table. The torque response efficiency of applied voltage space vector also varies with the different positions of the stator flux space vector within the same sector of the complex plane, since only one voltage space vector

is applied for the whole sector in Takahashi's switching strategy [Chapuis et al (1998)]. Torque dynamic equation, torque dynamic behaviour and efficiency of stator voltage space vectors are also analysed by [Chapuis et al (1998)] to give a modified switching scheme with emphasis on torque response at high speed.

The response of torque, stator flux, speed and stator phase current obtained using direct torque control with Takahashi's table is discussed in the next sub-section. These results are obtained by the simulation of DTC of induction motor. The models in the simulation were built with the assumption of ideal conditions. The discussion will look at the responses in torque mode, speed mode (closed loop speed control), and braking mode. Problems of DTC, which have been discussed above, will be visualised by means of results obtained from simulation.

5.2.2 Torque mode of operation

The responses of torque and stator flux in the torque mode of operation, where the input quantities to the DTC controller are electromagnetic torque and stator flux commands, are obtained using Matlab and Simulink. Simulated control system is the one already discussed in chapter 4 (figure 4.8).

The simulation procedure closely corresponds to the one of section 4.4. Voltage supply is again the voltage source inverter with the fixed DC link voltage of 580V. The torque command is set to rated motor torque value and the flux command is set to rated stator flux value. When the motor reaches rated speed, a load torque equal to rated motor torque is applied to the motor to stabilise the speed. During the period of load torque application, both torque and flux commands remain constant and rated. The hysteresis bands for torque and stator flux are ±1% of rated values. Computational step in the simulation is 1μs. The first 0.7 seconds after motor starting is simulated. Figure 5.3a illustrates machine's torque and load torque during described transient, stator flux response, rotor speed, and stator current. High flux ripples at low speed and high torque ripples at high speed are observed during the transient. Behaviour is similar to the one already reported in section 4.4.

As already noted, simulations do not include current limiting features. This explains the existence of a very high stator current peak in figure 5.3a, of around 60 A (or approximately 5 times of the rated stator peak current). When stator flux is established in the motor, stator current is reduced.

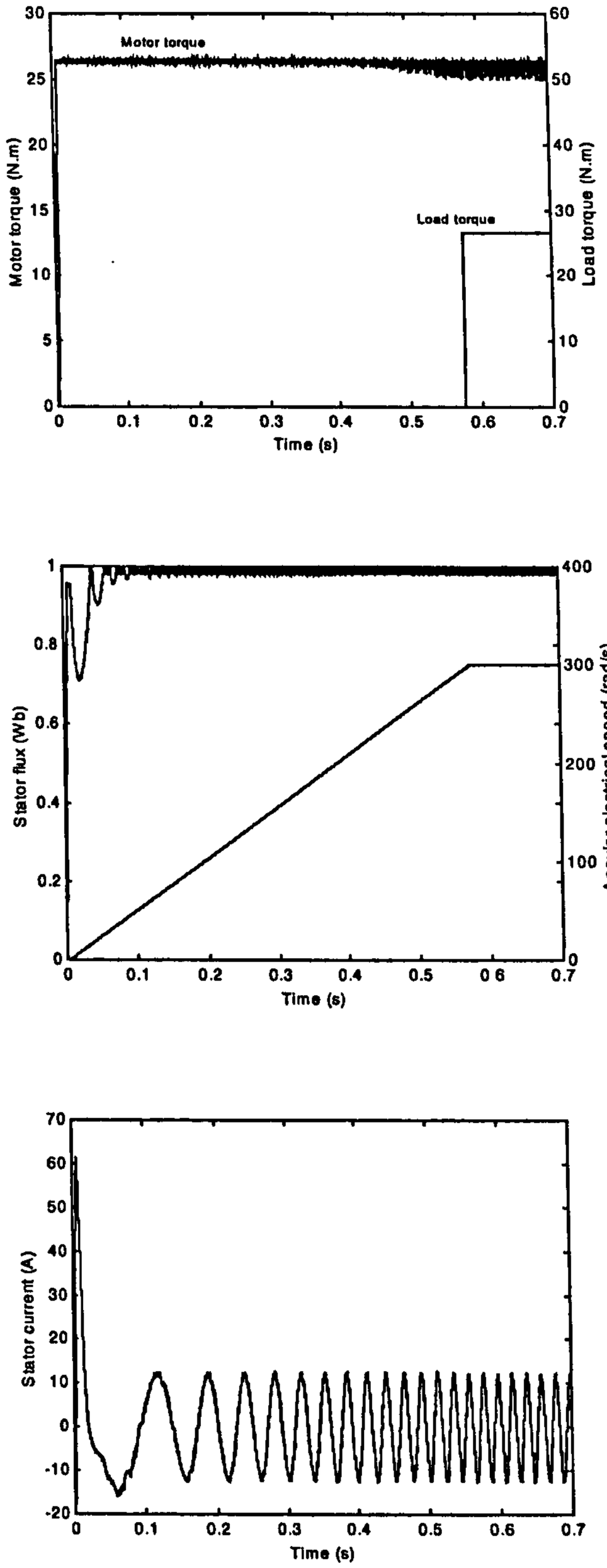

a)

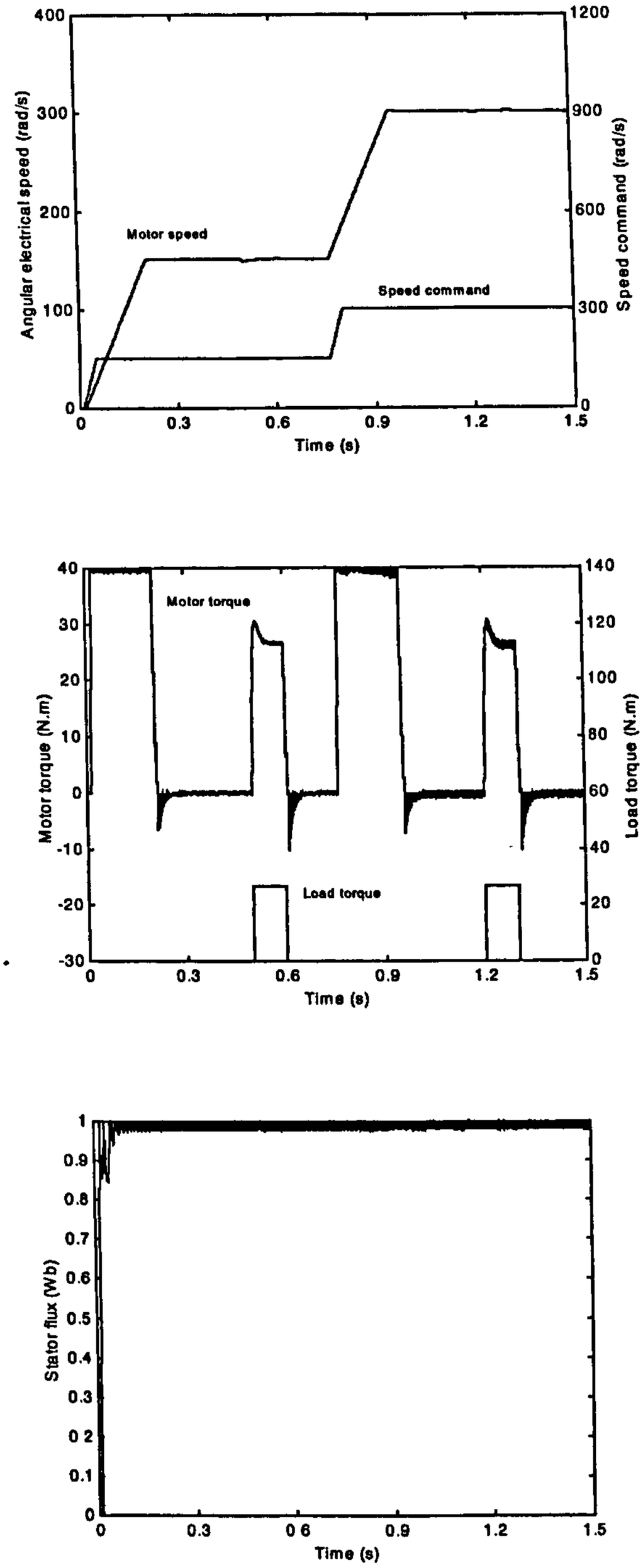

b)

Figure 5.3: a) Motor torque, load torque, stator flux, actual speed, and stator current in torque mode of operation, b) Actual speed, speed command, motor torque, load torque and stator flux in speed mode of operation.

Closer examination of stator flux response in figure 5.3a shows that substantial deviation of stator flux outside the prescribed hysteresis band of 1% takes place during approximately first 0.1 seconds (i.e. until speed reaches 52 rad/s or 17.4% of the rated

speed equal to 301.6 electrical rad/s). Deviations outside the hysteresis band become very small after this time interval and completely disappear after the first 0.4 seconds, when speed reaches 210 rad/s (or approximately 70% of the rated speed). In the remaining part of the acceleration transient and in the subsequent steady state operation, stator flux deviates by no more than ±1% from the reference value of 0.9889 Wb. Indeed the average value of stator flux is 0.9881 Wb, or 99.9% of the reference value.

Torque response in figure 5.3a is characterised by extremely quick initial build-up. Motor torque reaches the set reference value in less than 0.01 seconds and from then oscillates within the prescribed hysteresis band. Since the operation is in motoring, actual motor torque varies between the reference (equal to 26.5 N.m) and 99.9% of the reference (26.235 N.m). The average value is therefore 26.3675 N.m. However, once when the speed exceeds 210 rad/s (70% of the rated speed), torque ripple starts to increase. In rated speed operation, torque deviation is substantially larger than the prescribed hysteresis band of 1%. It is at most 6% so that the average torque developed by the motor reduces. It is now 26.2377 N.m instead of 26.3675 N.m. This means that the final achieved operating condition in figure 5.3a is only a quasi steady state operation because motor torque is slightly smaller than the load torque. In other words, speed in figure 5.3a is essentially reducing although at a very small rate so that the speed decrease is not visible in the figure.

5.2.3 Speed mode of operation

Simulated DTC scheme for speed mode of operation is the one illustrated in figure 4.9. It is assumed at this point that the actual speed of the machine is measured by an ideal sensor. Speed controller is of PI type.

Torque command is the output of the PI controller, whose input is the difference between the measured angular electrical speed and the speed command. Stator flux command is fed directly into the flux hysteresis comparator, which is the same as in the DTC torque drive. The PI controller is fine-tuned to obtain a fast, low-overshoot speed response in transient state and accurate steady state holding. PI controller with anti windup feature, which prevents excessively large signal to be fed into the cascaded devices, is used in the simulation. The output of the PI controller is limited to 1.5 times the rated motor torque. A ramped signal is applied to the PI controller as the speed command. The speed command first increases from zero to one half of the rated speed

and then stays at this value for a while. When steady state is established, rated load torque is at first applied and then removed to test load torque rejection behaviour of the speed drive. Motor is then accelerated to rated speed using once more a ramped speed command. The same sequence of transients related to load torque application and removal is repeated. The time interval up to 1.5 seconds after starting is simulated. Results related to torque, speed and stator flux response are shown in figure 5.3b.

Figure 5.3b shows that speed response of the motor is very fast indeed, with virtually no overshoot at all. Application and removal of the load torque lead to very small dip and overshoot, respectively, that are very quickly compensated by the speed controller. Since motor torque is limited to 1.5 times the motor rated torque, acceleration is faster than in the case of torque mode, illustrated in figure 5.3a. This fact is reflected in flux response in figure 5.3b. Since the torque builds to 1.5 times the rated value and acceleration is quicker, initial time period during which stator flux deviations exceed the hysteresis band is shorter and the flux deviations are smaller, when compared with figure 5.3a. However, initial stator current (not shown here) attains higher value than in figure 5.3a.

Stator flux ripple (figure 5.3b) settles within the prescribed hysteresis band once the motor exits the low speed region. In general, stator flux behaviour is very similar for torque and speed mode of operation, as was to be expected. Very much the same applies to the torque response as well. Torque in figure 5.3b is kept within the prescribed hysteresis band at low and medium speeds. However, in the vicinity of rated speed and at rated speed, torque ripple exceeds the hysteresis band. Since speed controller now exists, average value for torque is equal to the applied load torque in any steady state. This means that the torque reference, produced by the PI speed controller must now be somewhat larger than the actual motor average output torque.

5.2.4 Braking mode and low speed operation

The operation of the direct torque controlled induction machine with speed measurement in braking mode is investigated in this sub-section. The induction motor is at first accelerated to one half of the rated speed (150.8 rad/s). Speed command is then reduced to 10 rad/s. The machine is kept running at this speed for a while to obtain the flux and torque response at low speed. The first second after starting is simulated. Figure 5.4a shows speed command and actual speed of the induction motor. The actual

speed follows the speed command and in the steady state it has the same value as the speed command. Figure 5.4b shows the torque response. The torque is again limited to 1.5 times the rated torque and it attains this value during both acceleration and braking. During both steady states (at 150.8 rad/s and at 10 rad/s), the actual torque is zero. Torque response is very quick and symmetrical during acceleration and deceleration.

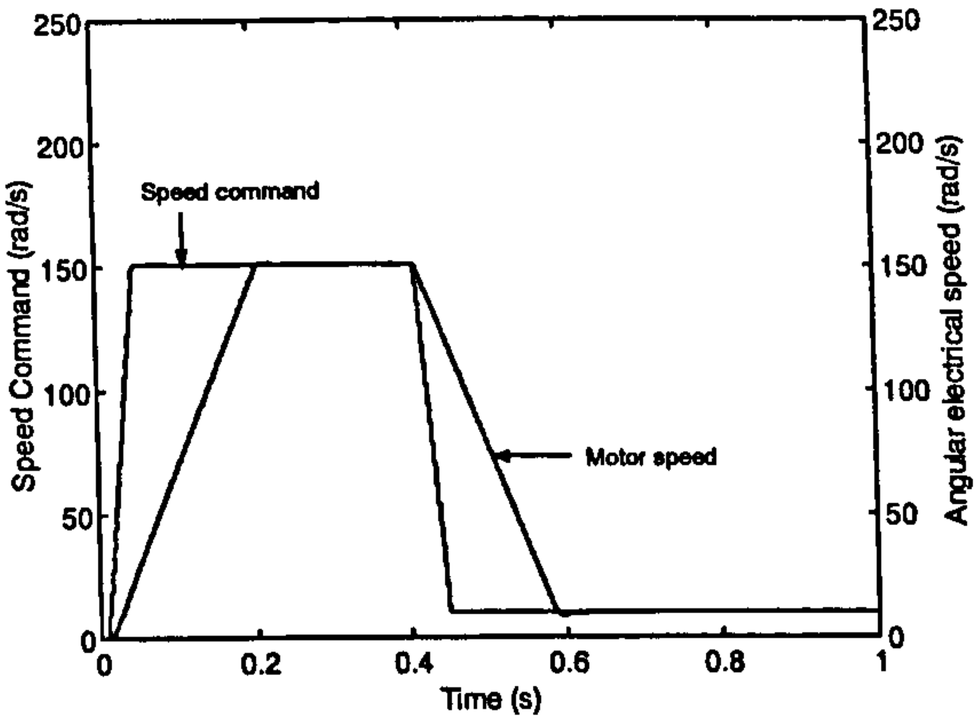

a)

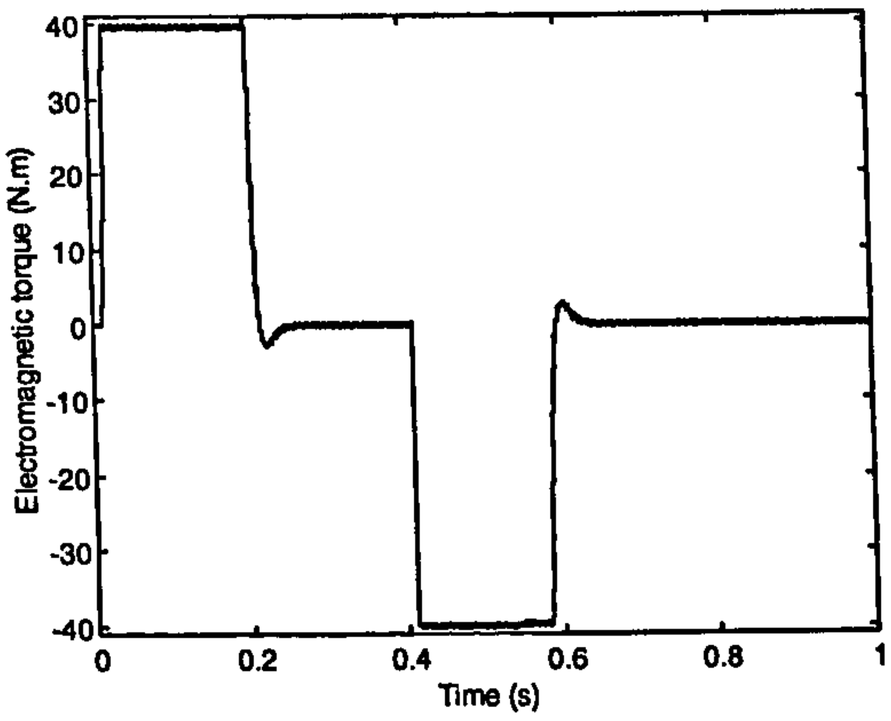

b)

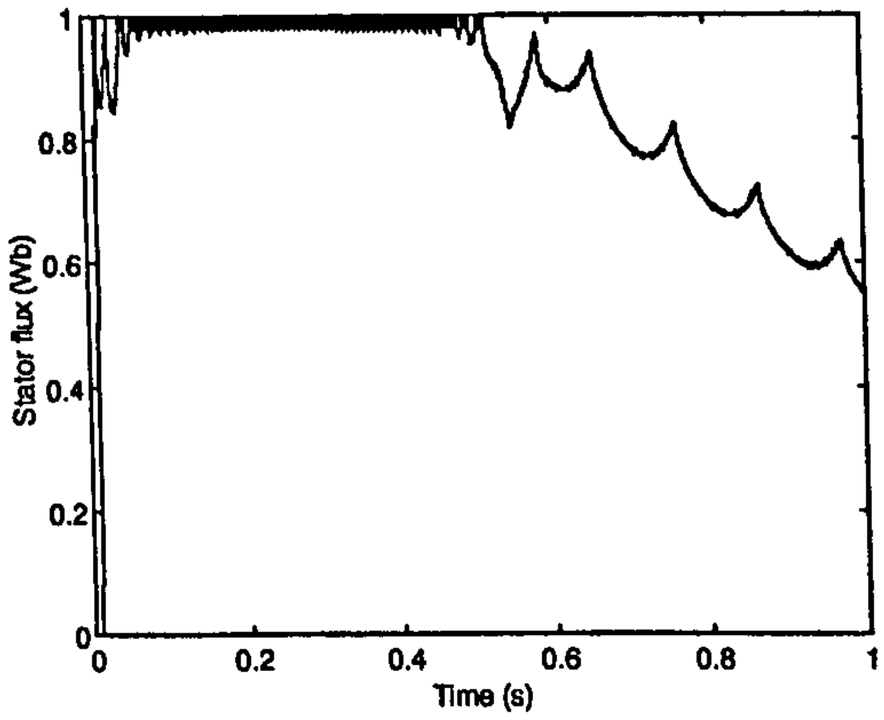

c)

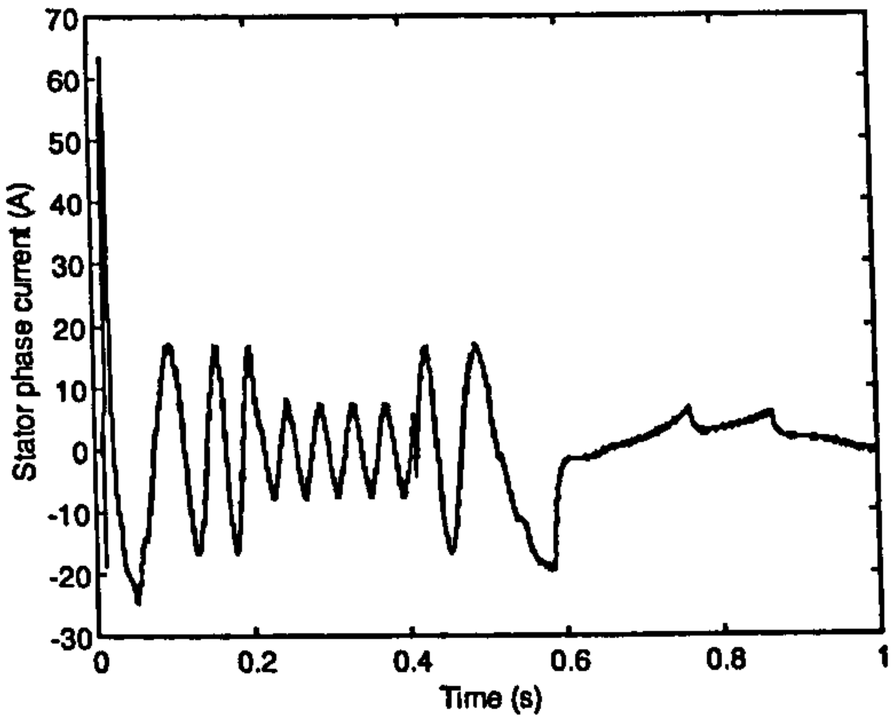

d)

Figure 5.4: Induction motor in low speed operation, a) actual speed and speed command, b) motor torque, c) stator flux, d) stator current.

Stator flux response during acceleration and at 150 rad/s is similar to the response obtained before in speed mode of DTC. The stator flux, however, is significantly weakened when speed is reduced from medium region to low region. When the actual speed reaches steady state at 10 rad/s, the stator flux has been reduced to approximately 55% of the rated flux, and it keeps decreasing during the operation at 10 rad/s. This weakened stator flux is the main disadvantage of Takahashi switching table. The control scheme is unable to maintain the flux at reference value at low and

zero speed. This leads to the under-excited state of the induction motor when operating at low speed with DTC.

The response of stator phase current is shown in figure 5.4d. As already noted in the previous sub-section, stator current peak value during acceleration to one half of the rated speed is unrealistically high (63 A) due to the omission of the current limiting from the simulation models.

Problems inherent to the Takahashi's switching table have led to development of a number of modified switching table. These will be discussed in the next section. Modified schemes aim at either improving flux response at low speed by reducing flux ripple and maintaining flux response within the limited range or at improving torque response at high speed by reducing torque ripple. Most of the modifications of the original switching scheme try to make different selection of voltage vectors while not increasing the frequency of the inverter and still obtaining the satisfactory improvements in the torque and/or flux response. Some other modified switching schemes improve the response of the drive at the expense of an increase in the switching frequency.

5.3 Modified switching tables

A number of modifications for Takahashi's switching table have been suggested in literature. Some of the existing solutions will be presented in this section. These solutions are selected because of their feasibility for practical implementation, simplicity of the algorithm, which does not require complicated software and hardware, and effectiveness in reducing torque and/or flux problems. A novel switching table for improved low speed and high speed control is presented at the end of this section.

5.3.1 Speed dependent switching table

The first of the modifications is the improvement of switching table proposed by [Casadei et al (1994)]. The authors first analyse different switching strategies for two-quadrant and four-quadrant operation, which have been suggested before and then introduce a new switching strategy, which is dependent on motor speed. The switching table for the two-quadrant operation is given in table 5.1. Voltage space vectors for positive motor speed are shown in the table. Active forward voltage vectors v_{k+1} and

v_{k+2} are used to increase torque. To decrease torque, the switching strategy uses either zero voltage vectors v_0 (method A), or radial voltage vectors v_k, v_{k+3} (method C), or a combination of radial and zero voltage vectors v_k, v_0 (method B). These switching schemes are used for the case when stator flux space vector rotates in one direction (positive direction for the switching strategies of table 5.1) and the machine's torque can be positive (for motoring) or negative (for braking).

Switching strategy for four-quadrant operation is given in table 5.2. The active backward voltage space vectors are used in this scheme instead of zero vectors or radial vectors for torque reduction. This strategy can be used when the stator flux space vector is required to rotate in two directions [Casadei et al (1994)]. However, this switching strategy results in high switching frequency of the inverter because of large voltage vector components tangential to the stator flux vector locus [Casadei et al (1994)]. The authors suggest a new switching scheme for four-quadrant operation, which is dependent on speed of the machine. The strategy is presented in table 5.3.

Table 5.1: Voltage vector selection strategies for two-quadrant operation [Casadei et al (1994)].

	$T_e\uparrow$	$T_e\downarrow$		
		A	B	C
$\psi_s\uparrow$	v_{k+1}	v_0	v_k	v_k
$\psi_s\downarrow$	v_{k+2}	v_0	v_0	v_{k+3}

Table 5.2: Voltage vector selection strategy for four-quadrant operation [Casadei et al (1994)].

	$T_e\uparrow$	$T_e\downarrow$
$\psi_s\uparrow$	v_{k+1}	v_{k-1}
$\psi_s\downarrow$	v_{k+2}	v_{k-2}

Table 5.3: Speed-dependent voltage vector selection strategy [Casadei et al (1994)].

High negative speed $(\omega_r < -\omega_{\lim})$			Low speed region $(-\omega_{\lim} \le \omega_r \le \omega_{\lim})$			High positive speed $(\omega_r > \omega_{\lim})$		
	$T_e\uparrow$	$T_e\downarrow$		$T_e\uparrow$	$T_e\downarrow$		$T_e\uparrow$	$T_e\downarrow$
$\psi_s\uparrow$	v_0	v_{k-1}	$\psi_s\uparrow$	v_{k+1}	v_{k-1}	$\psi_s\uparrow$	v_{k+1}	v_0
$\psi_s\downarrow$	v_0	v_{k-2}	$\psi_s\downarrow$	v_{k+2}	v_{k-2}	$\psi_s\downarrow$	v_{k+2}	v_0

Three different switching tables are used for three different ranges of speed. A speed limit is chosen to be about 20% of the rated speed and it defines the low speed region (where the absolute value of motor speed is less than or equal to the speed limit). It includes both positive and negative speeds. When the speed is positive (or negative) and outside the low speed region, another switching table is used. This switching table is similar to the one suggested by Takahashi for positive speed (or negative speed) to ensure the low switching frequency. When the speed falls into the low speed region, the switching table similar to the one for four-quadrant operation (table 5.2) is used. Because the machine operates at relatively low speed, the problem of high switching frequency of this switching table is avoided. Zero vectors are not used at low speed in this strategy; therefore, the problem of weakened stator flux in DTC at low speed is also avoided. This problem of Takahashi's switching table is observed in starting of the motor, during braking and during operation at low speed, as already mentioned. However, the problems related to zero vector application at high speed are not addressed in this strategy.

5.3.2 Switching table for zero speed control

The second suggestion for improvement of Takahashi's switching table was presented by [Alfonso et al (1999)]. This switching strategy is speed-independent and it concentrates on the reduction of stator flux demagnetisation (or flux weakening). Modifications are made in stator flux hysteresis comparator, stator flux complex plane division and switching table. The improvement also aims at avoiding an increase in switching frequency, which is practically dependent on machine parameters and DC link voltage of the inverter [Alfonso et al (1999)]. This modified strategy is a combination of Takahashi's switching table, which is considered the best from zero voltage application point of view and a modified switching table, called "magnetising look-up table" by the authors. Magnetising look-up table attempts to produce a strong magnetisation, independent of stator flux position [Alfonso et al (1999)].

The first modification in this scheme is the stator flux hysteresis comparator. The two-level hysteresis comparator, used in traditional DTC, has been replaced with a three-level hysteresis comparator shown in figure 5.5. This comparator will also determine the transition between the traditional switching table of Takahashi and the other one. When the stator flux error exceeds an upper limit, the stator flux is already

below the lower hysteresis band. The output of the hysteresis comparator goes to level 2 and DTC is switched to magnetising look-up table to produce strong magnetisation in the induction machine. When stator flux exceeds upper hysteresis band, the hysteresis comparator is turned off and DTC reverts to Takahashi's switching table.

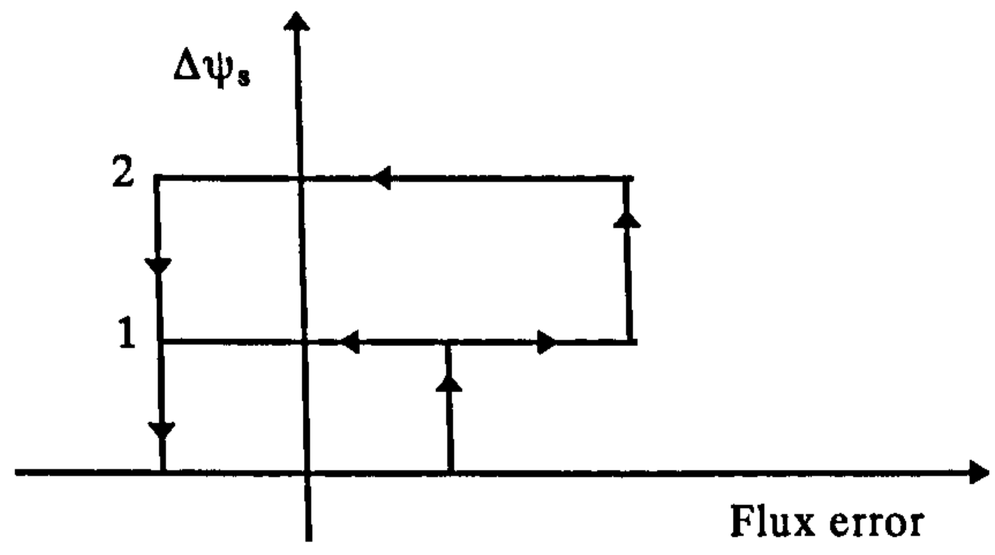

Figure 5.5: Asymmetric three-level hysteresis comparator [Alfonso et al (1999)].

The stator flux complex plane is also modified in this new strategy. The six original sectors for the traditional switching table are replaced by a set of new sectors, created by rotating the reference axis +30 degrees (for the positive speed; two-quadrant operation is considered in this strategy). The new sectors will be used for the magnetising look-up table, therefore, they are numbered from 7 to 12 to avoid the confusion with the original ones. The modified complex plane is shown in figure 5.6. The sectors in this new complex plane are bound by the inverter voltage vectors. Applying them in the respective sectors will give both strong magnetisation and fast increasing (or decreasing) torque at the same time [Alfonso et al (1999)].

The switching table with magnetising switching strategy is presented in table 5.4. Zero voltage vectors are not used in the magnetising look-up table; therefore, the demagnetisation of stator flux is avoided. Torque comparator output has the values of 1 and –1 only, so the zero voltage vectors are not applied to the induction machine.

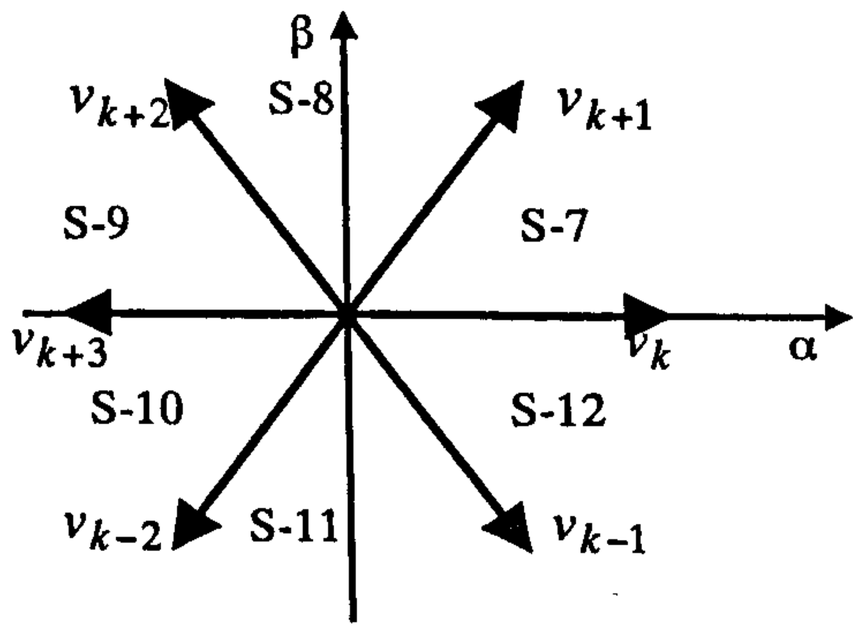

Figure 5.6: Sector division used for magnetising look-up table [Alfonso et al (1999)].

Table 5.4: Look-up table of [Alfonso et al (1999)].

$\Delta\psi_s = 1$	ΔT_e	Sector 1	Sector 2	Sector 3	Sector 4	Sector 5	Sector 6
	1	v_{k+1}	v_{k+2}	v_{k+3}	v_{k-2}	v_{k-1}	v_k
	0	v_{000}	v_{111}	v_{000}	v_{111}	v_{000}	v_{111}
	-1	v_{k-1}	v_k	v_{k+1}	v_{k+2}	v_{k+3}	v_{k-2}
$\Delta\psi_s = 0$	ΔT_e	Sector 1	Sector 2	Sector 3	Sector 4	Sector 5	Sector 6
	1	v_{k+2}	v_{k+3}	v_{k-2}	v_{k-1}	v_k	v_{k+1}
	0	v_{000}	v_{111}	v_{000}	v_{111}	v_{000}	v_{111}
	-1	v_{k-2}	v_{k-1}	v_k	v_{k+1}	v_{k+2}	v_{k+3}
$\Delta\psi_s = 2$	ΔT_e	Sector 7	Sector 8	Sector 9	Sector 10	Sector 11	Sector 12
	1	v_{k+1}	v_{k+2}	v_{k+3}	v_{k-2}	v_{k-1}	v_k
	-1	v_k	v_{k+1}	v_{k+2}	v_{k+3}	v_{k-2}	v_{k-1}

5.3.3 Switching table with increased switching frequency

Another improvement of the switching table was suggested by [Liu and Chen (1998)]. Modification of torque hysteresis comparator and switching scheme are carried out in this strategy. Five-level torque hysteresis comparator is used instead of three-level torque comparator. The inverter is switched twice in one sampling period to synthesise more than eight available voltage vectors (zero vectors and the other six active voltage vectors) [Liu and Chen (1998)]. Another six active voltage vectors are created in this way. Each of the new voltage vectors is synthesised by using two adjacent original voltage vectors in one sampling period, and each of these two voltage vectors is applied in one half of the sampling period. This concept is illustrated in figure 5.7 and by the following equation:

$$\underline{v}_{ij} = \frac{1}{2}\underline{v}_i + \frac{1}{2}\underline{v}_j \tag{5.7}$$

where $\underline{v}_i, \underline{v}_j$ are the voltage vectors of the inverter and $\underline{v}_{ij}$ is the voltage vector synthesised from these vectors.

The synthesised vectors, however, do not have the same magnitude and position as the original vectors. Therefore, applying these vectors to the induction machine will not give the same torque and flux response as those that would have been obtained with the original vectors. All the 12 non-zero, active voltage vectors are shown in figure 5.8.

These vectors will give more flexibility to control the stator flux space vector, and consequently, torque and stator flux response of the induction machine.

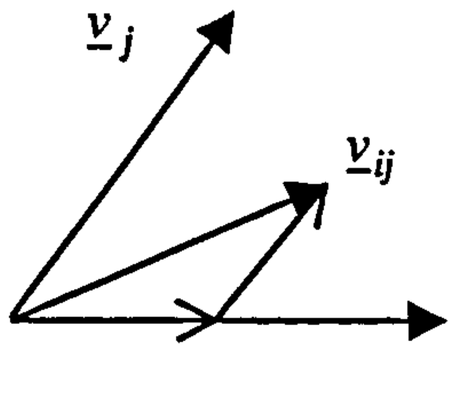

Figure 5.7: Voltage vector synthesis [Liu and Chen (1998)].

The torque hysteresis comparator used here has 5 levels and two hysteresis bands. The output of the comparator is similar to the output of the three-level hysteresis comparator used in the original strategy of Takahashi. It is equal to 1 if torque needs to be increased and equal to 2 if torque needs to be increased and already exceeds the inner hysteresis band. It is equal to 0 if there is no requirement for change in torque. Similarly, it is equal to –1 if torque needs to be decreased, and equal to –2 if torque needs to be decreased and already exceeds the inner hysteresis band. The modified switching table is presented in table 5.5. The switching frequency in this strategy has been doubled to obtain a better controllability of torque and stator flux.

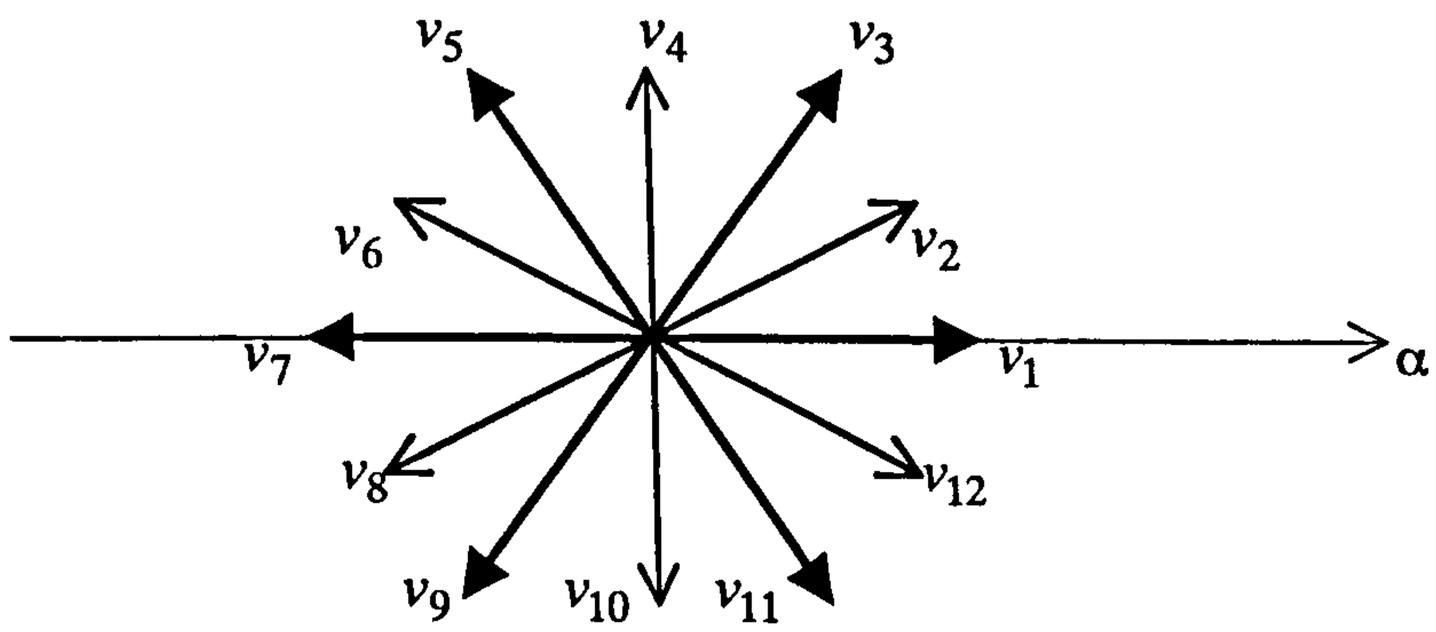

Figure 5.8: 12 distinct active voltage vectors [Liu and Chen (1998)].

Table 5.5: Switching table for DTC suggested by [Liu and Chen (1998)].

ΔT_e	2	1	0	-1	-2
$\Delta\psi_s = 1$	v_{2k+1}	v_{2k}	v_0	v_{2k+10}	v_{2k+9}
$\Delta\psi_s = 0$	v_{2k+3}	v_{2k+4}	v_0	v_{2k+6}	v_{2k+7}

5.3.4 Switching table for improved dynamic torque behaviour in four-quadrant operation

This control strategy was proposed by [El Hassan et al (1997)]. Equations for torque dynamic variation are derived from the differential equations of an induction machine model in stationary reference frame, given in chapter 3 and repeated here for convenience.

$$\begin{aligned} \underline{v}_s &= R_s \underline{i}_s + L_{\sigma s} \frac{d\underline{i}_s}{dt} + L_m \frac{d(\underline{i}_s + \underline{i}_r)}{dt} \\ 0 &= R_r \underline{i}_r + L_{\sigma r} \frac{d\underline{i}_r}{dt} + L_m \frac{d(\underline{i}_s + \underline{i}_r)}{dt} - j\omega_r \underline{\psi}_r \end{aligned} \tag{5.8}$$

It is assumed that: $L_m >> L_{\sigma s}, L_{\sigma r}$ and $L_m \frac{d(\underline{i}_s + \underline{i}_r)}{dt} \cong 0$; therefore, $\underline{i}_s \cong -\underline{i}_r$.

By subtracting the second equation of the model from the first one, a reduced model is obtained.

$$\underline{v}_s = (R_s + R_r)\underline{i}_s + (L_{\sigma s} + L_{\sigma r})\frac{d\underline{i}_s}{dt} + j\omega_r \underline{\psi}_r \tag{5.9}$$

In the stationary reference frame, the current derivative and flux derivative ($\frac{d\underline{\psi}_s}{dt} = \underline{v}_s - R_s \cdot \underline{i}_s$) are known. Therefore, torque derivative can be obtained, starting from the torque equation as in (5.10), and using equation (5.9), as follows [El Hassan et al (1997)]:

$$T_e = \frac{3}{2} P\left(\psi_{\alpha s} i_{\beta s} - \psi_{\beta s} i_{\alpha s}\right) \tag{5.10}$$

and

$$\frac{dT_e}{dt} = \frac{3P}{2(L_{\sigma s} + L_{\sigma r})}\left[\left(v_{\beta s}\psi_{\alpha r} - v_{\alpha s}\psi_{\beta r}\right) - \omega_r\left(\psi_{\alpha s}\psi_{\alpha r} + \psi_{\beta s}\psi_{\beta r}\right) - \frac{(R_s + R_r)}{P} T_e\right] \tag{5.11}$$

When a zero voltage space vector is applied, torque variation is expressed as in the following equation.

$$\frac{dT_e}{dt} = \frac{3P}{2(L_{\sigma s} + L_{\sigma r})}\left[-\omega_r\left(\psi_{\alpha s}\psi_{\alpha r} + \psi_{\beta s}\psi_{\beta r}\right) - \frac{(R_s + R_r)}{P} T_e\right] \tag{5.12}$$

In motoring, ω_r and T_e have the same signs. Therefore, the sign of torque variation can be determined from the direction of rotation, as shown in (5.13):

$$\begin{aligned} &\frac{dT_e}{dt} < 0 \text{ if } \omega_r > 0 \\ &\frac{dT_e}{dt} > 0 \text{ if } \omega_r < 0 \end{aligned} \tag{5.13}$$

During generating, ω_r and T_e have opposite signs. Therefore:

$$\frac{dT_e}{dt}=0 \text{ if } T_e=-\frac{P\left(\psi_{\alpha s}\psi_{\alpha r}+\psi_{\beta s}\psi_{\beta r}\right)}{\left(R_s+R_r\right)}\omega_r \tag{5.14}$$

$$\frac{dT_e}{dt}<0 \text{ if } T_e>-\frac{P\left(\psi_{\alpha s}\psi_{\alpha r}+\psi_{\beta s}\psi_{\beta r}\right)}{\left(R_s+R_r\right)}\omega_r \quad \text{(zoneB)} \tag{5.15}$$

$$\frac{dT_e}{dt}>0 \text{ if } T_e<-\frac{P\left(\psi_{\alpha s}\psi_{\alpha r}+\psi_{\beta s}\psi_{\beta r}\right)}{\left(R_s+R_r\right)}\omega_r \quad \text{(zoneA)} \tag{5.16}$$

Zone A and zone B are defined in the torque-speed plane as shown in figure 5.9.

The zero torque derivative line in T_e-ω_r plane as shown in figure 5.9a is the line $T_e=-\frac{P\left(\psi_{\alpha s}\psi_{\alpha r}+\psi_{\beta s}\psi_{\beta r}\right)}{\left(R_s+R_r\right)}\omega_r$. Stator flux, rotor flux, stator resistance and rotor resistance are required to calculate the location of torque derivative operating point for each pair of torque and rotor speed values. The control scheme is therefore more dependent on machine's parameters.

The zones defined in figure 5.9b are used to select appropriate voltage space vector when stator flux value is in those zones. Table 5.6 shows the switching table for this analytical control scheme of DTC. This switching table requires up to four inputs to decide which voltage space vector is to be applied to the induction machine, one input more than the traditional Takahashi's switching table.

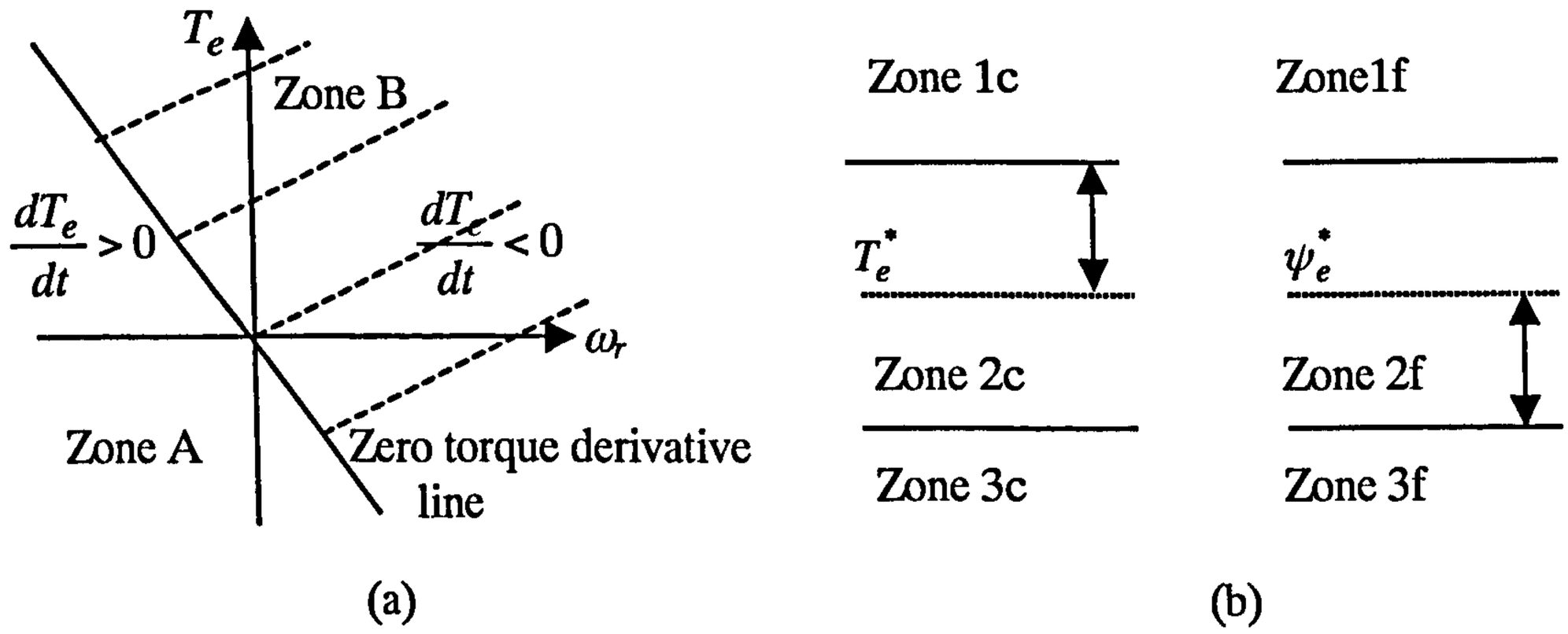

Figure 5.9: a) Sign of torque derivative variation in the torque-speed plane when a zero voltage vector is applied, and b) Flux and torque zones for voltage space vector selection [El Hassan et al (1997)].

Table 5.6: Switching table of [El Hassan et al (1997)]

ψ_s	3f	2f	1f	3f	2f	1f	3f	1f
T_e	3c	3c	3c	1c	1c	1c	2c	2c
Sector 1	v_2	v_0	v_0	v_6	v_6	v_5	v_1	v_0
Sector 2	v_3	v_7	v_7	v_1	v_1	v_6	v_2	v_7
Sector 3	v_4	v_0	v_0	v_2	v_2	v_1	v_3	v_0
Sector 4	v_5	v_7	v_7	v_3	v_3	v_2	v_4	v_7
Sector 5	v_6	v_0	v_0	v_4	v_4	v_3	v_5	v_0
Sector 6	v_1	v_7	v_7	v_5	v_5	v_4	v_6	v_7
ZONE A								
Sector 1	v_2	v_2	v_3	v_6	v_0	v_0	v_1	v_0
Sector 2	v_3	v_3	v_4	v_1	v_7	v_7	v_2	v_7
Sector 3	v_4	v_4	v_5	v_2	v_0	v_0	v_3	v_0
Sector 4	v_5	v_5	v_6	v_3	v_7	v_7	v_4	v_7
Sector 5	v_6	v_6	v_1	v_4	v_0	v_0	v_5	v_0
Sector 6	v_1	v_1	v_2	v_5	v_7	v_7	v_6	v_7
ZONE B								

5.3.5 A novel switching table for improved low speed and high speed control

The modified switching tables in sections 5.3.1 and 5.3.2 aim at improving performance at low speed by avoiding the use of zero vectors. However, at high speed, the modified switching table is essentially the same as the original one. Therefore, the main problem of DTC at high speed, high torque ripple, is not eliminated or reduced. Zero voltage vectors are used at high speed for torque decrease, to reduce switching frequency of the inverter. With respect to the switching table for zero speed control, the stator flux stays within the hysteresis bands at high speed. Therefore, the outputs of the stator flux hysteresis comparator are only 0 or 1. However, high flux ripples at low speed, caused by demagnetisation, would give the output of the comparator the value of 2. Zero vectors are then prevented from being applied. The demagnetisation problem is eliminated without dependence on machine speed. This would be a better solution for low speed problems of DTC. The effect of machine speed on non-zero voltage vector

performance at high speed has been investigated experimentally in [Bertoluzzo et al (1999), Chen and Li (1999)]. Torque ripple has been shown to vary from a positive value to a negative value when stator flux position rotates in positive direction within the *k*-th sector and voltage vector v_{k+1} is applied for the whole sector, while the machine is running at rated speed. The torque variation is supposed to be positive to increase electromagnetic torque. The performance deteriorates in the vicinity of the border between the *k*-th and the (*k*+1)-th sector. Similarly, with voltage vector v_{k+2}, torque variation varies from negative to positive, at rated speed, instead of being positive. This explains the high torque ripples at high speed, present with DTC.

A new switching table is suggested in [Pham-Dinh and Levi (2001b)]. Three-level flux hysteresis comparator and the rotation of +30 degrees of the reference frame, as suggested in section 5.3.2, are still used here. However, when the speed of the induction machine reaches 80% of the rated speed, another rotation of the reference frame is made. The reference frame is rotated –15 degrees from the stationary position, as shown in figure 5.10. The sector 1 is now spanning from -3π/12 to π/12, instead of -π/6 to π/6, the new sector is called 1M. This will avoid the situation of applying voltage vector v_{k+1} in the vicinity of the border between the *k*-th sector and the (*k*+1)-th sector. Voltage vector v_{k+2} is applied instead, to guarantee the positive torque change.

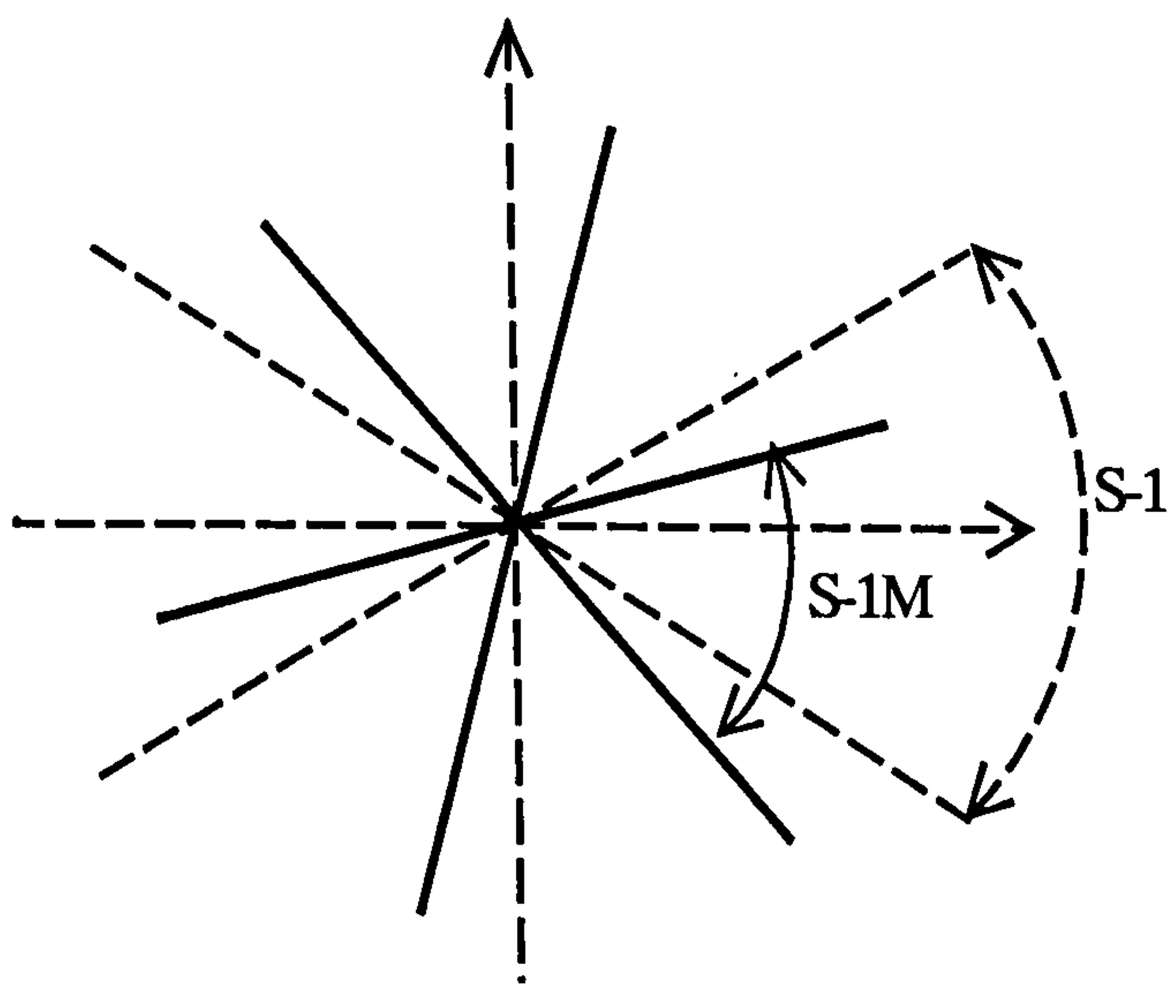

Figure 5.10: Complex plane division at high speed for the new switching table.

The new switching table for improvement of direct torque control in both low and high speed regions is shown in table 5.7.

Table 5.7: Switching table for improved low speed and high speed control.

$\Delta\psi_s = 1$	ΔT_e	S-1 or S-1M	S-2 or S-2M	S-3 or S-3M	S-4 or S-4M	S-5 or S-5M	S-6 or S-6M
	1	v_{k+1}	v_{k+2}	v_{k+3}	v_{k-2}	v_{k-1}	v_k
	0	v_{000}	v_{111}	v_{000}	v_{111}	v_{000}	v_{111}
	-1	v_{k-1}	v_k	v_{k+1}	v_{k+2}	v_{k+3}	v_{k-2}
$\Delta\psi_s = 0$	ΔT_e	S-1 or S-6M	S-2 or S-2M	S-3 or S-3M	S-4 or S-4M	S-5 or S-5M	S-6 or S-6M
	1	v_{k+2}	v_{k+3}	v_{k-2}	v_{k-1}	v_k	v_{k+1}
	0	v_{000}	v_{111}	v_{000}	v_{111}	v_{000}	v_{111}
	-1	v_{k-2}	v_{k-1}	v_k	v_{k+1}	v_{k+2}	v_{k+3}
$\Delta\psi_s = 2$	ΔT_e	Sector 7	Sector 8	Sector 9	Sector 10	Sector 11	Sector 12
	1	v_{k+1}	v_{k+2}	v_{k+3}	v_{k-2}	v_{k-1}	v_k
	-1	v_k	v_{k+1}	v_{k+2}	v_{k+3}	v_{k-2}	v_{k-1}

5.4 Simulation results of DTC using modified switching tables

Simulation results, obtained using switching tables (ST) of sections 5.3.1-5.3.3 and 5.3.5, which are called further on Casadei's, Alfonso's, Liu's and novel switching table, are described in this section. These methods are simple in terms of algorithm and computational capacity of the hardware required, and are therefore more viable in terms of practical realisation. Modification of section 5.3.4 is more dependent on machine parameters and also requires a more complicated switching table.

Speed mode of operation is analysed for the Casadei's, Alfonso's and Liu's switching tables. The responses are then compared with the responses obtained with the original Takahashi's switching table. These modified switching tables are aimed at improving flux response at low speed. The speed command is at first increased from zero to one half of the rated speed and is then reduced to 10 rad/s (ramped reference signal is used). Flux command is equal to rated stator flux at all times. Hysteresis bands

equal to 1% of rated values are used again for both flux and torque hysteresis comparators. Load torque is kept at zero and the first second after motor starting is simulated. The computational step in the simulations is 1μs. The switching frequency for the simulations of Casadei's, Alfonso's and novel switching table is therefore at most 1MHz, while the switching frequency of the simulation of Liu's table, however, is at most 500KHz. The torque, stator flux and speed responses obtained from the simulations of Casadei's and Alfonso's methods discussed are shown in figure 5.11. Torque, speed and stator flux obtained from the simulation using Liu's modification in both speed mode and torque mode are shown in figure 5.12. The corresponding responses with the novel switching table and Takahashi's switching table in torque mode are shown in figure 5.13.

The switching scheme proposed in section 5.3.5 is in fact a modification of the Alfonso's switching table for zero speed control to obtain high torque performance at high speed. Behaviour of the scheme at low and medium speed will therefore be the same as the one illustrated in figure 5.11 for Alfonso's switching method. The simulation is therefore carried out at rated speed. The operating mode of the control system is now torque mode so that the impact of the proposed modification on the torque response of the system can be observed better. Torque mode of operation using Liu's switching table is also simulated for the sake of comparing the torque performance at high speed for different switching tables (figure 5.12b) and response of DTC with Takahashi's switching table in torque mode is re-plotted here for this purpose. Torque and flux commands of rated values are the inputs of the control system. When the motor reaches rated speed, load torque of rated value is applied to keep the speed quasi constant. The first 0.7 seconds after motor starting is simulated for the torque mode of operation.

Simulations related to speed mode of operation have shown that flux response with modified switching tables improves, especially in the low speed region. For the Casadei's modification (figure 5.11a) the flux response always stays within the hysteresis band in the steady state at low speed. Flux ripples exceed hysteresis band during transients, but are significantly reduced compared to the flux ripples of Takahashi's switching table. Distortion in flux response when voltage space vector selection scheme is changed from switching table for high positive speed to switching table for low speed region does not cause distortion in torque response. Flux ripples are

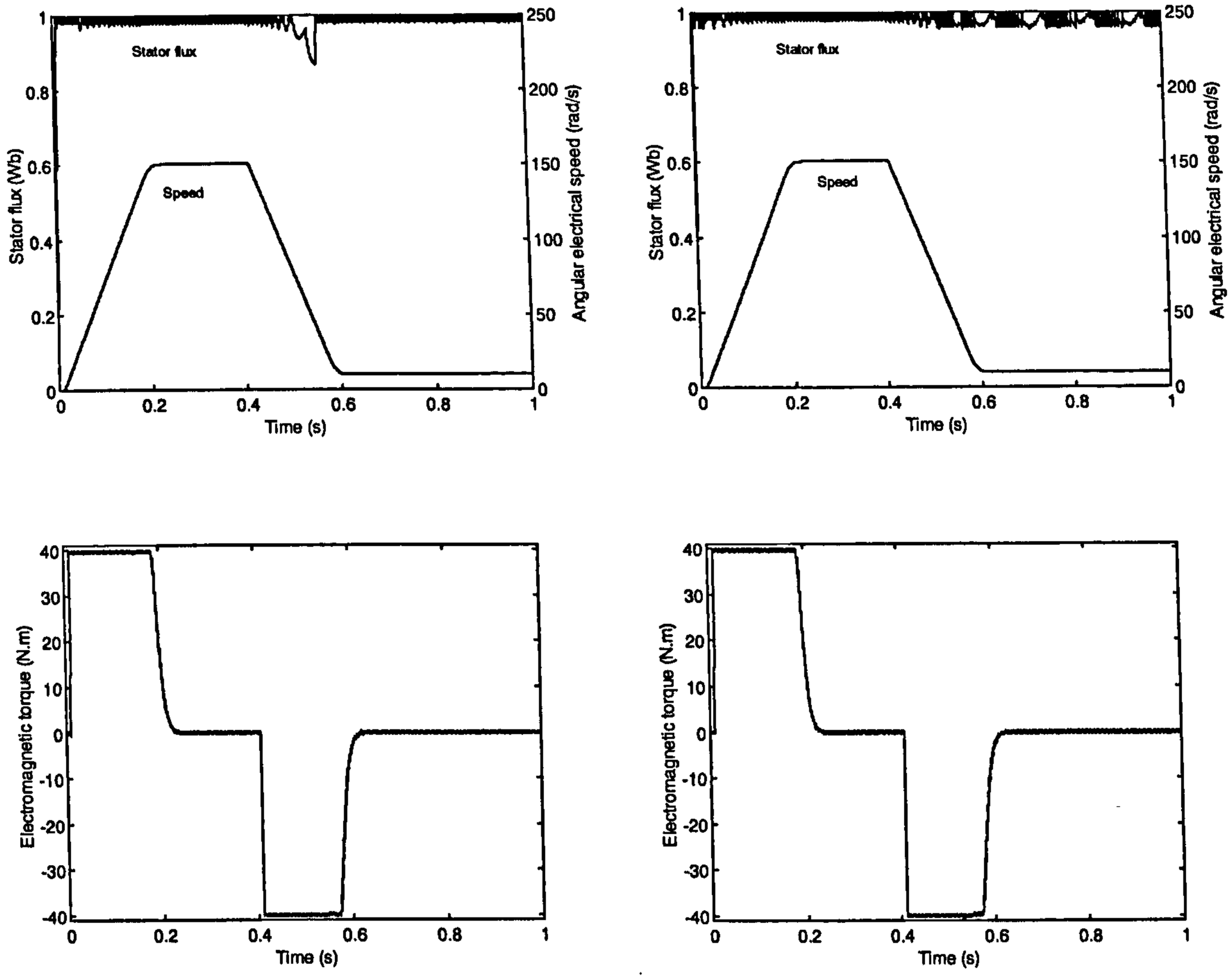

Figure 5.11: a) Torque, stator flux and speed response of DTC with modified Casadei's switching table, b) Torque, stator flux and speed response of DTC with Alfonso's switching table.

high when speed is reduced from medium to low value.

The flux response in DTC with the Alfonso's switching table (figures 5.11b) always stays within the outer hysteresis band. This hysteresis band is three times the inner hysteresis band, 3% of the rated flux. The flux response varies between 97% and 101% of the rated flux during the operation. At the medium and high speed, the flux stays within the inner hysteresis band. At low speed and in dynamic state, it stays within the outer hysteresis band. No uncontrolled flux ripple has been observed.

The flux response of DTC with Liu's switching table (figure 5.12) is also within the hysteresis band at low speed, and is slightly better than the flux response obtained with Casadei's switching table. However, in transient state, when speed is reduced from medium to low value, the flux ripples are significantly higher than those obtained in previous simulations. At low speed, the flux ripple is reduced, although flux is still

outside the hysteresis band when stator flux space vector is in the vicinity of the borders between the sectors in the complex plane. However, the flux response with this switching table at low speed is, in general, still better than the one obtained with Takahashi's table. In speed mode, torque is limited to 1.5 times the rated torque in all the simulations. Torque returns to zero value in the final steady state. The problem of high torque ripple does not take place during the operation of the drive because the speed is only in the low and medium regions.

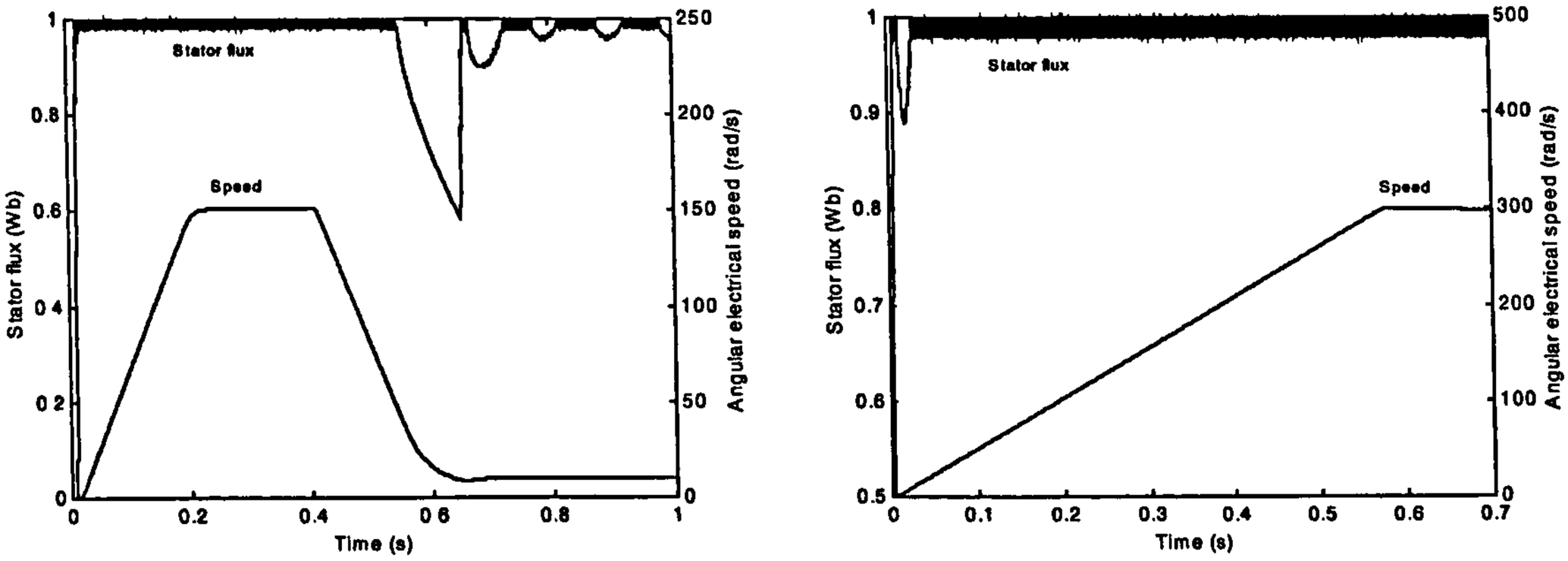

a) b)

Figure 5.12: Torque, stator flux and speed response of DTC with Liu's switching table: a) in speed mode of operation, b) in torque mode of operation.

In torque mode, it is observed that at high speed the flux response of DTC with the novel switching table deteriorates (figure 5.13). Flux ripple is about 5.5% of the rated flux (a large outer hysteresis band for flux control at low speed, 6%, is used in the simulation in torque mode to keep the zero-speed control off; this control scheme does not become active until the flux ripple exceeds the outer hysteresis band, otherwise the

reference frame will be rotated by +30 degrees). The flux responses of the DTC with Liu's switching table and Takahashi's switching table stay well within the hysteresis band of 1% (figures 5.12 and 5.13).

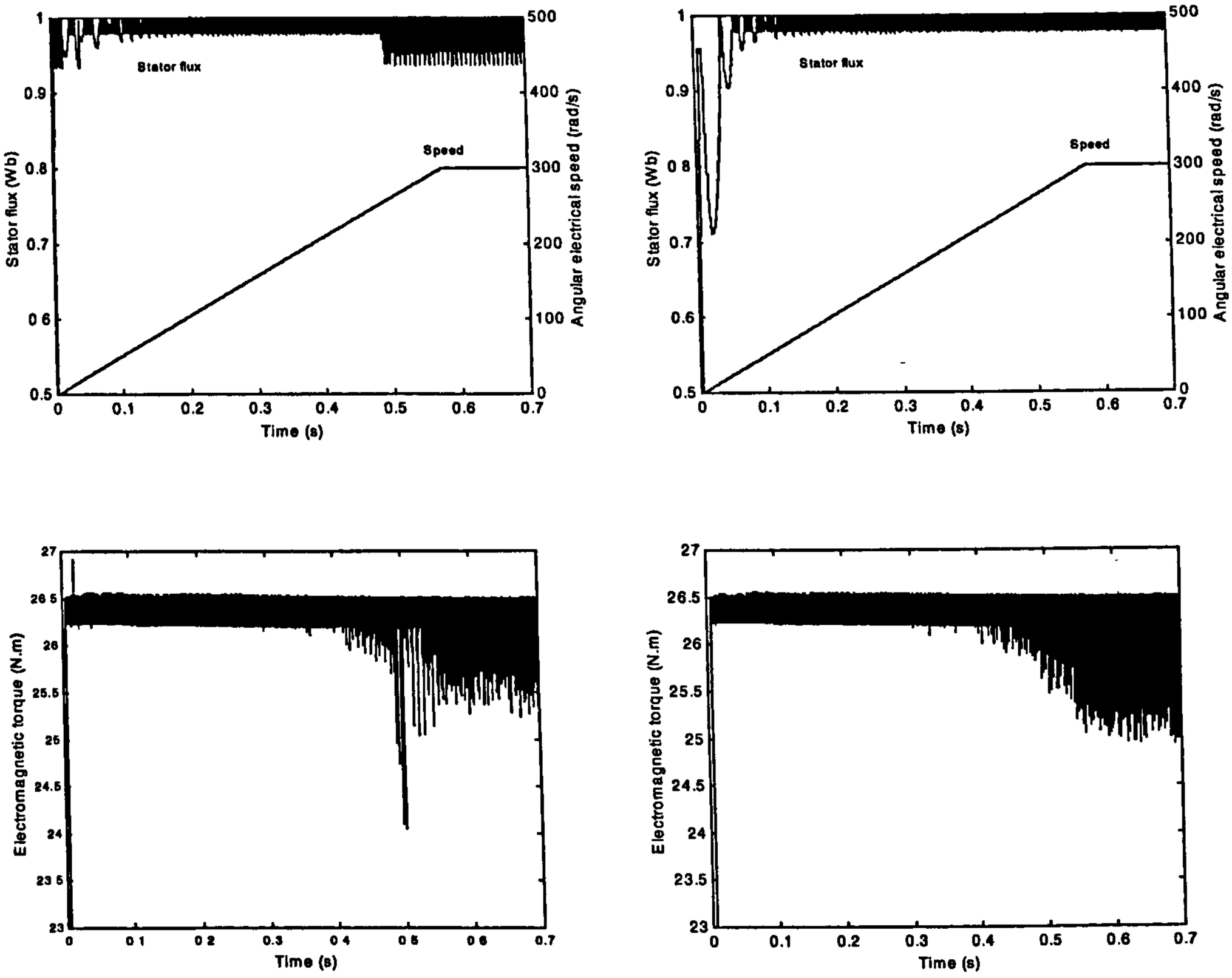

a) b)

Figure 5.13: Torque, stator flux and speed responses of DTC in torque mode with: a) novel switching table, b) original switching table of Takahashi.

Torque response of DTC with novel switching table of section 5.3.5, however, improves at high speed. Torque ripples are reduced at rated speed, although there are a few significant high torque ripples in the vicinity of rated speed (figure 5.13a). Torque response of DTC with Liu's control scheme, nonetheless, deteriorates at medium and high speed (figure 5.12b). The torque ripple is significantly higher when compared to the one of DTC with Takahashi's switching scheme. The Liu's control scheme aims at improving both torque and flux response. However, only flux response is improved in the low speed region, while torque response is worse when speed is increased. The highest torque ripples are observed at rated speed. The average torque in steady state at

rated speed of novel switching scheme is 26.2934 N.m, the equivalent number for Takahashi's switching scheme is 26.2377 N.m, and the equivalent number for Liu's switching scheme is 25.9681 N.m.

5.5 Summary

DTC with the Takahashi's switching table has been addressed in this chapter. The investigation has analysed the problems of traditional DTC in torque mode, speed mode, and breaking mode. The operation in all the speed regions (low, medium, and high) have also been investigated. The investigation has pointed out the typical problems of demagnetisation of stator flux at low speed and high electromagnetic torque ripple at high speed. Modifications of Takahashi's switching table to improve the performance of DTC have been discussed next. Two modifications aiming at avoiding stator flux demagnetisation at low speed, one modification for torque and flux improvement with higher switching frequency, one modification for torque dynamic behaviour improvement in four-quadrant operation, and one modification for high performance at both low and high speed have been outlined. The last one is the novel scheme developed in this thesis.

Simulations of the modified switching tables for flux response improvement at low speed, modified switching table with increased switching frequency and modified switching table for low-speed and high-speed control have been performed. The simulations show the effectiveness of the modified control schemes in improving flux and torque response of DTC. From the simulations, it has been observed that the modifications for flux improvement at low speed give significantly improved flux response. Good flux response at low speed and significantly higher torque ripples at medium and high speed are the results of the modification with increased switching frequency. The modification for low-speed and high-speed control proposed in section 5.3.5 gives both improved flux response at low speed and reduced torque ripples at high speed.

CHAPTER 6

DIRECT TORQUE CONTROL CONSIDERING THE IRON LOSS

6.1 Introduction

As already noted, the existence of iron loss is normally neglected in derivation of induction machine models. Consequently, operation of all the model-based high performance control schemes is characterised with certain amount of iron loss induced detuning. Impact of iron loss on operation of vector controlled induction machines has been examined in detail in recent past and numerous methods of iron loss compensation have been suggested, as reviewed in section 2.7. In contrast to such a situation with regard to vector control, it appears that a corresponding study has never been done in conjunction with direct torque control (DTC) of induction machines. The purpose of this chapter is twofold. A detailed simulation study is at first performed, so that the impact of iron loss on accuracy of the direct torque control is examined in detail. Torque mode of operation in the base speed region is considered primarily although examination of speed mode (with speed sensor) of operation is also included. On the basis of the results of detuning investigation, a simple iron loss compensation method is developed. Its accuracy is verified by simulation. Further simplifications of the iron loss compensation scheme are investigated and it is shown that, for certain machines, iron loss can be effectively compensated by simple deduction of a constant, iron loss related, torque component from the initial torque estimate. The main original results of this chapter have been published in Pham-Dinh and Levi (2001a), Levi and Pham-Dinh (2002), and Levi and Pham-Dinh (2001).

6.2 Iron loss representation and simulation process of DTC considering the core loss

6.2.1 Iron loss representation in machine model

The induction motor model, with included iron loss representation, is formulated on the basis of the dynamic space-vector equivalent circuit already described in

subsection 3.3.1 and displayed here again for convenience in figure 6.1 [Levi (1994), Levi (1996)]. Stationary reference frame ($\omega_a = 0$) is utilised. Equivalent iron loss resistance R_{Fe} is placed in parallel to the magnetising branch and is a function of the operating stator frequency, as indicated in figure 6.1. Such an approach to iron loss modelling has been used extensively in discussion of iron loss impact on vector controlled induction machines and in development of appropriate compensation schemes. However, due to inherent differences between the vector control and DTC, the circuit of figure 6.1 is, strictly mathematically, incorrect for representation of an induction machine subjected to DTC. This issue, already identified in subsection 3.3.1, is felt to be important and it therefore deserves further clarifications.

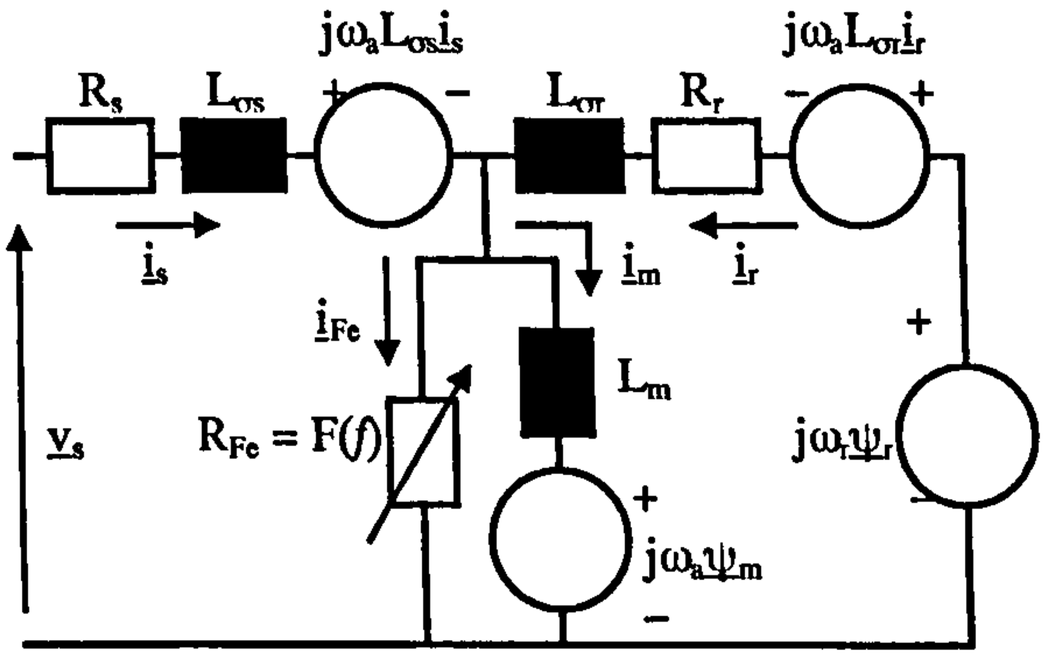

Figure 6.1: Space vector dynamic equivalent circuit of an induction machine with included iron loss representation.

As explained in subsection 3.3.1, the equivalent iron loss resistance in figure 6.1 models the fundamental component of the iron loss and is calculated from experimentally determined fundamental iron loss. PWM inverter supply inevitably leads to occurrence of higher voltage harmonics, which produce additional harmonic iron loss components. This however does not have any influence on the accuracy of the iron loss representation when vector control is under consideration. This is so because a vector controller is a fundamental harmonic controller and impact of iron loss on the operation of the drive can be analysed assuming ideal sinusoidal conditions in steady state operation [Levi (1994)]. When dynamics of a vector controlled induction motor drive are simulated, the inverter can be completely omitted from the drive model and the circuit of figure 6.1 is therefore completely valid. In contrast to vector control, DTC can only be analysed and simulated if the PWM inverter model is included, since the basic

DTC principles make use of the non-ideal inverter nature. When the circuit of figure 6.1 is applied in conjunction with DTC, the equivalent iron loss resistance seen by all of the PWM inverter output voltage harmonics will be the one that accurately represents the fundamental iron loss only. This is an inherent limitation of the application of the circuit of figure 6.1 in analysis of DTC of induction machines. Unfortunately, there appears to be no better solution to the problem. One would ideally need to use the theory of multiple reference frames, in which an appropriate circuit similar to the one of figure 6.1 would be devised for each voltage harmonic. Equivalent iron loss resistance values in these harmonic equivalent circuits could be obtained using the extension of the iron loss identification procedure proposed in [Levi et al (1996)]. However, since DTC relies on hysteresis control, voltage harmonics that will be present in the inverter output voltage cannot be determined in advance; moreover, output voltage spectrum is continuous, so that application of the multiple reference frame theory is not possible.

Since the circuit of figure 6.1 is used in simulation, the fundamental component of the iron loss is correctly represented, while all the higher harmonic components of the iron loss are, at least to some extent, modelled incorrectly. This means that the simulation results, obtained by means of the circuit of figure 6.1, will be correct with respect to the fundamental voltage harmonic behaviour, while the superimposed ripples due to higher voltage harmonics will be of questionable accuracy. This issue will be addressed again once when the simulation results are presented.

As already noted, fundamental iron loss component was determined experimentally, using the procedure of [Levi et al (1996)]. The testing was performed in the frequency range from 10 Hz up to 100 Hz. Base speed region, relevant for the analysis and simulation in this chapter, encompasses frequencies up to 50 Hz. Once when the fundamental iron loss component as function of the operating frequency is known, the equivalent iron loss resistance of figure 6.1 can be easily calculated. Figure 6.2 presents the measurement results related to the fundamental iron loss component (figure 6.2a) and corresponding equivalent iron loss resistance (figure 6.2b). The appropriate analytical approximation of the equivalent iron loss resistance, required for the circuit of figure 6.1, is shown in figure 6.2b as well. Analytical approximation of the fundamental iron loss, included in figure 6.2a, will be required later on for compensation purposes. These analytical functions, obtained using least squares fitting, are given with the following expressions, in terms of fundamental frequency:

$$P_{Fe}(\mathrm{W}) = \begin{cases} 0.00003808 f^4 - 0.004585 f^3 + 0.183 f^2 + 1.0254 f - 0.2784 & f \le 50\,\mathrm{Hz} \\ 0.00002087 f^4 - 0.0073 f^3 + 0.9658 f^2 - 57.684 f + 1468.3 & f > 50\,\mathrm{Hz} \end{cases}$$
$$R_{Fe}(\Omega) = \begin{cases} 128.92 + 8.242 f + 0.0788 f^2 & f \le 50\,\mathrm{Hz} \\ 1841 - 55275/f & f > 50\,\mathrm{Hz} \end{cases} \qquad (6.1)$$

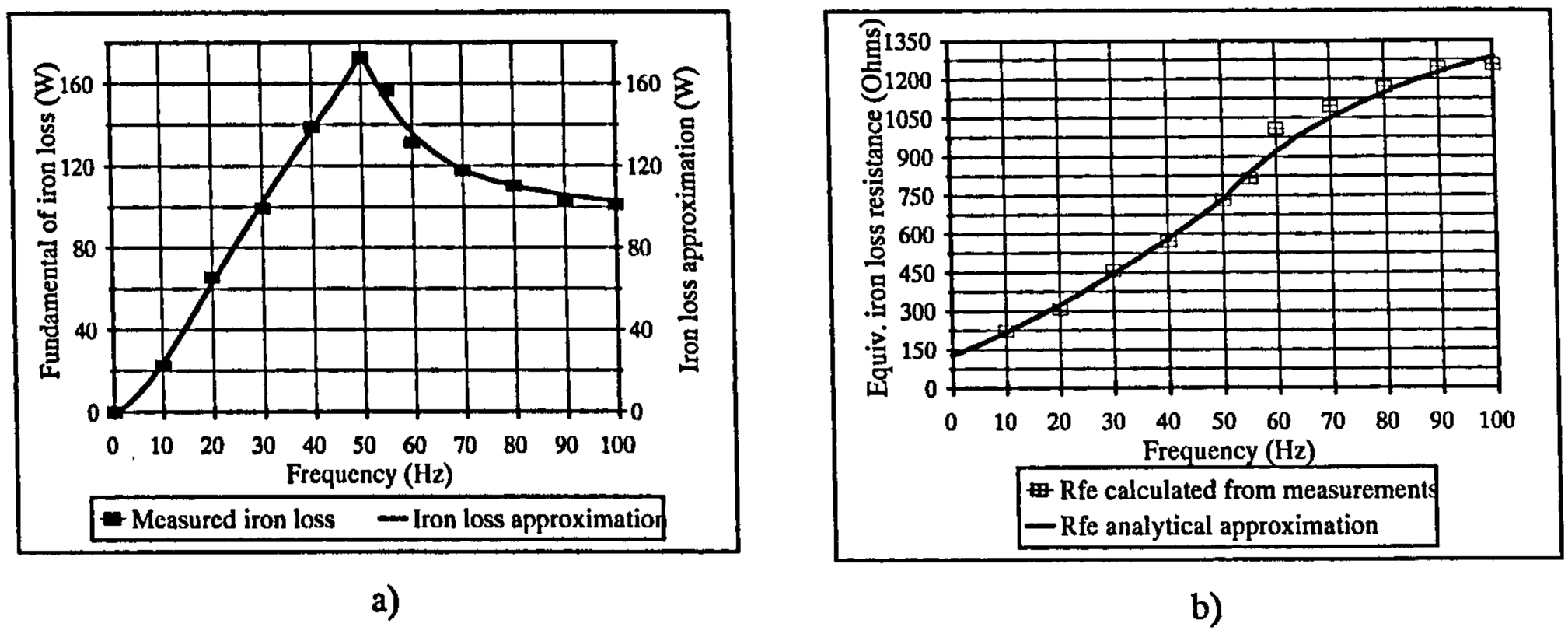

a) b)

Figure 6.2: Fundamental iron loss component a), and calculated equivalent iron loss resistance b): experimentally identified points and corresponding analytical approximations.

6.2.2 Simulation process of DTC considering the core loss

The DTC scheme used in the simulations throughout this chapter is the one explained in subsections 4.3.2 and 4.3.4. Since DTC is inherently sensorless, torque mode of operation in the base speed region is primarily under consideration in this chapter. Speed mode of operation with speed sensor is also examined at a later stage.

The control scheme is implemented in Simulink software. The model of the inverter, as described in section 3.4, is included in the simulation programs. The same 4 kW, 380 V, 8.7 A, 4-pole, 50 Hz, 26.5 Nm motor, whose iron loss characteristics are shown in figure 6.2, is used again (peak rated stator flux is 0.9889 Wb). DC link voltage is once more fixed to the value of 580 V at all times and hysteresis bands in DTC are set again to ±1% of the rated torque and rated stator flux (peak) values. The equations for stator fiux magnitude and position estimation, and torque estimation are (4.19), (4.21) and (4.28).

On the basic of the dynamic equivalent circuit of figure 6.1 and using the general machine model equations with included iron loss (subsection 3.3.1), the induction motor is represented with the system of equations (3.39) to (3.44).

For the display purposes, actual stator flux in the machine is calculated using:

$$\begin{aligned}\psi_{\alpha s} &= L_{\sigma s} i_{\alpha s} + L_m i_{\alpha m} = L_{\sigma s} i_{\alpha s} + \psi_{\alpha m} \\ \psi_{\beta s} &= L_{\sigma s} i_{\beta s} + L_m i_{\beta m} = L_{\sigma s} i_{\beta s} + \psi_{\beta m} \\ \psi_s &= \sqrt{\psi_{\alpha s}^2 + \psi_{\beta s}^2}\end{aligned} \tag{6.2}$$

During the simulation of the torque mode of operation, according to control scheme of figure 4.8, flux command is kept at rated value. A quasi steady state operation at certain speed is achieved by application of an appropriate load torque (since there is always some difference between the load torque and the average motor torque, speed of rotation is never perfectly constant). Torque reference and load torque profiles are shown in figure 6.3. Quasi steady state operation is established at one half of the rated speed and at rated speed, for load torque values equal to one half of the rated (13.25 Nm) and rated (26.5 Nm). Stator flux reference is equal to rated (peak) stator flux at all times. Control scheme for speed mode of operation is the one of figure 4.9.

It should be noted once more that no special care has been taken to limit the stator current during the drive starting (this being the same as in chapters 4 and 5). Stator current will therefore obtain such high values during initial part of the start-up, which could not be tolerated in an actual drive. The voltage source inverter is assumed to be ideal, which means that the voltage source can deliver infinitely high current. This is not the case for a realistic voltage source inverter with semiconductor switches, which can only provide a limited current to the motor. The problem of current limiting in DTC is beyond the scope of interest here, since it does not affect the results of the study in any way.

Simulation of speed mode of operation with speed sensor is carried out with the same machine model as the one used for torque mode. A PID controller with anti-windup is used as a speed controller. The output of the speed controller is passed through a limiter before going into the torque command input of the direct torque controller. The limiter sets the upper and lower limits for torque command, which are $\pm$ 1.5 T_{en}. The anti-windup saturation also has the same upper and lower limits as the output of the speed controller. The parameters of the speed controller are

$$K = 12, b = 1, T_i = 12/800, T_t = 10, T_d = 0, N = 1000$$

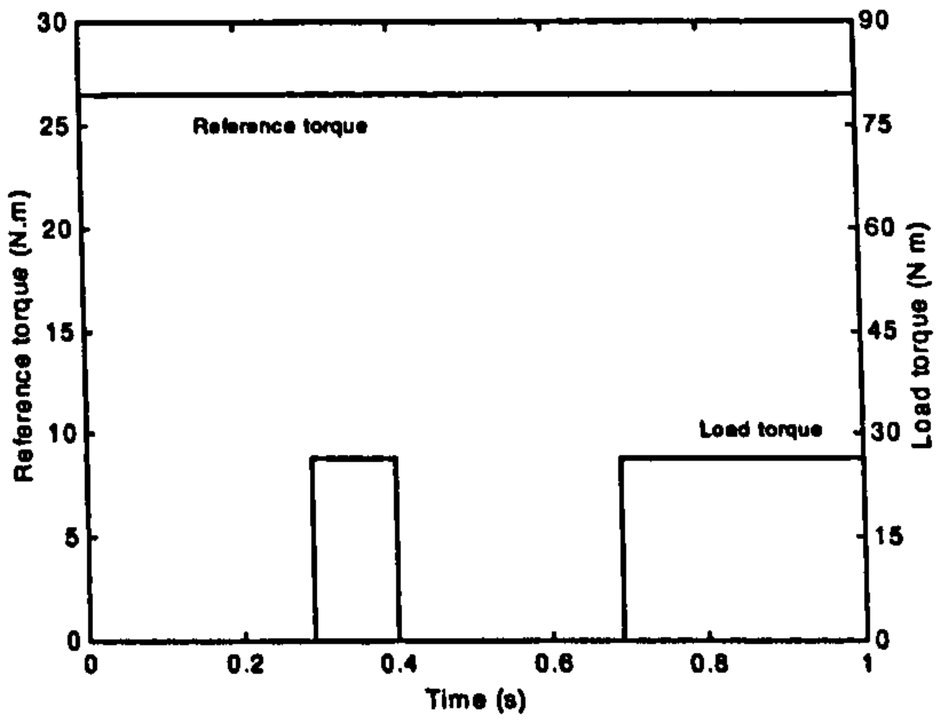

a)

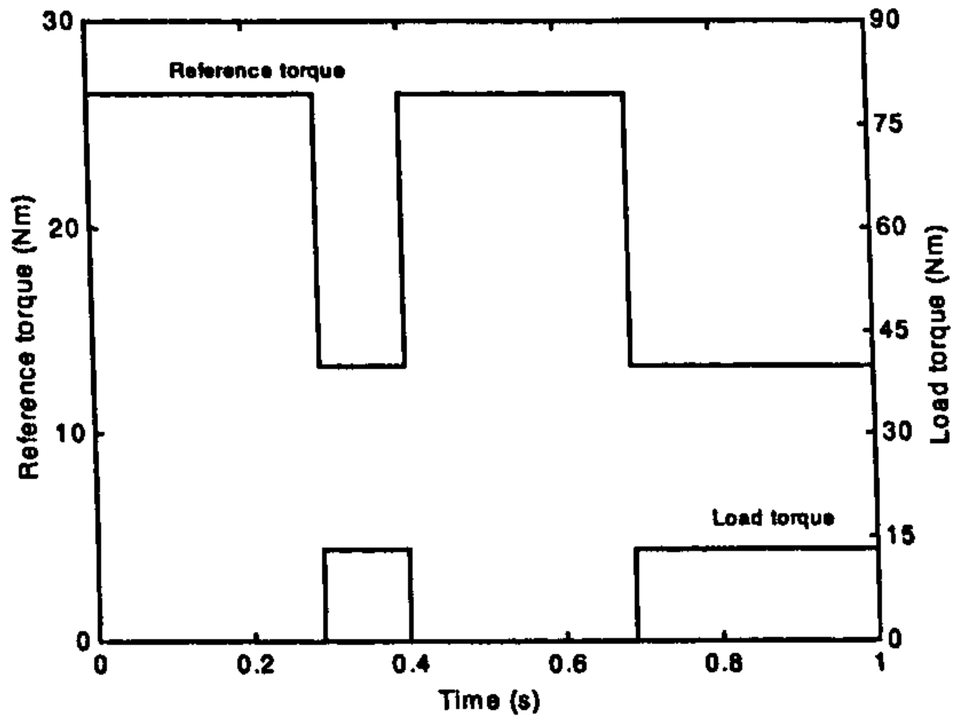

b)

Figure 6.3: Profiles of the reference torque and load torque, used in torque mode simulations, yielding quasi steady states with the rated load torque a) and one half of the rated load torque b).

6.3 Detuning due to iron loss in direct torque controlled induction motor drives

Standard constant parameter model of an induction machine without iron loss (section 3.2) is at first utilised. Figure 6.4 illustrates stator flux, motor torque and speed response that correspond to the two torque profiles of figure 6.3. Well-known problems with high stator flux ripple at low speed and high torque ripple at high speed are again evident. Stator flux is kept within the prescribed 1% hysteresis band, except at low speeds. Torque ripple stays within the 1% hysteresis band, except in vicinity of the rated speed. The traces of figure 6.4 constitute the basis for further evaluation of the impact of iron loss on behaviour of direct torque controlled induction motor drive. Stator flux and motor torque are averaged for steady state operation at both operating speeds, for the two load torque profiles. The values are summarised in table 6.1 (the 3rd and the 6th columns). Average torque value is approximately 0.5% (at one half of the rated speed) to 1% (at rated speed) below the torque reference, while the average stator flux value is negligibly smaller than the reference value.

The same simulation study is performed once more. The machine is now represented with the model (3.39)-(3.44), so that the iron loss is accounted for. Equivalent iron loss representation of (6.1) is utilised. In order to apply the correct value of the equivalent iron loss resistance within the machine model at each operating frequency, it is necessary to have the information regarding the instantaneous variation

of the stator frequency. This information is not readily available within the DTC scheme. Stator frequency is evaluated by filtering (cut-off frequency is 100 Hz) the instantaneous speed of the stator flux space vector, which is given with [Vas (1998)]

$$f = \frac{1}{2\pi} \frac{\psi_{\alpha s}\, d\psi_{\beta s}/dt - \psi_{\beta s}\, d\psi_{\alpha s}/dt}{\psi_{\alpha s}^2 + \psi_{\beta s}^2} \tag{6.3}$$

Evaluation of the stator frequency according to (6.3) is problematic in the low frequency region. Equivalent iron loss resistance in the motor model is therefore initially fixed to the value that corresponds to 10 Hz and equations (6.1) and (6.3) are applied once when this stator frequency is exceeded.

As discussed shortly, presence of the iron loss leads to a reduction in the motor output torque, so that the acceleration is slower. In order to arrive at the same quasi steady states as in figure 6.4 (one half of the rated speed and rated speed), the two instants of the load toque application in profiles of figure 6.3 are now delayed by 0.01 second and 0.015 second, respectively. Results of the simulations are given in figure 6.5, where stator flux, motor speed, motor torque and stator current are shown, again for the two profiles of figure 6.3. In addition, figure 6.6 shows motor torque at 50% of the rated speed with load torque equal to 50% and 100% of the rated torque, which result when iron loss is neglected and when iron loss is accounted for.

Stator flux and motor torque are once more averaged for steady state operation at both operating speeds, for the two load torque profiles, and the values are summarised in table 6.1 (the 4th and the 7th columns). Torque error is defined as difference of average values in steady state operation, obtained when iron loss is neglected and when iron loss is accounted for. It is further normalised with respect to rated motor torque and is given in the 5th column of table 6.1. Average stator flux value is in all the cases essentially identical to the value, which results when iron loss is neglected, so that no stator flux error takes place. Stator flux estimation is not affected by the inclusion of the iron loss, as explained in the following paragraph, and a negligibly small error in stator flux is assigned to the limited accuracy of the averaging procedure. Torque error is however substantial. The actual motor torque is considerably smaller than the reference torque, this being the net consequence of the iron loss existence. One observes that for the motor under consideration torque error appears to be independent of both the operating speed and the load torque value. It is in all the four studied operating points around 1.12 Nm or 4.2 % of the motor rated torque. This means

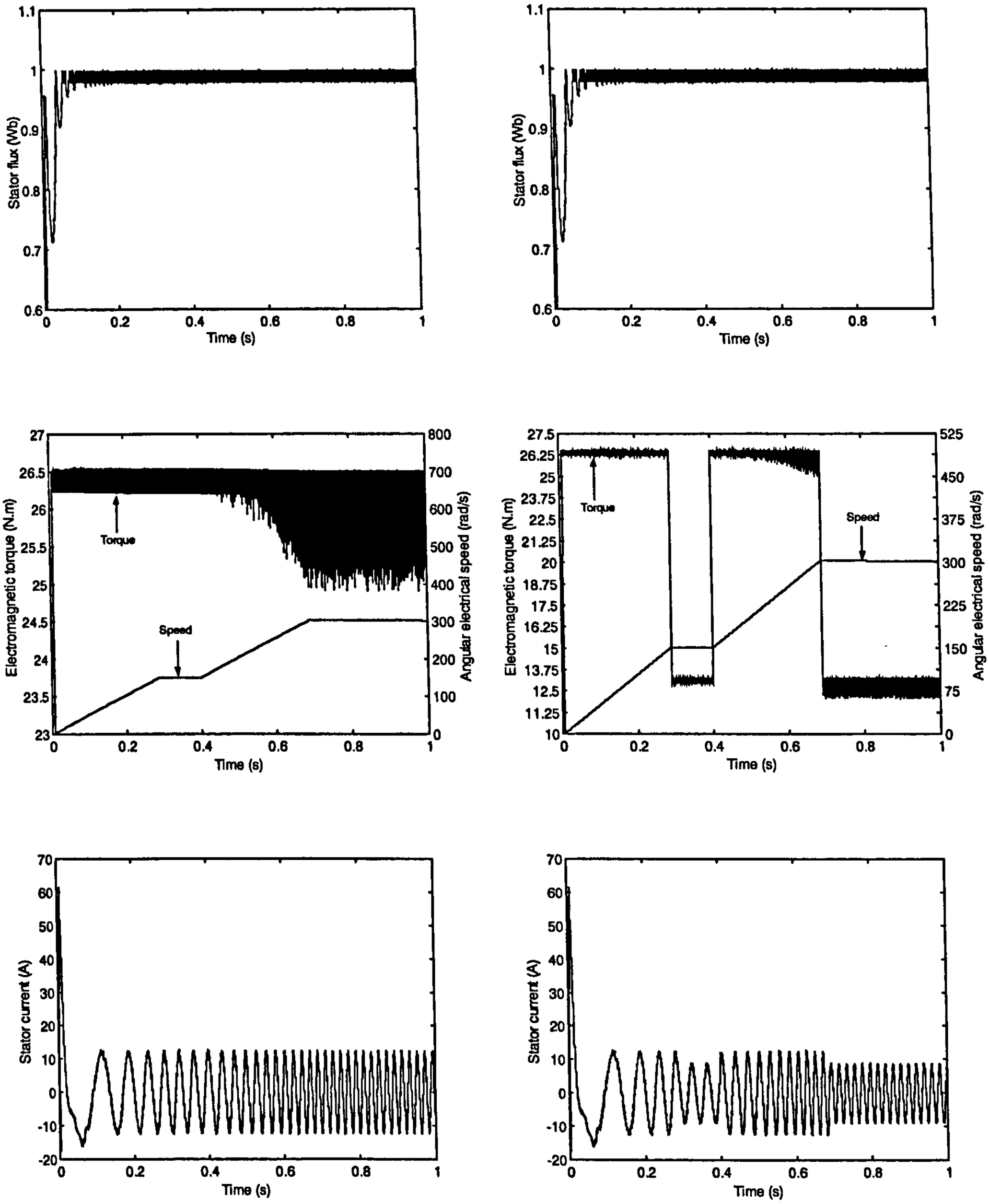

Figure 6.4: Stator flux, speed, torque and stator current of induction motor with DTC, when iron loss is ignored, for reference torque and load torque profile of: a) figure 6.3a, b) figure 6.3b.

that, lower the load torque is, higher the percentage torque error is when expressed with respect to the load torque value. It is interesting to note that the torque error of 4.2% very closely corresponds to the ratio of the fundamental iron loss at rated 50 Hz (173.4 W from (6.1)) to the rated motor power (4 kW), which comes to 4.3%. The use of this

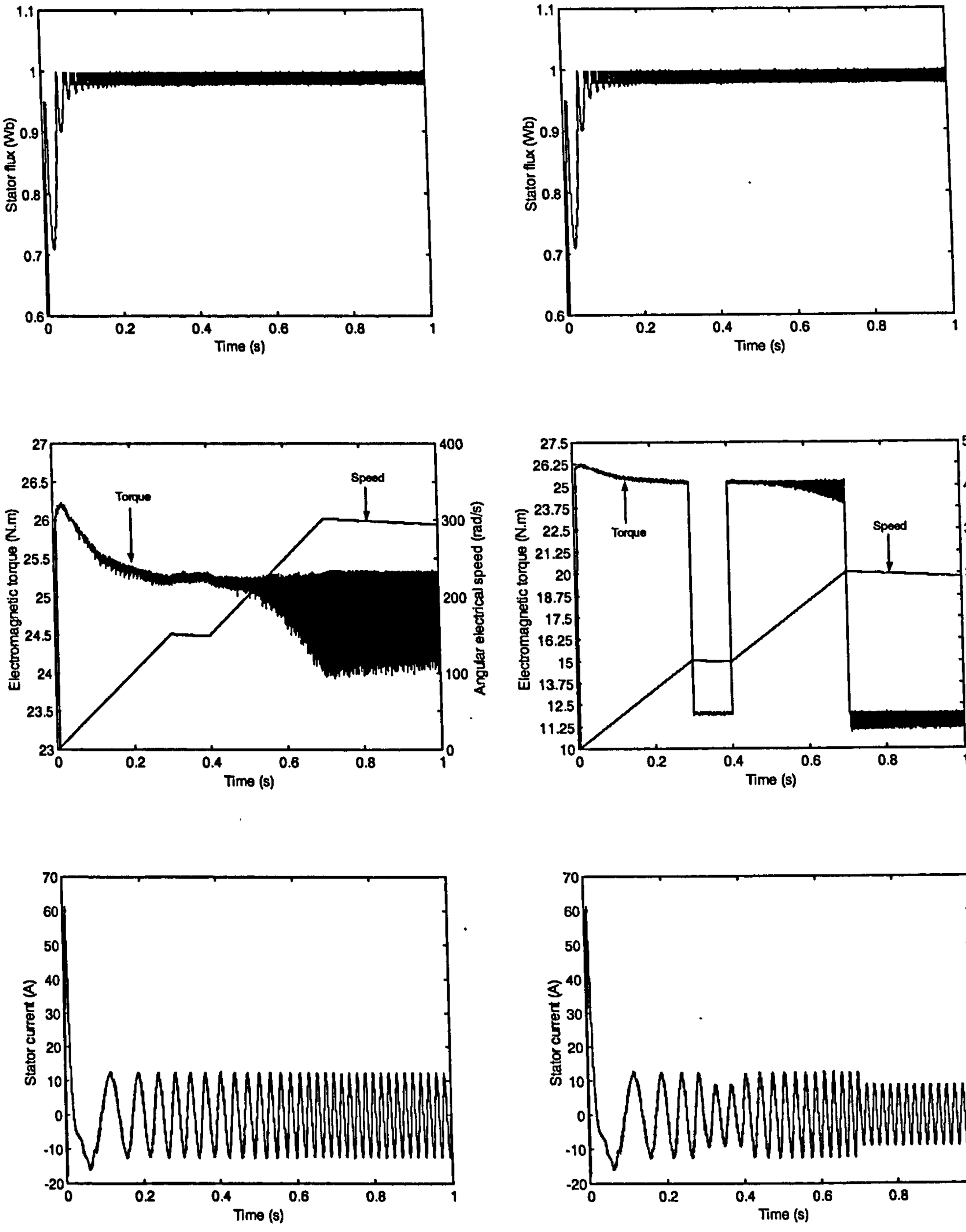

a) b)

Figure 6.5: Stator flux, speed, motor torque and stator current, when iron loss is included in the motor model, for the reference torque and load torque profile of: a) figure 6.3a, b) figure 6.3b.

fact will be made in the discussion of the iron loss compensation.

Comparison of the stator flux and motor torque traces in figures 6.4, 6.5 and 6.6 shows some interesting features. Inclusion of the iron loss representation in the machine model, using the circuit of figure 6.1, does not alter the amount of stator flux ripple. On

the other hand, torque ripple is significantly reduced at medium speeds. Since the stator flux magnitude and position are estimated from the motor stator voltages and stator currents, stator flux estimation automatically accounts for the iron loss. In other words, all the stator flux related estimates (magnitude, position and two-axis components) correctly reflect existence of the iron loss (that is, presence of the iron loss does not induce any detuning in these estimates). However, torque estimate used for closed loop torque control, differs from the actual motor torque. It is believed that the change in torque ripples is only an apparent consequence of the iron loss existence that does not take place in reality. As discussed in Section 6.2.1, equivalent iron loss resistance accurately models only the fundamental iron loss component. Utilisation of the same equivalent iron loss resistance for all the voltage harmonics is believed to be responsible for this change in the ripple characteristics of the drive.

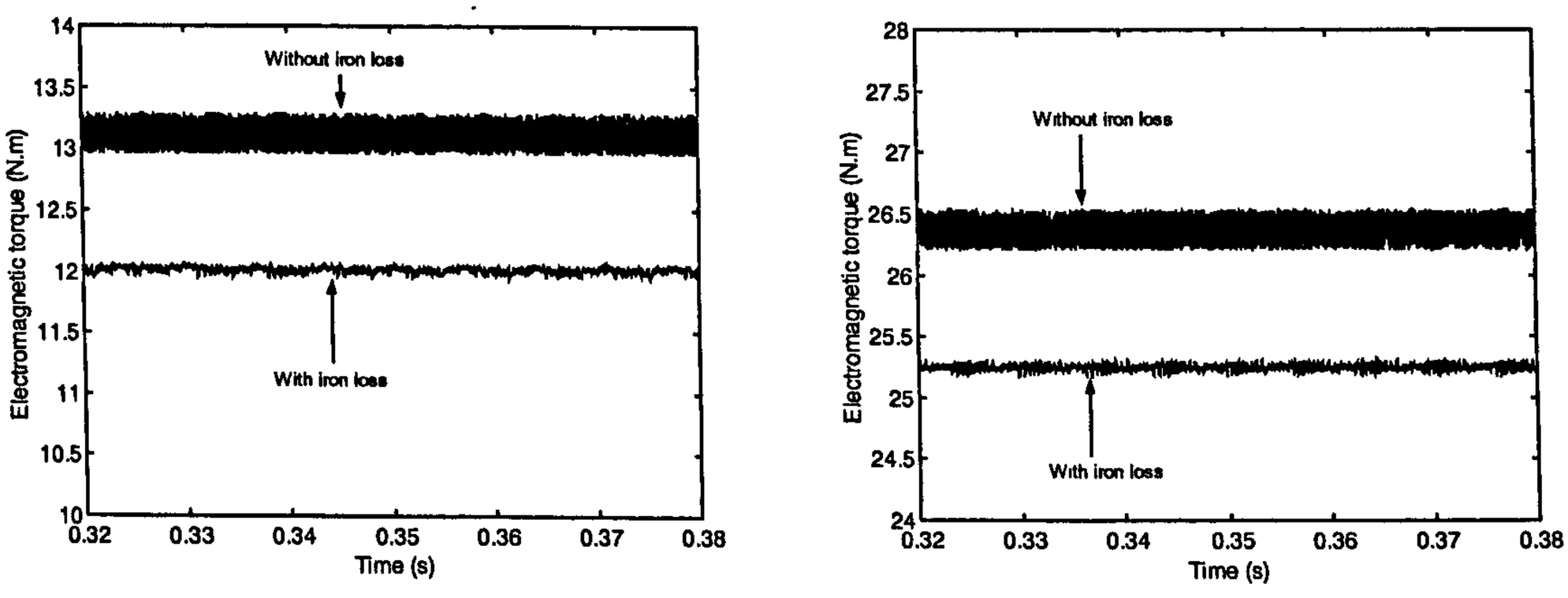

a) b)

Figure 6.6: Comparison of the motor torque, obtained with and without iron loss representation in the model, during quasi steady state operation at one half of the rated speed: a) with one half of the rated load torque and one half of the rated torque command, b) with rated load torque and rated torque command.

Closed loop speed control, using actual motor speed as the feedback signal, is investigated next. Stator flux, motor torque, motor speed and load torque of DTC induction motor drive in speed mode of operation are shown in figure 6.7 for two cases. Results of figure 6.7a are obtained with induction motor model without iron loss, while figure 6.7b applies to the case when iron loss representation is included in the motor model. Motor torque with included iron loss is smaller than the estimated torque in motoring, illustrated in figure 6.7 (stator flux is unchanged). Figure 6.8 shows the difference in speed and torque response (during operation in the torque limit) of the

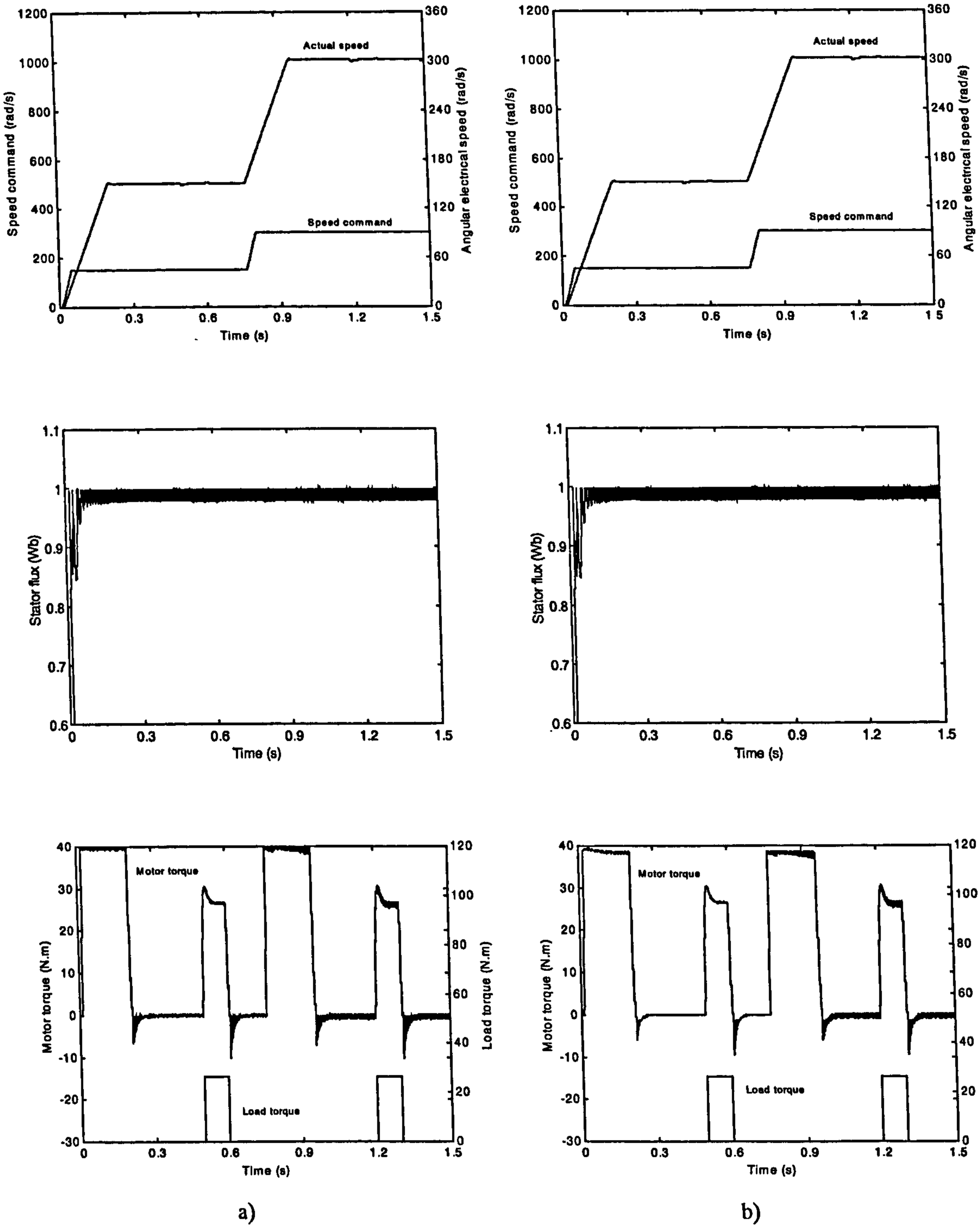

Figure 6.7: Behaviour of the DTC speed drive for the applied speed command and load torque profiles: a) core loss is neglected in the motor model, b) core loss is included in the motor model.

speed drive when iron loss is considered and when it is ignored. Figure 6.9 shows the acceleration and braking transient of DTC speed drive with and without iron loss. Stator flux of DTC speed drive in acceleration and braking is unchanged, regardless of the

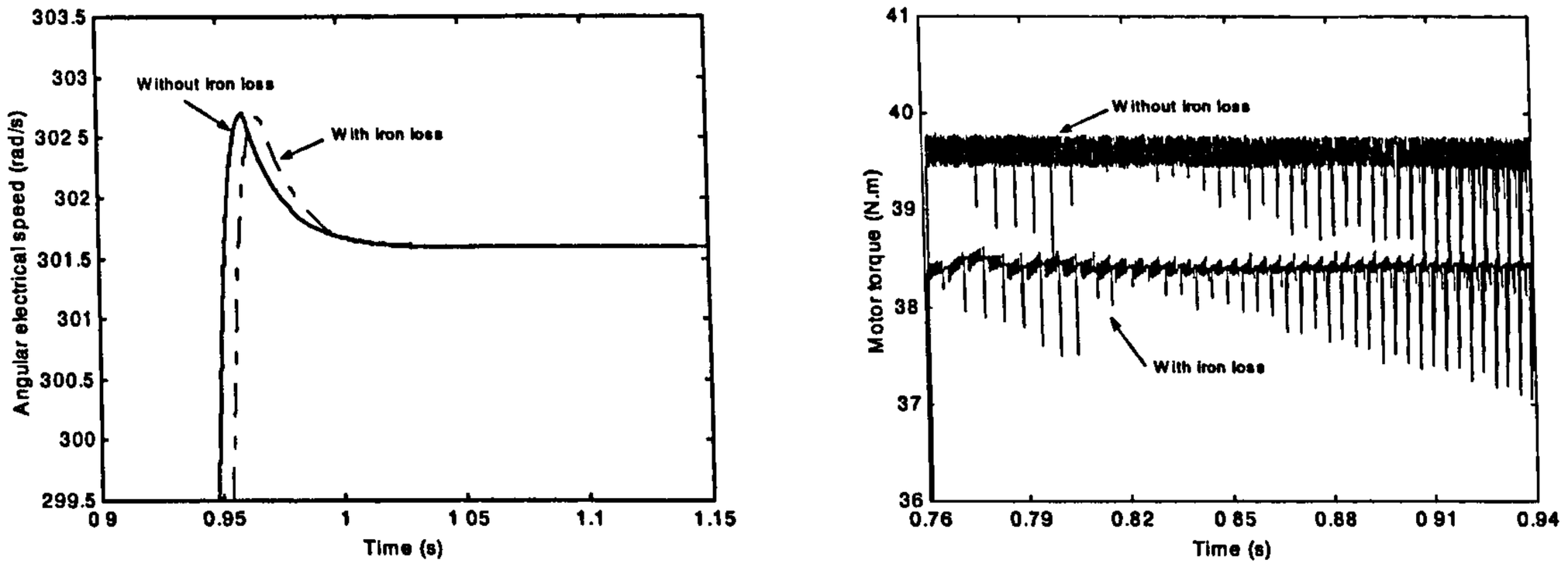

a) b)

Figure 6.8: Comparison of: a) motor speed, b) motor torque, when core loss is neglected and when core loss is accounted for (zoomed and overlapped traces of figures 6.7a and 6.7b).

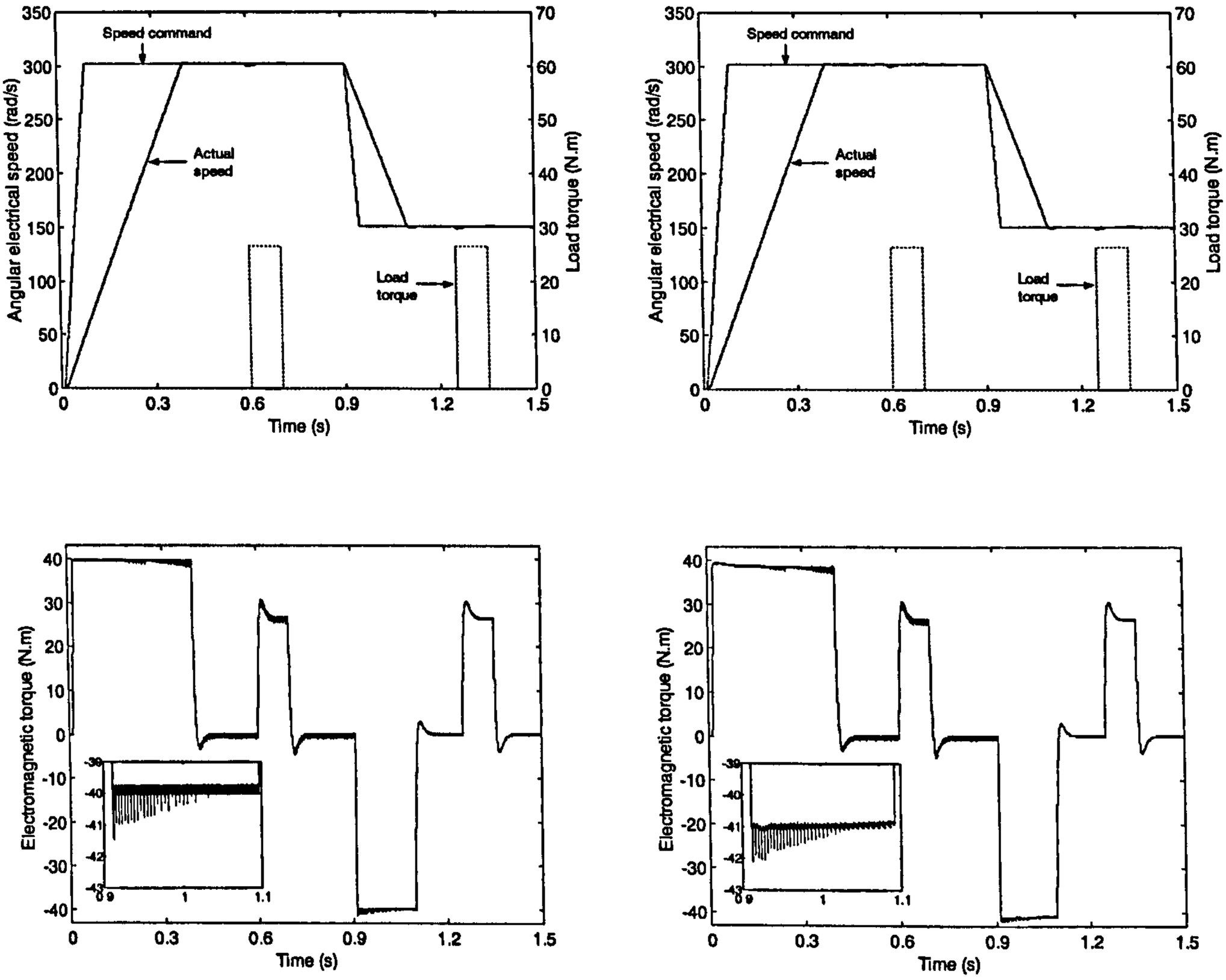

a) b)

Figure 6.9: Motor speed, speed command, load torque, and motor torque in acceleration and braking operation when: a) core loss is not included, b) core loss is included.

inclusion of core loss. Therefore, stator flux is not shown again in figure 6.9.

Table 6.1: Averaged motor torque and stator flux values in quasi steady state operation, with and without iron loss, and associated torque errors.

Load torque (Nm)	Quasi steady state speed	Average motor torque, no iron loss (Nm)	Average motor torque, with iron loss (Nm)	Torque error due to iron loss (Nm, %)	Average stator flux, no iron loss (Wb)	Average stator flux, with iron loss (Wb)
T_{en}	Rated	26.23	25.11	1.12 (4.23%)	0.9881	0.9881
T_{en}	0.5·rated	26.37	25.25	1.12 (4.23%)	0.9873	0.9873
$0.5 \cdot T_{en}$	Rated	13.022	11.907	1.115 (4.2%)	0.9882	0.9883
$0.5 \cdot T_{en}$	0.5·rated	13.12	12.01	1.11 (4.19%)	0.9877	0.9876

While the acceleration transient remains the same as before (figure 6.7b), an interesting feature of the impact of iron loss on the braking operation can be observed in figure 6.9b. During operation in the torque limit, actual motor torque is now greater than the estimated torque (by absolute value), leading to slightly faster deceleration (see zoomed inlets in figure 6.9).

6.4 Compensation of iron loss in direct torque controlled induction motors

On the basis of the considerations of the previous section, it follows that the only quantity that is affected by the iron loss is the motor torque. Compensation of the torque error is therefore considered, for both torque and speed mode of operation. Torque estimate of (4.21), used for the closed loop torque control, does not recognise the existence of the iron loss and therefore delivers a too high value of the estimated torque in motoring. While the same in general holds true in the case of vector control, the issue of iron loss compensation is grossly simplified in this scheme of DTC, since stator flux related estimates automatically account for the existence of the iron loss. It is only necessary to modify the torque estimate of (4.21) by deducting an iron loss related torque component, so that the new torque estimate for closed loop torque control is given with

$$T_e' = (3/2)P(\psi_{\alpha s} i_{\beta s} - \psi_{\beta s} i_{\alpha s}) - \Delta T_{Fe} \tag{6.4}$$

Since the output power is wrongly assumed to be $T_e \omega_m$ when iron loss is neglected, while the true output power is $T_e' \omega_m$, the torque increment of (6.4) that will provide compensation of the fundamental iron loss component can be obtained as

$$T_e\omega_m = T_e'\omega_m + P_{Fe}$$
$$\Delta T_{Fe} = P_{Fe}/\omega_m \qquad (6.5)$$
$$P_{Fe} = \Delta T_{Fe}\omega_m$$

It should be noted that (6.4) is valid for both motoring and braking and that the sign of the torque increment is always the same (that is, iron loss reduces the output torque available in motoring, while the shaft torque in braking is higher (by absolute value) than predicted by (4.21). Symbol ω_m in (6.5) stands for mechanical angular speed of rotor rotation ($\omega_m = \omega_r/P$), while P_{Fe} is the fundamental component of the iron loss.

As already discussed, fundamental iron loss component is a function of the operating frequency. Hence iron loss compensation requires that equation (6.1) is given in a form of the look-up table and that appropriate iron loss value is extracted in each operating point as a function of frequency. However, stator frequency is normally not readily available within the DTC. It therefore may be possible to use instead of stator frequency electrical rotor speed of rotation, since the speed value is likely to be either measured or estimated (and is needed anyway for application of (6.5)). The difference between the two, rotor slip frequency, is always rather small. In what follows the two compensation strategies, based on the torque increment calculation according to

$$\Delta T_{Fe} = \frac{P_{Fe}(f)}{\omega_m} \quad \text{or} \quad \Delta T_{Fe} = \frac{P_{Fe}(P\omega_m/2\pi)}{\omega_m} \qquad (6.6)$$

are investigated. For the reasons discussed in conjunction with (6.3), a constant torque increment, that corresponds to iron loss at 10 Hz, is applied during the initial part of the acceleration trajectory, until the frequency reaches 10 Hz. The same simulation study is repeated again and stator flux, torque and speed traces for the profiles of figure 6.3 are shown in figure 6.10 (for frequency based evaluation of the fundamental iron loss) and figure 6.11 (for speed based evaluation of the fundamental iron loss). Compensation of the torque error according to (6.4), (6.6) does not affect the stator flux. Stator flux traces remain to be exactly the same as in figure 6.5.

Torque is again averaged for operation at one half of the rated speed and at rated speed, for the both load torque profiles, and the values are summarised in table 6.2 for the both proposed compensation strategies. As can be seen from the values in table 6.2 and from the time-domain traces in figures 6.10 and 6.11, differences between the two compensation strategies are marginal. Residual torque error is for all the operating points and for the both compensation strategies below 1% (in six out of eight cases it is well below 0.5%). The compensation is not perfect however and the explanation for this

is rather simple. Analytical approximation of the equivalent iron loss resistance of (6.1) is used in the motor model, while analytical approximation of the fundamental iron loss of (6.1) is used within the controller. The mapping of these two functions is not ideal, so that a small residual torque error (of variable sign, table 6.2) can be expected in most of the operating regimes.

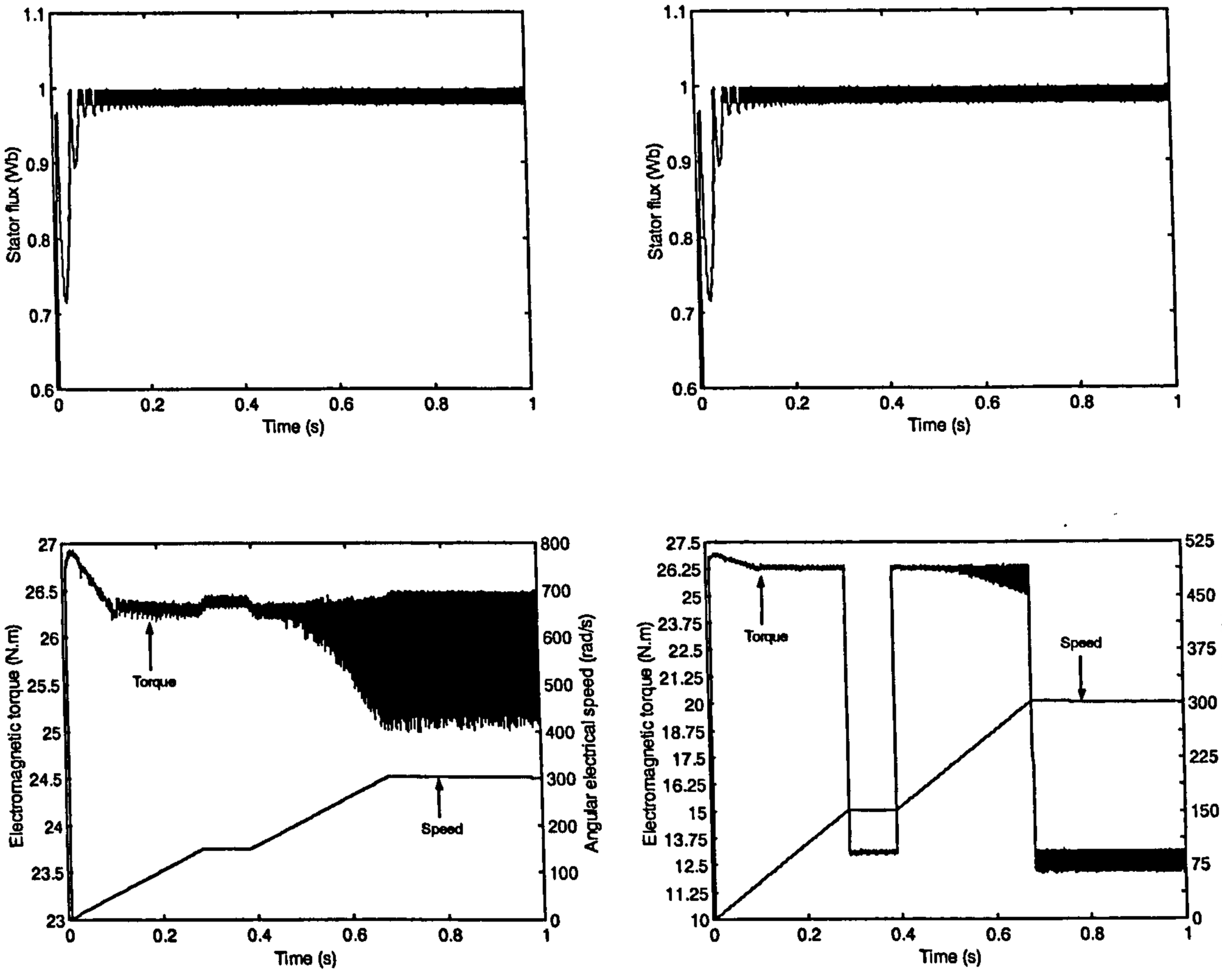

Figure 6.10: Stator flux, motor torque and speed variation with compensated iron loss, using frequency dependent calculation of the fundamental iron loss, with torque profiles of figure 6.3.

The proposed iron loss compensation method is universally valid for any induction machine subjected to DTC and the only necessary condition for its application is that the fundamental component of the iron loss has been determined during the drive commissioning as a function of the fundamental frequency. Depending on whether the information regarding stator frequency or the rotor speed is available, one or the other of the two possibilities suggested in (6.6) may be selected. However, in a number of cases the proposed compensation method can be considerably simplified, as discussed next.

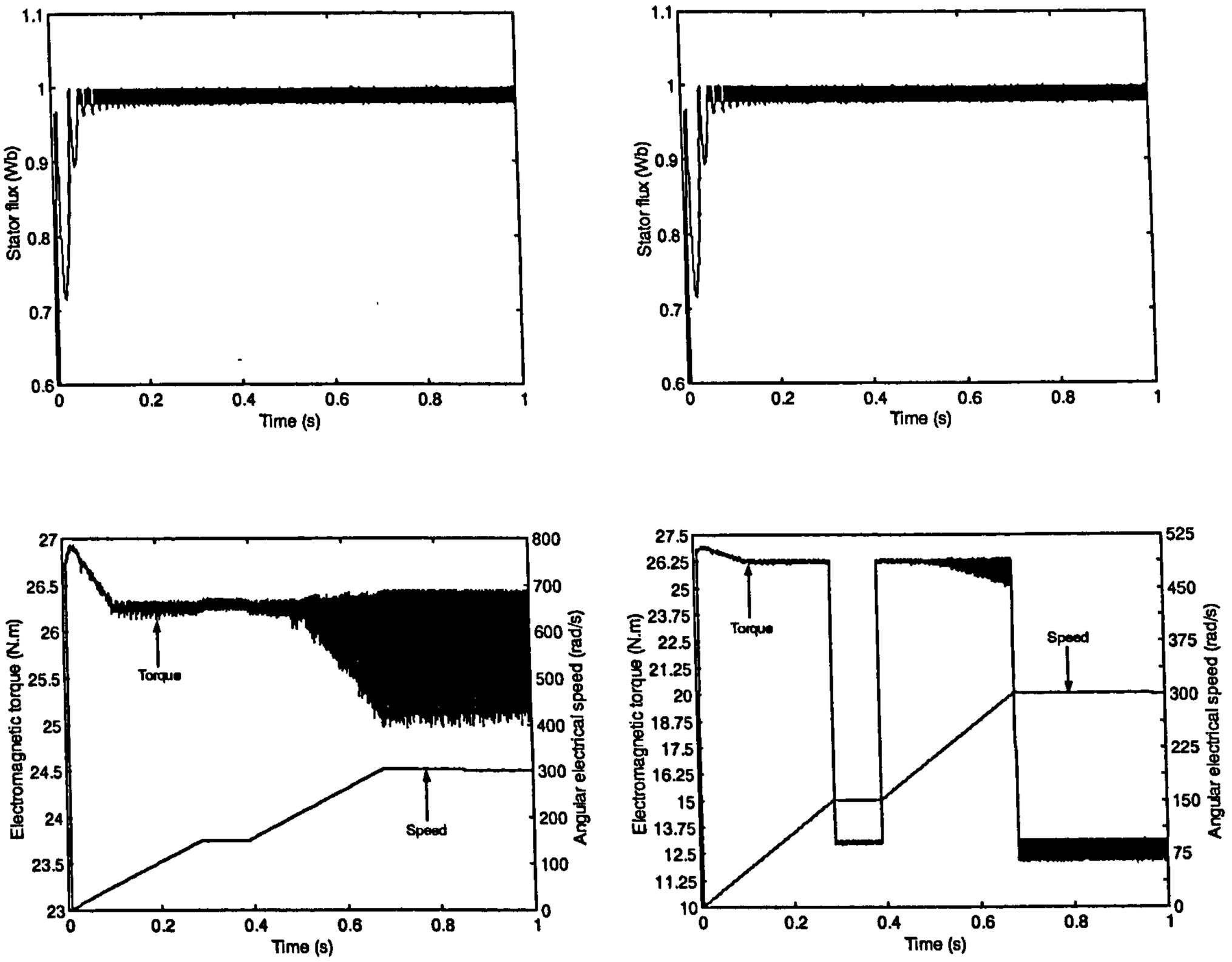

a) b)

Figure 6.11: Stator flux, motor torque and speed variation with compensated iron loss, using speed dependent calculation of the fundamental iron loss, with torque profiles of figure 6.3.

Table 6.2: Averaged motor torque values in quasi steady state operation for proposed iron loss compensation methods and associated residual torque errors.

Compensation methods	Load torque (Nm)	Quasi steady state speed	Average torque, no iron loss (Nm)	Average torque, compensated iron loss (Nm)	Residual torque error (Nm, %)
$P_{Fe} = F(f)$	T_{en}	rated	26.23	26.01	0.22 (0.83 %)
	T_{en}	0.5·rated	26.37	26.38	-0.01 (-0.04%)
	$0.5 \cdot T_{en}$	rated	13.022	12.922	0.1 (0.38%)
	$0.5 \cdot T_{en}$	0.5·rated	13.12	13.11	0.01 (0.04%)
$P_{Fe} = F(\omega_m)$	T_{en}	rated	26.23	26.08	0.15 (0.57%)
	T_{en}	0.5·rated	26.37	26.3	0.07 (0.26%)
	$0.5 \cdot T_{en}$	rated	13.022	12.95	0.072 (0.27%)
	$0.5 \cdot T_{en}$	0.5·rated	13.12	13.07	0.05 (0.19%)

Iron loss in an induction motor is a sum of the hysteresis loss and eddy current loss. Since the two components depend on supply frequency in a different way, it is often considered as satisfactory to regard the total fundamental iron loss in the base speed region as proportional to the frequency at power 1.6 [Wieser (1998)]. However, experimentally identified fundamental component of the iron loss very often exhibits almost linear variation with the stator frequency [Dittrich (1998), Noguchi et al (1997), Wieser (1998)]. Closer inspection of the variation of the fundamental iron loss with frequency in the range from 0 to 50 Hz for the motor under consideration here (figure 6.2a) shows that the almost linear correlation applies in this case as well. By approximating the iron loss in the base speed region with a linear dependence on frequency, one arrives at the simplest possible iron loss compensation strategy. It follows from (6.5)-(6.6) that the required torque increment is under these conditions constant and equal to

$$\Delta T_{Fe} = \frac{P_{Fen}}{P_n} T_{en} = \text{const.} \tag{6.7}$$

where index n stands for rated values and P_{Fen} is the fundamental iron loss at rated (50 Hz here) frequency. As the fundamental iron loss at 50 Hz equals 173.4 W, while rated motor power and torque are 4 kW and 26.5 Nm, respectively, the required torque increment is 1.15 Nm. This value is just slightly higher than the torque error of 1.12 Nm that was observed in table 6.1 as the characteristic difference between the motor average torque values with and without iron loss consideration. Use of this simple compensation method is illustrated in figure 6.12 for the torque mode of operation, where once more torque response is shown for the two load torque profiles of figure 6.3 (stator flux is not shown since it is not changed). Operation of the DTC scheme in the speed mode, with compensated iron loss, is illustrated in figures 6.13 and 6.14. Constant torque increment of 1.15 Nm is used. As can be seen from figure 6.14, the delay of the speed response, that exists when iron loss is not compensated (figure 6.8), is now completely eliminated.

The averaged quasi steady-state torque values at the two operating speeds for the load torque values are summarised in table 6.3, where the residual torque error is given as well. The error is reduced to a negligibly small value (that is well within the numerical accuracy of the procedure) in all the operating points, indicating that essentially a perfect cancellation of the iron loss caused detuning is achieved. It is interesting to note that a rather large overshoot of the motor torque now appears in the initial part of the acceleration, at very low frequencies. This overshoot is a consequence

of iron loss over-compensation, that takes place at frequencies below approximately 15 Hz. Measured fundamental iron loss in figure 6.2a illustrates very good linearity in the frequency range from 20 Hz to 50 Hz. However, the value at 10 Hz departs from this linear behaviour and is substantially smaller. Compensating torque increment of 1.15 Nm is therefore too high a value for very low frequency region, so that the over-compensation takes place and the overshoot occurs.

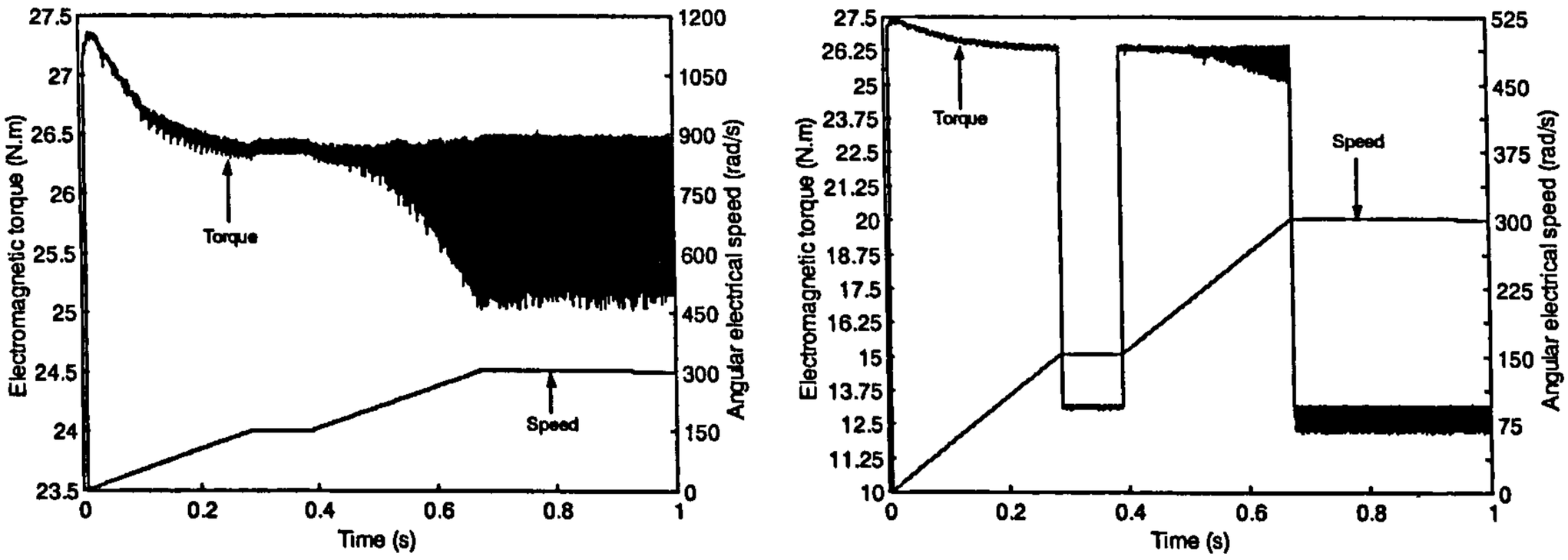

Figure 6.12: Motor torque and speed variation using constant torque increment of 1.15 Nm in the torque estimator for iron loss compensation, with torque profiles of figure 6.3.

Similar considerations apply to figures 6.10 and 6.11 as well, where an overshoot (of a smaller value, though) is evident during the start-up. It is a consequence of the application of the constant torque increment (that corresponds to the fundamental iron loss at 10 Hz) for all the frequencies below 10 Hz.

Table 6.3: Averaged motor torque values in quasi steady state operation and associated residual torque errors, when iron loss is compensated using a constant torque increment of 1.15 Nm.

Load torque (Nm)	Quasi steady state speed	Average torque, no iron loss (Nm)	Average torque (Nm), compensated iron loss ΔT_{Fe} = 1.15 Nm	Residual torque error (Nm, %)
T_{en}	rated	26.23	26.255	-0.025 (-0.1 %)
T_{en}	0.5·rated	26.37	26.395	-0.025 (-0.1%)
$0.5 \cdot T_{en}$	rated	13.022	13.038	-0.016 (-0.06%)
$0.5 \cdot T_{en}$	0.5·rated	13.12	13.18	-0.06 (-0.23%)

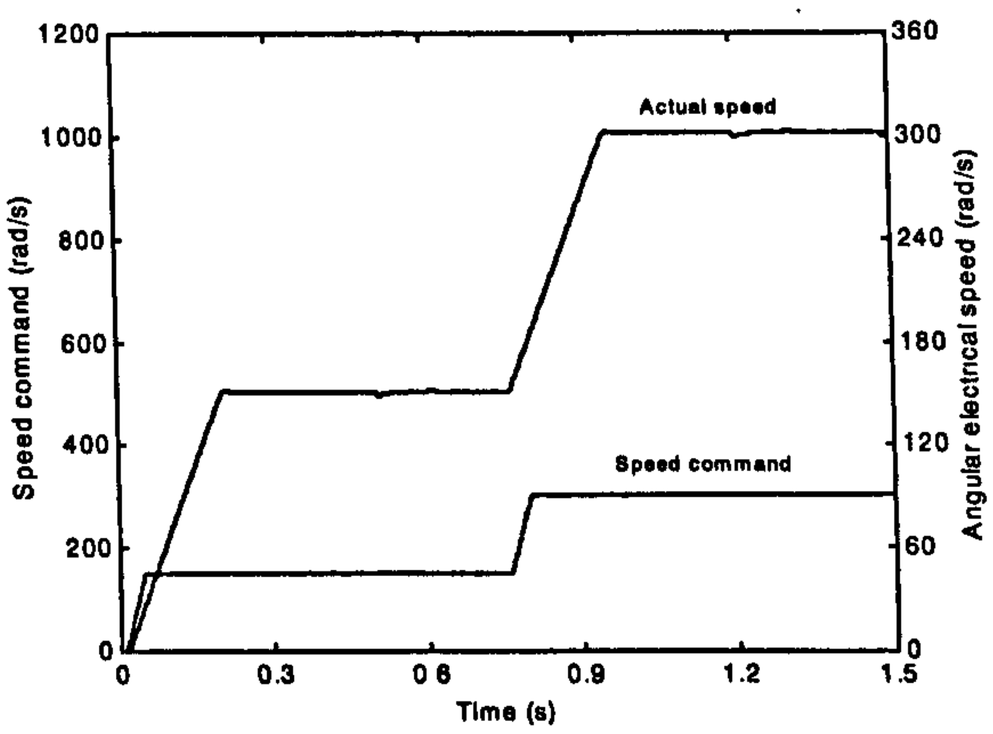

a)

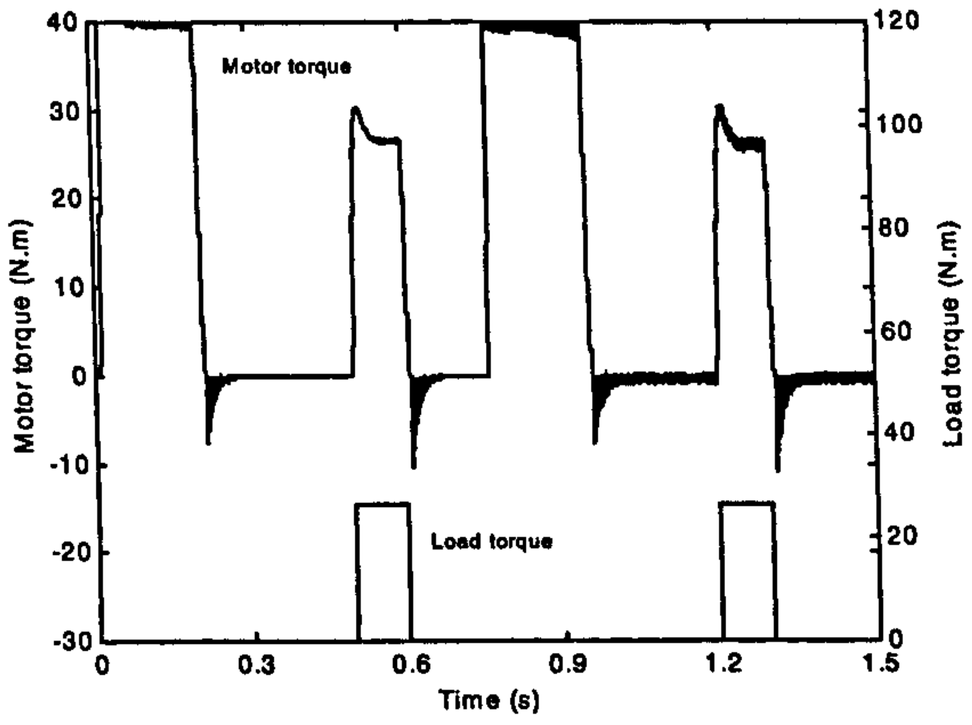

b)

Figure 6.13: Behaviour of the DTC speed drive, when core loss is included in the motor model and is compensated in the torque estimation.

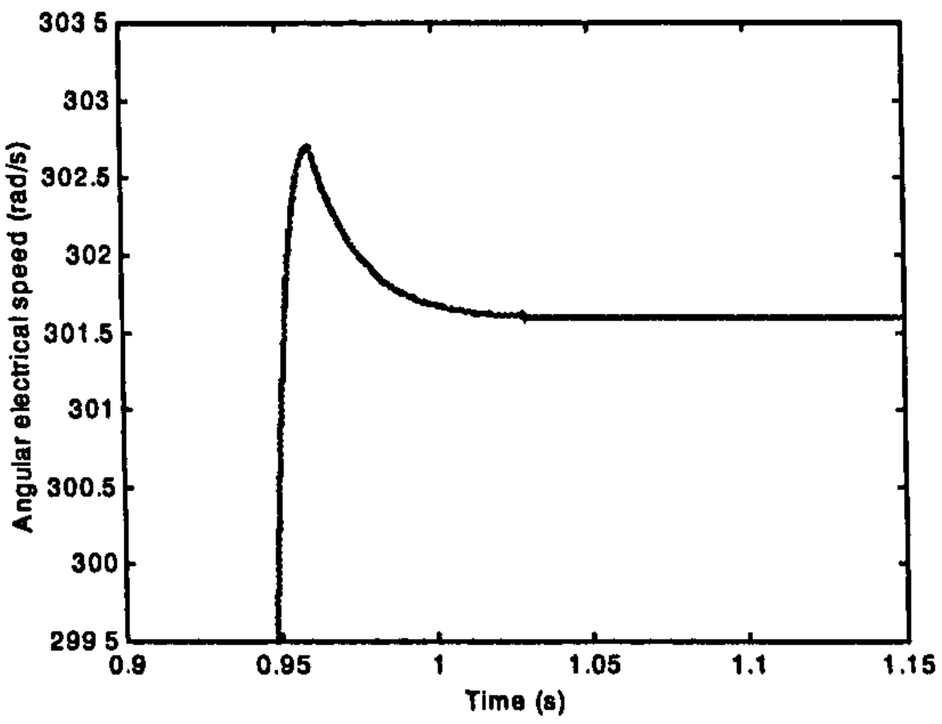

a)

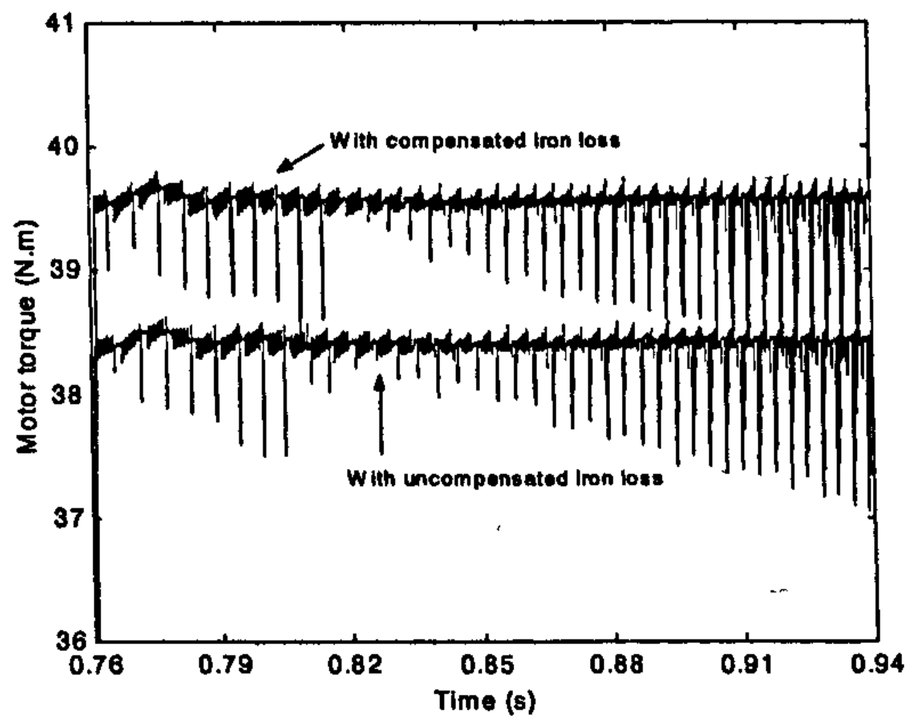

b)

Figure 6.14: a) Motor speed without core loss and with compensated core loss (extracts from figures 6.7a and 6.13), and b) motor torque with compensated and uncompensated core loss (extracts from figure 6.7b and 6.13).

6.5 Summary

This chapter analysed impact of the iron loss existence in an induction motor on accuracy of direct torque control. The approach to inclusion of the iron loss into the dynamic model of an induction motor is described, and the limitations of the method are addressed. Fundamental iron loss is identified experimentally and the equivalent iron loss resistance, required for the motor model, is obtained from these data. A detailed simulation study is performed for the torque mode of operation of the drive in the base speed region and the following conclusions are drawn:

- Iron loss existence does not affect the accuracy of stator flux magnitude and position estimation and the average stator flux in the motor is therefore unchanged.
- Iron loss significantly affects the output motor torque under all operating conditions. The standard torque estimation method over-estimates motor torque in motoring, so that the acceleration is slower than anticipated. Similarly, an under-estimate occurs in braking, so that deceleration becomes faster than expected. These conclusions are equally applicable when closed loop speed control is added to the DTC scheme. There is a substantial torque error in all the quasi steady states as well, typically over 4% of the motor rated torque for the machine studied here.

A simple method of torque error compensation is devised in the second part of the chapter. It is based on the power flow considerations, requires a functional dependence of the fundamental iron loss component on stator frequency (that needs to be stored as a look-up table), and involves one division (with motor speed of rotation). Since stator frequency may or may not be available within the DTC scheme, while information regarding the motor speed of rotation is likely to be available, two versions of the compensation method are analysed. The first one utilises the stator frequency in the process of fundamental iron loss extraction from the look-up table, while the second one approximates stator frequency with electrical frequency of rotor rotation. Both versions give very satisfactory compensation results, since the torque error is in the most of the operating conditions reduced to below 0.5% and is within the numerical accuracy of the calculations.

It is finally observed that for many induction motors, including the one studied here, variation of the fundamental iron loss with frequency in the base speed region closely corresponds to a linear relationship. In such a case it becomes possible to use the simplest possible compensation method, that essentially does not require any additional calculations (apart from one subtraction). The torque increment, used to compensate for the iron loss, becomes in this case a constant, frequency (and speed) independent quantity, that is determinable from the knowledge of the fundamental iron loss component at rated frequency and the motor rated power and torque. It is shown that

application of this simple compensation method enables almost perfect cancellation of the iron loss induced torque error in the frequency region where iron loss variation is practically proportional to frequency (15 to 50 Hz for the motor studied here).

CHAPTER 7

SENSORLESS DIRECT TORQUE CONTROL

7.1 Introduction

Sensorless control of induction motor has been researched extensively for the last ten years [Vas (1993, 1998)]. Speed of the rotor is estimated based on the measurements practically available when the induction motor is running, such as stator voltage and stator current measurements. The speed prediction techniques help to eliminate the utilisation of speed sensors, which are expensive and vulnerable in harsh operating environment. The speed estimation techniques do not depend on the control method used in an induction motor drive. The speed prediction methods, which have been proposed originally in conjunction with vector control, can be used in conjunction with direct torque control as well. Reliable and useful techniques should provide the estimated speed with an accuracy of 0.5% or better, in all the operating conditions, from zero speed to the highest speed, and should be independent of parameter variation effects [Vas (1998)].

This chapter will at first discuss different MRAS based speed estimation techniques for an induction motor. Then, discussion and simulations of sensorless direct torque control of induction motor with flux based MRAS speed estimators will be presented. These speed estimators will be stator flux based and rotor flux based. The particular attention will be paid to the compensation of the iron loss within a speed estimator, with the idea of improving the speed estimation accuracy. Two novel modified speed estimators of MRAS type with full iron loss compensation will be presented and verified by simulation.

7.2 MRAS based speed estimation

Measured stator voltage and currents are used for extracting the information about speed from two machine models. In the first model, certain state or other variable of the induction machine is calculated independently of the rotor speed (reference model). In the second model, the same variable is calculated from a different machine

model that is dependent on the rotor speed (adjustable or adaptive model). The estimated rotor speed is used in the second model as feedback signal. The difference between the variables from the two models is used to find the estimated value of the rotor speed through an adaptation mechanism, which tunes the adaptive model to obtain a satisfactory estimation of speed [Vas (1998)]. The general idea of the model reference adaptive system is shown in figure 7.1. The outputs of the reference and adaptive models in the figure 7.1 are shown as reactive power, without the loss of generality [Peng and Fukao (1994)]. The difference between the two estimated variables is formulated into an error signal. This signal is used as input into a PI controller, whose output is the estimated speed. The variables of an induction machine that can be used for a MRAS speed estimators are, as already noted, rotor flux, back EMF, reactive power and air gap power. Rotor flux based MRAS speed estimator is, however, the most frequently used MRAS speed estimator [Schauder (1992), Tajima and Hori (1993)]. It is for this reason that flux based speed estimators of MRAS type are selected for further work.

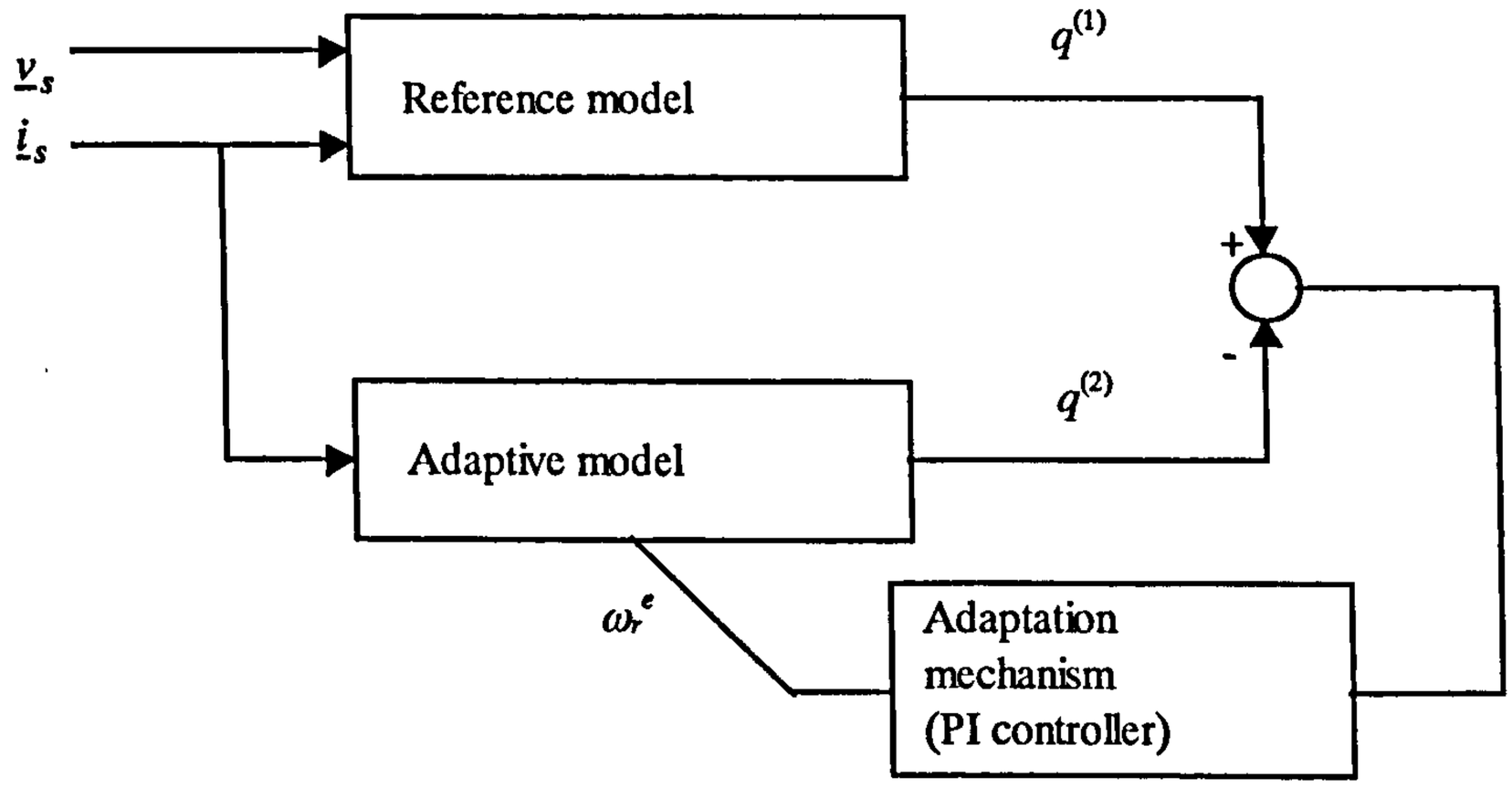

Figure 7.1: Conceptual block diagram of a MRAS speed estimator, using reactive power.

7.3 Mathematical models of speed estimators with flux based model reference adaptive system

7.3.1 Stator flux based MRAS speed estimator using standard constant parameter induction machine model

Equations and model for a stator flux based MRAS speed estimator using a standard constant parameter model of an induction machine are derived and discussed in

this subsection. Two different models for stator flux are used in the speed estimator. One is independent of the rotor speed and the other uses estimated rotor speed as a parameter, and these two models also have two different sets of inputs. Error quantity between the two outputs is the angle between the two flux space vectors. When the estimated speed is correct, the two vectors are aligned and the angle between them is zero, or the error quantity is zero. This angle will be driven to zero in the speed estimator to find the correct speed estimate.

In the stationary reference frame, equations for stator and rotor voltages of an induction motor are obtained from space vector equations in an arbitrary reference frame (3.27) by setting $\omega_a = 0$ (superscript *s* for stationary reference frame is omitted):

$$\begin{aligned} \underline{v}_s &= R_s \underline{i}_s + \frac{d\underline{\psi}_s}{dt} \\ 0 &= R_r \underline{i}_r + \frac{d\underline{\psi}_r}{dt} - j\omega_r \underline{\psi}_r \end{aligned} \tag{7.1}$$

Rotor current and rotor flux can be expressed from equations (3.28) as:

$$\begin{aligned} \underline{i}_r &= \frac{\underline{\psi}_s - L_s \underline{i}_s}{L_m} \\ \underline{\psi}_r &= \frac{L_r}{L_m}\underline{\psi}_s - \sigma \frac{L_r L_s}{L_m}\underline{i}_s \end{aligned} \tag{7.2}$$

where σ is once more the total leakage coefficient, $\sigma = 1 - L_m^2/(L_s L_r)$. Substitution of (7.2) into the second equation of (7.1) yields:

$$\begin{aligned} \underline{v}_s &= R_s \underline{i}_s + \frac{d\underline{\psi}_s}{dt} \\ 0 &= \frac{\underline{\psi}_s - L_s \underline{i}_s}{L_m} + \frac{T_r}{L_m}\frac{d\underline{\psi}_s}{dt} - \frac{T_r \sigma L_s}{L_m}\frac{d\underline{i}_s}{dt} - j\omega_r\left(\frac{T_r}{L_m}\underline{\psi}_s - \frac{T_r \sigma L_s}{L_m}\underline{i}_s\right) \end{aligned} \tag{7.3}$$

After some manipulation, the following equations are obtained:

$$\begin{aligned} \underline{v}_s &= R_s \underline{i}_s + \frac{d\underline{\psi}_s}{dt} \\ 0 &= \left(\frac{1}{T_r} - j\omega_r\right)\underline{\psi}_s + \frac{d\underline{\psi}_s}{dt} - \left(\frac{L_s}{T_r} - j\omega_r \sigma L_s\right)\underline{i}_s - \sigma L_s \frac{d\underline{i}_s}{dt} \end{aligned} \tag{7.4}$$

The differential equations are then re-arranged into state space form:

$$\begin{aligned} \frac{d\underline{\psi}_s^{(1)}}{dt} &= \underline{v}_s - R_s \underline{i}_s \\ \frac{d\underline{\psi}_s^{(2)}}{dt} &= \left(j\omega_r^e - \frac{1}{T_r}\right)\underline{\psi}_s + \left(\frac{L_s}{T_r} - j\omega_r^e \sigma L_s\right)\underline{i}_s + \sigma L_s \frac{d\underline{i}_s}{dt} \end{aligned} \tag{7.5}$$

where ω_r^e is the estimated rotor speed and superscripts (1) and (2) denote outputs of the reference and the adjustable models. They are written in the integral forms as follows:

$$\underline{\psi}_s^{(1)} = \int(\underline{v}_s - R_s \underline{i}_s)dt$$
$$\underline{\psi}_s^{(2)} = \int(j\omega_r^e - \frac{1}{T_r})\underline{\psi}_s dt + \int(\frac{L_s}{T_r} - j\omega_r^e \sigma L_s)\underline{i}_s dt + \sigma L_s \underline{i}_s \quad (7.6)$$

The first equation of (7.6) is used for the reference model because of its independence on rotor speed. The second equation of (7.6) is used for the adaptive model and it requires estimated rotor speed as a parameter. Resolution of (7.6) into α–β components gives:

$$\psi_{\alpha s}^{(1)} = \int(v_{\alpha s} - R_s i_{\alpha s})dt$$
$$\psi_{\beta s}^{(1)} = \int(v_{\beta s} - R_s i_{\beta s})dt \quad (7.7)$$

$$\psi_{\alpha s}^{(2)} = -\int\left(\omega_r^e \psi_{\beta s}^{(2)} + \frac{1}{T_r}\psi_{\alpha s}^{(2)}\right)dt + \int\left(\frac{L_s}{T_r} i_{\alpha s} + \omega_r^e \sigma L_s i_{\beta s}\right)dt + \sigma L_s i_{\alpha s}$$
$$\psi_{\beta s}^{(2)} = -\int\left(\omega_r^e \psi_{\alpha s}^{(2)} - \frac{1}{T_r}\psi_{\beta s}^{(2)}\right)dt + \int\left(\frac{L_s}{T_r} i_{\beta s} - \omega_r^e \sigma L_s i_{\alpha s}\right)dt + \sigma L_s i_{\beta s} \quad (7.8)$$

The error quantity between the stator flux output of the reference model and adaptive model is defined as:

$$\varepsilon = \psi_{\alpha s}^{(2)} \psi_{\beta s}^{(1)} - \psi_{\alpha s}^{(1)} \psi_{\beta s}^{(2)} \quad (7.9)$$

The inputs to the reference model (7.7) are stator voltages and stator currents. The inputs to the adaptive model (7.8) are stator currents and estimated speed. The error quantity is driven to zero by a PI controller, whose output is the estimated speed. This error quantity and the PI controller in the algorithm form the adaptive mechanism of a model reference adaptive system based speed estimator. The block scheme of the stator flux based MRAS speed estimator is shown in figure 7.2.

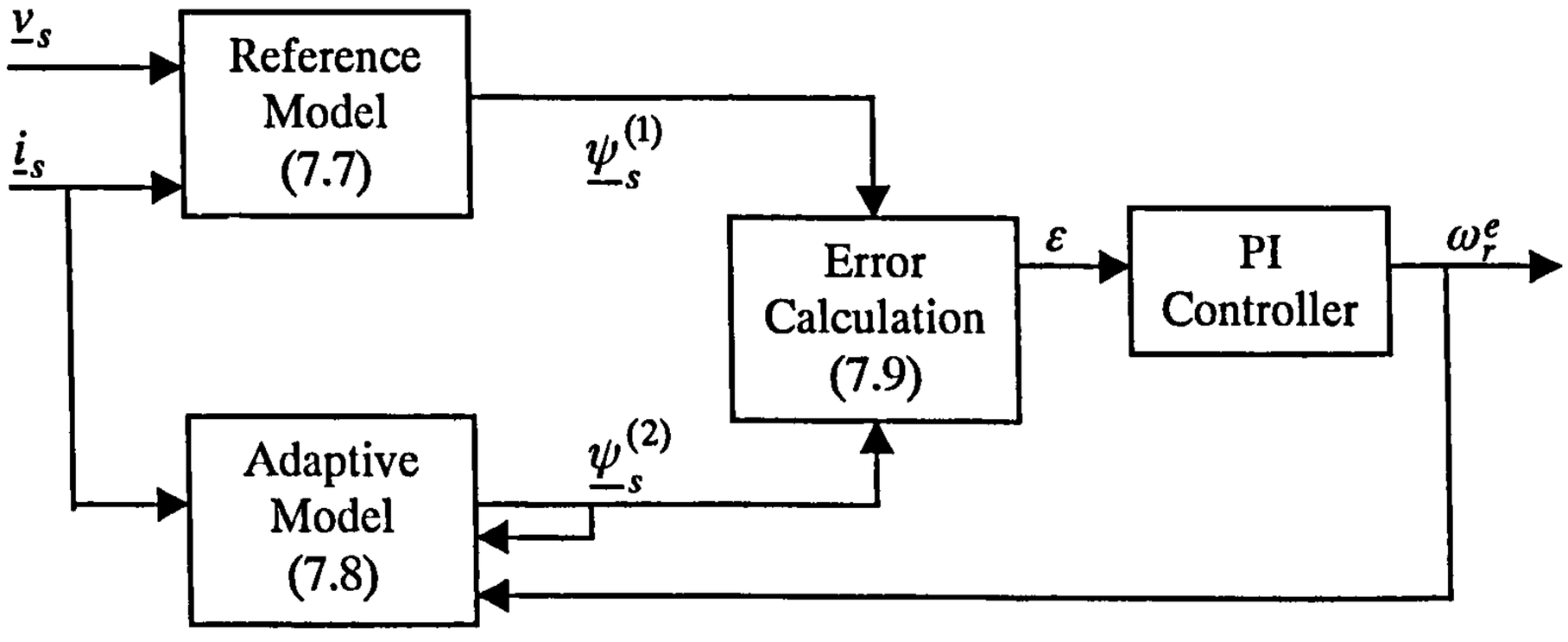

Figure 7.2: Block scheme of the stator flux based MRAS speed estimator.

7.3.2 Rotor flux based MRAS speed estimator using standard constant parameter induction machine model

Another MRAS speed estimator, which uses rotor flux equations for the reference model and adaptive model, is also analysed. The idea is the same as the one for the stator flux based MRAS speed estimator. The outputs of the models are now rotor flux space vectors. The reference model will be based on the rotor flux differential equation, which is independent of rotor speed. The adaptive model is based on the rotor flux differential equation with rotor speed as a parameter. The equations are obtained using (7.1) as the starting point, by eliminating rotor current and stator flux space vectors. The final form of the equations is [Schauder (1992)]:

$$\begin{aligned}\frac{d\underline{\psi}_r^{(1)}}{dt} &= \frac{L_r}{L_m}\left[\underline{v}_s - (R_s + \sigma L_s p)\underline{i}_s\right] \\ \frac{d\underline{\psi}_r^{(2)}}{dt} &= \left(j\omega_r^e - \frac{1}{T_r}\right)\underline{\psi}_r^{(2)} + \frac{L_m}{T_r}\underline{i}_s\end{aligned} \tag{7.10}$$

Here $p = d/dt$ is the differential operator, $\underline{\psi}_r^{(1)}$ is the rotor flux output of the reference model, and $\underline{\psi}_r^{(2)}$ is the rotor flux output of the adaptive model.

The inputs to the first of (7.10) are measured stator voltage and stator current. The inputs to the second of (7.10) are estimated speed and stator current. The block scheme of this speed estimator is the same as the one of the stator flux based MRAS speed estimator, shown in figure 7.2. The equations of the reference model, and the adaptive model, expressed in terms of α–β components in integral form, as well as the error quantity are:

$$\begin{aligned}\psi_{\alpha r}^{(1)} &= \frac{L_r}{L_m}\int(v_{\alpha s} - R_s i_{\alpha s})dt - \frac{L_r}{L_m}\sigma L_s i_{\alpha s} \\ \psi_{\beta r}^{(1)} &= \frac{L_r}{L_m}\int(v_{\beta s} - R_s i_{\beta s})dt - \frac{L_r}{L_m}\sigma L_s i_{\beta s}\end{aligned} \tag{7.11}$$

$$\begin{aligned}\psi_{\alpha r}^{(2)} &= -\int\left(\omega_r^e \psi_{\beta r}^{(2)} + \frac{1}{T_r}\psi_{\alpha r}^{(2)}\right)dt + \frac{L_m}{T_r}\int i_{\alpha s}dt \\ \psi_{\beta r}^{(2)} &= \int\left(\omega_r^e \psi_{\alpha r}^{(2)} - \frac{1}{T_r}\psi_{\beta r}^{(2)}\right)dt + \frac{L_m}{T_r}\int i_{\beta s}dt\end{aligned} \tag{7.12}$$

$$\varepsilon = \psi_{\alpha r}^{(2)}\psi_{\beta r}^{(1)} - \psi_{\alpha r}^{(1)}\psi_{\beta r}^{(2)} \tag{7.13}$$

7.3.3 A novel stator flux based MRAS speed estimator using induction machine model with iron loss representation

Modelling of an induction machine with the representation of iron loss was discussed in detail in section 3.3, where appropriate model equations were derived. These equations will be used in this and the subsequent section to propose two novel modified speed estimators with iron loss compensation. As already explained in section 3.3, equivalent iron loss resistor can be placed either in parallel to the magnetising branch of the machine or immediately after the stator resistance. The two possible situations are illustrated again, for the sake of convenience, in figure 7.3. The circuits are shown for the stationary reference frame.

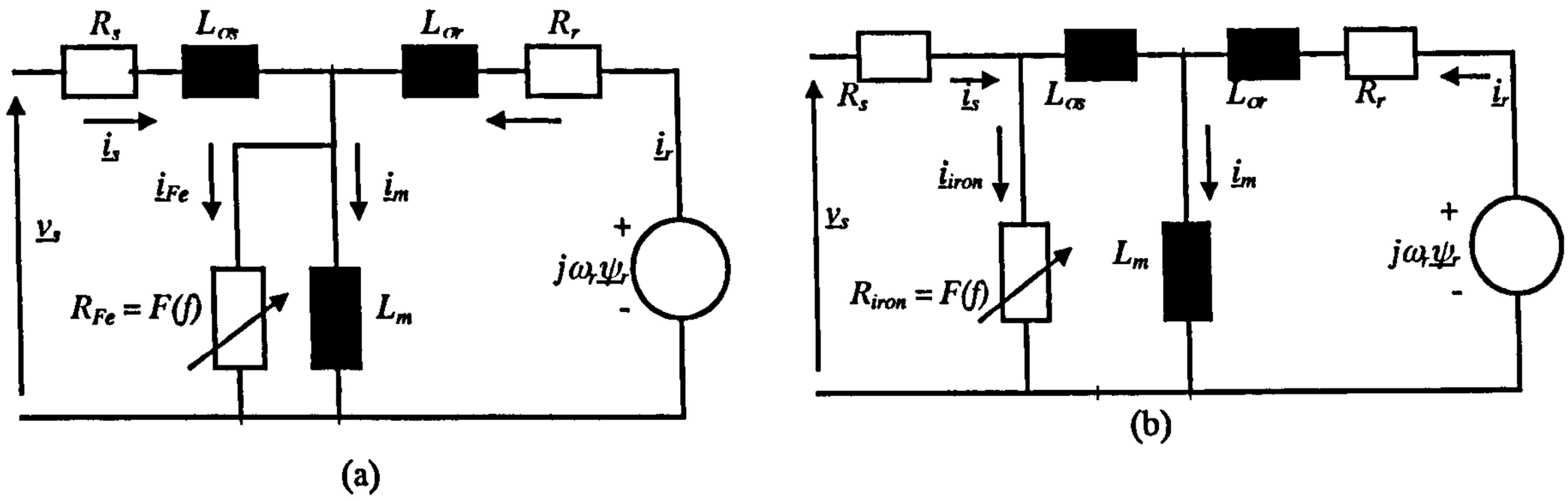

Figure 7.3: Equivalent circuits of an induction machine with iron loss representation (stationary reference frame).

Regardless of which of the two circuits of figure 7.3 is used for the estimator development, the equation of the reference model $\underline{\psi}_s^{(1)} = \int(\underline{v}_s - R_s \cdot \underline{i}_s)dt$ remains the same, since the iron loss is accounted for automatically in the equation. Representation of figure 7.3a has been already considered in chapter 6 in conjunction with compensation of iron loss in torque estimation for direct torque control. Mathematical model required for development of a modified adjustable model follows directly from the equations given in subsection 3.3.1 for the general, arbitrary reference frame, by setting $\omega_a = 0$:

$$0 = R_r \underline{i}_r + d\underline{\psi}_r / dt - j\omega_r \underline{\psi}_r \tag{7.14}$$

$$R_{Fe}\underline{i}_{Fe} = L_m \, d\underline{i}_m / dt \;\Rightarrow\; \underline{i}_{Fe} = T_{Fe}\frac{d\underline{i}_m}{dt} \tag{7.15}$$

$$\underline{\psi}_s = L_{\sigma s}\underline{i}_s + L_m\underline{i}_m \Rightarrow \underline{i}_m = \frac{\underline{\psi}_s - L_{\sigma s}\underline{i}_s}{L_m} \tag{7.16}$$

$$\underline{\psi}_r = L_{\sigma r}\underline{i}_r + L_m\underline{i}_m \Rightarrow \underline{i}_r = \frac{\underline{\psi}_r - L_m\underline{i}_m}{L_{\sigma r}} \tag{7.17}$$

$$\underline{i}_m + \underline{i}_{Fe} = \underline{i}_s + \underline{i}_r \tag{7.18}$$

where $T_{Fe} = L_m/R_{Fe}$. Substituting (7.17) into (7.14), the following equation is obtained:

$$0 = \left(\frac{1}{T_{\sigma r}} - j\omega_r\right)\underline{\psi}_r - \frac{L_m}{T_{\sigma r}}\underline{i}_m + \frac{d\underline{\psi}_r}{dt} \tag{7.19}$$

Substituting (7.15) and (7.16) into (7.18) leads to:

$$\underline{i}_r = \frac{\underline{\psi}_s - L_{\sigma s}\underline{i}_s}{L_m} + T_{Fe}\frac{d\underline{i}_m}{dt} - \underline{i}_s \tag{7.20}$$

Substituting (7.16) into (7.20) yields:

$$\underline{i}_r = \frac{\underline{\psi}_s - L_{\sigma s}\underline{i}_s}{L_m} - \underline{i}_s + \frac{T_{Fe}}{L_m}\left(\frac{d\underline{\psi}_s}{dt} - L_{\sigma s}\frac{d\underline{i}_s}{dt}\right) \tag{7.21}$$

Next, substituting (7.21) into (7.17), one gets:

$$\underline{\psi}_r = L_{\sigma r}\left[\frac{\underline{\psi}_s - L_{\sigma s}\underline{i}_s}{L_m} - \underline{i}_s + \frac{T_{Fe}}{L_m}\left(\frac{d\underline{\psi}_s}{dt} - L_{\sigma s}\frac{d\underline{i}_s}{dt}\right)\right] + L_m\left(\frac{\underline{\psi}_s - L_{\sigma s}\underline{i}_s}{L_m}\right) \tag{7.22}$$

Finally, substituting (7.22) into the equation (7.19) gives differential equation for the adaptive model of the speed estimator. However, it is a second order differential equation, which is far too complicated for practical implementation. The adaptive model of a MRAS speed estimator obtained using the machine model of figure 7.3a is therefore not convenient. The machine model with iron loss representation as in figure 7.3b is used instead. The equivalent iron loss resistor is labelled R_{iron} and $\underline{i}_{iron}$ is the current flowing through the resistor. The following equations are now obtained from the corresponding model of subsection 3.3.2:

$$\underline{i}_{iron} = \frac{\underline{v}_s - R_s\underline{i}_s}{R_{iron}} \tag{7.23}$$

$$\underline{i}_s' = \underline{i}_s - \underline{i}_{iron} = \underline{i}_s - \frac{\underline{v}_s - R_s\underline{i}_s}{R_{iron}} \tag{7.24}$$

$$\underline{\psi}_s = L_s\underline{i}_s' + L_m\underline{i}_r \Rightarrow \underline{i}_r = \frac{\underline{\psi}_s - L_s\underline{i}_s'}{L_m} \tag{7.25}$$

$$\underline{\psi}_r = L_r\underline{i}_r + L_m\underline{i}_s' \tag{7.26}$$

Substitution of (7.25) into (7.26) leads to:

$$\underline{\psi}_r = \frac{L_r}{L_m}\underline{\psi}_s - \sigma\frac{L_r L_s}{L_m}\underline{i}_s' \tag{7.27}$$

Substituting (7.25) and (7.27) into (7.14), the adaptive model is obtained as follows:

$$0 = \left(\frac{1}{T_r} - j\omega_r\right)\underline{\psi}_s + \frac{d\underline{\psi}_s}{dt} - \left(\frac{L_s}{T_r} - j\omega_r\sigma L_s\right)\underline{i}_s' - \sigma L_s\frac{d\underline{i}_s'}{dt} \tag{7.28}$$

or

$$\underline{\psi}_s^{(2)} = \int\left(j\omega_r^e - \frac{1}{T_r}\right)\underline{\psi}_s dt + \int\left(\frac{L_s}{T_r} - j\omega_r^e\sigma L_s\right)\underline{i}_s' dt + \sigma L_s\underline{i}_s' \tag{7.29}$$

Differential equation of the adaptive model can be expressed in terms of α–β components of flux and current in the following form:

$$\begin{aligned}
\psi_{\alpha s}^{(2)} &= -\int\left(\omega_r^e\psi_{\beta s}^{(2)} + \frac{1}{T_r}\psi_{\alpha s}^{(2)}\right)dt + \int\left(\frac{L_s}{T_r}i_{\alpha s}' + \omega_r^e\sigma L_s i_{\beta s}'\right)dt + \sigma L_s i_{\alpha s}' \\
\psi_{\beta s}^{(2)} &= \int\left(\omega_r^e\psi_{\alpha s}^{(2)} - \frac{1}{T_r}\psi_{\beta s}^{(2)}\right)dt + \int\left(\frac{L_s}{T_r}i_{\beta s}' - \omega_r^e\sigma L_s i_{\alpha s}'\right)dt + \sigma L_s i_{\beta s}'
\end{aligned} \tag{7.30}$$

where on the basis of (7.24)

$$\begin{aligned}
i_{\alpha s}' &= i_{\alpha s}\left(1 + \frac{R_s}{R_{iron}}\right) - \frac{v_{\alpha s}}{R_{iron}} \\
i_{\beta s}' &= i_{\beta s}\left(1 + \frac{R_s}{R_{iron}}\right) - \frac{v_{\beta s}}{R_{iron}}
\end{aligned} \tag{7.31}$$

The error quantity equation is the same as in the case without iron loss and it is repeated here for the sake of completeness:

$$\varepsilon = \psi_{\alpha s}^{(2)}\psi_{\beta s}^{(1)} - \psi_{\alpha s}^{(1)}\psi_{\beta s}^{(2)} \tag{7.32}$$

From the equations (7.30) it is evident that the differential equations for the adaptive model of the MRAS speed estimator with iron loss compensation are the same as the differential equations (7.8) when iron loss is ignored, with the exception that $i_{\alpha s}', i_{\beta s}'$ are used instead of $i_{\alpha s}, i_{\beta s}$. The differential equations for the reference model are also the same as those valid without iron loss compensation. It therefore follows that by using the circuit of figure 7.3b an extremely simple speed estimator with iron loss compensation can be constructed. The complexity added by the compensation is negligible, since only two additional algebraic equations (7.31) are needed.

Implementation of this modified speed estimator requires knowledge of the function $R_{iron} = F(f)$ (figure 7.3b). The values of this resistance can be calculated by

using the analogy between the two circuits in figure 7.3 and the knowledge of the equivalent iron loss resistance R_{Fe} of figure 7.3a. This resistance is given in chapter 6 with (6.1) and figure 6.2b. Corresponding approximation for R_{iron} is

$$R_{iron}(\Omega) = 1.73057953\ 10^{-8} f^6 - 4.60525860\ 10^{-6} f^5 + 4.34050219\ 10^{-4} f^4 - 1.92309101\ 10^{-2} f^3 + 5.50004221\ 10^{-1} f^2 + 3.27092043 f + 1.75344637\ 10^2 \quad (7.33)$$

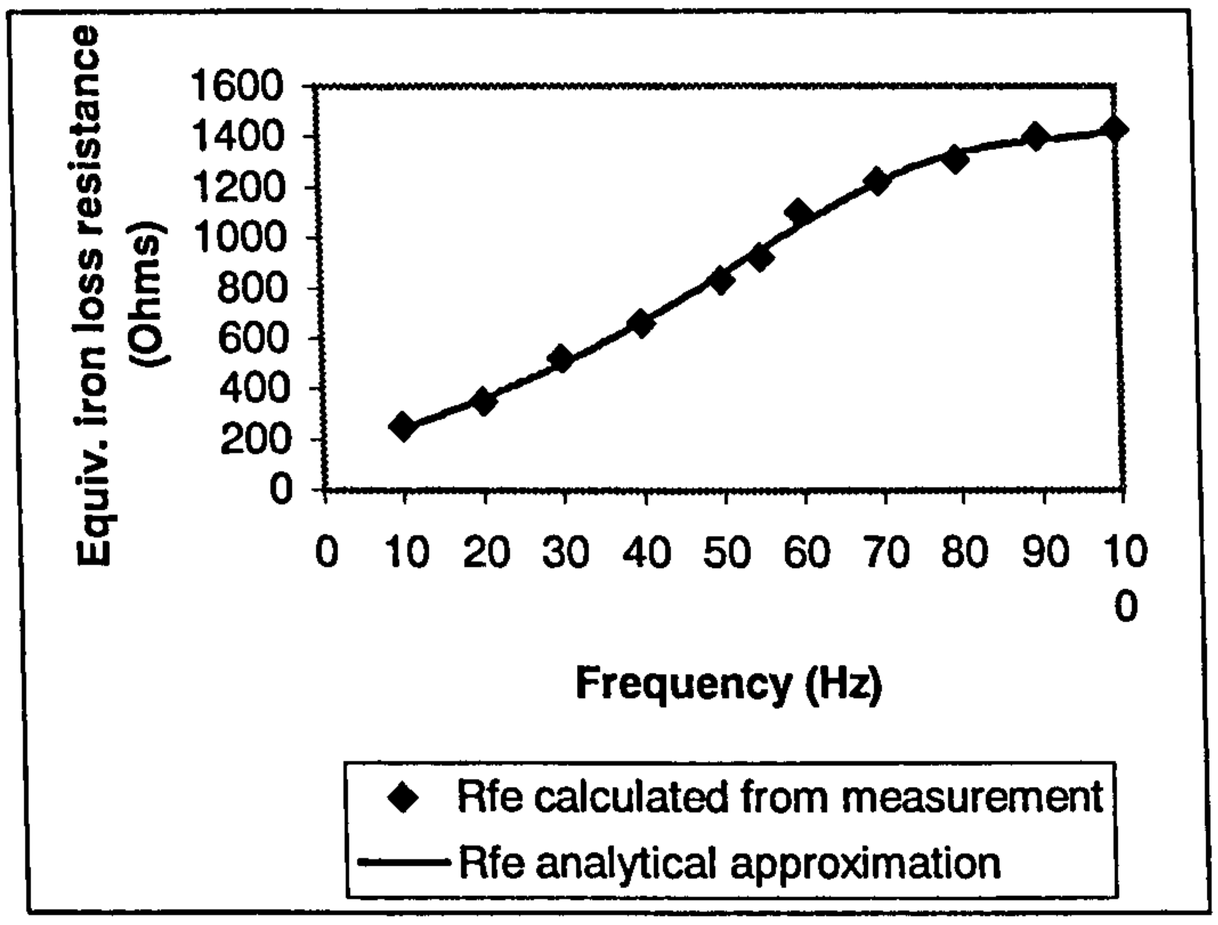

Figure 7.4: Equivalent iron loss resistance R_{iron}: experimentally identified points and corresponding analytical approximation.

7.3.4 A novel rotor flux based MRAS speed estimator using induction machine model with iron loss representation

The machine model of figure 7.3b is used again here to derive the differential equations for the reference model and the adaptive model of the MRAS speed estimator. It is also found that, similarly to the case with stator flux based MRAS speed estimator, the form of differential equations in adaptive model when iron loss is considered is exactly the same as the one for the adaptive model when iron loss is ignored. The only difference is that $\underline{i}_s'$ is used instead of $\underline{i}_s$. The reference model, when iron loss is included, is, however, not exactly the same as the one without iron loss, since both $\underline{i}_s$ and $\underline{i}_s'$ are used in the reference model with iron loss. The current $\underline{i}_s'$ remains to be given with (7.24) and (7.31).

The differential equations for the reference and the adaptive model are now:

$$\frac{d\underline{\psi}_r^{(1)}}{dt} = \frac{L_r}{L_m}\left(\underline{v}_s - R_s \underline{i}_s - \sigma L_s \frac{d\underline{i}_s'}{dt}\right) \quad (7.34a)$$

$$\frac{d\underline{\psi}_r^{(2)}}{dt} = \left(j\omega_r^e - \frac{1}{T_r} \right) \underline{\psi}_r^{(2)} + \frac{L_m}{T_r} \underline{i}_s^{'} \tag{7.34b}$$

The reference and adaptive models can be expressed in terms of α–β components of rotor flux, stator voltage and stator current as follows:

$$\begin{aligned}
\psi_{\alpha r}^{(1)} &= \frac{L_r}{L_m} \int \left(v_{\alpha s} - R_s i_{\alpha s} \right) dt - \frac{L_r}{L_m} \sigma L_s i_{\alpha s}^{'} \\
\psi_{\beta r}^{(1)} &= \frac{L_r}{L_m} \int \left(v_{\beta s} - R_s i_{\beta s} \right) dt - \frac{L_r}{L_m} \sigma L_s i_{\beta s}^{'}
\end{aligned} \tag{7.35}$$

$$\begin{aligned}
\psi_{\alpha r}^{(2)} &= -\int \left(\omega_r^e \psi_{\beta r}^{(2)} + \frac{1}{T_r} \psi_{\alpha r}^{(2)} \right) dt + \frac{L_m}{T_r} \int i_{\alpha s}^{'} dt \\
\psi_{\beta r}^{(2)} &= -\int \left(\omega_r^e \psi_{\alpha r}^{(2)} + \frac{1}{T_r} \psi_{\beta r}^{(2)} \right) dt + \frac{L_m}{T_r} \int i_{\beta s}^{'} dt
\end{aligned}$$

The error quantity remains to be given with (7.13).

The mathematical models of model reference adaptive systems discussed in this section are further used to build speed estimators in Matlab/Simulink. These Matlab/Simulink models of the speed estimators are then used for the simulation of sensorless direct torque control. The models, which include iron loss compensation, are used in conjunction with Simulink model of an induction machine, which includes iron loss (subsection 3.3.1, figure 7.3a). The speed estimators based on the equations for standard constant parameter induction machine model are used in conjunction with models of induction machines with and without iron loss (standard machine model). This will enable examination of not only the behaviour of MRAS based speed estimator when the system is completely ideal, but also the effects of iron loss when it is ignored in the speed estimator. The speed estimators presented here used the measured signals that are anyway required for standard DTC scheme of an induction machine, for the purpose of stator flux and torque estimation.

7.4 Sensorless direct torque control with stator flux based MRAS speed estimator

Simulation results, obtained using developed Simulink models, are discussed in what follows. It should be noted that the reference torque is limited to ±1.5 rated torque, while stator flux and torque estimation is the same as the one used in chapters 5 and 6. Application of the speed estimator with iron loss compensation requires

utilisation of the frequency dependent function $R_{iron} = F(f)$ of figure 7.4. The stator frequency is approximated in the compensation scheme with $f \cong \omega_r^e / 2\pi$, obtained as explained in chapter 6, section 6.3. Parameters of the direct torque controller are the same as the one used in previous chapters.

Speed estimators with stator flux based MRAS are used for the sensorless DTC of induction machine in the following simulations. The speed estimator without iron loss compensation is used first in conjunction with three models of the induction machine, standard constant parameter machine model, machine model with iron loss and machine model with iron loss and compensation for iron loss in the torque estimator of the DTC scheme. The speed estimator with iron loss compensation is then used with the machine model including iron loss and compensation of iron loss in the torque estimator. In each case, the simulation of acceleration of induction motor from standstill to one half of the rated speed and then to rated speed, with load rejection test at both speeds, deceleration from one half of the rated speed (medium speed region) to low speed and reversal from positive one half of the rated speed to negative one half of the rated speed are carried out. The signals of the system, such as motor angular electrical speed, estimated speed, motor torque and motor flux, are collected and analysed.

7.4.1 Simulations using standard constant parameter machine model

The simulations are carried out for the first 1.5 sec after starting of the induction motor. Simulation of the motor acceleration is carried out first. The induction motor is accelerated to one half of the rated speed (720 rpm) with rated stator flux command, then load torque equal to the motor rated torque is applied to test torque rejection capability of the speed controller. The motor is then accelerated to rated speed (1440 rpm). Again, the rejection test with rated load torque is carried out at this speed. Actual speed and estimated speed of the motor are observed and compared during the simulation. The deceleration of the sensorless DTC is the next simulation. The motor is decelerated from one half of the rated speed to 10% of the rated speed. Speed reversing of the induction motor from positive one half of the rated speed to negative one half of the rated speed is also simulated. These simulations will be carried out for the two direct torque controllers of an induction machine, direct torque controller with Takahashi's switching table and the controller with switching table suggested by [Casadei et al

(1994)] (subsection 5.3.1, table 5.3). A comparison between the speed, torque and stator flux responses from the two controllers is then made.

Actual speed of the motor, estimated speed from the estimator and load torque during the acceleration of the induction motor are shown in figure 7.5. Both controllers give good speed responses. The actual speed and the estimated speed are in good agreement. Load torque rejection properties are also good for both controllers. With regard to the speed response during acceleration, modified switching table of [Casadei et al (1994)] gives good response, comparable with the one obtained with Takahashi's switching table.

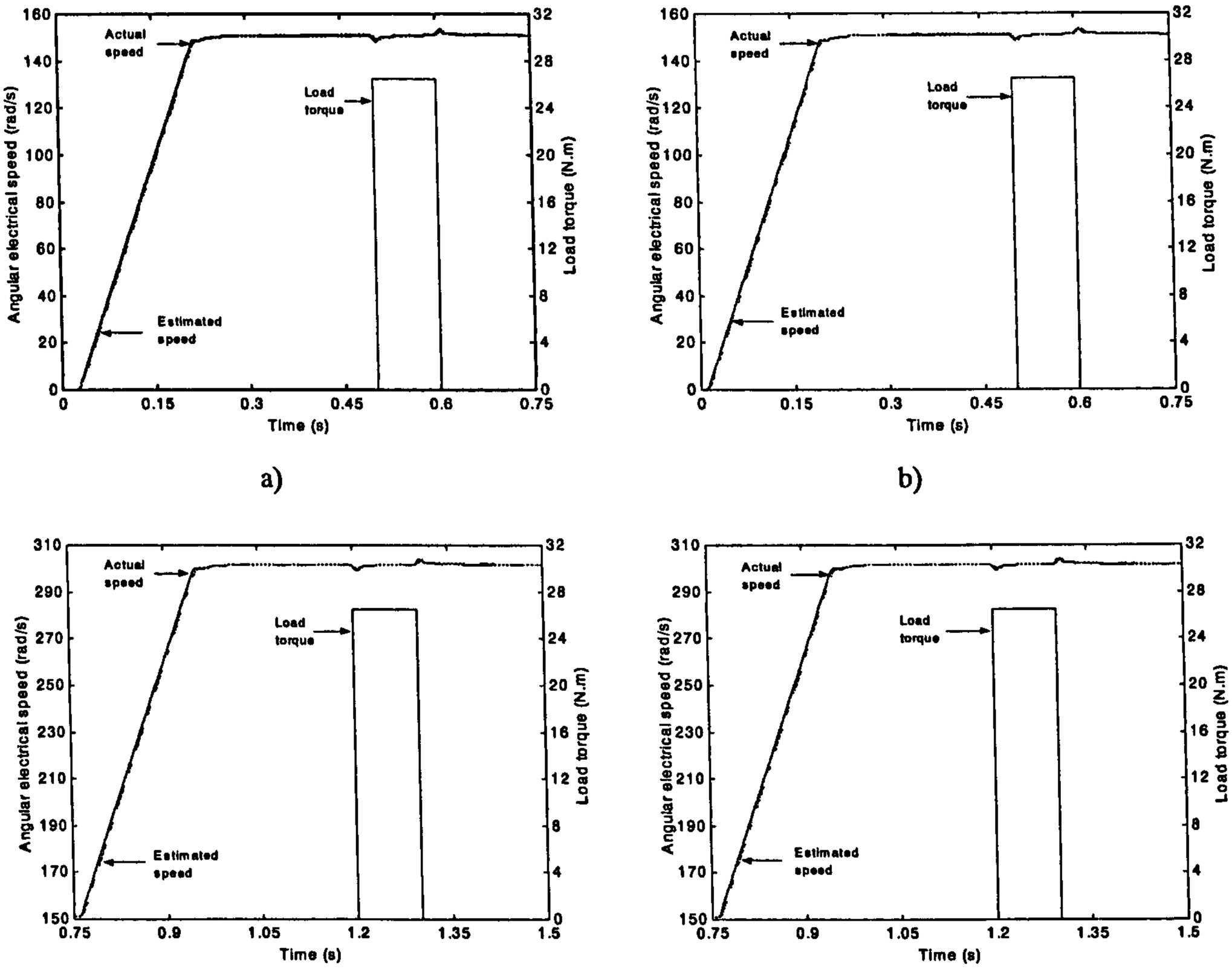

Figure 7.5: Sensorless direct torque control: a) acceleration to 0.5 p.u. speed with Takahashi's switching table, b) acceleration to 0.5 p.u. speed with Casadei's switching table, c) acceleration to rated speed with Takahashi's switching table, d) acceleration to rated speed with Casadei's switching table.

Deceleration transient and reversing transient are examined next and the results are given in figures 7.6 and 7.7, respectively. Speed response with DTC using

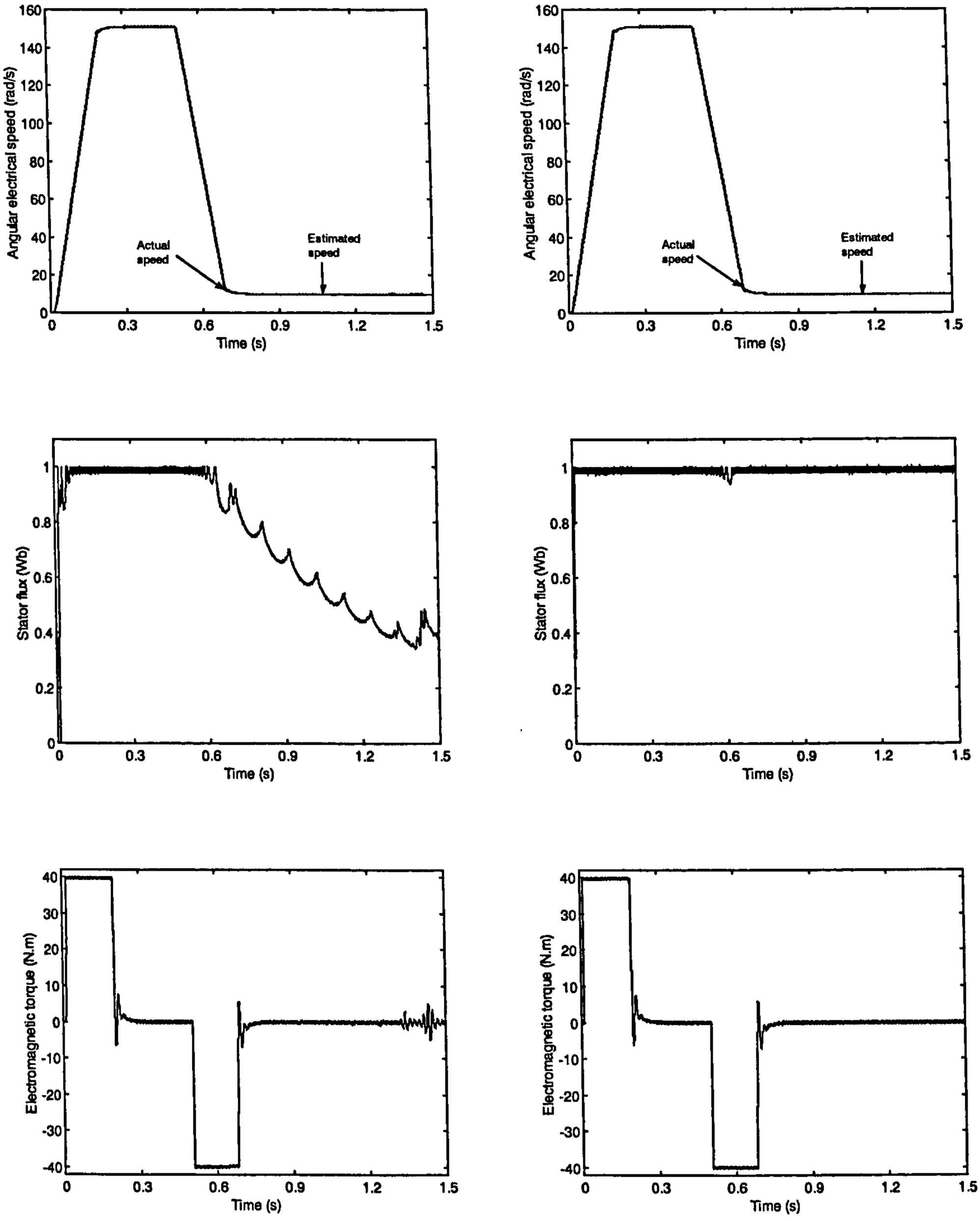

Figure 7.6: Deceleration to 10 rad/s of an induction machine with direct torque control: a) speed, stator flux and motor torque with Takahashi's switching table b) speed, stator flux and motor torque with Casadei's table.

Takahashi's switching table is the same as speed response with Casadei's switching table during the deceleration and in the low speed region. The stator flux response

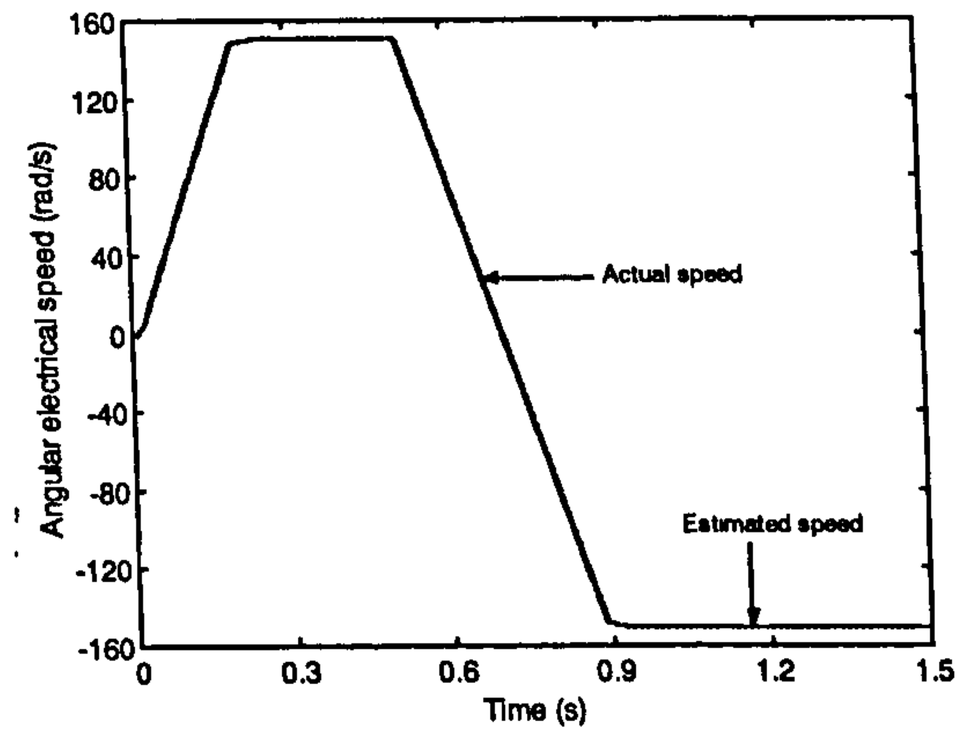

a)

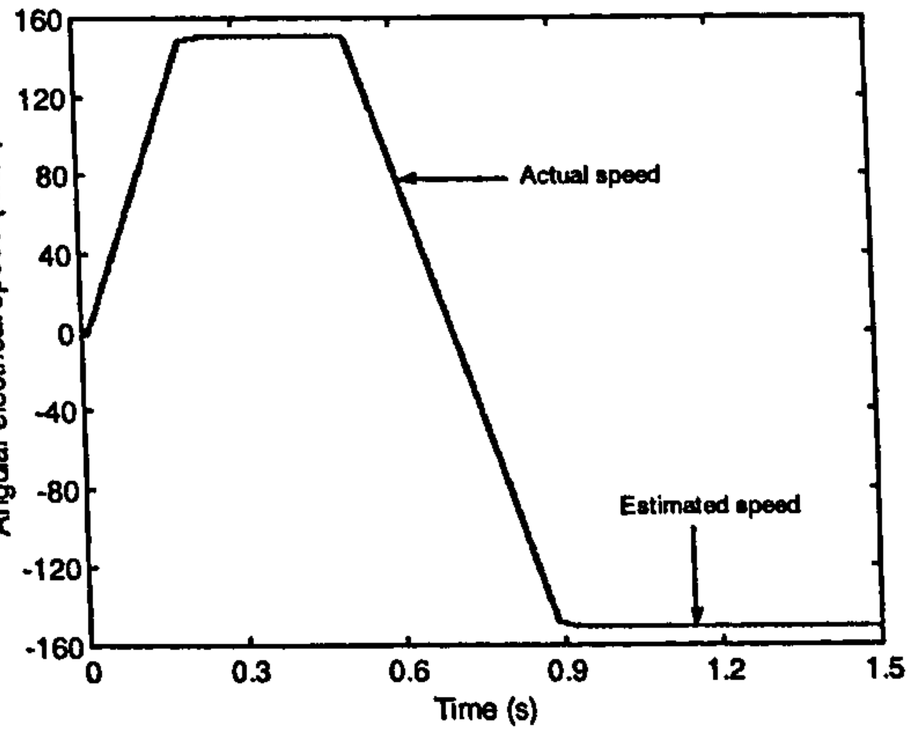

b)

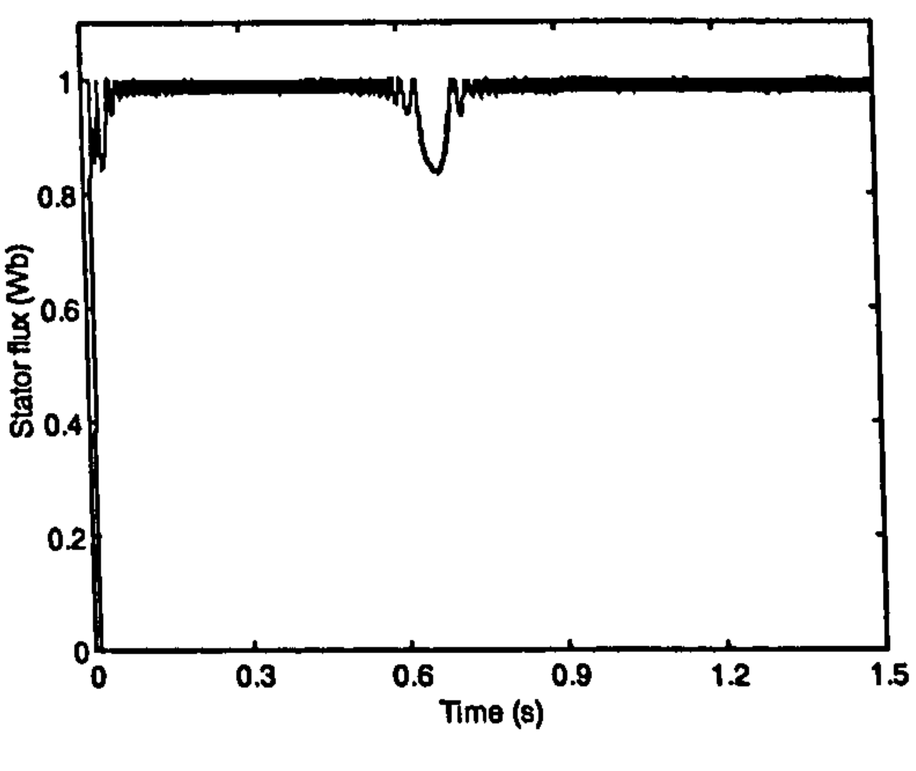

c)

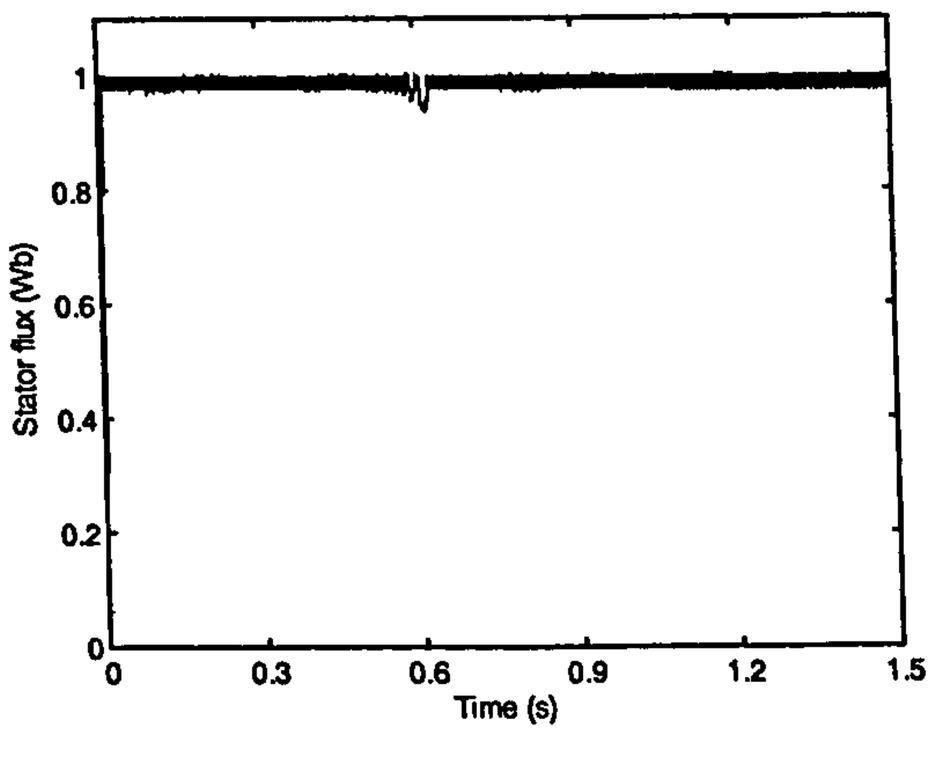

d)

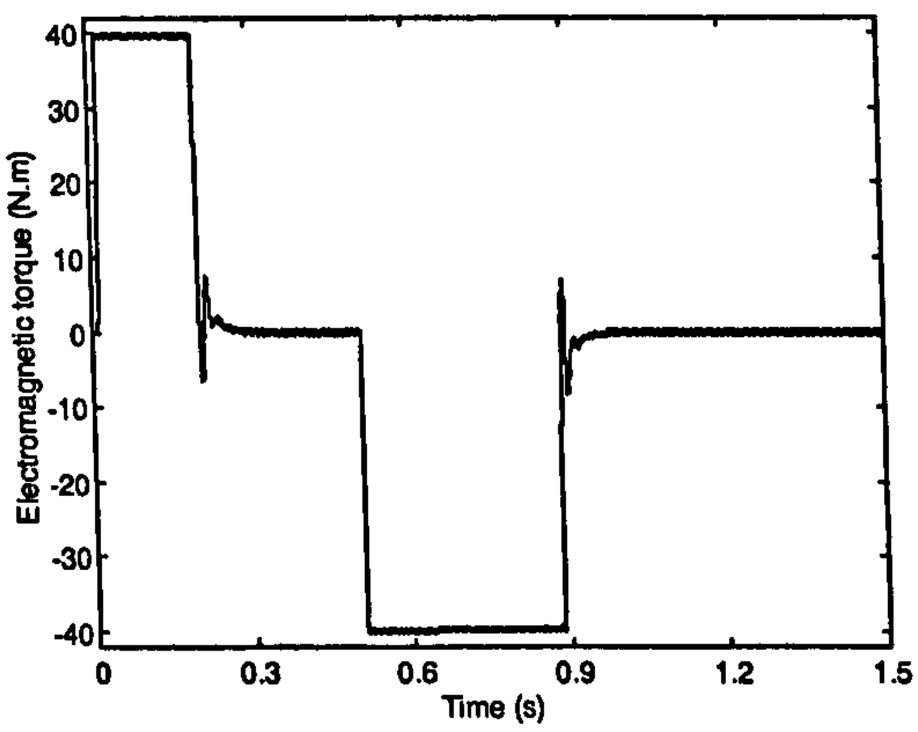

e)

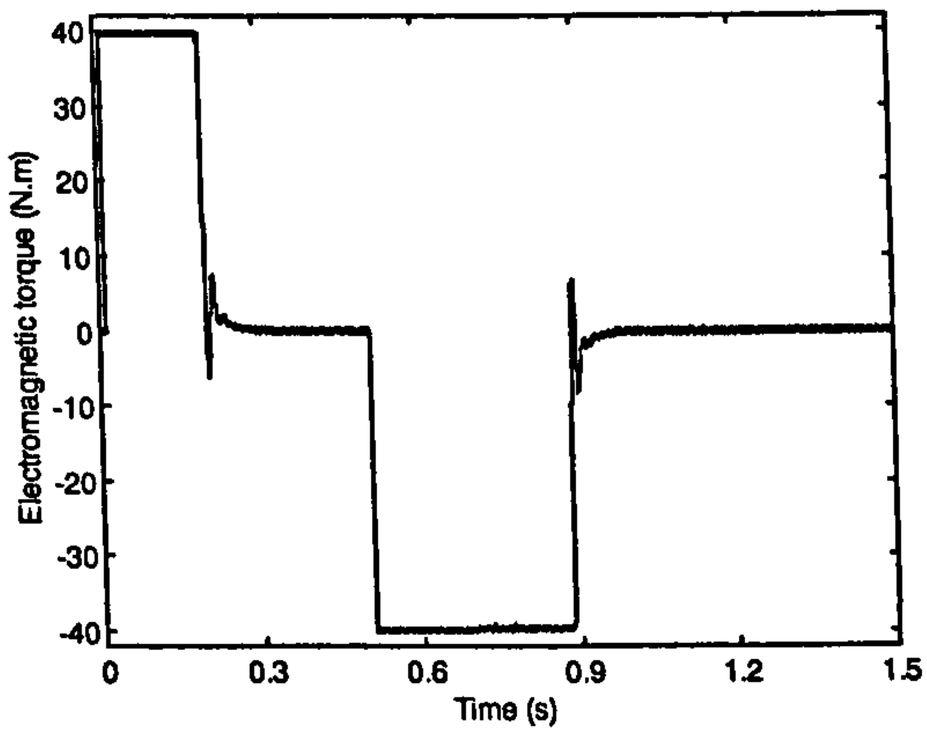

f)

Figure 7.7: Reversing from +0.5p.u. speed to –0.5p.u. speed with direct torque control: a) speeds, stator flux and torque with Takahashi's table, b) speeds, stator flux and torque with Casadei's table.

with Takahashi's switching table is severely weakened due to the applications of zero voltage vectors when the motor is operating in the low speed region.

The stator flux is reduced to nearly zero instead of being kept at rated value. Torque with Takahashi's switching table is distorted when the stator flux is reduced to below 0.4 Wb as shown in figure 7.6a. Distortion is not observed in torque response in the low speed region when the stator flux is weakened but still above 0.4 Wb. Estimated speed is, however, still consistent with measured speed when torque is distorted. The speed response with modified switching table of [Casadei et al (1994)] is equally good and stable in the low speed region as shown in figure 7.6b. Stator flux of the induction motor is, nonetheless, just slightly distorted during the deceleration, but then it remains within the hysteresis bands around the rated value. Torque response is not distorted during the deceleration.

Similarly, the stator flux of induction motor with Takahashi's switching table is weakened, down to 0.8 Wb, when the speed is in low speed region during the reversing transient (figure 7.7a). The stator flux is then brought back to within the hysteresis band when the speed is increased in the negative direction. Torque is therefore not affected by the flux weakening. Both estimated and measured speeds are also not distorted. From these simulations it can be concluded that sensorless DTC with switching table of Casadei (1994) gives better performance in all regimes of operation. It is for this reason that all the subsequent simulations are carried out with this switching table.

Figure 7.8 shows the error between the estimated speed and actual speed in steady state. These are zoomed extracts from figure 7.5.

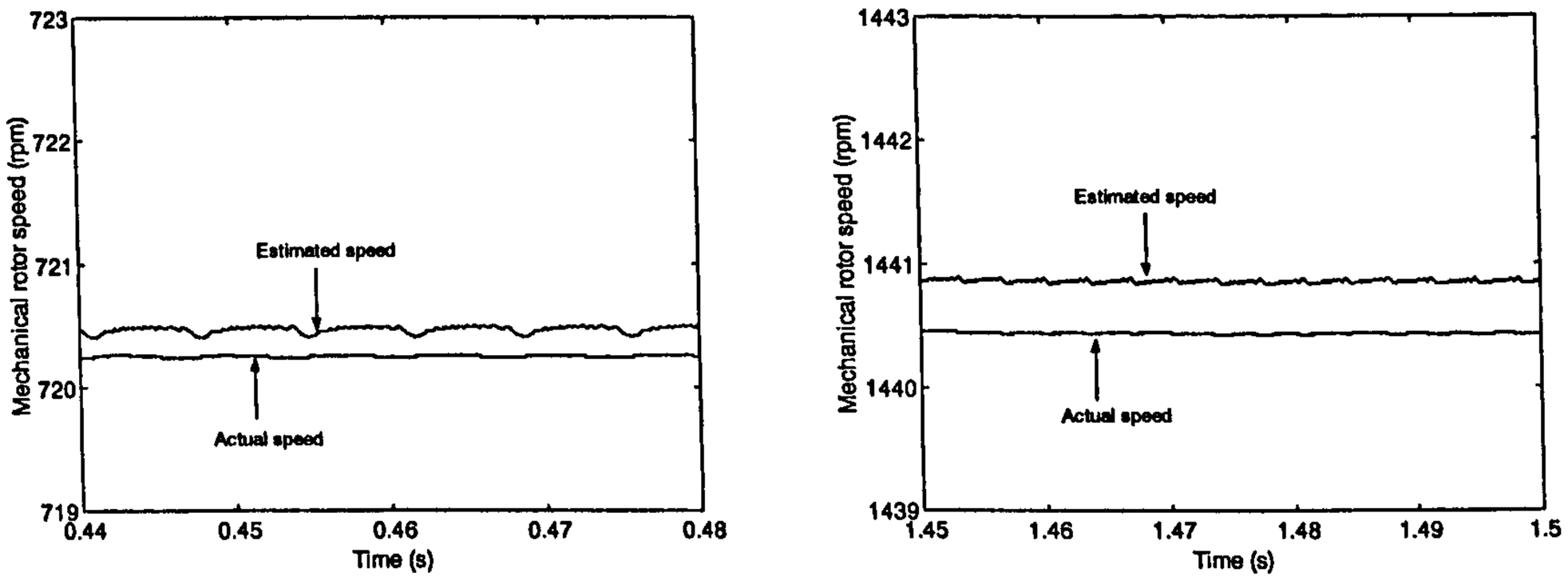

a) b)

Figure 7.8: Illustration of the speed estimation error in steady state with DTC (switching table of Casadei (1994)), a) at one half of the rated speed, b) at rated speed.

One expects that, since ideal operating conditions are under consideration and there is not detuning of any kind in the speed estimator, the actual and the estimated speed should be the same. Moreover, since a PI controller is used as the speed controller, the reference speed (720 rpm and 1440 rpm, respectively) must be equal to the speed used as feedback (estimated speed here) in any steady state. Indeed, when the actual speed was used as feedback in the same simulation, with the same programme, the reference and the actual speed were equal. However, estimated speed still deviated from the other two by approximately the same amount as in figure 7.8. Numerous attempts to rectify this anomaly by changing the parameters of the two PI controllers and the simulation programme were fruitless and no plausible explanation can be offered for the existence of speed errors in figure 7.8. This means that all the other values of steady state speed estimation error, shown further on, have to be considered in terms of their relative value with respect to those of figure 7.8.

7.4.2 Simulations using induction machine model with iron loss representation

Iron loss is now included in the simulation of the sensorless DTC. Iron loss resistance as a function of stator frequency is included in the machine model. The same simulation tests are carried out and, as stated above, DTC with switching table of [Casadei et al (1994)] is used. Figure 7.9 shows actual speed, estimated speed, stator flux and electromagnetic torque during the acceleration and load rejection tests. Figure 7.10 shows stator flux, torque and the speeds during deceleration and speed reversal.

The speed response during acceleration is always slower than the speed response obtained when iron loss is ignored. This is due to the reduction of the useful motor output torque caused by the iron loss. Stator flux ripples are unaffected as has been shown in chapter 6. Torque response of the induction motor initially goes negative at the starting of the motor, which is the reason of negative value of the actual speed. Torque response in the limit is below the set torque limit, due to the iron loss. The actual torque output is therefore less than the estimated torque. Actual speed and estimated speed are in rather good agreement during the deceleration and speed reversing. Both torque and flux responses during deceleration and speed reversing are also consistent with the ones obtained during acceleration.

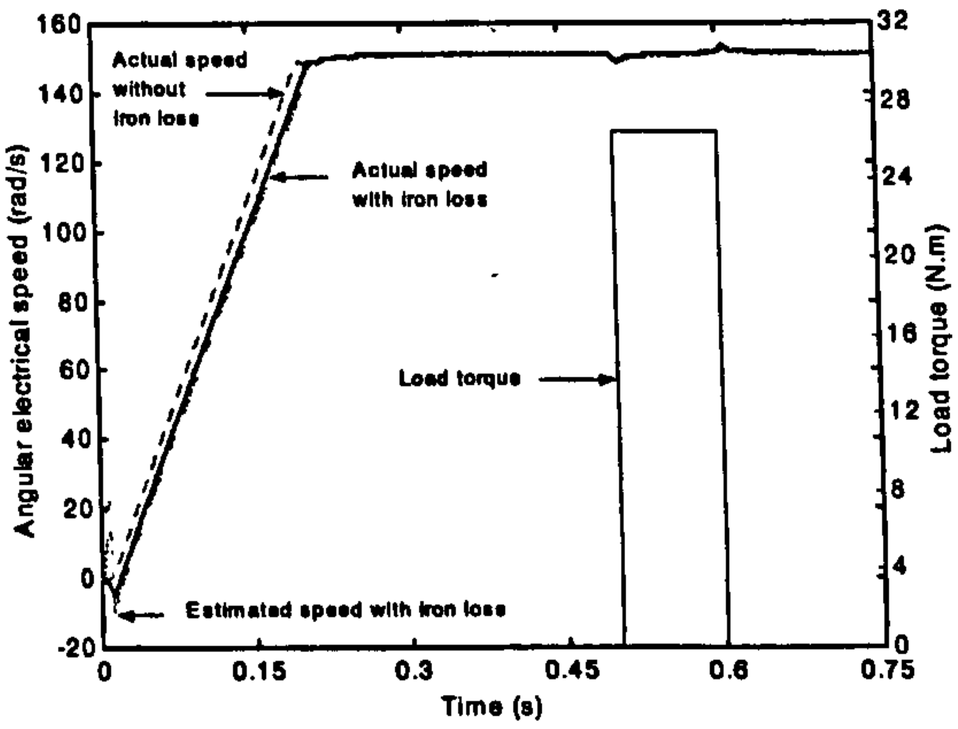

a)

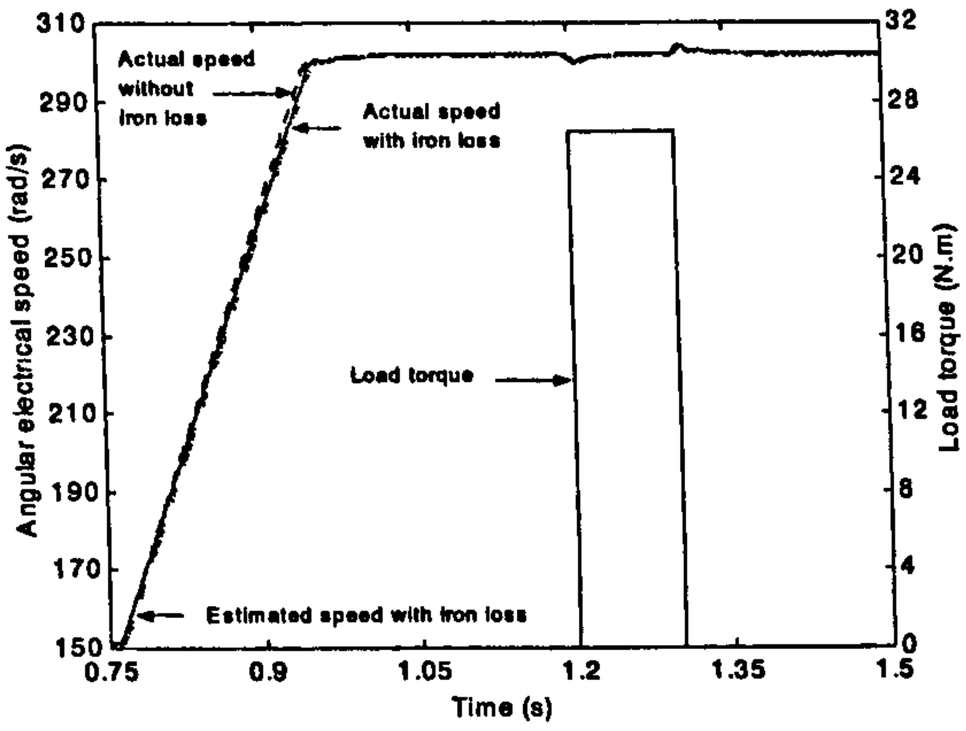

b)

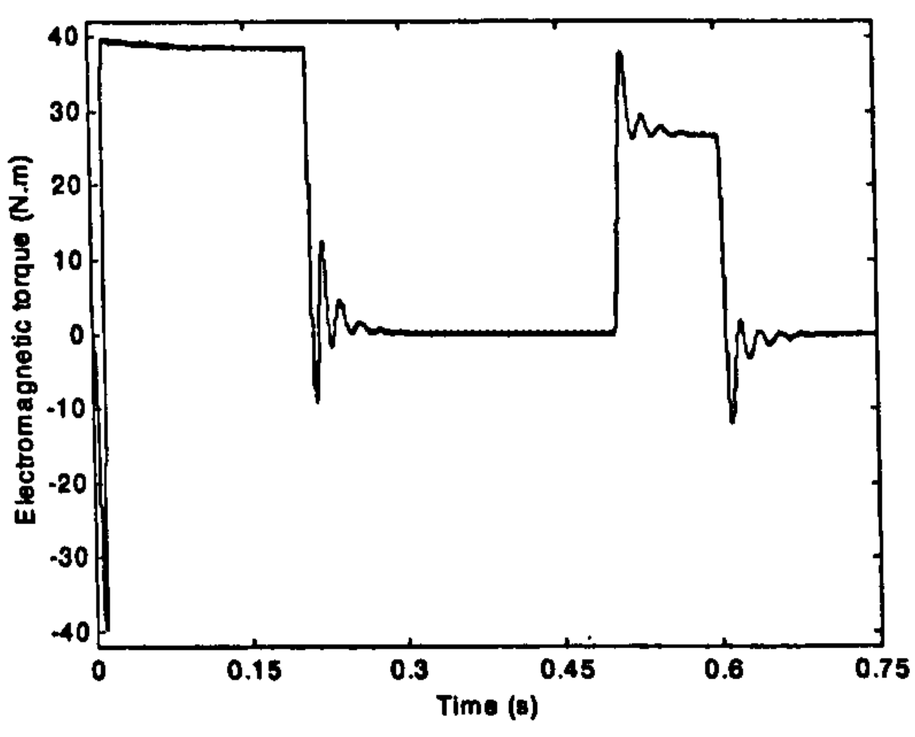

c)

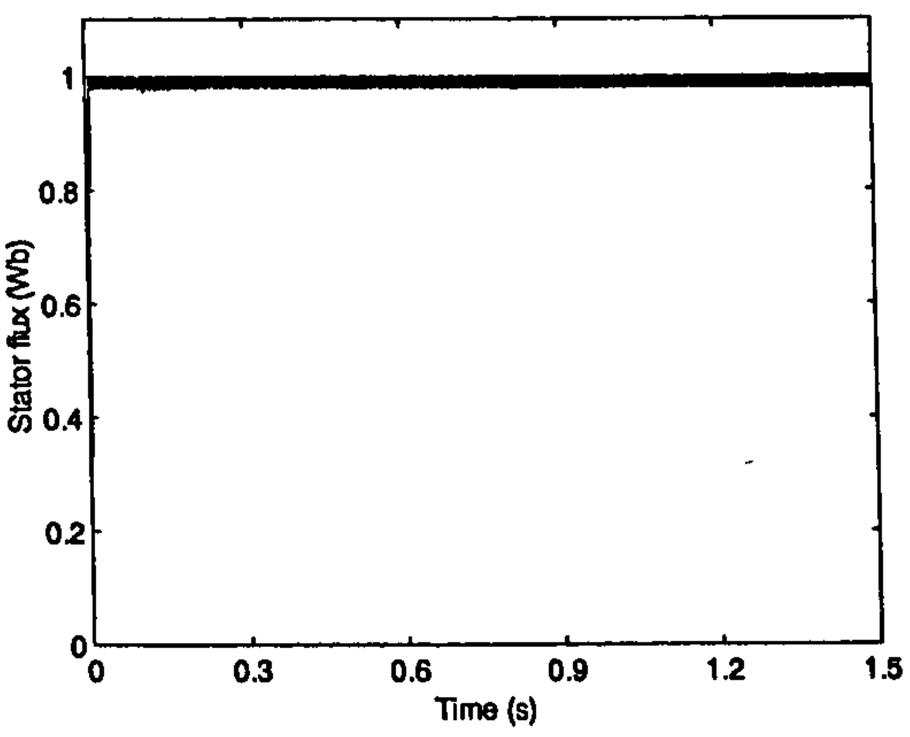

d)

Figure 7.9: Impact of iron loss on sensorless DTC: a) acceleration to one half of the rated speed, b) acceleration to rated speed, c) electromagnetic torque acceleration to 0.5 p.u. speed, d) stator flux acceleration to 0.5 p.u. speed. Load rejection transient encompassed by all traces. Iron loss is not compensated in any part of the DTC scheme.

7.4.3 Simulations using induction machine model with iron loss representation and iron loss compensation in torque estimator

A constant compensation torque increment of 1.15 Nm is introduced in the torque estimator. This compensation will account for the reduction in the available torque of the induction motor due to iron loss. The need for this compensation was elaborated in detail in chapter 6, where the origin of this constant torque increment was addressed as well. Acceleration transients are illustrated, together with load rejection, in figure 7.11.

Deceleration and reversing transients are studied once more and the results are shown in figure 7.12. The actual speed response of the induction motor with compensation of iron loss in the torque estimator is slightly faster than the actual speed

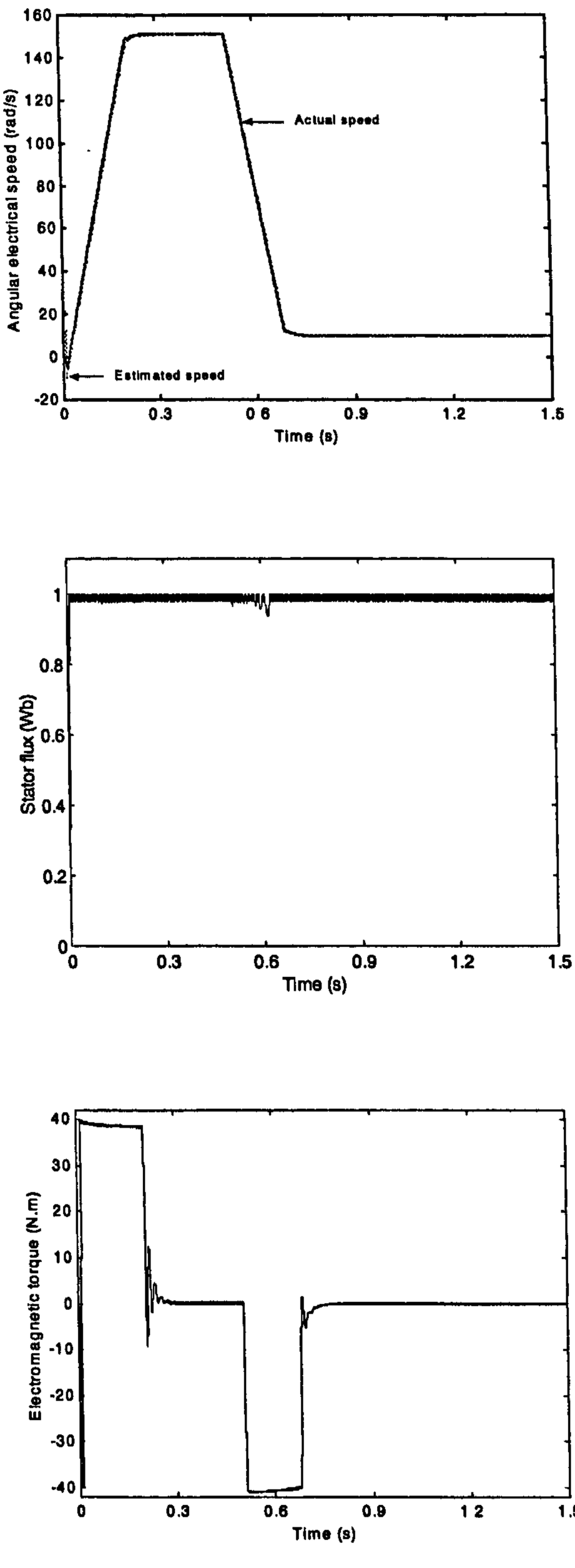

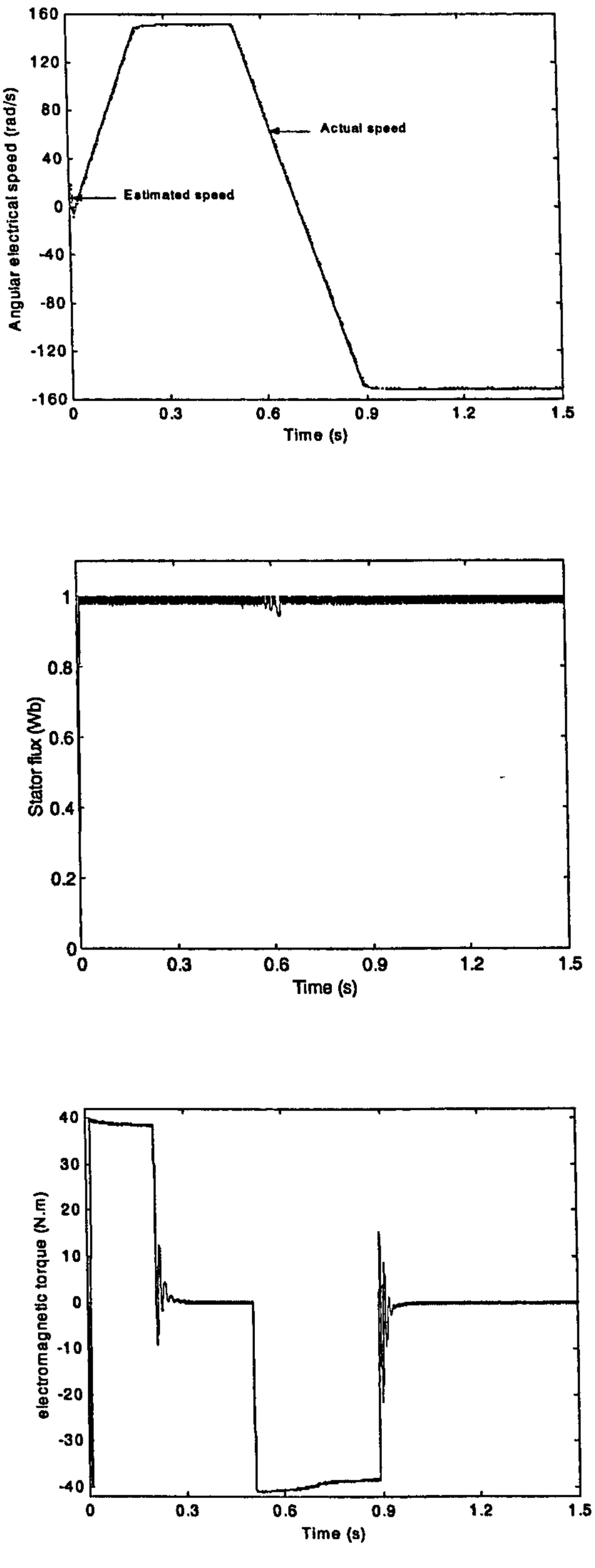

a) b)

Figure 7.10: Impact of iron loss on deceleration and reversing transient: a) speeds, stator flux and torque during deceleration to 10 rad/s, b) speeds, stator flux and torque during reversing from +0.5 p.u. speed to -0.5 p.u. speed. Iron loss is not compensated anywhere in the controller.

response when the iron loss is completely ignored in the controller, which is the same as the estimated speed response. The difference is more visible in the low speed region.

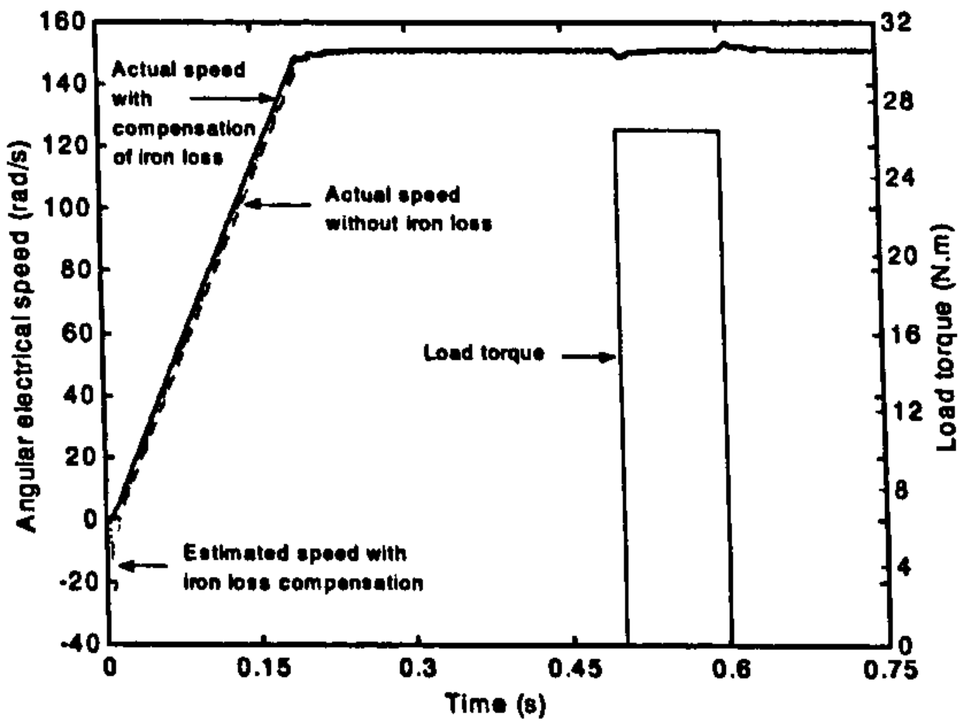

a)

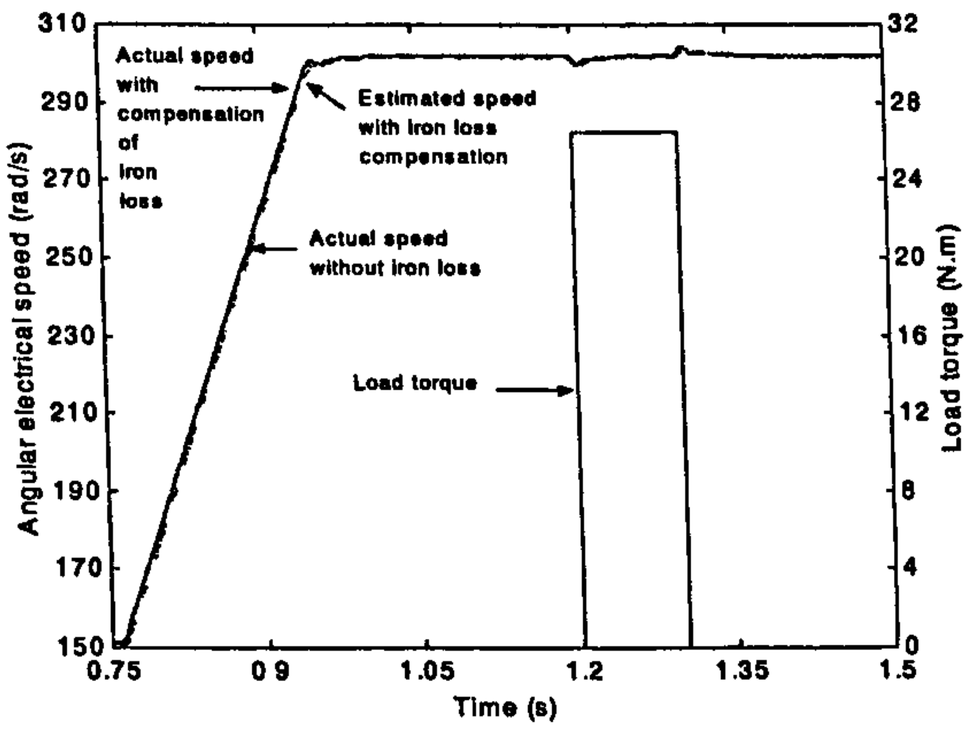

b)

Figure 7.11: Acceleration of the induction motor with iron loss compensation in the torque estimator, a) to one half of the rated speed, b) to rated speed.

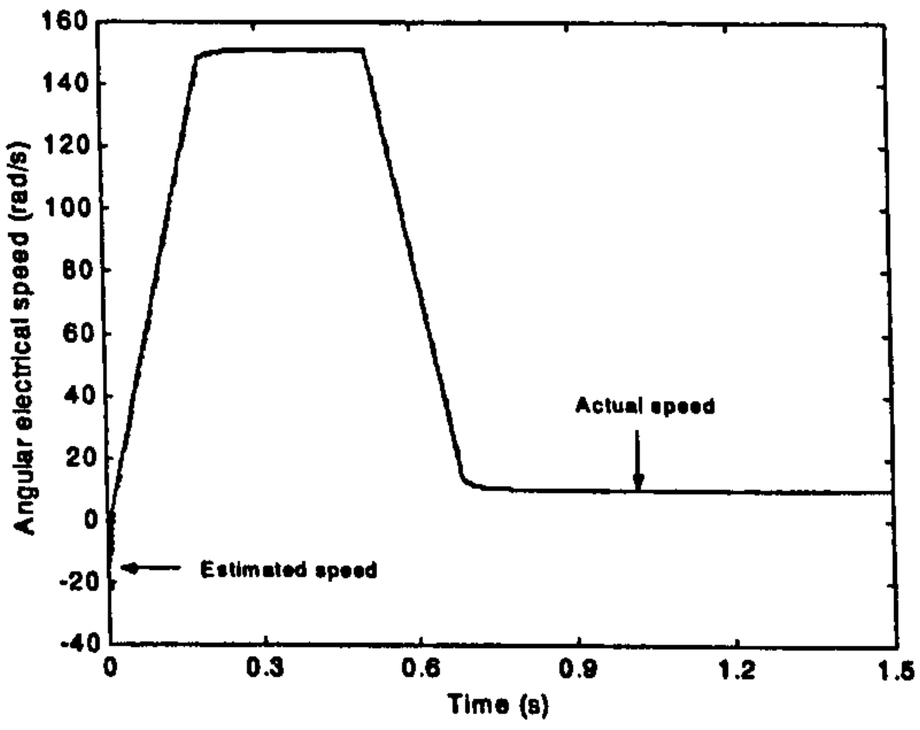

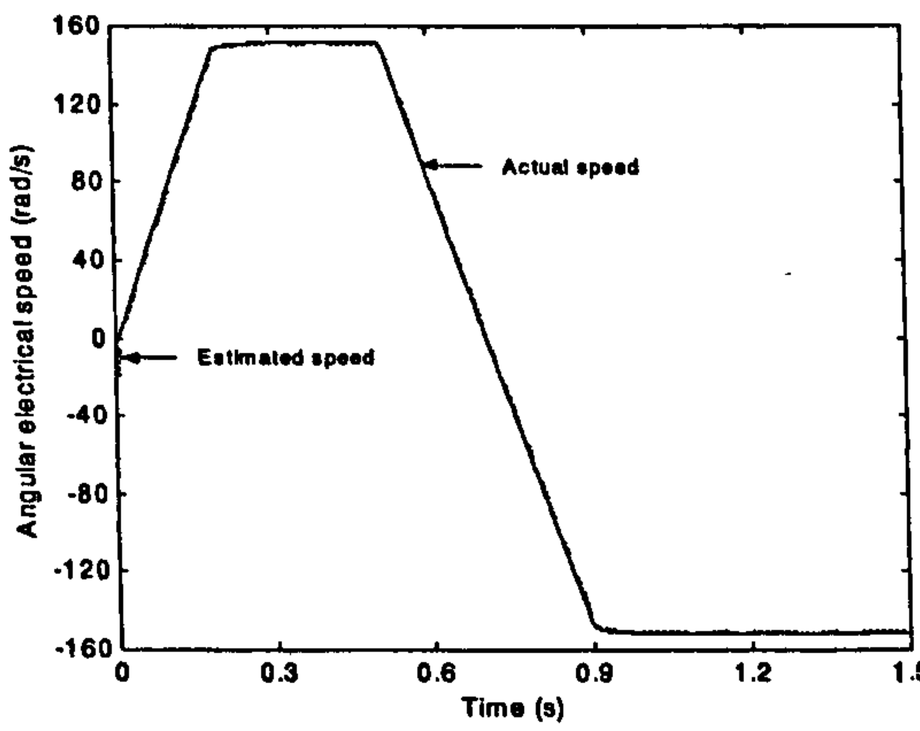

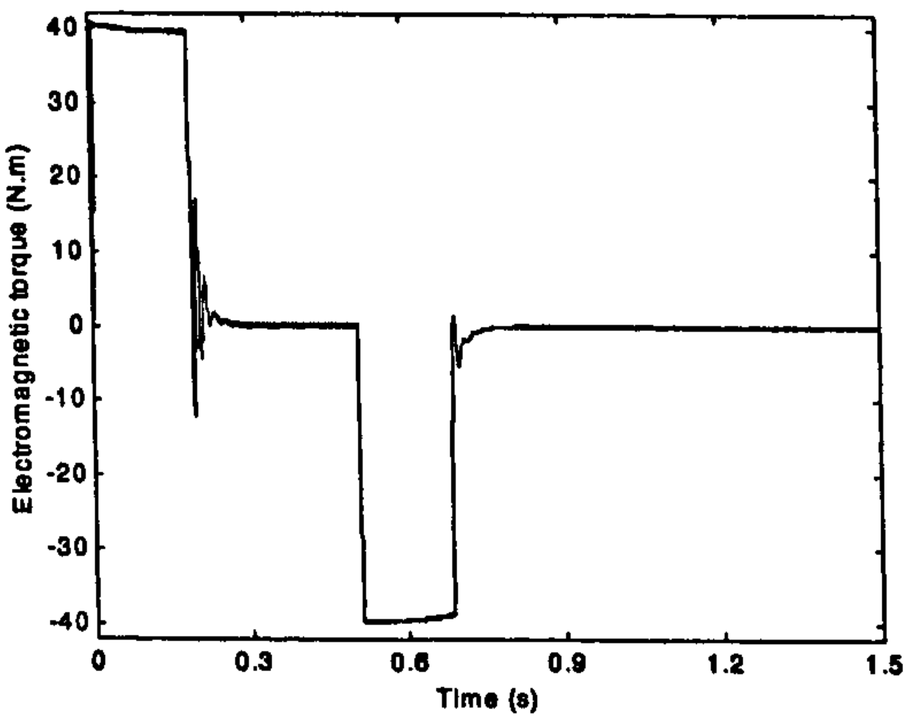

a)

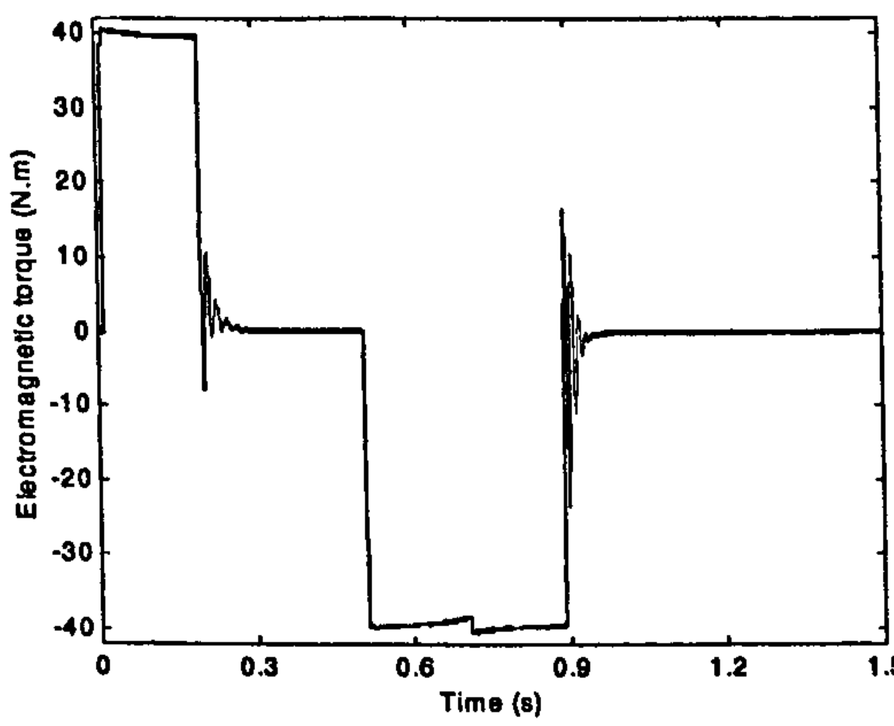

b)

Figure 7.12: Deceleration and reversing with iron loss compensation in the torque estimator. Speeds and torque during deceleration to 10 rad/s a), and during reversing b).

Flux responses are essentially the same as in the case without compensation, and therefore are not shown again here. Torque is over-compensated at the very low speed

during motoring. This is because the torque increment of 1.15 Nm is too high at low frequency. Over-compensation also happens during braking, when the absolute value of the estimated torque (estimated torque is negative in braking) is higher than the one of the actual torque (which is also negative). The compensation of iron loss in the torque estimator is speed-sign dependent. The increment is negative when actual speed is positive, and positive when the actual speed is negative.

Therefore, torque response is also over-compensated when the speed is low and negative. A small jump in the motor torque value can be observed during reversing transient (figure 7.12b) at the instant when speed changes sign. This is the consequence of the crude torque error compensation through a constant torque increment. It was verified during the course of investigation that such a jump does not take place when torque compensation is implemented using frequency dependent increment (section 6.4).

7.4.4 Simulations using induction machine model with iron loss representation and compensation for iron loss in both torque and speed estimators

The compensation of iron loss in the torque estimator fails to improve speed estimation accuracy. Iron loss compensation is therefore incorporated now in the speed estimator as well. The iron loss resistance R_{iron} is a function of frequency. Estimated speed frequency is used to calculate the iron loss resistance in the speed estimator instead of the stator frequency because of its practical availability within the controller. Figure 7.13 shows the estimated speed and the actual speed when iron loss is compensated in both the torque and speed estimators, along with actual speeds from the three previously studied cases (iron loss completely ignored, iron loss included in the motor model but without any compensation, and iron loss compensated in the torque estimator only). The speed traces apply to acceleration, load rejection transient and subsequent steady state. Deceleration transient is shown in figure 7.13f and figure 7.14.

Figure 7.13a shows good stability of the estimated speed at the starting of the induction motor. The estimated speed and the actual speed are in good agreement in low speed as well as high speed regions. Steady state error between the estimated speed and the actual speed is reduced when iron loss compensation is included, both at one half of

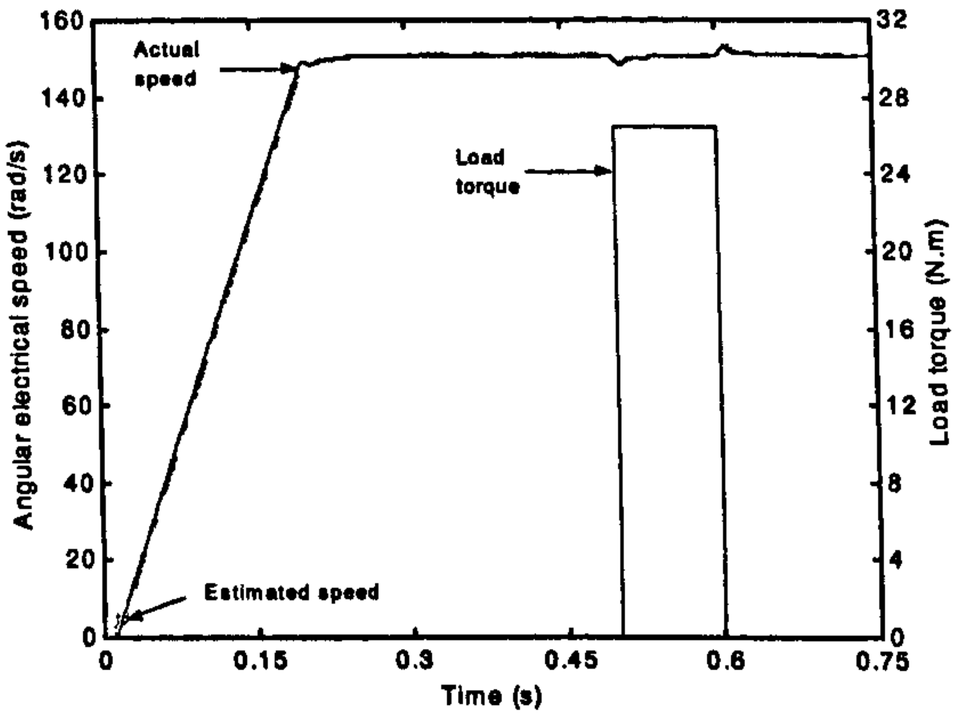

a)

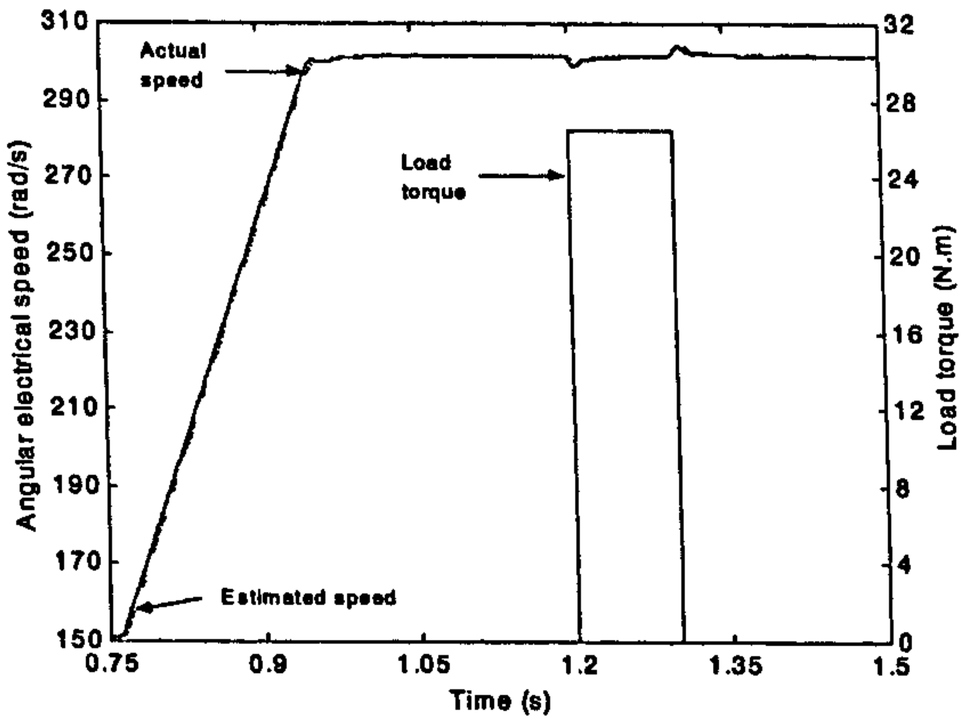

b)

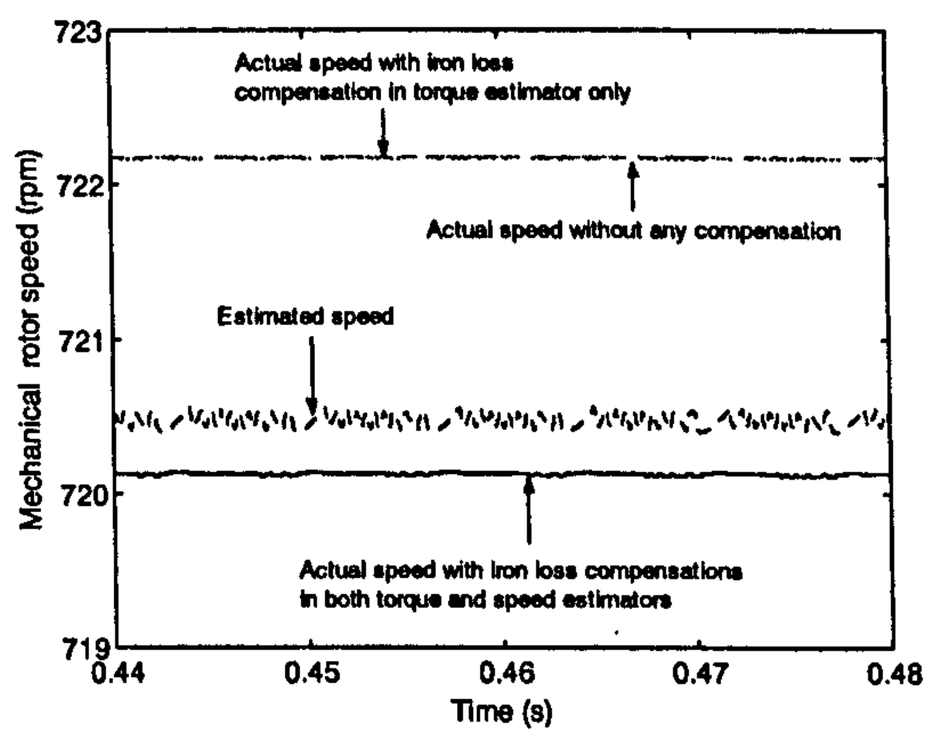

c)

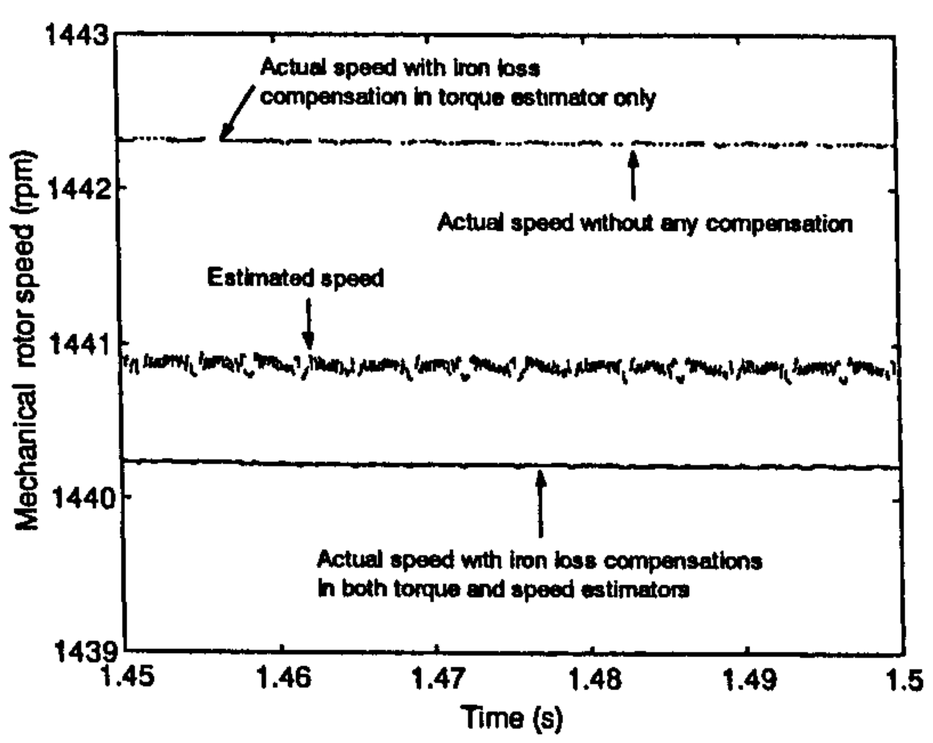

d)

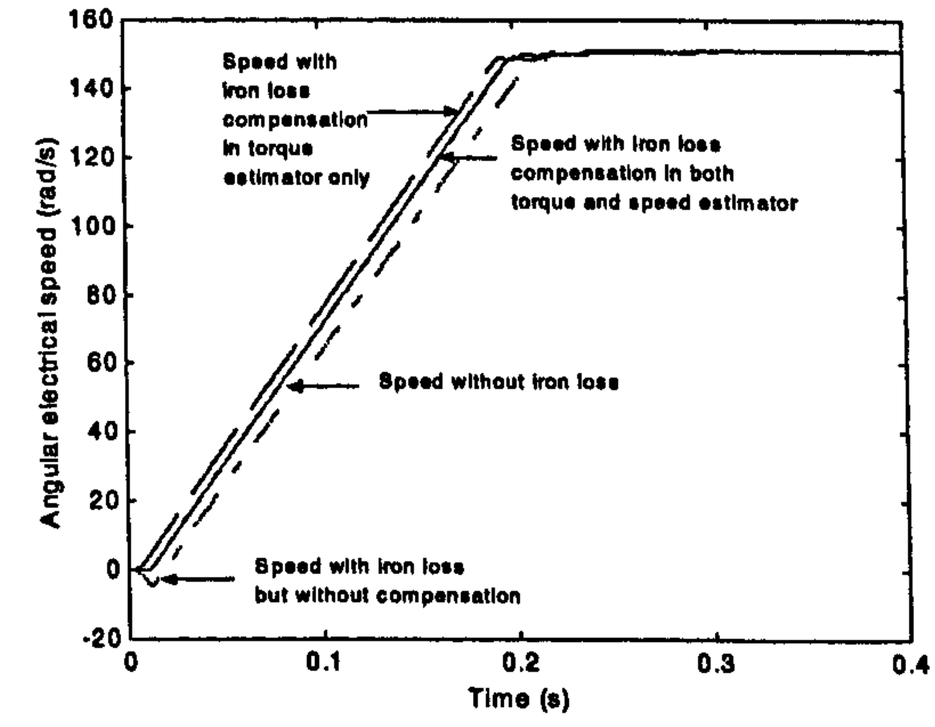

e)

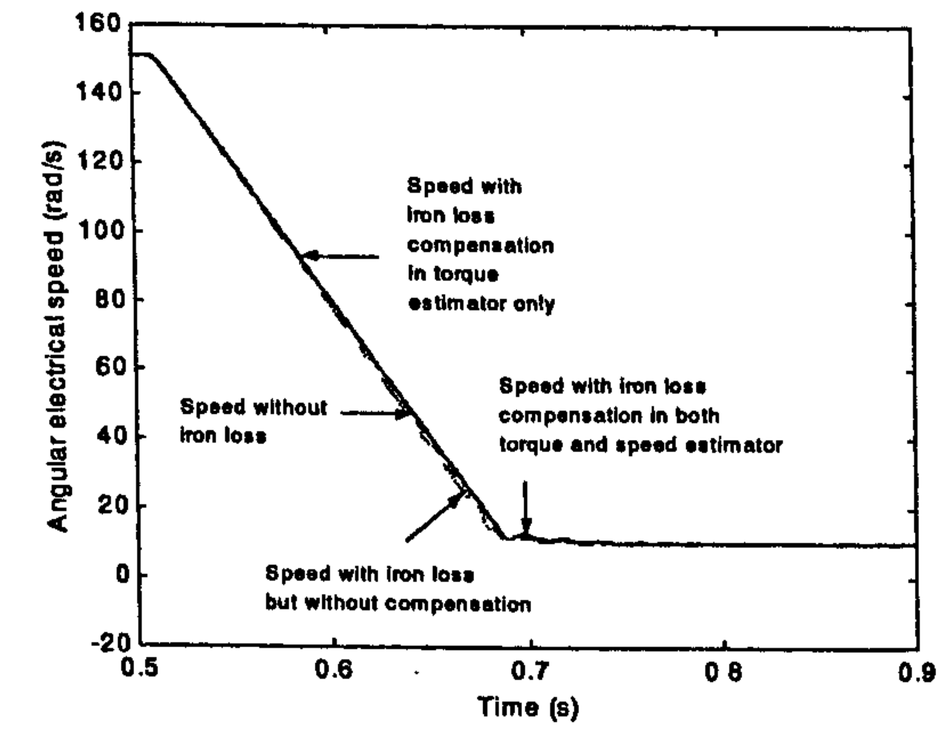

f)

Figure 7.13: Compensation of iron loss in both torque and speed estimators: a) acceleration to one half of the rated speed and load rejection transient, b) acceleration to the rated speed and load rejection transient, c) steady state errors between the estimated speed and the actual speed at one half of the rated speed, d) steady state errors between the estimated speed and the actual speeds at the rated speed, e) actual speeds of sensorless DTC during acceleration to one half of rated speed, f) actual speeds of sensorless DTC during deceleration to 10 rad/s.

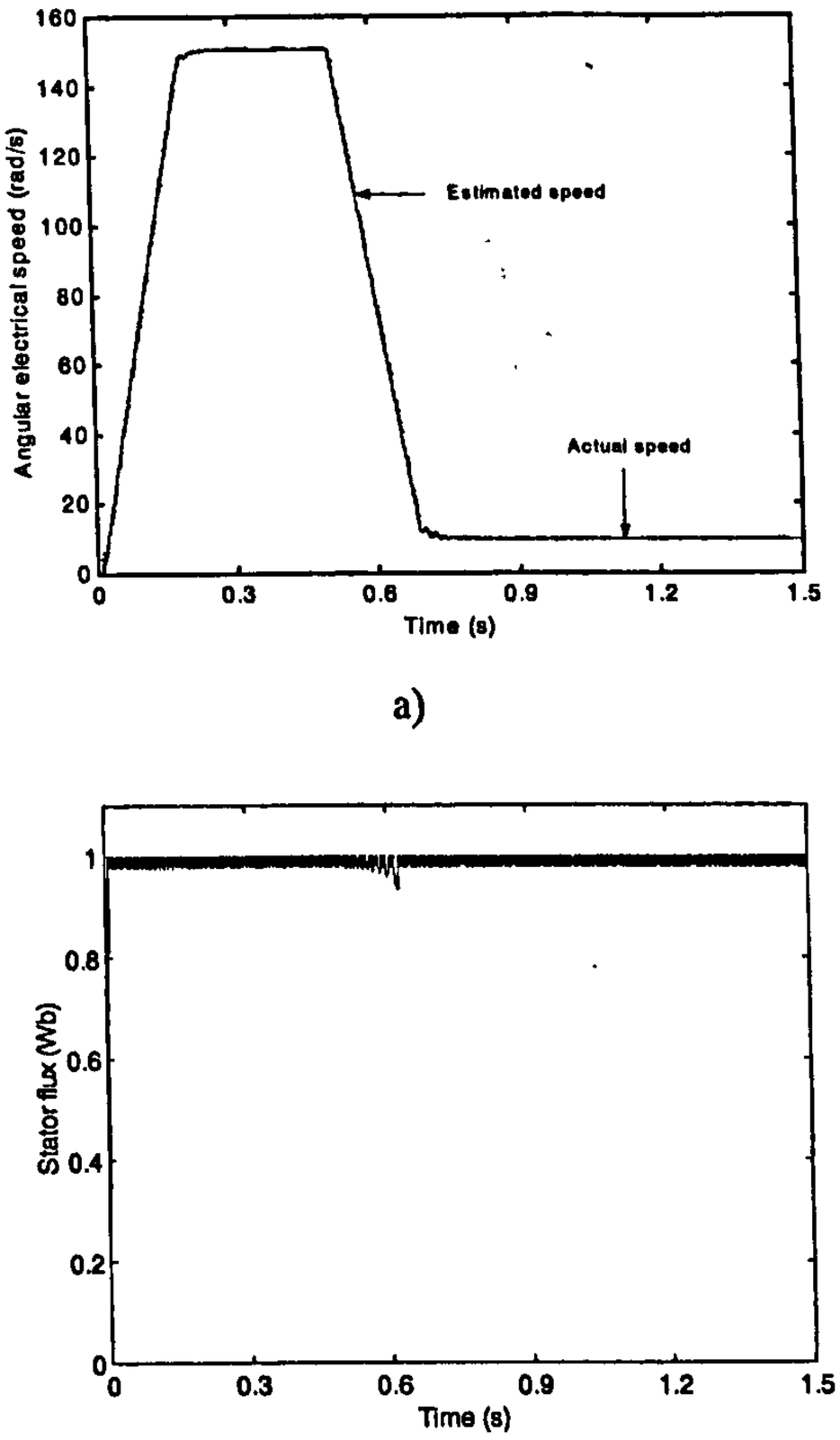

a)

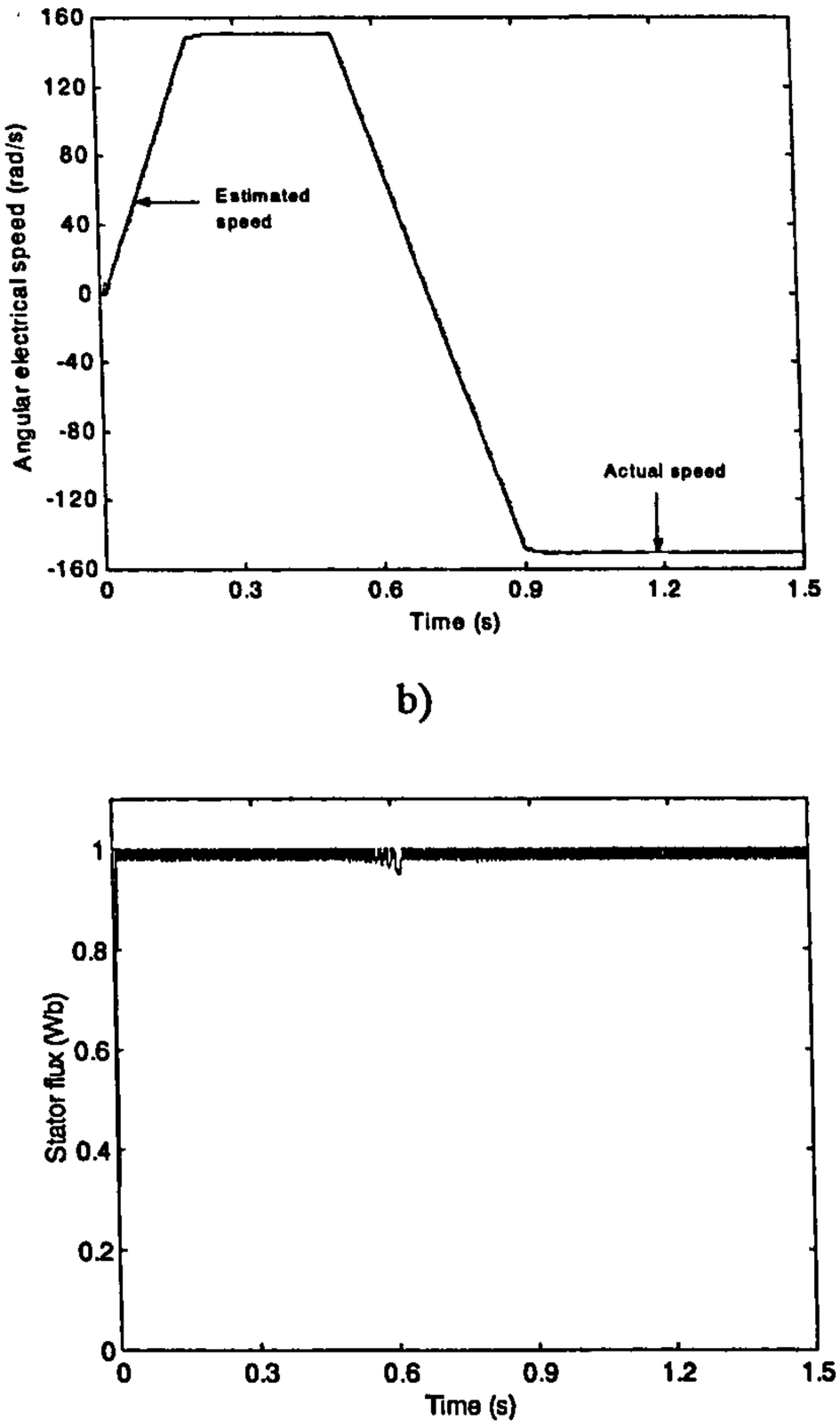

b)

c)

d)

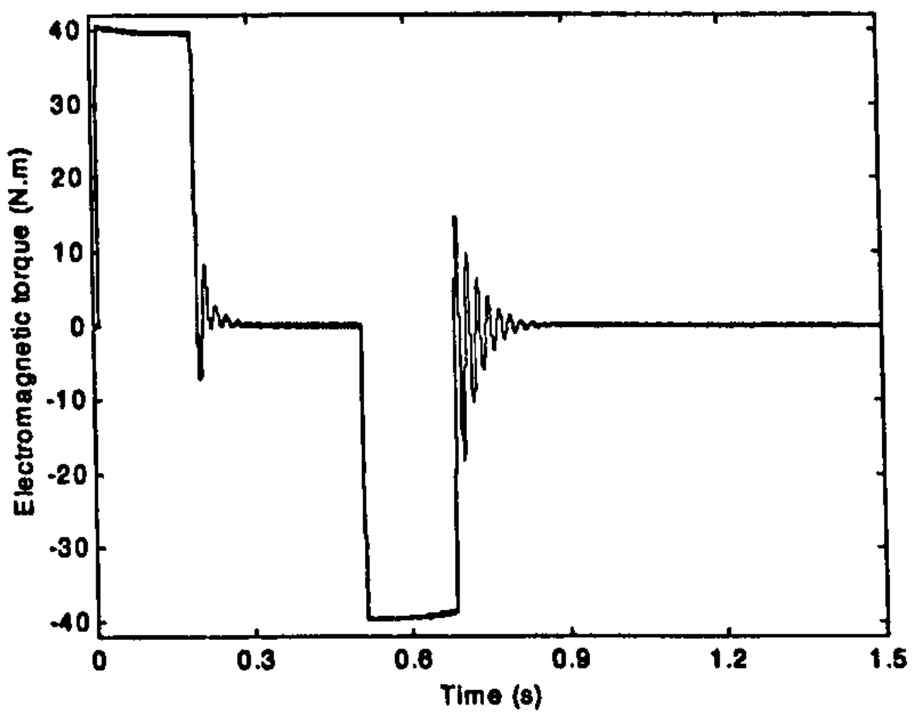

e)

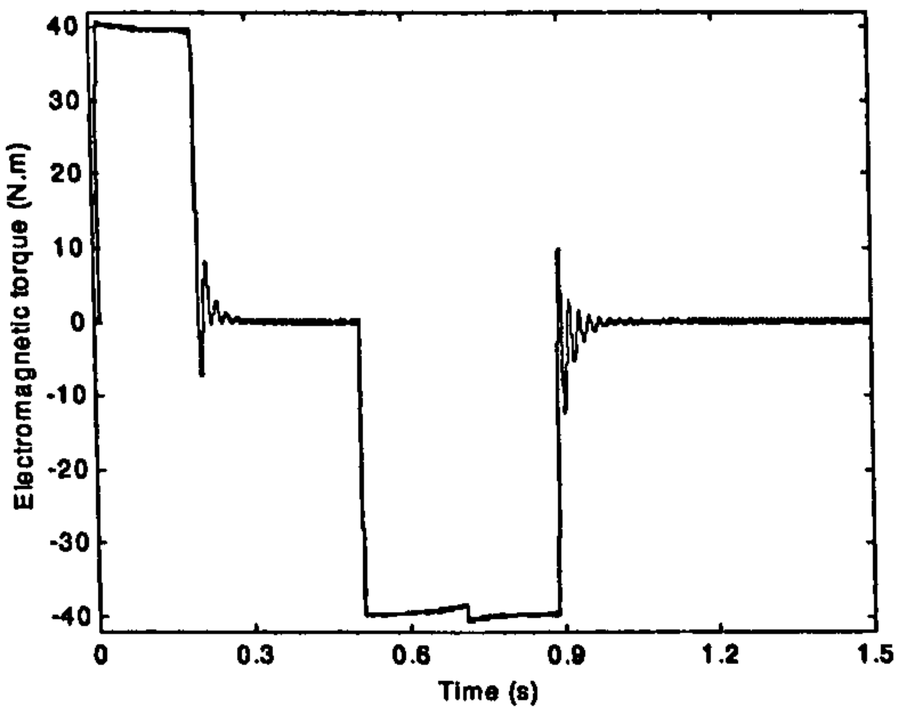

f)

Figure 7.14: Compensation of iron loss in both torque and speed estimation: a) speeds, stator flux and torque during deceleration to 10 rad/s, b) speeds, stator flux and torque during reversing from 0.5 p.u. speed to -0.5 p.u. speed.

rated speed and at the rated speed. Figures 7.13c and 7.13d show that there is hardly any improvement in the steady state error when only compensation in the torque estimator is incorporated in the system. Steady state errors in this case are almost the same as those

obtained without any compensation. Although of only 2rpm value, the errors are significantly larger than the residual error with full compensation. Compensation of the iron loss in the speed estimator reduces speed estimation error to well below 0.5 rpm at the lower speed, and to approximately 0.6 rpm at rated speed.

The speed estimation error is only insignificantly larger than the one shown in figure 7.8. This small difference is assigned to the use of rotor rotational frequency instead of the stator frequency and to non-ideal mapping of the two iron loss resistance functions, used within the motor model and the speed estimator equations. Actual speed during acceleration at low speed is consistent with the actual speed obtained with standard constant parameter machine model (figure 7.13e).

Figure 7.14 shows speeds (actual and estimated speeds), stator flux and electromagnetic torque of the induction motor with iron loss compensation, during deceleration and speed reversing. The speeds are consistent and stator flux and electromagnetic torque behave as expected.

The modified speed estimator, proposed in sub-section 7.3.3 and examined by simulation in this sub-section, has been presented in [Pham-Dinh and Levi (2002)].

7.5 Sensorless direct torque control with rotor flux based MRAS speed estimator

Very much the same description as the one given in the beginning of section 7.4 applies here as well. The same simulation procedure is followed and the same transients are studied. Parameters of the induction motor and the direct torque controller are unchanged. The switching table used throughout this sub-section is again Casadei's table [Casadei et al (1994)], for the reason explained in sub-section 7.4.

7.5.1 Simulations using standard constant parameter machine model

The simulations of induction motor acceleration, deceleration and speed reversal, similar to the simulations for stator flux based MRAS speed estimator, are carried out. Acceleration to one half of the rated speed and then full rated speed, with load disturbance testing at both speeds, is simulated first. Actual speed, estimated speed, load torque, stator flux and electromagnetic torque developed by the motor are shown in figure 7.15. Figure 7.15 also shows steady state speed estimation errors for both stator

and rotor flux based speed estimators. As can be seen, the actual speed is the same, while there exits a small speed estimation error (less than 0.5rpm) of opposite signs for the two estimations. The error with rotor flux based speed estimator is slightly larger than with stator flux based speed estimator. The same remarks apply here as those given in conjunction with figure 7.8. Actual and estimated speeds are in good agreement during the acceleration; load torque is rejected well at both one half and full rated speed. Stator flux, when modified switching table of Casadei (1994) is used, stays within the hysteresis bands for a wide range of speed. Electromagnetic torque follows torque command (which is the output of the speed controller) rapidly and accurately.

The simulation of deceleration from one half of the rated speed to 10 rad/s and speed reversal from positive to negative one half of rated speed are carried out next. Actual speed, estimated speed, stator flux and electromagnetic torque of the induction motor are shown in figure 7.16. Actual and estimated speeds are in very good agreement during both deceleration and speed reversal. Stator flux ripples exceed the hysteresis bands for very short time intervals. In both simulations, torque response of the induction motor is fast and robust.

7.5.2 Simulations using induction machine model with iron loss representation

The model of induction motor, which includes iron loss in the machine, is now used for the simulation of sensorless DTC with rotor flux based MRAS speed estimator. The iron loss resistance is a function of the stator frequency. This iron loss resistance is represented by the same function of frequency as in previous simulations. The same three simulations of acceleration, deceleration and speed reversal are carried out. The results are given in figures 7.17 and 7.18.

Problem with estimated speed during the starting up of the motor has been previously observed. When motor's speed reaches 20 rad/s, the actual speed and the estimated speed come into good agreement and remain to be so further on. Load rejection is good at both speeds. Motor torque response does not reach the set limit due to the existence of the iron loss. Except for this slight reduction, the torque response is very fast. Steady state speed estimation error obtained with rotor flux based MRAS speed estimator is compared to the case when iron loss is ignored. The error with the iron loss is significantly larger than the one without iron loss, approximately 2.5 rpm at

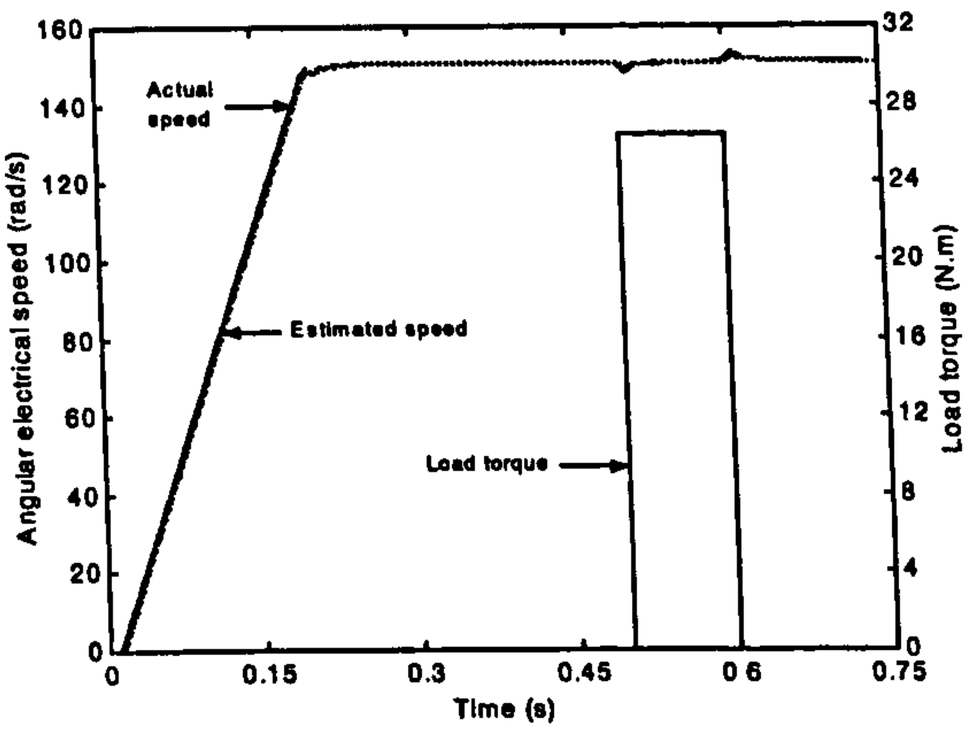

a)

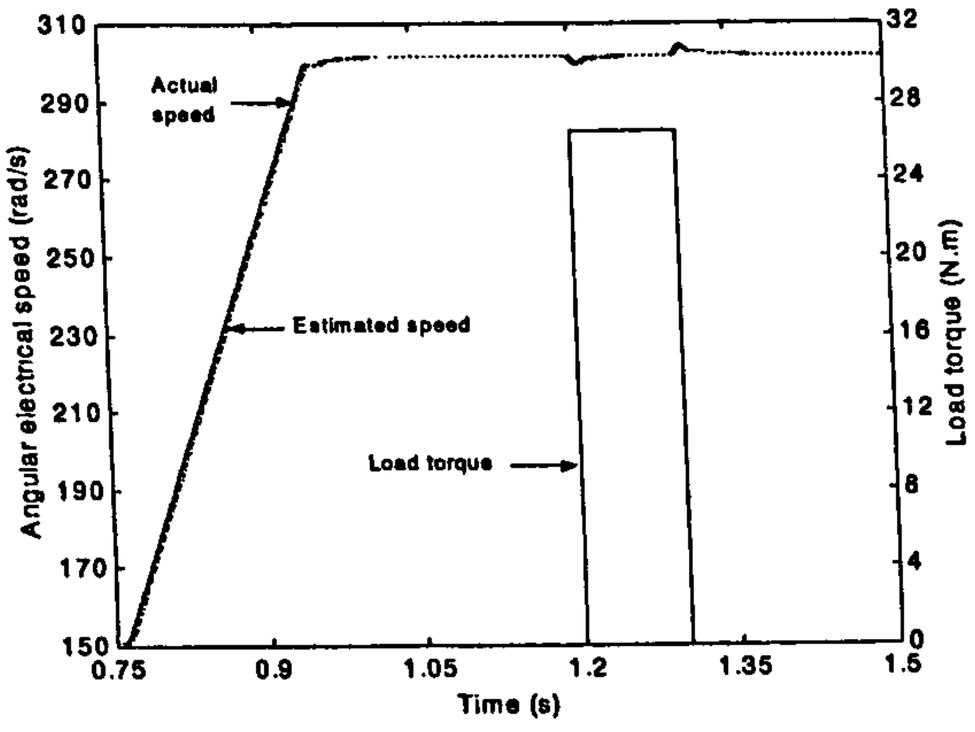

b)

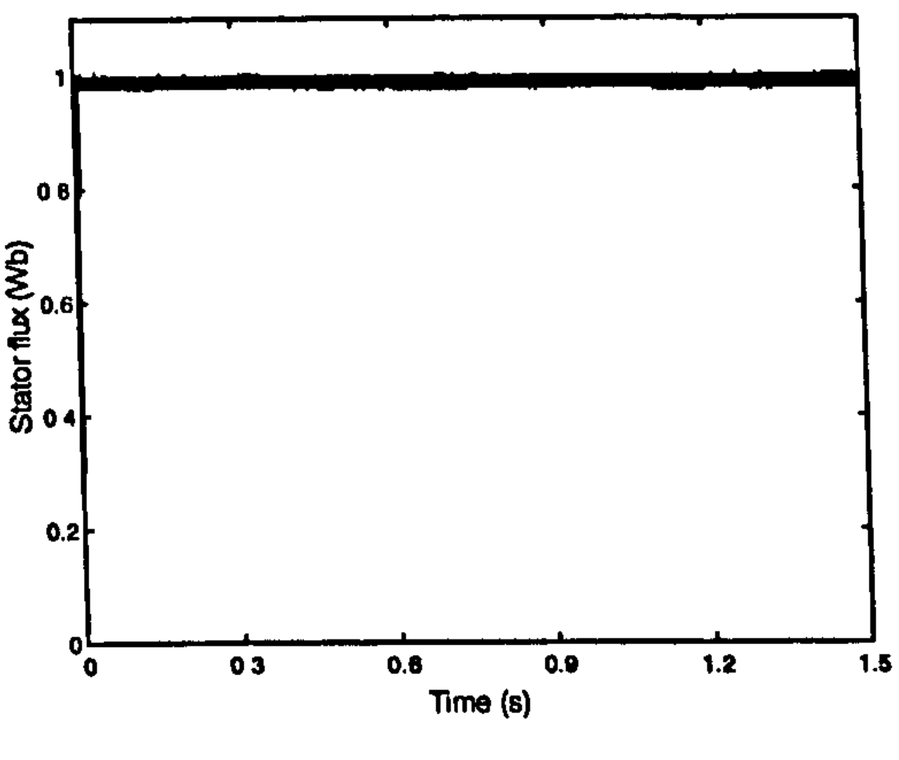

c)

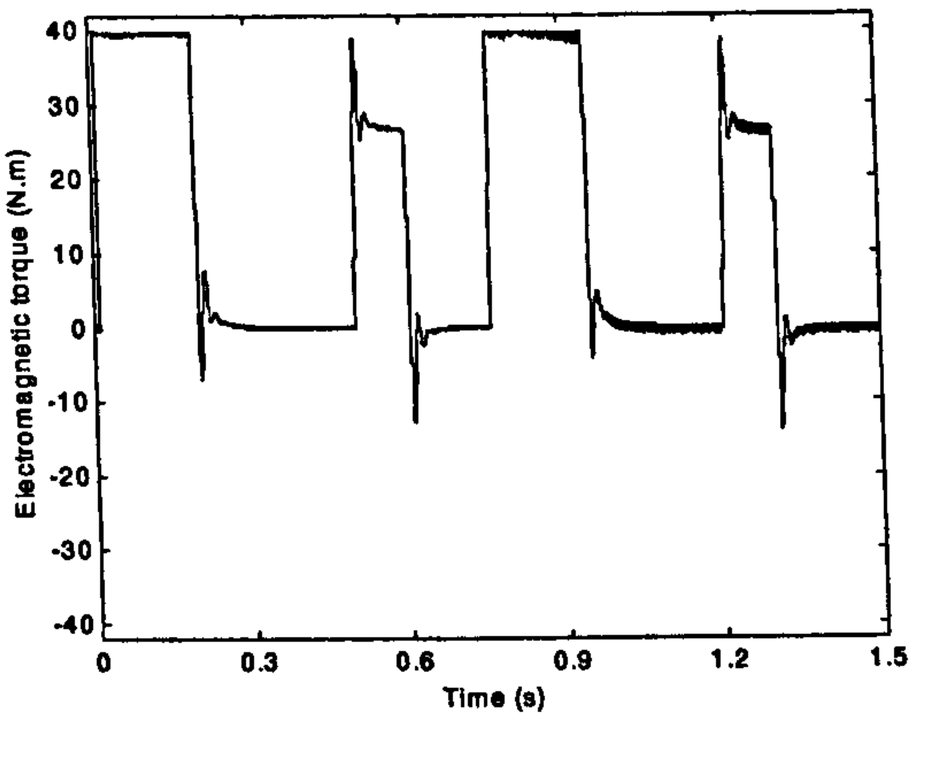

d)

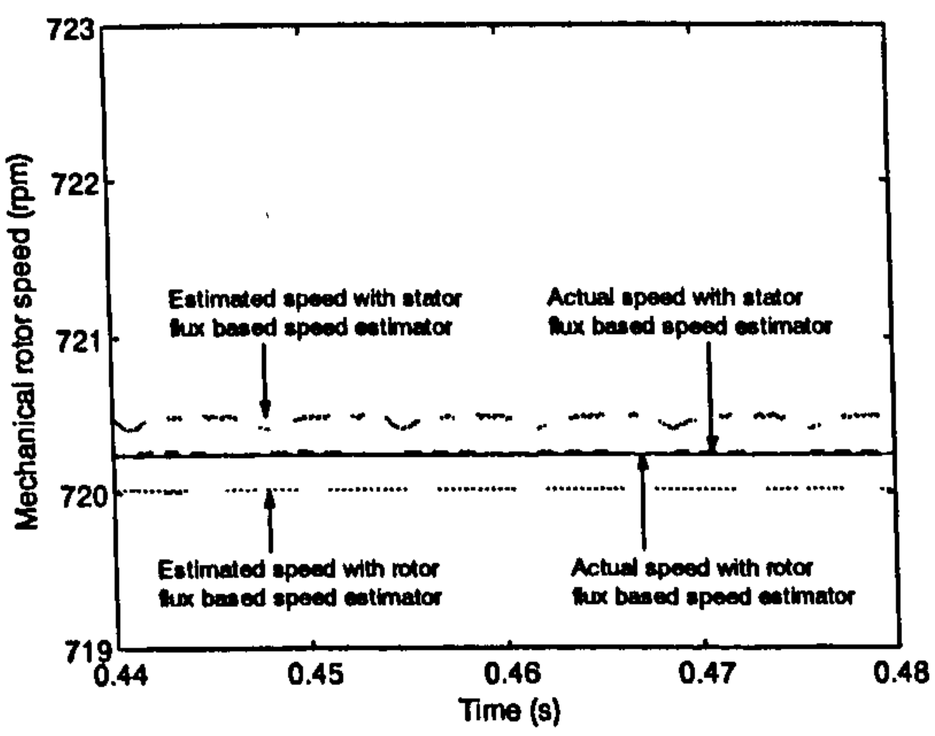

e)

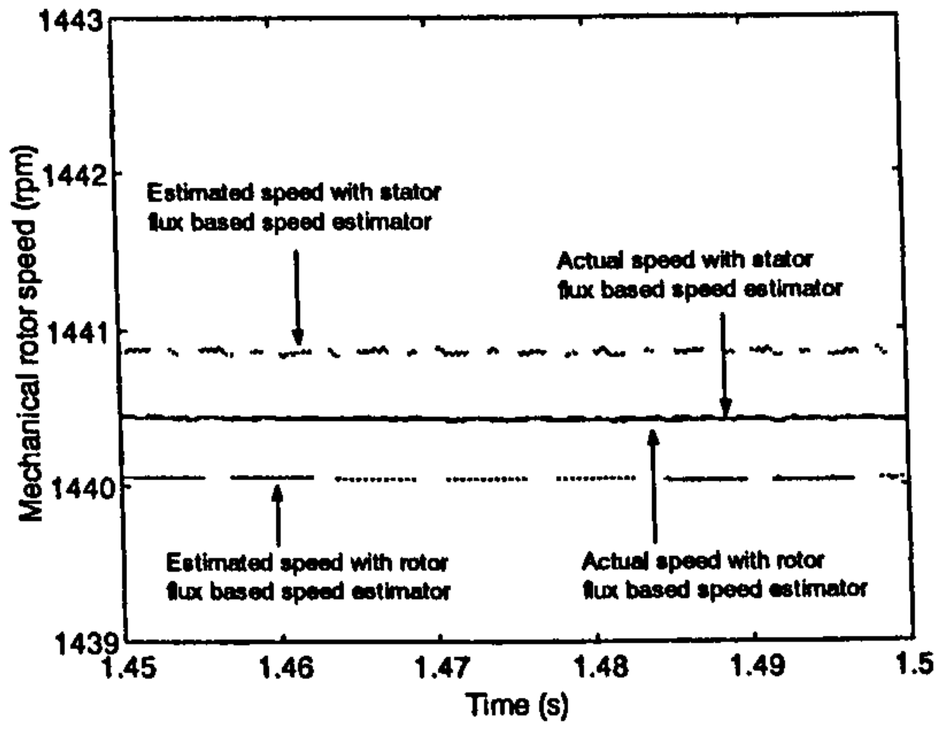

f)

Figure 7.15: Acceleration and load rejection of sensorless DTC with rotor flux based MRAS speed estimator: a) actual and estimated speeds, acceleration to one half of the rated speed, b) the speeds and load torque during acceleration from one half to full rated speed, c) stator flux during the accelerations, d) electromagnetic torque of induction motor during the accelerations, e) steady state speed estimation errors with stator flux based and rotor flux based MRAS speed estimators at one half of the rated speed, f) the same steady state errors at rated speed. Iron loss is neglected in the motor model.

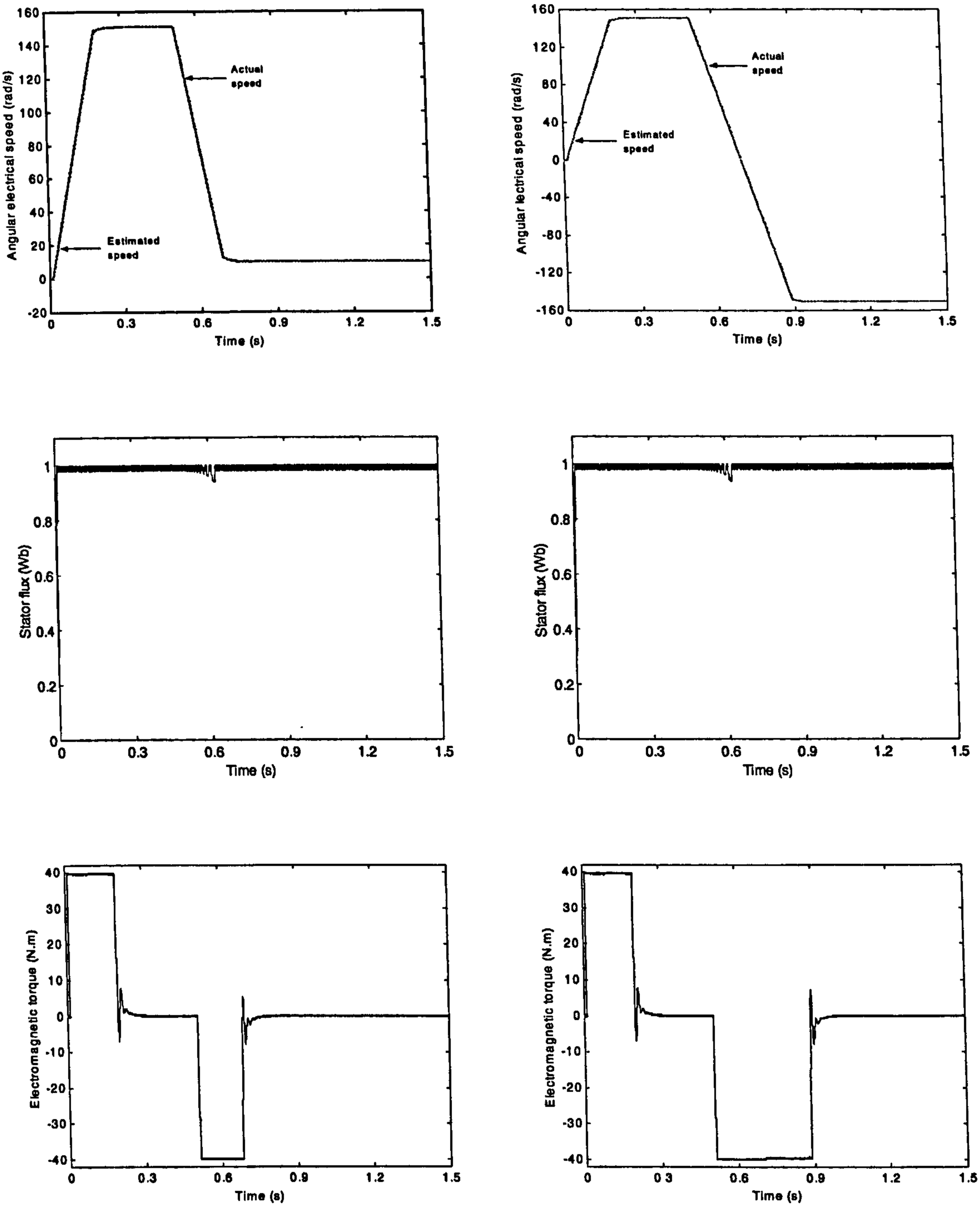

Figure 7.16: Deceleration and reversing transient of DTC using rotor flux based speed estimator: a) traces for deceleration to 10rad/s, b) traces for 0.5 p.u. to -0.5 p.u. speed reversing transient. Iron loss is neglected in the motor model.

one half of the rated speed and slightly higher at rated speed. Comparison of these values and those obtained when stator flux based MRAS speed estimator is used is also carried out. At both one half of the rated speed and at rated speed, the errors with rotor

flux based speed estimator are higher, especially at rated speed. The steady state errors discussed are shown in figures 7.17e and 7.17f. Speed estimation error in steady state operation is small, less than 3rpm. This value is consistent with the findings of [Levi et al (1999)], where the same rotor flux based MRAS speed estimator was examined in conjunction with sensorless rotor flux oriented control.

Simulations of deceleration and speed reversal are carried out next. Actual and estimated speeds are in good agreement during deceleration from one half of the rated speed to 10 rad/s and in steady state at that speed. Distortion in the estimated speed in the low speed region, as observed during start up, does not take place during deceleration (figure 7.18a). Similar considerations apply to the speed reversal (figure 7.18b). Despite some torque reduction due to iron loss, torque response during deceleration is fast and accurate. Torque reduction is more visible during speed reversal.

7.5.3 Simulations using induction machine model with iron loss representation and iron loss compensation in torque estimator

Iron loss compensation in torque estimator of the direct torque controller is implemented to improve the performance of the drive by reducing the torque error in the torque estimate. The same constant torque increment compensation of electromagnetic torque, as discussed in section 7.4.3, is used here as well. Traces of speed response (actual and estimated speeds), stator flux and torque response during acceleration, deceleration and speed reversal are collected to make a comparison with those reported in sub-section 7.5.2.

Distortion in estimated speed during start up is reduced, but not completely eliminated, as shown in figure 7.19a. The two speeds are in good agreement during acceleration and load rejection test. However, reduction in steady state speed estimation error is not achieved with the iron loss compensation in the torque estimator. The steady state error is almost exactly the same as the one in uncompensated operation at both one half of the rated speed and at rated speed, as shown in figures 7.19e and 7.19f. The steady state speed estimation errors in sensorless DTC with stator flux based MRAS speed estimator for the corresponding simulation are included in figures 7.19e and 7.19f. The errors of the rotor flux based speed estimator are generally larger, as has already been observed in sub-sections 7.5.1 and 7.5.2. Torque response is improved as torque reduction and torque distortion at start up are eliminated. Over-compensation is

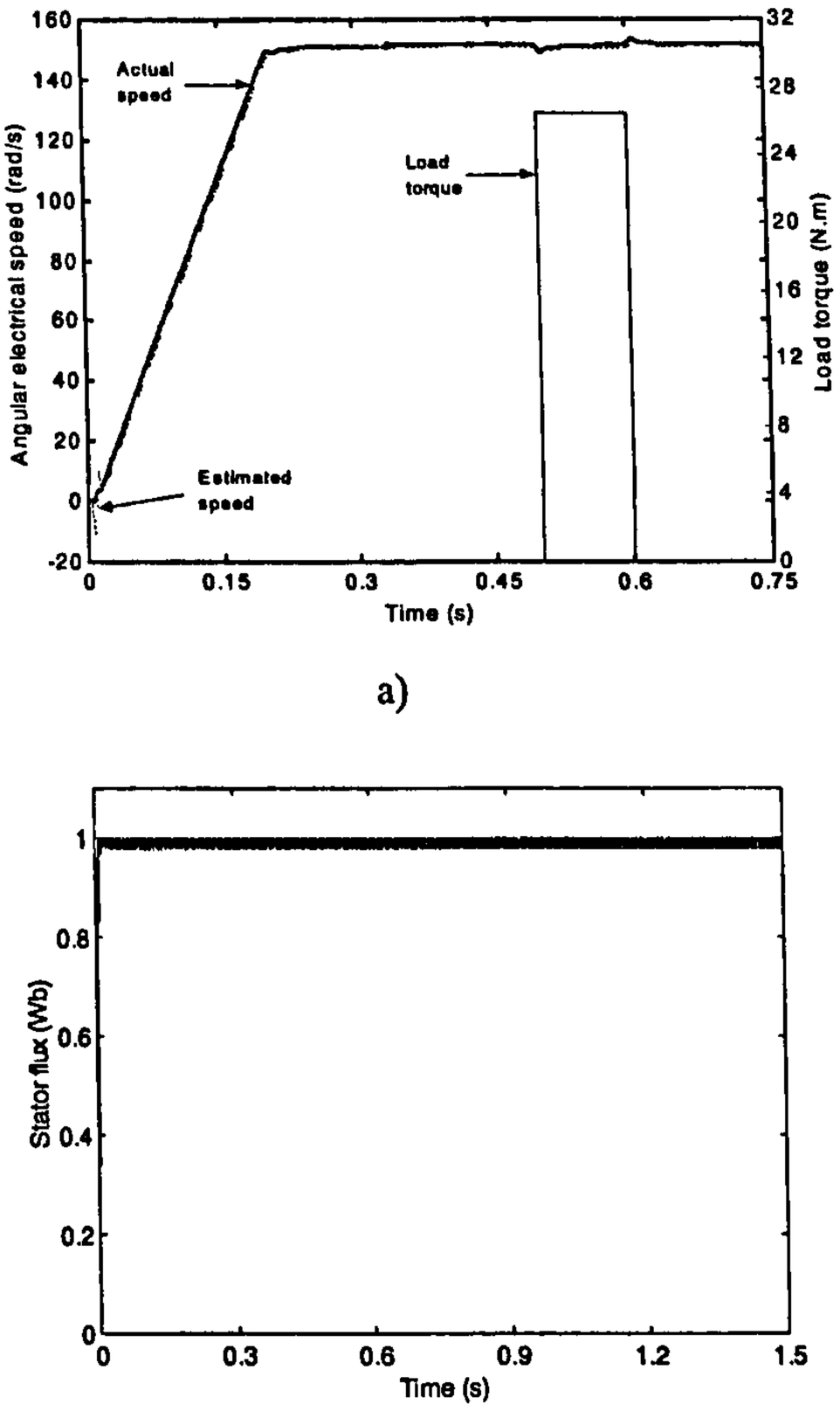

a)

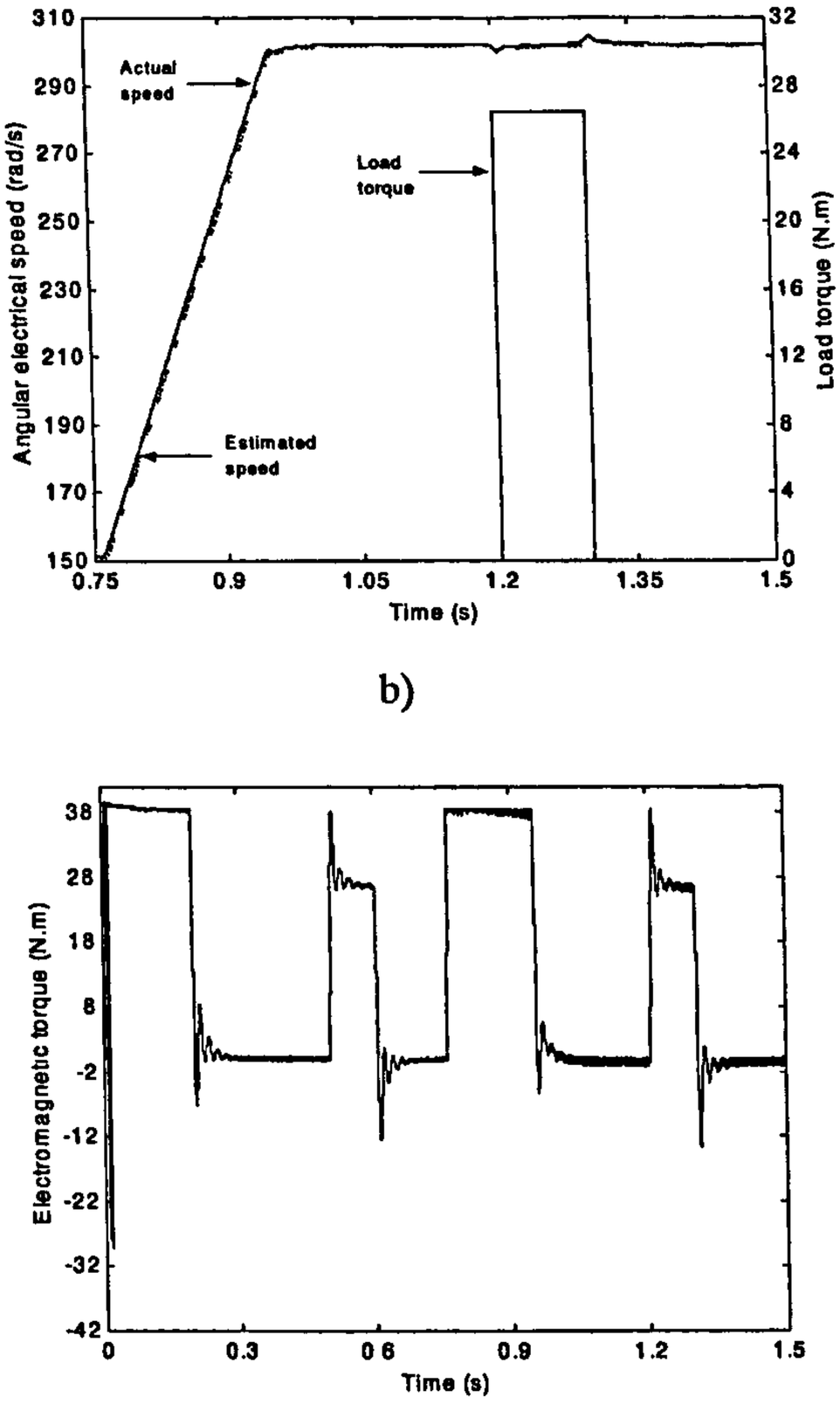

b)

c)

d)

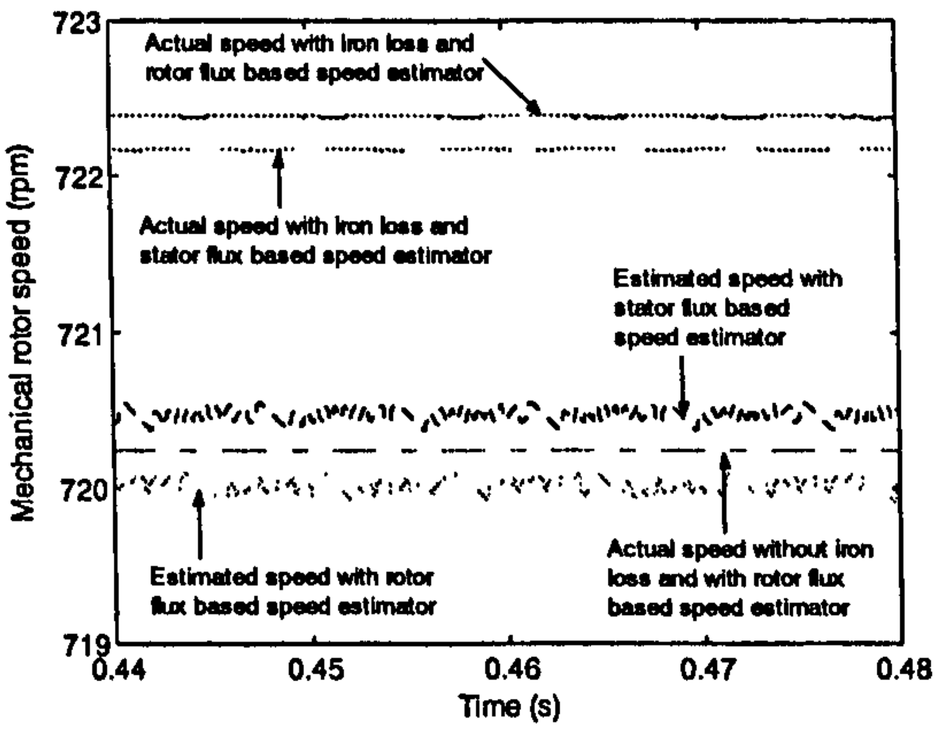

e)

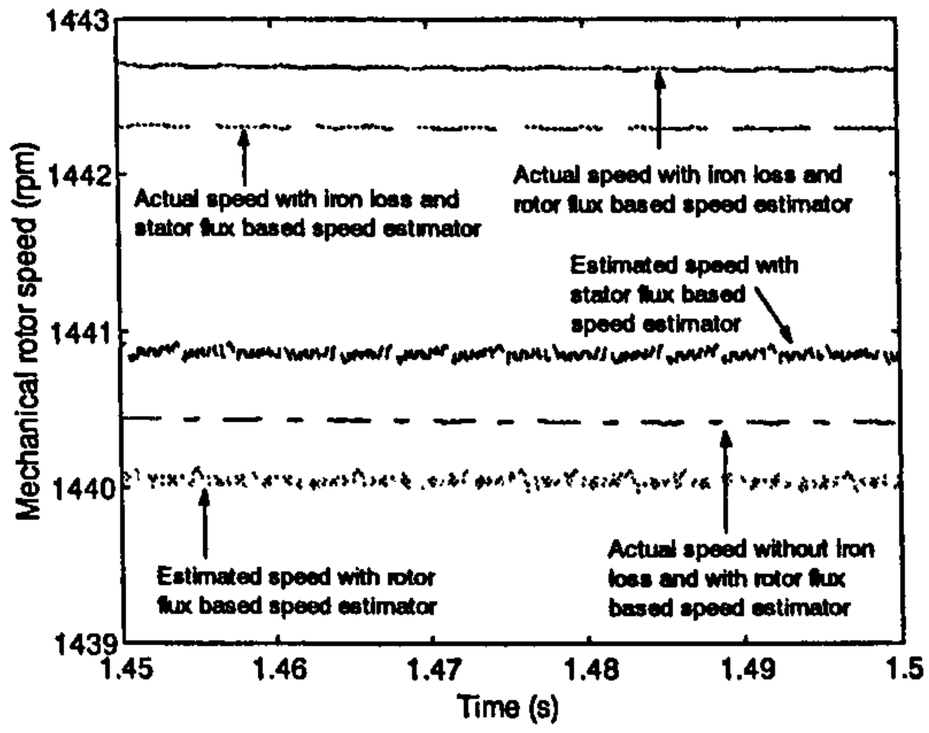

f)

Figure 7.17: Acceleration and load rejection transient of sensorless DTC with rotor flux based MRAS speed estimator: a) actual and estimated speeds and load torque during acceleration to one half of the rated speed, b) the speeds and load torque during acceleration to the rated speed, c) stator flux during the accelerations, d) electromagnetic torque during the accelerations, e) steady state speed estimation errors with stator flux based and rotor flux based MRAS speed estimators at one half of the rated speed, f) the steady state speed estimation errors at the rated speed. Iron loss is included in the motor model.

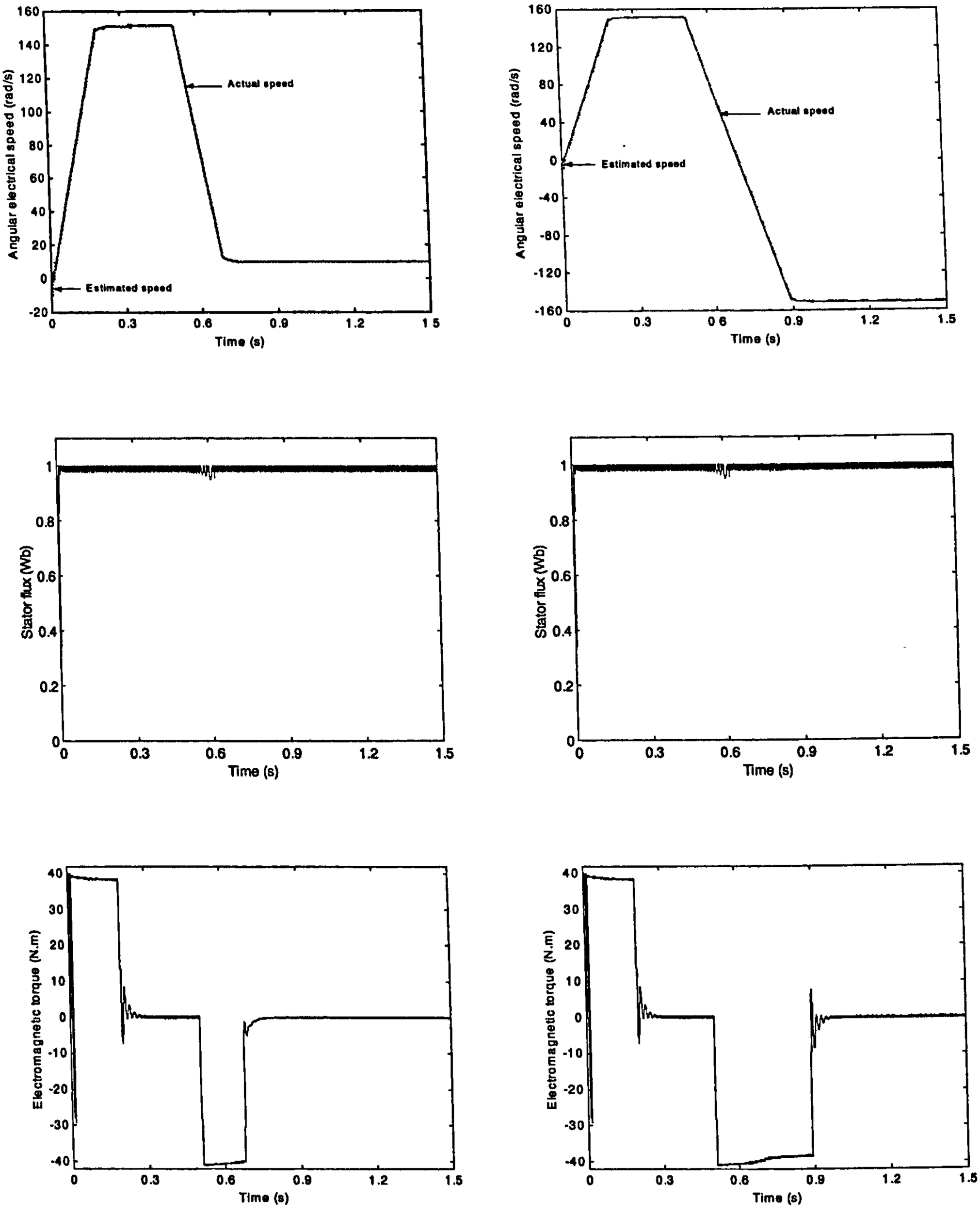

Figure 7.18: Deceleration of sensorless DTC with rotor flux based MRAS speed estimator from one half of the rated speed to 10 rad/s a) and reversing transient b): actual speed, estimated speed, stator flux and motor torque are shown. Iron loss is included in the motor model.

observed again in torque response at low speed. Other than that, torque response is very fast and accurate and this is exactly what the compensation is aimed at. Stator flux response is similar to the one without compensation. Torque, stator flux and speeds are

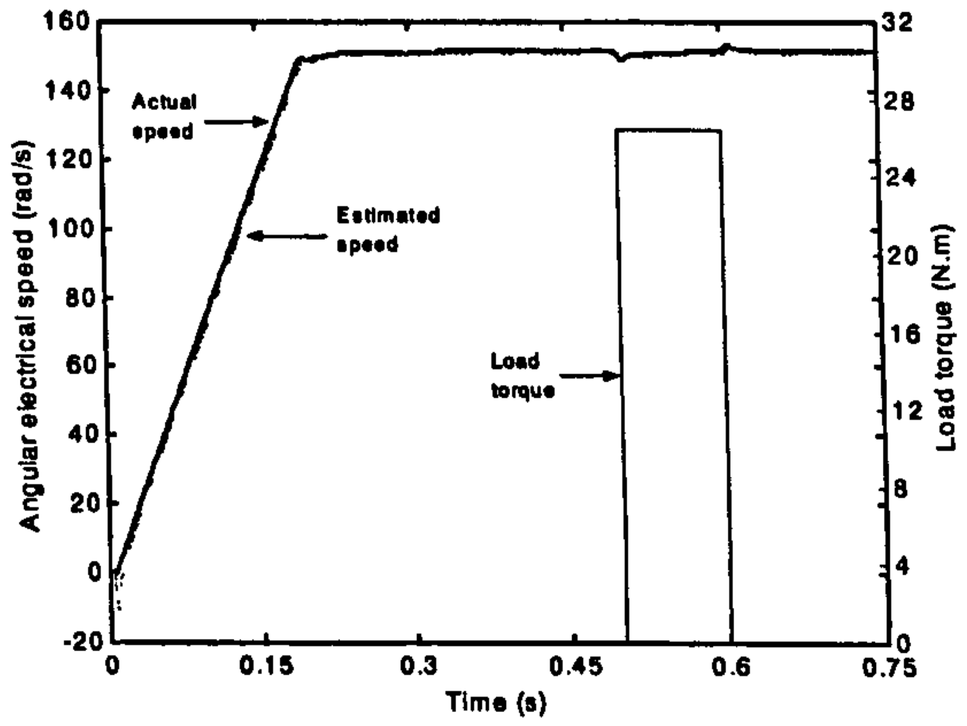

a)

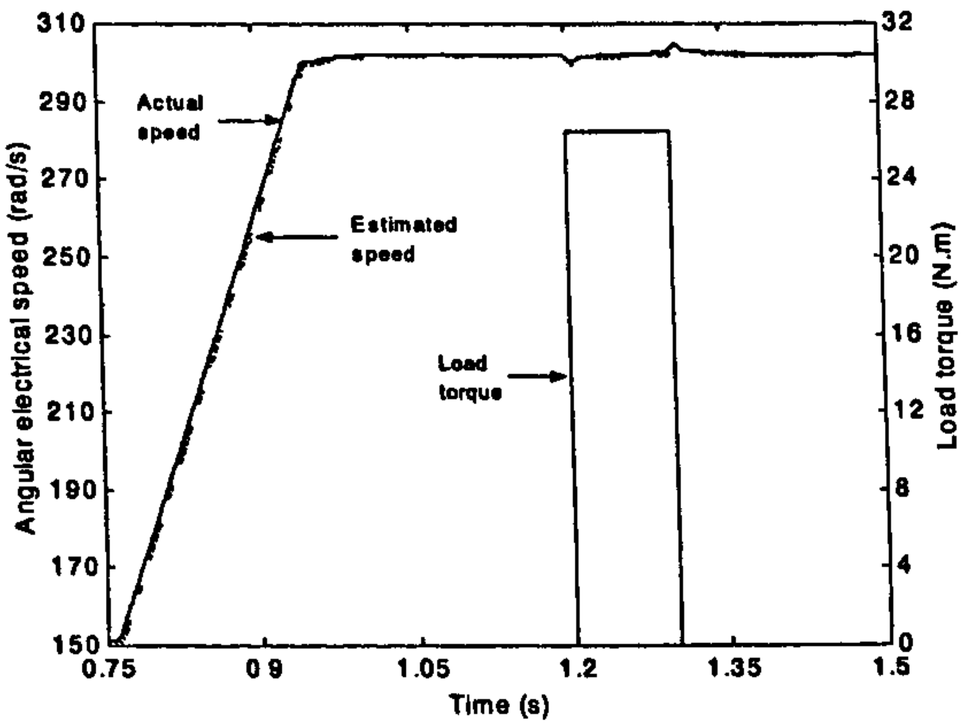

b)

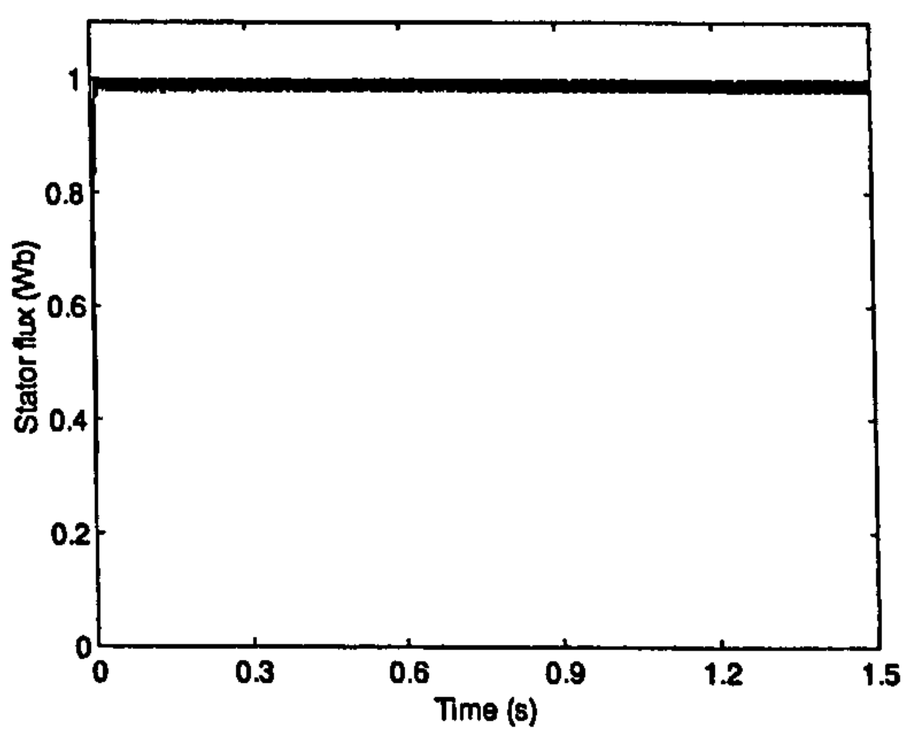

c)

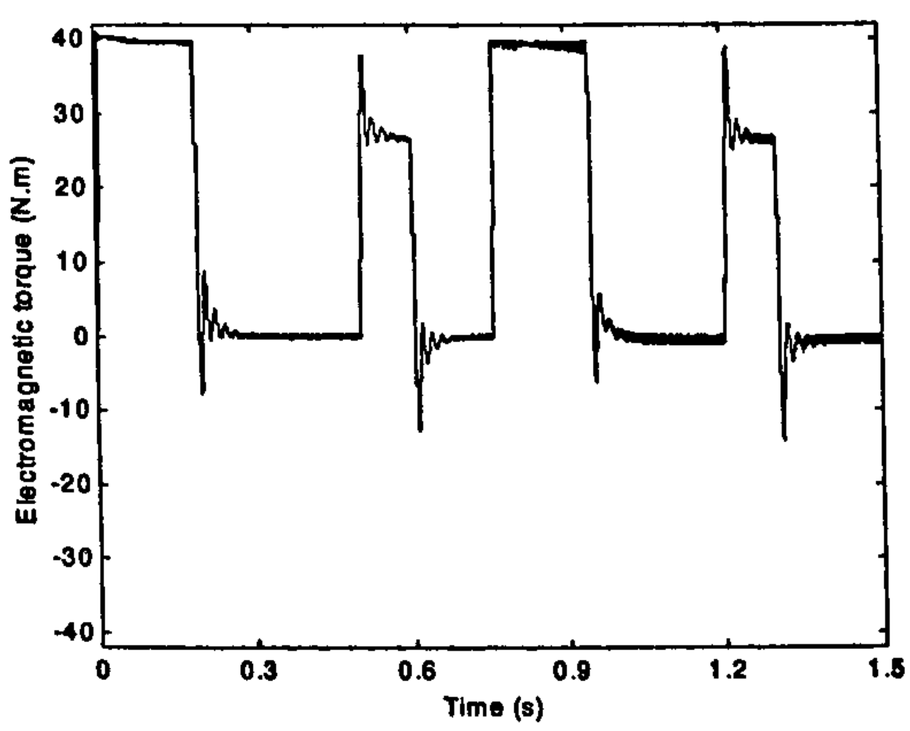

d)

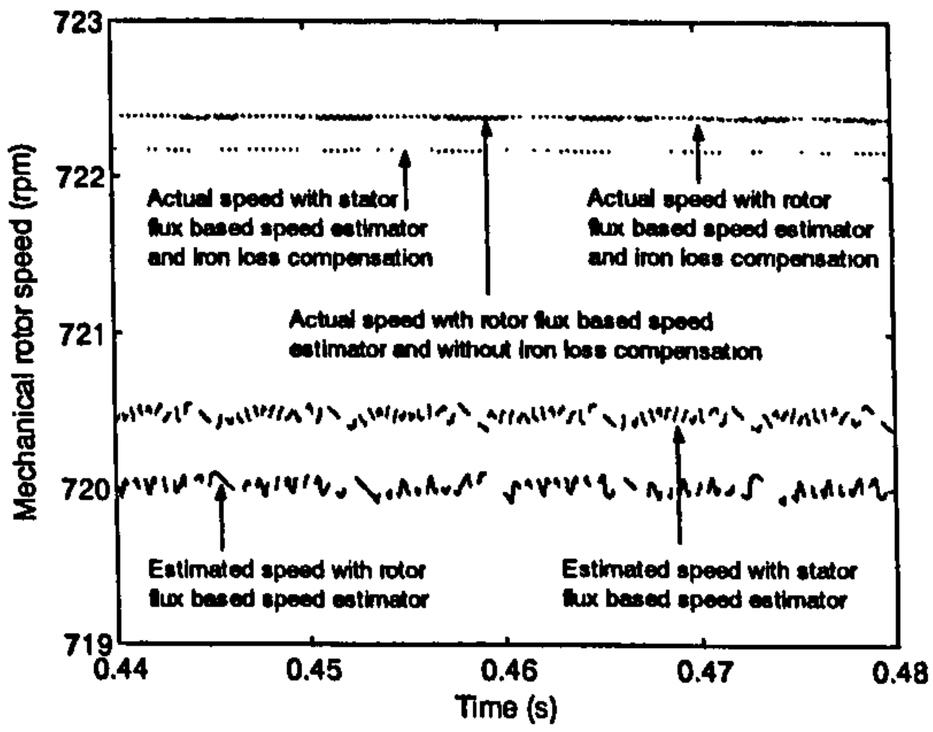

e)

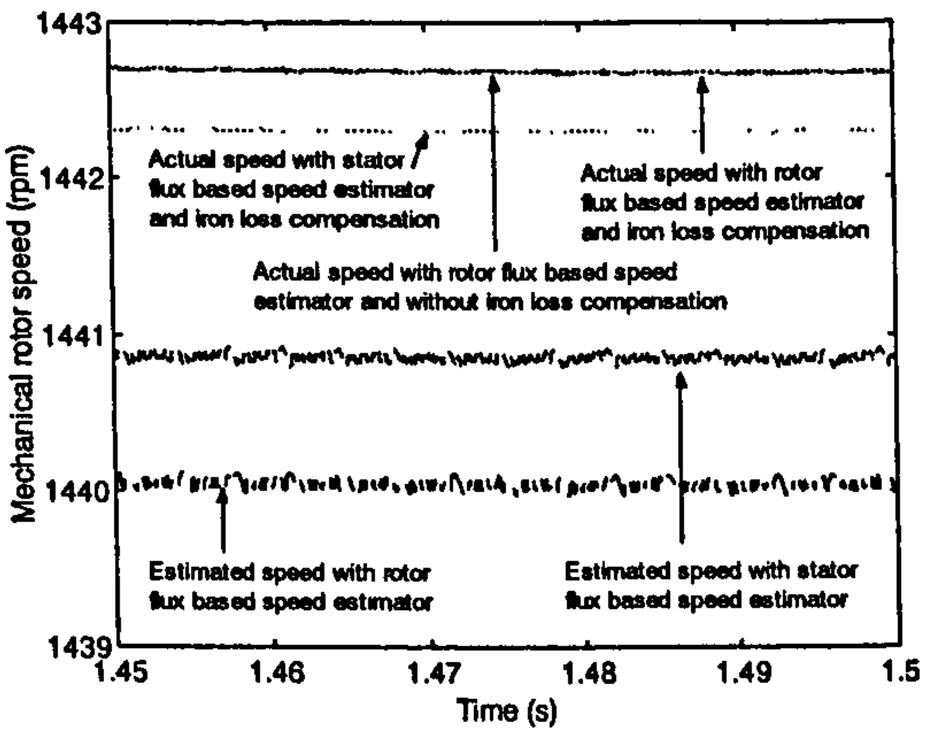

f)

Figure 7.19: Sensorless DTC with iron loss compensation in the torque estimator and rotor flux based MRAS speed estimator: a) speeds and load torque during acceleration to one half of rated speed, b) the speeds and load torque during acceleration to rated speed, c) stator flux during the accelerations, d) electromagnetic torque during the accelerations, e) steady state speed estimation errors with stator flux and rotor flux based MRAS speed estimators at one half of the rated speed, f) the same steady state speed estimation errors at rated speed.

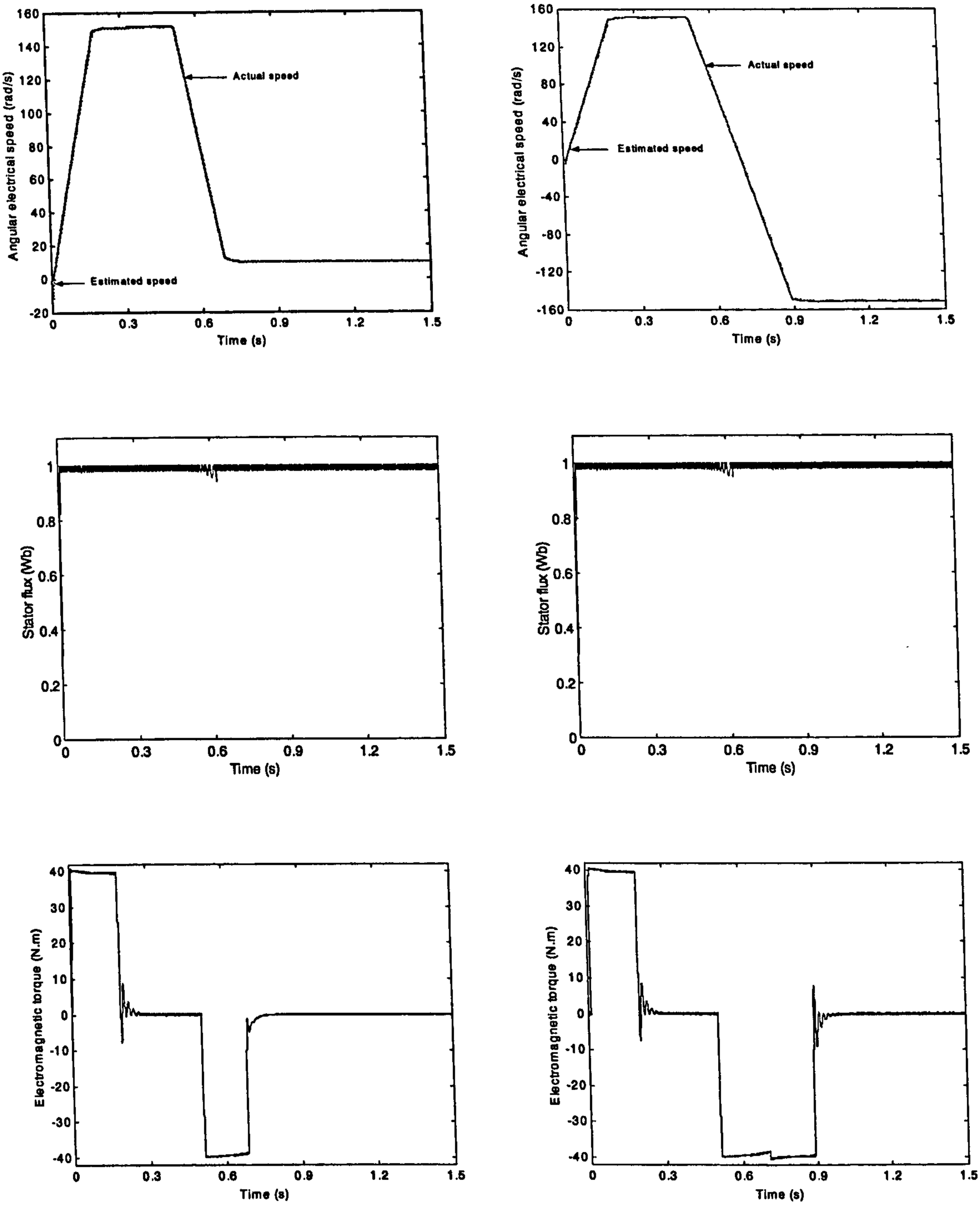

Figure 7.20: Deceleration and reversing transient of sensorless DTC with iron loss compensation in the torque estimator and rotor flux based MRAS speed estimator: a) deceleration from one half of the rated speed to 10 rad/s, b) reversing transient. Actual speed, estimated speed, stator flux and motor torque are shown.

also observed during simulations of the deceleration and speed reversal, figure 7.20. Very much the same considerations apply as those given in the previous paragraph.

7.5.4 Simulations using induction machine model with iron loss representation and compensation of the iron loss in both torque and speed estimators

Iron loss compensation in rotor flux based MRAS speed estimator is implemented in an attempt to eliminate or at least reduce the speed estimation error. It is also expected that the improved torque behaviour due to iron loss compensation in the torque estimator will not be adversely affected. The same frequency dependent iron loss resistance R_{iron} is used again. The same transients and the same traces are simulated and displayed, respectively.

The distortion in the estimated speed of the sensorless DTC at start up is removed, figure 7.21a. Actual and estimated speed are consistent with each other throughout the acceleration transients, as shown in figures 7.21a and 7.21b. Performance of the iron loss compensated speed estimator in terms of steady state speed estimation error is also investigated. Figures 7.21c and 7.21d show the steady state speed estimation error at one half of the rated speed and at rated speed, respectively, for the two cases when iron loss compensation is and is not implemented in the speed estimator. Iron loss compensation in the speed estimator reduces the steady state speed estimation error significantly. The error is less than 0.2 rpm at one half of the rated speed and slightly higher at full rated speed. Comparison of performance between rotor flux based speed estimator and stator flux based speed estimator (both with iron loss compensation) is also carried out in figures 7.21e and 7.21f. Steady state speed estimation error with rotor flux based speed estimator is smaller than the one of the stator flux based speed estimator at both speeds. The difference is more visible at rated speed. This is different from what has been observed regarding the steady state errors of the two speed estimators without iron loss compensation.

Simulations of deceleration and speed reversal of sensorless DTC with rotor flux based speed estimator with iron loss compensation are carried out next. Both actual and estimated speeds are consistent during deceleration and speed reversal, as shown in figures 7.22a and 7.22b. Figures 7.22a and 7.22b show that the stator flux response is similar to the traces obtained before. The improved performance of the torque response, obtained with iron loss compensation in the torque estimator, is not adversely affected when iron loss compensation is incorporated in the speed estimator. Torque reduction is not present in the torque response although excessive torque compensation at low speed

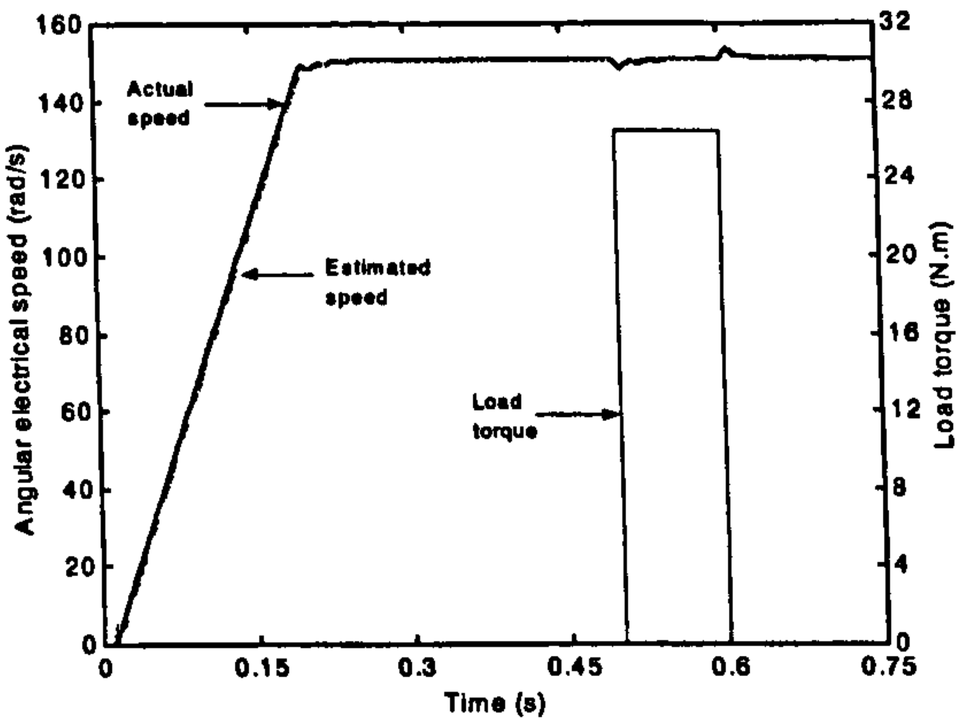

a)

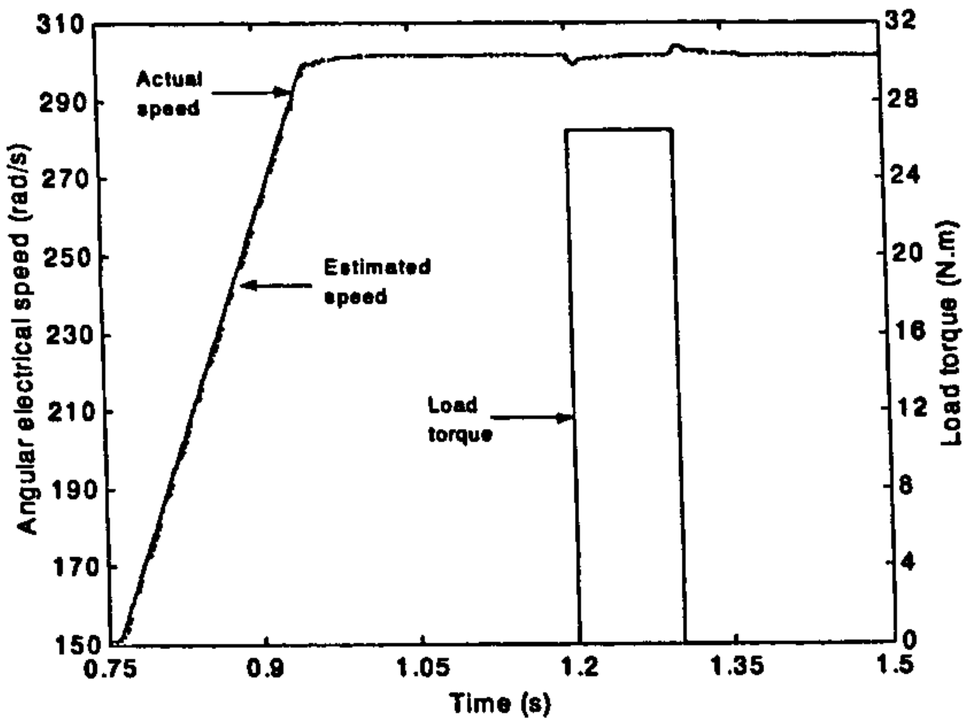

b)

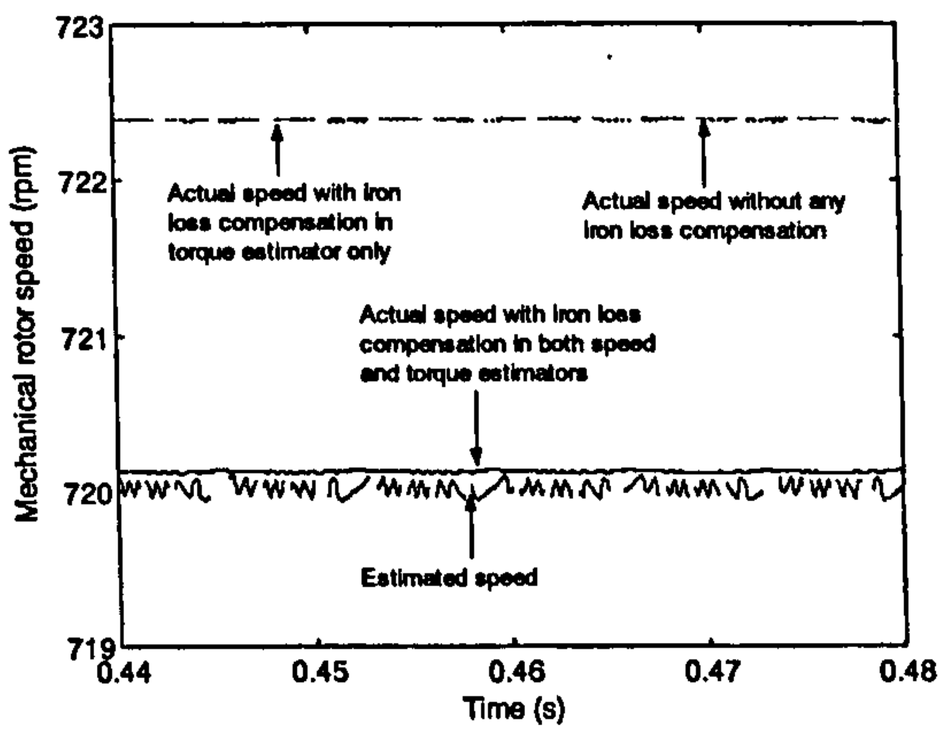

c)

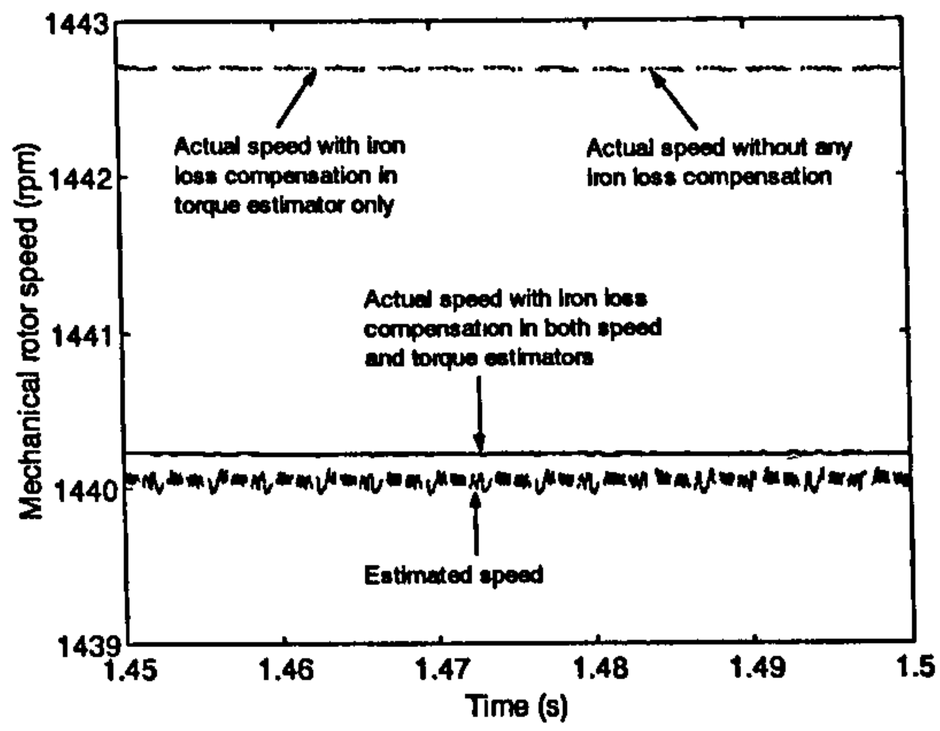

d)

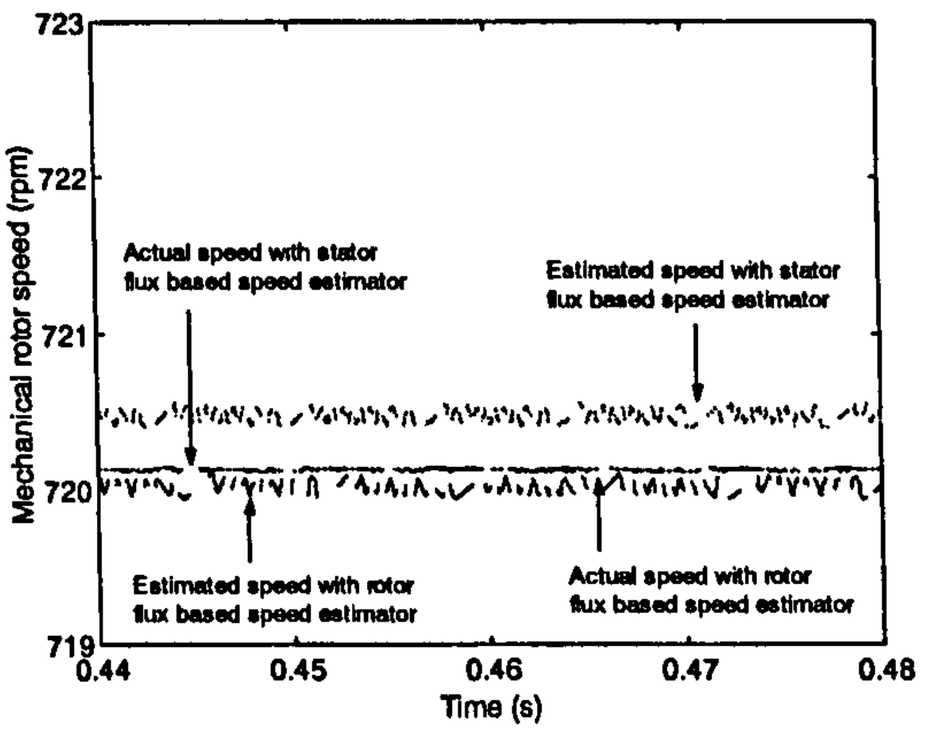

e)

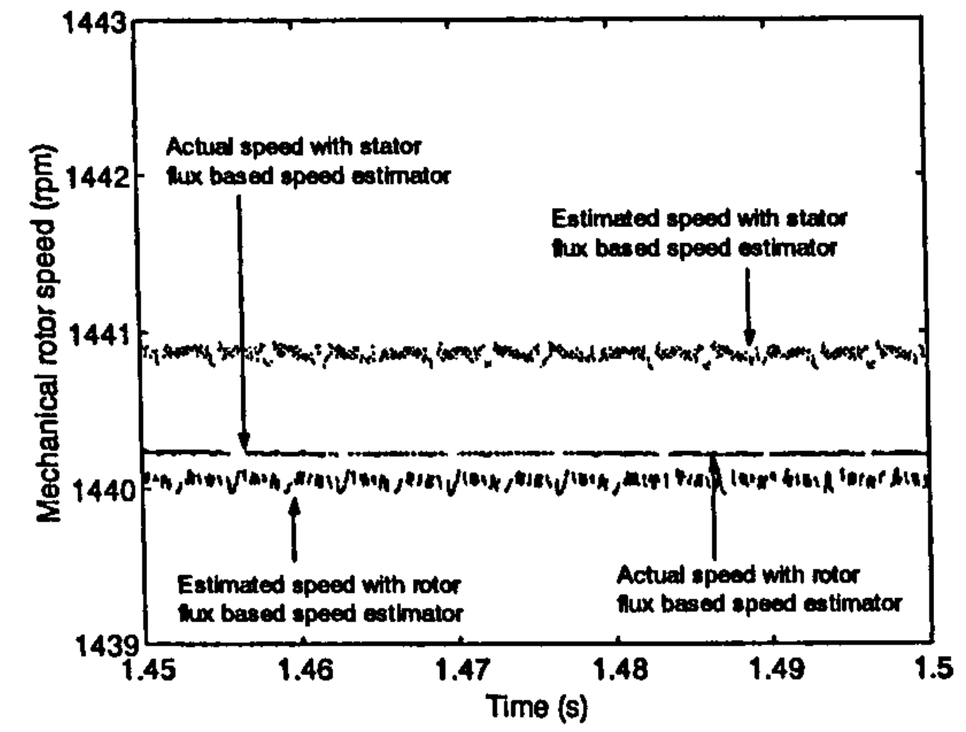

f)

Figure 7.21: Sensorless DTC with iron loss compensation in both speed and torque estimators and rotor flux based MRAS speed estimator: a) acceleration to one half of the rated speed, b) acceleration to the rated speed, c) actual and estimated speeds for different cases at one half of the rated speed, d) the same at rated speed, e) steady state speed estimation error in sensorless control with stator flux and with rotor flux based MRAS speed estimators at one half of the rated speed, f) the same at rated speed.

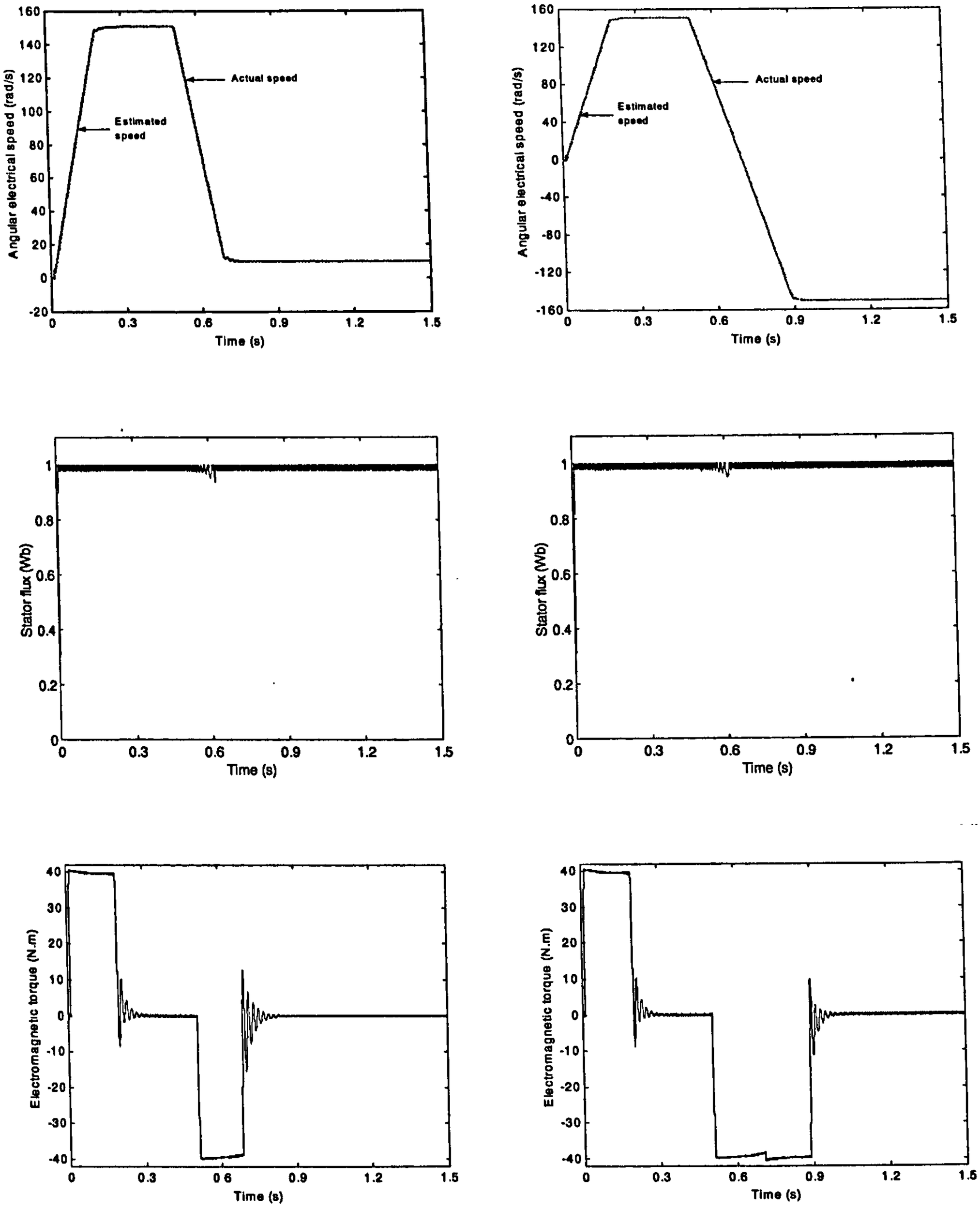

Figure 7.22: Deceleration of the sensorless DTC with iron loss compensation in both torque and speed estimators and rotor flux based MRAS speed estimator a), and reversing transient b). Traces of actual speed, estimated speed, stator flux and motor torque are shown.

can still be observed. Generally, torque response is fast and accurate as shown in figures 7.22a and 7.22b for the cases of deceleration and speed reversal, respectively.

7.6 Summary

Speed estimation methods for high performance induction motor drives have been reviewed in the first part of this chapter. A suitable speed estimator, which can give reliable and accurate estimation of rotor speed, is then selected for further analysis in conjunction with sensorless direct torque control. The selected speed estimator is based on model reference adaptive system and it can utilise various motor variables as the output of the reference and the adjustable model. Two versions are elaborated, with stator flux and rotor flux selected as the outputs of the reference and adaptive models, respectively. Next, a novel form of both speed estimators is proposed, such that the speed estimator includes compensation of the iron loss. A detailed simulation study is then performed. It is shown that the utilisation of the speed estimator with iron loss compensation in conjunction with the torque estimator with iron loss compensation enables practically complete elimination of both torque errors and speed estimation errors. It is shown as well that the typical speed estimation error when iron loss is not compensated is around 2 to 3rpm. Although this is a very small value indeed, inclusion of the iron loss compensation into the speed estimation is so simple that it seems worth doing.

It is also shown that the two elaborated speed estimators offer comparable performance under the same conditions. The fully compensated scheme with rotor flux based speed estimator appears to offer insignificantly lower speed estimation error, when compared to the stator flux based version of the speed estimator.

CHAPTER 8

EXPERIMENTAL INVESTIGATION

8.1 Introduction

Experimental investigations of performance of direct torque control and vector control are carried out in this chapter. A qualitative comparison of performance of the two control methods is then made based on the obtained data. A DSB drive of Vickers Electrics is used in experimentation related to vector control and an ABB drive is used for the analysis of direct torque control. Data regarding operation with and without load, at various speeds in the base speed region, are obtained for the ABB drive. The Vickers drive is investigated under no-load conditions only, since this drive has been dealt with extensively in a previous PhD project [Sokola (1998)].

8.2 Performance of the vector controlled drive system

8.2.1 Description of the drive system

The drive system is an indirect feed-forward current-fed rotor-flux oriented induction motor drive. It consists of a 2.3kW, 4-pole induction motor supplied from a current-controlled 8 A (continuous), 22 A (peak, short-term) voltage source inverter [Sokola and Levi (2001)]. An 8051 micro-controller and TMS30C14 digital signal processor are used in the vector controller. The drive system is controlled from a PC using the MS-DOS based control software.

The speed control and field orientation are digitally controlled, however, the current control loops are analogue and are implemented in the stationary reference frame. Ramp comparison current control method is used. The induction motor also includes a resolver as a position sensor. The current-regulated PWM voltage source inverter operates at 10 kHz switching frequency. Two current sensors are incorporated in the current control loops to provide feedback signals. The current limit for the q-axis current command is calculated based on the maximum allowed total stator current (22 A peak) and instantaneous stator d-axis current command.

The drive is capable of operating in both the base speed region and the field-weakening region. The maximum speed in the field-weakening region is 8000 rpm. The base speed can be selected by the user. To enable the operation of the induction motor in field-weakening region, rotor flux reference is reduced above the base speed, in inverse proportion to the speed [Sokola (1998)]:

$$\psi_r^* = \psi_r^n \frac{\omega_B}{\omega_r} \tag{8.1}$$

where ψ_r^n, ω_B are rated rotor flux and base speed respectively.

This approach will continue to treat the motor as current-fed in the field-weakening region. Therefore, the same control system structure is retained in the whole speed control range. The disadvantage of this approach is that the operation of the drive system is affected by the variation of the magnetising inductance. Magnetising inductance increases when the motor operates with the reduced rotor flux. The effects of the variation can be compensated by either embedding the magnetising curve in the control system [Levi et al (1990), Wieser (1997)] or by providing on-line identification of the magnetising inductance [Choi et al (1997)]. The approach implemented in this drive system is to incorporate the magnetising curve in the vector control scheme because of its simplicity. This method, however, requires the knowledge of the magnetising curve, which is identified during the commissioning of the drive. Detailed consideration of this issue can be found in [Sokola (1998)].

8.2.2 Measuring equipment

The drive has an analogue output, which gives a voltage signal proportional to speed. Speed traces of steady state and transient responses are recorded using Hewlett Packard spectrum analyser as a digital oscilloscope. Transient responses of stator currents can also be observed and collected by this analyser when it is used in conjunction with a Tektronix current probe and amplifier. The current signal is processed as a voltage signal on the analyser.

8.2.3 No-load operation of the vector controlled drive system

The base speed for the drive is selected as 1500 rpm. The induction motor is coupled to a DC generator, which is unloaded. Details of the appropriate magnetising curve approximation of the induction machine are entered during the drive set-up,

together with the value of the rated magnetising current (rated *d*-axis current command) [Sokola (1998)]. The correct value for slip gain of the drive in DSP units is 47 [Sokola (1998)]. This value is first entered into the drive, it is then varied to examine the effects of the de-tuning caused by incorrect slip-gain setting on the performance of the drive. Speed commands for acceleration and deceleration are step commands. The speed controller's parameters (proportional constant and integral constant) are kept constant for the whole experiment with the vector controlled drive. Default values are used for other parameters of the drive (digital filter parameters, current control loop parameters, the limit of the maximum peak current of the drive, etc.).

Transient speed responses of the unloaded induction machine are observed and recorded. The motor is accelerated to 100rpm, 300rpm, 500rpm, 700rpm, 900rpm, 1100rpm, 1300rpm and 1500rpm and then decelerated to 0rpm. The first two seconds of the transient are captured on the digital oscilloscope (this includes a short period before the transient response is triggered). The sampling frequency is set to 400 Hz. This means that 800 data points are stored for each trace. The transient response of stator phase current during acceleration is also observed and recorded.

Figure 8.1 shows speed of the induction motor during the acceleration and deceleration transient, together with stator phase current during some selected acceleration transients. The rotor speed response of the induction motor during accelerations from 0rpm to 100rpm, 300rpm, 500 rpm and 700 rpm are shown in figure 8.1a. There is a certain amount of noise in the signals. Low overshoots are observed in the low speed region (100rpm, 300rpm), however, higher overshoots are present in the medium speed region (500rpm, 700rpm) during acceleration. Motor speed settles down to the commanded value in 0.5 second after the motor starts accelerating when speed command is 100rpm and overshoot is low. At higher speed commands and with higher overshoot, motor speed response takes more time to settle down at the commanded value, about 1.5-1.7 seconds.

The overshoot, however, reduces when the speed command is higher than 700rpm. Less noise is observed in the signal at higher speed. Figure 8.1b shows the motor speed response when it is accelerated to 900rpm, 1100rpm, 1300rpm and 1500rpm. Overshoot is not present in the transient response for speed commands equal to 1100rpm, 1300rpm and 1500rpm. It takes the motor typically 1.2 to settle down to the commanded speed for commanded speeds equal to 1100rpm or above.

Similarly, transient responses of speed during deceleration are also observed and captured and the results are given in figures 8.1c and 8.1d. In the high speed region (1100rpm, 1300rpm, 1500rpm), no undershoot is observed in the transient responses. The motor goes down to standstill in around 1.1 seconds after the zero speed command is given. However, in medium speed region and low speed region (900rpm, 700rpm, 500rpm, and 300rpm) undershoots are present, especially at 700rpm (symmetrically to the response during acceleration). The motor takes up to 1.7 seconds to settle at standstill. Nevertheless, when the motor is decelerated from 100rpm to 0rpm, no undershoot is observed and the duration of the transient is about 0.5 second. More noise is observed in the signals in the medium and low speed regions.

Transient responses of stator phase current during the acceleration to 100rpm, 500rpm, 700rpm, and 1100rpm are shown in figure 8.1e and 8.1 f. The motor has been pre-magnetised before application of the speed command and the presence of the *d*-axis component of stator current is evident in the figures. As can be seen in stator current traces, speed command of only 100rpm does not require operation of the drive in the current (torque) limit of 22A (figure 8.1e). The same applies to the other small speed commands, such as 300rpm and 500rpm. However, for n* = 900rpm operation in the current limit begins to take place (figure 8.1f) and, as the speed command further increases, intervals with operation in the current limit become longer (for example, speed command of 1100rpm in figure 8.1f). Identical situation applies to deceleration transients, where the only difference is basically the sign of the stator *q*-axis current (and hence the phase of the stator phase current).

Different nature of the speed response during acceleration and deceleration, as function of the speed command setting, appears to be an inherent property of a high performance drive with a constant parameter PI speed controller. The setting of the PI controller parameters is usually done in such a way that an aperiodic speed response is obtained for rated step speed command. If speed command is lowered, an overshoot starts appearing, as observed in figure 8.1. Detailed experimental study of this phenomenon has recently been reported in [Ibrahim and Levi (2002)] and it suffices to say that the behaviour of the speed response observed here is in full agreement with findings of this reference.

Slip gain in the vector controlled drive is varied next in order to investigate the effects of incorrect slip gain (rotor time constant) setting on the performances of the drive. The slip gain is set 130%, 120%, 110%, 90%, 80%, and 70% of the correct value.

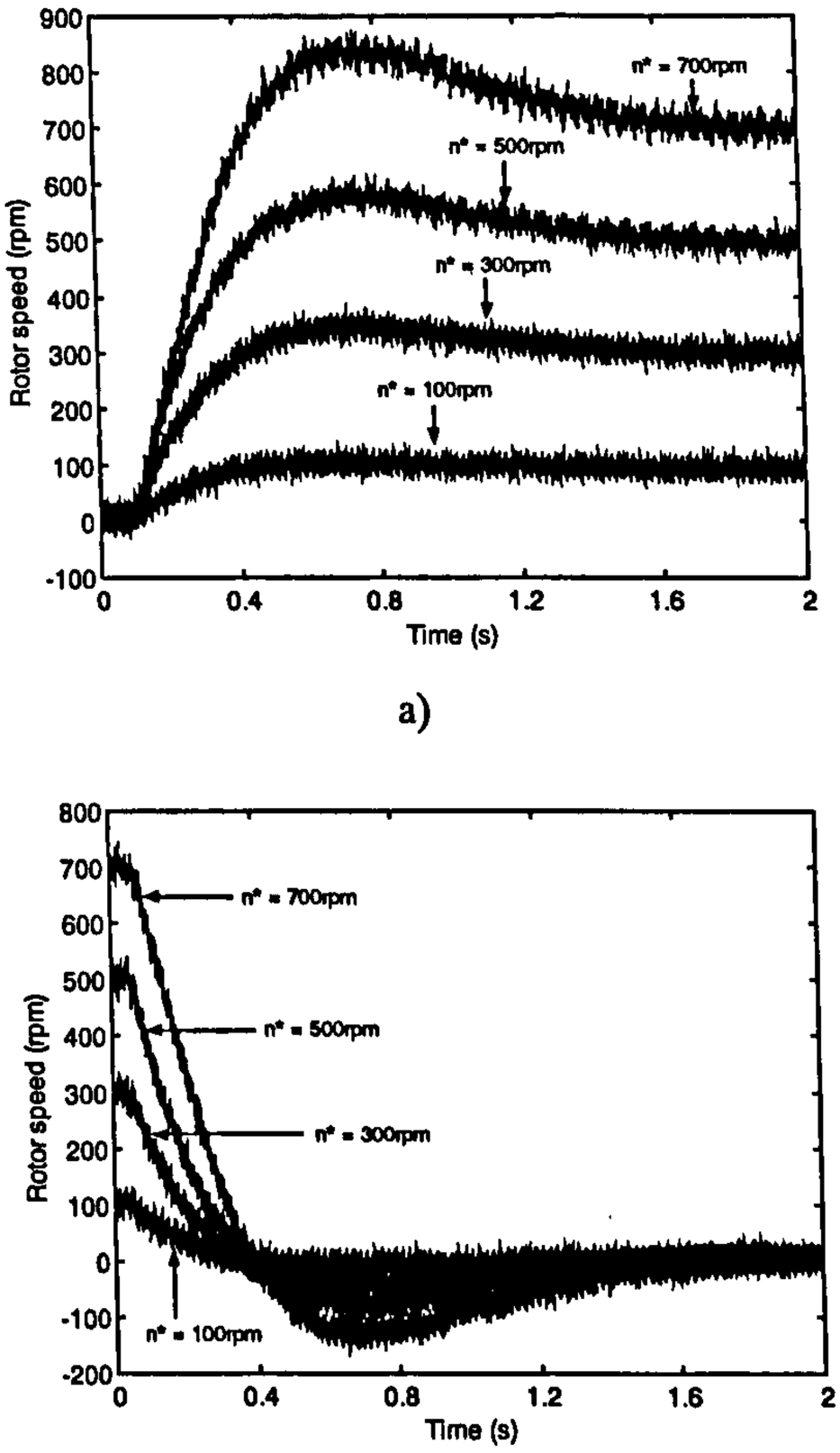

a)

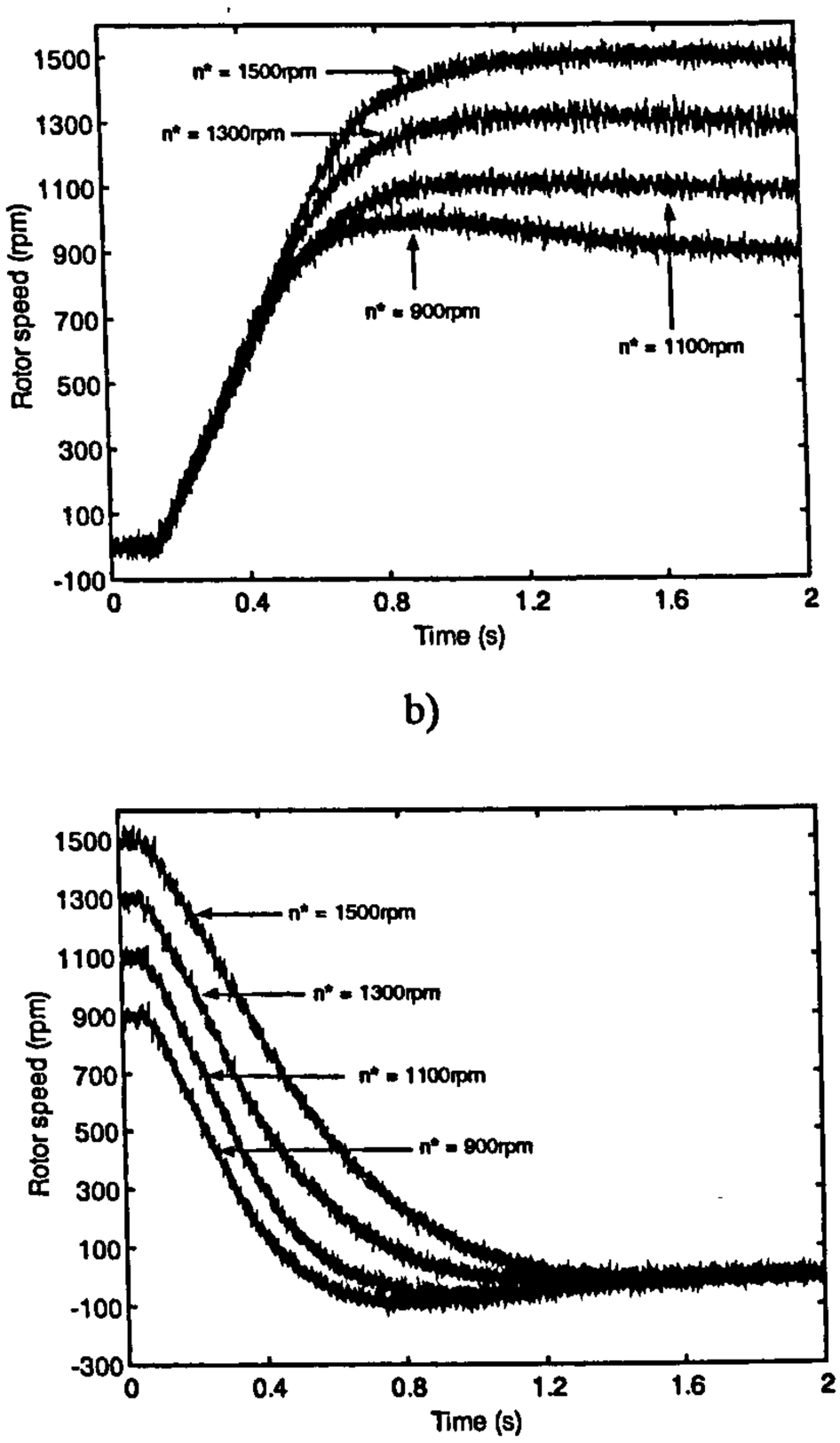

b)

c)

d)

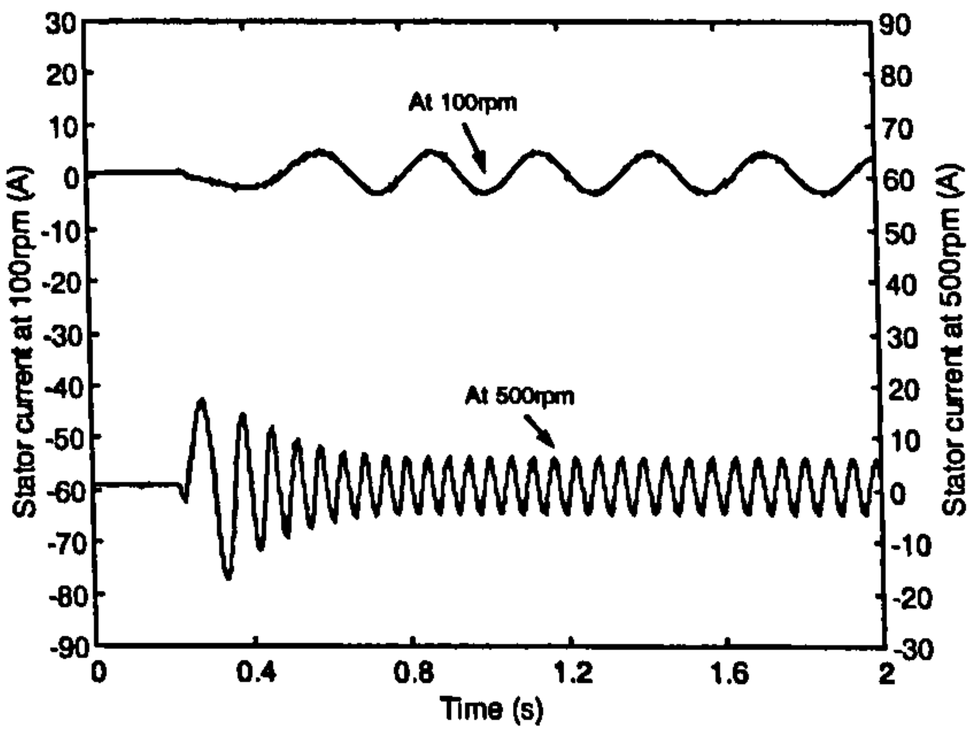

e)

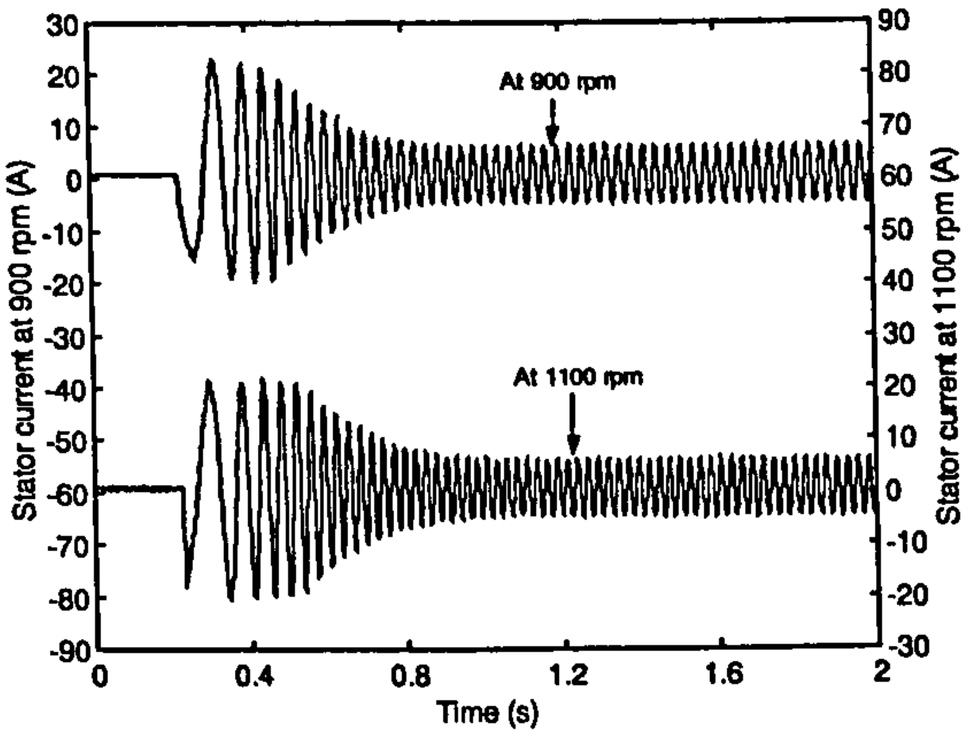

f)

Figure 8.1: Acceleration of the motor to: a) low and medium speeds; b) medium and high speeds. Deceleration of the motor: c) at medium and low speed; d) at high and medium speeds. Stator phase current during acceleration to: e) 100rpm and 500rpm; f) 900rpm and 1100rpm.

The transient responses of speed when the slip gain is set to 130% (30% increment) and 80% (20% decrement) of the correct value are shown in figure 8.2, for speed commands equal to 500rpm, 1100rpm and 1500rpm (figures 8.2a, 8.2c and 8.2e respectively).

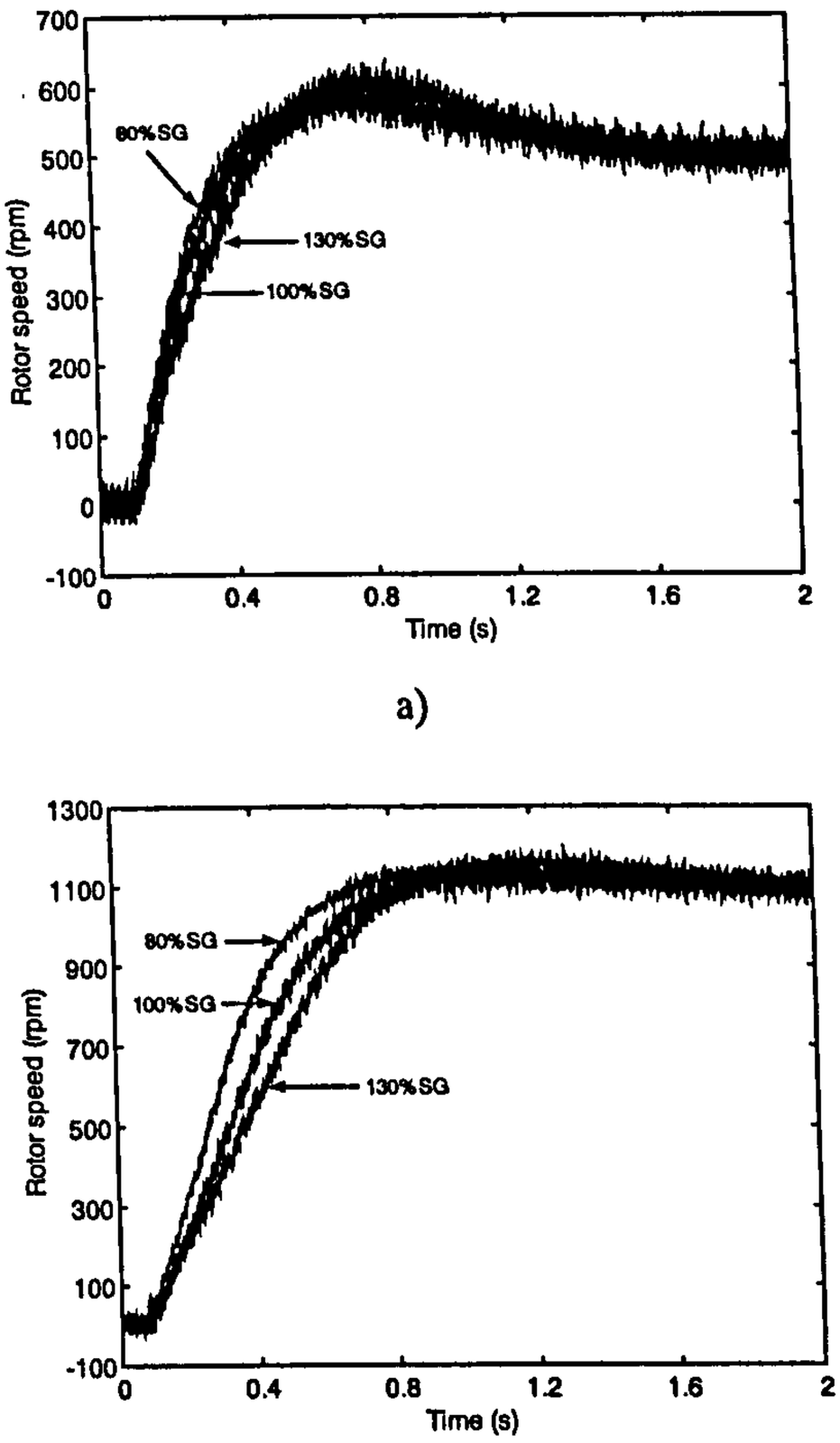

a)

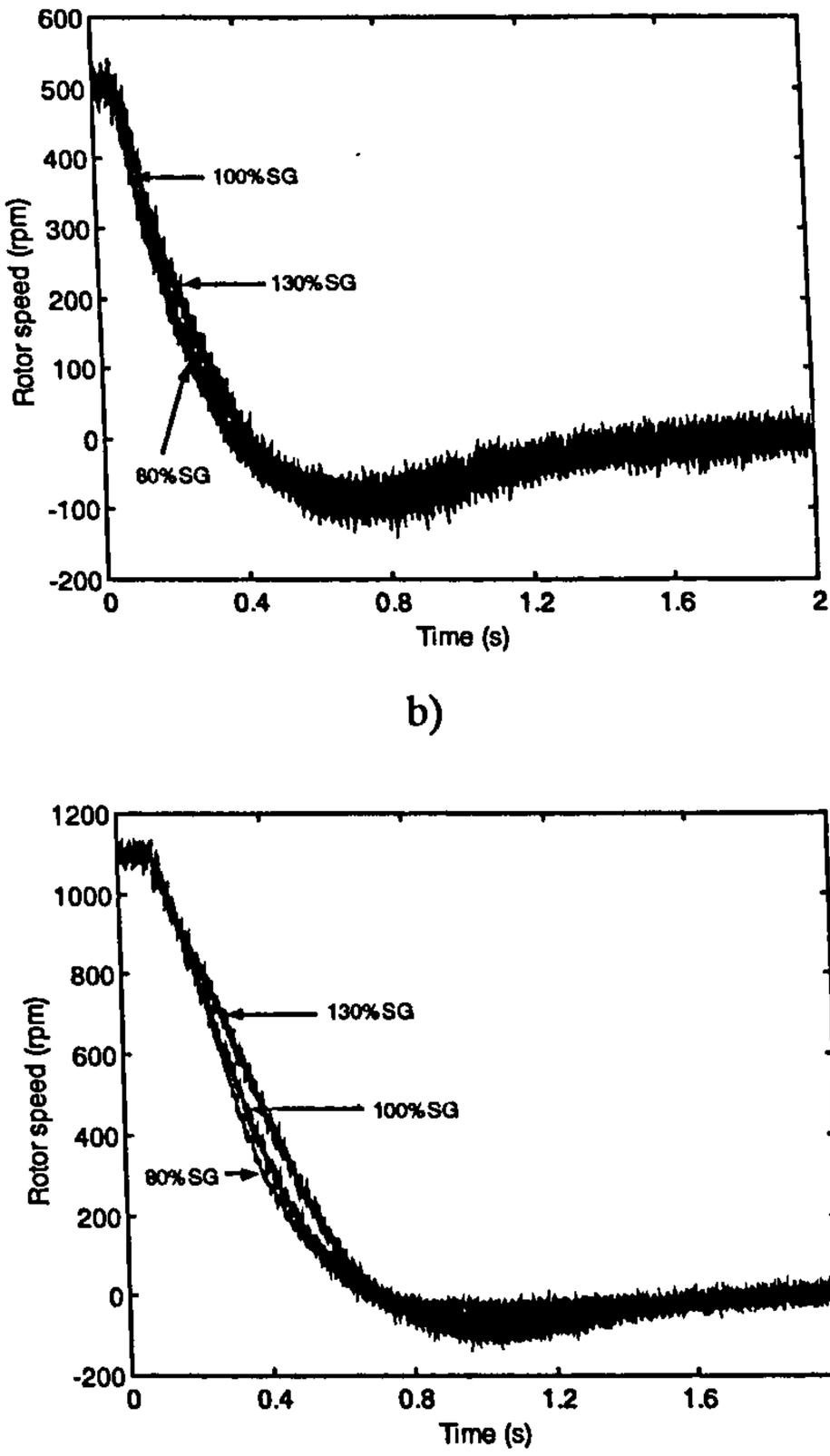

b)

c)

d)

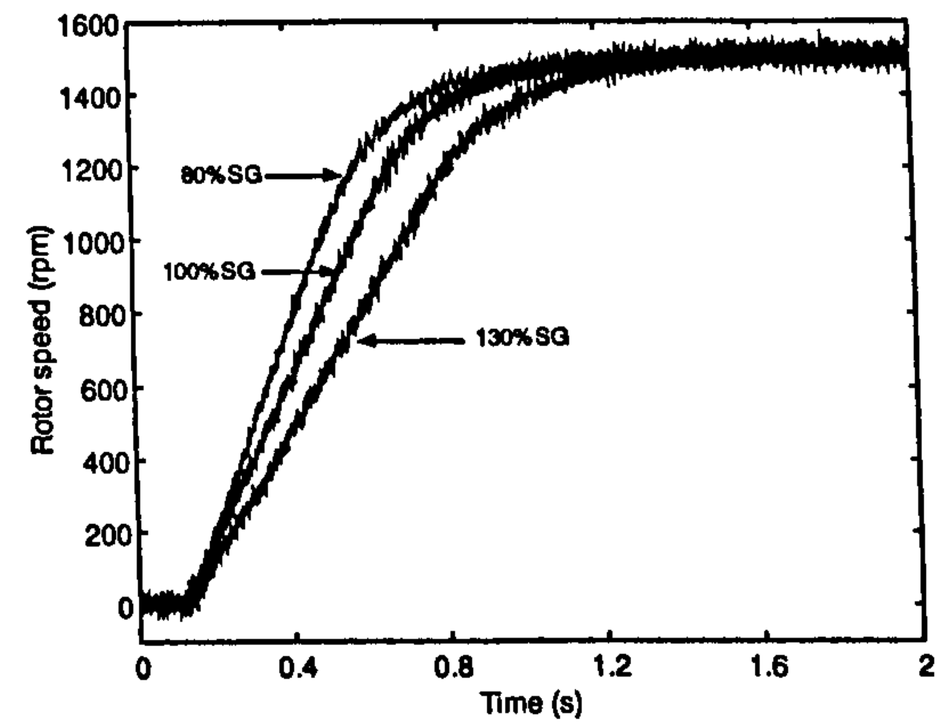

e)

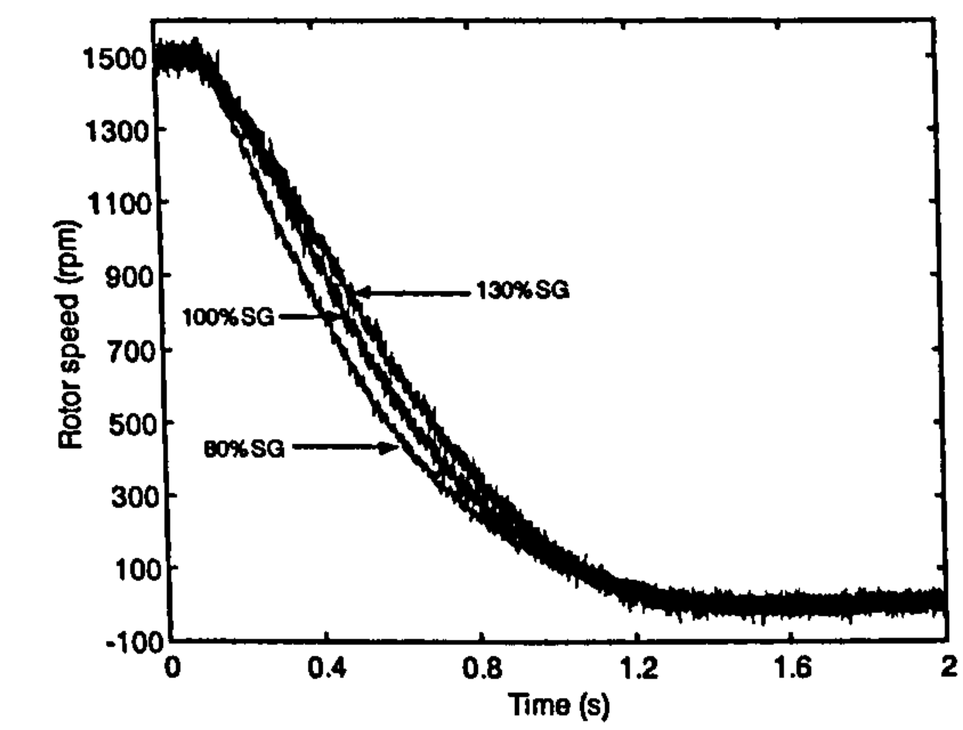

f)

Figure 8.2: Effects of incorrect setting of slip gain on transient responses of motor speed during: a) acceleration to 500rpm; b) deceleration from 500rpm; c) acceleration to 1100rpm; d) deceleration from 1100rpm; e) acceleration to 1500rpm; f) deceleration from 1500rpm.

Corresponding deceleration transients are illustrated in figures 8.2b, 8.2d, and 8.2f, respectively.

The transient responses are generally faster when the slip gain is too low, and slower when slip gain is too high in every speed region. Overshoots in the responses are slightly reduced when the slip gain is smaller, and slightly increased when the slip gain is higher, for the whole base speed region.

Stator current (RMS value of fundamental current) is reduced during steady state operation with light load (up to 50% of the rated load at the rated speed) and too high slip gain setting, and is increased when the slip gain setting is too low [Sokola and Levi (2001)]. The measurements of the stator current during the steady state of the drive with no-load operation are not repeated here. The reduction of the RMS value of the fundamental component of the stator current, when slip gain is high, is attributed to the decrease of flux controlling component of stator current, i_{ds}, which is also the dominant component when the load torque is light. However, when the load torque is increased, the torque controlling component in stator current is more dominant, and the RMS values of the fundamental stator currents for correct slip gain setting and higher setting are equal, especially in high speed region. And when the load torque is 100% of the rated torque at the rated speed, RMS value of stator current with higher slip gain setting is higher than the one with correct slip gain setting in high speed region [Sokola and Levi (2001)]. Therefore, operation with higher slip gain setting is beneficial, in terms of efficiency (copper loss and iron loss), only with light load torque.

Transient responses of speed in no load operation and incorrect slip gain setting shown in [Sokola and Levi (2001)] are also consistent with the responses obtained here during both acceleration and deceleration. Response time during acceleration increases for higher slip gain setting and decreases for lower slip gain settings. Due to the limit of stator current, higher transient torque can be developed with lower slip gain settings [Sokola and Levi (2001)], this will cause faster responses for lower slip gain setting. This difference in response time during acceleration will increase with higher load torque. However, the difference in response time during deceleration is more significant for lower load torque due to the role of load torque in braking process. Again, the response time is higher for high slip gain setting in no load operation. And the response time is not affected at all when the load torque is 100% of the rated torque at the rated speed.

8.3 Performance of the direct torque controlled drive

8.3.1 Description of the drive system

An ABB direct torque controlled drive system is installed and commissioned and then operated to investigate the performance of the first generation of industrial DTC drives. The system consists of a frequency converter (ACS 601) unit, a braking chopper for over-voltage protection, pulse encoder interface module, and a pulse encoder. The induction motor is a three-phase, star-connected, 50Hz, 4-pole, 2.2kW motor with rated stator current of 5A, rated stator voltage of 415V and rated speed of 1430rpm.

8.3.1.1 Description of the ACS 601 frequency converter

The ACS 601 frequency converter belongs to the ACS 600 product family of low voltage three phase frequency converters and converter modules for speed control of squirrel cage electric motors. The ACS products are used for majority of standard applications. The family also includes ACP 600 products, which are specifically designed for positioning, synchronising and other high precision control applications, ACC 600 products for crane drive applications and ACS 600 MultiDrive for multi-drive applications. The specific ACS 601 frequency converter used here includes a 6-pulse diode rectifier, and is of the wall-mounted type, suitable for applications with powers less than 5 kW.

Operational rectifier input voltage ratings are 380/400/415 V. Frequency of the mains input voltage must be in the range of 48-63 Hz, with maximum rate of change 17%/s. The maximum imbalance is ± 3% of nominal phase to phase input voltage. The converter can withstand a maximum short circuit current of 50 kA in 1 second. Fundamental harmonic power factor of input power is 0.97.

The average switching frequency of the converter is 3000 Hz. The output voltage range of the frequency converter is from zero to the input voltage (380/400/415 V). Frequency of the output voltage is in the range of 0-300 Hz. During the DTC mode of operation (there are two possible modes of operation for the converter: scalar *V/f* and DTC), the converter delivers the output voltage with frequency from 0 to $3.2 \cdot f_{FWP}$, where f_{FWP} is frequency at field weakening point initiation and it is calculated as follows:

$$f_{FWP} = \frac{V_{main}}{V_{motor}^{n}} \cdot f_{motor}^{n} \tag{8.2}$$

and $V_{main}, V_{motor}^{n}, f_{motor}^{n}$ are the input voltage to the frequency converter, rated motor voltage and rated motor frequency, here $f_{FWP} = 50\,\text{Hz}$. The converter's output frequency resolution is 0.01 Hz. Power limit at the output is 1.5 times of typical motor power during heavy-duty use (50% to 100% overload capacity). Automatic over-current trip is 3.5 times the rated rms output current in heavy-duty use or 21.7 A (the rated rms output current in heavy-duty use is 6.2 A). However, default current limit set by the control panel (or DriveWindow software) is 200% of the rated rms output current in heavy-duty use or 12.4 A. Efficiency of the frequency converter is approximately 98% at nominal power level. Air temperature during the operation of the converter should be from 0°C to 40°C.

The frequency converter can also be connected to many optional peripheral modules such as field-bus adapter modules, I/O extension modules, pulse encoder interface module, double pulse encoder interface module, a personal or laptop computer. These peripheral units are linked with the frequency converter by fibre optic cables for mutual communication. An extra circuitry needs to be installed inside the converter to support optical communication when this equipment is used in conjunction with the converter. Control of the frequency converter can be carried out from the control panel, which can be removed from the converter to enable the user to control the converter from a remote location through a cable connecting the converter and the control panel, or from a PC equipped with the ABB DriveWindow software.

The computer communicates with the converter through fibre optical cables. A special circuitry needs to be installed in the computer to convert digital signal to optical signal and vice versa. All the control functions of the frequency converter can be done by either the software or the control panel. However, the control panel has higher authority when the control parameters of the converter need to be changed, therefore, parameter setting should be done on the control panel. Nevertheless, the software can provide data acquisition. All the actual signals and values of parameters in the drive can be acquired by the software. The signals can also be observed during transient and steady state operation of the frequency converter. Up to six signals can be observed and acquired simultaneously by the software. The maximum sampling frequency of software is 1 kHz. There are two modes of sampling, normal mode and fast mode. The

maximum sampling frequency for the normal mode is 100 Hz, above 100 Hz is the fast mode of operation of the data sampling. However, operation in the fast mode could cause hanging-up or crashing of the PC if the speed of PC microprocessor is not fast enough and the dynamic memory is not big enough. It is not recommended to use the fast mode of operation. Another reason for not using this mode is that Windows is not a real-time operating system. It means that, in practice, even if the measurements are done cyclically, they are not done with equal time intervals. Load caused by drivers in Windows kernel may cause interrupts in measurements. These interrupts can hide the phenomena one is trying to monitor, especially when the monitoring interval is small [ABB Industry Oy (2002)]. Data acquisition interval in both normal and fast modes varies also because of load caused by the operating system kernel and high priority programs due to non real-time characteristic of Windows.

The actual sampling frequency of DriveWindow software used in this direct torque controlled drive (100 Hz) is therefore lower than the sampling frequency of the universal spectrum analyser used for data acquisition and observation of the vector controlled drive (400 Hz). However, the total number of data points collected by the software is much higher than in the case of the spectrum analyser. The software can continuously collect the data for almost 25 days. The number of data points collected by the software is in practice limited by the amount of virtual memory in the PC.

The frequency controller can operate with several application programs or macros. These macros are Factory, Hand/Auto Control, PID Control, Sequential Control, and Torque Control. Factory macro is suitable for applications such as conveyers and other industrial constant torque applications. It is also suitable for applications to be run for long periods with constant speed different from the nominal speed of the motor and vibration endurance test benches needing variable speeds of vibrating motors. It can also be used for testing of rotating machines and other applications, which need traditional external control. Control functions of this macro can be performed on control panel or by DriveWindow software.

Hand/Auto Control macro is used for the processes requiring automatic motor speed control with PLC, for example, and manual speed control with an external control panel. The control functions are carried out on peripheral devices, which communicate with the frequency converter through the I/O extension modules.

PID Control macro is suitable for applications with different closed loop control systems such as pressure control, level control and flow control. These applications are

booster pumps of municipal water supply systems, automatic level control of water reservoirs, booster pumps of district heating systems and speed controls of different types of material handling systems where the material flow has to be regulated. The controlling functions are made externally and then transmitted to the frequency converter through I/O extension modules.

Torque Control macro is used in processes requiring torque control such as mixer or slave drives. Torque reference comes from a PLC or some other process automation system or control panel. Again, I/O extension modules are required for controlling of the frequency converter. Sequential Control macro is for processes requiring motor speed control in addition to the adjustable speed with 1 to 15 constant speeds and/or with two different acceleration/deceleration times. The control can be performed automatically with a PLC or some other process automation system or by using normal speed selection switches.

Only Factory macro is used in the experiment. No I/O extension modules are therefore connected to the converter. This macro operates in speed control mode. Speed feedback signal can be from either pulse encoder or speed estimator inside the converter. Speed feedback signals can be selected by either the control panel or DriveWindow software. Parameters of the speed controller incorporated in the converter, such as gain, integration time, derivation time, derivation time used in compensation of acceleration, and slip gain of the speed controller (in order to compensate for the steady state error), can also be adjusted by the user. The speed controller output is the reference for the torque controller. The torque reference limits can be set up by the user. The values of speed controller parameters are tuned automatically when the Motor ID Run is performed. Motor ID Run is carried out when the drive system is started up for the first time. These values then can be stored in the drive or the control panel. It is not necessary to perform the Motor ID Run every time the system is started afterwards.

Full Motor ID Run is performed on the induction motor in this experiment when the drive system was first started up. During the Motor ID Run, the converter will identify the characteristic parameters of the motor for the optimum control of the motor. However, the parameters identified during the ID run can not be viewed and edited by the user. The ID Run will take about 1 minute. Performing the Motor ID Run will guarantee that the best possible control accuracy is achieved. Before this process is carried out, the motor must be de-coupled from the load or driven equipment. Although

Motor ID Run is not compulsory before using the frequency converter, it is recommended when the following requirements exist:

- Operation point is near zero speed.
- Operation with torque range above the motor nominal torque within wide speed range and without any pulse encoder.

Reduced Motor ID Run can be performed instead of full Motor ID Run described above in some applications. De-coupling of the motor and the load (or driven equipment) is not required for the reduced ID Run. The applications in which reduced Motor ID Run is sufficient include:

- The applications in which the mechanical losses are higher than 20% of rated power (i.e. the motor can not be de-coupled from the driven equipment).
- The applications in which flux reduction is not allowed while the motor is running (i.e. in case of a braking motor in which the brake switches are on if the flux is reduced below a certain level).

8.3.1.2 Pulse encoder interface module (ABB-NTAC-02)

This equipment is an optional device for the ACS 601 frequency converter. The module offers an interface for a digital pulse encoder connection, converting digital signals into optical signals. This module and other I/O extension modules are connected to the converter via an optical DDCS-protocol communication link. All the optically communicating equipment is connected to the application and motor control board inside the frequency converter, which acts as a master, checking these modules cyclically. The modules respond to the master's enquiries. These modules are mounted outside the frequency converter. This module can also communicate with other external modules by optical fibre cables. Power supply of the interface module is from the 24 V (DC) voltage source inside the frequency converter.

8.3.1.3 Description of the NBRA-653 braking chopper

A braking chopper is used to protect the frequency converter against over-voltage damage when the motor brakes. A braking resistor is used to dissipate the power caused by the over-voltage. The chopper connects the braking resistor to the intermediate circuit of the frequency converter whenever the voltage in the intermediate

circuit exceeds the maximum limit, which is 1.21·1.35·415V in this experiment where the supply voltage to the frequency converter is 415V. The energy generated by the motor during a fast deceleration causes the voltage to rise in the intermediate circuit of the frequency converter. Energy consumption by the resistor lowers the voltage until the braking resistor can be disconnected.

The chopper and the resistor are rated so that the power equal to the short-term overload capacity of the ACS 600 can be handled during the braking. The short-term overload capacity for a Normal Use rated ACS 600 is 110% of the rated output power, and for a Heavy-duty Use rated ACS 600 is 150% of the rated output power. The rating of the braking resistor here is 5kW.

The braking chopper is also equipped with an 'enable' input and a relay output. The input can be connected to a temperature sensitive switch mounted in the resistor assembly to protect the resistor against over temperature. This input is not used. The relay output indicates chopper faults. In this experimental rig, the fault monitoring of the braking chopper is carried out by the frequency converter.

8.3.1.4 Description of the load - DC motor

A permanent magnet DC motor is coupled with the induction motor to be used as a DC generator. The DC motor is rated at 1.5 kW when the form factor is 1.05, and the maximum armature current is 9.0 A. It is rated at 1.1 kW when the form factor is 1.40 and the maximum armature current is 7.0 A. The rated armature voltage of the DC motor is 180 V, and the rated speed is 1800 rpm. A resistor bank is connected to the armature terminals of the DC motor for loading. The load resistor is set at 80 Ω, 34.3 Ω, 24 Ω and 17.2 Ω to obtain the armature current at the terminals of the DC generator of 1.80 A, 3.90 A, 5.40 A and 7.40 A at the rated speed of the induction motor (1430 rpm), respectively.

8.3.1.5 The complete DTC experimental rig

Figure 8.3 shows the components and the connections of the experimental rig. The arrows indicate communication cables and the directions of communication, the other connections indicate power cables. The braking chopper and the pulse encoder interface module are shown in the figure by their code names (NBRA-653 and NTAC-02, respectively).

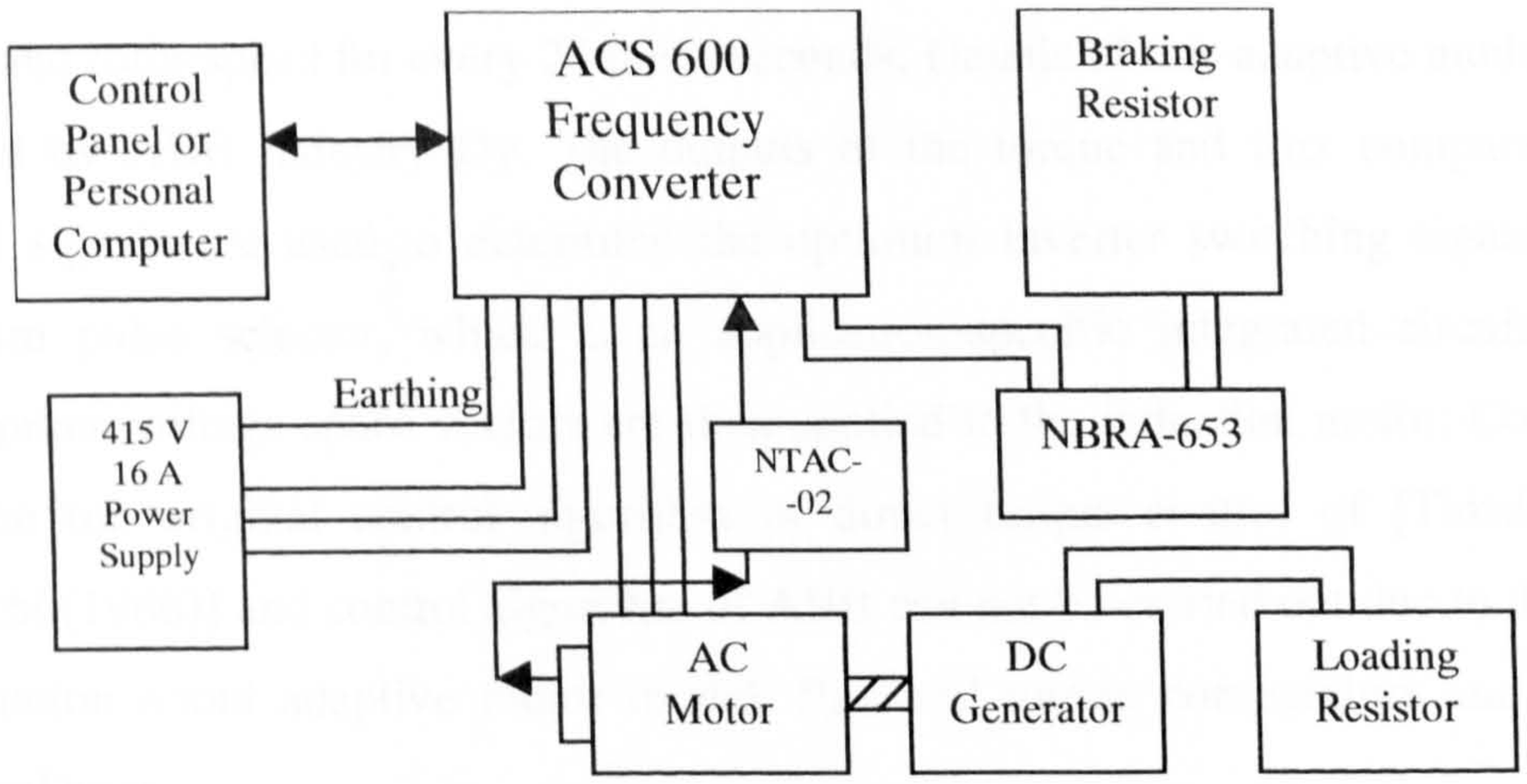

Figure 8.3: The schematic outlay of the DTC induction motor rig.

8.3.1.6 Control algorithm of the ABB DTC drive

Figure 8.4 shows the schematic control algorithm of the ABB direct torque controlled drive [ABB Industry Oy (2002)].

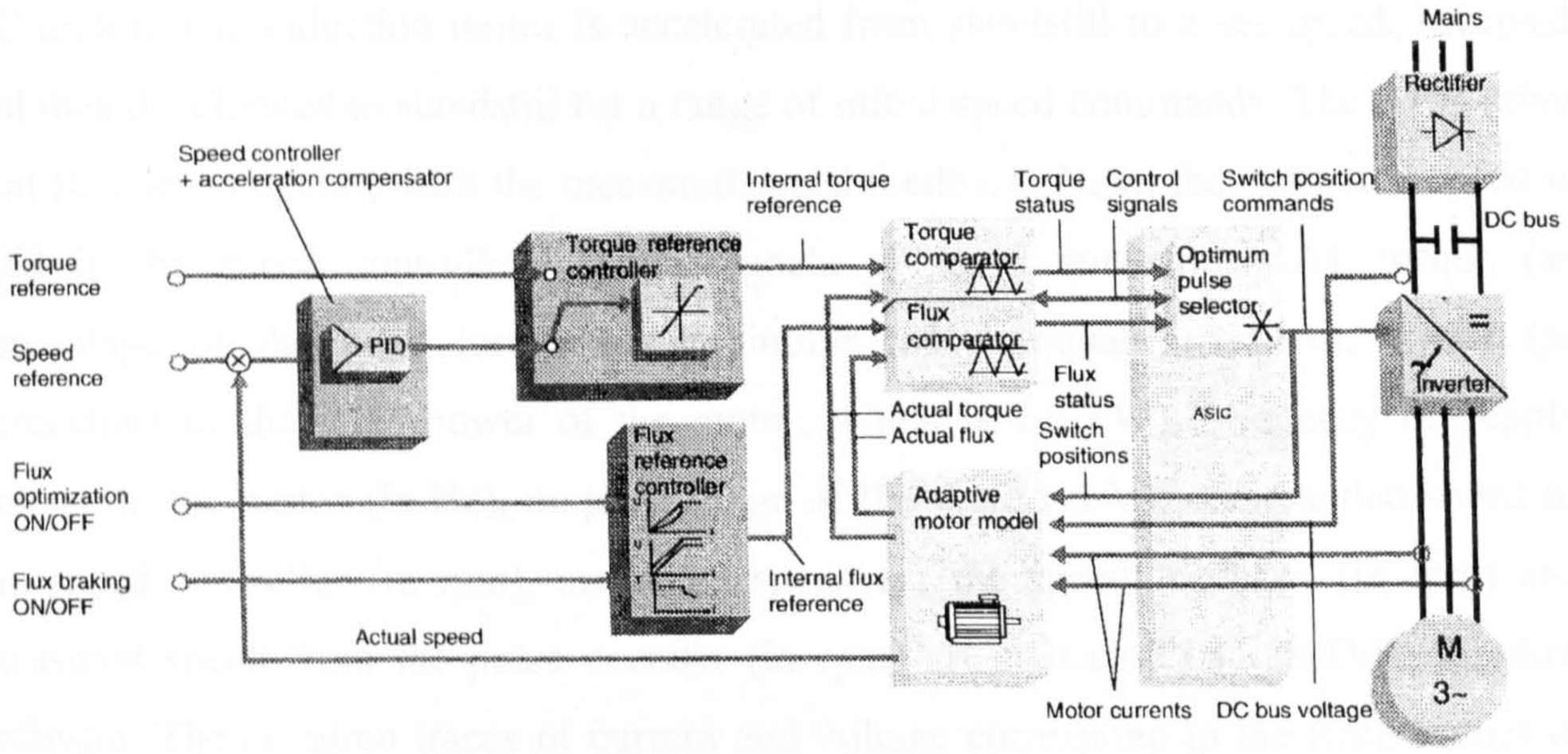

Figure 8.4: Control algorithm of ABB direct torque controlled drive [ABB Industry Oy (2002)].

The torque and flux reference for the direct torque controller are internal signals and are from the outputs of the torque reference controller and flux reference controller, respectively. Inputs of the torque reference controller are either from the external torque reference signal (Torque Control macro) or from the output of the PID speed controller (all the macros). However, there is no input for external flux reference in flux reference controller. The estimated stator flux and torque are from the adaptive motor model, which uses measured stator phase currents and reconstructed stator phase voltages (calculated from the DC bus voltage and the switching signals) to estimate stator flux,

torque and rotor speed for every 25 microseconds. Details of this adaptive model are not released by ABB Industry Oy. The outputs of the torque and flux comparators and control signals are used to determine the optimum inverter switching signals by the optimum pulse selector, which is an application-specific integrated circuit (ASIC). Appropriate voltage space vectors are then applied to the induction motor. Comparison between the original control algorithm of direct torque control of [Takahashi and Noguchi (1986)] and control algorithm of ABB can not be carried out due to the lack of information about adaptive motor model, flux and torque comparators and optimum pulse selector.

8.3.2 Performance of the direct torque controlled drive under no-load conditions

The drive is connected to the induction motor, which is disconnected from the DC motor. The induction motor is accelerated from standstill to a set speed, reversed and then decelerated to standstill for a range of initial speed commands. The ABB drive is at first set to operate with the measured speed feedback. Next, the estimated speed is used in the speed controller. Actual signals of stator current (in A), torque (as percentage of the rated torque of the motor, which equals 15 N.m), power (as percentage of the rated power of the motor, which is 2.2 kW), frequency of supply voltage to the motor (in Hz), output voltage of the drive (in V), commanded speed of the speed controller (in rpm), estimated speed for the speed feedback (in rpm) and measured speed from the pulse encoder (in rpm) are collected by the DriveWindow software. The acquired traces of current and voltage correspond to the RMS values of input current and motor line voltage.

Figure 8.5 shows the responses of the motor speed during acceleration from zero speed, reversing and deceleration to zero speed in low, medium and high speed regions using measured speed feedback. Figure 8.6 compares the variations in speed responses when estimated speed feedback and measured speed feedback, respectively, are used in the speed control loop. Figure 8.7 shows the corresponding responses of stator current. Similarly, figure 8.8 shows the responses of motor torque, figure 8.9 the responses of motor power, figure 8.10 the responses of frequency of input voltage to the motor, and figure 8.11 the output voltage of the drive during the three transients.

The speed signals obtained from the direct torque controlled drive and the DriveWindow software have less noise than the ones obtained from the vector controlled drive with Hewlett Packard universal spectrum analyser. Speed response time of speed during the acceleration and deceleration in DTC drive is much shorter than the one observed with the vector controlled drive for all speed commands. However, although the two motors used in the two drives are almost of the same power rating (2.3 kW and 2.2 kW, respectively), the principal difference between the two sets of experiments is that here the induction motor is not coupled to DC machine (and hence the only inertia is of the motor itself), while in the vector controlled rig the DC motor was coupled to the induction motor all the times (and the inertia was therefore substantially higher). Furthermore, current limit setting as percentage of the rated motor current is not the same either. Therefore, on the basis of the presented results one must not conclude that DTC yields a faster response (although this is commonly claimed by ABB). As a matter of fact, it is obvious that in the vector controlled drive maximum torque is developed practically instantaneously as the machine is pre-magnetised (stator current traces in figure 8.1f). Due to the almost instantaneous step torque response, speed response is initially a linear function of time (for example, figure 8.1b). This however does not apply in a DTC drive, since the machine can not be pre-magnetised at zero speed with zero load torque. This is confirmed in figures 8.7a and 8.7b where the stator current at standstill is zero. Consequently, speed response (figures 8.5a and 8.5b) is not initially linear and is slower in the first part of the transient than in the vector controlled rig.

Overshoots in speed responses obtained in DTC drive are lower than in the speed responses in vector controlled drive, especially in low and medium speed regions, during both acceleration and deceleration. Overshoots of speed responses in DTC drive appear to be independent of operating speed of the drive during acceleration, however, they slightly vary with speed setting during deceleration, especially for decelerations to standstill from 700 rpm and 1300 rpm. This apparent difference between the DTC drive and the vector controlled drive behaviour has a rather simple explanation. As the DTC drive accelerates very rapidly to the set speed due to the very small inertia, current limit is not entered for any of the speed commands (figure 8.7a and 8.7b). This means that the speed controller operates in the linear region at all times, in contrast to the speed controller in vector controlled drive where the output gets saturated during operation in

the current limit (this is especially pronounced for higher speed settings in figure 8.1f and is a consequence of much higher total inertia of the drive).

Both drive systems result in correct steady state speed holding. Overshoots in speed responses become higher for speed settings equal to or below 700 rpm and at 1300rpm during reversing, as shown in figures 8.5e and 8.5f.

Speed responses with estimated speed feedback and measured speed feedback in the speed controller during acceleration from zero to 50 rpm, 100rpm, 500 rpm, 700rpm, 1100rpm, 1430rpm and subsequent reversing are shown in figure 8.6. During acceleration at very low speed (50 rpm) and low speed (100 rpm), speed responses with measured speed feedback have lower overshoot and shorter response time. During the reversing transients, speed response with measured speed feedback at 50 rpm has lower overshoot and shorter response time than the one with estimated speed feedback. The speed response with measured speed feedback at 100 rpm appears to have higher overshoot (but shorter response time) than the other one. This is probably only an apparent difference, caused by the low sampling rate of signals. Similarly, during the acceleration from zero speed into medium speed region, the speed responses with speed encoder have lower overshoot and are faster. During the reversing at 700 rpm, the quality of speed response with measured speed feedback is similar to the other one. In high speed region, the speed response with measured speed feedback has lower overshoot and shorter settling time during the acceleration and reversing at 1100rpm. The speed responses during reversing at the rated speed are equally good with or without speed encoder.

The actual signal of stator phase current obtained by the DriveWindow software (RMS value) is shown in figure 8.7. As already noted, the induction motor is not pre-magnetised before starting-up in direct torque control (zero current value prior to speed command application). Current remains below the current limit during acceleration, due to small inertia and rapid achievement of the set speed. Stator current attains higher RMS value during deceleration and reversing at all speeds. These are shown in figures 8.7c, 8.7d, 8.7e and 8.7f. One observes, by comparing stator current during deceleration and reversing transients (figures 8.7c to 8.7f), one interesting difference. RMS of stator current during acceleration exhibits substantial oscillations. However, this does not happen during deceleration and reversing. The explanation is believed to be in the fact that during acceleration, there is a simultaneous building up of both flux and torque of the machine. In contrast to this deceleration and reversing take place when the machine

is fully fluxed. This at the same time explains why for example reversing transient (speed change $\Delta n = 2|n^*|$) takes a much shorter time interval than the acceleration to the same set speed (speed change $\Delta n = n^*$). During steady state operation of the unloaded induction motor, the stator current settles at about 2.5 A at all speeds.

Motor torque is shown as percentage of the rated torque of the induction motor in figure 8.8. Torque is building very slowly during the acceleration from standstill for all speed commands (figure 8.8a and 8.8b). This is an inherent disadvantage of DTC, when compared to vector control, caused by the lack of possibility to excite the machine at zero speed with zero load torque. Due to no-load acceleration with small inertia, only a very small torque is required to bring the motor to the commanded speed during acceleration (less than rated in all cases shown in figures 8.8a and 8.8b). During deceleration and reversing (figures 8.8c to 8.8f) much higher torque values are encountered (up to twice the rated torque), explaining why these transients take much less time than the acceleration transient from standstill. One observes in torque traces for deceleration and reversing a rather oscillating behaviour, which is the consequence of oscillatory speed responses. One notes as well that the torque and speed oscillations in figures 8.8c to 8.8f do not have always an one to one correspondence. This is an inevitable consequence of measuring error and very low sampling rate (100 Hz) for all displayed signals.

Figures 8.9a and 8.9b display output power during acceleration and it is of course positive. However, power is negative during deceleration. Figures 8.9c and 8.9d show the power dissipated by the braking resistor connected to the DTC frequency converter through the braking chopper during the deceleration to standstill. It is up to 75% of the rated power of the motor when the motor is decelerated from the rated speed for the unloaded induction motor. Similar considerations apply to the reversing transient, figures 8.9 e and 8.9f. Power is at first negative during braking and then becomes positive as the machine accelerates in the other direction of rotation.

Figure 8.10 shows the responses of output frequency of the DTC drive, which are consistent with the response of speed of the induction motor during acceleration, deceleration and reversing at all speeds. Both the speed and the output frequency have the same response time and consistent behaviour during deceleration and reversing.

Figures 8.11a and 8.11b imply that the RMS value of the output voltage of the DTC drive takes more time to settle down to steady state than the speed of the induction

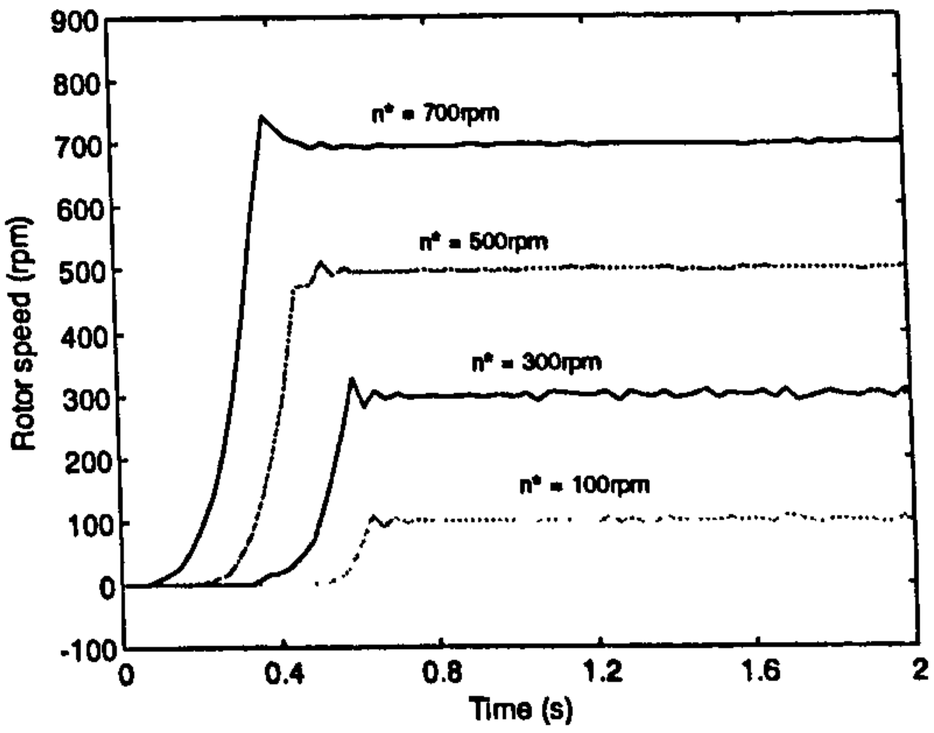

a)

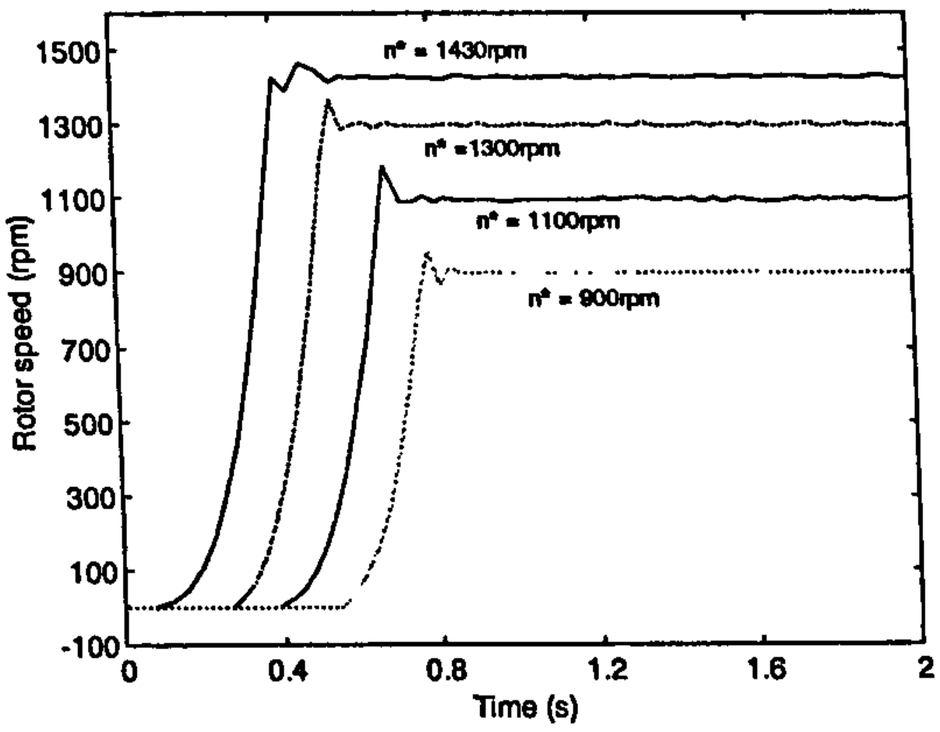

b)

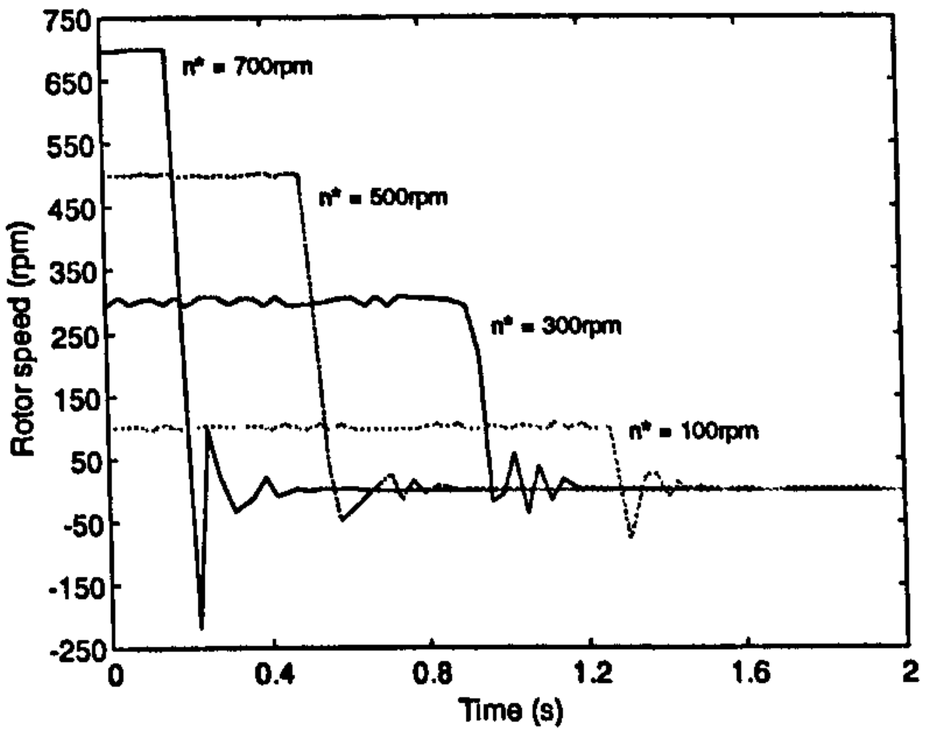

c)

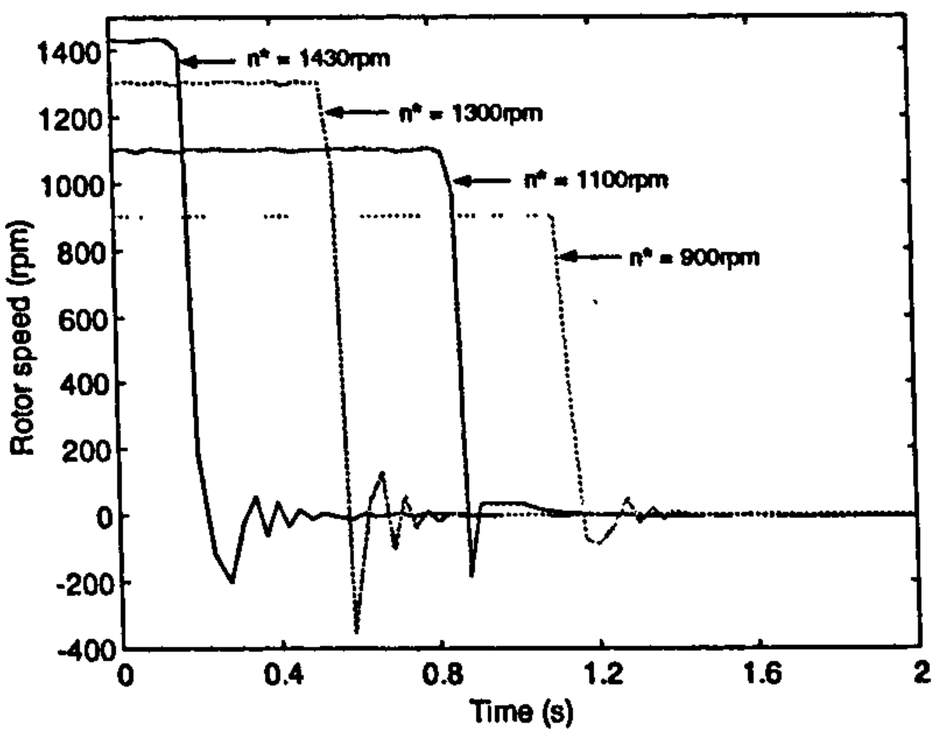

d)

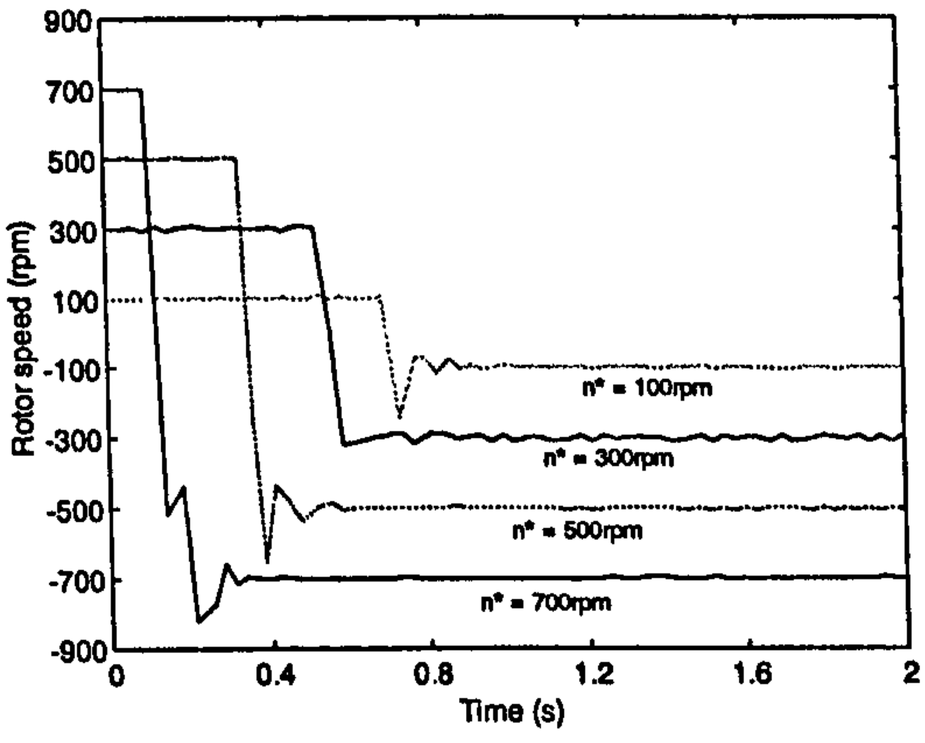

e)

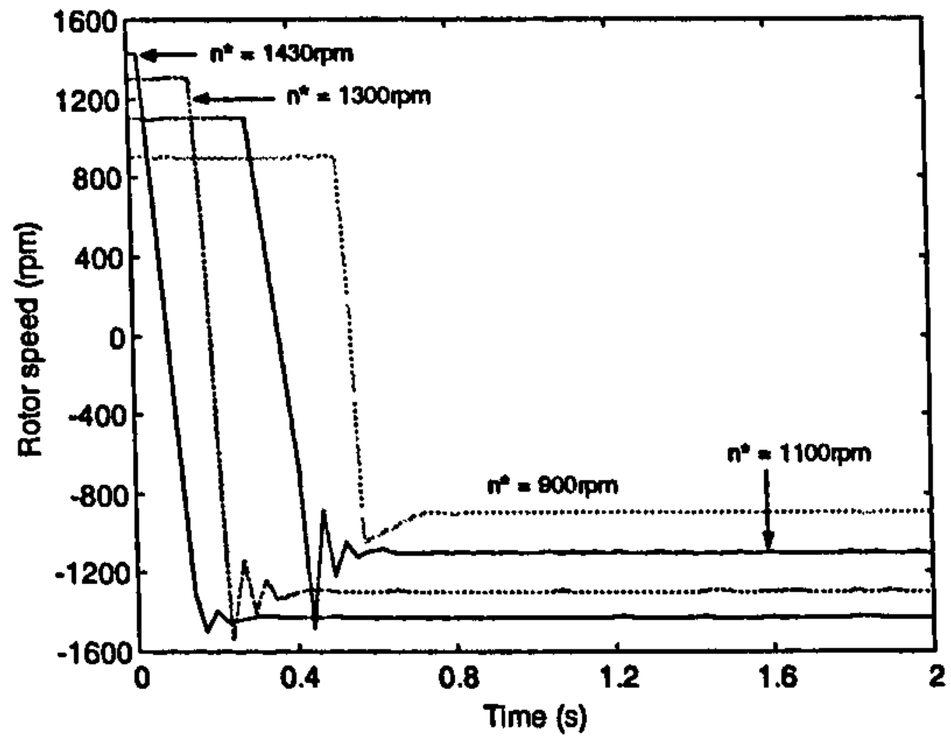

f)

Figure 8.5: Rotor speed of a direct torque controlled and unloaded induction motor during: a) acceleration, 100rpm to 700rpm, b) acceleration, 900rpm to 1430rpm, c) deceleration, 100rpm to 700rpm, d) deceleration, 900rpm to 1430rpm, e) reversing, 100rpm to 700rpm, f) reversing, 900rpm to 1430rpm.

motor during acceleration at starting-up of the motor. This happens in all speed regions, and no explanation can be given for this behaviour. However, the transient responses of

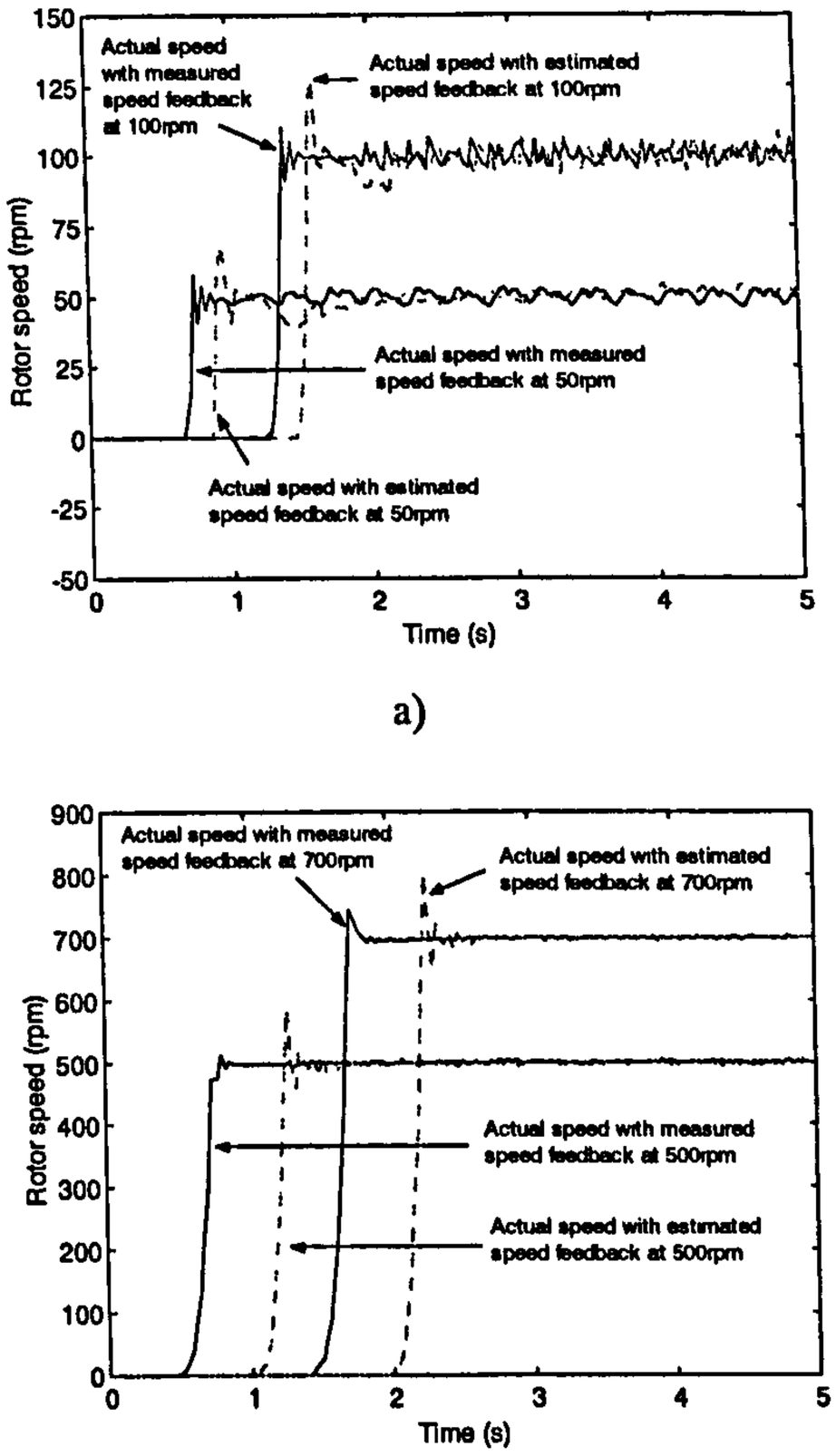

a)

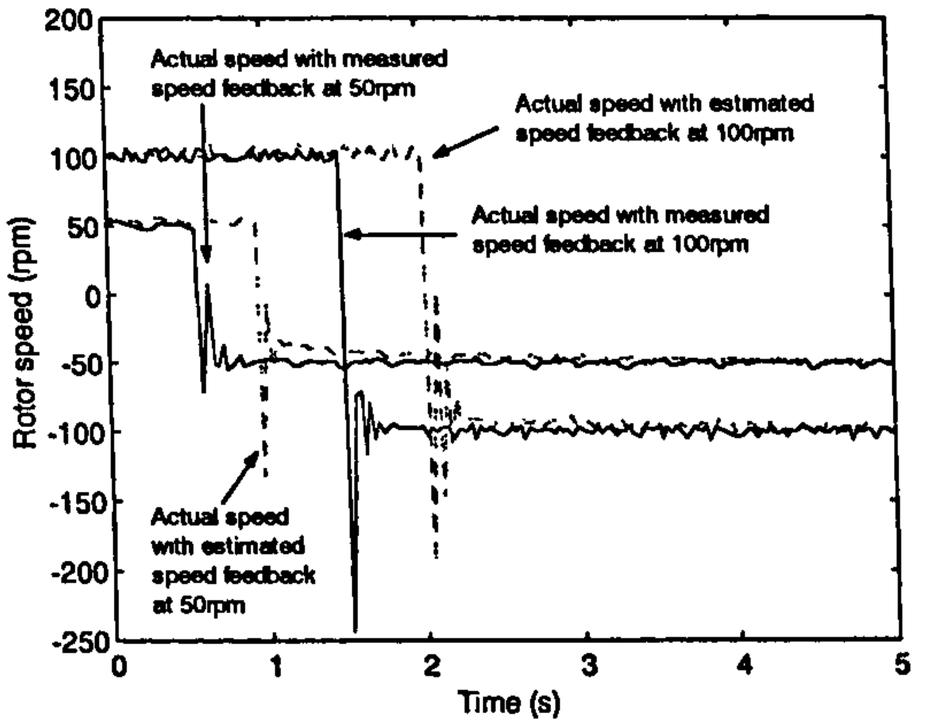

b)

c)

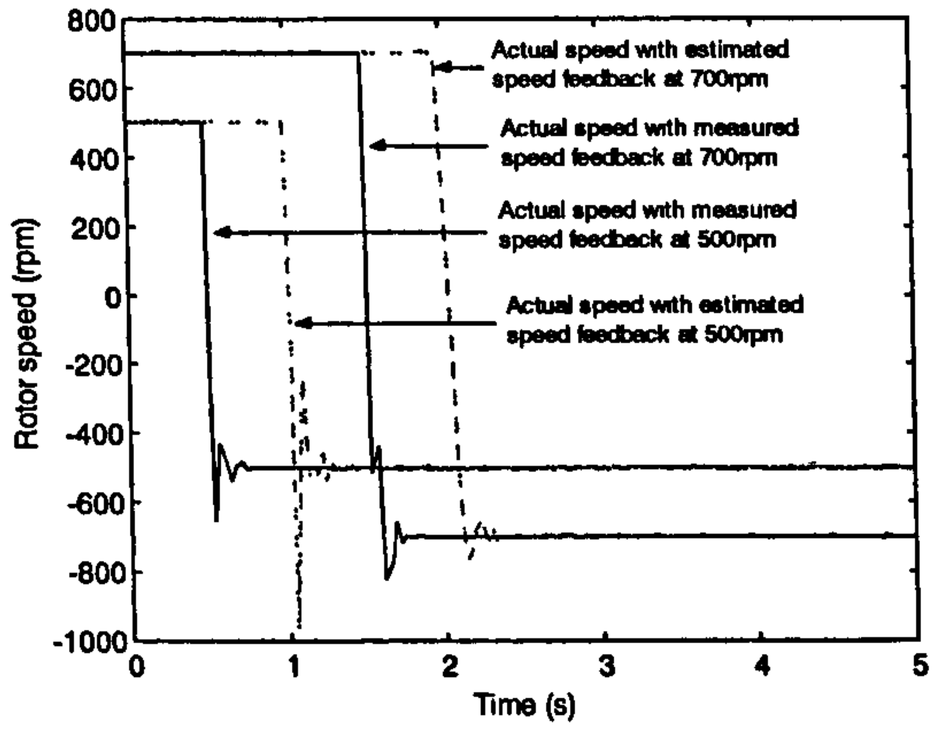

d)

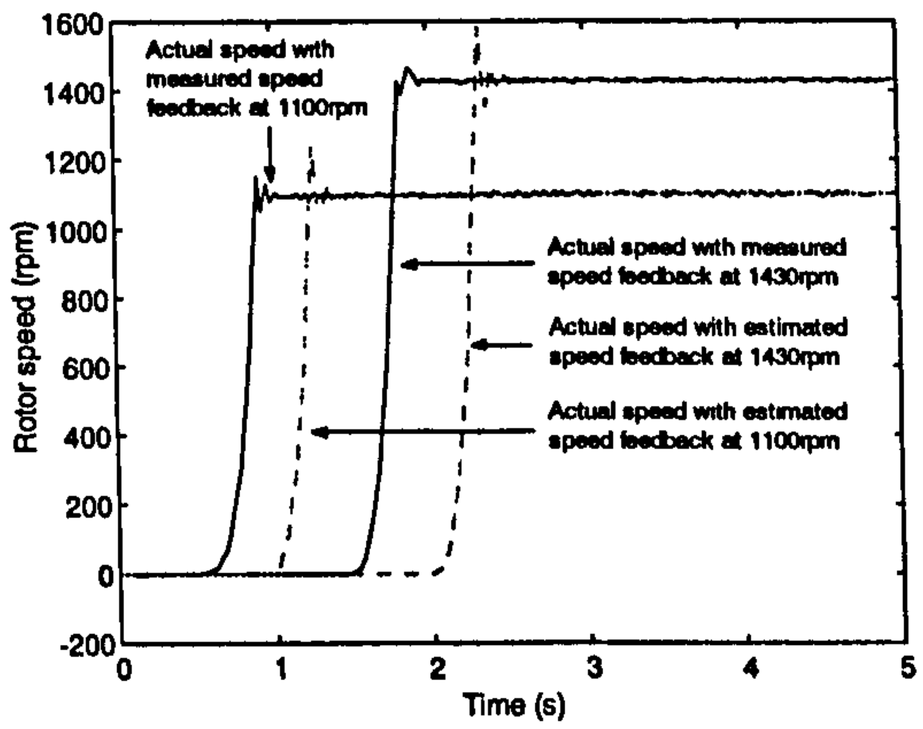

e)

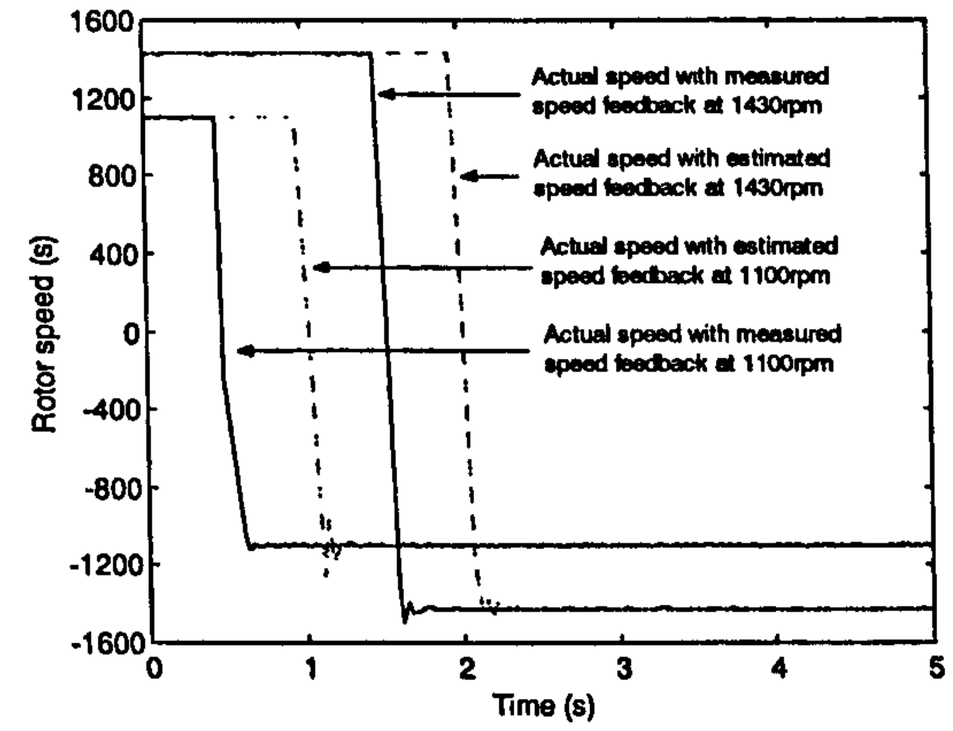

f)

Figure 8.6: Rotor speeds with measured speed feedback and estimated speed feedback of an unloaded induction motor with DTC drive during a) acceleration in low speed region, b) reversing in medium speed region, c) acceleration in medium speed region, d) reversing in medium speed region, e) acceleration in high speed region, f) reversing in high speed region.

the output voltage are faster during deceleration to standstill and reversing. The output voltage is reduced during the transient responses, then quickly brought back to the

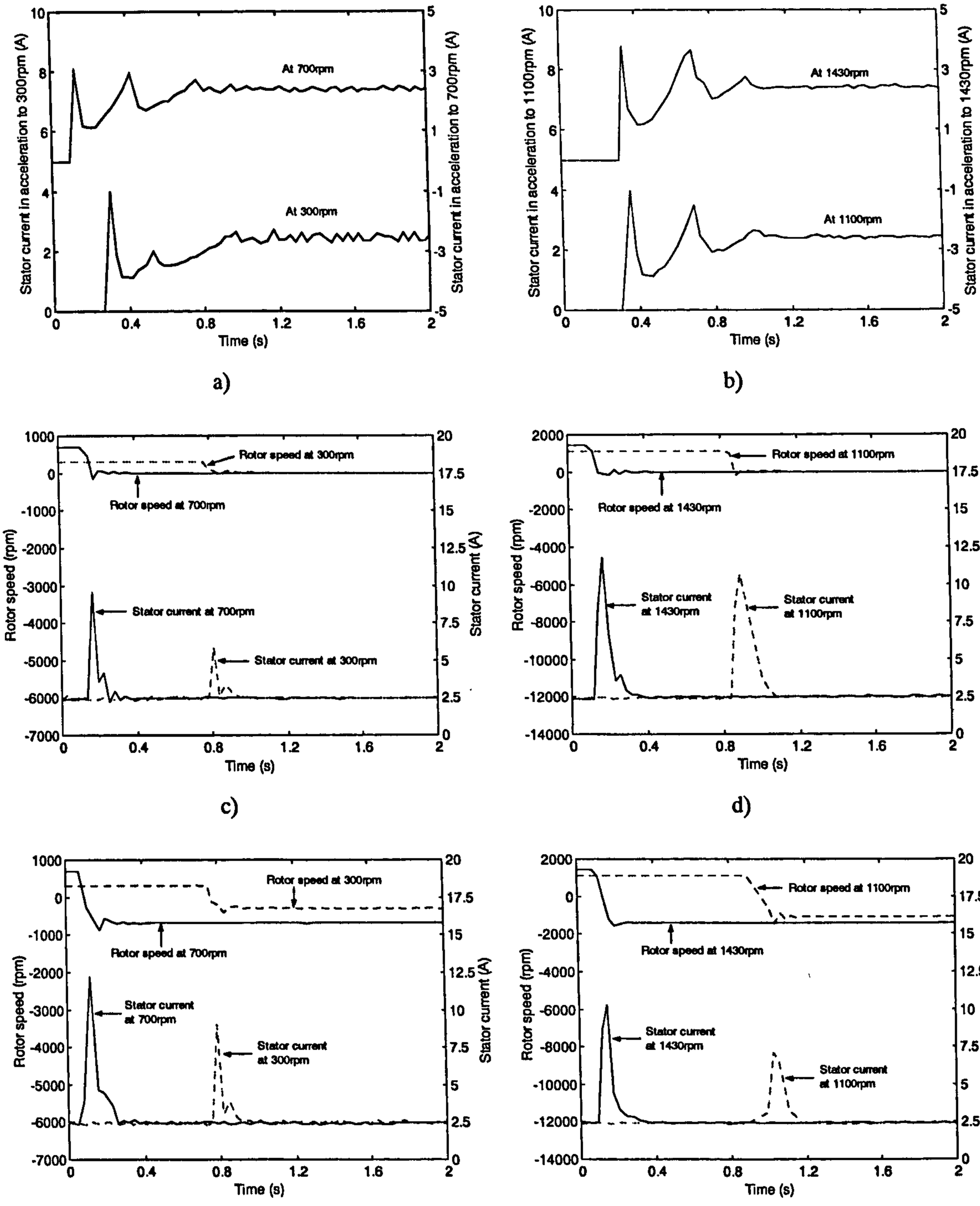

Figure 8.7: Stator phase current of an unloaded induction motor during: acceleration from stand still to a) 300 rpm and 700rpm, b) 1100 rpm and 1430 rpm; deceleration to standstill from c) 300 rpm and 700 rpm, d) 1100 rpm and 1430 rpm; reversing from e) 300 rpm and 700 rpm, f) 1100rpm and 1430 rpm.

steady state level. Figure 8.11c and 8.11d also show that the output voltage is oscillatory during steady state operation at zero speed. Finally, figures 8.11e and 8.11f seem to

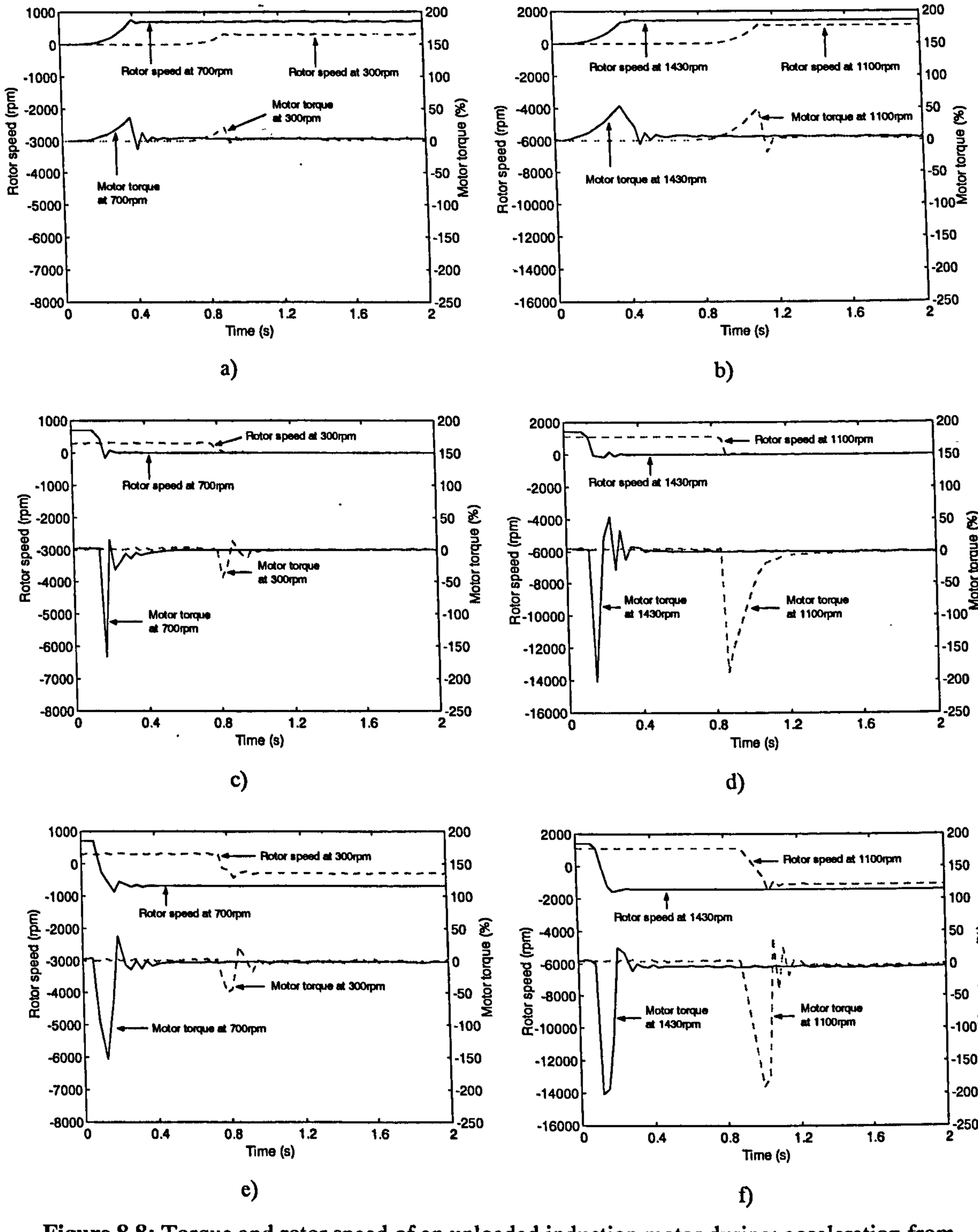

Figure 8.8: Torque and rotor speed of an unloaded induction motor during: acceleration from standstill to a) 300 rpm and 700rpm, b) 1100 rpm and 1430 rpm; deceleration to standstill from c) 300 rpm and 700 rpm, d) 1100 rpm and 1430 rpm; reversing from e) 300 rpm and 700 rpm, f) 1100rpm and 1430 rpm.

indicate that, during reversing, the output voltage does not ever come anywhere close to zero value, although frequency of course passes through zero. Having in mind the

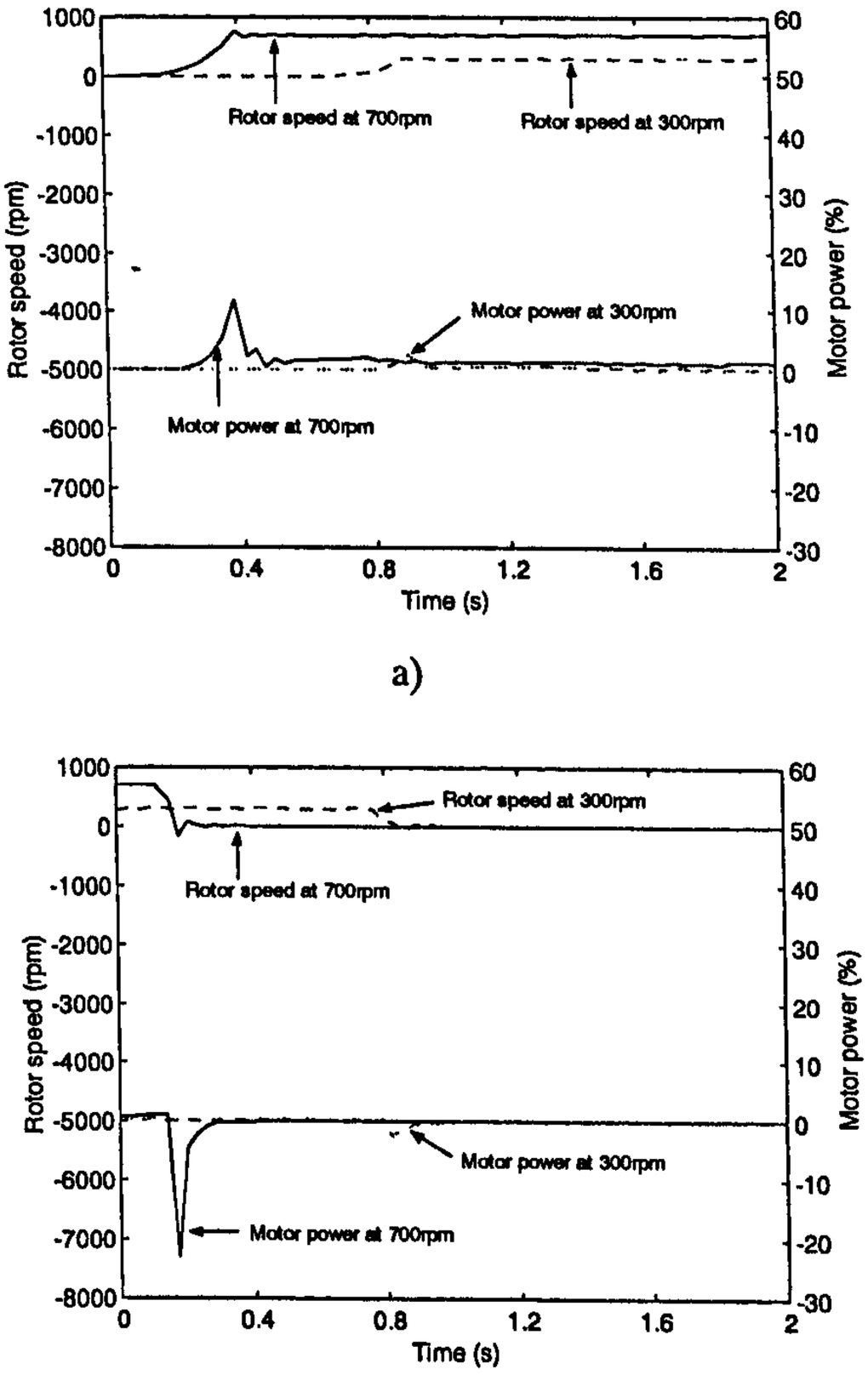

a)

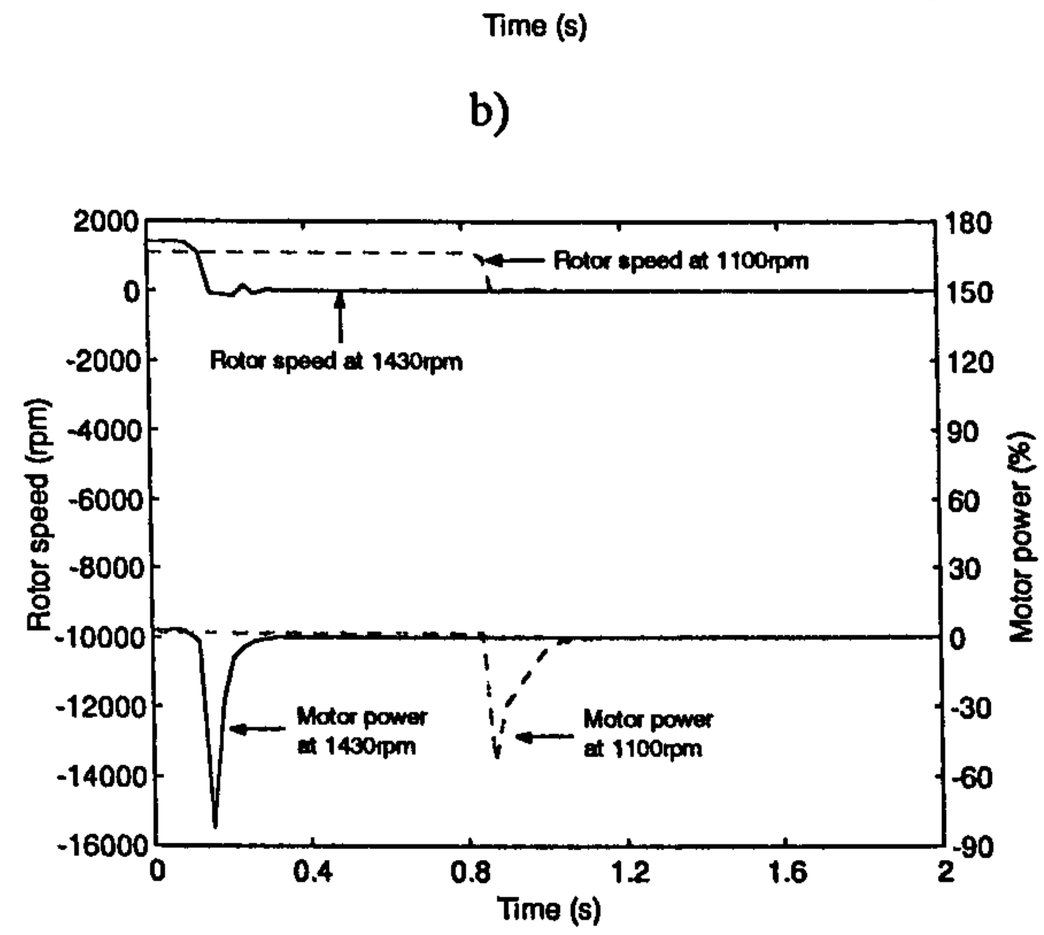

b)

c)

d)

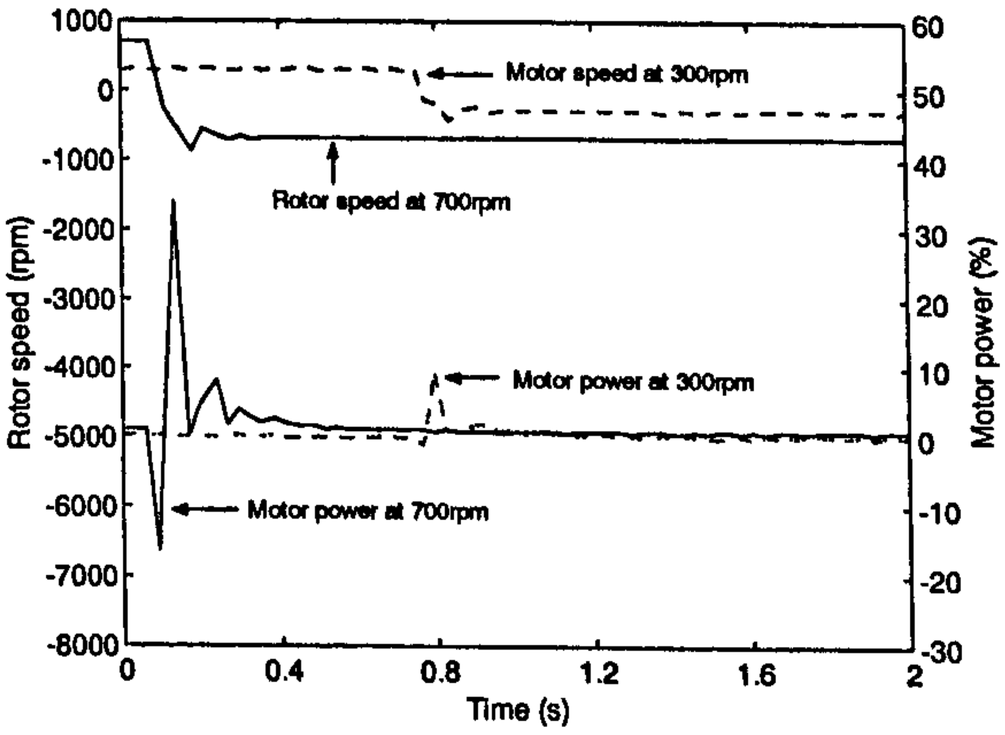

e)

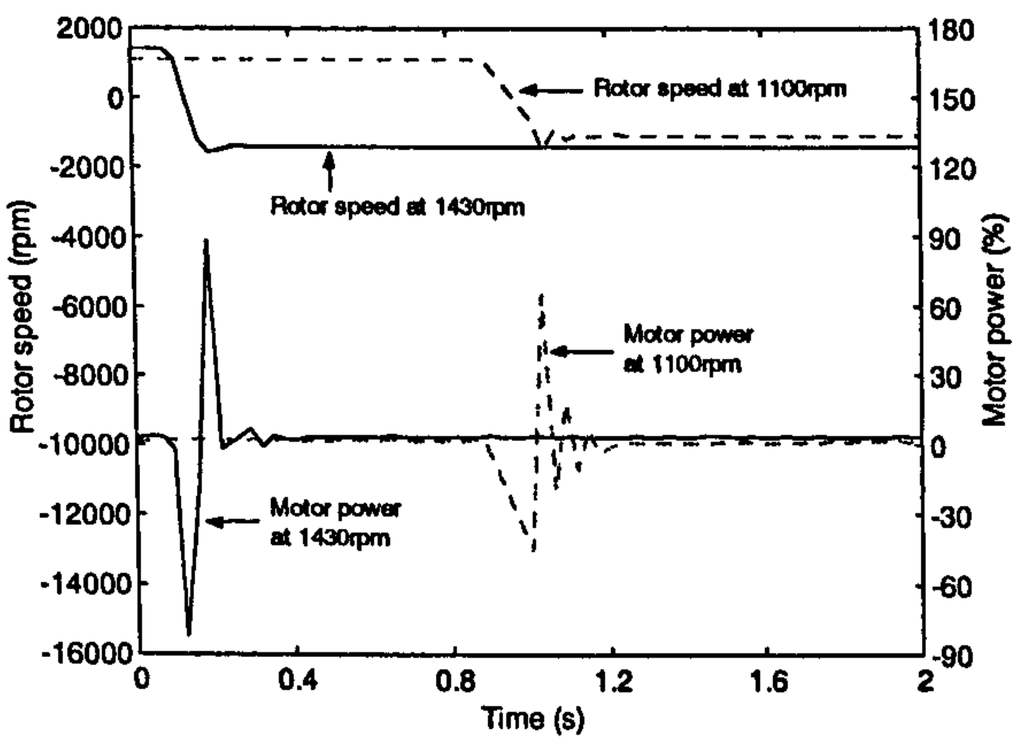

f)

Figure 8.9: Power and rotor speed of an unloaded induction motor during: acceleration from standstill to a) 300 rpm and 700rpm, b) 1100 rpm and 1430 rpm; deceleration to standstill from c) 300 rpm and 700 rpm, d) 1100 rpm and 1430 rpm; reversing from e) 300 rpm and 700 rpm, f) 1100rpm and 1430 rpm.

problems that exist for DTC operation in vicinity of zero speed, one possible explanation is that the drive switches from DTC to V/f control law at low frequencies

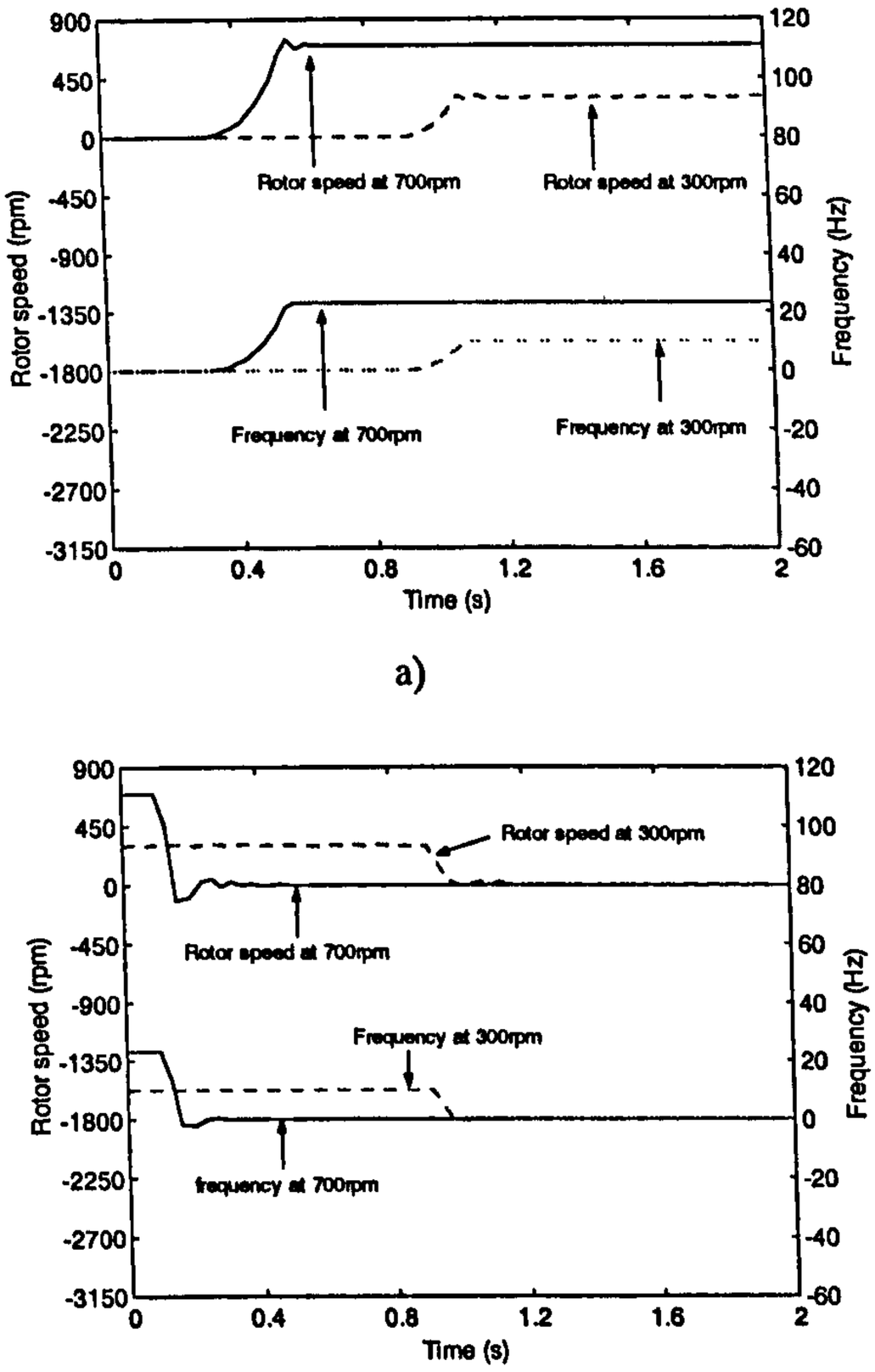

a)

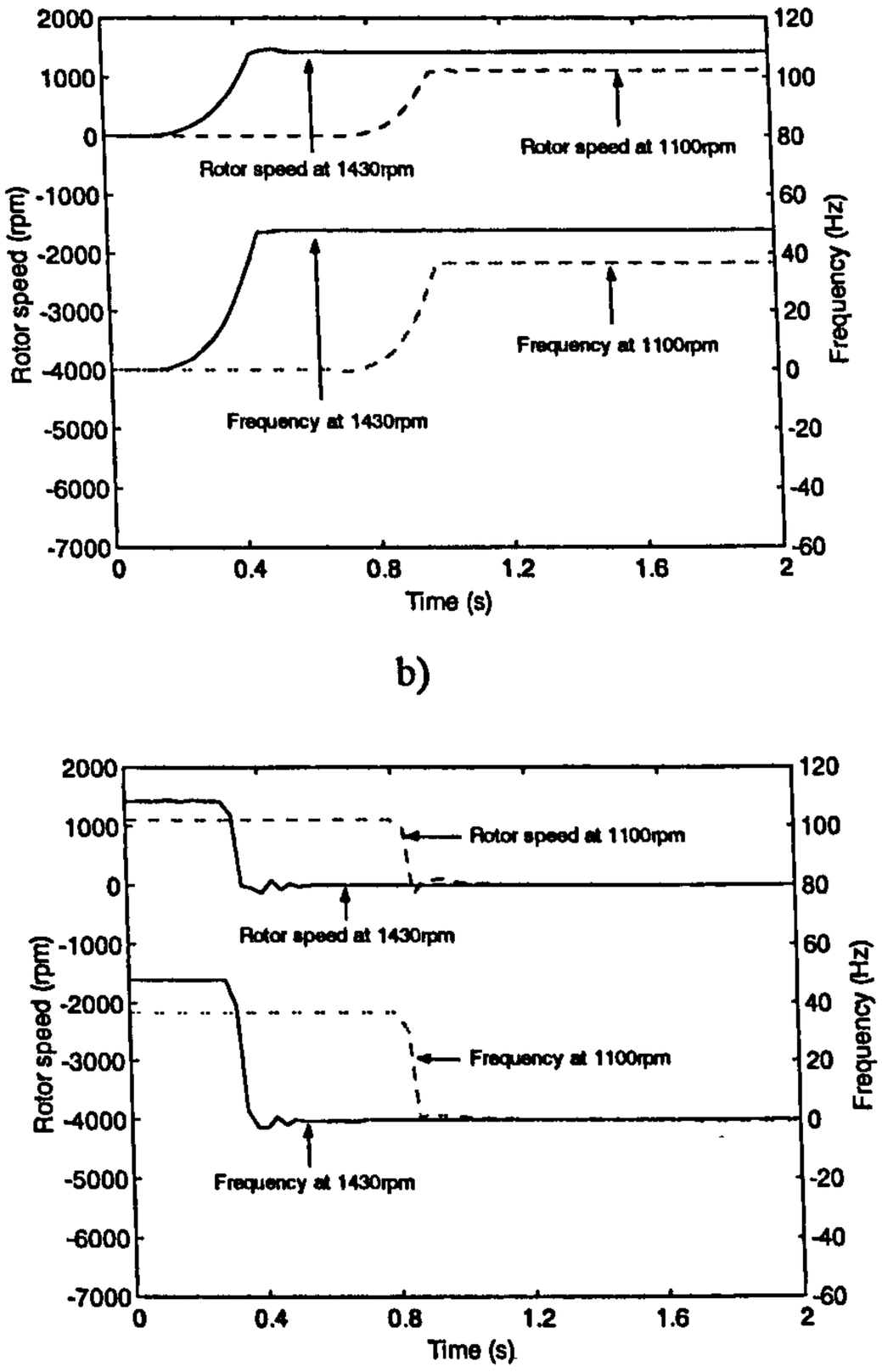

b)

c)

d)

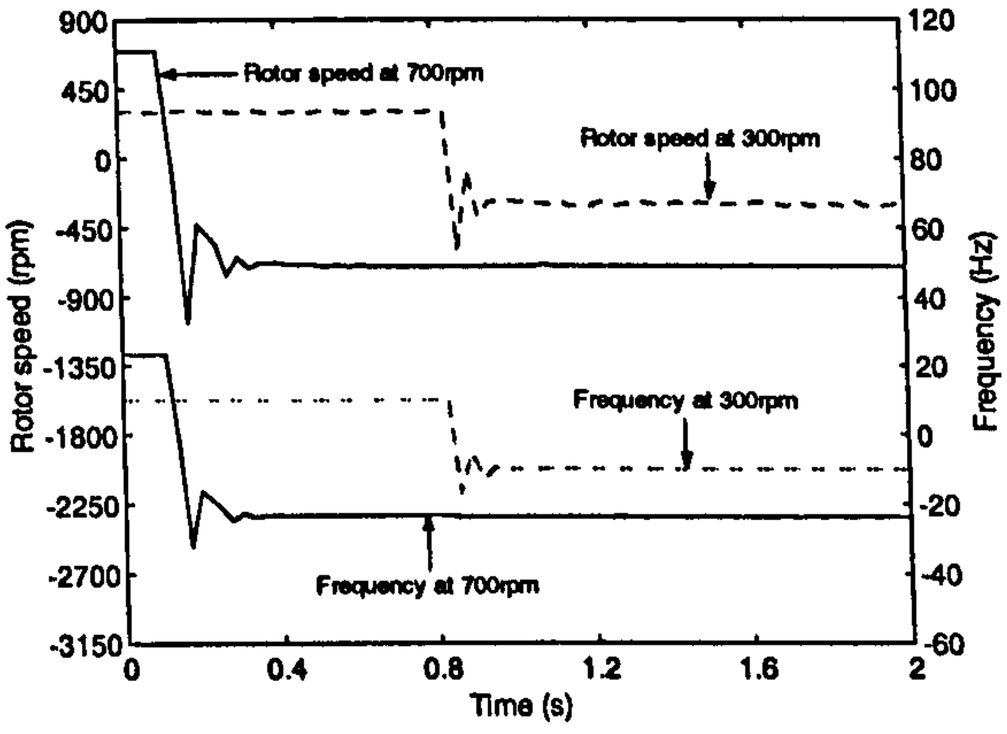

e)

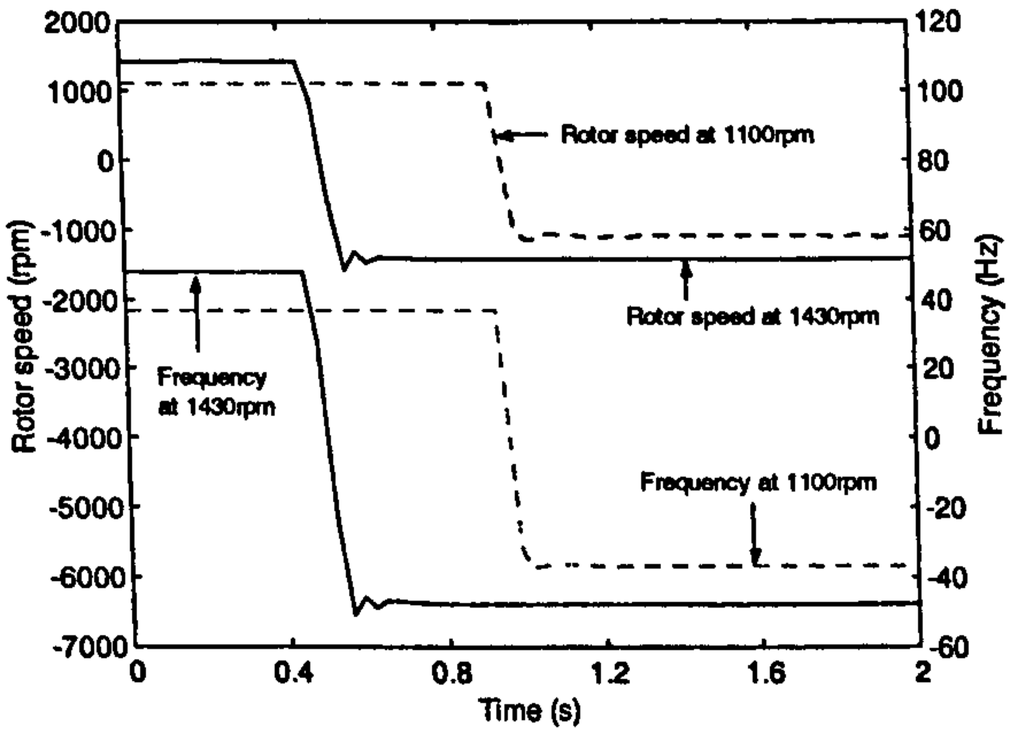

f)

Figure 8.10: Output frequency of the frequency converter and rotor speed of an unloaded induction motor during: acceleration from standstill to a) 300 rpm and 700rpm, b) 1100 rpm and 1430 rpm; deceleration to standstill from c) 300 rpm and 700 rpm, d) 1100 rpm and 1430 rpm; reversing from e) 300 rpm and 700 rpm, f) 1100rpm and 1430 rpm.

and provides a substantial voltage boost at very low frequencies.

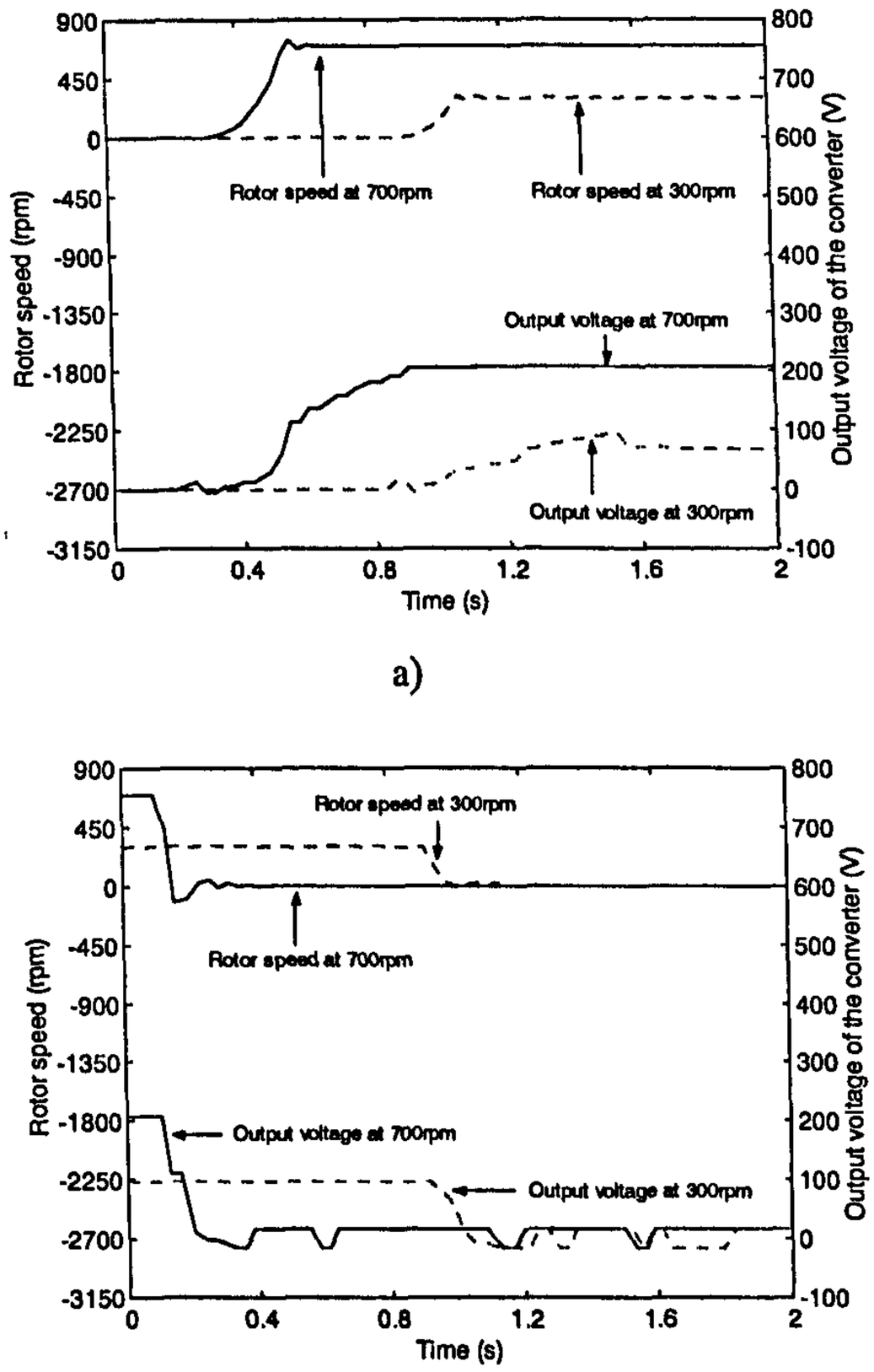

a)

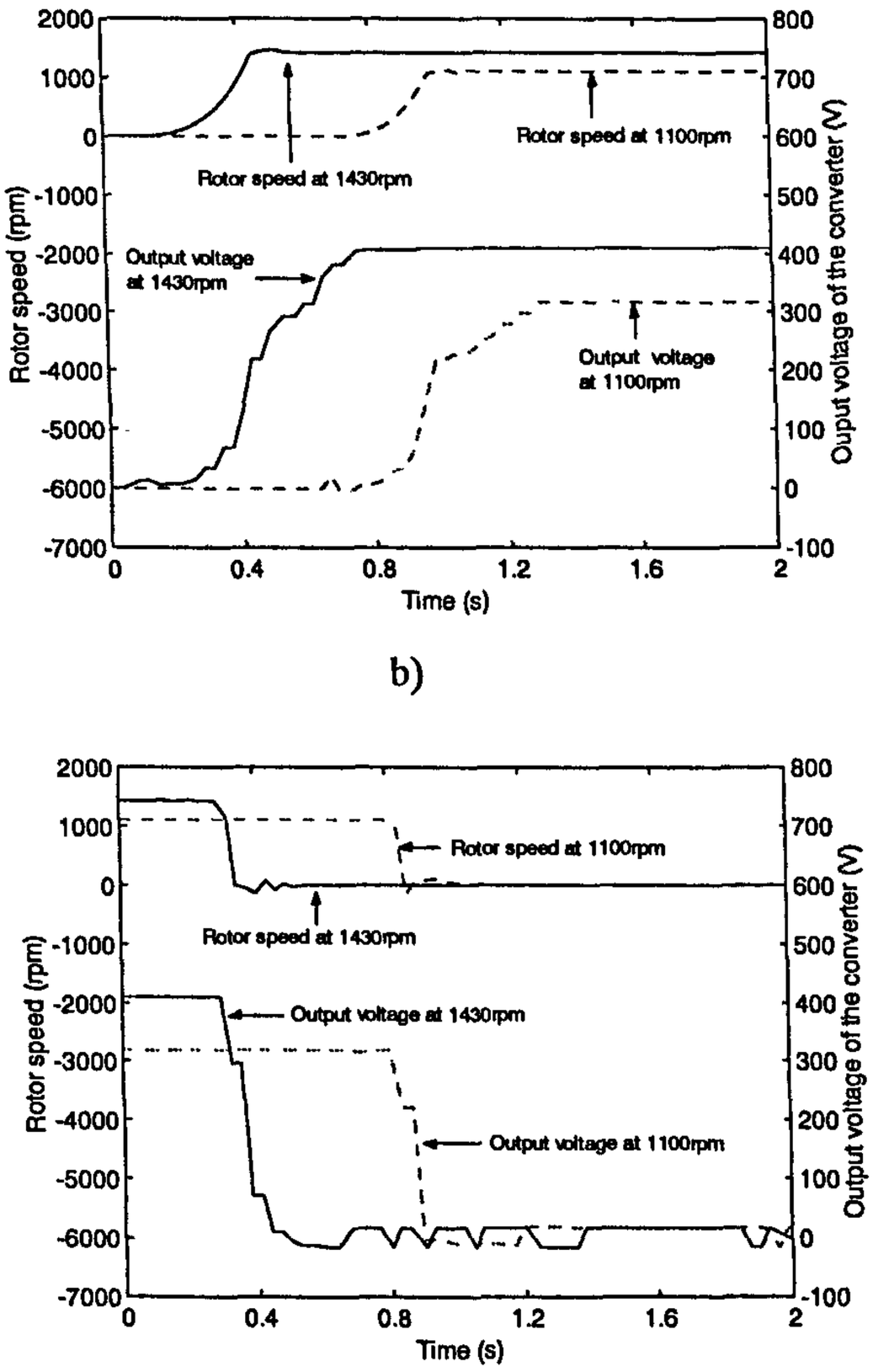

b)

c)

d)

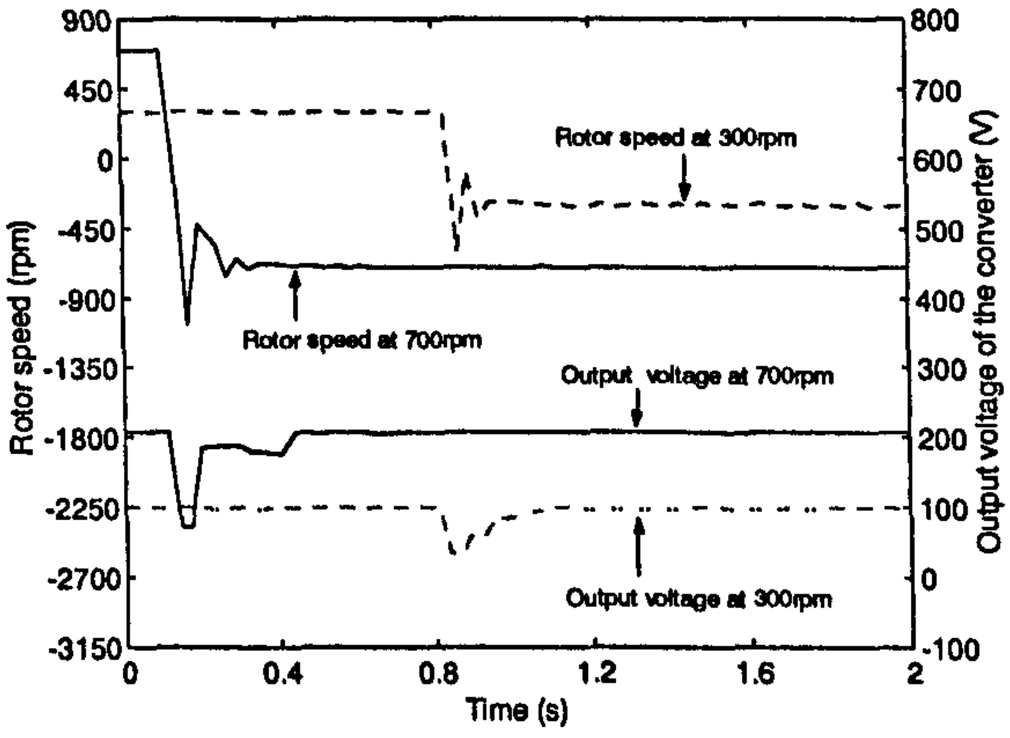

e)

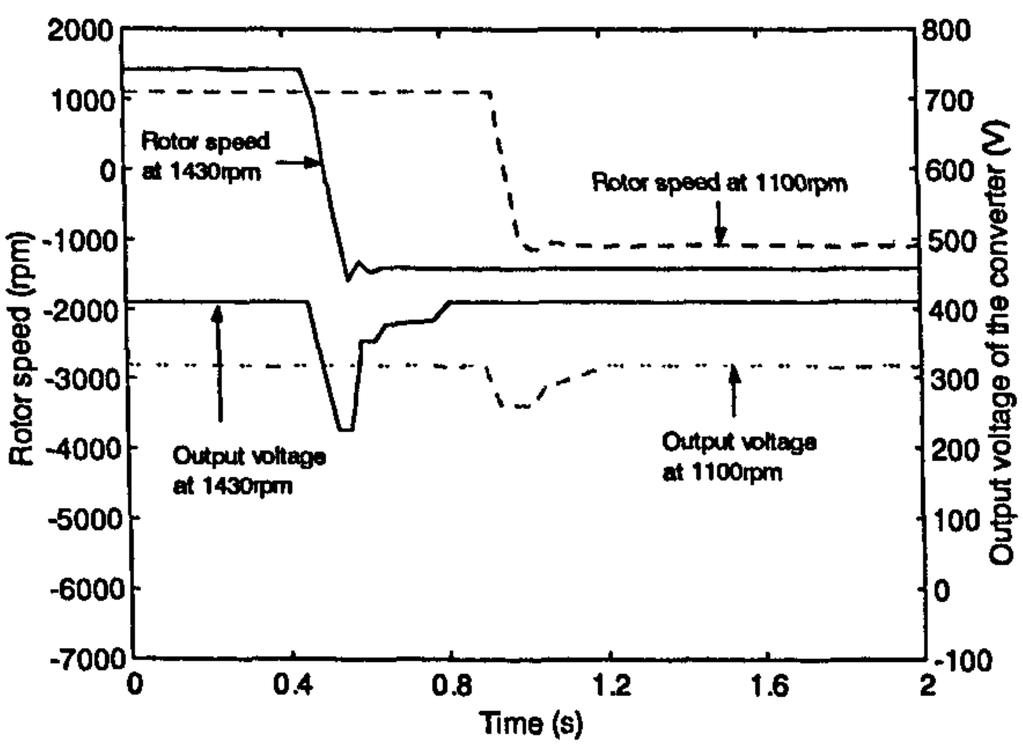

f)

Figure 8.11: Output voltage of the frequency converter and rotor speed of an unloaded induction motor during: acceleration from stand still to a) 300 rpm and 700rpm, b) 1100 rpm and 1430 rpm; deceleration to standstill from c) 300 rpm and 700 rpm, d) 1100 rpm and 1430 rpm; reversing from e) 300 rpm and 700 rpm, f) 1100rpm and 1430 rpm.

8.3.3 Performance of a direct torque controlled drive with a loaded induction motor

The induction motor is now coupled with the permanent magnet DC motor, which is used as a loading generator. The armature terminal of the DC motor are connected to a loading resistor with variable resistance. The resistance of the loading resistor is set at 80 Ohms, 34.3 Ohms, 24 Ohms and 17.2 Ohms to obtain the armature current at the terminals of the DC generator of 1.80 A, 3.90 A, 5.40 A and 7.40 A at the rated speed of the induction motor, respectively. Again, the induction motor is accelerated from standstill to a wide range of speeds, decelerated from the steady state speed to standstill and reversed. The same signals (actual speed, estimated speed, stator phase current, torque, motor power, output frequency and output voltage of the converter) are collected by the DriveWindow software. The function Autotune Run in the software enables automatic adjustment of the PI speed controller parameters to the connected load. This function is executed each time when the drive was turned on, meaning that speed controller parameters should have been matched always to the load. However, as will be shown shortly, speed response with connected load is considerably worse than under no-load conditions, especially at higher reference speed settings, with very long settling time.

Figure 8.12 shows the variation of torque with speed of the direct toque controlled induction motor when the load resistor of the DC generator is set at four different values. The measured values in figure 8.12 were obtained in steady state operation for different set speeds and different resistor values by means of the drive's DriveWindow software. Because the excitation of the generator is constant, torque is linearly proportional to rotor speed. The experimental data show torque is linearly related to speed at each setting of the loading resistor. Because of the limitation of the armature current, the induction motor can only be loaded up to about 60% of the rated torque at the rated speed, when the loading resistor is 17.2 Ohms.

Figures 8.13 to 8.19 show measured variables of the induction motor when the loading resistor is set to 17.2 Ω. Although the experiments were conducted for other settings of the resistor as well, only results for 17.2 Ω are given here, since no important differences were observed between the other results and those given in figures 8.13 to 8.19. Figure 8.13 shows the rotor speed of the loaded induction motor during acceleration from standstill, deceleration to zero speed and reversing. Figure 8.14 shows

the rotor speeds with both measured and estimated speed feedback in the speed controller, in low, medium and high speed regions. Figures 8.15 to 8.19 show the profiles of stator phase current, motor torque, motor power, output frequency and output voltage of the DTC drive during acceleration, deceleration and reversing at 300 rpm, 700 rpm, 1100 rpm, and 1430 rpm.

Although the initial part of the speed transient shows rapid increase in speed, the required reference speed value is attained only after a substantial amount of time (time scale in figures 8.13a and 8.13b is up to seven and ten seconds, respectively). This is believed to be a consequence of the PI speed controller parameter setting. Overshoots and oscillations are reduced at all speeds, compared to the no-load case, during the acceleration from standstill as shown in figures 8.13a and 8.13b. Overshoots and oscillations are also reduced during deceleration to zero speed and reversing as shown in figures 8.13c to 8.13f.

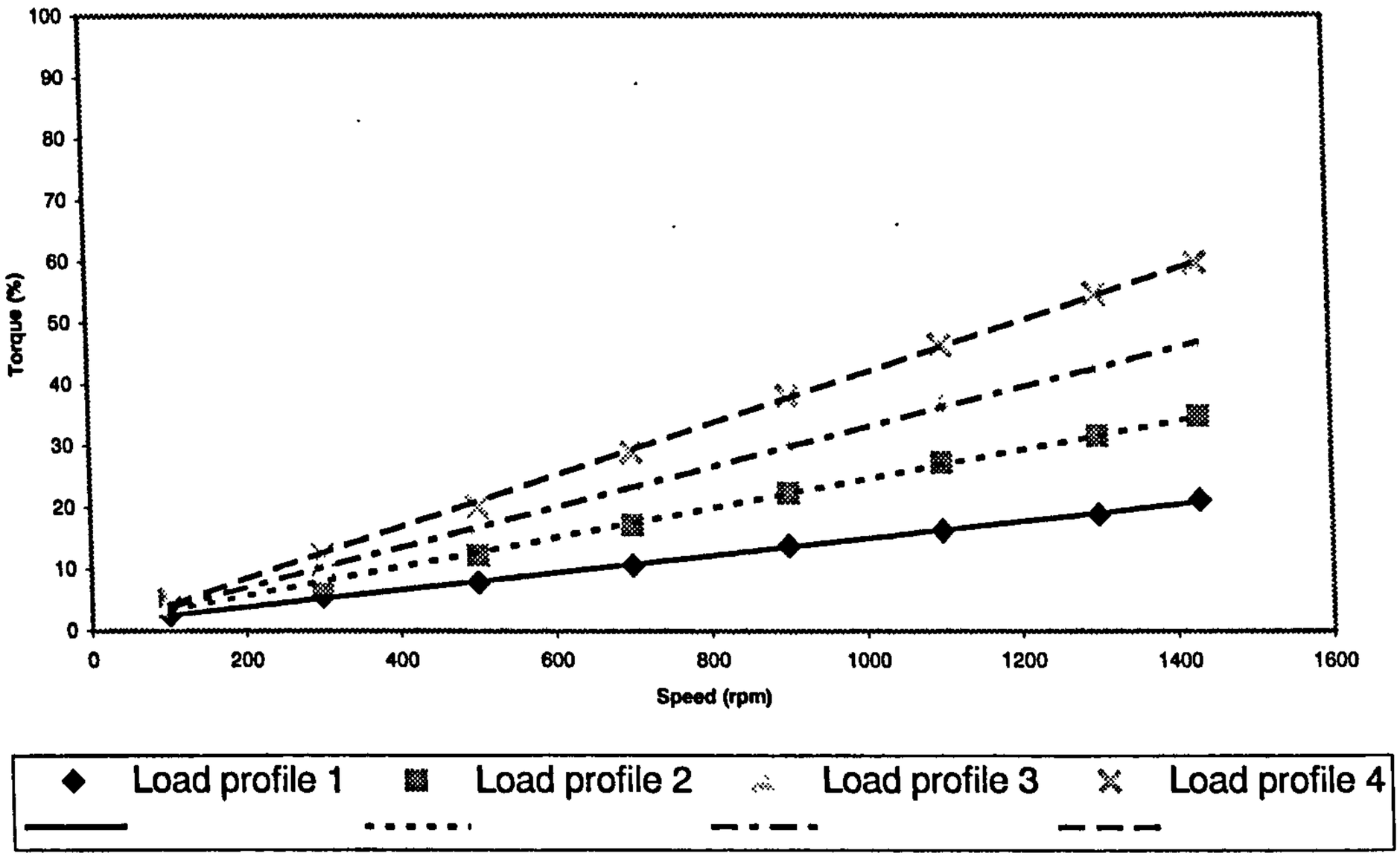

Figure 8.12: Variation of torque of the direct torque controlled induction motor when the load resistance of the DC generator is at 80 Ohms (load profile 1), 34.3 Ohms (load profile 2), 24 Ohms (load profile 3) and 17.2 Ohms (load profile 4).

During the acceleration of the induction motor with speed dependent load, rotor speed has lower overshoot and less oscillation when the measured speed feedback is used in low speed region (at 50 rpm and 100 rpm) than with estimated speed feedback (figure 8.14). Overshoots and oscillations are also significantly reduced during the

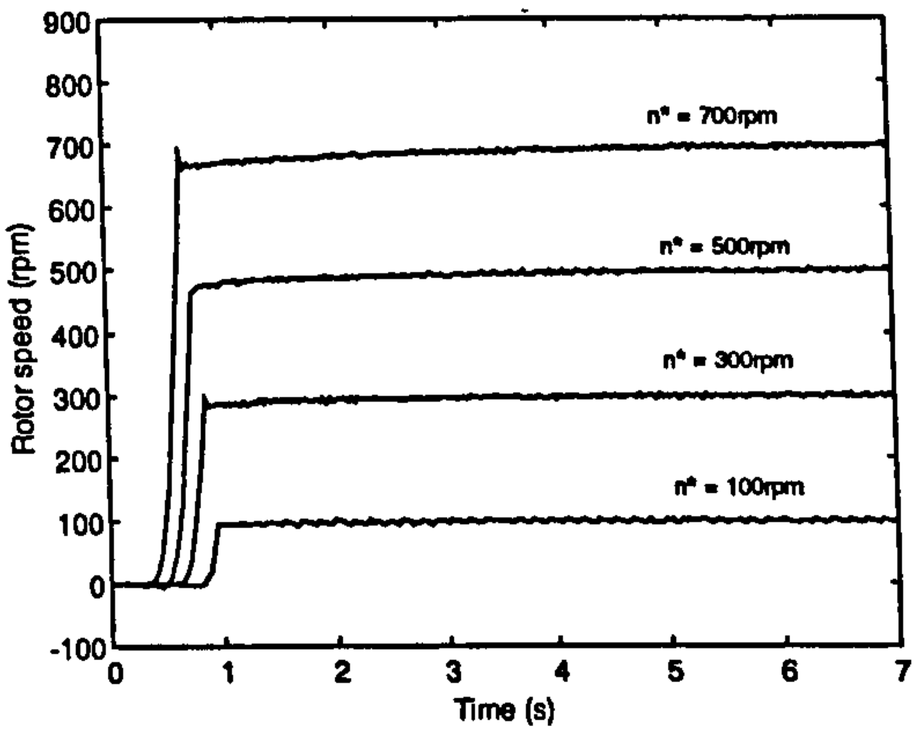

a)

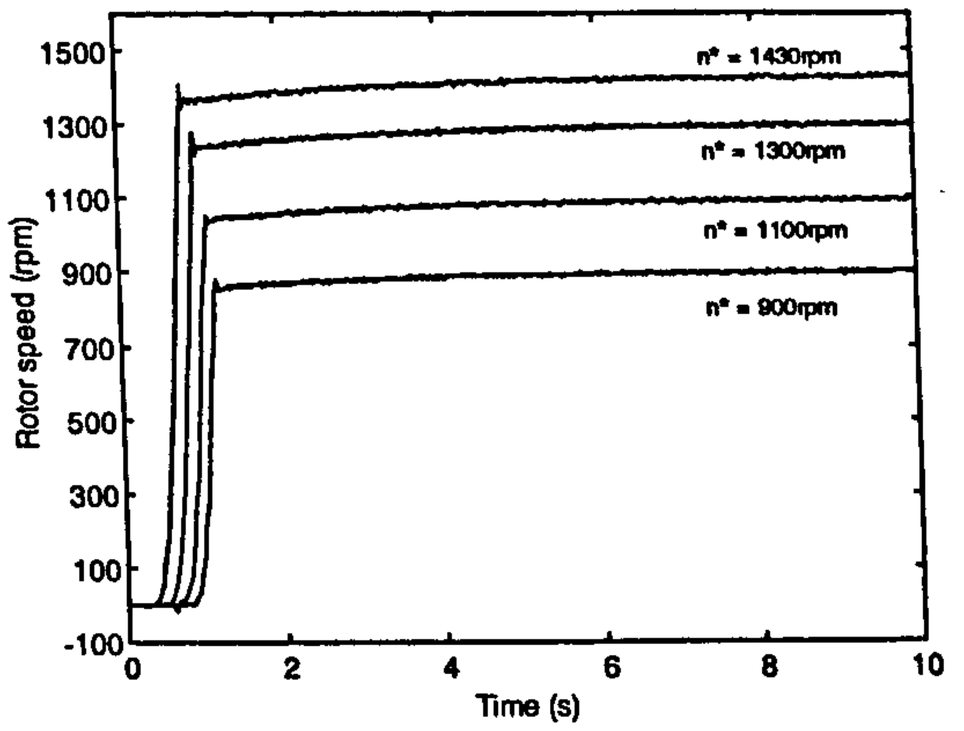

b)

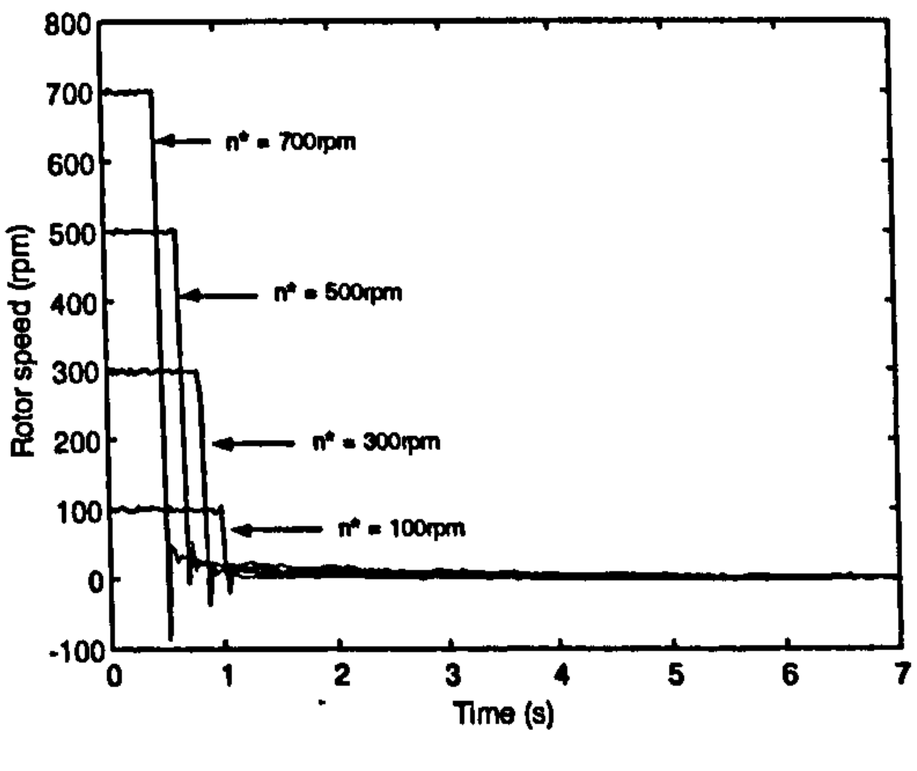

c)

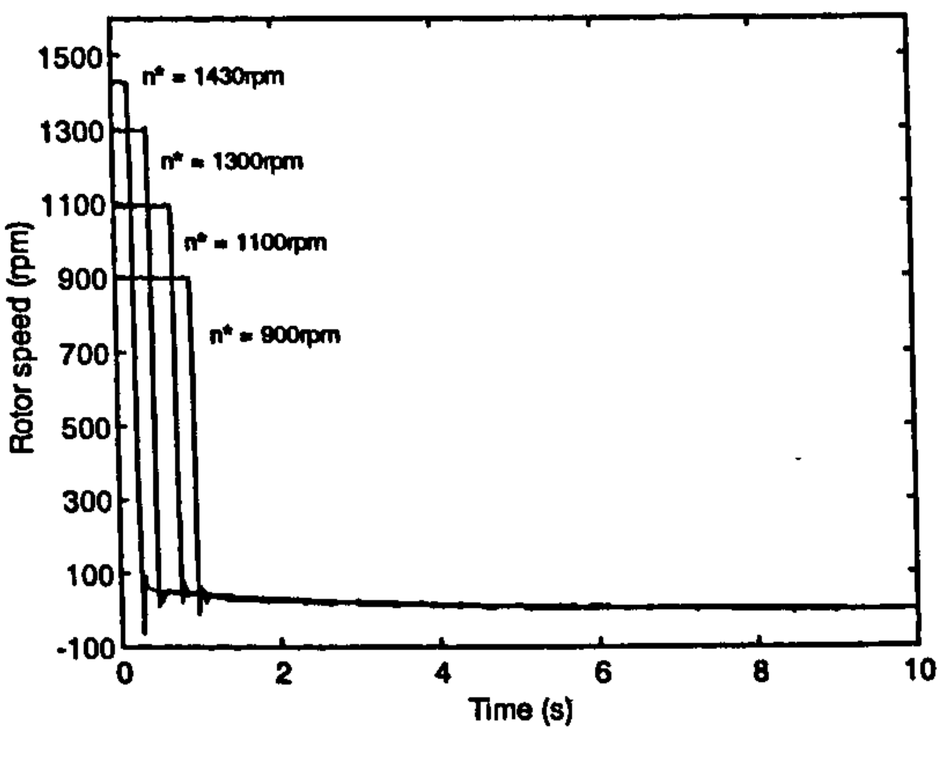

d)

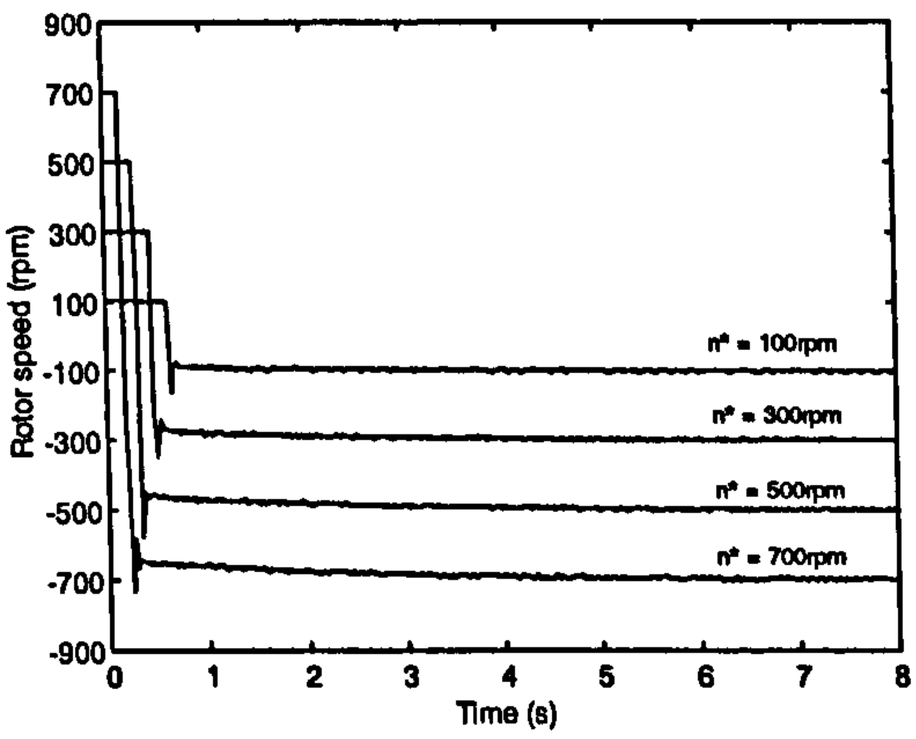

e)

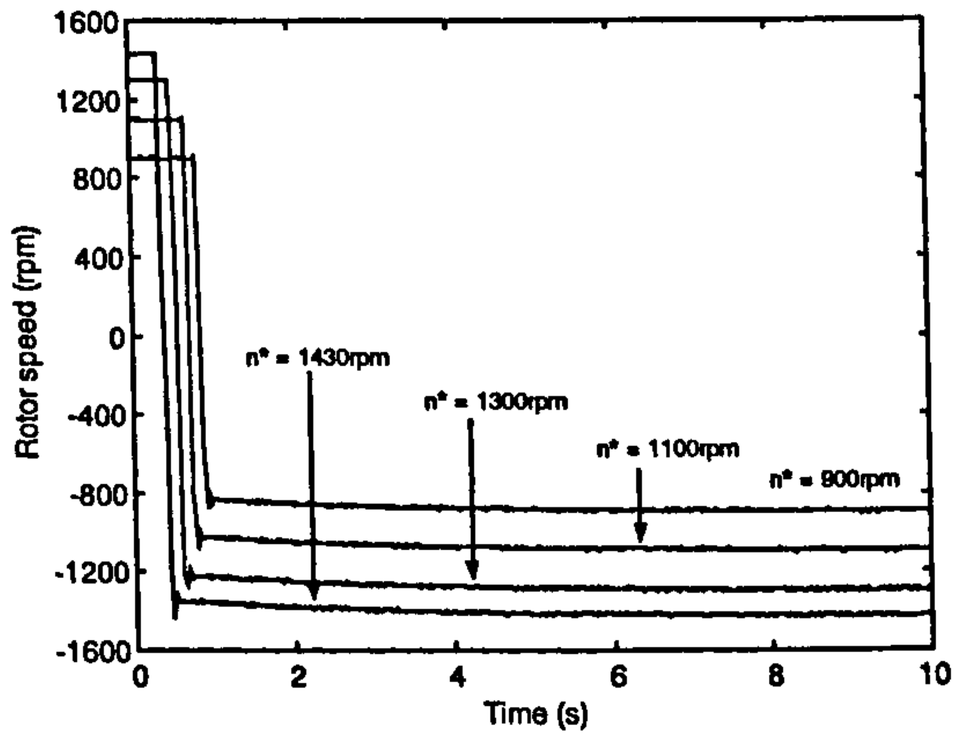

f)

Figure 8.13: Rotor speed of a direct torque controlled and loaded induction motor during: a) acceleration, 100rpm to 700rpm, b) acceleration, 900rpm to 1430rpm, c) deceleration, 100rpm to 700rpm, d) deceleration, 900rpm to 1430rpm, e) reversing, 100rpm to 700rpm, f) reversing, 900rpm to 1430rpm.

reversing from respective speeds when the motor is loaded as shown in figure 8.14b. Figures 8.14c to 8.14f show similar reductions in the medium and high speed region (at

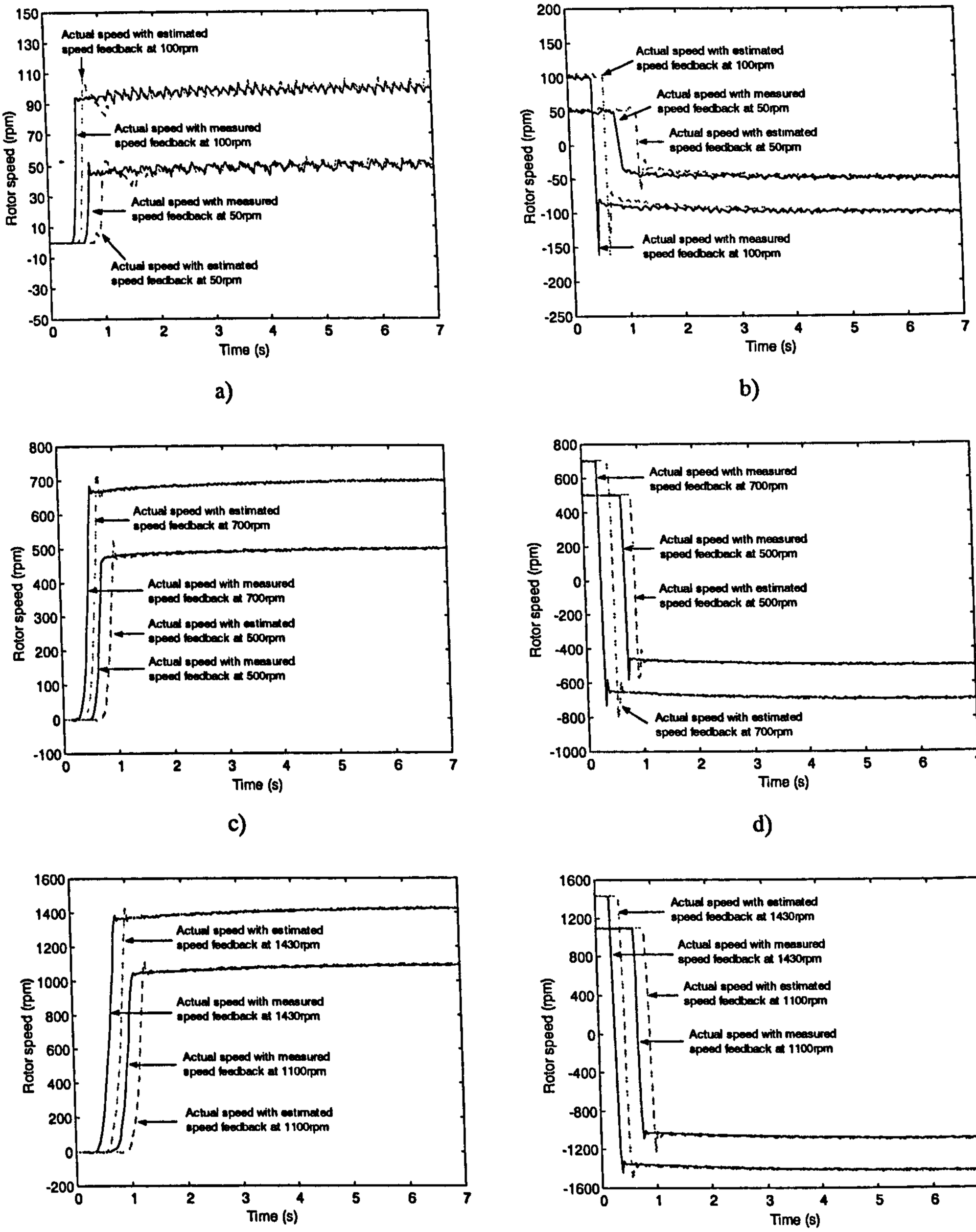

Figure 8.14: Rotor speeds with measured speed feedback and estimated speed feedback of a loaded induction motor with DTC drive during a) acceleration in low speed region, b) reversing in medium speed region, c) acceleration in medium speed region, d) reversing in medium speed region, e) acceleration in high speed region, f) reversing in high speed region.

500 rpm, 700 rpm, 1100 rpm and 1430 rpm respectively) in both acceleration and reversing. The responses of speed in medium and high speed regions are more

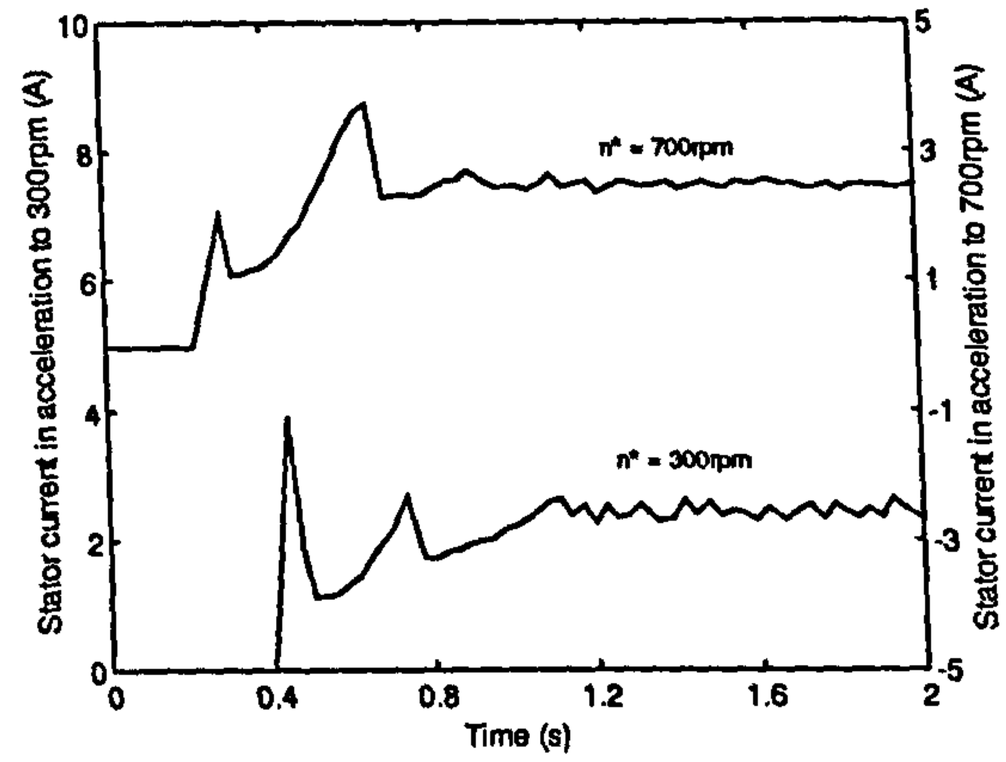

a)

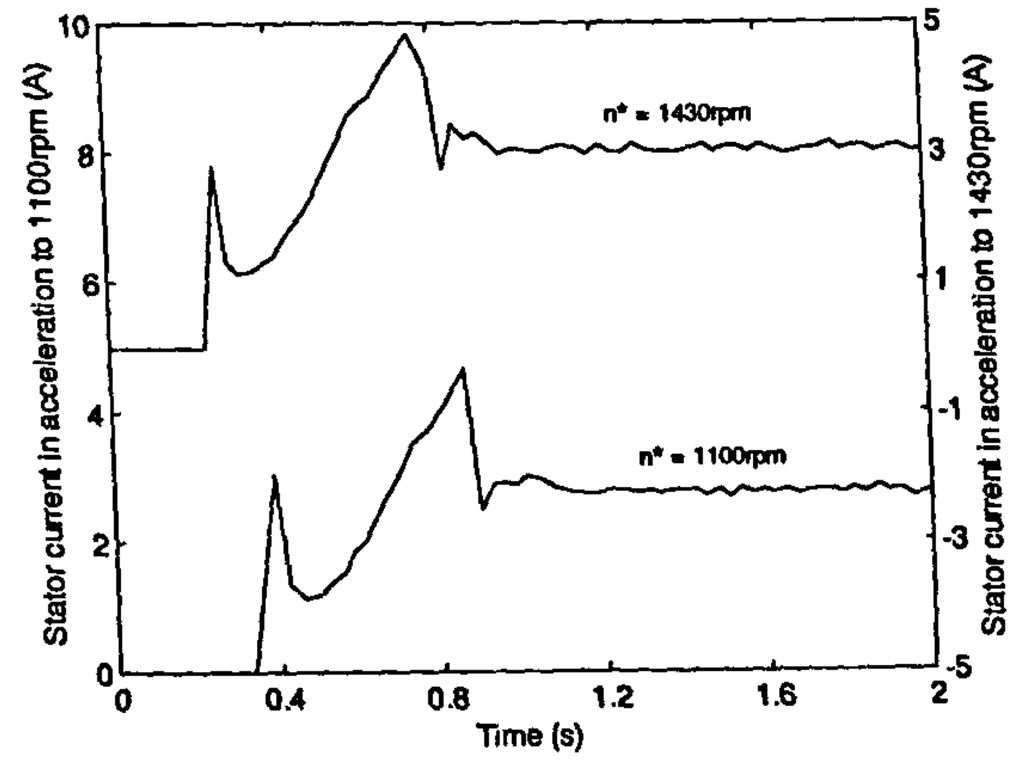

b)

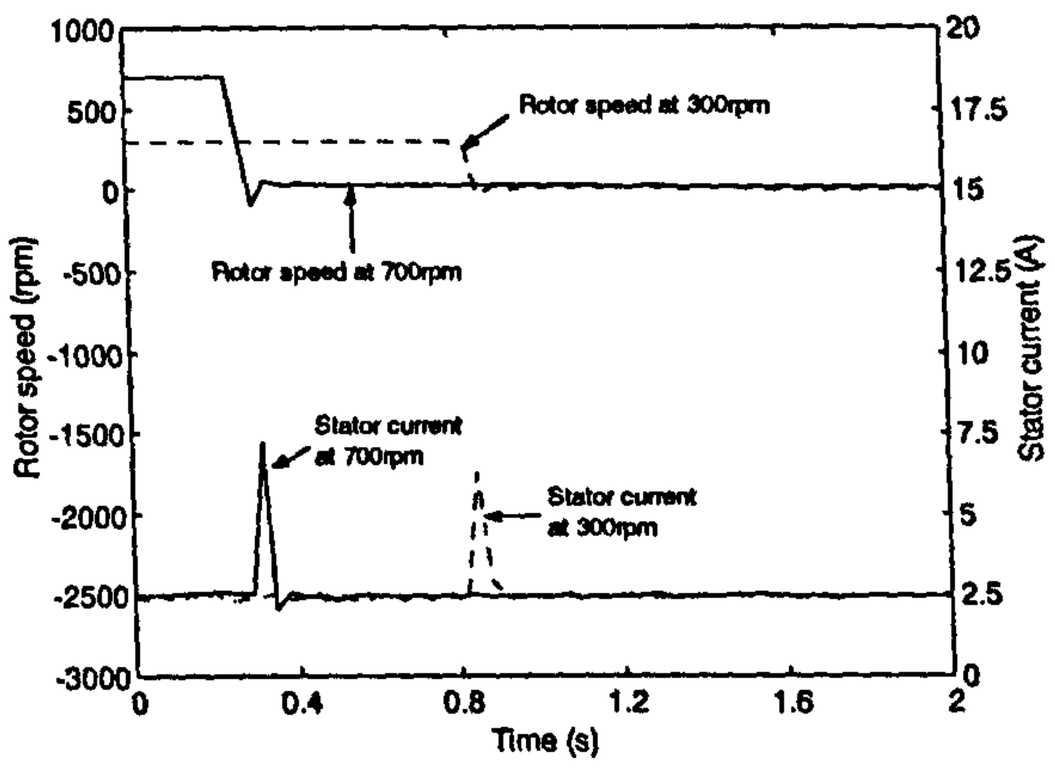

c)

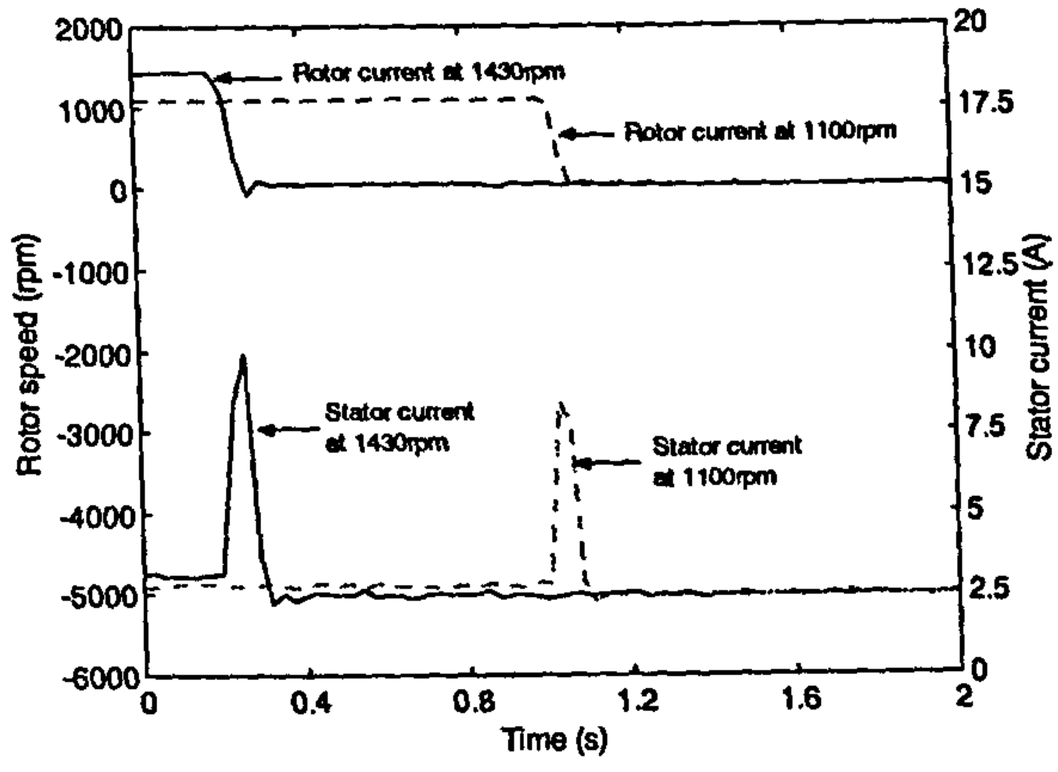

d)

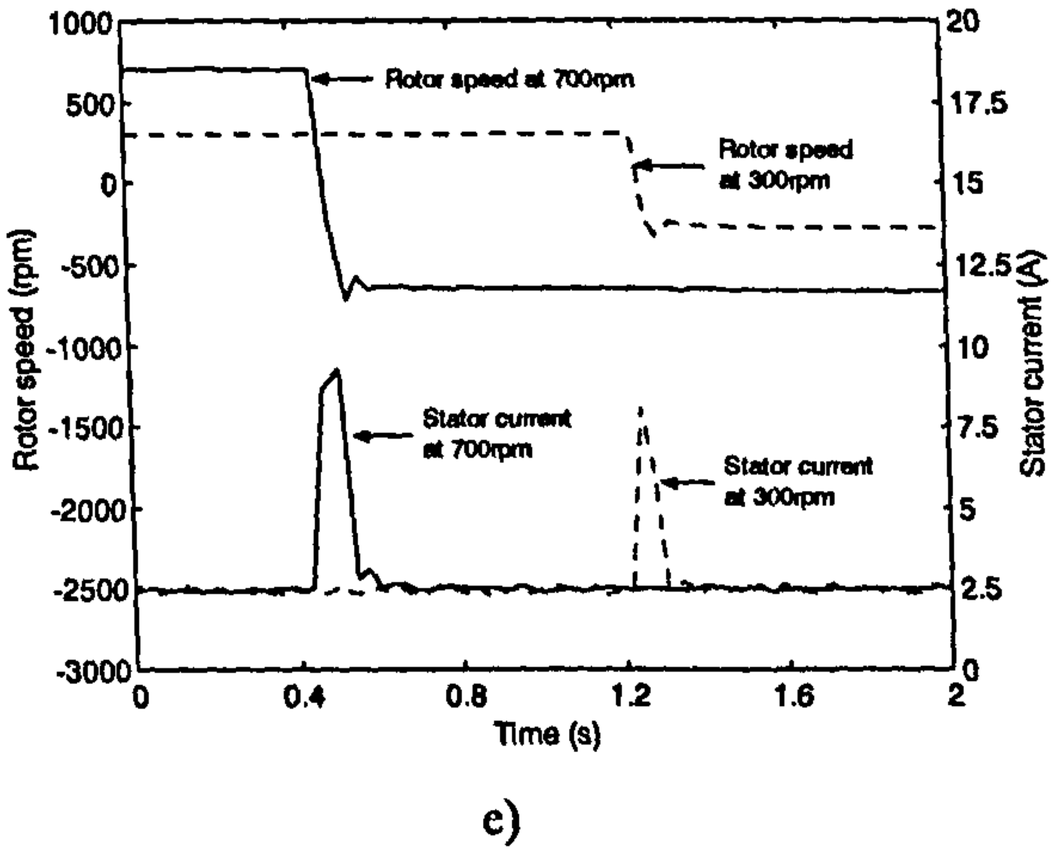

e)

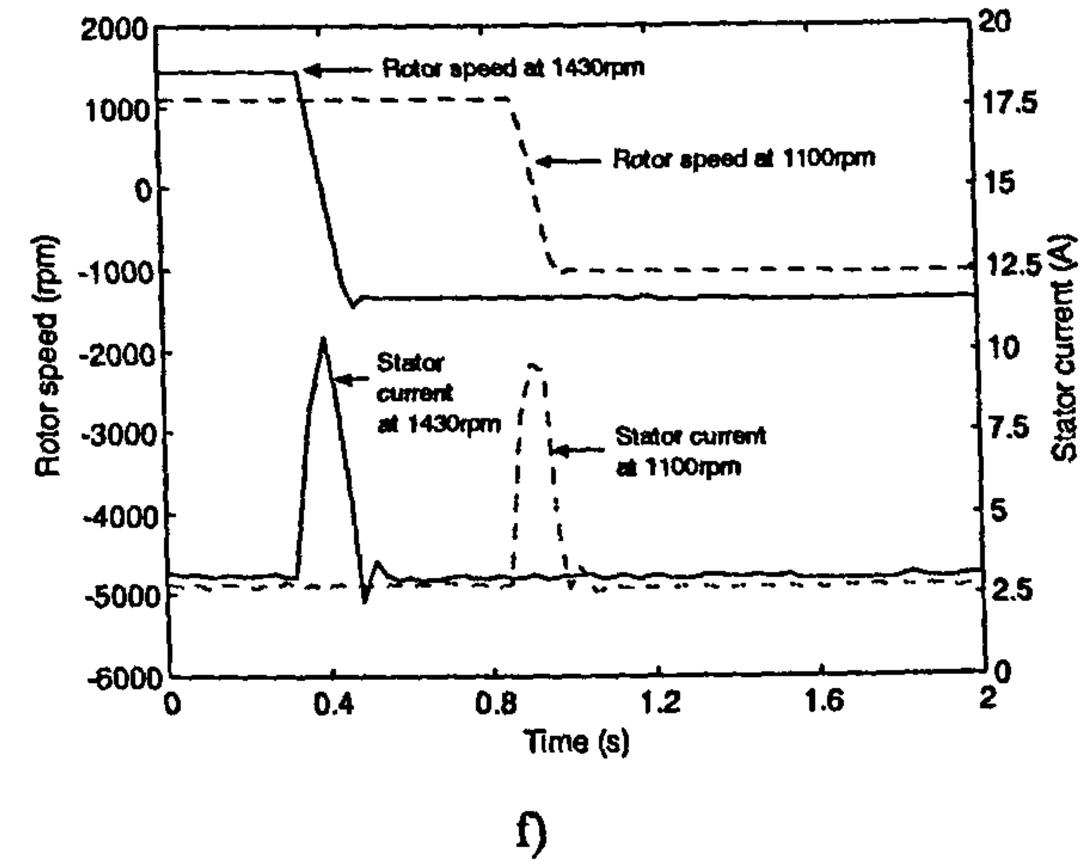

f)

Figure 8.15: Stator phase current of the loaded induction motor during: acceleration from standstill to a) 300 rpm and 700rpm, b) 1100 rpm and 1430 rpm; deceleration to standstill from c) 300 rpm and 700 rpm, d) 1100 rpm and 1430 rpm; reversing from e) 300 rpm and 700 rpm, f) 1100rpm and 1430 rpm.

consistent with the loaded motor for both measured and estimated speed feedback.

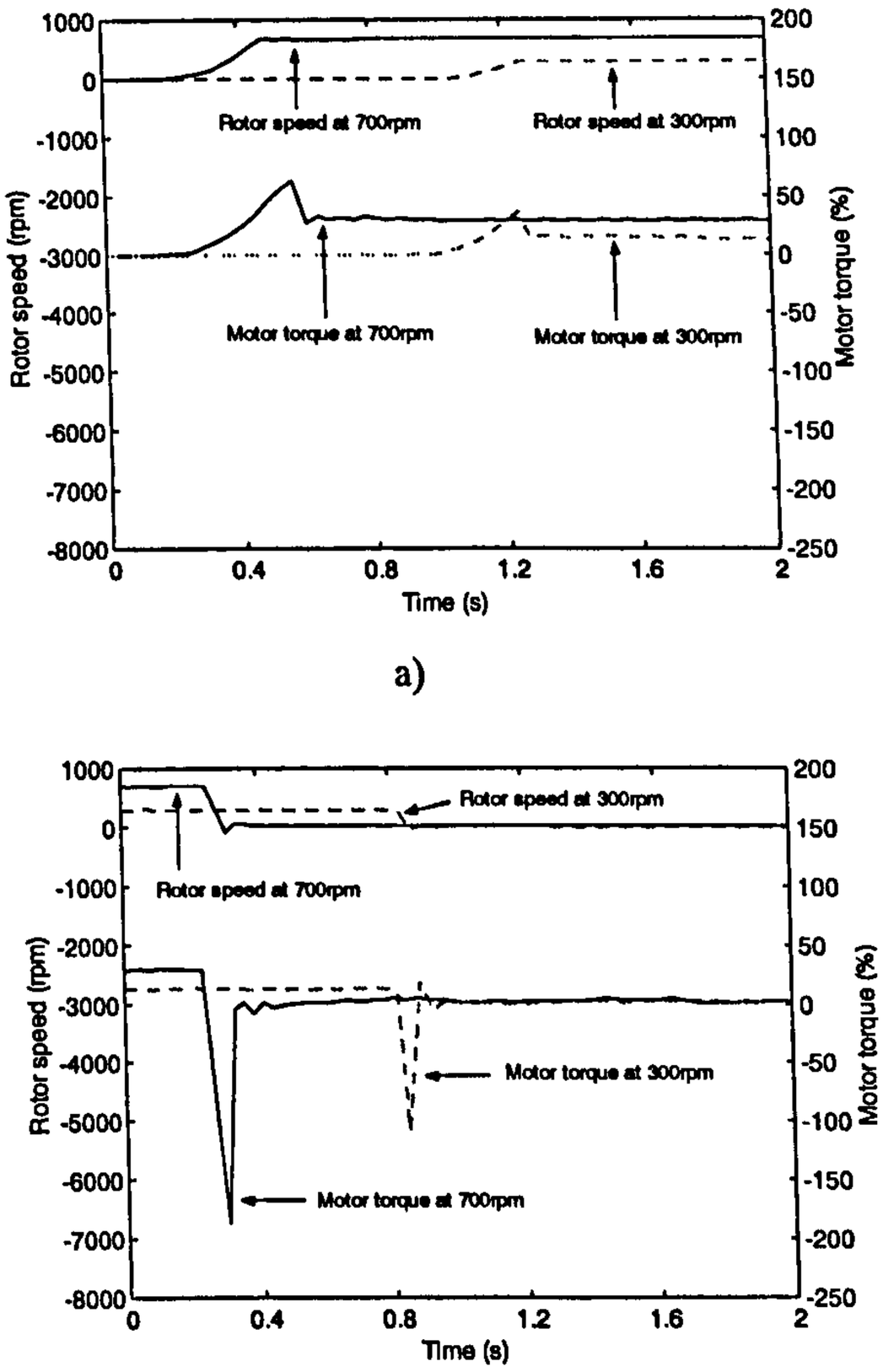

a)

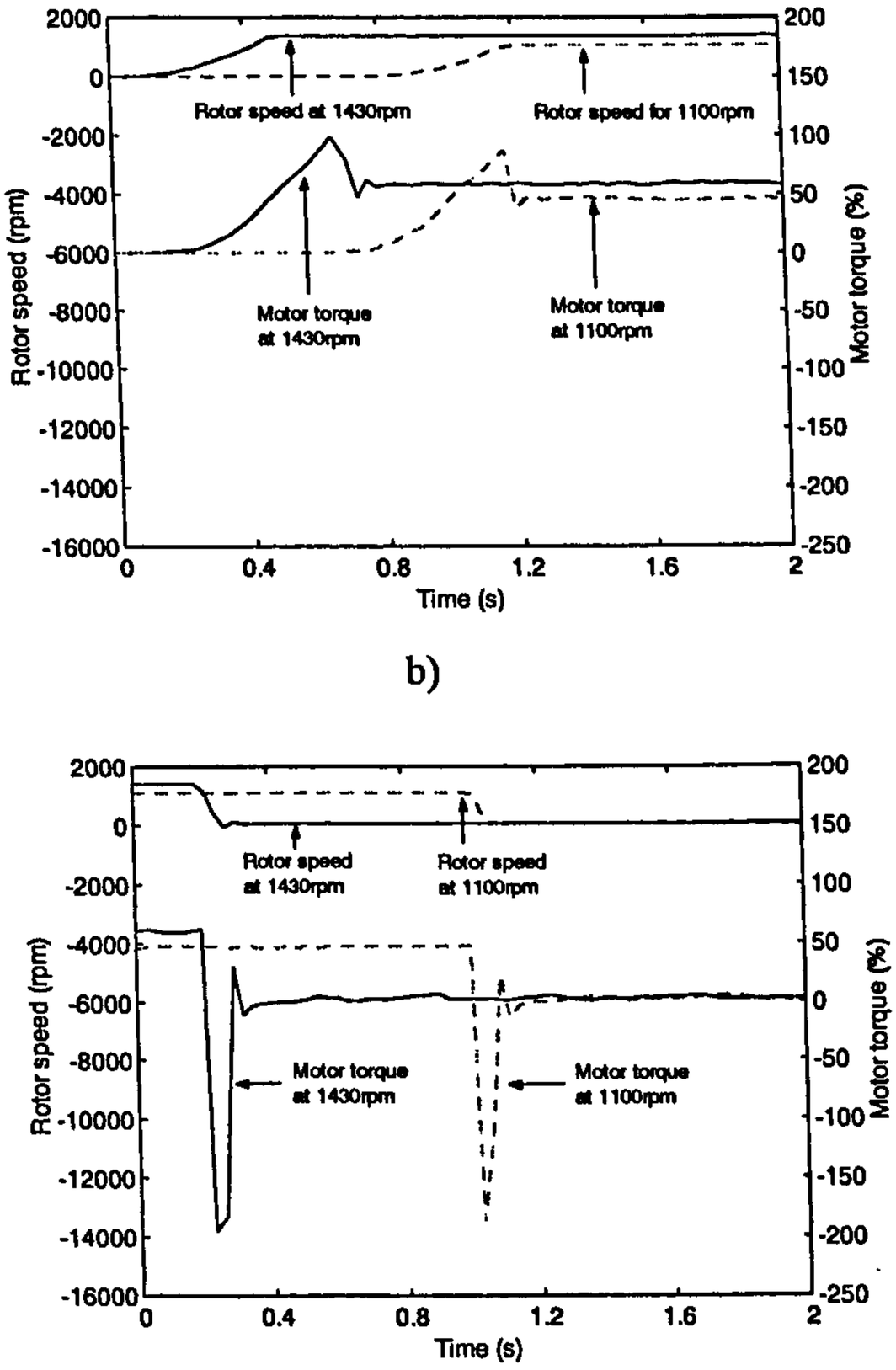

b)

c)

d)

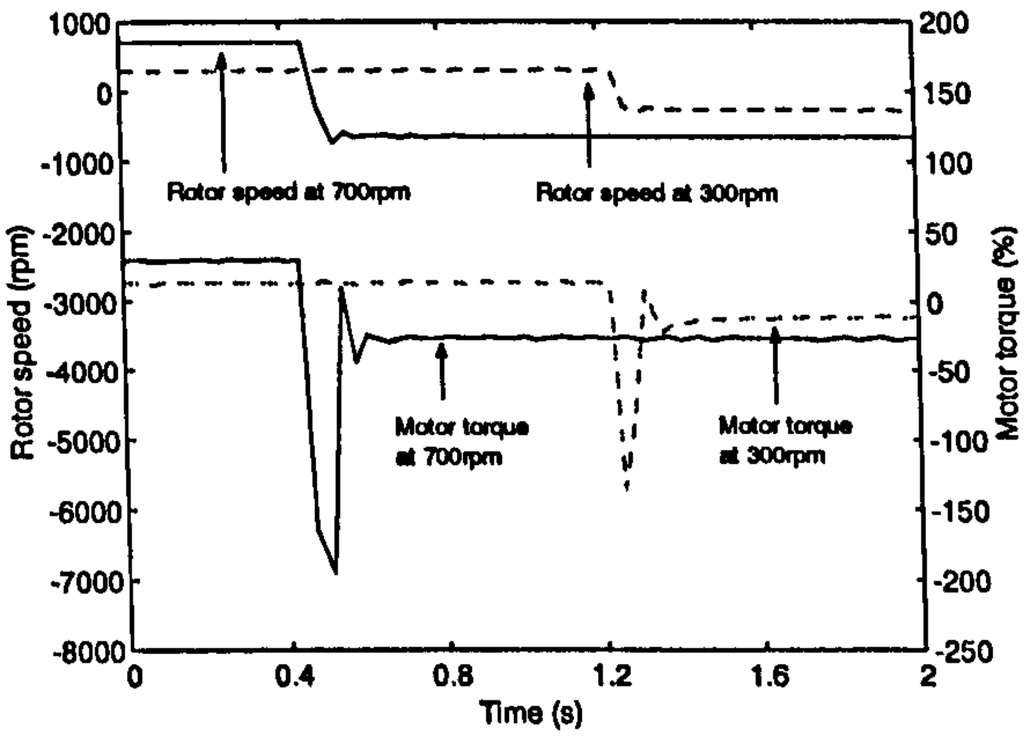

e)

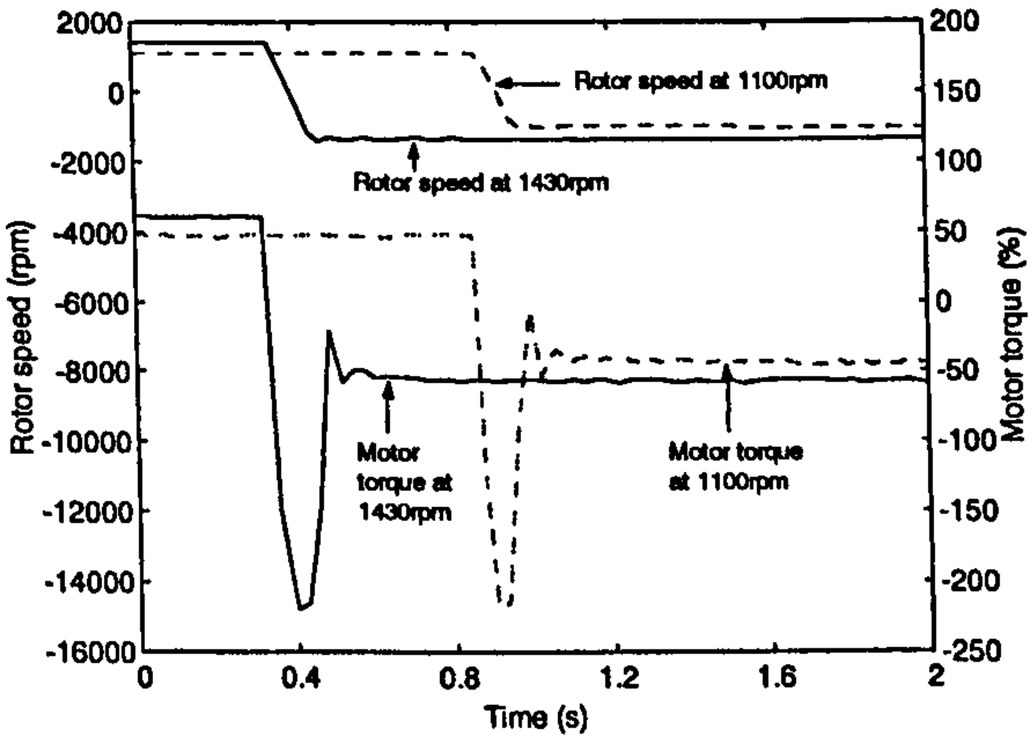

f)

Figure 8.16: Torque and rotor speed of the loaded induction motor during: acceleration from standstill to a) 300 rpm and 700rpm, b) 1100 rpm and 1430 rpm; deceleration to standstill from c) 300 rpm and 700 rpm, d) 1100 rpm and 1430 rpm; reversing from e) 300 rpm and 700 rpm, f) 1100rpm and 1430 rpm.

Stator phase current (figure 8.15) has higher maximum value at medium and high speed during the starting up transient when the induction motor is loaded. In low

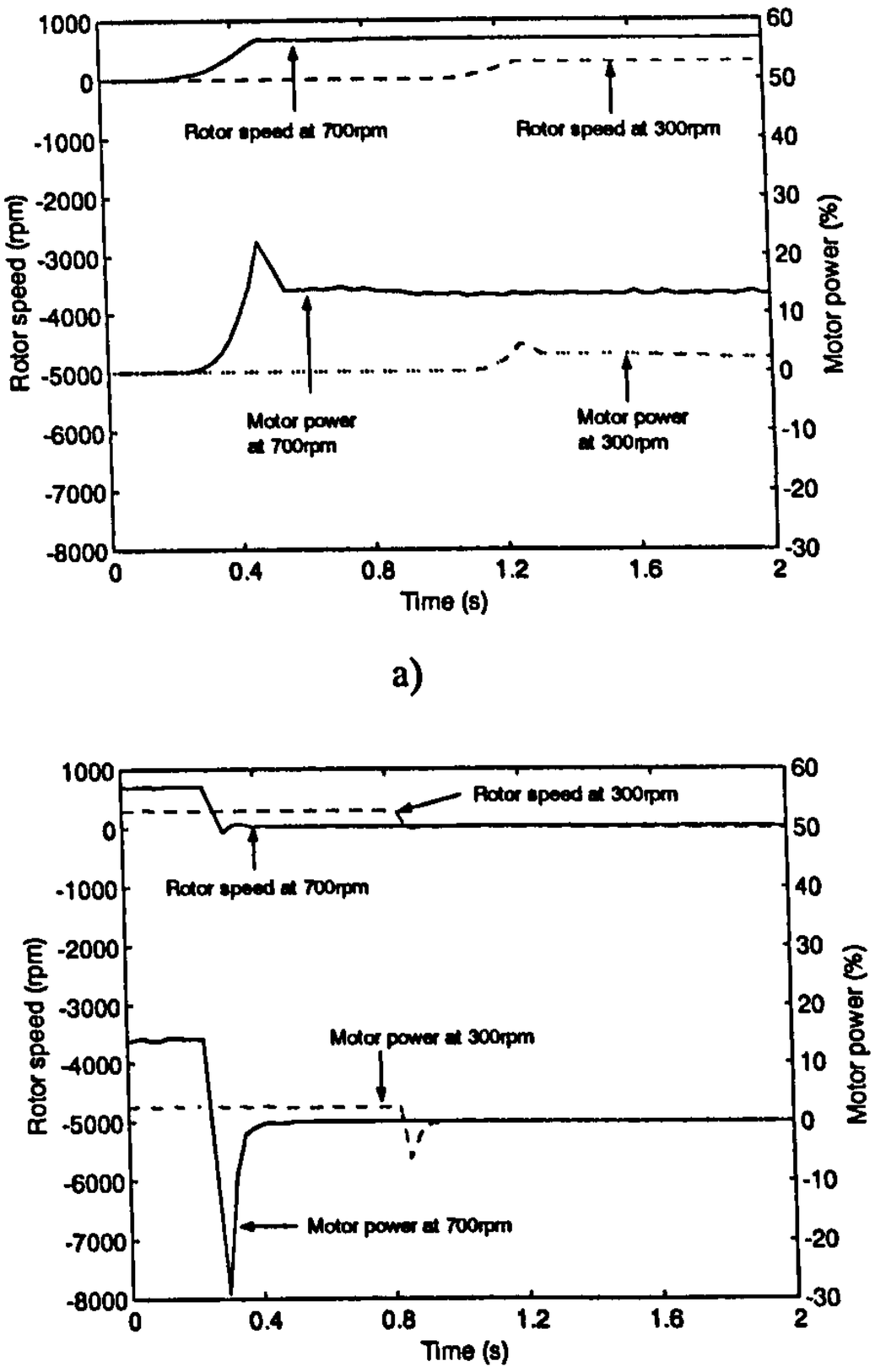

a)

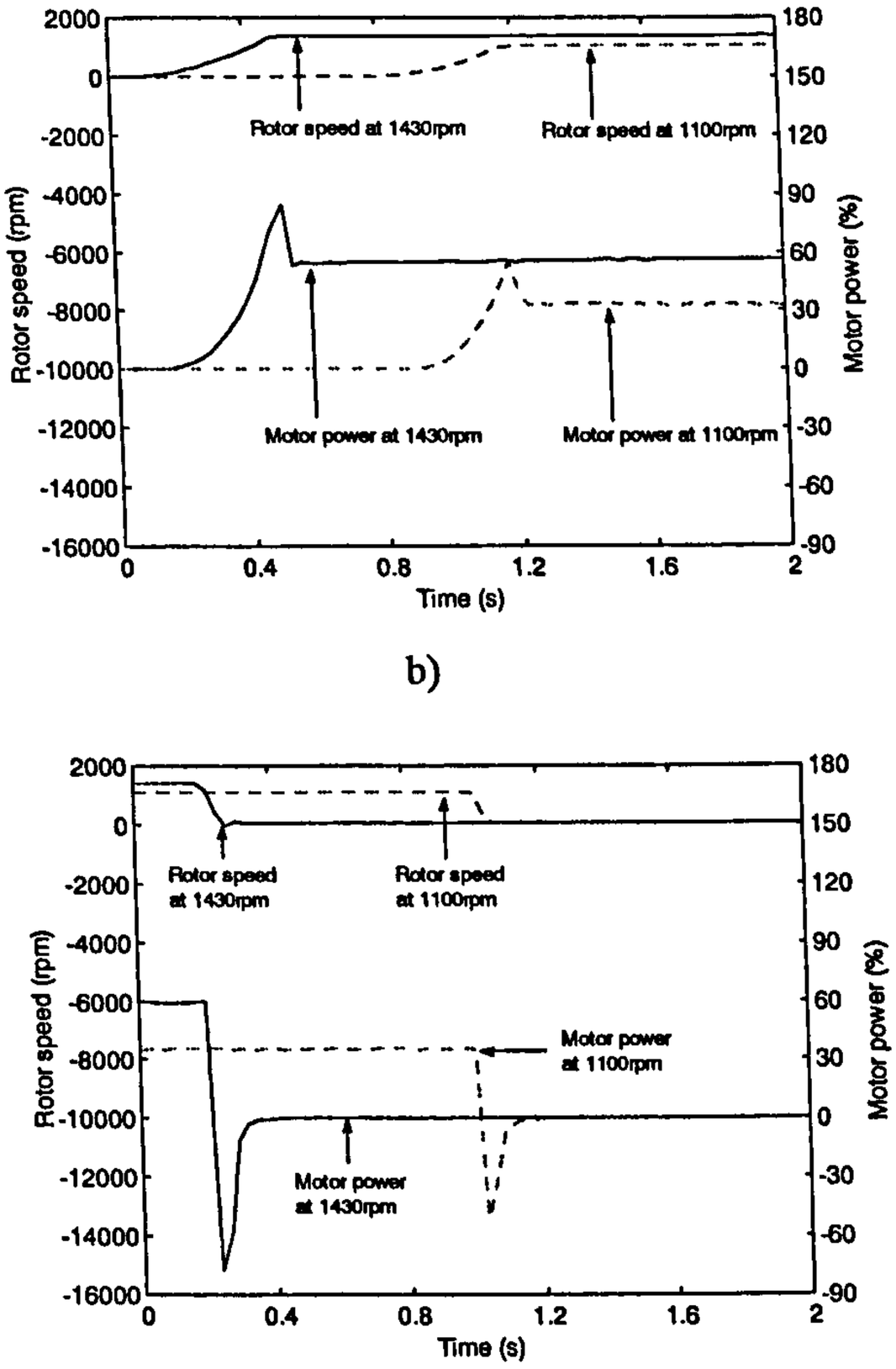

b)

c)

d)

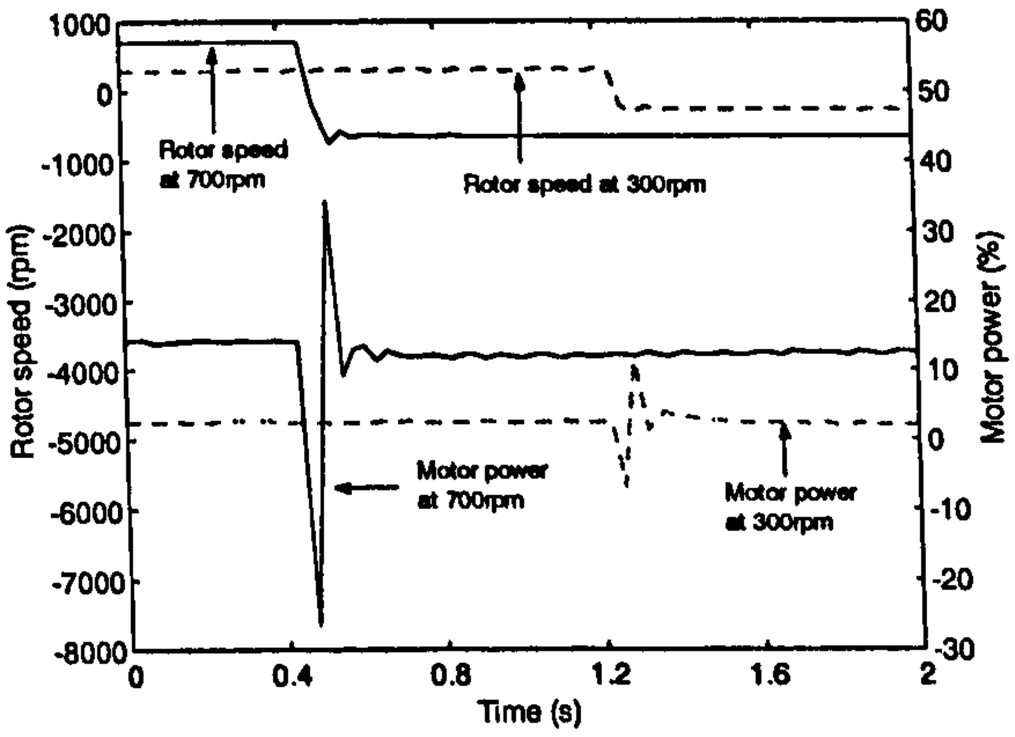

e)

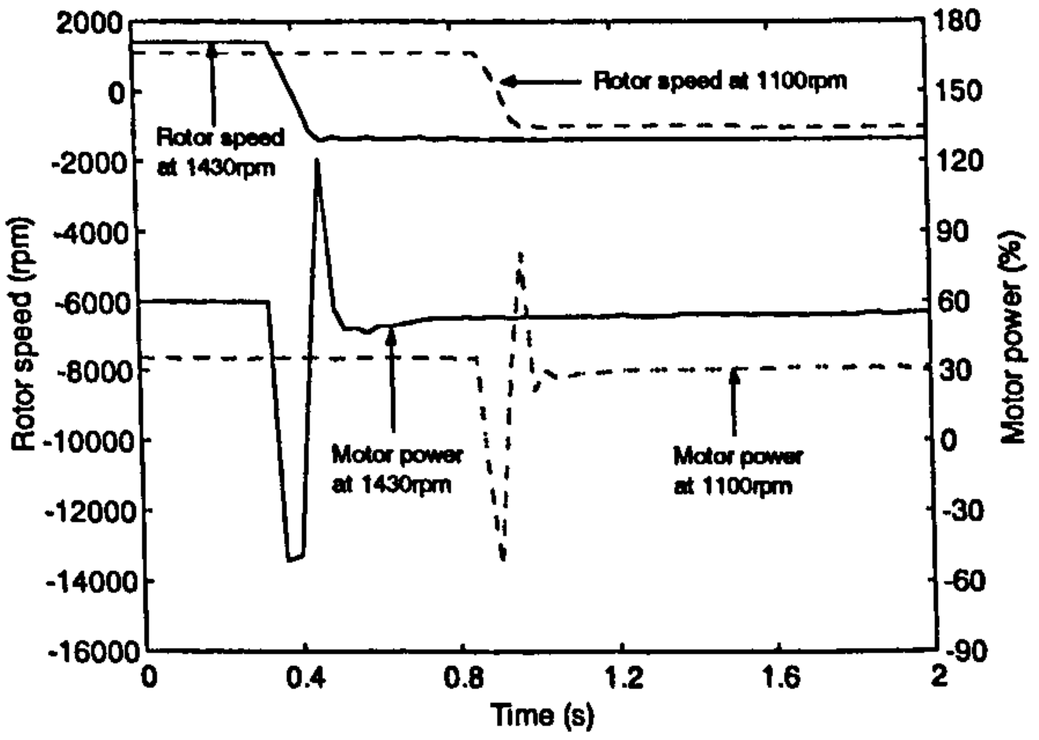

f)

Figure 8.17: Power and rotor speed of the loaded induction motor during: acceleration from standstill to a) 300 rpm and 700rpm, b) 1100 rpm and 1430 rpm; deceleration to standstill from c) 300 rpm and 700 rpm, d) 1100 rpm and 1430 rpm; reversing from e) 300 rpm and 700 rpm, f) 1100rpm and 1430 rpm.

speed region, the maximum is unchanged during acceleration from standstill due to low load torque value. The response time of stator current is not affected by the load, stator

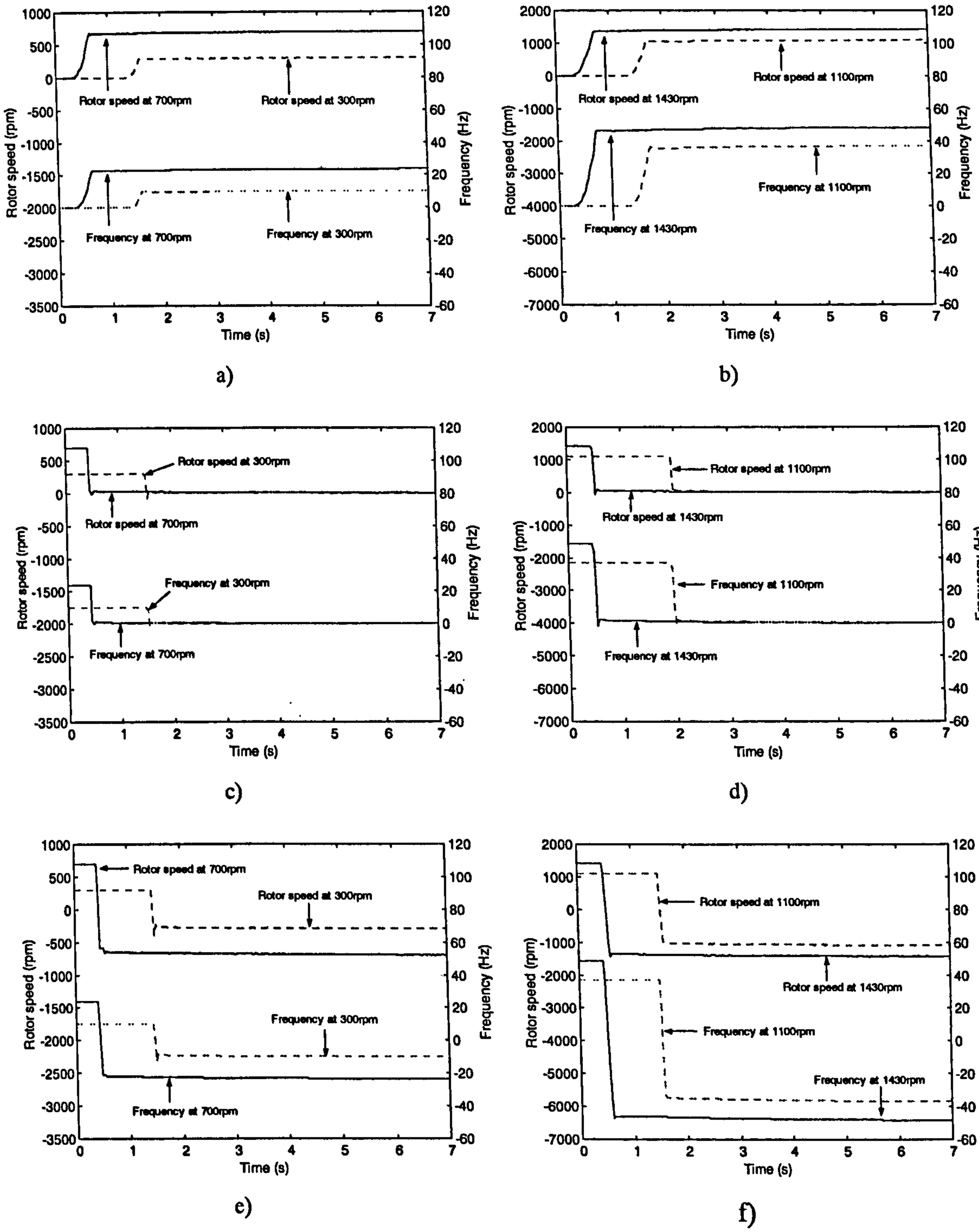

Figure 8.18: Output frequency of the frequency converter and rotor speed of the loaded induction motor during: acceleration from stand still to a) 300 rpm and 700rpm, b) 1100 rpm and 1430 rpm; deceleration to standstill from c) 300 rpm and 700 rpm, d) 1100 rpm and 1430 rpm; reversing from e) 300 rpm and 700 rpm, f) 1100rpm and 1430 rpm.

current quickly reaches steady state value at all speeds. However, the steady state current is higher for the loaded motor in high speed region, while steady state current is

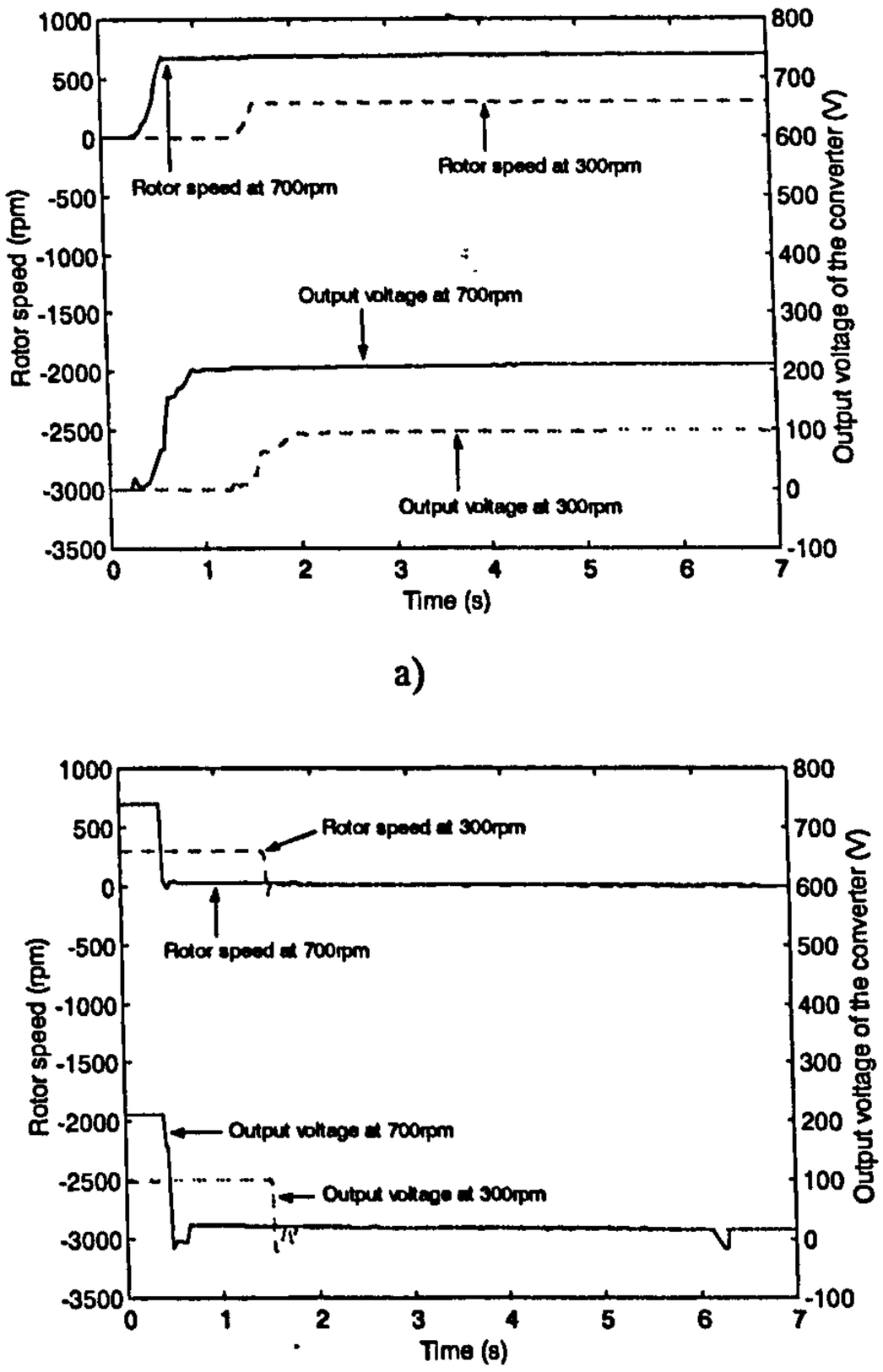

a)

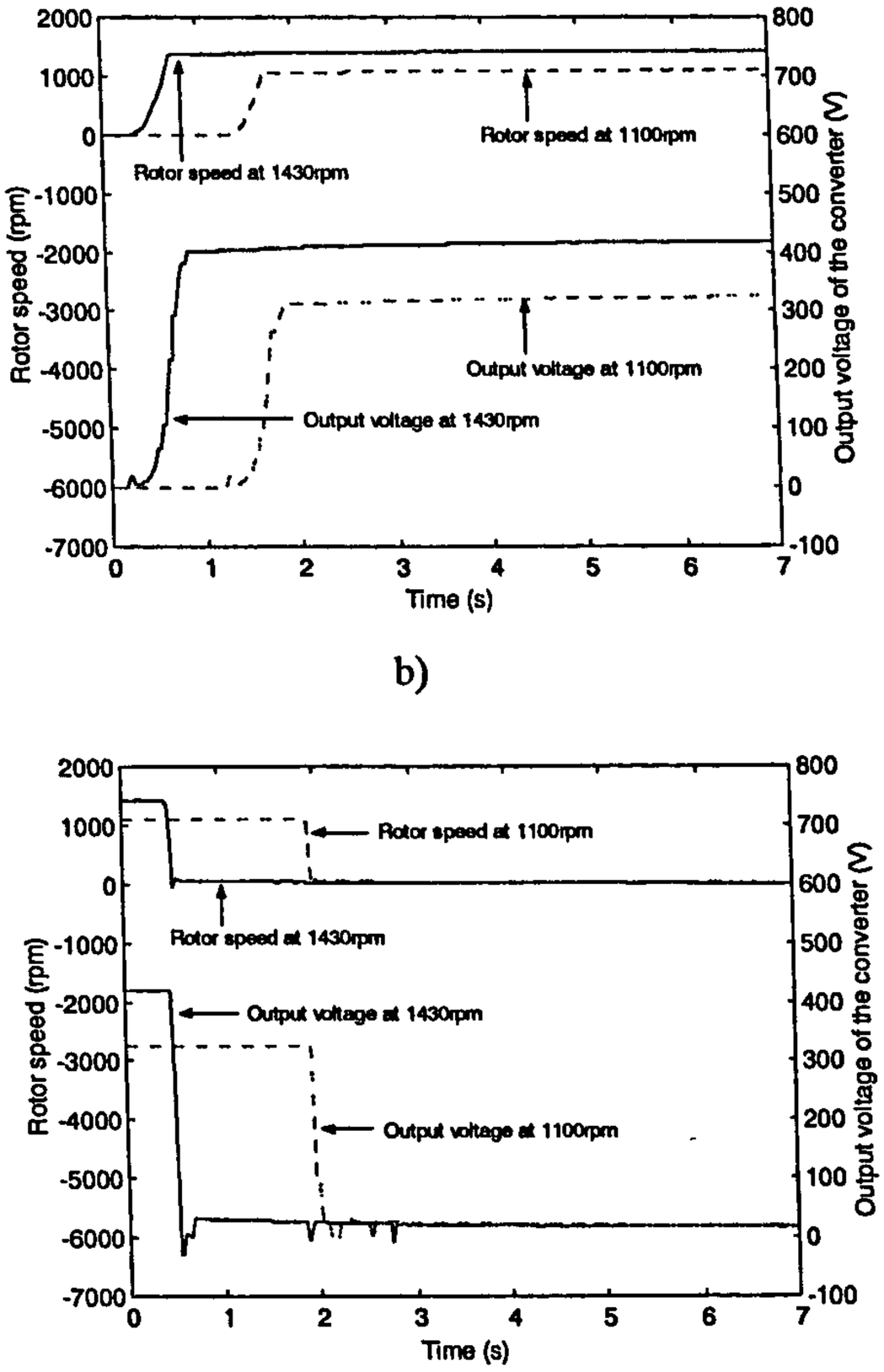

b)

c)

d)

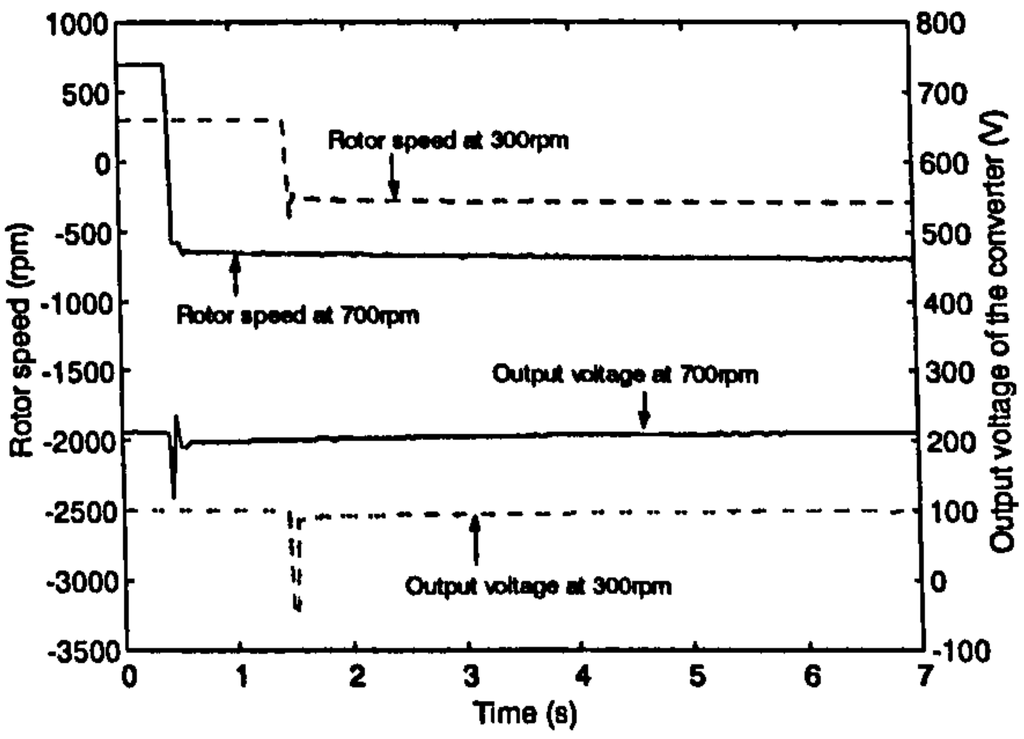

e)

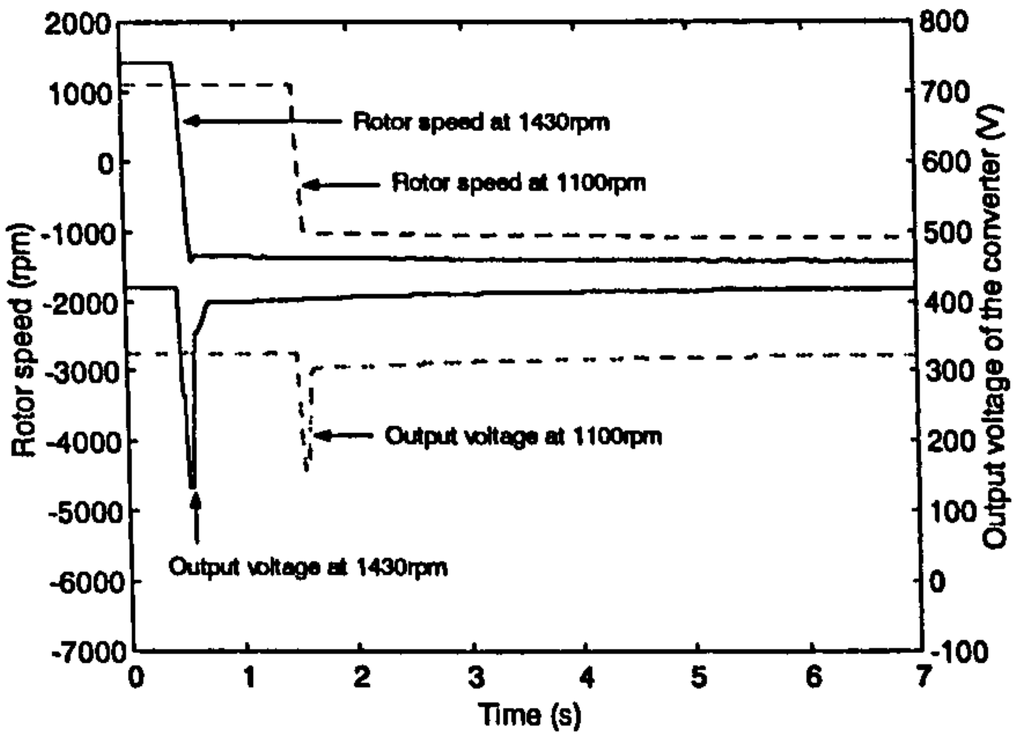

f)

Figure 8.19: Output voltage of the frequency converter and rotor speed of the loaded induction motor during: acceleration from stand still to a) 300 rpm and 700rpm, b) 1100 rpm and 1430 rpm; deceleration to standstill from c) 300 rpm and 700 rpm, d) 1100 rpm and 1430 rpm; reversing from e) 300 rpm and 700 rpm, f) 1100rpm and 1430 rpm.

not significantly changed in medium and low speed, due to relative low values of the load torque. Maximum of the stator current is predominantly unchanged when the motor

is loaded during deceleration to standstill. This is so since the same maximum braking torque is developed by the motor, figure 8.16.

Torque response is relatively slow when the rotor speed increases during the acceleration from standstill. The torque then settles down to the steady state value when speed reaches the commanded value, as shown in figures 8.16a and 8.16b. Steady state values of torque increase with steady state speeds due to the linear dependence of load torque on speed, as already shown in figure 8.12. Torque responses are consistent for all speed regions during the acceleration. Torque peak values are about 200% of the rated torque during the decelerations to zero speed in the medium and high speed region as shown in figures 8.16c and 8.16d. The maximum torque is lower in the low speed region and is about 120% of the rated torque of the induction motor. The torque peak values are further increased during the reversing in all speed regions, as shown in figures 8.16e and 8.16f. Torque responses are also consistent in all speed regions during the decelerations and reversing when the induction motor is loaded.

Motor power behaviour (figure 8.17) closely corresponds to the motor torque response, discussed above. Motor power in steady states increases with increase in steady state speeds due to the increment in the load torque and speed.

Figure 8.18 shows that the responses of the output frequency of the frequency converter are consistent with the rotor speed in low, medium as well as high speed regions for all the three types of transient responses of speed. The same applies to responses of the output voltage of the frequency converter (figure 8.19).

8.4 Summary

Investigations of the performance of a vector controlled induction motor drive and a direct torque controlled drive have been carried out in this chapter. Measurements of the actual rotor speed and stator current of the vector controlled drive have been done for a series of transient. Details of the structure of the drive are also discussed. Investigation of the detuning effects caused by of the incorrect setting of slip gain of the drive is also carried out. Measurement of speed with different settings of slip gain has been done and differences in behaviour have been discussed.

Measurements on the direct torque controlled induction motor under no-load conditions (such as reference speed, measured speed, estimated speed, stator phase

current, motor power, motor torque, output frequency of the drive, and output voltage of the drive) are made by using data acquisition software (DriveWindow). The chapter also presents a description of the software as well as of the structure and components of the direct torque controlled drive. A comparison of performance of both drive types is then made with the obtained data with regard to no-load operation.

A permanent magnet DC motor is then coupled with the direct torque controlled induction motor and is used as a loading generator. The armature terminal of the DC generator is connected to a resistor with varying resistance in order to vary the load torque of the induction motor. The same data acquisition software is used for collecting the same actual signals of the motor in the direct torque controlled drive. Comparison between the performance of the drive with and without load is then made.

Although the experiments were conducted on two different induction machines with very different overall inertia, it can be said that both the vector controlled drive and the direct torque controlled drive offer very good dynamic performance. A clear advantage of the vector controlled drive is shown to be the possibility of machine's pre-magnetisation at standstill. This leads to fast acceleration transients from standstill, which can not be obtained with a direct torque controlled drive.

CHAPTER 9

CONCLUSION

9.1 Summary and conclusions

Direct torque control of induction motor is investigated in this research project. At first, a review of literature is carried out. Numerous aspects of direct torque control, which have been studied before, are discussed. These include the origin and nature of direct torque control, power supplies for direct torque controlled drives, look-up tables for voltage space vector selection, estimation of electromagnetic torque and stator flux, impact of stator resistance variation on accuracy of direct torque control, considerations of iron loss in high performance drives, and sensorless direct torque control. Problems and solutions for each aspect of direct torque control are summarised. Some of the solutions are used further in the research project for development of modified control schemes for direct torque control.

Developments of mathematical models for induction machine and voltage source inverter, required for simulation of direct torque control, are presented next. A constant parameter standard machine model in an arbitrary common reference frame is elaborated. The model in the stationary reference frame is used for simulations of direct torque control due to its simplicity and the independence of DTC on co-ordinate transformation. Induction machine models with iron loss consideration are further discussed. The iron loss is represented with an equivalent iron loss resistance. This resistance is placed either in parallel with the magnetising branch or in parallel immediately after the stator resistance. Modelling of a voltage source inverter is finally presented. The semiconductor switches in the model of the voltage source are assumed to be ideal and the DC link voltage of the inverter is treated as constant.

Principles of vector control and direct torque control are further elaborated in the thesis. Both rotor flux oriented control and stator flux oriented control are reviewed. Control schemes for indirect vector control (indirect feed-forward rotor flux oriented control and indirect feed-forward stator flux oriented control) and direct feedback vector control (with either rotor flux orientation or stator flux orientation) are further presented. Principles of direct torque control are covered next. Torque production

mechanism in induction motor is highlighted in order to explain how torque and stator flux can be controlled by varying the magnitude of stator flux space vector and the relative angular position between stator flux space vector and rotor flux space vector. The variation is obtained with the application of appropriate voltage space vectors in a short time period to meet both torque and flux control demands. Basic control schemes of direct torque control in both torque mode of operation and speed mode of operation are presented. Switching table or optimised method for selection of voltage space vectors, based on the states of torque and flux hysteresis controllers, is described. The switching table is the classical one, which was originally suggested in the mid-eighties. The selection is based on the output of flux and torque hysteresis controllers and the relative position of the stator flux space vector in the complex plane. Knowledge of the accurate position of the stator flux vector is not necessary, only the sector where the vector is located in the complex plane is required. Zero voltage space vectors of the voltage source inverter are used when no change in torque is required to keep the switching frequency of the inverter at a low level. Methods for estimating the stator flux and electromagnetic torque of the induction motor are elaborated. Direct torque control does not require online co-ordinate transformation. Information about speed is therefore unnecessary, except for closed-loop speed controller. An open loop speed estimator (model based method with no corrective part) used in commercial ABB direct torque control drive is reviewed.

Upon review of the mathematical modelling of an induction motor and principles of vector control and direct torque control, the research further focuses on three particular aspects of direct torque control. The first one is a comparison of performance obtainable with vector control and direct torque control. The second aspect is the choice of an appropriate switching table for direct torque control. The third aspect is the impact of iron loss existence on accuracy of direct torque control and means for iron loss compensation in sensored and sensorless mode of operation. An original contribution is offered in relation to all three aspects. The most important contributions of the thesis are believed to be those related to the third aspect.

The first aspect, a comparison between behaviour of a vector controlled induction motor drive and a direct torque controlled drive, is a theme which is covered in two chapters of the thesis (chapter 4 and chapter 8) in a different way. It is argued in chapter 4 that the only way to perform a valid comparison is to select a specific stator flux oriented control scheme in torque mode of operation and with hysteresis current

control. A simulation comparison between stator flux oriented control (SFOC) and direct torque control is carried out in torque mode of operation. Both control methods rely on stator flux control and use the same principle for stator flux position calculation. The comparison is based on torque, stator flux, and stator current responses obtained from simulations of both control methods using the constant parameter standard induction machine model. The comparison has found that speed, stator flux, and torque dynamic responses with both SFOC and DTC are essentially identical. It has also been found that stator flux and stator current ripples are considerably smaller in SFOC. Torque ripple is found to be substantially smaller in DTC at low and medium speeds, while at high speeds torque ripple with DTC exceeds the one with SFOC.

The findings of this comparison seem to go against conclusions of some of the existing comparisons, which invariably compare DTC with indirect RFOC. It is the belief of the author that any valid comparison must compare like-for-like and that the results of the analysis, arrived at in this thesis, are representing a true reflection of the relative performance of the two control methods.

More attention is devoted next to the second aspect, a choice of an appropriate inverter switching scheme. Theoretical analysis of the problems such as high flux ripple at low speed and high torque ripple at high speed is given. The torque deviation due to the applied voltage space vector, leading to high torque ripple at high speeds and low torque ripple at low speeds, is investigated. Effects of different applied voltage vectors on the stator flux space vector behaviour at different locations within one sector of the complex plane are also analysed. The analysis explains the reason for high flux ripple at low speed especially when the stator flux space vector is in the vicinity of the border between two adjacent sectors in the complex plane. Consequences of the application of zero voltage space vectors for the sake of low switching frequencies are discussed. This helps to explain the problem of high torque ripple at high speeds and demagnetisation phenomenon at low speed. Simulations of direct torque control with classical switching table in torque and speed mode of operation are performed to examine the problems. The responses of speed, flux and torque confirm the existence of the above mentioned problems associated with Takahashi's switching table.

The second aspect of direct torque control, covered in detail in the thesis, is the selection of the optimum stator voltage space vector. Several existing modifications of the classical switching table of Takahashi, which have been suggested in literature, are reviewed. These solutions are selected for presentation because of their feasibility for

practical implementation, simplicity of the algorithm and effectiveness in reducing torque and/or flux ripple problem. Simulations of direct torque control with the modified switching tables are carried out to verify the improvement. A speed dependent switching table is examined first. This switching table aims at reducing the flux ripple in low speed region by not applying zero voltage space vectors in the low speed region (less than 20% of the rated speed of the induction motor). However, the problem of high torque ripple at high speed is not solved by this switching table. Another switching table for improvement of flux response at low speed only is the so-called switching table for zero speed control. When the flux error exceeds an outer hysteresis band, a magnetising look-up table is used instead of the traditional switching table of Takahashi. This magnetising look-up table uses a redefined complex plane of stator flux space vector where the axes are rotated by 30 degrees (for positive speed, two-quadrant operation). A switching table with increased switching frequency is looked at next. This switching table aims at improving both flux and torque response by increasing the number of applied voltage space vectors to the induction machine. Additional voltage space vectors are created from the six basic non-zero voltage space vectors of the voltage source inverter. A new voltage space vector is the vectorial sum of two adjacent basic non-zero voltage space vectors, and each is applied in one half of the sampling period. The switching frequency is therefore doubled. Both flux and torque responses are slightly improved at the expense of increased switching loss. A switching table for improved dynamic torque behaviour in four-quadrant operation is the last existing solution examined in the thesis. The selection of the voltage space vector is made not only on the basis of the outputs of the three-level hysteresis comparators of flux and torque but also using the sign of rate of change of torque in time domain. It is determined from the values of stator flux, torque, speed, stator resistance and rotor resistance. Due to the complexity and high dependence on the accuracy of machine parameters of the algorithm, simulation for this switching table is not carried out. A novel switching table for improved low speed and high speed control is further suggested. This is a further modification of the existing switching table for zero speed control. A new complex plane of the stator flux space vector where the axes are rotated by –15 degrees (positive speed, two-quadrant operation) is used when the motor speed reaches 80% of the rated speed. Traditional switching table of Takahashi is still utilised with this new complex plane. The new switching strategy improves torque response at

high speed at the expense of higher flux ripple at high speed, and reduces flux ripple at low speed.

The third and major theme of research in the thesis, impact of iron loss on accuracy of direct torque control and means for compensation, is elaborated in chapters 6 and 7. Investigation of detuning of direct torque control of induction motor due to core loss is carried out. An induction machine model with iron loss representation is used for the investigation of the iron loss impact on the direct torque control accuracy. The equivalent iron loss resistance represents accurately only fundamental component of the iron loss and is a function of operating frequency. Simulations of torque mode of operation and speed mode of operation with speed sensor are carried out with traditional switching table of Takahashi. Simulations have shown that average torque in steady state operation in both medium speed region and high speed region deviates about 4.2% of the rated torque due to the iron loss existence. Flux responses are not affected by the presence of iron loss, since stator flux estimation automatically takes into account iron loss existence in the machine. The problem of torque deviation caused by the fact that the torque estimator does not recognise the existence of the iron loss means that the estimated torque is higher than the actual torque in motoring. An iron loss related torque component is therefore introduced in the torque estimator with the idea of providing compensation. However, the iron loss related torque component is operating frequency dependent, and stator frequency is not obtainable in practice. An approximation by replacing stator frequency with angular electrical speed is used instead. Simulations show the reduction of residual torque error of the average torque in steady state for both stator frequency dependent compensation and angular electrical speed compensation to lees than 0.9% of the rated torque. Torque error in the steady state in the medium speed region is smaller than in the high speed region. Due to the almost linear behaviour of iron loss in the base speed region, an alternative compensation with a constant iron loss related torque component in the torque estimator is suggested. A constant torque compensation of 1.15 N.m is made in the torque estimator of the direct torque controller. Simulations have shown that the residual torque error of the average torque is less than 0.1% of the rated torque when the constant torque increment compensation is used.

Sensorless direct torque control is further investigated, since direct torque control is inherently sensorless. Information about speed is not required by the direct torque controller due to its independence on co-ordinate transformation. Speed

estimator is only necessary for speed mode of operation. Criteria for selection of speed estimator are also independent of the operation of the direct torque controller. Model reference adaptive systems (MRAS) are used for estimating the speed. Flux based models are utilised for both adaptive and reference systems, and both stator flux and rotor flux MRAS speed estimators are used to estimate the speed. A stator flux based model, which is independent of speed, is developed from the constant parameter standard machine model for the reference model of the speed estimator. Another stator flux based model with speed as a variable is also developed from the same machine model for the adaptive model of the speed estimator. Iron loss compensation is at first not incorporated in models. Error quantity between the output of the two models, or speed tuning signal, is used to drive a PI controller (or speed tuning mechanism) whose output is the estimated speed itself. The estimated speed is also used as a variable in the adaptive model. Similarly, mathematical modelling of a rotor flux based MRAS speed estimator is developed from the constant parameter standard machine model. Mathematical models for flux based MRAS speed estimators with iron loss compensation are further developed. The models are obtained from a machine model with parallel equivalent iron loss resistance placed immediately after stator resistance. This machine model gives a less complicated system of first order differential equations, compared with the other machine model in which the equivalent iron loss resistance is placed in parallel with the magnetising branch. The equivalent iron loss resistance is therefore a different function of operating frequency.

Simulations of sensorless direct torque control with speed dependent switching table (a modification of the classical switching table, as already discussed in detail in chapter 5) are carried out. This switching table is used to avoid demagnetisation in induction motor during deceleration and reversing. The two types of flux based MRAS speed estimators, with and without iron loss compensation, are used in the simulations. Effects of iron loss on performance of the speed estimators are also examined by performing comparison between the responses obtained with different speed estimators. Iron loss increases speed response time in all speed regions and also leads to a steady state error between the estimated speed and the actual speed. Stator flux based MRAS speed estimator with iron loss compensation improves the performance of the drive, since the compensation of iron loss in the torque estimator only can not eliminate speed estimation error. Similar improvement is also obtained with the rotor flux based MRAS speed estimator with iron loss compensation. Rotor flux based MRAS speed estimator

with iron loss compensation, however, gives slightly lower estimation error in steady state than the corresponding stator flux based one. On the basis of the analysis of the iron loss impact on operation of a direct torque controlled induction motor drive it can be concluded that the error in torque estimation is more important that the error in speed estimation (which does not exceed 3 rpm). This means that compensation of the iron loss induced torque estimation error should be incorporated into the DTC algorithm, while compensation of the iron loss in the speed estimation process is optional. It should be pointed out though that compensation of the iron loss in the flux based MRAS estimator is an easy and straightforward task, as shown in chapter 7.

The first aspect of the original research, a comparison between a vector controlled and a DTC induction motor drive, is revisited in chapter 8. Experimental comparison between an industrial vector controlled drive and an industrial direct torque controlled drive is carried out. A DSB drive of Vickers Electrics and an ACS-601 drive of ABB have been used for vector control experimental rig and DTC experimental rig, respectively. Since vast majority of industrial vector controlled drives are with indirect RFOC, it was not possible to compare SFOC with DTC as the case was in chapter 4. Furthermore, due to the numerous differences between the two experimental rigs, the comparison in the experimental work is restricted to qualitative rather than quantitative observations. Operation under no-load conditions in base speed region is investigated with indirect RFOC drive. The induction motor is accelerated and decelerated in the speed mode of operation. Operation in base speed region with and without load is examined with the direct torque controlled drive. The induction motor is accelerated, decelcratcd and reversed in the speed mode of operation. Microsoft Windows based software (ABB DriveWindow) is used for data acquisition and monitoring of the drive. It is concluded that both drives offer excellent dynamic performance. Vector controlled drive has an advantage of shorter response time at starting due to pre-magnetisation at standstill. No obvious advantage of the DTC drive was observed in the experiments.

9.2 Future work

The problem of pure integration, related to DC drift and initial value, has been ignored in this project, although pure integrators have been used in stator flux estimator and speed estimator. Further work with alternatives for pure integrators being used in

flux and speed estimators should be done in the future. Alternative stator flux estimators, which are less sensitive to accuracy of the measured voltage and current, and variation of stator resistance, should be utilised in the direct torque controller for future research. Compensation for detuning of stator flux and torque estimation due to the variation of stator resistance with temperature should also be researched. Novel modifications for the classical switching table to provide high quality of flux response at low speed and torque response at high speed should also be designed. Experimental investigation of the iron loss compensation in torque estimator and speed estimator is envisaged as yet another future research direction.

CHAPTER 10

REFERENCES

ABB Industry Oy (2002), DriveWindow's user manual, Helsinki, Finland.

Abbondanti,A., and Brennen,M.B. (1975), Variable speed induction motor drives use electronic slip calculator based on motor voltages and currents, *IEEE Transactions on Industry Applications*, Vol. 11, No. 5, pp. 483-488.

Alfonso,D., Gianluca,G., Ignazio,M., and Aldo,P. (1999), An improved look-up table for zero speed control in DTC drives, *European Conference on Power Electronics and Applications EPE'99*, Lausanne, Switzerland, CD-ROM.

Attaianese,C., Nardi,C., Perfetto,A., and Tomasso,G. (1999), Vectorial torque control: A new approach to torque and flux control of induction motor drives, *IEEE Transactions on Industrial Applications*, Vol. 35, No. 6, pp. 1399-1405.

Beguenane,R., Benbouzid,M.E.H., and Capolino,G.A. (1995), Design of slip frequency detector with improvement accuracy for induction motor rotor parameters updating, *European Conference on Power Electronics and Applications EPE'95*, Sevilla, Spain, pp. 3.417-3.422.

Beguenane,R., Benbouzid,M.E.H., and Capolino,G.A. (1996), Rotor parameter updating for induction motor vector control by non-invasive slip frequency measurement, *International Conference on Electrical Machines ICEM'96*, Vigo, Spain, Vol.3, pp. 153-157.

Bertoluzzo,M., Buja,G., and Menis,R. (1999), Analytical formulation of the direct torque of induction machines, *IEEE International Symposium on Industrial Electronics ISIE'99*, Bled, Slovenia, pp. PS14-PS20.

Boldea,I., and Nasar,S.A. (1987), Unified treatment of core losses and saturation in the orthogonal axis models of electric machines, *IEE Proceeding, Part B*, Vol. 134, No. 6, pp. 353-363.

Boldea,I., and Nasar,S.A. (1992), *Vector control of AC drives*, Boca Raton, Florida CRC Press.

Briz,F., Degner,M.W., Diez,A., and Lorenz,R.D. (2001), Measuring, modelling, and decoupling of saturation-induced saliencies in carrier-signal injection-based sensorless AC drives, *IEEE Transactions on Industry Applications*, Vol.37, No.5, pp. 1356-1364.

Casadei,D., Grandi,G., Serra,G., and Tani,A. (1994), Switching strategies in direct torque control of induction machines, *International Conference on Electrical Machines ICEM'94*, Paris, France, pp. 204-209.

Casadei,D., Serra,G., and Tani,A. (1995), Direct flux and torque control of induction machine for electric vehicle applications, *IEE International Conference on Electrical Machines and Drives*, IEE Conference Publication No. 412, pp. 349-353.

Casadei,D., Serra,G., and Tani,A. (1997), Analytical investigation of torque and flux ripple in DTC schemes for induction motors, *IEEE Annual Conference of the Industrial Electronics Society IECON'97*, New Orleans, LA, pp. 552-556.

Casadei,D., Grandi,G., Serra,G., and Tani,A. (1998a), The use of matrix converters in direct torque control of induction machines, *IEEE Annual Meeting of Industrial Electronics Society IECON'98*, Aachen, Germany, pp. 744-749.

Casadei,D., Serra,G., and Tani,A. (1998b), Improvement of direct torque control performance by using a discrete SVM technique, *IEEE Power Electronics Specialists Conference PESC'98,* Fukuoka, Japan, pp. 997-1003.

Casadei,D., Serra,G., and Tani,A. (2000), Implementation of a direct torque control algorithm for induction motors based on discrete space vector modulation, *IEEE Transactions on Power Electronics,* Vol. 15, No. 4, pp. 769-777.

Casadei,D., Matteini,M., Serra,G., Tani,A., and Blaabjerg,F. (2001), Direct torque control using matrix converters: improvement of the input line current quality, *European Power Electronics Conference EPE'01*, Graz, Austria, CD-ROM.

Chapuis,Y.A., and Roye,D. (1998), Direct torque control and current limitation method in start up of an induction machine, *IEE Conference on Power Electronics and Variable Speed Drives PEVD'98*, London, UK, IEE Conference Publication No. 456, pp. 451-455.

Chapuis,Y.A., Poure,P., and Braun,F. (1998), Torque dynamic correction of direct torque control for induction machine using a DSP, *International Conference on Power Conversion and Intelligent Motion PCIM'98*, Nuremberg, Germany, pp. 241-250.

Chen,J., and Li,Y. (1999), Virtual vectors based predictive control of torque and flux of induction motor and speed sensorless drives, *IEEE Industrial Applications Society Annual Meeting IAS'99*, Phoenix, Arizona, CD-ROM paper No. 59_3.

Choi,D.H., Cho,S.B., and Hyun,D.S. (1997), Improved torque response by tuning of the magnetising inductance under field weakening operation region, *IEEE Industrial Applications Society Annual Meeting IAS'97*, New Orleans, Louisiana, USA, pp. 418-425.

Choi,J.W., Chung,D.W., and Sul,S.K. (1996), Implementation of field oriented induction machine considering iron losses, *IEEE Applied Power Electronics Conference APEC'96,* San Jose, California, pp. 375-379.

Cilia,J., Asher,G.M., Bradley,K.J., and Sumner,M. (1997), Sensorless position detection for vector-controlled induction motor drives using an asymmetric outer-section cage, *IEEE Transactions on Industry Applications*, Vol. 33, No. 5, pp. 1162-1169.

Cilia,J., Asher,G.M., Shuli,J., Sumner,M., Bradley,K.J., and Ferrah,A. (1998), The estimation of the fundamental frequency in sensorless vector controlled induction motor drives using a real-time adaptive filter, *International Conference on Electrical Machines ICEM'98*, Istanbul, Turkey, pp. 1017-1021.

Conroy,B.P., Sumner,M., and Alexander,T. (1995), Application of encoderless vector control techniques in a medium performance induction motor drive, *European Conference On Power Electronics and Applications EPE'95*, Seville, Spain, pp. 3.469 - 3.474.

Consoli,A. (2000), AC Machine sensorless control techniques based on high frequency signal injection, *9th International Conference on Power Electronics and Motion Control EPE-PEMC'2000*, Kosice, Slovak Republic, pp. 1-98 - 1-103.

Consoli,A., Russo,F., Scarcella,G., and Testa,A. (1999a), Low and zero speed sensorless control of synchronous reluctance motors, *IEEE Transactions on Industry Applications*, Vol. 35, No. 5., pp. 1050-1057.

Consoli,A., Scarcella,G., and Testa,A. (1999b), Sensorless control of permanent magnet synchronous motors at zero speed, *IEEE Industrial Application Society Annual Meeting IAS'99*, Phoenix, Arizona, pp. 1033-1040.

Consoli,A., Scarcella,G., and Testa,A. (2000), A new zero-frequency flux-position detection approach for direct-field-oriented-control drives, *IEEE Transactions on Industry Applications*, Vol. 36, No. 3, pp. 797-804.

De Donker,R., Profumo,F., and Pastorelli,M. (1990), Self-tuning of induction motor servo drives using the universal field oriented controller, *IEEE Power Electronics Specialists Conference PESC'90*, San Antonio, TX, pp. 649-655.

Degner,M.W., and Lorenz,R.D. (1997), Position estimation in induction machines utilising rotor bar slot harmonics and carrier frequency signal injection, *Power Conversion Conference PCC'97*, Nagaoka, Japan, pp. 69-72.

Degner,M.W., and Lorenz,R.D. (1998), Using multiple saliencies for the estimation of flux, position, and velocity in AC machines, *IEEE Transactions on Industry Applications*, Vol. 34, No. 5, pp. 1097-1104.

Degner,M.W., and Lorenz,R.D. (2000), Position estimation in induction machines utilising rotor bar slot harmonics and carrier-frequency signal injection, *IEEE Transactions on Industry Applications*, Vol. 36, No. 3, pp. 736-742.

Depenbrock,M. (1985), Direkte Selbstregelung (DSR) fur hochdynamische Drehfeldantriebe mit Stromrichterschaltung, *Etz Archiv,* Vol. 7, No. 7, pp. 211-218.

Depenbrock,M. (1988); Direct self-control (DSC) of inverter-fed induction motors, *IEEE Transactions on Power Electronics,* Vol. 3, No. 4, pp. 420-429.

Dittrich,A. (1998), Model based identification of the iron loss resistance of an induction machine, *International Conference on Power Electronics and Variable Speed Drives PEVD'98,* London, UK, IEE Conference Publication No. 456, pp. 500-503.

Dixon,J.W., and Rivarola,J.N. (1996), An improved method to measure speed in induction motors, based on induced irregularities, *IEEE Applied Power Electronics Conference APEC'96*, San Jose, CA, pp. 399-404.

Du,T., Vas,P., Stronach,A.F., and Brdys,M.A. (1994), Applications of Kalman filters and extended Luenberger observers in induction motor drives, *International Intelligent Motion Conference PCIM'94*, Nurnberg, Germany, pp. 369-386.

El Hassan,I., Roboam,X., De Fornel,B., and Westerholt,E.V. (1997), Torque dynamic behaviour of induction machine DTC in 4 quadrant operation, *IEEE*

International Symposium on Industrial Electronics ISIE'97, Guimaraes, Portugal, pp. 1034-1038.

Ferrah,A., Bradley,K.G., and Asher,G.M. (1992a), A FFT-based novel approach to noninvasive speed measurement in induction motor drives, *IEEE Transactions on Instrumentation and Measurement*, Vol. 41, No. 6, pp. 797-802.

Ferrah,A., Bradley,K.G., and Asher,G.M. (1992b), Sensorless speed detection of inverter fed induction motors using rotor slot harmonics and fast Fourier transform, *IEEE Power Electronics Specialist Conference PESC'92*, Toledo, Spain, pp. 279-286.

Ferrah,A., Bradley,K.J., Hogben,P.J., Woolfson,M.S., and Asher,G.M. (1996), A transputer-based speed identifier for induction motor drives using real-time adaptive filtering, *Proc. IEEE Industrial Application Society Annual Meeting IAS'96*, San Diego, CA, pp. 394-400.

Ferrah,A., Bradley,K.J., Hogben-Laing,P.J., Woolfson,M.S., Asher,G.M., Sumner,M., Cilia,J., and Shuli,J. (1998), A speed identifier for induction motor drives using real-time adaptive digital filtering, *IEEE Transactions on Industry Applications*, Vol.34, No.1, pp. 156-162.

Garcia,G.O., Santisteban,J.A., and Brignone,S.D. (1994), Iron loss influence on a field-oriented controller, *The 20th Annual Conference of the IEEE Industrial Electronics Society IECON'94*, Bologna, Italy, pp. 633-638.

Griva,G., Profumo,F., Bojoi,R., Bostan,V., Cuibus,M., and Ilas,C. (2001), General adaptation law for MRAS high performance sensorless induction motor drives, *IEEE Power Electronics Specialist Conference PESC'01*, Vancouver, Canada, pp. 1197-1202.

Habetler,T.G., and Divan,D.M. (1991), Control strategy for direct self control using discrete pulse modulation, *IEEE Transactions on Industry Applications*, Vol. 27, No. 5, pp. 893-901.

Habetler,T.G., Profumo,F., Pastorelli,M., and Tolbert,L.M. (1992), Direct torque control of induction machines using space vector modulation, *IEEE Transactions on Industry Applications*, Vol. 28, No.5, pp. 1045-1053.

Habetler,T.G., Profumo,F., Griva,G., Pastorelli,M., and Bettini,A. (1998), Stator resistance tuning in a stator-flux oriented drive using an instantaneous hybrid

flux estimator, *IEEE Transactions on Power Electronics,* Vol. 13, No. 1, pp. 125-133.

Hintze,D., and Schröder,D. (1992), Induction motor drive with intelligent controller and parameter adaptation, *IEEE Industrial Application Society Annual Meeting IAS'92,* Houston, Texas, pp. 970-977.

Holliday,D., Fletcher,J.E., and Williams,B.W. (1995), Non-invasive rotor position and speed sensing of asynchronous motors, *European Conference on Power Electronics and Applications EPE'95*, Sevilla, Spain, pp. 1.333-1.337.

Hu,J., and Wu,B. (1998), New integration algorithms for estimating motor flux over a wide speed range, *IEEE Transactions on Power Electronics,* Vol. 13, No. 5, pp. 969-977.

Hurst,K.D., and Habetler,T.G. (1997), A comparison of spectrum estimation techniques for sensorless speed detection in induction machines, *IEEE Transactions on Industry Applications*, Vol.33, No.4, pp. 898-905.

Hurst,K.D., Habetler,T.G., Griva,G., and Profumo,F. (1994), Speed sensorless field-oriented control of induction machines using current harmonic spectral estimation, *IEEE Industrial Application Society Annual Meeting IAS'94*, Denver, CO, pp. 601-607.

Hurst,K.D., Habetler,T.G., Griva,G., Profumo,F., and Jansen,P.L. (1997), A self-tuning closed-loop flux observer for sensorless torque control of standard induction machines, *IEEE Transactions on Power Electronics*, Vol. 12, No. 5, pp. 807-815.

Hurst,K.D., Habetler,T.G., Griva,G., and Profumo,F. (1998), Zero-speed tacholess IM torque control: Simply a matter stator voltage integration, *IEEE Transactions on Industry Applications*, Vol. 34, No. 4, pp. 790-795.

Ibrahim,Z., and Levi,E. (2002), A comparative analysis of fuzzy logic and PI speed control in high-performance AC drives using experimental approach, *IEEE Transactions on Industry Applications*, Vol. 38, No. 5, pp. 1210-1218.

Jacobina,C.B., Filho,J.E.C., and Lima,A.M.N. (2000), On-line estimation of the stator resistance of induction machines based on zero-sequence model, *IEEE Transactions on Power Electronics*, Vol. 15, No.2, pp. 346-353.

Jansen,P.L., and Lorenz,R.D. (1995a), Transducerless field orientation concepts employing saturation-induced saliencies in induction machines, *IEEE Industrial Application Society Annual Meeting IAS'95*, Orlando, Florida, pp. 174-181.

Jansen,P.L., and Lorenz,R.D. (1995b), Tranducerless position and velocity estimation in induction machines and salient AC machines, *IEEE Transactions on Industry Applications*, Vol. 31, No. 2, pp. 240-247.

Jansen,P.L., and Lorenz,R.D. (1996), Transducerless field orientation concepts employing saturation-induced saliencies in induction machines, *IEEE Transactions on Industry Applications*, Vol. 32, No. 6, pp. 1380-1393.

Jiang,J., and Holtz,J. (1997), High dynamic speed sensorless AC drive with on-line model parameter tuning for steady-state accuracy, *IEEE Transactions on Industrial Electronics*, Vol. 44, No. 2, pp. 240-246.

Jung,J., and Nam,K. (1998), A vector control scheme for EV induction motors with a series iron loss model, *IEEE Transactions on Industrial Electronics,* Vol. 45, No. 4, pp. 617-624.

Kang,J.K., and Sul,S.K. (1999), New direct torque control of induction motor for minimum torque ripple and constant switching frequency, *IEEE Transactions on Industry Applications*, Vol. 35, No. 5, pp. 1076-1082.

Kazmierkowski,M.P., and Tunia,H. (1994), *Automatic Control of Converter-Fed Drive*, Elsevier, New York.

Kazmierkowski,M.P., and Kasprowicz,A.B. (1995), Improved direct torque and flux vector control of PWM inverter-fed induction motor drives, IEEE Transactions on Industrial Electronics, Vol.42, No.4, pp. 344-350.

Kerkman,R.J., Seibel,B.J., Rowan,T.M., and Schlegel,D.W. (1996), A new flux and stator resistance identifier for AC drive systems, *IEEE Transactions on Industry Applications,* Vol. 32, No. 3, pp. 585-593.

Krause,P.C., Wasynczuk,O., and Sudhoff,S.D. (1995), *Analysis of electric machinery*, IEEE Press, New York.

Kreindler,L., Moreira,J.C., Testa,A., and Lipo,T.A. (1992), Direct field orientation controller using the stator phase voltage third harmonic, *IEEE Industrial Application Society Annual Meeting IAS'92*, Houston, Texas, pp. 508-516.

Kubota,H., and Matsuse,K. (1992), Compensation for core loss of adaptive flux observer-based field-oriented induction motor drives, *IEEE Industrial Electronics Society Annual Meeting IECON'92*, San Diego, CA, pp. 67-71.

Lai,Y.S., Lin,J.C., and Wang,J.J. (2000), Direct torque control induction motor drives with self-commissioning based on Taguchi methodology, *IEEE Transactions on Power Electronics*, Vol. 15, No.6, pp. 1065-1071.

Le-Huy,H. (1999), Comparison of field oriented control and direct torque control for induction motor drives, *IEEE Industrial Application Society Annual Meeting IAS'99*, Phoenix, Arizona, CD-ROM paper No. 28_1.pdf.

Lee,S.B., Habetler,T.G., Harley,R.G., and Gritter,D.J. (2000), A stator and rotor resistance estimation technique for conductor temperature monitoring, *IEEE Industrial Application Society Annual Meeting IAS'00*, Rome, Italy, CD-ROM paper No. 09_04.pdf.

Leonhard,W. (1996), *Control of electrical drives*, Springer-Verlag, Berlin, 2nd Edition.

Levi,E. (1994), Impact of iron loss on behaviour of vector controlled induction machines, *IEEE Industrial Application Society Annual Meeting IAS'94*, Denver, Colorado, pp. 74-80.

Levi,E. (1995), Impact of iron loss on behaviour of vector controlled induction machines, *IEEE Transactions on Industry Applications*, Vol.31, No.6, pp. 1287-1296.

Levi,E. (1996), Rotor flux oriented control of induction machines considering the core loss, *Electric Machines and Power Systems*, Vol. 24, No. 1, pp. 37-50.

Levi,E., and Pham-Dinh,T. (2001), Impact of iron loss on direct torque control of induction machines and its compensation, *European Power Electronics Conference EPE'01*, Graz, Austria, CD-ROM paper No. PP00047.pdf.

Levi,E., and Pham-Dinh,T. (2002), DTC of induction machines considering the iron loss, *Electrical Power Components and Systems*, Vol. 30, No. 6, pp. 557-579.

Levi,E., Vukosavic,S., and Vuckovic,V. (1990), Saturation compensation schemes for vector controlled induction motor drives, *IEEE Power Electronics Specialists Conference PESC'90*, San Antonio, Texas, USA, pp. 591-598.

Levi,E., Vuckovic,V., and Sokola,M. (1995), Rotor flux estimation in vector controlled induction machines incorporating the iron loss compensation, *European*

Conference on Power Electronics and Applications EPE'95, Seville, Spain, pp. 3.997-3.1002.

Levi,E., Sokola,M., Boglietti,A., and Pastorelli,M. (1996), Iron loss in rotor flux oriented induction machines: identification, assessment of detuning and compensation, *IEEE Transactions on Power Electronics,* Vol. 11, No. 5, pp. 698-709.

Levi,E., Wang,M., and Williams,D. (1999), Evaluation of iron loss influence on speed estimation in sensorless MRAC-based field-oriented induction machines, *European Transactions on Electrical Power ETEP*, Vol. 9, No. 2, pp. 77-84.

Liu,Y.H., and Chen,C.L. (1998), A novel regulation scheme for direct torque controller, *International Conference on Power Conversion and Intelligent Motion PCIM'98*, Nuremberg, Germany, pp. 269-273.

Lüdtke,I., and Jayne,M.G. (1995), A comparative study of high performance speed control strategies for voltage-sourced PWM inverter-fed induction motor drives, *Proceeding of IEE International Conference on Electric Machines and Drives,* IEE Conference Publication No. 412, pp. 343-348.

Manjrekar,M.D., Lipo,T.A., Chang,S.G., and Kim,K.S. (1998), Flux tracking methods for direct field orientation, *International Conference on Electrical Machines ICEM'98*, Istanbul, Turkey, pp. 1022-1029.

Marwali,M.N., and Keyhani,A. (1997), A comparative study of flux based MRAS and back emf based MRAS speed estimators for speed sensorless vector control of induction machines, *IEEE Industrial Application Society Annual Meeting IAS'97*, New Orleans, LA, pp. 160 - 166.

Matsuse,K., Taniguchi,S., Yoshizumi,T., and Namiki,K. (1999a), A speed sensorless vector control of induction motor operating at high efficiency taking core loss into account, *IEEE Industrial Application Society Annual Meeting IAS'99,* Phoenix, Arizona, CD-ROM Paper No. 28_3.

Matsuse,K., Yoshizumi,T., Katsusa,S., and Taniguchi,S. (1999b), High-response flux control of direct-field-oriented induction motor with high efficiency taking core loss into account, *IEEE Transactions on Industry Applications,* Vol. 35, No. 1, pp. 62-69.

Mir,S., Elbuluk,M.E., and Zinger,D.S. (1998), PI and fuzzy estimators for tuning the stator resistance in direct torque control of induction machines, *IEEE Transactions on Power Electronics,* Vol. 13, No. 2, pp. 279-287.

Mizuno,T., Takayama,J., Ichioka,T., and Terashima,M. (1990), Decoupling control method of induction motors taking stator core loss into consideration, *International Power Electronics Conference IPEC'90,* Tokyo, Japan, pp. 69-74.

Monmasson,E., Naassani,A.A., and Louis,J.P. (2001), Extension of DTC concept, *IEEE Transactions on Industrial Electronics*, Vol. 48, No. 3, pp. 715-717.

Moreira,J.C., and Lipo,T.A. (1990), Direct field orientation using the third harmonic component of the stator voltage, *International Conference on Electrical Machines ICEM'90*, Cambridge, Massachusetts, pp. 1237-1242.

Moulahoum,S., Touhami,O., and Benhaddadi,M. (1998), Iron loss in vector controlled induction machine, *International Conference on Electrical Machines ICEM'98*, Istanbul, Turkey, pp. 169-174.

Nillesen,M.E., Duarte,J.L., Pasquariello,M., and Del Pizzo,A. (2000), Direct torque control with the application of a predictive pulse width c ontrol, *IEEE Annual Meeting of Industrial Applications Society IAS'00*, Rome, Italy, CD-ROM paper 33_05.pdf.

Noguchi,T. and Hiraishi,D. (1999), Core loss compensation of direct field-oriented induction motor incorporating robust parameter identification, *IEEE Industrial Electronics Society Annual Conference IECON'99*, San Jose, CA, pp. 1409-1414.

Noguchi,T., Nakmahachalasint,P., and Watanakul,N. (1997), Precise torque control of induction motor with on-line parameter identification in consideration of core loss, *Proceeding of Power Conversion Conference PCC'97,* Nagaoka, Japan, pp. 113-118.

Novotny,D.W., and Lipo,T.A. (1996), *Vector control and dynamics of AC drives,* Clarendon Press, Oxford.

Peng,F.Z., and Fukao,T. (1994), Robust speed identification for speed-sensorless vector control of induction motors, *IEEE Transactions on Industry Applications*, Vol. 30, No. 5, pp. 1234-1240.

Perelmuter,V. (2000), Three-level inverters with direct torque control, *IEEE Annual Meeting of Industrial Applications Society IAS'00*, Rome, Italy, CD-ROM paper 33_04.pdf.

Pham-Dinh,T. and Levi, E. (2000), Induction motor direct torque control versus vector control: A comparison, *Universities Power Engineering Conference UPEC'00*, Belfast, UK, CD-ROM paper No. P150.pdf.

Pham-Dinh,T., and Levi,E. (2001a), Core loss in direct torque controlled induction motor drives: Detuning and compensation, *IEEE Power Electronics Specialist Conference PESC'01*, Vancouver, Canada, pp. 1429-1434.

Pham-Dinh,T. and Levi, E. (2001b), Modified switching tables for direct torque control, *Universities Power Engineering Conference UPEC'01*, Swansea, UK, CD-ROM paper No. P534.pdf.

Pham-Dinh,T., and Levi,E. (2002), Sensorless DTC of induction machines with complete core loss compensation, *IEE International Conference on Power Electronics Machines and Drives PEMD'02*, Bath, UK, pp. 98-103.

Purcell,A., and Acarnley,P. (1998), Multi-level hysteresis comparator forms for direct torque control scheme, *Electronics Letters*, Vol. 34, No. 6, pp. 601-603.

Rasmussen,H., Vadstrup,P., and Børsting,H. (1999), Rotor field oriented control with adaptive iron loss compensation, *IEEE Industrial Application Society Annual Meeting IAS'99*, Phoenix, Arizona, CD-ROM Paper No. 28_2.

Schauder,C. (1992), Adaptive speed identification for vector control of induction motor without rotational transducers, *IEEE Transactions on Industry Applications*, Vol. 28, No. 5, pp. 1054-1061.

Schofield,J.R.G. (1998); Variable speed drives using induction motors and direct torque control, *Digests of IEE Colloquium on 'Vector Control Revisited'*, London, pp. 5/1-5/7.

Schroedl,M. (1988), Detection of rotor position of permanent magnet synchronuous machines at standstill, *International Conference on Electrical Machines ICEM'88*, Pisa, pp. 195-197.

Schroedl,M. (1992), Sensorless control of induction motors at low speed and standstill, *International Conference on Electrical Machines ICEM'92*, Manchester, UK, pp. 863-867.

Schroedl,M. (1993), Digital implementation of a sensorless algorithm for permanent magnet synchronous motors, *European Conference on Power Electronics and Applications EPE'93*, Brighton, UK, pp. 430-435.

Sokola,M. (1998), *Vector control of induction machines using improved machine models*, PhD Thesis, Liverpool John Moores University, Liverpool, UK.

Sokola,M., and Levi,E. (2001), Experimental evaluation of parameter variation effects in indirect rotor-flux oriented induction-motor drives, *European Transactions on Electrical Power*, Vol. 11, No. 2, pp. 107-117.

Späth,H. (1983), Steuerverfahren für Drehstrommaschinen, Springer Verlag, Heidelberg.

Staines,C.S., Asher,G.M., and Bradley,K.J. (1998), A new method for sensorless derivation of an induction motor shaft position and other machine characteristics, *International Conference on Electrical Machines ICEM'98*, Istanbul, Turkey, pp. 902-907.

Tajima,H., and Hori,Y. (1993), Speed sensorless field-orientation control of the induction machine, *IEEE Transactions on Industry Applications*, Vol. 29, No. 1, pp. 175-180.

Takahashi,I., and Noguchi,T. (1986), A new quick-response and high-efficiency control strategy of an induction motor, *IEEE Transactions on Industry Applications*, Vol. IA-22, No.5, pp. 820-827.

Takahashi,I., and Ohmori,Y. (1989); High performance direct torque control of an induction machine, *IEEE Transactions on Industry Applications,* Vol. 25, No. 2, pp. 257-264.

Tan,Z., Li,Y., and Li,M. (2001), A direct torque control of induction motor based on three-level NPC inverter, *IEEE Power Electronics Specialist Conference PESC'01*, Vancouver, Canada, pp. 1435-1439.

Tang,L., and Rahman,M.F. (2001), A new direct torque control strategy for flux and torque ripple reduction for induction motor drives by using space vector modulation, *IEEE Power Electronics Specialist Conference PESC'01*, Vancouver, Canada, pp. 1440-1445.

Tiitinen,P. (1996); The next generation motor control method, DTC direct torque control, *IEEE International Conference on Power Electronics, Drives and Energy Systems for Industrial Growth PEDES'96,* New Delhi, India, pp. 37-43.

Tiitinen,P., Pohjalainen,P., and Lalu,J. (1995),The next generation motor control method: Direct torque control (DTC), *European Power Electronics Journal,* Vol. 5, No. 1, pp. 14-18.

Trzynadlowski,A.M. (1994), *The field orientation principle in control of induction motors*, Kluwer Academic Publishers, Norwell, Massachusetts.

Turl,G., Sumner,M., and Asher, G.M. (2001), A hybrid sensorless induction motor control strategy for high performance drive applications, *IEEE Power Electronics Specialist Conference PESC'01*, Vancouver, Canada, pp. 20-25.

Vas,P. (1990), *Vector control of AC machines*, Oxford University Press, New York.

Vas,P. (1992), *Electrical machines and drives - A space-vector theory approach*, Oxford Clarendon Press.

Vas,P. (1993), *Parameter estimation, condition monitoring, and diagnosis of electrical machines*, Oxford University Press, New York.

Vas,P. (1998), *Sensorless vector and direct torque control*, Oxford University Press, New York.

Vas,P., and Rashed,M. (1999), DSP implementation of sensorless DTC induction motor and permanent magnet synchronous motor drives with minimised torque ripples, *European Conference on Power Electronics and Applications EPE'99*, Lausanne, Switzerland, CD-ROM paper.

Wang,M. (1999), *Parameter variation effects in sensorless vector controlled induction machines*, PhD dissertation, School of engineering, Liverpool John Moores University, United Kingdom.

Wang,M., Levi,E., and Jovanovic,M. (1999), Compensation of parameter variation effects in sensorless indirect vector controlled induction machines using model based approach, *Electric Machines and Power Systems,* Vol. 27, No. 9, pp. 1001-1027.

Wee,S.D., Shin,M.H., and Hyun,D.S. (1999), Stator flux-oriented vector control of induction motors considering iron-loss, *Annual Conference of the IEEE Industrial Electronics Society IECON'99,* San Jose, California, pp. 945-950.

Wieser,R.S. (1995), High dynamic torque calculator for inverter fed induction machines, *European Conference on Power Electronics and Applications EPE'95*, Seville, Spain, pp. 3.771-3.776.

Wieser,R.S. (1997), Optimal rotor flux regulation for fast accelerating induction machines in the field weakening region, *IEEE Industrial Applications Society Annual Meeting IAS'97*, New Orleans, Louisiana, USA, pp. 401-409.

Wieser,R.S. (1998), Some clarifications on the impact of AC machine iron properties on space phasor models and field oriented control, *International Conference on Electrical Machines ICEM'98*, Istanbul, Turkey, pp. 1510-1515.

Wu,R., and Slemon,G.R. (1991), A permanent magnet motor drive without a shaft sensor, *IEEE Transactions on Industry Applications*, Vol. 27, No. 5, pp. 1005-1011.

Wu,X.Q., and Steimel,A. (1997), Direct self control of induction machines fed by a double three-level inverter, *IEEE Transactions on Industrial Electronics*, Vol. 44, No. 4, pp. 519-527.

Xu,X., De Donker,R., and Novotny,D.W. (1988a), Stator flux orientation control of induction machines in the field weakening region, *IEEE Industrial Application Society Annual Meeting IAS'88*, Pittsburgh, PA, pp. 437-443.

Xu,X., De Donker,R., and Novotny,D.W. (1988b), Stator flux oriented induction motor drives, *IEEE Power Electronics Specialists Conference PESC'88*, Kyoto, Japan, pp. 870-876.

Zhen,L., and Xu,L. (1995), A mutual MRAS identification scheme for position sensorless field orientation control of induction machines, *IEEE Industrial Application Society Annual Meeting IAS'95*, Orlando, FL, pp. 159-165.

Zhen,L., and Xu,L. (1998), Sensorless field orientation control of induction machines based on a mutual MRAS scheme, *IEEE Transactions on Industrial Electronics*, Vol. 45, No. 5, pp. 824-831.

Zinger,D.S., Profumo,F., Lipo,T.A., and Novotny,D.W. (1990), A direct field-oriented controller for induction motor drive using tapped stator windings, *IEEE Transactions on Power Electronics*, Vol. 5, No. 4, pp. 446-453.

APPENDIX A: INDUCTION MOTOR DATA

$P_n = 4$ kW

$n_n = 1440$ rpm

$T_{en} = 26.5$ N.m

$V_n = 380$ V

$I_n = 8.7$ A

50 Hz

Star connected

$2P = 4$

$R_s = 1.37\ \Omega$

$R_r = 1.10\ \Omega$

$L_m = 0.141$ H

$L_{\sigma s} = 4.87$ mH

$L_{\sigma r} = 7.96$ mH

$\psi_{sn} = 0.9889$ Wb (peak)

PAGE/PAGES EXCLUDED UNDER INSTRUCTION FROM UNIVERSITY